Understanding the role of dietary sulforaphane in regulating metabolic pathways using genomic approaches

Federico Bernuzzi

Quadram Institute of Bioscience

A thesis submitted to the University of East Anglia for the Degree of Doctor of Philosophy

October 2021

This work was supported by the UKRI Biotechnology and Biological Sciences Research Council (BBSRC) Norwich Research Park Biosciences Doctoral Training Partnership grant number BB/M011216/1, the BBSRC Institute Strategic Programme Food Innovation and Health BB/R012512/1 and its constituent project BBS/E/F/000PR10347 (Theme 4, Regulation of Metabolic Homeostasis)

Abstract:

Introduction:

Sulforaphane (4-methyl sulfinylbutyl isothiocyanate), a phytochemical derived from broccoli, has been linked to many health benefits in model systems, primarily through the activation of NRF2 (Nuclear factor erythroid-2 related factor), which regulates cellular antioxidant response. Recent evidence suggests that SF may improve glucose regulation in diabetic patients, but the molecular pathways or the role of NRF2 are yet unclear. This work set out to assess the molecular mechanisms by which SF regulates energy metabolism in the liver under conditions that represent different cellular metabolic states.

Methods:

Established liver hepatocellular carcinoma cells (HepG2) were treated with physiological concentrations of SF (10 μM) under varying glucose concentrations; no (0 mM), basal (5 mM), and high glucose (25 mM). Metabolic phenotyping was undertaken using the Seahorse Extracellular Flux Analyser, untargeted metabolomics, and subsequent experiments with stable isotope tracers of glucose and glutamine, coupled with Gas-Chromatography and Mass Spectrometry (GC-MS). Whole transcriptome was obtained through Illumina RNA sequencing. Finally, the genome-editing technique CRISPR-Cas 9 was applied to assess whether NRF2 mediates the metabolic changes.

Results:

Real time energy production assessed using the Seahorse Extracellular Flux Analyser demonstrated that SF reduced both mitochondrial respiration and glycolysis in HepG2 cells in a high glucose environment. At the same time, the expression of GSH biosynthetic genes and levels of reduced glutathione (GSH) were significantly increased. To support GSH synthesis, SF altered levels of the three amino acids that are the biosynthetic building blocks; namely, increased intracellular utilization of glycine and glutamate, by redirecting the latter away from the TCA cycle, as well as increased the import of cysteine from the media. To support the cellular antioxidant enzyme response, SF also altered pathways generating NADPH, the necessary cofactor for these oxidoreductase reactions, namely pentose phosphate pathway (PPP) and 1C-metabolism. Firstly, SF increased genes in the PPP pathway, including glucose-6-phosphate dehydrogenase, the rate limiting enzyme, and increased the PPP metabolite ribulose-5-phosphate, suggesting that excess glucose is likely redirected towards PPP, away from glycolysis. Secondly, SF upregulated genes in the folate cycle, namely 10-formyltetrahydrofolate dehydrogenase (ALDH1L1) and monofunctional C1-

tetrahydrofolate synthase (MTHFD1L) and utilized serine as a methyl donor for THF to support the 1C metabolism. Finally, SF downregulated the biosynthesis of the unsaturated fatty acids gene set, which is an NADPH consuming pathway. Finally, transcriptomic and targeted metabolomics LC-MS analysis of NRF2KD HepG2 cells generated using CRISPR-Cas 9 genome editing revealed that the above metabolic effects are mediated through NRF2.

Conclusions:

The results suggest that SF rewires central metabolism to suppress the metabolic dysregulation induced by excessive glucose and identify glucose biosynthesis and 1C-metabolism as key mechanistic pathways.

Table of Contents

Abbreviations

1C	One Carbon Metabolism
2-DG	2-Deoxy-d-Glucose
ACTB	Beta-Actin
ANOVA	Analysis of Variance
ARE	Antioxidant Response Element
ATP	Adenosine 5-Triphosphate
BG	Basal Glucose
BMI	Body Mass Index
BSE	Broccoli sprout extract
CPT1a	Carnitine Palmitoyltransferase
CRISPR Cas9	Clustered Regularly Interspaced Short Palindromic Repeats Cas 9
CVD	Cardiovascular Diseases
DAG	Diacylglycerols
DEG	Differentially Expressed Genes
DMEM	Dulbecco's Modified Eagle Medium
DMSO	Dimethyl Sulfoxide
DNA	Deoxyribonucleic acid
DPBS	Phosphate Buffer Saline
ECAR	Extracellular Acidification Rate
EMEM	Eagle's Minimum Essential Medium
ER	Endoplasmic Reticulumn
FADH	Flavin Adenine Dinucleotide
FASD	Fatty Acid Desaturase
FASN	Fatty Acid Synthease
FBS	Fetal Bovine Serum
FDR	False Discovery Rate
FCCP	Carbonyl cyanide-p-trifluoromethoxyphenylhydrazone
G6PD	Glucose-6-Phospahte Dehydrogenase
GCK	Glucokinase
GCLC	Glutamate Cysteine Ligase Catalytic Subunit
GCLM	Glutamate Cysteine Ligase Regulatory Subunit
GC-MS	Gas Chromatography-Mass Spectrometry
GI	Gastrointestinal
GLDC	Glycine Decarboxylase
GPx	Glutathione Peroxidase
GR	Glutathione Reductase
GSEA	Gene Set Enrichment Analysis
GSH	Reduced Glutathione
GSL	Glucosinolates
GSSG	Glutathione Disulfide
GSTM	Glutathione S-transferase
HCC	Hepatocelluar Carcinoma
HDL	High-Density Lipoprotein
HepG2	Hepatocellular Carcinoma Cell Line
HG	High Glucose
HMOX1	Heme Oxygenase
I3C	Indole-3-carbinol

IL	Interleukin
IMP	Inosine Monophosphate
IR	Insulin Resistance
ITC	Isothiocyanate
KEAP1	Kelch-like ECH-associated protein 1
KEGG	Kyoto Encylopedia of Genes and Genomes
LC-MS	Liquid Chromatography-Mass Spectrometry
LDL	Low-Density Lipoprotein
MetX	Metabolic Syndrome
MID	Mass Isotopic Distribution
mTOR	Mammalian Target Of Rapamycin
NaCl	Sodium chloride
NADH	Nicotinamide Adenine Dinucleotide
NADPH	Nicotinamide Adenine Dinucleotide Phosphate
NAFLD	Non-Alcholic Fatty Liver Diseases
NASH	Non-Alcholoic Steatohepatitis
NES	Normalized Enrichment Score
NG	No Glucose
NQO1	NAD(P)H Dehydrogenase Quinone 1
NRF2	Nuclear Factor Erythroid 2-Related Factor 2
NRF2KD	Nuclear Factor Erythroid 2-Related Factor 2 Knock Down
OCR	Oxygen Consumption Rate
PCA	Principal Component Analysis
PHGDH	Phosphoglycerate Dehydrogenase
PPAR	Peroxisome Proliferator Activated Receptor
PPP	Pentose Phosphate Pathway
qRT-PCR	Quantitative Real-Time Polymerase Chain Reaction
Rlog	*Regularised logarithm*
RNA-Seq	RNA-Sequencing
ROS	Reactive Oxygen Species
SCD	Stearoyl-CoA Desaturase
SF	Sulforaphane
SHMT1/2	Serine Hydroxymethyl Transferase 1/2
SIRT	Sirtuin
SREBF	Sterol Regultaroy Element Binding Transcription Factor
SRXN	Sulfiredoxin
SSP	Serine Synthetic Pathway
STZ	Streptozocin
SULT	Sulfotransferases
T2D	Type 2 Diabetes Mellitus
TALDO	Transaldolase
TCA	Tricarboxylic Citric Acid
TKT	Transketolase
TNFα	Tumour necrosis factor-α
TXN	Thioredoxin
TXNRD	Thioredoxin Reductase
UCP	Uncoupling Protein

Acknowledgments

It has been an incredible 4 years. Words cannot express how privileged I feel to have undertaken such fantastic opportunities; I am so grateful to everyone who has helped me along the way. I have met some amazing people, developed a worldwide network, and since a doctorate is not challenging or stimulating enough, I had the “pleasure” of finishing the last 18 months of my Ph.D. during the COVID-19 pandemic. Four years ago, I was not sure whether I made the right choice. Now finishing, I can safely say it has been one of the best choices of my life. The success and achievements of this thesis are not down to a single person but a combination of individuals who deserve to be recognized.

Dr. Maria Traka, my primary supervisor, whom in these last four years has been like a second mother. Thank you for your patience and perseverance, especially during the first year of my Ph.D., when I was often confused about what was happening, and in general for believing in me that I could succeed and complete the project. I just hope you enjoyed learning from me, as much as I have enjoyed learning from you.

Dr. Tamas Korcsmaros, despite the thesis, being very limited on Networks, (I tried my best!!) nevertheless, thank you for letting me participate in all the lab meetings. It has been fascinating to hear this side of science. It was also a pleasure hearing all the constructive feedback you gave me throughout my Ph.D., inspiring me to develop into a great scientist. Wishing you all the best with your future scientific career at Imperial.

Professor Richard Mithen, although our time spent in the group was short, I am extremely grateful for firstly allowing me to work as a technician for your group before starting my Ph.D. I enjoyed attending the lab meetings and hearing you present and learning beside you.

Professor Karsten Hiller, I cannot express how thankful I am for haven allowed me to spend six weeks in your lab. You made me fall in love with the field of metabolomics, and the science that your group does at BRICS is fascinating; not to mention living in Braunschweig was lovely, it is such a beautiful city. A special mention as well to Dr. Tobias Ludwig and Dr. Wei Hu, for training me how to carry out the stable isotope tracer’s experiment. I appreciated it a lot and Mr. Andre Martens for all your invaluable help with the data analysis (I still have nightmares of Metabolite Detector).

Dr. Perla Troncoso-Rey, you have been an incredible bioinformatician. At the start of my Ph.D., programming was a skill that daunted me, but with your incredible support, I am more confident now (I still have a lot to learn though). I enjoyed working alongside you, learning all sorts of tricks, converting extremely complex data frames in metabolic

pathways overnight. I am optimistic that I can utilize the skills for future research jobs to help to advance our scientific knowledge in health and disease.

Dr. Naiara Beraza, thank you for allowing me to work alongside you, to develop further expertise.

Dr. Wesley Folwer and Dr. Aleks Gontayczk, for training me on how to carry out Western Blotting and genotyping, two skills particularly useful during my CRISPR/Cas 9 work

Dr. Shikha Saha, the wizard of analytical chemistry. It feels like Shikha when I came to you with a problem, you always had a solution or an answer. It was great fun working alongside you, developing methods on the LC-MS, and teaching me how to analyze the data.

Throughout my Ph.D. I have met and made some amazing friends. Dr. Jenna Helleur, Dr. Sophie Prosolek, Dr. Dan Yara, Dr. Priscilla Day-Walsh, Miss Gemma Beasy, Miss Jasmine Percival, Mr. Emad Shehata, and Mr. Danny Ward. I like to think that it's through this friendship that we helped each other preserve through our Ph.D. especially during times that our research was going nowhere. A special thanks to Dr. Ebenezer Foster-Nyarko, who throughout these four years you were constantly challenging me to develop as a scientist either in the meetings that we used to have or the Journal Club you set up and for reviewing my thesis chapters.

I would like to thank UKRI and BBSRC for funding this work and allowing me to have taken the PIPs placement. Thank you to Mr. Malcolm and Miss Bernie Williams for the short but amazing experience at myDNAhealth and for getting me into public engagement. Wishing you all the best with the future of the company. A big thank you to the UEA Innovation team (especially Dr. Rosemary Bass) for allowing me to participate in i-Teams giving me insight into how to translate research into a commercial product.

A special mention goes to my family, especially my parents, sister, and Billi (the family dog, you helped me to de-stress a lot when I was back home) without their support and love I would not be the person that I am today.

And finally, to my Catholic community: The Singles For Christ and Couples For Christ and reverend Fr Andrew Eburne and Fr Laurie Locke. I have never realized the power of prayers. The last twelve months have been tough a lot of work. Coming in at 6 am leaving around 7 pm. Often doing long hours during the weekend as well. Yet I still persevered. I am sure that your prayers allowed me to keep going. Prayers do work, they always have and always will.

CHAPTER 1: An Introduction To Metabolic Dysregulation, The Importance of Sulphur Compounds in Cruciferous Vegetables And The NRF2 System

Chapter 1 Figure

Chapter 1 Tables

1.0 Chapter 1: General Introduction

1.1 Summary of thesis:

This thesis contains the results of a research project that focused on assessing how sulforaphane (SF) modulates hepatic metabolism using *in vitro* models. Initially, an *in vitro* model that mimics metabolic dysregulation was developed by challenging an immortalized liver cancer cell line, HepG2, with physiological concentrations of SF along with the presence of fatty acids and/or various concentrations of glucose. This was done to assess whether non-nutrient bioactives such as SF can mitigate the effects of a western diet. The subsequent investigation involved carrying out a

transcriptome and metabolomics analysis of HepG2 challenged with various glucose concentrations (none, basal, and high) in the presence of SF. The glucose environments were used to mimic different metabolic states. The investigation aimed to underpin the molecular mechanism on how SF may maintain healthy hepatic metabolism.
Finally, a novel liver cell line that lacks the transcription factor NRF2 was developed using the genome-editing technique, CRISPR/Cas 9. Promoted by the transcriptome and metabolomics analysis findings, a time-course transcriptome analysis was conducted between WT and NRF2KD cells with SF in the presence of high glucose. This was done to assess whether NRF2 or other proteins mediate the metabolic changes induced by SF.

The general introduction introduces the liver as the central metabolic organ and how diet can impact hepatic metabolism. An emphasis has been placed on how the Western diet can result in dysregulation of hepatic metabolism, resulting in chronic diseases such as type 2 diabetes, cardiovascular diseases, non-alcoholic fatty liver diseases, and potentially even cancer. The following section covers the potential health benefits of cruciferous vegetables in reducing the development of such pathologies. It describes how glucosinolates (GSLs) are found in high levels in these vegetables and their breakdown to the active isothiocyanates (ITCs), emphasising how SF may be responsible for the observed health benefits. The final section is a detailed literature review on the transcription factors NRF2 and its dual role: the antioxidant response and the emerging evidence on how it regulates metabolism. The output of this thesis will hopefully continue to build on the scientific evidence that future treatment and prevention of many metabolic diseases may fall back on the ancient statement by Hippocrates, “Let food be thy medicine”.

1.2 Obesity and its consequences:

Cellular metabolism can be defined as a series of chemical reactions in living organisms to maintain life. These can be catabolic, such as the breakdown of glucose to pyruvate to ultimately produce ATP, or anabolic, such as the synthesis of proteins and nucleotides (DeBerardinis and Thompson, 2012). Through poor lifestyle choices such as:

1. A diet refined in processed carbohydrates and sugars,
2. Little exercises,
3. Irregular sleep patterns, etc.,

What may occur over the long term is an imbalance in metabolic homeostasis. This can lead to increased weight gain, and over time, potentially developing metabolic disorders such as type 2 diabetes, cardiovascular diseases, and potentially even cancer (Bremer *et al*., 2012).

One of the main features of current lifestyles is the frequent consumption of food; overeating highly caloric dense foods that are less satiating, which results in increased appetite, ensuing in a vicious cycle of snacking throughout the day, resulting in a large part of the day being spent in the postprandial state. In healthy individuals who are insulin sensitive, the glucose load is rapidly cleared from the blood and distributed to various cells and tissues. Insulin resistant individuals, however, manifest some degree of hyperinsulinemia to force glucose into peripheral tissue. Over the long term, the recurrent intake of high caloric dense food can result in the β-cells of the pancreas failing to produce sufficient insulin, resulting in increased circulation of blood glucose. The outcome can result in the formation of insulin resistance, diabetes, and metabolic syndrome (see section 1.2.1). Diabetes occurs when the β-cells can longer produce enough insulin to maintain euglycemia.

Extensive research has shown that these diets high in glucose and high fats mediate inflammation, resulting in a build-up of oxidative stress that may alter cellular physiological processes (Herieka and Erridge, 2014, Emerson *et al*., 2018). Oxidative stress is a phenomenon caused by an imbalance between the production and accumulation of reactive oxygen species (ROS) in cells and tissues and the ability of a biological system to detoxify these products (Pizzino *et al*., 2017). The increased build-up of ROS will result in the activation of the transcription factor NF-ƙB, which induces the expression of the following cytokines: tumour necrosis factor-alpha (TNFα) and interleukin 6 (IL6), thereby promoting inflammation (Elmarakby and Sullivan, 2012, Rahman *et al*., 2002) (**figure 1.1**). Oxidative stress, moreover, may also promote cells into cellular senescence via cellular damage (MacKellar *et al*., 2010). In addition, excessive high caloric intake from either processed carbohydrates and/or high-fat diets will cause more substrates to enter the TCA cycle, resulting in more electrons being donated to the electron transport chain (Teodoro *et al*., 2013). What may occur is that the additional electrons might build at the complex III protein present in the respiratory chain, resulting in electrons being picked up by oxygen, further increasing the production of superoxide, creating a vicious cycle (Brownlee, 2001).

High processed/refined carbohydrate diets also result in significant blood glucose peaks post meals, resulting in large amounts of insulin being secreted. Over time, less insulin will bind to its receptor on cells, resulting in insulin resistance. Constant insulin secretion essentially drives fatty acid biosynthesis, as insulin upregulates the activity of

transcription factors related to fatty acid biosynthesis (Blaak *et al*., 2012, Wong and Sul, 2010).

Due to these lifestyle changes, the prevalence of obesity has rapidly increased over the last 10-15 years. Obesity is a medical condition in which an individual has accumulated excessive body fat that may negatively affect their health. Being obese puts individuals at increased risk of developing metabolic syndrome, type 2 diabetes, non-alcoholic fatty liver disease (NAFLD), cardiovascular diseases, and cancer. The leading underlying cause of these conditions is dysregulation of liver metabolism and the development of insulin resistance. Insulin resistance is a medical condition in which cells fail to respond to insulin. Glucose produced from the liver contributes to hyperglycemia in type 2 diabetic patients (Magnusson *et al*., 1992, Meyer *et al*., 1998). In healthy livers, glucokinase (GCK) promotes glucose utilization; studies using Zucker diabetic obese rats have shown much lower GCK expression. Similarly, overexpression of GCK in these rats decreases hyperglycemia (Torres *et al*., 2009). This, in turn, can promote endoplasmic reticulum (ER) stress, thereby promoting insulin resistance in the liver and damaging β-cells of the pancreas (Back and Kaufman, 2012, Lozano *et al*., 2016).

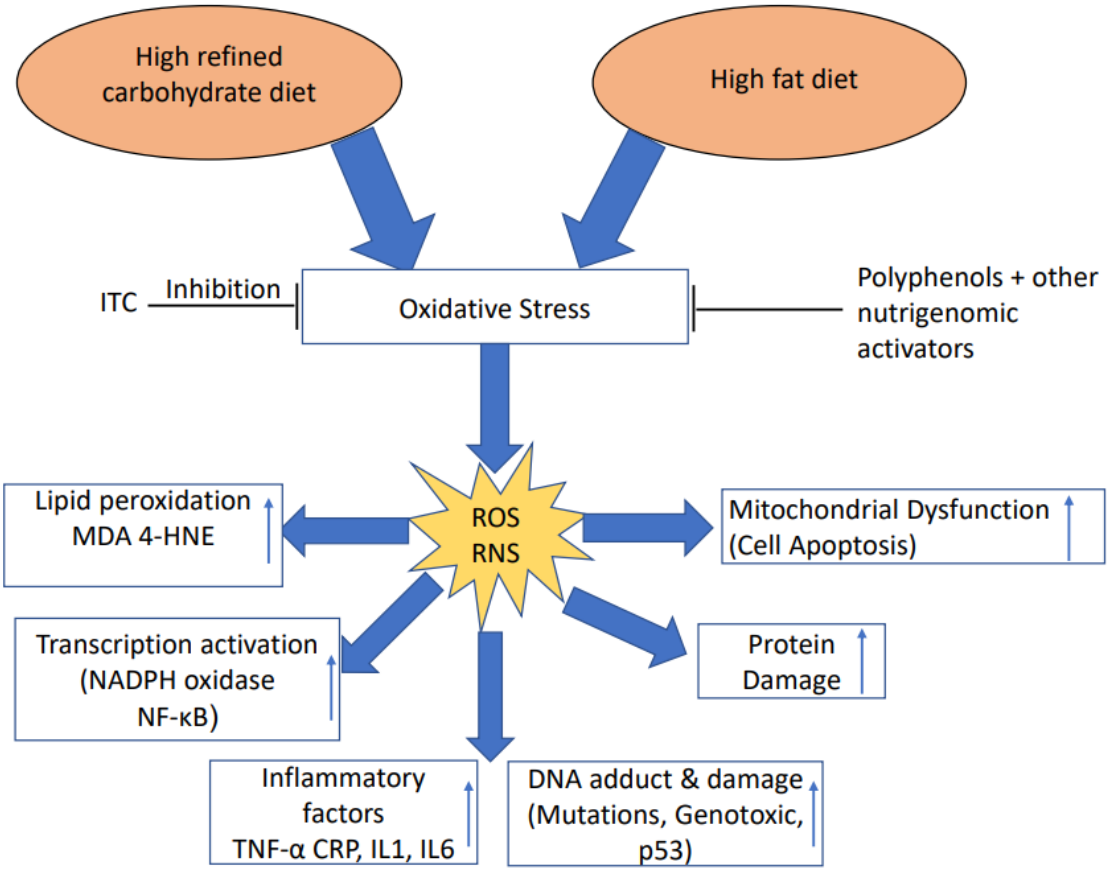

Figure 1.1 **The interplay between a Western diet, resulting in increased oxidative stress leading to more ROS produced, which can result in the formation of human pathologies over the long term.** RNS (Reactive Nitrogen Species), MDA (malondialdehyde), 4-HNE (4-hydroxynonena), CRP (C-reactive protein), p53 (tumour protein p53).

1.2.1 REDOX Balance and Metabolic Control

In biological organisms, reactive oxygen species (ROS) are by-products of normal oxygen metabolism. The primary sources of ROS arise from the protein complexes I and III of the electron transport chain, in the form of free-radical intermediates such as a superoxide ion ($O2^-$), resulting from the partial reduction of oxygen (Ray *et al*., 2012). Production of these ROS is an unavoidable and inherent consequence of healthy mitochondrial function. ROS have been shown to have a dual role; at low levels, these ROS are needed for cellular function, as they can act as important signalling molecules (Ray *et al*., 2012). A build-up of these ROS, if left untreated, can lead to impaired physiological function through:

- Cellular damage of DNA results in the formation of DNA adducts, causing impaired DNA replication and leading to mutations (Juan *et al*., 2021) (**figure 1.1**).

- Oxidation of amino acids damages proteins (resulting in altered protein structure) (Juan *et al*., 2021).
- Oxidation of polyunsaturated fatty acids results in lipid peroxides (Juan *et al*., 2021).

When ROS overwhelm the cellular antioxidant defence mechanism, oxidative stress occurs. Formation of the following human pathologies, including cancers (Trachootham *et al*., 2009), neurodegenerative disorders (Shukla *et al*., 2011), cardiovascular diseases (Paravicini and Touyz, 2006) and ageing (Haigis and Yankner, 2010), has been linked with increased oxidative stress. These ROS can also arise from exposure to exogenous sources such as heavy metals (Muthukumar and Nachiappan, 2010), cigarette smoke, alcohol intake, or UV radiation. Under homeostasis, cellular ROS are balanced by the cell's antioxidant capacity, more commonly referred to as the cellular REDOX status. Two critical enzymes that help clear ROS are superoxide dismutase and catalase. Superoxide dismutase converts superoxide's into hydrogen peroxide (H_2O_2), which is then neutralised by catalase into water. The primary REDOX sensor of the cell and, therefore, an essential part of the antioxidant response is the tripeptide glutathione (Pizzorno, 2014) (see chapter 5 for more detailed information about glutathione). The critical residue that allows glutathione to bind ROS and neutralise ROS is through cysteine, which can be reversibly oxidised in response to subtle changes in the cellular environment, acting as a biological ROS sensor (Pizzorno, 2014).

1.2.2 REDOX, Diet and Health

Although certain foods such as berries and chocolate have antioxidant properties due to the polyphenols and turmeric (through curcumin) (Hewlings and Kalman, 2017, Carlsen *et al*., 2010), the scientific evidence remains unclear whether antioxidant-rich foods can reduce certain diseases. Chocolate, for example, is rich in flavonoids, and these compounds have been previously reported to have free radical scavenging properties and chelation of transition metals ions and can also modulate specific signalling pathways (Williams *et al*., 2004). It is thought that through these processes, antioxidants can slow or prevent DNA damage, ultimately leading to reduced disease risk and potentially increasing longevity.

Whilst dietary antioxidants can be obtained from various fruits and vegetables, broccoli is perhaps one of the most studied sources of antioxidant non-nutrients (see **section 1.3**). SF derived from the breakdown of the glucosinolate glucoraphanin has been shown to increase the cellular antioxidant capacity through upregulation of antioxidant

detoxification pathways through activation of the transcription factor NRF2 (Itoh *et al*., 1999) (see **NRF2 section 1.5**).

1.2.3 Metabolic syndrome (MetS)

At the centre of insulin resistance is MetS. Although there is no current definition of MetS, it is commonly described by clustering of at least three out of the five medical conditions: abdominal obesity, high blood pressure, high blood sugar, high serum triglycerides, and low serum high-density lipoprotein (HDL), with the vital sign of metabolic syndrome being characterized by central obesity (Saklayen, 2018). Table 1.0 represents a detailed summary of all the clinical symptoms.

What is still not fully understood is the trigger of MetS; whether MetS is caused either by obesity or insulin resistance or due too much further metabolic damage. MetS is thought to result in a dysregulation of the body's ability to store and utilize energy. Chronic physical inactivity coupled with a persistent poor diet has been suggested as the leading hypothesis for driving the development of MetS (Bremer *et al*., 2012). MetS has become one of the most significant healthcare burdens in the developed world. In the US alone, 1 in 3 adults are estimated to live with the disease, and the problem is increasingly affecting the UK (Saklayen, 2018).

Table 1.0: Detailed Classification of all the possible clinical symptoms that can result in Metabolic Syndrome

Symptom	Classification
Fasting Blood Glucose	Glucose ≥ 110 mg/dL
Obesity	WHR > 0.9 in men
	WHR > 0.85 in women
	BMI ≥ 30kg/m2
Triglycerides	≥ 150 mg/dL
Total Cholesterol	> 200 mg/Dl
HDL Cholesterol	< 40 mg/dL in men
	< 50 mg/dL in women
Hypertension	≥ 140/90 mmHg
Microalbuminuria	Albumin/creatinine ratio > 30 mg/g
	Albumin excretion rate > 20 mcg/min

It is predicted that the National Health Services (NHS) will spend 17% of their entire budget (£16.9 billion) on diabetes management alone by the financial year of 2035/36, with further spending required to cover other MetS-related comorbidities (https://www.diabetes.org.uk/about_us/news_landing_page/nhs-spending-on-diabetes-to-reach-169-billion-by-2035). Currently there is no specific treatment for MetS. Instead, general practitioners will often treat each patient separately by prescribing the

following drugs depending on the patient's symptoms: angiotensin converting enzymes (ACE) inhibitors to treat hypertension, statins to treat hypercholesterolemia, and metformin to reduce fasting blood sugars. As these prescriptions are expensive, affordable alternative treatments are under investigation (Stedman *et al*., 2019).

Dietary interventions represent a cost-effective and straightforward approach. Specific dietary interventions have already been put into practice. These include daily physical exercises (at least 30 minutes a day) along with other calorie restricted diets; by either reducing saturated fats or reducing the intake of dietary carbohydrates (de la Iglesia *et al*., 2016). Recent evidence suggests that modulating the gut microbiome may be a potential strategy. At the centre of diet and health, the gut microbiome has recently been shown to be crucial in maintaining human health.

The gut microbiome is an ecosystem of bacteria, fungi, archaea, and viruses that inhabit the gastrointestinal tract (Thursby and Juge, 2017). A diverse microbiota has been associated with the production of a wide range of metabolites that may have anti-inflammatory and anti-oxidant activity (Wang *et al*., 2020). Observational studies have shown that patients with MetS have decreased beneficial microbes coupled with increased proliferation of potentially harmful ones (Wang *et al*., 2020, Moran-Ramos *et al*., 2017). For example, one study identified that individuals who had MetS and were obese had a decrease in the following bacteria: *Fecalibacterium, Oscillibacter*, and *Alistipes*, as well as having reduced levels of serum metabolites related to gut microbial patterns, compared to lean individuals (Thingholm *et al*., 2019). These bacteria are commonly associated with the fermentation of dietary fiber. Mechanistic studies using obese mice have instead shown that supplementing with the prebiotic oligofructose resulted in a 100-fold increase in the abundance of *Akkermansia* (Plovier *et al*., 2017). In addition, non-nutrient bioactive compounds, some of which the microbiome produce, are promising strategies to prevent or delay the onset of MetS through their effect on lipid and glucose homeostasis (NRF2 metabolism 1.9.5/1.9.6).

1.2.4 Non-alcoholic fatty liver diseases

Systemic insulin resistance and MetS are also underlying factors for developing non-alcoholic fatty liver disease (NAFLD). NAFLD represents a spectrum of disorders, ranging from the accumulation of lipids in the liver (hepatic steatosis), where the levels of lipids present around the liver are more significant than 5% (Fabbrini *et al*., 2009). More severe steatosis results in liver scarring and inflammation (referred to as non-alcoholic steatohepatitis, NASH). Patients who develop NASH have a 2.5% increased risk of dying per year (Chalasani *et al*., 2018). In the worst scenario, NAFLD can evolve into hepatocellular carcinoma or liver failure (Fabbrini *et al*., 2009). Lipid accumulation

in the liver further promotes hepatic insulin resistance, forming a vicious cycle. NAFLD is currently the most common liver disorder worldwide, estimated at 25% of the world's population (Marjot *et al*., 2019). Over 90% of obese, 60% diabetic and up to 20% of normal-weight people would develop NAFLD at some point in their life (Younossi *et al*., 2018). NAFLD is also the leading cause of chronic liver diseases. Like MetS, the current treatment for NAFLD is weight loss through lifestyle changes: mainly through dietary changes and increased exercise (Kenneally *et al*., 2017). Within the last couple of years, preliminary studies have shown that several different strategies are being investigated to potentially ameliorate the condition (Glen *et al*., 2016, Tilg *et al*., 2017).

The primary feature of NAFLD is the accumulation of lipids in the form of triglycerides on the liver. To date, however, it is not fully understood how and why these triglycerides accumulate. It has been proposed that oxidative stress, through ROS production, hormonal imbalances, and mitochondrial abnormalities, all appear to play a role in the formation of the disease (Friedman *et al*., 2018). Ongoing research has also suggested the possibility that increased consumption of fructose is a driver of the disease. Consumption of high levels of fructose prompts *de novo* lipogenesis while at the same time inhibiting β-oxidation. The enzyme fructokinase can rapidly metabolize fructose, resulting in its depletion, thereby reducing the intracellular levels of ATP. This decrease in ATP results in increased oxidative stress, resulting in impaired liver function along with excessive lipids accumulating in the liver (Marjot *et al*., 2019). The cell's metabolic state drives hexokinase (also called glucokinase) activity. On the other hand, Fructokinase is not controlled by the cell metabolic state.

1.2.5 MetS and cardiovascular diseases

Being insulin resistant can also increase the risk of developing cardiovascular diseases (CVDs). CVDs are another cluster of diseases related to diet and lifestyle choices and are largely preventable. It is estimated that up to 90% of CVD may be prevented (O'Donnell *et al.*, 2016). CVDs involve the heart or blood vessels. The most common CVDs include coronary heart diseases such as angina and myocardial infarction (the latter more commonly referred to as heart attack) (Flora and Nayak, 2019). Other common examples of CVDs include (Flora and Nayak, 2019):

1. Stroke,
2. Heart failure,
3. Hypertensive heart disease,
4. Cardiomyopathy,
5. Arrhythmia (irregular heartbeat),
6. Thrombosis and many others.

Common risk factors for the development of CVDs include hypertension, smoking, T2DM, lack of exercise, obesity, hypercholesterolemia, poor diet, and excessive alcohol consumption.

Coronary heart diseases, heart attack, and stroke all result in the formation of atherosclerotic plaques, leading to the gradual build-up of fat (cholesterol) in the walls of the coronary arteries of the heart or other arteries (Alfarisi *et al*., 2020). The outcome of atherosclerotic plaque is damage to the vascular endothelium. Low-density lipoprotein (LDL) cholesterol builds up and results in local inflammation, resulting in inflammatory cells such as macrophages being recruited to the site. Over time, these macrophages engulf the cholesterol and become foam cells. A cholesterol core (arterial plaque) is formed as these foam cells die. The formation of an arterial plaque reduces blood flow by impairing the elastic properties of the endothelium due to the build-up of calcium phosphate and lipids on the muscular layer of the blood vessels (Insull, 2009). However, this is rarely fatal, as people with coronary artery diseases might have one, two, or several plaques distributed throughout their coronary arteries and live for an extended period without any symptoms. Only when the plaque raptures can it result in complications to the individual. What may occur over time is that the plaque becomes unstable and ruptures, thereby promoting the formation of a blood clot that blocks the artery (Reed *et al*., 2017). Blockage of the artery can result in blood no longer being supplied to specific tissues. This can result in muscle damage, potential tissue death, and eventually a myocardial infarction (Alfarisi *et al*., 2020).
For stroke, the underlying mechanism is similar, where the restriction of blood supply to the brain often leads to cell death (Lo *et al*., 2003).

Apart from Africa, CVDs are the leading cause of death worldwide. In 2016, around 17.9 million people died of CVDs: representing 31% of all global deaths. Out of these, 85% were due to heart attacks and strokes (Wang et al., 2016). Currently, 7.6 million people in the UK live with CVDs (British Heart Foundation: https://www.bhf.org.uk/what-we-do/news-from-the-bhf/contact-the-press-office/facts-and-figures). Even though CVDs are related to lifestyle choices, blood lipid modification remains the primary preventative measure against CVD, and lipid-lowering statins are now estimated to total 1 million prescriptions per week in the UK (Rabar *et al*., 2014, Trusler, 2011). It is estimated that 7 million people in the UK are on statin medication, raising financial and ethical concerns (Mann, 2019). Therefore, future therapies for the management of CVD should consider promoting dietary preventions, as these remain one of the most cost-effective and efficient methods of preventing CVD (Barton *et al*., 2011, Funtikova *et al*., 2015).

1.2.6 Metabolic syndrome and cancer:

Another disease driven mainly by lifestyle is cancer. Cancer refers to a group of diseases involving the abnormal growth of tissues. Epidemiological studies have also shown an association between obesity, diabetes, and certain cancer types. These include liver, breast, colorectal and endometrial cancers (Esposito *et al*., 2012, Li *et al*., 2020a, Friberg *et al*., 2007). The molecular mechanism of how MetX can drive cancer is still not fully understood. Several hypotheses have been proposed, including inflammation, oxidative stress, and insulin resistance. In particular, insulin resistance and excessive production of insulin can promote increased cell proliferation and cell growth from hormones such as Insulin-like growth factor 1 (IGF1) while at the same time reducing cell apoptosis (Jee *et al*., 2005).

1.2.7 The hallmarks of cancer and cancer vs normal metabolism

While cancer consists of a large family of diseases and each cancer cell has its distinct metabolic capability, all tumour cells show several common features. Initially, a paper published by Hanahan and Weinberg summarized these common features as the six hallmarks of cancer (Hanahan and Weinberg, 2000). These include:

1. Uncontrolled proliferation,
2. Avoiding cell death,
3. Resistance to growth suppressors,
4. The induction of angiogenesis,
5. Infinite replicability, and
6. Invasion/ metastasis to adjacent tissue.

In 2011 the publication was updated, and now it is widely accepted that there are ten hallmarks of cancer. The remaining four include:

1. The deregulation of cellular energetics (notably the inhibition of aerobic glycolysis commonly referred to as the Warburg effect),
2. The ability to evade the immune system,
3. Genomic instability (chromosome abnormalities), and
4. Inflammation (Hanahan and Weinberg, 2011).

Regardless of being healthy or malignant, all cells produce energy from the catabolism of metabolic substrates, the most common being glucose. This energy comes in the form of ATP. ATP consists of a nitrogenous base—a ribose sugar with three phosphate groups attached to it. Hydrolysis of ATP to adenosine diphosphate or monophosphate (AMP) results in the release of energy that drives many processes in living cells. During

aerobic glycolysis, a normal cell will metabolize glucose through glycolysis, generating two ATP molecules. The product of glycolysis is pyruvate, which enters the TCA cycle. This generates nicotinamide adenine dinucleotide (NADH) and flavin adenine dinucleotide ($FADH_2$) required to produce ATP through oxidative phosphorylation.

The product of this process will ultimately produce thirty-four molecules of ATP. Most cancer cells instead produce their energy from glycolysis followed by lactic acid fermentation even in the presence of abundant levels of oxygen (**figure 1.2**). This metabolic process, also called anaerobic glycolysis, is commonly known as the Warburg effect after its discovery by Otto Warburg in the late 1920s (Vander Heiden *et al*., 2009). While anaerobic glycolysis is less efficient than oxidative phosphorylation (as only 4 ATP molecules compared to 34 per molecule of glucose are produced), it allows increased production of metabolites that form the building blocks of cellular growth. This allows rapid and uncontrolled division. To compensate for this energetic inefficiency, cancerous cells often display an increased capacity for glucose (or glutamine) uptake, alongside increased glycolytic rate (Vander Heiden *et al*., 2009). In a few cases, cancer cells prefer the amino acid glutamine as an energy source, as it provides nitrogen bases for the synthesis of nucleotides (DNA and or RNA) (Pavlova and Thompson, 2016, Zheng, 2012). In addition, the primary energy source of cancer stem cells is oxidative phosphorylation by metabolizing the amino acid glutamine (Yadav *et al*., 2020). It has been shown that mutations in tumour suppressor genes and oncogenes are responsible for turning a healthy cell into a malignant one. The Warburg effect is considered to be a result of these mutations rather than a cause (Grandér, 1998).

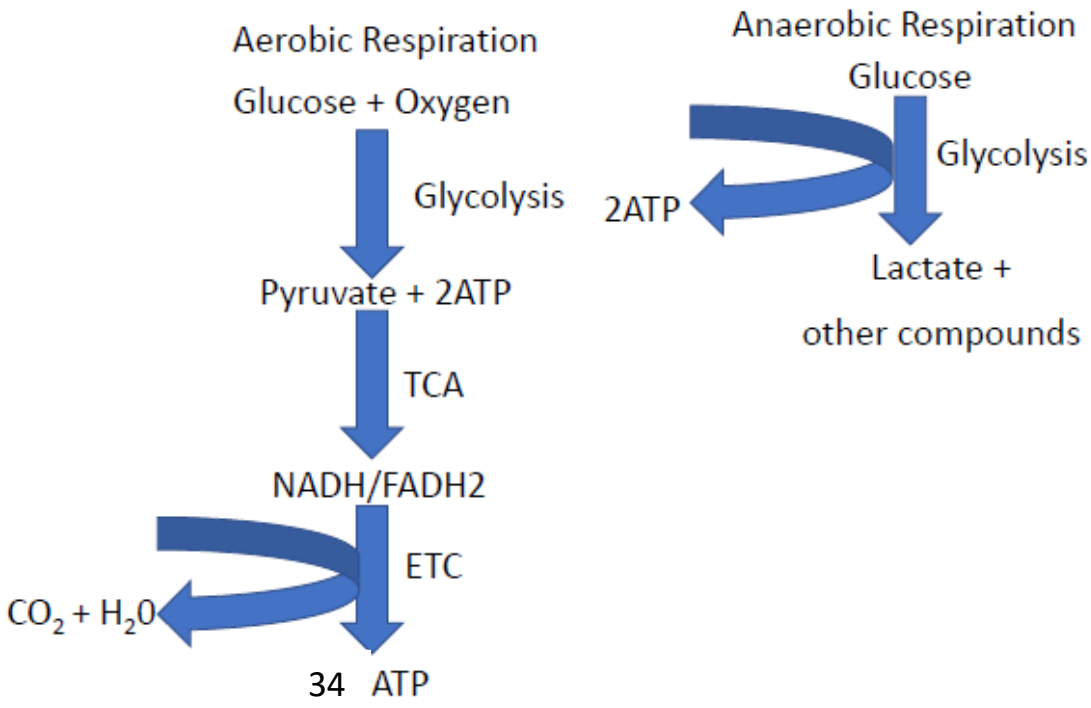

Figure 1.2. **Schematic showing the difference between aerobic and anaerobic respiration**.

1.2.8 The liver

Central to maintaining a healthy metabolism is the liver. The liver is the central metabolic organ of the body, whose main function is to govern energy metabolism. In humans, it is found in the right upper quadrant of the abdomen, directly below the diaphragm. Four lobes of different sizes form it: left and right lobes and the caudate and quadrate lobes. It is connected to two large blood vessels: the hepatic artery that carries blood rich in oxygen and the portal vein. A human adult liver weighs approximately 1.5 kg (Abdel-Misih and Bloomston, 2010). The unique feature of this organ is the ability to regenerate itself.

The liver is composed of four distinct cell types: hepatocytes, hepatic stellate cells, Kupfer cells, and sinusoidal epithelial cells, each of which are highly specialized for specific functions. The predominant parenchymal cell type within the liver are hepatocytes, which account for approximately 80% of the liver's mass (Ding *et al.*, 2016). A liver cell is defined as a hepatocyte. It is involved in a wide range of cellular and metabolic functions such as protein synthesis and storage, along with the catabolism of amino acids, carbohydrate metabolism, synthesis of cholesterol, bile acids/salts and phospholipids, as well as the detoxification of xenobiotic substrates (Ding *et al.*, 2016). As a result, hepatocytes play a fundamental role in metabolic homeostasis and xenobiotic detoxification; thus, these cell lines have become an important model for assessing cellular and systemic metabolic homeostasis and testing

new pharmacological drugs. Red blood cells and clotting factors such as fibrinogen and various prothrombin proteins are synthesized in the liver (Jelkmann, 2001).

1.2.9 Glucose homeostasis

Once food has been digested in the gastrointestinal (GI) tract, glucose, amino acids, and lipids are absorbed into the bloodstream and transported to the liver through the portal vein. One of the many functions of the liver is to act as a carbohydrate buffer, ensuring glucose levels in the blood remain constant. In the postprandial state, the β-cells of the pancreas will secrete insulin. Insulin reaches the liver through systemic circulation and will bind to insulin hepatic receptors (Edgerton *et al*., 2006). Insulin stimulation will inhibit gluconeogenesis and allow the liver to convert glucose into glycogen. The glucose is then transported to various organs through hexose transporters and stored for further use. The liver is capable of synthesizing and storing 100g of glycogen. If glycogen reservoirs are fully occupied, the glucose is converted to fatty acids (Rui, 2014).

During intense exercise, the muscles break down the stored glycogen and small amounts of protein. During this process, alanine and lactate are produced. These molecules are transported to the liver and are used as a precursor for the synthesis of glucose (gluconeogenesis).

1.2.10 Fatty acid and cholesterol homeostasis

Fatty acids in the liver can be esterified with G3P to form triacylglycerol (TAG), which can then be stored as lipid droplets in the liver (**figure 1.3**). Alternatively, glucose and TAG can be released into the bloodstream in the fasted state—the latter circulates as very-low density lipoprotein (VLDL) to provide energy. Under prolonged fasting or during times of starvations, adipose tissues undergo lipolysis and release non-esterified fatty acids (NFEAs). These are transported to the liver and oxidized in the mitochondria of hepatocytes (liver cells) by β-oxidation, generating ketone bodies (ketogenesis). Ketone bodies provide an alternative energy source (Rui, 2014).

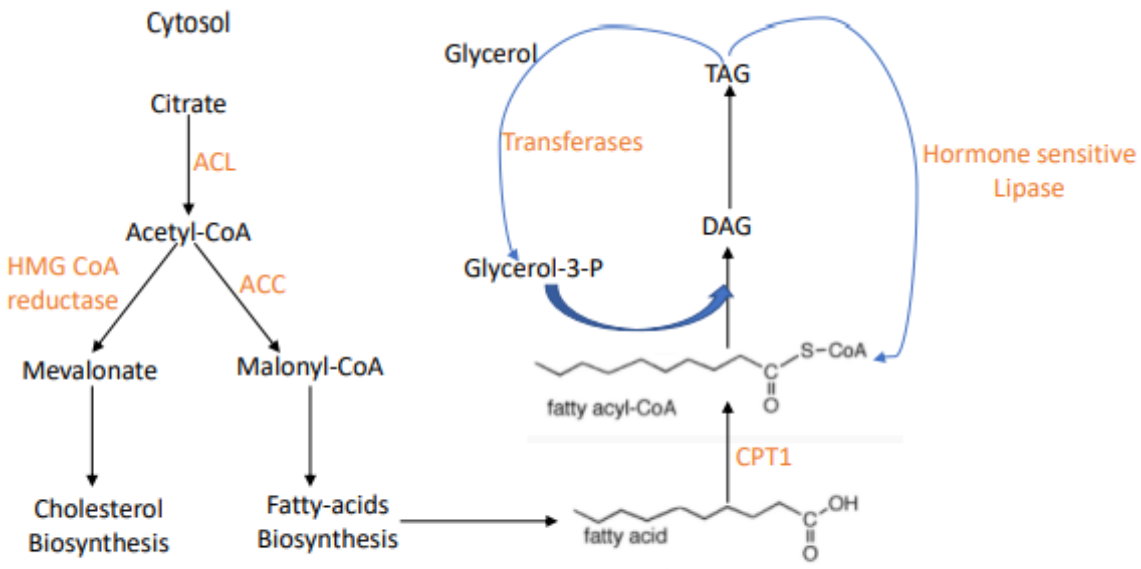

Figure 1.3. **Summary schematic on fatty acid metabolism**. The starting molecule is citrate generated from the TCA cycle. Citrate is then transported to the cytoplasm and generated Acetyl CoA. acetyl-CoA is the building block for either fatty acid or cholesterol biosynthesis. Fatty acids can then undergo condensation with G3P to generate TAG.

Cholesterol, a sterol essential for forming animal cell membranes, is also synthesized in the liver. Approximately two-thirds of cholesterol (66%) is synthesized in the liver, with the remaining third obtained through diet. The biosynthesis of cholesterol is a complex multi-step process. It begins with two molecules of acetyl-CoA condensing to form acetoacetyl-CoA. Acetoacetyl CoA then condenses with an additional molecule of acetyl CoA through the action of the enzyme 3-hydroxy-3-methylglutaryl-CoA (HMG CoA) reductase (**figure 1.3**). This enzyme is the pharmacological target of statins, as statins work by lowering cholesterol levels by inhibiting the activity of HMG CoA reductase.

As cholesterol is insoluble in the blood, it is transported throughout the body by lipoproteins. Several lipoproteins have been identified, but the most common ones are the high-density lipoprotein (HDL), whose primary function is to carry cholesterol from the peripheral tissue back to the liver, and LDL, which carries cholesterol from the liver to the peripheral tissue. The LDL can then bind to the LDL receptor of cells, allowing the absorption of cholesterol in the cells for the synthesis of membranes. The activity of the LDL receptor present on the surface of cells is tightly regulated by the sterol regulatory element-binding protein (SREBP). Cells with abundant cholesterol levels will have the synthesis of LDL receptors blocked to prevent additional cholesterol from

being taken up. Likewise, when a cell is deficient in cholesterol, SREBP induces transcription of the LDL receptor. When this process becomes dysregulated, many LDL molecules appear in the blood. These LDL molecules become oxidized. To prevent further damage, macrophages are recruited to engulf the oxidized LDL, resulting in foam cells building up. These macrophages often become trapped on the walls of blood vessels, resulting in the formation of atherosclerotic plaque (Weingärtner *et al*., 2010).

Cholesterol also serves as a precursor for bile acids. Primary bile acids are synthesized within the liver and conjugated with glycine or taurine to form a combination of eight possible bile acids through other receptors. These are then secreted into the lumen of the intestine. The primary function of bile acids is to help the digestion of fats and oils. They do this through the formation of micelles which can be absorbed into the enterohepatic circulation (Chiang and Ferrell, 2018).

1.3 Cruciferous vegetables:

Epidemiological evidence from both prospective cohort and retrospective case-control studies have shown an inverse association between consumption of cruciferous vegetables and the risk of developing a wide range of cancers including lung, stomach, colorectal, breast, bladder, and prostate, along with a reduction in developing myocardial infarction (Traka and Mithen, 2008). Broccoli belongs to the family of cruciferous or *Brassicaceae* (*Cruciferae*). This family encompasses a wide range of vegetables, including brussels sprouts, cauliflower, cabbage, kale kohlrabi (all *Brassica oleracea* cultivars), along with radish (*Raphanus sativus*), mustard (*Sinapis alba*), and rapeseed *(B. napus*) (Mandrich and Caputo, 2020). Along with many other vegetables, these are high in vitamins, minerals, and soluble fiber. The unique feature of these vegetables is the production of glucosinolates (GSLs); secondary metabolites that these plants produce as a defence mechanism against pests and insects, characterized by sulfur atoms which are responsible for their pungent smell and taste Therefore, due to the evidence of the health benefits that cruciferous vegetables provide, it would make sense to study how the benefits come about. While vegetables are loaded with vitamins and fiber, they also contain substances known as phytochemicals. Phytochemicals are non-nutrient molecules that interact with DNA to modulate multiple signalling pathways within cells. To date, more than 5,000 different phytochemicals have been discovered, our knowledge of their mechanism of action is limited to a few (Liu, 2013). There is increasing evidence of the abundance of these substances in broccoli, hence its beneficial effects on human health (Yagishita *et al*., 2019, Quirante-Moya *et al*., 2020, Juge *et al*., 2007). (Fahey *et al*., 2001) (**figure 1.4**).

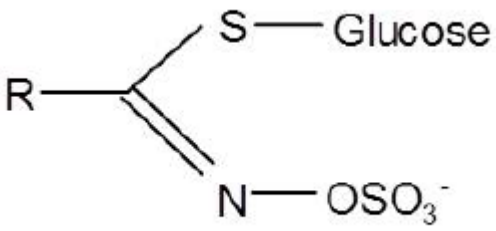

Figure 1.4: Glucosinolate structure.

The unique characteristic of each glucosinolate is the presence of both the sulfur-linked β-D glucopyranose and a sulphonate oxime group. In figure 1.4, the R refers to the side chain, which is variable and that determines its aliphatic, aryl, and indole characteristics (**figure 1.4**).

To date, more than 130 different GSLs have been identified from different plants. The profiles of these compounds vary depending on the species of the plant and the growth conditions, being aliphatic, aromatic v-methylthioalkyl, or heterocyclic depending on its structure (Agerbirk and Olsen, 2012, Holst and Williamson, 2004). As GSLs are very stable within the plant, the hydrolysis process is controlled enzymatically by the only thioglucosidase enzyme identified, namely myrosinase. In the plant *Arabidopsis thaliana,* which also belongs to the family of *Cruciferae,* it has been shown that GSLs were present in the phloem and endoderm, whereas the myrosinase is present in a different tissue, the phloem parenchyma (Blažević *et al*., 2016). When the plant cells are damaged either through chewing or mild cooking, the GSLs and enzymes come into contact to allow the hydrolysis reaction to occur (Herr and Buchler, 2010). As excessive cooking has been shown to denature the activity of myrosinase, this conversion can still happen through particular microbes within the GI tract that possess the myrosinase enzyme. Initially, the breakdown of GSLs results in the formation of an unstable aglucone. Under neutral pH, the aglucone rearranges to form isothiocyanates and thiocyanates, while under acidic conditions, small amounts of nitriles are produced (**figure 1.5)** (Rungapamestry *et al*., 2006, Wittstock and Burow, 2010).

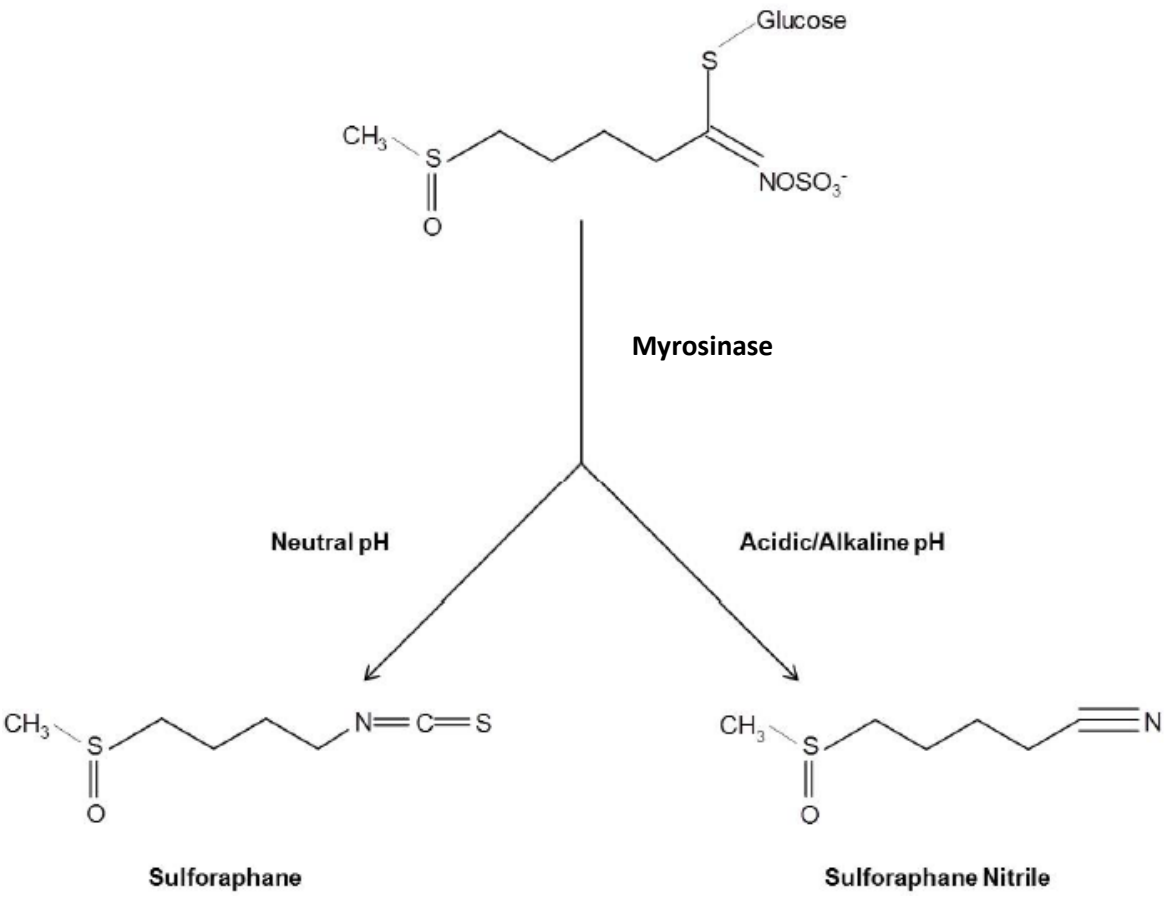

Figure 1.5. Breakdown of glucoraphanin to sulforaphane through myrosinase in different pH conditions.

1.4 ITCs and sulforaphane:

Evidence from both *in vitro* and *in vivo* studies has shown that the chemopreventive activity of cruciferous vegetables comes down to the isothiocyanates (ITCs). The most widely studied ITCs include SF and erucin (alkyl isothiocyanates), although within the last couple of years, *in vitro* studies on indole-3-carbinol (indolyl glucosinolates) has also been assessed to explore its role in cancer prevention (Katz *et al*., 2018, Lee *et al*., 2019).

SF is the best understood and studied ITC through both *in vitro* and *in vivo* studies. It is derived from the GSL glucoraphanin, which is the predominant GSL found in broccoli (**figure 1.6**). SF, compared to other phytochemicals such as quercetin (found in soy), curcumin (found in turmeric), beta-carotene (present in carrots), and resveratrol (found in red wine), is the most potent activator of the nuclear factor erythroid 2-related factor, transcription factor (NRF2) (see Section 1.5) (Houghton *et al*., 2016).

In the gut, formation of SF leads to it being readily conjugated to glutathione (GSH), forming dithiocarbamates. This reaction is catalysed by glutathione-S-transferase enzymes (GSTs). This process increases its stability and allows it to be distributed around the body. ITCs have been shown to accumulate intracellularly by reaching concentrations in the mM range (Zhang and Talalay, 1998). Following consumption of standard broccoli, 2 µM of ITCs in plasma was identified while high-GSL broccoli consumption and resulted in 7.4 µM of ITCs in plasma (Gasper *et al*., 2005). The conjugates are then transported to the kidney subsequently metabolized via the mercapturic acid pathway. This comprises a series of reactions. Firstly, glutamine and glycine residues of the ITC-GSH conjugate are removed. In the final step, the cystine residue undergoes N-acetylation to ultimately form N-acetylcysteine (NAC) conjugate (Zhang, 2000, Shapiro *et al*., 2006) (**figure 1.6**). Up to 60% of the NAC conjugate can be identified in urine samples.

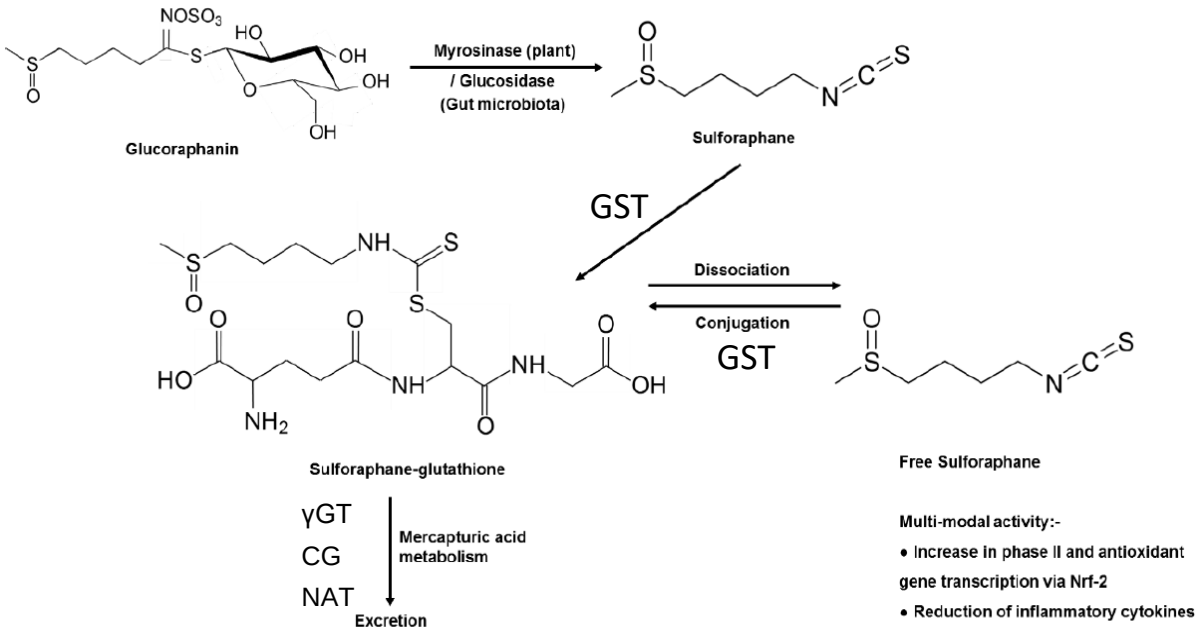

Figure 1.6: Glucoraphanin metabolism in humans. Abbreviations GST= Glutathione-S-transferase; γGT= γ-glutamyltranspeptidase; CG= cysteinylglycinase; NAT= *N*-acetyltransferase

After ingestion, glucoraphanin is broken down to sulforaphane through the action of the myrosinase enzyme, present either within the plant tissue or through specific gut microbes found in the colon that contain this enzyme. Sulforaphane is then absorbed and transported to the liver through the hepatic portal vein where it conjugates with glutathione and is metabolized through the mercapturic acid pathway or dissociate to induce the transcription factor NRF2. The conjugation between sulforaphane and

glutathione can occur enzymatically, more specifically it has been suggested it is likely to occur via the activity of the GSTs family (Zhang *et al*., 1995).

In humans, 3 mammalian GST gene families exist and are categorized in the following families: cytosolic, mitochondrial, and microsomal. From the GSTs identified, only a small subgroup has been studied in terms of their effects on the conjugation of ITCs. These are GSTA1, M1, M4, and P1 (Kolm *et al*., 1995). The GSTM1 enzyme is the most efficient at catalyzing the conjugation reaction, followed by GSTP1 (Kolm *et al*., 1995). It has been identified that many genes in this family harbor polymorphism; for example, both GSTM1 and GSTT1 have been reported to have a null mutation, resulting in loss of function of the gene (Hayes *et al.*, 2005, Hayes and Strange, 2000). The frequency of homozygous null GSTM1 genotype varies between 39% up to 63%, whilst for the GSTT1, this frequency varies between 10% to 21% for whites, but in asian individuals can be as high as 64% (Cotton *et al*., 2000). Whether GSTM1 polymorphism is either beneficial or detrimental remains to be answered, as epidemiological studies have provided conflicting results. For example, a study assessing GSTM1-positive individuals from the United States has shown that those who frequently consumed broccoli or cruciferous vegetables have increased protection from cancer development compared to GSTM1-null individuals (Joseph *et al*., 2004, Spitz *et al*., 2000). In contrast, studies conducted in Asia concluded that GSTM1 and GSTT1 null individuals who regularly consume cruciferous vegetables may gain greater protection than GSTM1 and GSTT1 positive individuals (Seow *et al*., 1998, Chung *et al.*, 1998).

1.5 NRF2

Research on broccoli and its importance for human health dates back to the early 90s. Zhang and colleagues were the first to show that SF is a potent activator of phase II enzymes. Elimination of toxic xenobiotics from cells is split into three different stages: phase I, II, and III. The first phase, which is mainly carried out by cytochrome P450 enzymes, involves transferring a hydroxyl, carboxyl, or an amino group to the toxic compound (Lin *et al*., 2016). Phase II enzymes are also referred to as transferases as they can transfer the modified metabolite to hydrophilic molecules through the addition of these molecules: glucuronyl transferases, glutathione transferases, sulfotransferases, amino acid transferases, and N/O methyltransferases (Shen and Kong, 2009), making the toxic xenobiotic more hydrophilic. This facilitates the excretion of the toxic compound by phase III enzymes, a series of drug transporter proteins such as multidrug resistance (MDR) pump, which are a type of efflux pump, allowing cells to secrete the toxic substrate. These hydrophilic molecules include glucuronic acid,

The family of phase II enzymes includes NAD(P)H: quinone reductase (NQO1) along with the glutathione-S-transferases. Both are involved in the detoxification of steroids and the environmental toxin benzo(a)pyrene (Zhang *et al*., 1992, Prochaska *et al*., 1992, Singletary and MacDonald, 2000). At that time, Zhang concluded that the anticarcinogenic properties of broccoli were due to SF. The problem remained that the exact mechanism through which this occurred was still not fully understood. Only two years later, the transcription factor NRF2 was discovered (Moi *et al*., 1994).

NRF2 belongs to the family of cap'n collar (CNC) proteins. The human NRF2 protein consists of 605 amino acids, while that found in rats and mice contains 597 amino acids. Emerging evidence has shown that NRF2 plays a dual role; besides its involvement in controlling pathways involved in fighting oxidative stress, it has also been identified to contribute to metabolism by regulating pathways involved in nicotinamide adenine dinucleotide phosphate (NADPH) and ATP production (Thimmulappa *et al*., 2002, Holmström *et al*., 2013).

NFR2 is formed by seven highly conserved domains, referred to as the NRF2-ECH homology domains. Each domain conducts a specific function (Itoh *et al*., 1995). Present within the Neh1 domain is the (CNC) leucine-rich region. This region is where NRF2 can dimerize with Maf proteins, allowing it to bind onto the DNA (Hirotsu *et al*., 2012). The Neh2 domain is where the Kelch-like ECH-associated protein 1 (KEAP1) binds, thereby controlling the activity of NRF2 (Itoh *et al*., 1999). The C-terminal region of the Neh3 domain contains a sequence of 16 amino acids that are involved in the transcription activation of NRF2. Studies have shown that the deletion of this region results in the CNC leucine rich region becoming inactive. In addition, this region can also interact with the chromodomain of the helicase DNA-binding protein 6 (Nioi *et al*., 2005).

The Neh4 and Neh5 regions are domains that recruit either the cAMP response element-binding protein (CREB)-binding protein (CBP) or receptor-associated coactivator (RAC)3 (Katoh *et al*., 2001). The Neh6 domain also negatively regulates NRF2, through the interaction with the β-transducin repeat-containing protein (β-TrCP) (McMahon *et al*., 2004).

The most recent domain that was identified is Neh7. This domain contains a specific region that allows it to interact, through protein-protein interaction with the DNA binding domain of the retinoid X receptor α (RXRα). This inhibits the activity of NRF2 by preventing coactivators' binding to the Neh4 and the Neh5 domains (Wang *et al*., 2013) (**figure 1.7**).

The Kelch domains of KEAP1 bind onto the DLG and ETGE motifs of the Neh2 domain of NRF2, and these sites are then ubiquitinated. Similarly, the WD-40 domain of β-TrCp bind onto the DSGIS and DSAPGS motifs, resulting in a series of reaction that leads to the ubiquitination of the Neh6 domain.

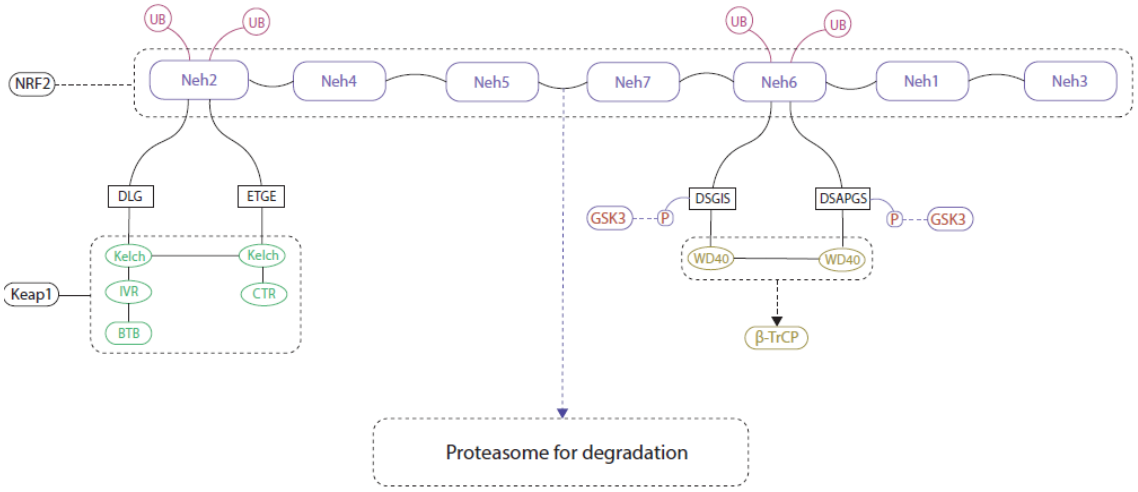

Figure 1.7: Inhibition of NRF2 through the interaction of the Kelch domains of KEAP1, represented by the green circles, and the WD40 domains from β-TrCp, shown by the yellow circles.

1.6 Regulation of NRF2

1.6.1 Transcriptional and post-translational regulation of NRF2

The two major pathways through which xenobiotics induce gene expression include:

- Regulation through the aryl hydrocarbon receptor (AhR)
- Activation of NRF2

The binding of polycyclic aromatic carbons (PAHs) to the AhR results in AhR binding to the xenobiotic response element (XRE) in the promoter regions of specific inducible genes, for example, CYP1A1 and CY1B1 (Denison *et al*., 1989, Denison *et al*., 1988).

Transcriptional activation of the NFE2L2 gene also occurs through the AhR, as present on the promoter of the NFE2L2 gene; there are both an XRE site and two XRE-like sequences. The induction of NRF2 results in it regulating the AhR, indicating that a feedback loop exists between the two transcription factors (Miao *et al*., 2005). Furthermore, metabolites produced by the human Aldo-Keto reductase gene (AKR1C), also controlled by NRF2, has been shown to bind to the AhR, leading to its activation, thereby demonstrating a further complex cross-talk (Burczynski *et al*., 1999, Burczynski

and Penning, 2000). Upstream the transcription start site, present on the promoter of the NFE2L2 gene, there is also two antioxidant response element (ARE)-like sequences. As a result, NRF2 can bind and increase its expression (Kwak *et al*., 2002). At the same time, downstream from the transcription start site, the NFE2L2 gene also contains an NF-ƙB binding site, allowing it to be induced in the presence of inflammatory stimuli (Rushworth *et al*., 2012).

With regards to post-translation regulation, most of the NRF2 activity is regulated at the protein level. NRF2 is constantly targeted to be degraded by the 26S proteasome through the action of several E3 ubiquitin ligases such as cullin-RING ubiquitin ligase, more commonly referred to as CRL, the S-phase kinase-associated protein 1 (SKP1), cullin-1 (CUL1), F-box protein E3 ubiquitin ligase, called SCF (Tebay *et al*., 2015). The rapid turnover of NRF2 allows the cells to accumulate newly translated protein so that in the case of redox stressors and metabolic stimuli, NRF2 is no longer ubiquitinated and sent for proteasomal degradation.

1.6.2 Regulation by KEAP1

As NRF2 is activated under stress, and as it controls a wide range of biological functions, biological processes that NRF2 regulates will feedback and inhibit its function. This will avoid it becoming overexpressed, both at the transcriptional and translational levels. The first protein identified to inhibit the function of NRF2 was KEAP1. Initially, it was thought that KEAP1 inhibited NRF2 by preventing newly synthesised NRF2 from translocating to the nucleus (Kang *et al*., 2004). Studies later confirmed that KEAP1's actual role is to ubiquitinate NRF2. KEAP1 is formed by four domains which are the following:

1. N-terminal region (NTR) also referred to as the conserved N-terminal broad complex,
2. Tram-track and Bric- à-Brac (BTB) domains. This domain contains the cysteine 151 residue, one of the important cysteine residues for stress sensing.
3. The intervening region (IVR) domain also contains two important cysteine residues (Cys273 and Cys288) for stress sensing.
4. The double glycine repeat (DGR) and the C-terminal region (CTR) domain fold to form a β-propeller structure, where Keap1 interacts with the Neh2 domain of NRF2 (Canning *et al*., 2013, Ogura *et al*., 2010, Padmanabhan *et al*., 2006).

The special feature of this protein is its relative richness in cysteine residues. Most proteins have on average a total of 2% cysteine residues. By contrast, KEAP1 contains 4% (Hansen *et al*., 2009). In addition, some of these thiol groups are highly reactive,

having a pK_a value lower than that of a free thiol and therefore existing as a thiolate anion (S^-). The thiolate anion is surrounded by polar and basic amino acids which function to stabilize it (McMahon *et al*., 2010, Paulsen and Carroll, 2010). The following model has been proposed to depict KEAP1's ubiquitination of NRF2. Initially, KEAP1 binds on the high affinity ETGE motif, followed by the low affinity DLG motif present on the Neh2 domain, through a "hinge and latch" mechanism.

This results in ubiquitin tags being added onto the CNC-bZIP region of NRF2 (Tong *et al*., 2006, Fukutomi *et al*., 2014). Once ubiquitin tags have been added, NRF2 is sent for proteasome degradation. The importance of KEAP1 in regulating the activity of NRF2 has been shown in both murine (Wakabayashi *et al*., 2003) (where it was knocked out) and human cell lines (through knockdown) (Devling *et al*., 2005). Mutation of either the DLG or ETGE motif leads to KEAP1 no longer being able to degrade NRF2 (**figure 1.8**). Similarly, KEAP1 activity can also be inhibited by a wide range of chemicals that act as electrophiles such as tert-Butylhydroquinone (tBHQ), SF, curcumin, 2-cyano-3,12-dioxoolea- na-1,9(11)-dien-28-oicacid-imidazoline(CDDO-Im), tricyclic bis-(cyanoenone)-31(TBE-31), and diethyl maleate (McMahon *et al*., 2010, Yamamoto *et al*., 2008, Fourquet *et al*., 2010, Kobayashi *et al*., 2009). The residue Cys-273 recognizes and reacts with cyclopentanone prostaglandins such as 15-deoxy-$^{\Delta 12,14}$-prostaglandin, while alkenes such as acrolein and 4-hydroxynonenol react with Cys-288 (Kobayashi *et al*., 2009, McMahon *et al*., 2010). The Cys-151 residue found within the BTB domain is where SF and other electrophiles such as tBHQ and nitric oxide (NO) bind, resulting in NRF2 activation (**figure 1.8**). Site-directed mutagenesis studies have instead revealed that mutation of Cys-151 to alanine results in NRF2 no longer being induced (Zhang and Hannink, 2003). Instead, the replacement of Lys-131, Arg-135, and Lys-150 which surround Cys-151 to methionine results in a weaker binding affinity of SF, tBHQ, and NO, resulting in reduced expression of NRF2 target genes (McMahon *et al*., 2010). A further electrophilic cysteine-434 is found in the DGR domain of KEAP1. This cysteine reacts with 8-nitroguanosine-3',5'-cyclic monophosphate (8-nitro-cGMP), a by-product of NO, and results in S-guanylation of KEAP1, resulting in induction of NRF2 target genes (Fujii *et al*., 2010) **(figure 1.8)**.

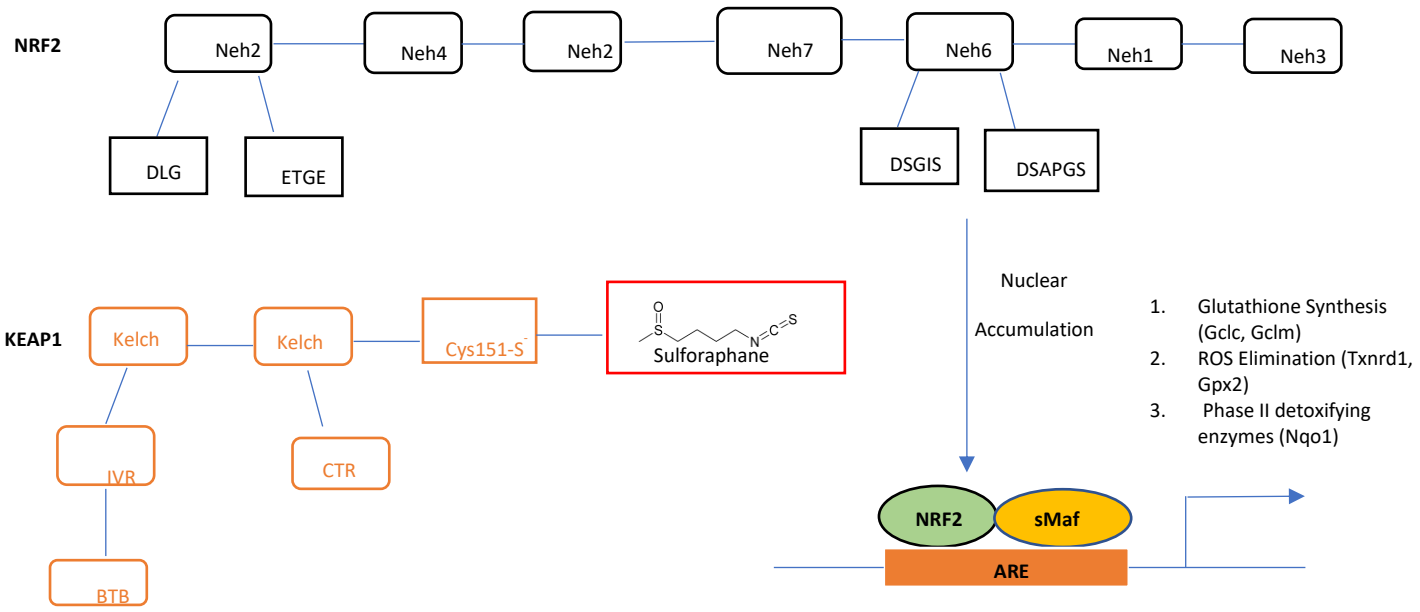

Figure 1.8*:* Schematic of the active NRF2 protein that allows induction of its target genes. Activation of NRF2 through the binding of the SF onto the Cys151 residue of KEAP1, shown by the yellow boxes. NRF2 accumulates and translocates to the nucleus, where it binds to an additional protein known as sMaf. The protein-protein interaction enables NRF2 to bind onto the ARE response and induces the expression of antioxidant and phase II detoxification genes.

1.7 The antioxidant response system

Disruption of KEAP1 allows NRF2 to translocate from the cytoplasm and accumulate in the nucleus (see **figure 1.8** for the functional structure of NRF2). There, it heterodimerizes with the small musculoaponeurotic fibrosarcoma (sMaf) protein (Itoh *et al*., 1997). To date, it is known that NRF2 can interact with three Maf proteins: MafF, MafG, and MafK (Hirotsu *et al*., 2012). The binding of NRF2 to Maf was identified by knocking out all three Maf proteins in fibroblasts (Hirotsu *et al*., 2012). The results revealed reduced antioxidant response, indicating that these sMaf proteins are crucial for recruiting NRF2 to the promoter site of the DNA (Katsuoka *et al*., 2005, Blank, 2008).

The region where the NRF2-sMaf heterodimers bind is referred to as the antioxidant response element (ARE) (**figure 1.8**). This site was first identified in the promoter region of genes that were induced by synthetic phenolic antioxidants such as the metabolite ter-butyl hydroquinone (tBHQ) being one of the strongest inducing agents (Hayes *et al*., 2000). Rushmore and colleagues first reported the ARE in the early 90s (Rushmore and Pickett, 1993). Rushmore identified that the promoter region of the

gene glutathione S-transferase A2 (GSTA2) found in rats had a sequence that was responsive to tBHQ and β-naphthoflavone (β-NF); but not to the classic ligand dioxin which binds to the aryl hydrocarbon receptor (AhR) (Rushmore and Pickett, 1990). Rushmore went on to demonstrate that this region was required for induction of genes by aromatic compounds such as 3-methylcholanthrene and diphenols such as catechol and hydroquinone (Rushmore *et al*., 1991). At the same time, Daniel and colleagues found that the promoter region of the gene GSTA1 in mice also contained an identical region. Friling and her colleagues went on to name that region the electrophile response element (EpRE), as they showed that it responded to electrophiles such as trans-4-phenyl-3-buten-2-one and dimethyl fumarate, as well as to tBHQ and β-NF (Friling *et al*., 1990). This region is now commonly referred to as ARE. Prestera and colleagues were the first to show that the phytochemical, SF, can induce gene expression through ARE (Prestera *et al*., 1993). Shortly after identifying the ARE sequence in rodent GST genes, it was discovered that that the regulatory region of both rat and human NQO1 gene also had an ARE sequence, also induced by tBHQ and β-NF (Favreau and Pickett, 1991, Jaiswal, 1991). Since its discovery, this region has been identified to contain the following motif: 5'- $^{A}/_{G}$ TGA$^{C}/_{G}$NNNGC$^{A}/_{G}$-3', where N represents redundant residues. In some circumstances, both the N nucleotides and the flanking sequences of the ARE may influence the function of a gene (Nioi *et al*., 2003, Hayes *et al*., 2010, Wasserman and Fahl, 1997).

1.7.1 Identification of NRF2 target genes

The discovery that both GST and NQO1 had a specific motif recognized by NRF2 led scientists to explore further and identify whether additional genes have similar functions. One group that played a prominent role was that of Masayuki Yamamoto. This group was the first to show that in mice that had NRF2 knocked out and administered with butylated hydroxyanisole (BHA) in the liver, both the various GST genes and NQO1 were not induced (Itoh *et al*., 1997).

Thimmulappa and colleagues carried out a transcriptional profile of small intestines from wild type ($NRF2^{+/+}$), and knockout mice ($NRF2^{-/-}$) treated with vehicle or sulforaphane for a week (Thimmulappa *et al*., 2002). The group also showed for the first time that NRF2 played a crucial role in the cellular detoxification pathways of glutathione conjugation and glucuronidation. The glucuronidation pathway eliminates many lipophilic xenobiotics by converting them to water-soluble compounds. This occurs through the presence of UDP-glucuronic acid (Thimmulappa *et al*., 2002). Furthermore, Thimmulappa and colleagues were the first to demonstrate the importance of NRF2 in regulating several genes involved in different aspects of

metabolism—not only in NADPH production, such as glucose-6-phosphate dehydrogenase (G6PD), but also the dependence of malic enzymes and 6-phosphogluconate dehydrogenase (6PGD) on NRF2. Soon after the study was published, a subsequent study identified an ARE sequence in the promoter region of the malic enzymes (Li *et al*., 2002). However, Yamamoto and the group identified an ARE sequence in G6PD and 6PGD several years later (Mitsuishi *et al*., 2012).

Due to its vital role in redox homeostasis and metabolism, either excessive or very little NRF2 activation can lead to physiological consequences. Perturbation of the transcription factor via knockout or knockdown leads to:

- Reduced cell proliferation (Reddy *et al*., 2008),
- Alteration in cell differentiation (Hochmuth *et al*., 2011, Tsai *et al*., 2013, Paul *et al*., 2014),
- An alteration in the unfolded protein response (Cullinan and Diehl, 2004),
- The increased build-up of toxic xenobiotics (Higgins *et al*., 2009, Niso-Santano *et al*., 2010, Kensler *et al*., 2007),
- Increased hepatic steatosis (Chowdhry *et al*., 2010, Meakin *et al*., 2014),
- Increased sensitivity to inflammation (Meakin *et al*., 2014, Chowdhry *et al*., 2010, Rangasamy *et al*., 2005, Thimmulappa *et al*., 2006, Cho *et al*., 2010), and
- A reduced ability of the liver to regenerate (Wakabayashi *et al*., 2010).

Similarly, overexpression of NRF2, which can occur through inhibition of KEAP1 activity or mutation in NRF2 found in the lung carcinoma cell line A549, results in the overproduction of GSH and NADPH. This leads to reductive stress and can result in the aggregation of misfolded proteins and cardiac hypertrophy (Brewer *et al*., 2013, Whitehead *et al*., 2013, Rajasekaran *et al*., 2007). Studies have also shown that overexpression of NRF2 may also increase the expression of the oxidized-LDL scavenger receptor cluster differentiation 36 (CD36), which can lead to the formation of foam cells and therefore increase the risk of atherosclerosis (Ishii *et al*., 2004, Sussan *et al*., 2008).

Studies on phase I-III enzymes began during the 1990s and early 2000s. For example, sulforaphane treatment to both human retinal pigment epithelial cells (ARPE-19) and HaCaT keratinocytes resulted in a twofold increase in the levels of GSH, and this was sustained for several days. The treatment was found to protect against the following oxidants and electrophiles:

- Menadione,
- *Tert*-butyl hydroperoxide,

- 4-hydroxynonenal and
- Peroxynitrite (Gao *et al*., 2001).

Studies using wild type mouse embryonic fibroblasts (MEF) treated with SF, and HaCaT cells with KEAP1 knockdown showed increased levels of the glutathione biosynthetic genes subunits: the modifier (GCLM) and the catalytic subunit (GCLC). It has also been shown that NRF2 regulates the expression of some glutathione-S-transferase (GST) and glutathione peroxidases 2 (GPX2)—both phase II enzymes responsible for detoxifying epoxide and hydrogen peroxide (Higgins *et al*., 2009).

Furthermore, human cell culture studies have shown that treating human K562 erythroleukemia cells with tBHQ and human K-1034 RPE cells with SF resulted in increased expression of thioredoxin 1 (TXN1) (Kim *et al*., 2003, Hawkes *et al*., 2014, Malhotra *et al*., 2010). Murine studies have shown that TXN1 plays an important role in protecting them against retinal light damage (Tanito *et al*., 2005). Upregulation of both GSH and TXN1 also leads to upregulation of reductases such as glutathione reductase (GSR), thioredoxin reductase 1 (TXNRD1), and sulfiredoxin (SRXN1). TXN1 contains two redox sensitive cysteine residues. These two residues are reduced by TXNRD1 through NADPH. TXN1 helps control the activity of many transcription factors (p53 and HIF-1α through oxidoreductive modification of the protein.

Another well-established phase II enzyme is NQO1, which catalyzes the reduction of quinones to hydroquinones. P450 reductases can oxidize Quinones to semiquinone. These molecules are highly unstable (due to the presence of a free radical) and tend to react with oxygen to generate ROS, leading to oxidative damage in cells. NQO1 prevents this process by utilizing NADPH to generate hydroquinones that can then be either glucuronidated by UDP-glucuronosyltransferase (UGT) or sulfonated by sulfotransferases (Dinkova-Kostova and Talalay, 2000, Miura *et al*., 2011).

Studies on the following human cell lines: HaCaT keratinocytes, MCF10A mammary cells, IMR-32 neuroblastoma, and U937 lymphoma cells treated with sulforaphane or tbHQ or knockdown of KEAP1, showed strong induction of another group of phase I enzymes AKR1B10, AKR1C1, AKR1C2, and AKR1C3. These enzymes belong to the family of Aldo-Keto reductase (Jung *et al*., 2013). These oxidoreductases also utilize NADPH to catalyze the conversion of a wide range of xenobiotics. For example, AKR1A1 is involved in reducing the chemotherapy drug doxorubicin to doxorubiciniol (Bains *et al.*, 2008). Instead, AKR1C1 and ARK1C2 are involved in metabolizing tibolone (treatment for postmenopausal conditions) and the oral contraceptive northeynodrel (Steckelbroeck *et al*., 2006, Jin *et al.*, 2012). In humans, several of these enzymes, such as AKR1B10, AKR1C1, AKR1C2, and AKR1C3 also play an important

role in clearing the build-up of lipid peroxidation by products such as 4-hydroxy-2-nonenal and 4-oxo-2-nonenal (Martin and Maser, 2009, Burczynski *et al*., 2001).

1.8 NRF2 and glucuronidation

Another mechanism through which NRF2 is involved in xenobiotic metabolism is through glucuronidation. This process involves the transfer of glucuronic acid, derived from UDP-glucuronic acid to a xenobiotic substrate by the enzyme UGT. For example, the product of heme metabolism, bilirubin, is eliminated by this pathway through the enzyme UDP-glucuronosyltransferase 1A1 (UGT1A1), which is also an NRF2 target (Thimmulappa *et al*., 2002). UDP-glucuronic acid is generated from G6P through a series of reactions. The first step involves the conversion of G6P to glucose-1-phosphate (G1P) by phosphoglucomutase. Then UDP is attached to the glucose molecules by UDP-glucose pyrophosphorylase to generate UDP-glucose. In the final step, UDP-glucose is converted to UDP-glucuronate by UDP-glucose dehydrogenase another enzyme whose activity is also regulated by NRF2 (Wu *et al*., 2012, Thimmulappa *et al*., 2002).

1.9 Part 2: NRF2 and its role in metabolism

The final section of the general introduction covers literature on NRF2 within the last 10 years. More specifically, it focuses especially on the recent discovery that NRF2 can also act as a central metabolic regulator by regulating a wide range of different metabolic pathways. Selected metabolic pathways which are of particular interest for this thesis are discussed.

1.9.1 NRF2 and glycolysis:

One of the most recent studies showing a link between NRF2 and glycolysis was conducted by Bollong and colleagues. This study identified novel crosstalk between glucose metabolism and the NRF2 antioxidant pathway (Bollong *et al* 2018). The administration of a small synthetic molecule, CBR-470-1, to IMR32 cells directly inhibited the glycolytic enzyme phosphoglycerate kinase 1 (PGK1). Inhibition of PGK1 led to the accumulation of a metabolite, methylglyoxal. This compound directly inhibits KEAP1 through post-translational modification by forming a methylimidazole cross link between cysteine151 and arginine135 residues of KEAP1. NRF2 activation was confirmed through western blotting and RNA-sequencing followed by Gene Set Enrichment Analysis (GSEA), showing enrichment of NRF2 target genes. The compound also induced transcript levels of NQO1 and HMOX1 in other cell lines such as HEK293T, SH-SY5Y, and primary lung fibroblasts. Depleting NRF2 through short

hairpin showed that CBR-470-1 activity depends on NRF2. The findings were then assessed *in vivo*, by administrating mice with 20 or 100 $mgkg^{-1}$ of analog of CBR-470-1. The results showed a dose-dependent increase in the transcript levels of NQO1 and HMOX1 in several organs (Bollong *et al*., 2018).

1.9.2 NRF2 and its role in the pentose phosphate pathway

Following the entry of glucose into the cells, glucose gets phosphorylated by hexokinase to glucose-6-phosphate (G6P). At this stage, G6P can continue through glycolysis to generate two molecules of pyruvate, which are then directed into the tricarboxylic acid (TCA) cycle to produce ATP through oxidative phosphorylation, or it can enter the pentose phosphate pathway (PPP) (**figure 1.9**). The quantity of glucose present in the cells will dictate how glucose will be metabolized. Under high glucose availability, via the activation of PI3K-Akt, the glucose is redirected to anabolic reactions such as the PPP. Yamamoto and colleagues were the first to show that the enzymes G6PD, PGD, transaldolase (TALDO), and transketolase (TKT) have an ARE sequence and are thus NRF2 targets (Mitsuishi *et al*., 2012). Further, Furthermore, Yamamoto and colleagues showed that siRNA knockdown of NRF2 leads to increased glycolytic intermediates (G6P, fructose-6-phosphate, dihydroxyacetone phosphate, pyruvate, and lactate) in the cells (Mitsuishi *et al*., 2012). In cancer cells where NRF2 is constitutively active, knockdown of NRF2 results in the downregulation of these enzymes involved in the PPP. Similarly, in human breast epithelial cells (MCF10A) that are treated with SF or KEAP1 knockdown, an increase in the PPP enzymes is observed (Agyeman *et al*., 2012). It has been shown that by controlling the activity of G6PD and PGD, the NADPH that is generated is utilized to maintain glutathione in its reduced state (**figure 1.9**) (Singh *et al*., 2013, Mitsuishi *et al*., 2012).

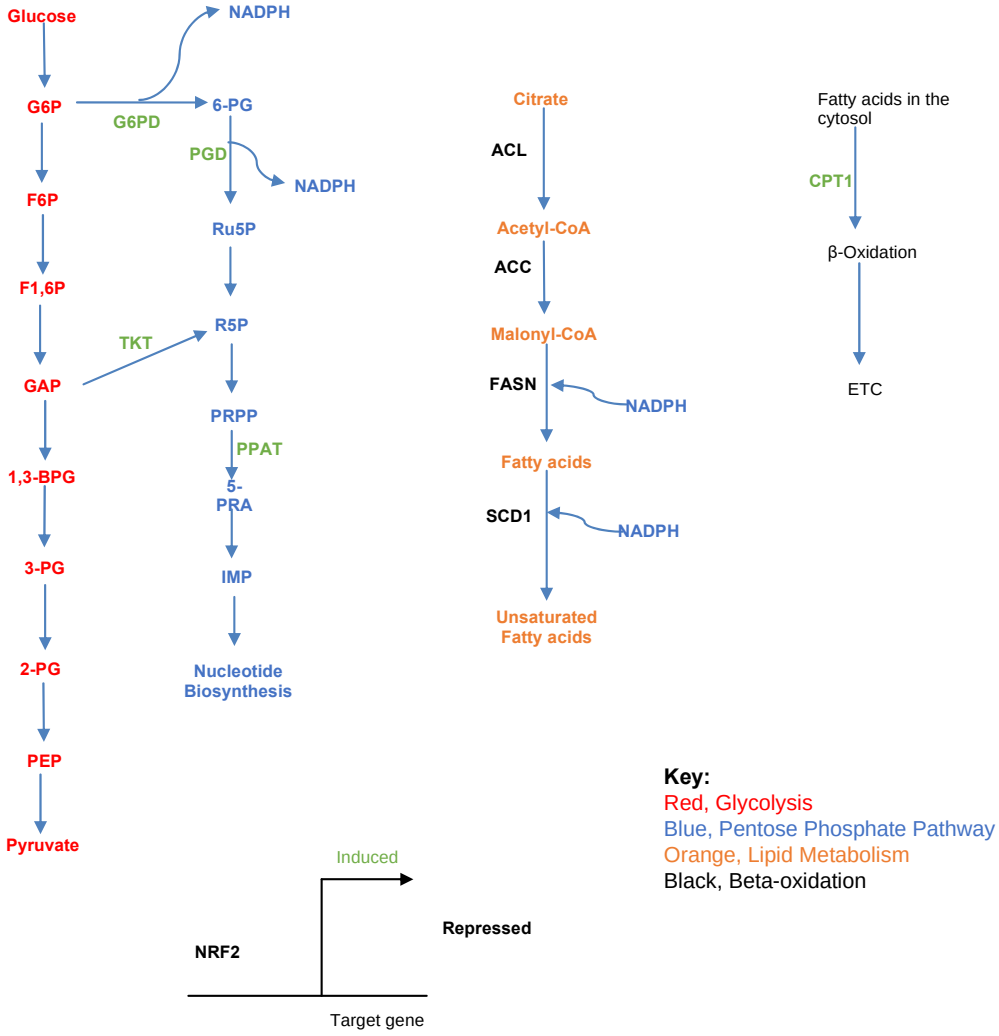

Figure 1.9: NRF2 and its contribution in crucial metabolic pathways such as the Pentose Phosphate Pathway and Lipid Metabolism. Green denotes the genes induced by NFR2, while black shows genes that NRF2 represses. NRF2 increases the expression of critical enzymes involved in PPP, leading to NADPH production required for cellular growth and antioxidant response. NRF2 also suppresses lipid biosynthesis. Lipid biosynthesis consumes a large amount of NADPH. Therefore, by suppressing lipid synthesis, the NADPH can be redirected for the antioxidant response.

1.9.3 The TCA cycle

The first step in the TCA cycle is the formation of acetyl-CoA by pyruvate dehydrogenase (PDH). Acetyl-CoA can then condense with oxaloacetate to generate citrate, which is transferred to the cytoplasm to synthesise lipids or converted to isocitrate by aconitase. Isocitrate is converted to α-ketoglutarate (α-KG) by isocitrate dehydrogenase (IDH). α-KG is further converted to succinyl-CoA by α-KG dehydrogenase. Succinyl-CoA is oxidized to fumarate by the succinate dehydrogenase (SHD) complex and then hydrated to malate by fumarate hydratase (FH). In the final step, malate is oxidized to regenerate oxaloacetate by malate dehydrogenase, continuing the cycle (**figure 1.10**).

Evidence that NRF2 regulates the TCA activity has been recently discovered. Firstly, NRF2 can increase the levels of PDH, leading to increased substrates entering the TCA cycle and, therefore, increasing the cycle's activity (Singh *et al*., 2013). PDH has not yet been identified to have an ARE sequence. NRF2 also directly regulates the activity of malic enzyme 1 (ME1) and Isocitrate dehydrogenase (IDH1), both of which generate NADPH. ME1 is a mitochondrial enzyme that metabolizes malate to pyruvate, while IDH1 converts isocitrate to α-ketoglutarate. Both enzymes have been shown to have ARE sequences (Mitsuishi *et al*., 2012). It has also been recently identified that pyruvate carboxylase is a potential NRF2-MafG target gene (Hirotsu *et al*., 2012). Pyruvate carboxylase catalyzes the carboxylation of pyruvate to oxaloacetate (**figure 1.10**). Emerging evidence has shown that NRF2 also appears to regulate mitochondrial biogenesis and physiology. It was identified that NFR2 knockdown in colon cancer cells results in reduced oxygen consumption and ATP production (Kim *et al*., 2011). In contrast, when NRF2 is overexpressed, these cell lines have higher basal mitochondrial membrane potential and higher oxygen consumption rates, resulting in higher basal ATP levels, suggesting that NRF2 is involved in oxidative phosphorylation (Holmstrom *et al*., 2013).

NRF2 also regulates the expression of various subunits of the cytochrome C oxidase protein (Agyeman *et al*., 2012, Holmstrom *et al*., 2013, Carrasco-Pozo *et al*., 2017), in addition to regulating mitochondrial respiration by providing electron carries such as NADH / $FADH_2$ for complex I and II. Other studies have shown that NRF2 can both positively (Hota *et al*., 2012, Piantadosi *et al*., 2011, Athale *et al*., 2012) and negatively regulate (Uruno *et al*., 2013, Zhang *et al*., 2013b) the mRNA levels of the nuclear respiratory factor 1 (NRF1). This protein regulates the activity of the five protein complexes of the respiratory chain, along with PGC-1α.

Under oxidative stress, uncoupling protein 3 (UCP3) is upregulated by NRF2 to reduce the build-up of superoxides (Anedda *et al*., 2013). Finally, it has been recently stated that NRF2 can regulate mitochondrial bioenergetics through PPARγ and PPARγ coactivator 1 beta (PGC-1β) (Chorley *et al.*, 2012, Dinkova-Kostova and Abramov, 2015, Itoh *et al*., 2015), although future studies are required to gain a mechanistic understanding of how this process occurs.

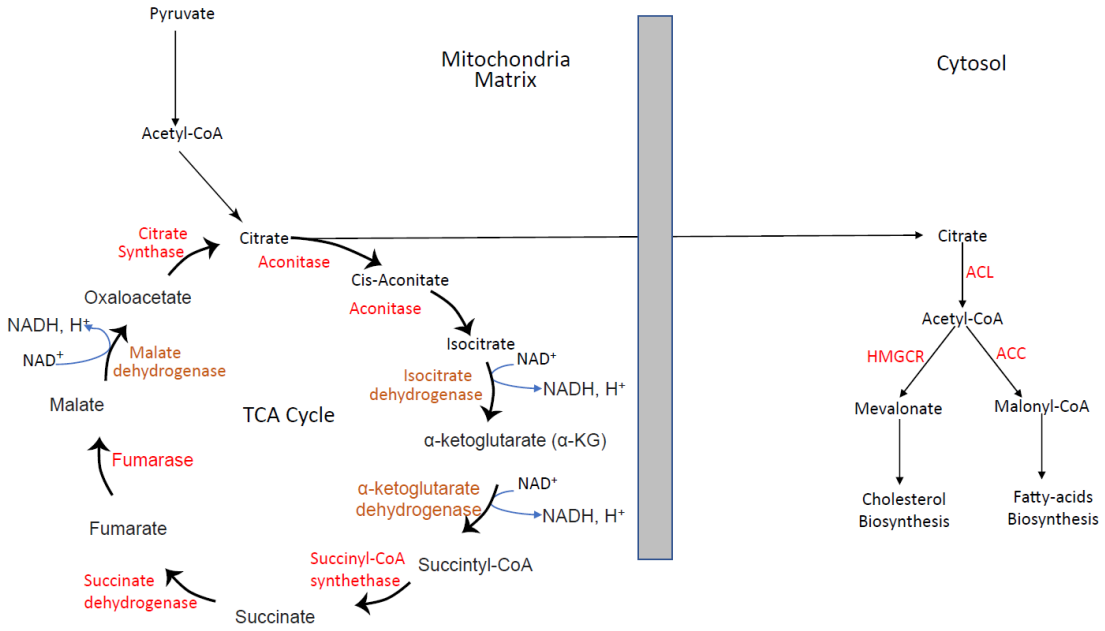

Figure 1.10: Summary of the TCA cycle on the left and lipid homeostasis on the right. Enzyme highlighted in orange represent NRF2 targets.

1.9.4 Glutamine metabolism

The most abundant amino acid in human serum is glutamine, with concentrations of around 500 µM (Lin *et al*., 2016). Proliferating cells are highly dependent on glutamine, as it is both a nitrogen and carbon source for the TCA cycle. NRF2 controls both the uptake and metabolism of glutamine in cells. For example, NRF2 can control the expression of the glutamine transporter SLC1A5 and asparagine synthetase (ASNS), whose function is to produce asparagine and glutamate from aspartate and glutamine (Averous *et al*., 2004). In addition, the first step of glutaminolysis, which comprises the conversion of glutamine to glutamate by glutaminase, is also an NRF2 target (Agyeman *et al*., 2012). Glutamate can then be either converted to α-ketoglutarate through the action of glutamate dehydrogenase or redirected for glutathione biosynthesis. The conversion of glutamate to glutathione occurs through the glutamate-cystine ligase GCLC/GCLM genes, key NRF2 targets along with the amino acids cysteine and glycine. Knockdown of NRF2 results in the glutamine pool being reduced, resulting in a reduction in the biosynthesis of glutathione (Mitsuishi *et al*., 2012). A recent study showed that KRAS, driven lung cancers with a mutation in KEAP1, resulting in constitutive NRF2 activation, rely heavily on glutaminolysis and the addition of a glutaminase inhibitor CB-839 disrupts their proliferation (Romero *et al*., 2017).

1.9.5 NRF2 and lipid metabolism

Biosynthesis of lipids begins with citrate an intermediate of the TCA cycle being transported to the cytosol, where it is converted to acetyl-CoA by ATP-citrate lyase (ACL*)*. Acetyl-CoA is then converted to a three-carbon intermediate known as malonyl-CoA by acetyl-CoA carboxylase (ACC). The two-carbon chain, acetyl-CoA, dimerizes with the three-carbon chain malonyl-CoA to produce a four-carbon intermediate (Figure 1.6). Elongation of the carbon chain occurs by fatty acid synthase (FASN) to produce saturated fatty acids. Insertion of a double bond occurs through fatty acid desaturase (FADS), leading to the synthesis of unsaturated fatty acids such as palmitoleic and oleic acid (Rui, 2014) (**figures 1.9 and 1.10**).

Evidence of a role of NRF2 in lipid metabolism was first identified by Tanaka *et al.,* (Tanaka *et al*., 2008). The study showed that NRF2 knock out mice that were placed on a high-fat diet (65% of the total calories came from lard) or control (7% calories came from fat) for four weeks had an increased expression of the following genes: ACC1, FASN, fatty acid elongase and the sterol regulatory element-binding protein-1c (SREBF1) a key transcription factor in lipid regulation. Treatment of the NRF2 activator

SF in the human liver cell line HHL5 inhibited both the protein and mRNA levels of SREBF1 by blocking the expression of PERK (Tian *et al*., 2018).

A second study assessed, through a 'gene-dose response model', the levels of 52 genes involved in lipid biosynthesis and 21 fatty acid synthesis genes from livers of wild type, NRF2 knockout, KEAP1 knockdown (KEAP1-KD), and KEAP1 knockout (KEAP1-KO) mice. The study results showed that out of these 52 genes, 36 were highly expressed in the NRF2 knockout mice. The study also showed that NRF2 could inhibit the expression of specific genes involved in fatty acid desaturation, such as FADS1 and FADS2. NRF2-null mice had a 56% and 52% increase in mRNA levels of FADS1 and FADS2, respectively. On the other hand, the KEAP1-KO had a 46% and 32 % decrease in the mRNA of FADS1 and FADS2, respectively (Wu *et al*., 2011).

Other studies have shown that NRF2 is involved in downregulating the function of both stearoyl CoA desaturase (SCD1) and ACC (Kitteringham *et al*., 2010, Tanaka *et al*., 2012). Downregulation of ACC also leads to an increase in β-oxidation, as levels of malonyl-CoA are reduced. Malonyl-CoA inhibits the function of carnitine palmitoyltransferase (CPT1a), a protein that is involved in transporting long-chain fatty acids from the cytosol to the mitochondria for β-oxidation (Hayes and Dinkova-Kostova, 2014). Additional studies also support the evidence that knockdown of NRF2 inhibits the expression of genes involved in β-oxidation such as acyl-CoA oxidase 1 and 2 (ACOX1), (ACOX2), CPT1a, and CPT2. Similarly, the activation of NRF2 in the lungs of mice leads to the expression of genes involved in fatty acid oxidation and lipases (Pang *et al*., 2014).

Nagata and colleagues (Nagata *et al*., 2017) were the first to assess how glucoraphanin (GR), the precursor of sulforaphane, impacts fatty acid metabolism. In their study, C57BL/6GJSlc mice were placed into four groups:

1. Normal chow diet (NC),
2. NC-GR,
3. High Fat Diet (HFD) and
4. HFD-GR.

Firstly, the study showed that GR supplementation could reduce steatosis through two different methods: the downregulation of lipid biosynthesis genes such as FASN, SREBF1 and the peroxisome proliferator-activated receptor (PPARγ) and increasing the expression of brown-fat genes (increased caloric expenditure) such as UCP1, cell death activator (CIDEA), and elongation of very long chain fatty acids protein (ELOVL3). Specific genes related to the NAPDH oxidase subunits, such as $gp91^{phox}$, $p22^{phox}$, $p47^{phox,}$ and $p67^{phox}$, along with proteins involved in the production of reactive

oxygen species were also downregulated. Finally, supplementation also decreased inflammation by reducing the number of M1- macrophages accumulating in the liver and increasing anti-inflammatory M2-like macrophages. This resulted in reduced mRNA levels of TNF-α and the NADPH oxidase (Nagata *et al*., 2017).

A follow-up study to (Nagata *et al.* 2017*)* also reported similar results. In that study, mice on a high-fat diet were supplemented with either broccoli or GR from broccoli seeds. Both broccoli and GR supplementation led to a significant reduction in serum levels of the lipids, triglycerides, total cholesterol, and LDL cholesterol. Glucose tolerance tests also showed that both broccoli and the GR group had improved glucose tolerance. Similarly, a homeostatic model assessment of insulin resistance (HOMA-IR) revealed an increase in insulin sensitivity. Both groups showed a reduction in mRNA of FASN, ACC, and SREBP, although only FASN reached statistically significant. The mice supplemented with GR had a statistically significant increase in mRNA of both CPT1 and ACOX1, whereas, those with the broccoli supplementation, only ACOX significantly increased. Compared to previous mice studies, the detailed assessment of how GR affected the gut microbiota composition was novel about the study. GR decreased the Firmicutes to Bacteroidetes ratio; by increasing the number of *Bacteroidetes,* and significantly decreasing *Lachnospiraceae*. A high ratio of Firmicutes to Bacteroidetes is commonly observed in obese individuals. Redundancy analysis plots (RDA) revealed that *Bacteroidaceae,* positively correlated with antioxidant genes SOD and CAT, while *Lachnospiraceae, Ruminococcaceae,* and *Desulfovibrionaceae* significantly enriched in HFD, positively correlated with serum TG, TC, and HDL-C (Xu *et al*., 2020).

Lipid metabolism in the liver is controlled by the nuclear receptor PPARα. This transcription factor controls the expression of several genes involved in lipid transport, β-oxidation, ketogenesis, lipogenesis, and cholesterol metabolism. During fasting conditions or low energy availability, PPARα is activated. Studies have shown that upon NRF2 activation, levels of PPARα decrease (Yates *et al*., 2009). Data from microarray studies on mice fasted for 24h and PPARα knocked out showed significant downregulation in mRNA levels of NRF2 compared to wild-type mice. No change was however observed in the PPARα knockout mice that were fed. These results suggest a potential feedback loop between NRF2 and PPARα during fasting conditions, although the exact mechanism is still not fully understood (Sanderson *et al*., 2009). During fasted state, activation of NRF2 could be through several mechanisms. One could be through transcriptional activation by PPARα. A second may be through the increased production of ROS resulting from oxidation of fatty acids, leading to increased protein stability of NRF2, or it may be a combination of both.

Zhang and colleagues investigated the effects of NRF2 deletion on mice placed on a 24h fast. The results showed that hepatic glycogen, gluconeogenesis, was not affected by the absence of NRF2 (Zhang *et al*., 2013b). An additional finding was that fasted wild type mice failed to induce NRF2 target genes. The study also showed that ROS levels were higher in the NRF2 deficient mice due to the inability to induce the antioxidant genes. A second study reported a similar finding. Here, mice that had NRF2 upregulated through KEAP1 knockdown and were placed on a 24h fast also failed to induce its target genes. The results, however, showed a small and significant induction of NQO1 (Xu *et al*., 2013).

In summary, while the role of NRF2 in lipid metabolism is still not fully understood, as lipid biosynthesis consumes large amounts of NADPH in the cells, a possible explanation may be that NRF2 is involved in blocking this process so that the NADPH can be utilized for the antioxidant response instead.

1.9.6 NRF2 and glucose homeostasis

Impaired glucose homeostasis leads to a phenomenon known as IR. IR is characterized by the failure of cells to respond to insulin leading to high blood glucose. Over the long term, this can result in type 2 diabetes mellitus (T2DM). Long-term complications of T2DM include damage to small blood vessels (microvasculature) found on the retina, kidney, and peripheral nerves (Papatheodorou *et al*., 2018).

Insulin is produced in the β-cells of the pancreas. Diabetes mellitus can occur by either the destruction of the β-cells, resulting in type 1 diabetes, or by insufficient insulin production leading to type 2 (Cnop *et al*., 2005). Oxidative stress has been suggested as a possible mechanism that may result in damage to the β-cells (Fujimoto *et al*., 2011). Patients with T2DM have increased DNA damage of the pancreatic islets in addition to a reduced β-cell mass (Sakuraba *et al*., 2002).

Studies using animal models have shown that NRF2 plays a crucial role in the protection of β-cells. For example, β-cells obtained from mice with NRF2 deleted have increased ROS production, resulting in increased DNA adducts and ultimately apoptosis of β-cells within the islets. The induction of NRF2 blocks this process (Yagishita *et al.*, 2014). NRF2 can preserve the destruction of β-cells; by mopping up free radicals and reducing inflammation derived from the nuclear factor-kappa βeta pathway. It can also enhance the activity of cellular degradation systems such as apoptosis, autophagy, and proteasomal degradation (Li *et al*., 2014, Lee *et al*., 2012). Damage to β-cells through oxidative stress may also affect insulin secretion, although this relationship is not fully understood. While some studies show that ROS blocks

insulin secretion by reducing the production of ATP and increasing the activity of glyceraldehyde 3-phosphate dehydrogenase (GAPDH) (McEvoy *et al*., 2015), the general evidence seems to suggest that oxidative stress is necessary for insulin to be released (Saadeh *et al*., 2012, Leloup *et al*., 2009). In addition, what is still not fully understood is whether NRF2 affects insulin secretion. Data from NRF2 knockout mice have revealed that they have decreased insulin secretion. NRF2 deficiency has also been reported with reduced blood glucose, enhanced insulin signalling, and decreased fat and body weight (Saha et al., 2010, Yu et al., 2011b, Zhang et al., 2012b, Meakin et al., 2014, Meher et al., 2012).

One of the pioneering studies to assess the role of NRF2 in glucose homeostasis was through a mice model of type 1 diabetes by administration of the drug streptozotocin (STZ). This compound destroys β-cells of the pancreas. The study showed that NRF2 knockout mice administered with STZ followed by intraperitoneal glucose injection had worsened blood glucose and higher levels of serum β-hydroxybutyrate, triglycerides, and fatty acids compared to wild type mice. STZ treatment to the NRF2-null mice also resulted in reduced hepatic glycogen, enhanced expression in the gluconeogenesis genes glucose-6-phosphatase (G6PC*)* and phosphoenolpyruvate carboxylase (PCK), and reduced glycolysis. Administration of the NRF2 activator, oltipraz, lowered blood glucose in the WT mice but did not affect the NRF2 null mice administered with STZ (Aleksunes *et al*., 2010).

A second study that assessed the role of NRF2 in glucose homeostasis was in db/db mice (a model for type 2 diabetes). Db/db mice are characterized by a mutation in the diabetes gene db gene encoding for the ObR (leptin receptor), whereas ob/ob mice (see next page) are characterized by a mutation in the ob gene, which encodes leptin (Coleman, 1978). One of the study findings was db/db mice placed on a high-fat diet (HFD) with KEAP1 knockdown had genes involved in energy utilization such as CPT1b and the mitochondrial uncoupling protein 3 (UCP3) in skeletal muscles upregulated. Knockout of NRF2 instead resulted in diminished expression of UCP3 and CPT1b. The study also showed mRNA levels of several gluconeogenesis genes such as G6PC*,* fructose-1,6-biphosphatase (FBP1)*,* and peroxisome proliferator-activated receptor-gamma coactivator 1-alpha (PGC1α) in the db/db KEAP1 KD mice were reduced. The study concluded that NRF2 might reduce T2DM through a combination of factors:

- Promoting antioxidant enzymes in the pancreas, thereby inhibiting ROS,
- Increasing the expression of genes related to energy consumption in skeletal muscle, and finally,
- Downregulating gluconeogenesis related genes (Uruno *et al*., 2013).

In vitro studies using murine hepatocytes have shown that NRF2 can inhibit the expression of G6P and other genes involved in gluconeogenesis, despite induction of gluconeogenesis using a cAMP analogue (David *et al*., 2017). Further, a more recent study using mouse models showed that NRF2 might improve insulin resistance suppressing oxidative stress in the hypothalamus, which may affect metabolic regulation (Yagishita *et al*., 2017).

Excessive body fat accumulation results in obesity. Obesity increases the risk of developing insulin resistance and T2D. Studies using ob/ob mice have shown that induction of NRF2 suppresses weight gain and increases the consumption of oxygen in the skeletal muscle, leading to an increased ATP production as well as improved cellular uptake of glucose (Uruno *et al*., 2013, Holmstrom *et al*., 2013, Kahn *et al*., 2006).

One of the most recent studies that assessed SF regulation in glucose homeostasis was conducted through both *in vitro* and *in vivo* studies. The *in vitro* work consisted of administering rat hepatoma (H4IIE) cells with a high concentration of saturated fat palmitic acid (250 µM) to induce diabetogenic conditions. A 16 h pre-treatment of PA led to a 34% increase in glucose production, while 24 h SF treatment (at 3 µM) led to a 45% reduction in glucose. This study also showed that SF treatment significantly downregulated several genes in gluconeogenesis, such as G6PC*,* PCK1, FBP1, and the glucose-6-phosphatase catalytic subunit. Conversely, the knockdown of NRF2 revealed no effect on insulin signalling, as the phosphorylation status of the insulin receptor substrate 1 (IRS1) and the protein AKT were not changed (Axelsson *et al*., 2017). The *in vivo* study consisted of a randomized, double-blind controlled study for 12 weeks, where 102 type 2 diabetes patients of Scandinavian origin had either mild or severe T2D (severe diabetes was defined as having an HbA1c over 50 mmol/mol) took part. The participants were placed into either a placebo or a capsule containing broccoli sprout extract (BSE) with a high concentration of glucoraphanin (the equivalent of 150 µM SF). The severe T2D was further split into two groups: non-obese and obese to reduce any possible confounders. Fasting blood glucose and Hb1Ac measurements were taken before and at the end of the study. Firstly, the results revealed a significant change in fasting blood glucose between the intervention (8.3 ± 0.3 mM) compared to the placebo group (9 ± 0.4 mM) (Axelsson *et al*., 2017). Hb1Ac levels also changed; the placebo group had 57 mmol/mol while the BSE treated was 53 mmol/mol. Regression analysis revealed a clear correlation between the reduction of fasting blood glucose and a decrease in HbA1c. However, it is worth mentioning that BSE treatment was only effective in obese patients with dysregulated T2D (Axelsson *et al*., 2017).

A potential newly identified mechanism through which SF can reduce/prevent cardiomyopathy complications caused by T2D is through the AMP-activated protein kinase (AMPK). In this study, WT and (AMPKα2) KO mice were firstly placed on an HFD for 3 months to induce insulin resistance. To cause hyperglycemia, both WT and KO mice were then intraperitoneally injected with streptozocin (STZ). Upon treatment, mice were then gavaged with or without SF for 3 months while still being fed a high-fat diet or chow for the control group. Mice were then sacrificed at 3- and 6-months post SF treatment. The study showed that in the WT mice placed on an HFD followed by STZ administration, SF could inhibit cardiomyopathy through two different pathways: inhibiting lipid metabolism through AMPK activation and the NRF2 antioxidant response. pAMPK upregulation by SF enhanced oxidation of fatty acids in the mitochondria by upregulating the CPT1b and PGC1-α pathways. pAMPK was also able to inhibit the SCD-1 gene involved in synthesising unsaturated fatty acids. Finally, the study discovered a novel mechanism through which NRF2 could induce the antioxidant response. Phosphorylation of AKT by pAMPK, which led to increased GSK3β, could induce NRF2. NRF2 upregulated genes in the antioxidant response, such as HMOX1 and catalase (CAT), thereby reducing oxidative stress and fibrosis of cardiac tissue (Sun *et al*., 2020).

1.9.7 NRF2 and cardiovascular diseases

As mentioned in section 1.2.3, CVDs are the world's leading causes of death, and lifestyle choices can largely prevent these. Within the last couple of years, research on NRF2 has suggested that its activation may also play a role as a potential target for cardiovascular diseases (da Costa *et al*., 2019, Satta *et al*., 2017). A summary of the latest research on NRF2 and its role in the management of CVDs has also been presented.

Increased ROS results in the oxidation of LDL cholesterol. This contributes to the formation of foam cells, eventually resulting in arterial plaque. Several different mechanisms have been proposed to explain how NRF2 may attenuate the progression of atherosclerosis. One proposed mechanism is through the induction of the antioxidant response. For example, mice that lack GPx-1, a direct NRF2 target gene, have increased oxidation of LDL-cholesterol, resulting in a greater number of foam cells developing (Cheng *et al*., 2013). Similarly, mice that are both HMOX1 and apolipoprotein E deficient have increased oxidative stress and develop atherosclerotic lesions at a faster rate (Yet *et al*., 2003). Deletion of HMOX1 in macrophages has also been shown to increase a build-up of lipids, resulting in a greater number of foam cells formed and an increase in the number of pro-inflammatory cytokines (Orozco *et al*.,

2007). What was also identified in a human study is that participants with carotid artery disease had increased expression of HMOX1, and this correlated with an unstable plaque phenotype. The study concluded that it was not fully understood whether the upregulation of HMOX1 in these patients was an atheroprotective response to reducing the plaque's ROS levels or if HMOX1 contributes to increased plaque vulnerability (Cheng *et al*., 2009).

A second mechanism via which NRF2 may delay the progression of CVDs is by modulating the migration and proliferation of vascular smooth muscle cells (VSMCs) (Ashino *et al*., 2013). Studies have shown that NRF2 deletion increases PDGF-induced migration of VSMCs, and these mice also have higher neointima hyperplasia. It has been hypothesized that NRF2 induction can suppress neointima hyperplasia by inducing apoptosis of VSMCs and reducing the proliferation of VSMCs (Ashino *et al*., 2016, Kim *et al*., 2009). In addition, it has also been shown that NRF2 induction attenuates the circulation of calciprotein particles (CPP), thereby reducing the calcification of VSMCs (Aghagolzadeh *et al*., 2017). Figure 1.11 represents a summary figure of the various pathways NRF2 regulates.

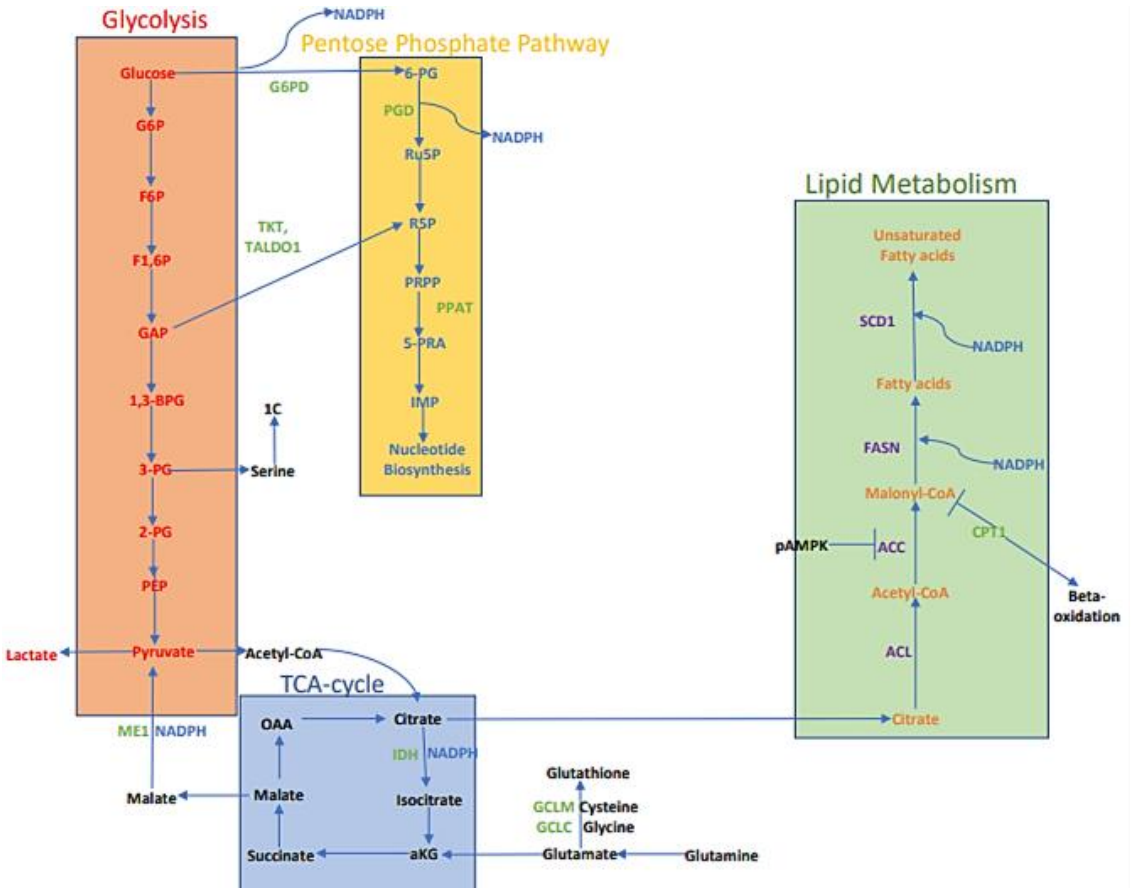

Figure 1.11. **Regulation of metabolic pathways involved in central metabolism by the transcription factor NRF2**. NRF2 positively regulates G6PD and PGD of the oxidative arm of PPP and TALDO1 and TK of the nonoxidative arm of the PPP. Regulation of these two genes and ME1 allows NADPH production, which is then redirected for Glutathione function. NRF2 regulates the rate limiting enzymes GCLM and GCLC involved in glutathione biosynthesis. At the same time, NRF2 inhibits the function of ACC, FASN and SCD1 involved in the biosynthesis of saturated and unsaturated fatty acids, which is an NADPH consuming process. The expression of genes for phosphoribosyl pyrophosphate amidotransferase (PPAT) and involved in de novo purine biosynthesis, also regulated by NRF2. The lower levels of SCD1 may influence positively AMP-activated protein kinase (AMPK), thus further suppressing ACC1 activity.

1.10 Aims:

Due to the emerging role of NRF2 in regulating metabolism, there is an unresolved question of whether some of the mechanistic basis of the beneficial effects of SF intake involves regulation of key metabolic pathways and whether this is mediated primarily through NRF2. In addition, understanding the role of NRF2 as a metabolic regulator and the process through which this occurs is still unclear. Despite the liver being the central metabolic organ, very few studies have assessed NRF2 metabolic activity *in vitro* using liver cell lines.

This thesis aims to test the hypothesis that NRF2 is the key mediator of broccoli bioactivity in modulating key metabolic pathways in the liver. This was investigated through:

1. Using an *in vitro* model of liver metabolic imbalance and understanding how physiological levels of SF impacts hepatic metabolism challenged with a range of fatty acids and glucose concentrations.
2. Assessing the effect of physiological concentrations of SF in inducing different transcriptional changes in hepatocytes challenged with different concentrations of glucose.
3. Assessing how physiological concentrations of SF redirects glucose and glutamine to metabolic pathways in hepatocytes challenged with different concentrations of glucose.
4. Applying the genome editing technique (CRISPR/Cas 9) to develop a novel liver cell line that lacks NRF2, to assess the extent to which the metabolic changes are mediated primarily by NRF2.

CHAPTER 2: MATERIALS AND METHODS

Chapter 2 Figures

Chapter 2 Tables:

2.0 Chapter 2: Materials and Methods

2.1 Preparation of sulforaphane

R, S-sulforaphane (Catalog: S8044, LKT Laboratories) was dissolved in 100% dimethyl sulfoxide (DMSO, Sigma catalog: D2650) to achieve a 5.5 M concentration and a 100 mM master stock solution stored at -20°C. 10 µL of the 100 mM stock solution was diluted to a 1 mM working solution. From the 1 mM solution, sulforaphane was diluted to final concentrations in the culture medium just before the addition to the cultures. The final concentration of DMSO in the culture was < 0.01%.

2.2 Cell Culture

HepG2 cells a human hepatocarcinoma cell line (isolated from an American 15-year-old male) were obtained from the American Type Culture Collection (ATCC, HB-8605). HepG2 was cultured in EMEM (Eagle's Minimum Essential Medium ATCC 30-2003)

containing 10% fetal bovine serum (FBS) (Gibco catalogue:10082147), 100 μml^{-1} penicillin, and 100 μml^{-1} streptomycin (Catalogue:15140122 Gibco). Cells were maintained at 37 °C in a 5% CO_2 environment. The cells were cultured in a T75 flask or grown on 6-well plates from passage 7 to 18.

2.3 WST-1 Assay

The WST-1 assay works by the conversion of the tetrazolium salt WST-1 (4-[3-(4-iodophenyl)-2-(nitrophenyl)2H-5-tetrazolio]-1,3-benzene disulfonate) into formazan by mitochondrial dehydrogenase enzymes. This assay indirectly measures the viable cells. By progressively increasing the concentrations of the treatment, a reduction in viability results in fewer metabolically active cells. As a result, a reduction in mitochondrial dehydrogenase activity results in a more significant number of cells being unable to carry out the conversion of the dye. The product of the enzymatic reaction, formazan, is a deep red colour that enables a spectrophotometric assay to allow quantitative determination of the number of viable cells.

The WST-1 (Sigma, catalog: 000000005015944001) assay was performed according to the manufacturer's instructions. For this assay, HepG2 were seeded at 2×10^4 cells per well in a 96-well plate with EMEM containing 10% FBS. 72 h after seeding, the wells were washed with 1XDPBS and treated with varying SF concentration (10-700 µM) for 2 h or 2-200 µM for 24 h in EMEM serum-free media. Briefly, after 2 or 24 hours of cell treatments, 10 µL (per 100 µL media) of WST-1 reagent was added to each well. The cells were incubated in a humidified atmosphere containing 5% CO2 at 37°C for up to 3 h. The metabolic conversion of the WST-1 reagent to formazan was quantified by measuring the absorbance using a spectrophotometer at 450 nm with a reference wavelength of 610nm. Medium-only was used for the blank correction to compensate for any absorbance contribution of the basal colour from the phenol red present within the medium. The percentage of viable cells was calculated using the following formula:

Cell viability (%) = optical density (OD) of the treatment group/OD of the control group x100

2.4 RNA extraction

HepG2 cells were seeded on a 6-well plate (2×10^5 cells/well). On the day of the treatment, the media was removed and the wells washed twice with 1X DPBS (14190144 Gibco) and 10 µM of SF or control (DMSO) in serum-free DMEM without glucose (Catalogue: 11966025 Gibco) supplemented with 1 mM sodium pyruvate

(11360070 Gibco), and 5.5 mM or 25 mM glucose (A2494001 Gibco) or 10 mM galactose (G5388 Sigma). For the continuous SF treatment RNA was extracted at 2, 4, 6, and 24 h. For the transient expression, 2, 10, and 25 µM of SF were added for 2 h. After 2 h, the media was removed, washed once with 1XDPBS, and serum-free media was added. RNA was then extracted following 2, 4, 6, and 22 h post media change. For all experimental procedures, following the desired time point:

1. Media was removed from six well plate
2. Cells were washed twice with 1XDPBS,
3. Buffer RLT with β-ME (444203 Sigma), to control and sulforaphane treated cells, were lysed directly on the 6-well plate.

RNA was then extracted using the RNeasy Qiagen kit (Ref:74004) according to the manufacturer's instructions. RNA abundance and integrity were assessed using the Nanodrop ND-1000 spectrophotometer. Briefly, triplicate readings for RNA quantification were performed per sample, and the average was calculated. The purity of the RNA was deduced from the ND plot and the 260/280 ratios. A 260/280 nm ratio greater than 2 was taken to indicate a pure sample, while 260/230 ratios less than 2 were taken as indicative of contaminants such as salts that absorb at 230 nm.

2.5 Quantitative real time-PCR analysis

For the quantification of gene expression, the Taqman® RNA to CT 1-step kit was used (Primer Design, catalog: OSPLUS). RNA extracted from the cells was used as the starting material to produce the complementary DNA strand based on the RNA sequence. The DNA was then amplified for the detection of target genes. Identification of target genes occurred through the fluorescent signal generated using dual-labeled probes. The 5' end of the probes was labeled with reporter dye such as FAM (6-carboxyfluorescein) and a quencher dye at the 3' end, e.g., TAMRA (6-carboxytetramethylrhodamine). When the two dyes are near each other, no fluorescent signal is generated. However, when the Taq polymerase amplifies the complementary DNA strand where the probe is bound, the 5' nuclease activity of the polymerase cleaves the probe, resulting in the reporter and quencher dyes being decoupled and a fluorescent signal is released. With each progressive cycle that occurs, the fluorescent signal increases, which can be used to determine the relative expression level of the target gene.

The expression of the genes HMOX1, NQO1, CPT1a, FAS, G6PD, PG6D, TKT, GCLC, TXRND1, and ACTB were measured by real-time PCR using an Applied Biosystems 7500 Step One Plus detector instrument. RNA from these genes was monitored using commercial probe sets, all of which were purchased from Integrated DNA technologies

Table 2.1. Quantitative real-time-PCR reactions were performed by adding 5 µl of the RNA (4 µgµL^{-1}) to 15 µL of Mastermix (probe, and water). To normalize the expression of the target genes, an endogenous control, also known as a housekeeping gene, was used to account for potential differences in the total RNA in each sample. For normalization of the target genes used in the present study, the housekeeping gene chosen was beta-actin, ACTB (Hs.PT.39a.22214847).

The samples were loaded onto a 96-well semi-skirted fast plate (Alpha Laboratories, catalog: LW2214) using the CAS-1200 robot. A no-template control (NTC) was loaded (RNase-free water provided by Qiagen kit) to ensure no RNA contamination, followed by each of the samples—including three biological and three technical replicates. The PCR program on the Step One Plus software was set at 48 °C for 30 min to allow reverse transcription, 95 °C for 10 min to activate the Taq polymerase, followed by 40 cycles of 95 °C for 15 seconds for denaturation and 60 °C for 1 min to anneal and extend the target gene DNA.

At the end of the run, the threshold cycle (CT) values for each reaction were calculated, and a standard curve of known total RNA quantities was used to calculate the amount of the target RNA. The standard curve for each gene was also used to calculate the amplification efficiency. The output from the Step One Plus software comprised a linear plot with the equation of the line, amplification efficiency, and the R^2 value. The amplification efficiency usually varies between >96% and less than 115%, where a reaction that has been 100% efficient will result in the gradient of the standard curve being -3.32. This means that the CT difference between two sequential 2-fold dilutions will equal 1. The R^2 value of the standard curve line represents how well the CT values for each sample lie on the best fit. Values >0.99 are highly accurate.

Table 2.0: List of primer sequences used in qRT-PCR

All primers were purchased as pre-designed qPCR probe assays from Integrated DNA Technologies (IDT) with double quenched probes (5'FAM / ZEN / 3' IBFQ).

Assay ID	Gene	Species	RefSeq	Transcripts hit	Detects all variants	Exon location	Design score
Hs.PT.58.3368888	PGD	Human	NM_002631	NM_002631	Yes	6 - 7	17.6013
Hs.PT.58.20384174	FASN	Human	NM_004104	NM_004104	Yes	3 - 4	16.8263
Hs.PT.58.3359761	SREBF1	Human	NM_001005291	NM_001005291, NM_004176	Yes	6 - 7	16.7304
Hs.PT.58.20474921	TKT	Human	NM_001064	NM_001064, NM_001135055, NM_001258028, NR_047580	Yes	9 - 10	16.7025
Hs.PT.58.27558354	G6PD	Human	NM_001042351	NM_001042351	No	1 - 3	16.5602
Hs.PT.39a.22214847	ACTB	Human	NM_001101	NM_001101	Yes	1 - 2	0

Primer 1	Primer 2	Probe	Amplicon	Start pos.	End pos.
CCATACTCTATCCCGTTGTGC	AGACCATCTTCCAAGGCATT	CTCCCTCATCTCCCACCCAGTCA	118	551	668
CGGAGTGAATCTGGGTTGATG	TTTGATGCCTCCTTCTTCGG	CCATCGTGTGTGCCTGCTTGG	125	295	419
CTGCTTGAGTTTCTGGTTGC	CTACCGCTCCTCCATC\AATG	TTATTCAGCTTTGCCTCAGTGCCCA	145	1286	1430
CATGCGAATCTGGTCAAAGG	CCGCTTCATCGAGTGCTAC	AGGACGGTGCCCTTCTGCA	136	1243	1378
GTATCCGACTGATGGAAGGC	TCCGGAGAGAAGTCTGAGTC	AGCTCGACAGCGTCATGGCA	150	56	205
CCTTGCACATGCCGGAG	ACAGAGCCTCGCCTTTG	TCATCCATGGTGAGCTGGCGG	110	30	139

RefSeq	Transcripts hit	Detects all variants	Exon location	Design score	Primer 1
NM_002631	NM_002631	Yes	6 - 7	17.6013	CCATACTCTATCCCGTTGTGC
NM_004104	NM_004104	Yes	3 - 4	16.8263	CGGAGTGAATCTGGGTTGATG
NM_001005291	NM_001005291, NM_004176	Yes	6 - 7	16.7304	CTGCTTGAGTTTCTGGTTGC
NM_001064	NM_001064, NM_001135055, NM_001258028, NR_047580	Yes	9 - 10	16.7025	CATGCGAATCTGGTCAAAGG
NM_001042351	NM_001042351	No	1 - 3	16.5602	GTATCCGACTGATGGAAGGC
NM_001101	NM_001101	Yes	1 - 2	0	CCTTGCACATGCCGGAG

Primer 2	Probe	Amplicon	Start pos.	End pos.
AGACCATCTTCCAAGGCATT	CTCCCTCATCTCCCACCCAGTCA	118	551	668
TTTGATGCCTCCTTCTTCGG	CCATCGTGTGTGCCTGCTTGG	125	295	419
CTACCGCTCCTCCATCAATG	TTATTCAGCTTTGCCTCAGTGCCCA	145	1286	1430
CCGCTTCATCGAGTGCTAC	AGGACGGTGCCCTTCTGCA	136	1243	1378
TCCGGAGAGAAGTCTGAGTC	AGCTCGACAGCGTCATGGCA	150	56	205
ACAGAGCCTCGCCTTTG	TCATCCATGGTGAGCTGGCGG	110	30	139

2.6 Oil Red O assay

Oil Red O, also known as Sudan Red 5B, is a fat-soluble diazo dye used for staining lipids. The dye is dissolved in a solvent, usually isopropanol. This means that the dye can enter the cells and stain the lipids bright red while the excess is removed by washing with water. An advantage of this protocol is that the Oil Red O stain can be eluted from the cells using isopropanol without dissolving the lipids themselves; thus, the level of staining can be quantified spectrophotometrically.

For the Oil Red O assay, HepG2 were seeded at 3×10^5 cells per ml in a 6-well plate. The following day, media was removed, washed twice with 1X DPBS, and serum-free MEM (Gibco, catalog: 51200-038) media was added along with 10 µM SF pre-treatment. Following 24 h SF pre-treatment, the media was removed, washed twice with 1X DPBS, and the cells treated with 0.2 mM BSA-palmitate conjugate or control (BSA/DMSO) for 24 h. After 24 h palmitate treatment, cells were washed twice with 1X DPBS and fixed with 10% formalin for 1 h. After fixation, cells were washed once with ddH_2O and then twice with 60% isopropanol and stained with Oil Red O working solution (2.5 g of Oil Red O (Sigma, catalog: O9755) in 100% isopropanol) for 20 min at room temperature. Cells were washed again with ddH_2O to remove unbound staining. To quantify Oil Red O content levels, 100% isopropanol was added to each well; after shaking at room temperature for 5 min. Finally, 200 µL of each sample was added to a 96-well plate, and the density of samples was read at 492 nm on a spectrophotometer.

2.7 Seahorse Assays:

I used the Seahorse BioScience (Agilent) to assess metabolism measuring the oxygen consumption rate (OCR) and extracellular acidification rate (ECAR). These measure the rate of oxidative phosphorylation and glycolysis respectively. The Seahorse can also assess additional metabolic pathways such as fatty acid metabolism in real time. The assay works through the acute injections of up to four test compounds. These compounds stress the cells, thus enabling the assessment of the potential changes in energy production (Ferrick *et al*., 2008).

OCR was measured in real-time using the XF_p extracellular analyzer (Agilent Technologies, Seahorse Biosciences) according to the manufacturer's protocol. Briefly, cells were seeded at a density of 5×10^4 cells/well in six wells of the eight-well Seahorse plate and grown for 48 h. For both the OCR and the ECAR assays, the Seahorse XF_p sensor cartridge (Agilent Technologies) was hydrated a day before the treatment using XF calibrant (Agilent Technologies) and placed in a 37°C non-CO_2 incubator.

Before running the assays, the media was replaced with Seahorse Base Media (DMEM) (Agilent, catalog: 102353-100) containing 4 mM glutamine (Gibco, catalog: A2916801, 1 mM sodium pyruvate (Giblco, catalog: 11360070). The plates were then placed in a non-CO2 incubator for 45 min to 1 h and then placed in the XF_p extracellular flux analyzer for calibration. Oligomycin (Catalog: 75351), Carbonyl cyanide-p-trifluoromethoxyphenylhydrazone (FCCP) (Catalog: C920), rotenone, and

antimycin A (Catalog: R8875/A8674) were purchased from Sigma- Aldrich and diluted in DMSO to generate 10 mM stock solutions which were stored at -20 ºC until required.

The Seahorse cartridge was prepared during the plate incubation in the non-CO_2 incubator. The stock drug compounds were diluted to working concentrations using the Seahorse media. Mitochondrial activity was evaluated by sequential injections of four components that affect its activity, as summarised in table 2.1 and figure 2.1.

Table 2.1: Summary of the compounds added to the Seahorse cartridge to the stress the mitochondrial for the Seahorse Mito stress kit

Port ID	Compound Added	Injection Volume	Port Concentration	Final Well Concentration
A	Oligomycin	20	10 µM	1 µM
B	FCCP	22	5 µM	0.5 µM
C	Rotenone/Antimycin A	25	5 µM	0.5 µM

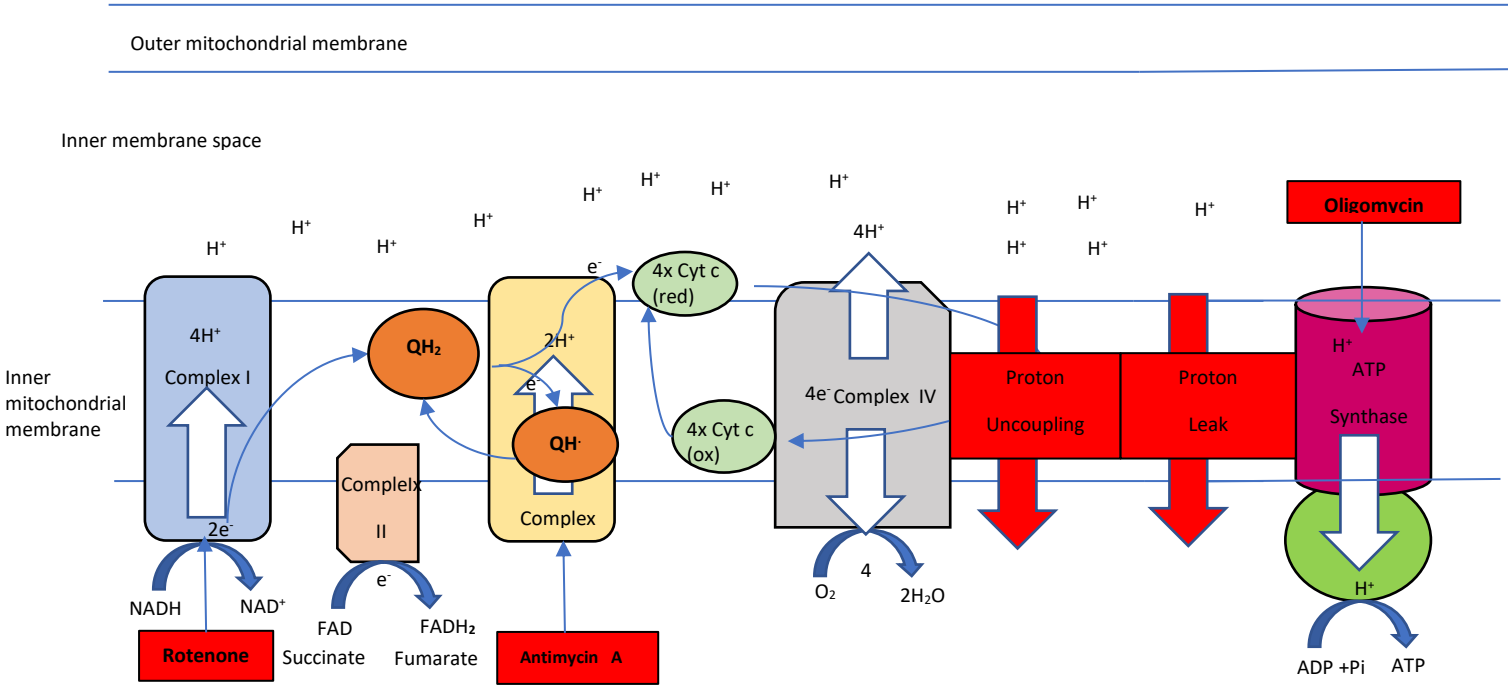

Figure 2.1. Summary of how the drug compounds affect the mitochondrial electron transport chain.

For the extracellular acidification rate (ECAR)-XF_p glycolysis rate assay (Agilent Technologies), cells were seeded at a density of 5×10^4 cells/well in 6 wells of the 8-well Seahorse plate and grown for 48 h. On the day of the treatment, media was removed, and the wells were washed twice as described above. Before running the assays, the media was replaced with Seahorse base media (DMEM, 102353-100 Agilent) containing 4 mM glutamine (Gibco, catalog: A2916801). The plate was then

placed in a non-CO2 incubator for 1 h before putting it in the XF_p extracellular flux analyzer for calibration. Following calibration, glycolysis function was assessed by sequential injections of two components that affect its activity, as summarised in table 2.2 and figure 2.2. For both the OCR and ECAR assays, protein from each well was extracted to normalize for variation in cell number. Briefly, cells were lysed with 1X lysis buffer (Cell Signalling Technology, catalog: 9803S), lysates were centrifuged at 17,000 g at 4 °C for 10 min. Protein concentrations were then quantified using the bicinchoninic protein assay (Sigma catalog: BCA1-1KT).

Table 2.2: Summary of the compounds added to the Seahorse cartridge to assess glycolytic function through the glycolysis stress test

Port ID	Compound Added	Injection Volume	Port Concentration	Final Well Concentration
A	Glucose	20	100 mM	10 mM
B	Oligomycin	22	10 µM	1 µM
C	2-DG	25	500 mM	50 mM

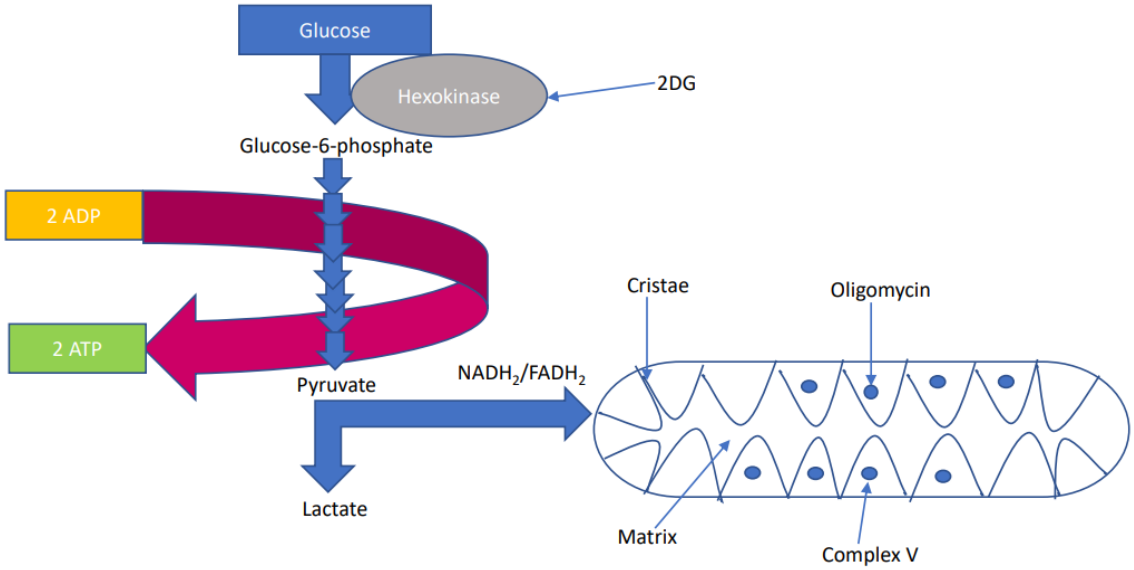

Figure 2.2. Summary of how the drug compounds affect glycolysis

2.8 RNA Sequencing and gene expression analysis

RNA sequencing often abbreviated to RNA-seq is a technology that uses next-generation sequencing (NGS) to reveal the presence and quantity of RNA at a given time point to asses the transcriptome (Stark *et al*., 2019). Before RNA-seq, gene expression studies were conducted using microarrays; although RNA seq offers many more advantages. For example, it doesn't require specific probes, and it can detect novel transcripts, alternative splicing junctions, new single nucleotide variants, allele-

specific expression, and other changes that arrays cannot identify (Rao *et al*., 2019). In addition, RNA seq can look at different populations of RNA such as total RNA, miRNA, tRNA, and ribosomal profiling. In this analysis, polyA sequencing was performed which only assesses mRNA. Compared to microarray experiments, the high specificity and sensitivity of RNA-seq can capture not only a higher percentage of differentially expressed genes but also genes that are usually low expressed (given the adequate sequencing depth) more accurately than microarray without the requirement for hybridization (Rao *et al*., 2019).

HepG2 cells were seeded on a 6 well plate (2×10^5 cells/well). Before sequencing RNA quality was first checked on the 2100 Bioanalyzer using the Agilent RNA 6000 Nano Reagents. RNA that had an RNA Integrity value (RIN) > 7 was sent for sequencing. For chapter 4 RNAseq analysis, RNA samples were then sent to Macrogen (South Korea). Macrogen then conducted the following: samples were ribo depleted through the TruSeq RNA-Poly A. Sequencing of 36 libraries was performed on an Illumina NovaSeq 2x using 100-bp paired-end reads, generating 30 million reads/library.

The RNA-sequencing data analysis was divided into two steps: processing the raw RNA-sequencing data to estimate genes counts and then the comparative analysis of the transcriptomics data (**figure 2.3**). The data processing was performed by the QIB bioinformatician Dr. Perla Troncoso Rey following the protocol for the *"new Tuxedo"* suite for short reads (Pertea et al., 2016a) and using the HPC environment managed by *the Norwich Bioscience Institute's Computing infrastructure for Science, CiS* (Pertea et al., 2016b). The new Tuxedo suit includes computational tools for the alignment of RNA-seq reads to a reference genome, the assembly of transcripts, quantification of gene and transcript expression, and differential expression analysis.

The first part of the analysis started with the processing of raw RNA-seq data to remove Illumina adapter sequences, low-quality and short reads using *Trim Galore!* v.0.6.5 . Adaptor sequences were removed with an overlap of a minimum of 5 bases (*--stringency 5*). For this analysis, the quality control (based on the 'Phred33' score) removed reads with a quality of less than 30 (-q 30) and reads shorter than 60 bp (-length 60).

The alignment of high-quality reads was performed with *HISAT2* v.2.1.0 (Kim *et al*., 2015) to the ensembl's human reference genome GRCh38, release 97 (July 2019) . *HISAT2* is an ultrafast splice-aware aligner based on the principles of some of the most widely used aligners; the Burrows-Wheeler aligner (BWA) and Bowtie (Li and Durbin, 2009), which uses the Burrow-Wheeler transform to store the reference genome in a

highly compressed form. Using the Ferragina-Manzini, FM, indexing, Bowtie, and BWA can search a genome very rapidly.

The alignments were then assembled into full-length transcripts and quantified in each sample using *StringTie* v.1.2.2 (Pertea et al., 2016a). *StringTie* creates as many isoforms as needed to explain the data, and estimates the expression levels of all known genes and transcripts. After the initial assembly, the assembled transcripts were merged to create a uniform set of transcripts for all samples (Pertea et al., 2016a). The merged transcripts were then compared to the reference human annotation and statistics on this comparison were calculated using *gffcompare* v.0.9.8 (Pertea and Pertea, 2020). Finally, the read alignments and the merged transcripts were used to re-estimate abundances (where necessary) and create transcript and gene counts for further analyses.

The complete bioinformatics pipeline, differential gene expression (DGE) analyses, and statistical analysis follow the QIB's GitHub repository for RNA-seq analysis in the following link: https://github.com/quadram-institute-bio science/FIH-RNAseq-analysis. Detailed information on how the comparative analysis of the transcriptomics data was carried out has been explained in chapters 4 and 6. Finally, plots for the genes vs the logFC were constructed using ggplot2 (3.1.0). Network analysis was conducted on Cytoscape 3.7.2.

For the RNAseq analysis conducted in chapter 6 RNA was extracted from Wild Type and NRF2KD HepG2 treated with 10 μM SF at 3, 9, and 24 h or control (DMSO) in serum-free DMEM without glucose (catalog: 11966025 Gibco) supplemented with 1 mM sodium pyruvate (catalog: 11360070 Gibco) and 25 mM glucose (catalog: A2494001 Gibco). RNA was sent to GeneWiz (Essex, United Kingdom). Both quality control and sequencing were carried out by GeneWiz through BioAnalyzer. Samples were then ribo depleted through the TruSeq RNA-Poly A. Sequencing of 36-324 libraries was performed on an Illumina NovaSeq 2x using 150-bp paired-end reads, generating 35 million reads/library. Processing the raw RNA-sequencing data to estimate genes counts were carried as mentioned above. Differentially expressed genes were obtained though, through the DESeq2 package. See chapter 6 for an in-depth explanation.

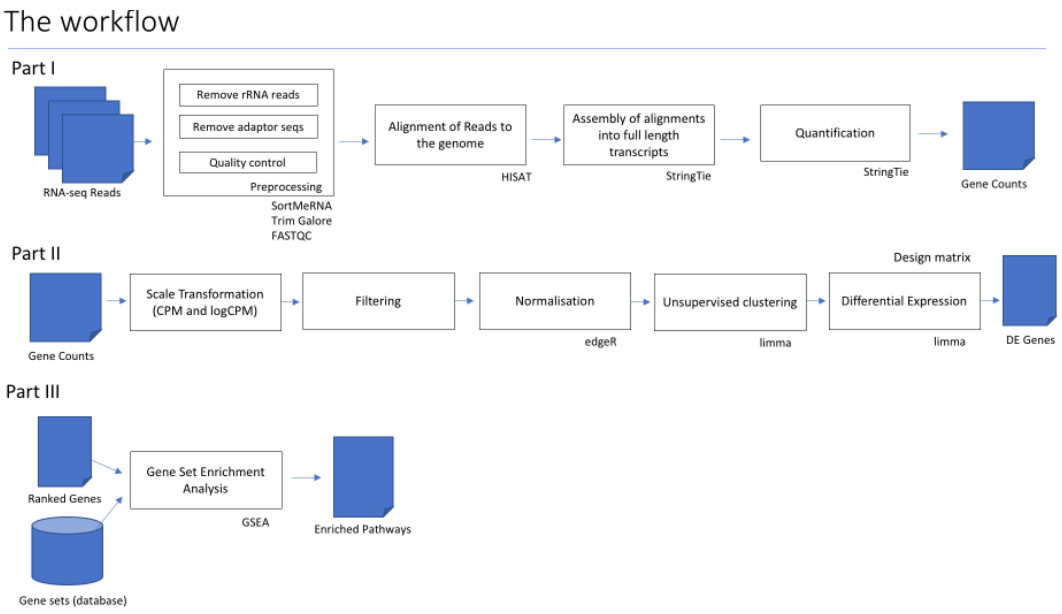

Figure 2.3. Summary of RNAseq data analysis pipeline

2.9 Gas chromatography/Mass spectrometry (GC-MS):

For the $^{13}C_6$ glucose assay, HepG2 cells were seeded at a density of 3×10^5 cells/well on a 6-well plate and grown for 48 h. On the day of the assay, cells were washed once with 1XDPBS and incubated for a further 24 h with DMEM (Sigma, catalog: D5030) supplemented with $^{13}C_6$ glucose (Sigma, catalog: 389374) and $^{12}C_5$ glutamine (Roth, catalog: HN08.2), sodium pyruvate (Sigma, catalog: P8574) and sodium bicarbonate (Sigma, catalog: S5761) with 10 µM of SF or control (DMSO) without serum.
For the $^{13}C_5$ glutamine assay, HepG2 cells were treated as described for the $^{13}C_6$ glucose assay except using $^{12}C_6$ glucose and $^{13}C_5$ glutamine (Sigma, catalog: 605166).
For the 1-2-13C_6 glucose assay, HepG2 cells were treated as described for the $^{13}C_6$ glucose assay except using 1-2-$^{13}C_6$ glucose tracer (Sigma, catalog: 453188) and $^{12}C_5$ glutamine.

Following 24 h incubation, the plate was washed once with 2 ml of 0.9% sodium chloride (NaCl) (Sigma, catalog: S3014). The intracellular metabolite was extracted by adding 400 µL each of methanol (-20 °C) and double distilled water (4 °C) containing 1 µgml^{-1} of the internal standard (IS) D6-glutaric acid (CDN isotopes catalog: D-5227). Cells were scraped and transferred to a tube containing 400 µL of chloroform (-20 °C) and vortexed for 20 min at 1400 rpm at 4 °C (Eppendorf ThermoMixer C). Polar, aqueous, and non-polar phases were separated by centrifugation (21,000g at 4 °C for 5 min) and 300 µL of the polar phase was transferred to a GC glass vial. Vials were dried vacuum-centrifuged at 4 °C, capped, and stored at -80 °C for further analysis.

Extraction of the extracellular metabolites was carried out using a methanol/water mixture (8:1 v/v). The water fraction contained the IS D6-glutaric acid 2 $ugml^{-1}$. 20 µL of medium were added to 180 µL of ice-cold methanol/water mixture (8:1 v/v) and vortexed for 10 min at 1400 rpm at 4 °C (Eppendorf ThermoMixer C). Polar, aqueous, and non-polar phases were separated by centrifugation (10 min at 17,000g for 4 °C) and 80 µL of the polar phase was transferred to a GC glass vial. Vials were dried vacuum-centrifuged at 4 °C, capped, and stored at -80 °C for further analysis.

Derivatisation of the samples (carried out at the BRICS from the Technical University of Braunschweig) was performed with an Axel Semrau Chronect Robotic Pal RTC directly before GC-MS measurement. 15 µL of 2 % methoxyamine hydrochloride in pyridine were added to the samples and agitated for 60 min at 40 °C. Afterward, an equal volume of N-Methyl-N-(trimethylsilyl) trifluoroacetamide was added and shaking continued for 30 min at the same temperature. 1 µL of each derivatized sample was injected in splitless mode into an SSL injector heated to 270 °C. The gas chromatographic separation was performed on an Agilent 7890B GC equipped with a 30 m ZB-35 + 5 m duraguard column (Phenomenex). Helium was used as a carrier gas with a flow rate of 1 ml min^{-1}. Initially, the GC oven temperature was held at 80 °C for 6 min. Afterward, the temperature was raised by 6 °C/min until 300 °C was reached and finally held for 10 min. Then, the temperature was increased to 325 °C at 10 °C/min and held for an additional 4 min, resulting in a total run time of 59.167 min for one sample. The GC system was coupled to an Agilent 5977B MSD. Electrical ionization of the metabolites was performed at 70 eV. The MS ion source was constantly heated to 230 °C and the quadrupole to 150 °C. For the untargeted approach, full scan mass spectra were acquired from m/z 70 to m/z 800. For the labeling experiments, the connected detector was operated in selected ion monitoring. GC-MS chromatograms were processed using the in-house developed software, MetaboliteDetector, v3.320200313 (Hiller *et al*., 2009). Mass isotopomer distributions were calculated according to the chemical formulas from Wegner *et al*. (Wegner *et al*., 2014).

Table 2.3: Deconvolution and parameter settings on the metabolite detector used to obtain the MID

The MID values were then exported to an Excel spreadsheet, where the values were imported into GraphPad Prism. Statistical analysis was carried out using a two-way ANOVA.

Parameters	Values
Peak height	5
Peak threshold	5
Deconvolution width	5
Bins/scan	10
Baseline adjustment	Off

2.10 Liquid Chromatography/Mass Spectrometry (LC-MS)

2.10.1 Analysis of glutamine, glutamic acid, pyroglutamic acid, and glutathione in basal and high glucose

The concentration of glutamine, glutamic acid, pyroglutamic acid, and oxidized/reduced glutathione in the cell and media were assessed through LC-MS.

Before performing the extraction, the cells were treated with 10 µM SF or control (DMSO) in media without glucose (Gibco, catalog: 11966025) and supplemented with 5 and 25 mM glucose (Gibco, catalog: A2494001) to represent the basal and high glucose environments. For the extraction, cells were washed once with 10 mL ice-cold 0.9% NaCl (Sigma, catalog: S3014) and harvested using 0.05% (w/v trypsin (Gibco, catalogue: 25200056). After cell count with the Countess™ (ThermoFisher Scientific Ref: AMQAX2000), the cell suspensions were centrifuged at 1,200g for 10 min at room temperature. The supernatant was discarded, and the cells were resuspended in 10 ml of 0.9% warm sodium chloride (Sigma, catalog: S3014), before centrifugation at 1,200g for 10 min. The supernatant was then removed and 0.5 mL of perchloric acid (0.3 mM) was added (Sigma, catalog: 50439). The mixture was kept on ice for 10 min followed by further centrifugation at a higher speed of 12,000 g at 4 ^{o}C for 10 min. The supernatant (50µl) was transferred to HPLC vials (Fisher Scientific, catalog: 10003264) and stored at -20 until further analysis. I performed triplicate readings per sample.

Metabolites were also extracted from the media. Briefly, 1ml of the culture medium was collected before harvesting HepG2 cells with trypsin, and 10% perchloric acid (3 mM) (Sigma, catalog: 50439) was added. Samples were kept on ice for 10 min followed by further centrifugation at a higher speed of 12,000 g at 4 ^{o}C for 10 min. The supernatant (50 µl) was transferred into HPLC vials and stored at -20 ^{o}C until further analysis

A standard curve was produced with 1mgml^{-1} concentration for glutamine, glutamic acid, pyroglutamic acid, all purchased from Sigma-Aldrich: glutamine (catalog: G3126), glutamic acid (catalog: G1251), pyroglutamic acid (catalog: 83160). A separate standard curve was prepared for oxidized glutathione (catalog: G4376) and reduced glutathione (catalog: G6013). Finally, for all chemicals, a five-point standard curve was produced with a 10-fold serial dilution, in either water for cell samples or DMEM media for media samples over the range of 1000 µgml^{-1} to 0.01 µgml^{-1}.

For LC-MS/MS analysis, the Agilent 1200 Series with 6490 Triple Quad LC-MS mass spectrometer was used, carried out at the Quadram Institute through the support of the senior analytical chemist Dr Shikha Saha. The HyperCarb UPLC column was used to separate glutamic acid, glutamine, and pyroglutamic acid (50X2.1, ThermoFisher), oxidized/reduced glutathione were separated using Luna Omega Polar 1.6 µM Polar C18 (Thermofisher) column, and the temperature for both columns was set to 30 °C. For the chromatographic separation gradient, mobile phases were used. Mobile phase A was 0.1% formic acid in water and mobile phase B was 0.1 % formic acid in methanol.

For the separation of all compounds, the mobile phase gradient was started from 1% B for 2 min, 2 % B by 4.1 min, 10% B by 5 min, 20% B by 6 min. After 1 min the column was washed up with 90% B and re-equilibrated for 2 min by 1% B. The flow rate was 0.1 ml/min.

The LC eluent flow was sprayed into the mass spectrometer interface without splitting. All ions were monitored using mass spectrometry in multiple reaction monitoring modes (MRM) in positive polarity with electrospray ionization (ESI) source. The source parameters were:

1. A gas temperature of 200 ˚C with a gas flow of 16 l/minute,
2. A sheath gas temperature of 300 ˚C with a sheath gas flow of 11 l/minute,
3. A nebulizer pressure of 50 psi and capillary voltage of 3500 °C. 4

The quantification was performed using a matrix match calibration curve. Identification was achieved based on the retention time and product ions. Table 2.4 summarises the monitored ions and the optimized MS operating parameters of the analyte.

Table 2.4: Summary of LC-MS/MS parameters

Analyte	Retention time (mins)	Precursor ion (m/z)	Production (m/z)	Collision energy	Cell accelerator energy	Polarity
Glutamine	1.04	147.16	83.9	18	4	Positive
Glutamine	1.04	147.16	56	30	4	Positive
Glutamic acid	1.22	148.14	83.4	14	44	Positive
Glutamic acid	1.22	148.14	56	30	4	Positive
Pyroglutamic acid	4.44	130.0	84	10	4	Positive
Pyroglutamic acid	4.44	130.0	56	30	4	Positive
Glutathione	3.6	308.33	84	42	4	Positive
Oxidized Glutathione	3.60	308.33	76	26	4	Positive
Glutathione	4.436	613.64	355.1	22	4	Positive
Oxidized Glutathione	4.436	613.64	231	30	4	Positive

2.10.2 Analysis of folate and methionine cycle and transsulfuration pathway metabolites in basal and high glucose

Analysis of the following metabolites: betaine, cysteine, cystine, homocysteine, homocystine, glutamic acid, glycine, serine, methionine, S-adenosyl-methionine (SAM), and S-adenosylhomocysteine (SAH) in the cell and media were quantified using the Agilent 1200 Series LC 6490 Triple Quad LC-MS mass spectrometer. Briefly, following the metabolite extraction (as described above), 20 µL of the supernatant from both cell and media samples were added to 180 µL of 60% of acetonitrile.

50 µL of this solution was added to the HPLC vials. Triplicate readings were performed per sample. A mix standard curve was produced with 1mgml^{-1} concentration for cysteine, cystine, glutamic acid, glycine, serine and methionine, all purchased from Sigma-Aldrich: betaine (catalogue: B2629), cysteine (catalogue: C-7755), cystine (catalogue: C-8755), L-homocysteine (catalogue: 69453), L-homocystine (catalogue: H6010) glutamic acid (catalogue: G1251), glycine (catalogue: G-7126), serine (catalogue: S-4500), methionine (catalogue: M9625), SAM (catalogue: A7007), SAH (catalogue: A9384). For all metabolites, a five-point standard curve was produced with a 10-fold serial dilution, in either water for cell samples or DMEM media (catalogue: 11966025 Gibco) for media samples over the range of 100 µgml^{-1} to 0.001 µgml^{-1}. Finally, 20 µL of the standards prepared in both water and media were added to 180 µL of 60% acetonitrile, 50 µL of which was added to HPLC vials. The Acquity BEH Amide (2.1×100mm,1.7µm particle size) including a Van Guard™ UPLC BEH Amide pre-column (2.1×5 mm, 1.7 µm particle size) (Waters, Milford, USA) was used to separate the amino acids. The column was maintained at a temperature of 35 °C, and 2 µL of

the sample volume was injected. Two mobile phases were used for the run: solvent A (10 mM ammonium formate in 85 % acetonitrile containing 0.15% formic acid) and solvent B (10 mM ammonium formate in Milli Q-water containing 0.15 % formic acid pH 3.0). Chromatographic separation was achieved at a flow rate of 0.4 $mLmin^{-1}$.

2.10.3 Amino acid analysis between WT and NRF2 KD HepG2

The extraction method used to extract metabolites in section 2.10.1 and 2.10.2 lacked a quencher. Therefore, the downstream analysis yielded variable results, most likely because the metabolites had already begun to degrade. Analysis of amino acids in WT and NRF2KD cells (chapter 6) therefore were extracted using a completely different method.

WT and NRF2KD HepG2 cells were seeded at a density of 3×10^5 cells/well on a 6-well plate and grown for 48 h. On the day of the assay, cells were washed once with 1XDPBS and incubated for another 3, 9, and 24 h with DMEM without glucose (Gibco, catalog: 11966025), supplemented with 1 mM sodium pyruvate (Gibco, catalog: 11360070) and 25 mM glucose (Gibco, catalog: A2494001) with DMEM without FBS, along with 10 µM SF or its control DMSO. Cells were plated in quadruplicates plus an extra plate for cell counting. Cells were counted using the Invitrogen™ Countess™ automated cell counter based on the manufacturer's instructions to give the total number of cells per well.

Following removal of media, the cells were washed once with 0.9% NaCl (4 °C). Metabolite extraction was performed by adding 500 µL of metabolite extraction buffer (MEB) per million cells, consisting of 50% methanol, 30% acetonitrile, and 20% Milli Q water, kept at -20 ^oC. Plates were incubated at 4^oC on a shaker for 5 min, followed by 24h incubation at -80 ^oC. Following incubation, cells were scraped and the insoluble material was transferred to a pre-chilled Eppendorf tube, vortexed for 15 min at 1400 rpm at 4 °C (Eppendorf ThermoMixer C), followed by centrifugation 18,000g at 4 °C for 20 min. The supernatant, 80 µL was transferred to an LC-MS vial and was dried vacuum-centrifuged at room temperature for 30 min. For the analysis, vials were resuspended with 50 µl of 60% acetonitrile.

2.11 CRISPR Cas 9 transfection

The clustered regularly interspaced short palindromic repeats (CRISPR) system is one of the main mechanisms for bacteria and archaea to protect themselves from foreign genetic material, from pathogens such as bacteriophages and plasmids (Marraffini,

2015). This process utilizes a Cas protein. On average about twenty nucleotides present at the 5'end of the guide RNA (gRNA), guide the Cas to the target sequence in the DNA through RNA-DNA complementary base pairing. The Cas-gRNA complex can then cleave the foreign DNA, (in this case, it is the NRF2 genomic sequence) as it can recognize a protospacer adjacent motif (PAM) (Jiang and Doudna, 2017).

Cell transfection in a 6-well plate was carried out using lipofectamine CRISPRMAX. A reverse transfection protocol was used for HepG2 cells. HepG2 cells were transfected the same day they were passaged. Briefly, DMEM media (Gibco, catalog: 31880230) was removed, the flask was washed twice with 1X DPBS (Gibco, catalog: 14190144) and 1.5 mL of 0.05% trypsin (Gibco, catalog: 25300054) was added per flask. Flasks were incubated at 37 ^{o}C 5% CO_2 for 5-10 min, followed by neutralization with DMEM + 10% FBS (Gibco, catalogue:10082147). The cell suspension was added to 50 mL falcon, spun at 1000g for 5 min, the media was removed and the cells were resuspended in 1X DPBS further spun at 1000g for 5 min and finally resuspended in 20 ml of Opti-MEM reduced serum (Gibco, catalog: 31985070) media without FBS nor pen/strep.

During the centrifugation step, the Cas9 ribonucleoprotein and lipofectamine CRISPRMAX reagent were prepared in separate 2 ml Eppendorf tubes. Tube 1 (the control) was prepared by adding 777 µL of Opti-MEM with 12.5 µg of GeneArt platinum Cas9 nuclease and 144 µL of Cas9 plus reagent (Invitrogen, catalog: A36499). Tube 2 was prepared by the addition of 777 µL of Opti-MEM with 12.5 µg of GeneArt platinum Cas9 nuclease, 144 µL of Cas9 plus reagent, and 2.5 µg of sgRNA (Table 2.5). The solution was incubated at room temperature for 5-10 min. In two separate 2 ml Eppendorf tubes, 9 µL of lipofectamine CRISPRMAX (Invitrogen, catalog: CMAX00003) was added to 116 µL of Opti-MEM and incubated at room temperature for 5 min. After incubation, the Cas9 RNPs were added to the lipofectamine CRISPRMAX solution and incubated for 15-20 min at room temperature (Yu *et al*., 2016). In the meantime, cells were counted and $2X10^5$ cells per ml were seeded per well. The Cas9 RNP/lipofectamine CRISPRMAX solution was added dropwise onto the suspension of the cells. At around 9 h post-transfection, the media containing the transfection reagent was removed and replaced with DMEM supplemented with 10% FBS and pen/strep. The transfected cells were incubated for 48-72 h before analysis.

Table 2.5: guide RNA sequences used to target the NRF2 gene including the positive control HPRT1

Gene	Sequence	PAM	Strand	Reference
NRF2	TCGATGTGACCGGGAATATC	AGG	+	A35510 CRISPR746137_SGM (ThermoFisher Scientific)
NRF2	GCGACGGAAAGAGTATGAGC	TGG	-	A35510 CRISPR746131_SGM (ThermoFisher Scientific)
NRF2	GGAGTAGTTGGCAGATCCAC	TGG	+	Hs.Cas9.NFE2L2.1.AE (IDT)
HPRT1	GCAUUUCUCAGUCCUAAACA		+	A35524 (Thermo Fisher Scientific)

2.11.1 Genomic cleavage assay

The GeneArt Genomic Detection Assay kit was used to assess genomic modification efficiency according to the manufacturer's instructions (ThermoFisher Scientific, catalog: A24372). Briefly, 48 h and 72 h post-transfection, the cells were washed with 1X DPBS followed by the addition of 500 µL of trypsin per well. The cells were harvested by centrifugation at 1000g for 5 min, then lysed with 50 µL of cell lysis buffer with 2 µL of proteinase K. Upon treatment with proteinase K, the samples were placed in a thermocycler set to the following conditions: 15 min for 68 ^{o}C followed by 95^{o}C for 10 min. The cell lysate (3 µL) was then used for PCR amplification with AmpliTaq Gold 360 master mix along with the addition of 1 µL of each of the forward and reverse primers (Table 2.6). The PCR program was set at 95 ^{o}C for 10 min for one cycle, then at 95 degrees for 30 s, 55 degrees for 30 s, and 72 degrees for 30 s for a total of 40 cycles. The final extension was set at 72 ^{o}C for 7 min. The resulting PCR product (3 µL) was added to 7 µL nucleotide-free water along with 2.5 µL of loading dye (New England Biolabs, catalog: B7025S) and visualized using a 2% agarose gel. The PCR product (1 µL) was mixed with 1 µL of 10X detection reaction buffer and 7 µL of water, and then subjected to denaturation and re-annealing on a thermocycler set to 95 degrees for 5 min, 95-85 ^{o}C, -2 ^{o}C/s, followed by 85-25^{o}C -0.1 degree/s. Finally, 1 µL of 10x detection enzyme (T7 Endonuclease I) was added to each sample and incubated on a thermocycler at 37 ^{o}C for 1 h. The digested product was analyzed with a 2% agarose gel. The summary of the CRISPR transfection and the GCD assay is shown in figure 2.4.

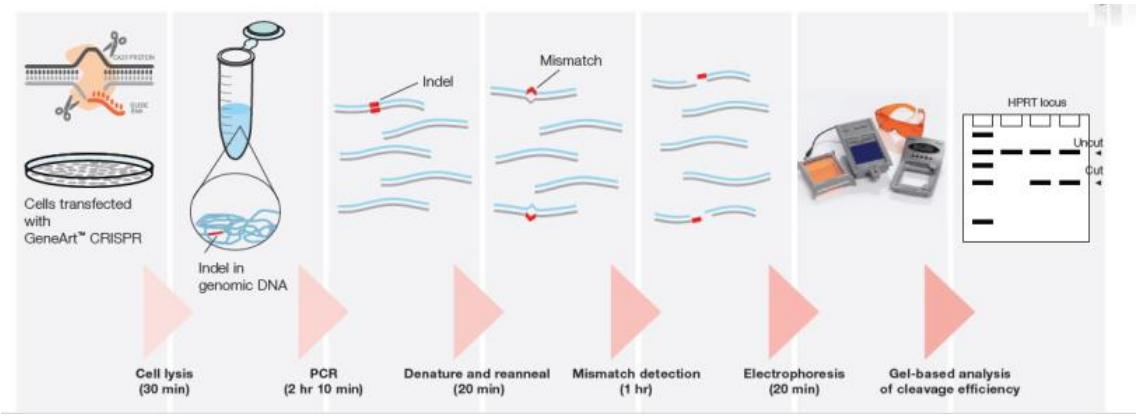

Figure 2.4 Schematic summary of how the CRISPR system is carried out *in vitro*. After the cells have been transfected with the Cas9 protein along with the gRNA, after 48-72 h, cells are lysed. DNA is amplified through PCR, and then a T7 Endonuclease I is added, which will cleave and INDEL generated by the editing. The DNA is then run on an agarose gel to identify the efficiency of the editing. Courtesy to ThermoFisher Scientific for providing the image.

Table 2.6: Primer sequences used for the PCR reaction for Genomic Cleavage Detection Assay

Gene	Forward 5' to 3'	Reverse 5' to 3'
NRF2	AGCACCCTCCAATCCTTCCT	AAGAGCCAGCTGGGCAATAA
NRF2	TGCCCTTTAGTGACCTCTACC	TGTACCTGGGAGTAGTTGGC
NRF2	GCTTGCCACACACAGTAACG	TCAGTCAGCGACGGAAAGAG
HPRT1	GAATATGTCCCAGATAGCAC	GTTCTCAGTGGCCACCTGC

2.11.2 Clone isolation

Following 72 h post-transfection, transfected cells (with the Cas9 and gRNA RNP) were washed with 1XDPBS, 500 µL of trypsin added to each well of a 6 well-plate and incubated for 10-15 min at 37 ^{o}C in 5% CO_2. Trypsin was neutralized with 1.5 ml of DMEM with 10% FBS and 100 µml^{-1} penicillin, and 100 µml^{-1} streptomycin. Cells were then centrifuged at 300g for 5 min. Following centrifugation, the cells were resuspended in DMEM with 10% FBS +pen/strep and diluted to a density of 8 cells ml^{-1} through serial dilution using the Countess™. The diluted cell suspension (100 µL) was added to the interior wells of seven 96-well plates. The plates were incubated at 37 °C in 5% CO_2. The media was changed every three days. Brightfield and phase contrast images were obtained on the AxioImager M2 fitted with a halogen light source, using 5x, 10x, and 20x EC Plan-Neofluar objectives with an AxioCam 105 cMOS colour camera and operated by Zen 2 (Blue edition) software (Carl Zeiss Ltd, Cambridge, UK). Images obtained were 2560 x 1920 with a 2.2 µm^2 pixel size and 1:1 binning. Images were analysed and altered for brightness and contrast with FIJI free image analysis software (Schindelin *et al*., 2012)

2.12 NRF2 protein quantification

Following 72h post-transfection, the supernatant from the transfected cells was removed, washed once with 1X DPBS, and then treated with 10 µM SF diluted in EMEM serum-free media. Following treatment for 16 hours, the culture supernatant was removed, washed twice with 1X DPBS (Gibco) and 200 µL of 1X cell lysis buffer (Cell Signalling Technologies, catalog: #9803S), containing a protease and phosphatase cocktail inhibitor (Cell Signalling Technologies, catalog: #5872S) and phenylmethylsulfonyl fluoride (PMSF), (Sigma-Aldrich, catalog: 93482-50ML-F) was added to each well and incubated for 5 min at 4°C. The wells were then scraped, cell debris removed, and placed into Eppendorf tubes. Tubes were vortexed briefly and kept on ice for 15 min, with vortexing every 5 min. After 15 min, 1 µL of benzonase nuclease (Sigma-Aldrich, catalog: E1014-25KU) was added to each tube. The cell extract was centrifuged at 14000g for 10 min at 4 °C. According to the manufacturer's instructions, the protein supernatant was removed and quantified using a bicinchoninic acid (BCA) assay (Sigma-Aldrich, catalog: BCA1-1KT).

Briefly, known concentrations ranging from 0-1000 $mgml^{-1}$ of bovine serum albumin (ThermoFisher Scientific, catalog: 23209) were compared to the protein samples, diluted 1:10 in Napi buffer (50 mM pH6 containing 5 mM of EDTA). After adding 200 µL BCA working reagent to 25 µL of protein samples to the 96-well plates (50:1 dilution between BCA and copper (II) sulfate solution), the samples were incubated for 30 minutes at 37°C without CO_2. The absorbance was measured at 562 nm using the Fluorostar Optima plate reader (BMG Labtech). Once quantified, the supernatant was stored at -20°C until the Western blot analysis.

2.12.1 Gel electrophoresis

Protein samples (30 µg) were heated at 70 °C for 10 min in 4x NuPAGE LDS sample buffer (Invitrogen, catalog: NP0007) and 10x NuPAGE sample reducing agent (Invitrogen, catalog: NP0009). Samples were centrifuged briefly to remove any air bubbles present before loading onto the gel. The samples (10 µL) were separated on a 15 well, 10% NuPAGE Bis-Tris gels (Invitrogen, catalog: NP0301BOX) through a diluted MOPS SDS running buffer (20X) (Invitrogen, catalog: NP000102) with the presence of an antioxidant (Catalogue: NP0005) for 55 min at 200 V at room temperature, using the XCell SureLock™ Mini-Cell (Invitrogen, catalog: EI0001).

2.12.2 Immunoblotting

Upon completion of the electrophoresis, the sponges, filter paper, and gel were soaked in diluted transfer buffer (Invitrogen, catalog: NP00061) containing 10% (v/v) methanol and antioxidant and assembled onto the XCell IITM Blot Module (Invitrogen, catalog: EI9014). The blot module was then placed in the XCell SureLockTM Mini-Cell Electrophoresis system, and the tank was filled with transfer buffer. Proteins were electrotransferred onto a polyvinylidene-difluoride (PVDF) membrane (Sigma-Aldrich, catalogue:10600016) for 3 h at 30 V.

The transfer of proteins from the gel to the membrane was determined through ponceau S staining (Sigma-Aldrich, catalog: P7170-1L). The membrane was washed several times with Mili Q water to ensure the ponceau staining was removed, cut depending on the size of protein of interest, before being blocked with 5 % bovine serum albumin (Catalogue: A2153-50G Sigma-Aldrich) in 1XDPBS (Fisher Scientific, catalog: BR0014G) containing 0.1% Tween-20 (Fisher Scientific, catalog: BP337-100) (PBS-T) for 60 min at 25 °C. Membranes were then incubated with the primary antibody, NRF2 (1:1000 CST Rabbit mAB #12721S) and β-actin (1:5000 CST Rabbit mAB #4970S) in blocking buffer for 16 h at 4 °C with gentle agitation. After incubation with primary antibody, the membranes were washed 3 times for 10 min, 5 min, and 5 min respectively with (PBS-T) and incubated with secondary antibody anti-rabbit IgG HRP-conjugated (1: 5000 CST #7074P2) in blocking buffer for 90 min at 25°C with gentle agitation (Table 2.7). Membranes were washed 3 times for 10 min, 5 min, and 5 min respectively with (PBS-T) and incubated with enhanced chemiluminescent detection reagent (BIO-RAD Laboratories Ltd, catalog: 1705061).

Table 2.7: List of primary antibodies used for Western Blotting

Protein	Reference/Species	Provider
Anti-NRF2	D1Z9C mAb Rabbit	Cell Signaling Technologies (CST
Anti-β-actin	13E5 mAb Rabbit	Cell Signaling Technologies (CST
Anti-Rabbit HRP Conjugate	7074S	Cell Signaling Technologies (CST)

2.13 Statistical analyses

I used the Graph Pad Prism 9.2 software for all the statistical analysis, unless where otherwise stated.

2.13.1 WST-1 Assay

Optical density (OD) values from the 450nm reading (corrected with data from 610nm) were used to determine the percentage of viable cells. For all treatments, the percentage viability was calculated against the untreated control cells. In experiments carried out with ranging doses of treatments, following the assumption of normality, one-way ANOVA was performed, followed by Tukey's multiple comparison tests. The results were represented as means ± SD.

2.13.2 qRT-PCR

In experiments carried out with ranging doses of treatments, if the data met the assumptions of normality, one-way ANOVA was performed, followed by Tukey's comparison tests. In the experiments carried out over a period with single-dose treatments, Student t-tests were performed for data that met assumptions of normality. Results were represented as means ± SD.

2.13.3 Oil red O assay

The obtained optical density (OD) values were corrected by subtracting the value found with isopropanol alone, and these raw data values were used for the analysis. In experiments carried out with ranging doses of treatments, following the assumption of normality, one-way ANOVA was performed, followed by Tukey's multiple comparison tests. The results were presented as means ± SD

2.13.4 RNAseq

Detailed analysis on how the RNAseq data were analyzed including how the raw reads were converted to gene counts and how the gene counts were then converted to the differentially expressed genes has been explained in chapters 4 and 6.

2.13.5 Seahorse analysis

Data files from Wave (the output of the Seahorse Analyzer) were exported to GraphPad Prism version 9.2. Each of the glucose levels was analyzed separately. Values of basal respiration and respirations following injection of oligomycin, FCCP, and rotenone were analyzed by doing a student t-test (DMSO vs SF) after the assumptions of normality were met. Results are represented as means ± SD.

2.13.6 GC-MS analysis

Deconvolution of mass spectra, peak picking, integration, retention time calibration, and mass isotopic distribution (MID) determination was performed using

MetaboliteDetector. Compounds were identified by retention time and mass spectrum with an in-house library. Settings for deconvolution and compound detection are shown in table 2.3. Intensities were normalized by the internal standard D6-Glutaric acid. MID of metabolites were then exported into an Excel spreadsheet. Values were then imported in GraphPad Prism. Following the assumption of normality, statistical analysis was performed using a two-way ANOVA through Tukey multiple comparisons. To assess how SF treatment with respect to the control DMSO affected the various mass isotopomers (M0, M1, M2) in the two glucose environments, multiple testing was carried out and corrected using Benjamini-Hochberg. The two factors included glucose concentrations (basal and high), and the treatments, DMSO and sulforaphane. Results are represented as means ± SD.

2.13.7 LC-MS analysis

Here, the data files were explored and analysed using the MassHunter Workstation software (Agilent). The peak areas of the analytes were determined and the peak area ratio (peak area of analyte/peak area of its companion internal standard) was used to determine the concentration of the analyte. Following the assumption of normality, statistical analysis was performed using a two-way ANOVA through Tukey multiple comparisons. The two factors included glucose concentrations (basal and high), and the treatments, DMSO and sulforaphane. Results are represented as means ± SD.

2.13.8 Western blots

Blot images obtained through the BioRad bioanalyzer were transported in Fiji and quantified (Schindelin *et al*., 2012). The quantified values were then transported to Excel, where the target protein was normalized to the housekeeping protein (β-actin). The results were presented as means ± SD. A Student t-test was performed to assess the effect of SF on NRF2 protein compared to the control DMSO.

CHAPTER 3: How does sulforaphane modulate hepatic metabolism?

Chapter 3 Figures

3.1 Introduction:

As stated in the general introduction (see **chapter 1)**, insulin resistance (IR) is a pathological condition, in which cells fail to respond to insulin. Over a prolonged period, IR can result in the development of a wide range of conditions such as type 2 diabetes and cardiovascular diseases, (Vazquez *et al*., 2007, Sung *et al*., 2012, McAuley and Mann, 2006).
Central to IR is the dysregulation of glucose homeostasis as well as other metabolic processes in the liver.

Due to being extensively studied and well characterized, the work conducted throughout the thesis has been carried out using a hepatocellular carcinoma cell line (HepG2) (Donato *et al*., 2015). HepG2 cell line was first derived in 1975, during "the lobectomy of a 15-year-old Argentinian Caucasian male with a well differentiated hepatocellular carcinoma". HepG2 is widely used in tissue culture, as it behaves similarly to that of normal differentiated liver tissue. For example, HepG2 secretes major plasma proteins and is responsible for cholesterol and bile acid metabolism, lipid metabolism and transport, glycogen synthesis, and insulin signalling (Donato *et al*., 2015). Confluent HepG2 monolayers have been shown to express normal levels of low-density lipoprotein (LDL) receptors and are known to internalize cholesterol-containing chylomicrons (Javitt, 1990). They are also easy to handle and have a stable phenotype (Donato *et al.*, 2015). In addition, HepG2 also display an epithelial, polarised morphology when grown in solid surface conditions and exhibit rudimentary bile cuniculi formations between adjacent cells in culture (Sormunen *et al*., 1993). Despite having similar levels of total lipoproteins and cholesterol to that of primary hepatocytes, HepG2 markers of lipoproteins do differ from those found in blood plasma under physiological conditions. For example, ApoB is the predominant apolipoprotein expressed in HepG2 instead of ApoA found in plasma (Dashti and Wolfbauer, 1987).

Another crucial metabolic process regulated by the liver is glucose metabolism and insulin signalling. It has recently been identified that compared to primary hepatocytes, hepatoma cells, including HepG2, have higher basal phosphorylation of AKT and constitutively activate RAS-MAPK signalling. The hepatoma cells also showed a reduction in the phosphorylation of GSK by insulin, suggesting insensitive to the effects of insulin along with decreased glucose production (Nakajima *et al*., 2000, Molinaro *et al*., 2020).
One of the main difficulties in studying insulin resistance and diabetes using HepG2 is the choice of substrate used to induce IR. For example, some studies stimulate HepG2

with high glucose levels, whilst others involve the addition of the fatty acid palmitate. Palmitate has become an established method to induce hepatic insulin resistance. Several studies have reported that palmitate treatment inhibits insulin signalling, and the fatty acid results in the ubiquitination and the degradation of several key insulin signalling molecules simultaneously, promoting insulin resistance (Ishii *et al*., 2015). Lee and colleagues showed that palmitate induced insulin resistance through the activation of specific kinases within the insulin signaling cascade but did not accumulate triglycerides within HepG2 (Lee *et al*., 2010). Another study showed that palmitate treatment also leads to suppression of several subunits of the respiratory chain, leading to increased oxidative stress resulting in the oxidative damage of mitochondrial DNA (García-Ruiz *et al*., 2015).

Besides the above insulin resistance can be induced by culturing HepG2 under supra-physiological concentrations of glucose. Although mitochondrial function remained intact, culturing HepG2 under high glucose results in increased lipid accumulation along with a subsequent increase in markers of non-alcoholic fatty liver. (Su *et al*., 2019). Further, Chandrasekaran and colleagues reported that exposure to HepG2 in 50 mM glucose resulted in increased ROS as well as lipid peroxidation, protein carbonyl, and 3-nitryrosin adduct formation (Chandrasekaran *et al*., 2010). The consensus seems to allude that whether high glucose or palmitate are added, both substrates lead to increased oxidative stress, and several studies have reported that oxidative stress is a potential mechanism resulting in IR (Hurrle and Hsu, 2017).

Since its discovery, SF has yielded promising results. Specifically, it has induced anti-inflammatory effects in a wide range of *in vitro* and animal models (Juge *et al*., 2007) and has recently been linked as a metabolic regulator (Hayes and Dinkova-Kostova, 2014). A notably interesting finding arising from several human studies is that the pharmacokinetics of sulforaphane indicate that it is secreted from the body within a few hours, but its effect in terms of reducing oxidative stress lasts for a long time (Gasper *et al*., 2005). This suggests that short stimulation of the NRF2 pathway is sufficient to cause long-term gene expression changes. At present, *in vitro* studies in hepatocytes showing the effect of SF in modulating metabolism are still not clear. Moreover, we do not know how intermittent activation of NRF2 through either cruciferous vegetable intake or NRF2 modulating drugs can offer long term protection from radical damage. Only one study has assessed the intermittent activation of NRF2 using astrocytes cells (Bergstrom *et al*., 2011).

To address these gaps in our knowledge, this chapter aimed to use an *in vitro* model of liver metabolic dysregulation (potentially insulin resistance) to understand how

physiological levels of SF impact hepatic metabolism. This was tested through the following objectives

1. To identify NRF2 induction following SF treatment by measuring two direct targets of NRF2: HMOX1 and NQO1 using quantitative real-time PCR.
2. To identify how SF affects lipid metabolism, assessed through Oil Red O after stimulating HepG2 with palmitate and monitoring two genes involved in lipid metabolism.
3. To determine how SF affects mitochondrial and non-mitochondrial respiration using the Seahorse BioScience Flux Analyzer after HepG2 challenged with differing concentrations of glucose to represent metabolic dysregulation.

The hypothesis driving the research presented in this chapter was that SF could attenuate lipid accumulation and improve mitochondrial function.

3.2 Results:

3.2.1 SF induces the antioxidant response and metabolic genes involved in metabolism

Physiological concentrations of SF in the liver (the concentration that would be expected to be found circulating in the body following the consumption of cruciferous vegetables such as broccoli) have been suggested to range from 2 up to 10 µM. I, therefore, used a 10 µM concentration of SF for my work. To ensure that the concentration of sulforaphane was not cytotoxic, the first experiment that was carried out was cell viability, through the cell proliferation WST-1 assay. Although WST-1 is referred to as a cell proliferation assay, it measures the activity of Complex II, succinate dehydrogenase, (an enzyme in the respiratory chain), therefore resulting in more of a metabolic assay. By progressively increasing the concentration of SF, cells become less viable decreasing Complex II activity. Most importantly, figure 3.1 shows that no significant reduction was seen in cell viability compared to the control with concentrations of 10 µM, indicating it was safe to use.

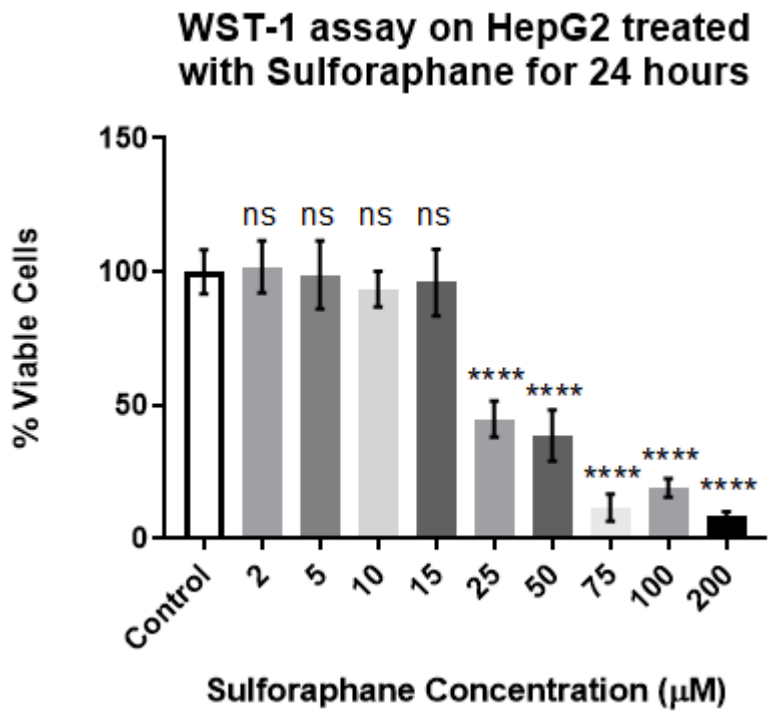

Figure 3.1. **The viability of HepG2 following treatment with SF for 24 h.** The viability of HepG2 exposed to various concentrations of SF was measured through WST1 assay using absorbance (450 nm) as a relative measure of metabolic activity. All values are expressed as mean ± SD from six independent wells, (technical replicates, although the experiment was repeated three times and this representative of other experiments). Statistical analysis was performed through a One-Way ANOVA, following a Tukey post-hoc comparing the concentrations to the control. **Control vs 25 μM SF** p<0.0001, **control vs 50 μM SF** p<0.0001, **control vs 75 μM SF** p<0.0001, **control vs 100 μM SF** p<0.0001, and **control vs 200 μM SF** p<0.0001.

To understand NRF2 activation in HepG2, the kinetics of two well established direct targets of NRF2, known to have an ARE sequence HMOX1 and NQO1 and shown to play an important role in upregulating the antioxidant response were investigated. Additionally, to assess whether SF affects genes involved in metabolism, two additional genes were also measured: CPT1a and FASN. CPT1a is involved in the beta-oxidation of long chain fatty acids, by adding carnitine to long chain fatty acids, so that they can diffuse from the cytoplasm into the mitochondrial matrix. FASN is involved in the *de novo* synthesis of saturated fatty acids. Following continuous treatment of physiological concentrations 10 μM SF RNA was extracted from HepG2 at the following time points: 2,4,6 and 24 h, representing acute and long-term exposure.

Following treatment, the antioxidant response gene HMOX1 was immediately induced. mRNA levels of HMOX1 increased by 3-fold after 2 h (95% CI, 1.162 to 2.346, p= 0.0012), reaching a 9-fold increase after 6 h (95% CI, 0.589 to 1.463 p= 0.0095) and

returning to basal levels after 24 h (**figure 3.2 a)**. NQO1 on the other hand responded slower to SF. After 6 h mRNA increased by 1.5-fold (95% CI -0.4450 to -0.2550, p=0.0005), but a large increase was observed after 24 h, almost a 3-fold increase (95% CI, -2.619 to -2.1 p< 0.0001 (**figure 3.2 b)**.

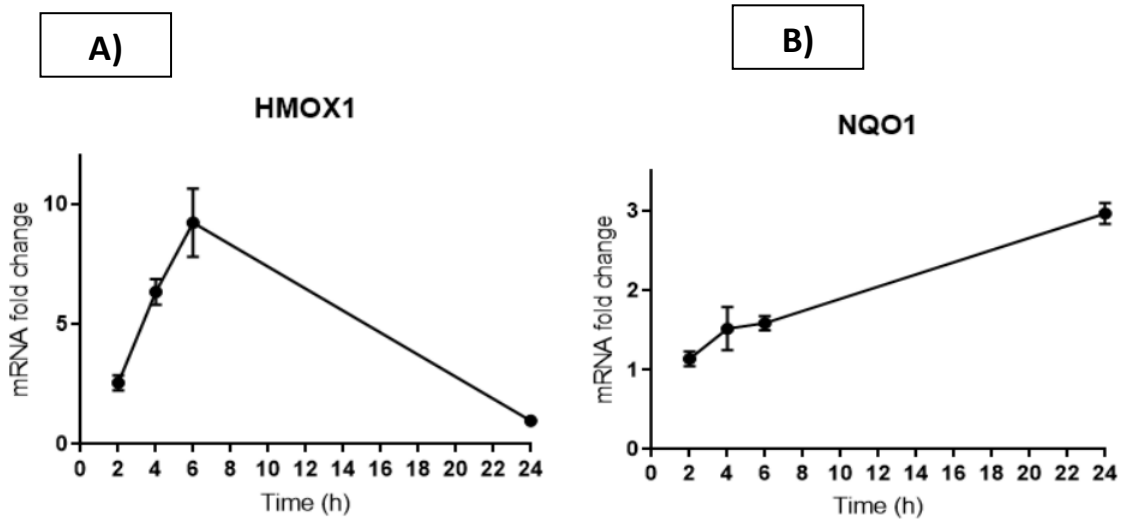

Figure 3.2. Effect of continuous 10 μM SF treatment on two NRF2 target genes in HepG2. A) HMOX1 and B) NQO1. Cells were cultured in basal glucose (5 mM) and RNA was extracted at 2, 4, 6, and 24 h time points before gene expression was assayed by qRT-PCR. Samples were normalized to the Housekeeping control beta-actin and mRNA fold change was determined by dividing each normalized treatment by the average of the normalized control. All values are expressed as mean ± SD from three biological replicates. Statistical analysis was determined by a t-test between treatment compared to its respective control, (* = $p < 0.05$, *** = $p < 0.001$, **** = $p < 0.0001$).

Interestingly, the induction of the metabolic genes following SF treatment was only observed after 24 h. The activity of FASN after 24 h of continuous 10 μM SF treatment led to a 50% decrease in activity (95% CI -0.6528 to -0.2901, p= 0.002), along with a 2.5-fold increase in CPT1a activity (95% CI 1.427 to 1.923, p< 0.0001) (**figure 3.3 a and b**).

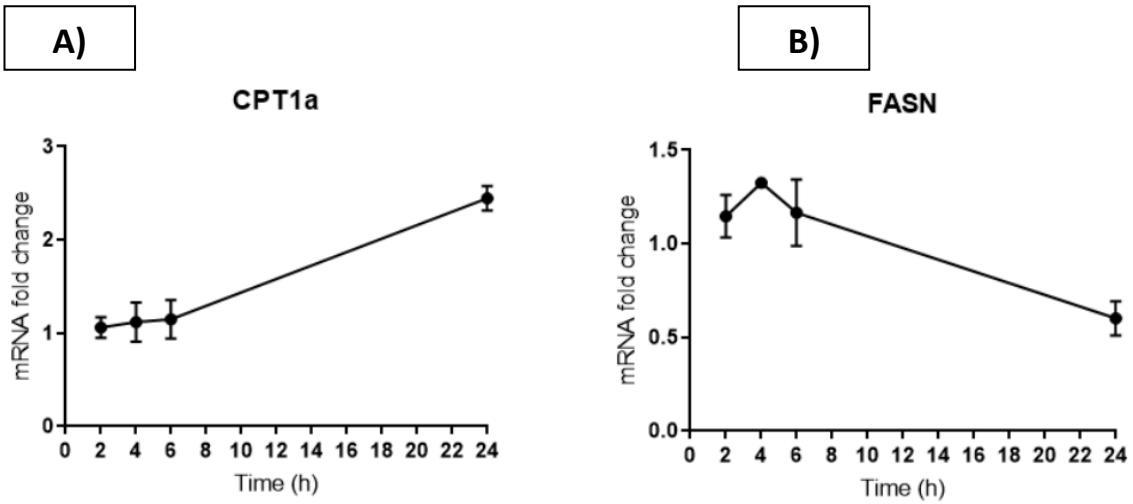

Figure 3.3.**Effect of continuous 10 µM SF treatment on two metabolic genes in HepG2.** A) CPT1a and B) FASN. Cells were cultured in basal glucose (5 mM), and RNA was extracted at 2, 4, 6, and 24 h time points before gene expression was assayed by qRT-PCR. Samples were normalized to the Housekeeping control beta-actin, and mRNA fold change was determined by dividing each normalized treatment by the average of the normalized control. All values are expressed as mean ± SD from three biological replicates. Statistical analysis was determined by a t-test between treatment compared to its respective control, (* = $p < 0.05$, *** = $p < 0.001$, **** = $p < 0.0001$).

To better understand whether a brief exposure of SF was similar to the short exposure that tissues are exposed to following consumption of a meal rich in broccoli can lead to prolonged changes in gene expression, HepG2 cells were treated with 2.5, 10, and 25 µM SF. The higher concentration of SF was used to potentially understand what effects consuming broccoli with a higher dose of glucoraphanin (such as that found in Beneforte) could have on human health (Traka *et al*., 2013). Firstly, a second cell viability was carried out to make sure that the 25 µM SF was not cytotoxic. The results revealed that up to 100 µM SF for 2 h did not affect the viability of HepG2, (**figure 3.4**).

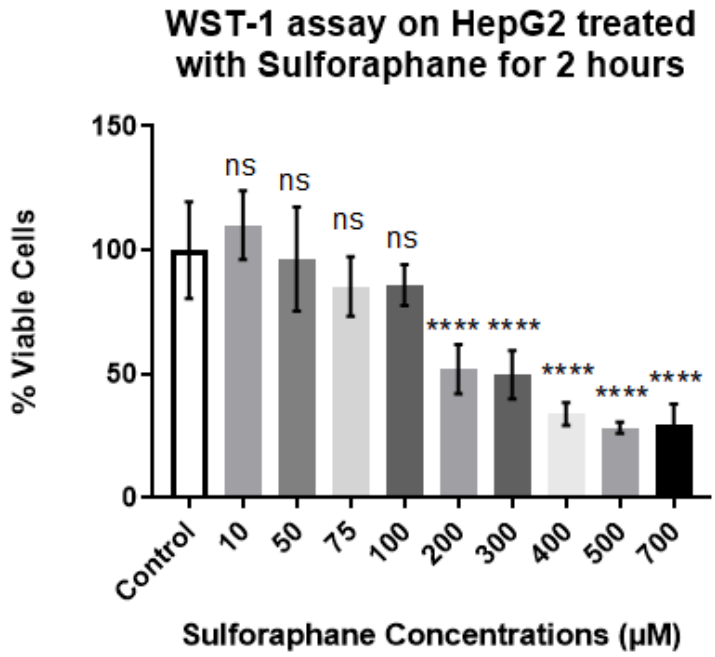

Figure 3.4. The viability of HepG2 following treatment with SF for 2 h. The viability of HepG2 exposed to various concentrations of SF was measured through WST1 assay using absorbance (450 nm) as a relative measure of metabolic activity. All values are expressed as mean ± SD from six independent wells (technical replicates, although the experiment was repeated three times and this representative of other experiments). Statistical analysis was performed through a One-Way ANOVA, following a Tukey post-hoc comparing the concentrations to the control. **Control vs 200 µM SF** p<0.0001, **control vs 300 µM SF** p<0.0001, **control vs 400 µM SF** p<0.0001, **control vs 500 µM SF** p<0.0001, and **control vs 700 µM SF** p<0.0001.

The results obtained from the brief SF exposure experiment (**figures 3.5 and 3.6**) resemble those shown in figures 3.2 and 3.3. After 2 h of sulforaphane treatment, mRNA levels of HMOX1 rose, to just under 2-fold for 2.5 µM (95% CI -1.097 to -0.3120, p=0.0022), 2-fold for 10 µM (95% CI -1.500 to -0.7152, p=0.001), and 2.8-fold for 25 µM concentrations (95% CI -2.224 to -1.439, p<0.0001). mRNA levels of HMOX1 following exposure of the small dose of SF remained active only 2 h post SF washout (95% CI -1.271 to -0.2776, p=0.006) (**figure 3.5 a)**.

For the 10 µM SF dose, mRNA levels of HMOX1 peaked at 4 h post treatment resulting in a 3.5-fold increase (95% CI -2.898 to -1.134, p=0.0005). The higher dose, on the other hand, HMOX1 mRNA peaked at 6 h post treatment, resulting in a 6-fold increase in HMOX1 mRNA (95% CI -6.934 to -5.171p <0.0001). Despite the higher SF dose, after 24 h, the results showed HMOX1 mRNA levels returned to baseline (**figure 3.5 a**).

NQO1 gene expression also followed a similar trend as HMOX1, with the greatest effect being seen at 25 µM dose. The addition of 2.5 µM SF after 2 h resulted in a slight increase in NQO1 (95% -0.4654 to -0.001912, p=0.048) and remained high 2 h after

the removal of SF from the media (95% -0.8626 to -0.09510, p=0.017) (**figure 3.5 b)**. The 10 µM dose only began to induce the mRNA of NQO1 after 4 h, resulting in a 2-fold increase (95% CI -1.156 to -0.3884, p=0.0011), whereas the high dose of SF resulted immediately in a 1.5-fold increase in the mRNA of NQO1(95% CI -0.7061 to -0.2427, p=0.001) (**figure 3.5 b**). mRNA of NQO1 appeared to continue to accumulate even at 24h, and the biggest effect was seen with 25 µM resulting in nearly a 3-fold increase (95% CI -2.540 to -1.407, p <0.0001), while 10 µM resulted in a 1.8-fold increase (95% CI -1.591 to -0.3242, p=0.0077) (**figure 3.5 b**).

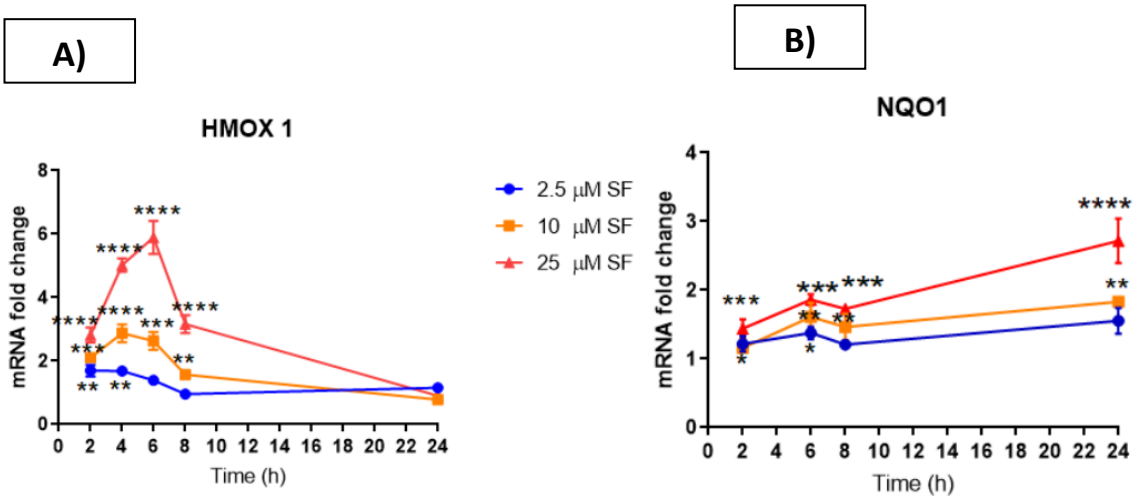

Figure 3.5 Effect of 10 µM SF treatment on two NRF2 target genes in HepG2 following short SF exposure. A) HMOX1 and B) NQO1. Cells were cultured in basal glucose (5 mM) and treated with 2.5,10 and 25 µM SF for 2 h only. RNA was extracted at 2, 4, 6, 8, and 24 h time points before gene expression was assayed by qRT-PCR. Samples were normalized to the Housekeeping control beta-actin and mRNA fold change was determined by dividing each normalized treatment by the average of the normalized control. All values are expressed as mean ± SD from three biological replicates. Statistical analysis was determined by a One Way ANOVA between control and treatments followed by Tukey post hoc (* = $p < 0.05$, *** = $p < 0.001$, **** = $p < 0.0001$).

Levels of CPT1a and FASN were also assessed. Interestingly, 2.5 µM did not affect the mRNA of CPT1A. SF treatment 25 µM after 2 h instantly led to a slight increase resulting in a 1.3-fold change in the mRNA of CPT1a (95% CI -0.4847 to -0.04481, p=0.02) (**figure 3.6 a**). At this dose, mRNA continued to increase up to 10h, followed by a slight decrease, but still resulted in a 2-fold increase after 24 h (95% CI -1.399 to -0.7054, p<0.0001) (**figure 3.6 a**). In contrast, 10 µM dose only began having an effect after 6h post SF treatment, resulting in a 1.5-fold increase (95% CI -0.9583 to -0.2952, p=0.0016) and after 24h, the levels returned almost to baseline (95% CI -0.7321 to -0.03879, p=0.03), (**figure 3.6 a**). For FASN, progressive doses of SF did lead to a

decrease in mRNA but failed to reach statistical significance (**figure 3.6 b**). Significant downregulation of the mRNA of FASN was observed at a much higher SF dose of 50 and 75 µM. However, these results were not included as high levels of SF in the human plasma are unlikely.

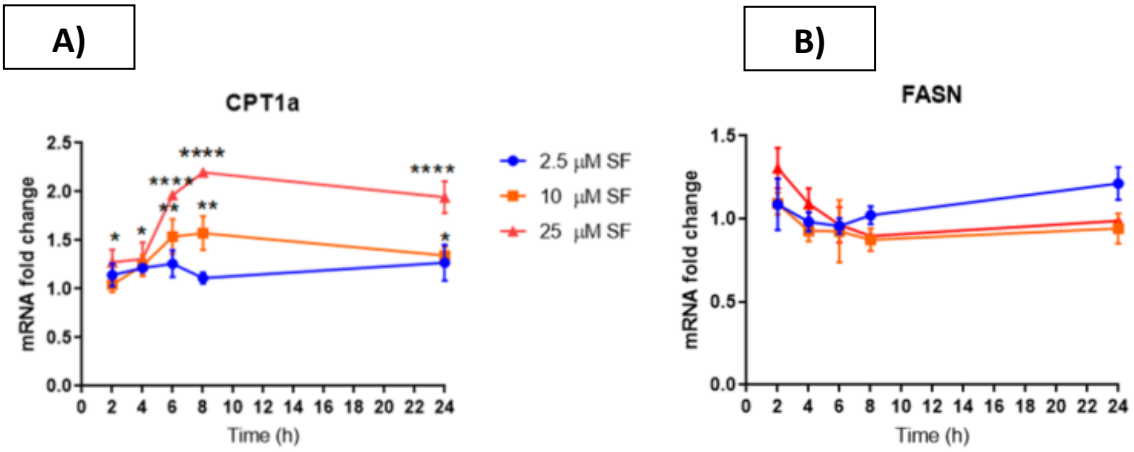

Figure 3.6. **Effect of 10 µM SF treatment on two metabolic genes in HepG2 following short SF exposure**. A) CPT1a and B) FASN. Cells were cultured in basal glucose (5 mM) and treated with 2.5,10 and 25 µM SF for 2 h only. RNA was extracted at 2, 4, 6, 8, and 24 h time points before gene expression were assayed by qRT-PCR. Samples were normalized to the Housekeeping control beta-actin, and mRNA fold change was determined by dividing each normalized treatment by the average of the normalized control. All values are expressed as mean ± SD from three biological replicates. Statistical analysis was determined by a One Way ANOVA between control and treatments followed by Tukey post hoc (* = $p < 0.05$, *** = $p < 0.001$, **** = $p < 0.0001$).

3.2.2 SF attenuates lipid accumulation in an *in vitro* model of NAFLD

In light of these *in vitro* findings, suggesting that physiological concentration of SF appeared to have a substantial effect in modulating genes involved in fatty acid metabolism, the next question that I asked was whether SF could mitigate the consequences following the consumption of a high fat meal. This was established by treating HepG2 cells with the saturated fatty acid palmitate (PA). PA was used since it is the most abundant saturated fatty acid (Carta *et al*., 2017). Exposure of PA to HepG2, therefore challenging hepatocytes with lipids, has been shown to represent an *in vitro* model of NAFLD.

Lipid accumulation was assessed through an Oil Red O Assay. Oil Red O is a fat-soluble dye that can bind onto lipids so that the absorbance can thus be quantified. Due to the presence of lipids in the serum (FBS), HepG2 cells were starved for 24 h. Following starvation, cells were treated with 0.2 mM PA for 24 h. PA treatment led to a significant increase in lipid accumulation (**figure 3.7**).

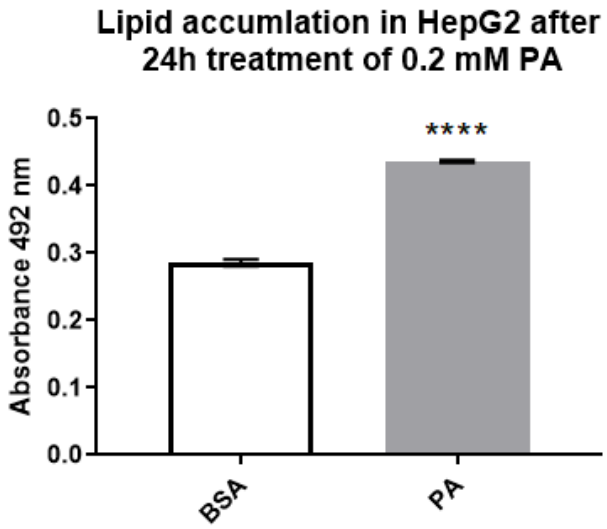

Figure 3.7. **Lipid accumulation determined by Oil Red O Assay.** HepG2 were cultured in EMEM, basal glucose media with 0.2 mM palmitate for 24 h. Following 24 h, lipid accumulation was measured at an absorbance of 492 nM. All values are expressed as mean ± SD from three biological replicates. Statistical analysis was performed through a t-test comparing the treatment to the control, BSA vs PA, $p<0.0001$.

The Seahorse Analyser was then used to assess how lipid accumulation could affect mitochondrial bioenergetics by measuring the Oxygen Consumption rate through the Mito Stress Test. Treatment of PA showed that increased accumulation of lipids on HepG2 suppressed mitochondrial activity, forcing the cells to become more glycolytic (**figure 3.8**).

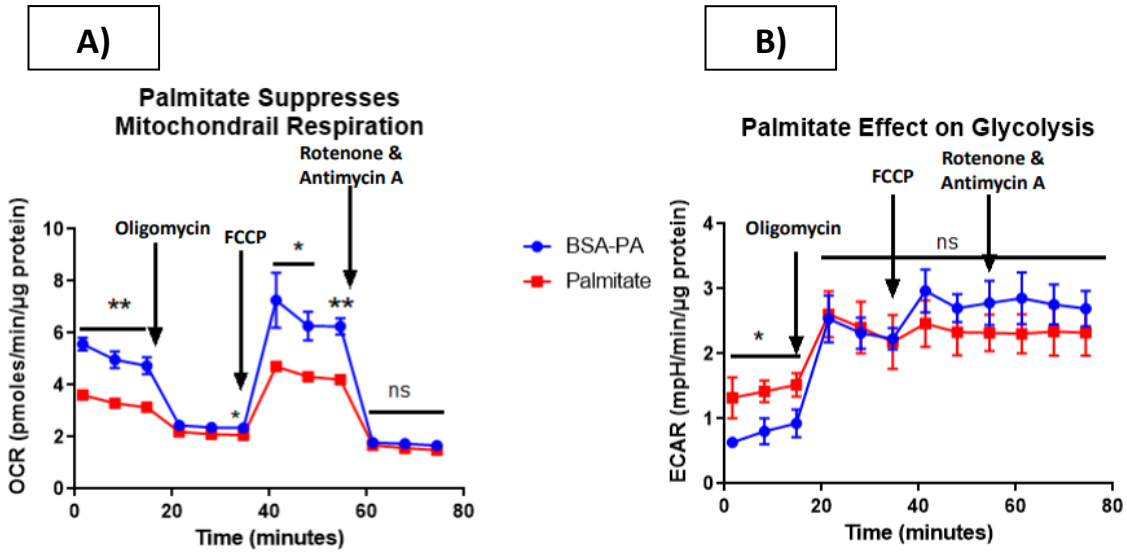

Figure 3.8. **Assessing HepG2 energy production in the presence of Palmitate**. HepG2 were cultured in EMEM basal glucose media with 0.2 mM Palmitate for 24 h. A) Mitochondrial and B) non-mitochondrial respiration was measured in the form of oxygen consumption rate (OCR) and extracellular acidification rate (ECAR), respectively. Experimental wells are shown in red, and controls are depicted in blue. All values are expressed as mean ± SEM from three biological replicates.

It was then determined whether SF could mitigate the effects induced by palmitate. Co-treatment of 10µM SF and PA for 24 h had no effect in reducing lipid accumulation, on the contrary, resulting instead an even further slight increase in the intracellular concentration of lipids **(figure 3.9 a and figure 3.10 d)**. Interestingly, however, in a separate experiment, where HepG2 cells were pre-treated with 10 µM SF for 24 h, followed by PA treatment for 24h, the barplot of the SF treatment and palmitate group resembled that of SF treatment samples only, thereby showing that SF was able attenuated lipid accumulation shown in (**figure 3.9 b**).

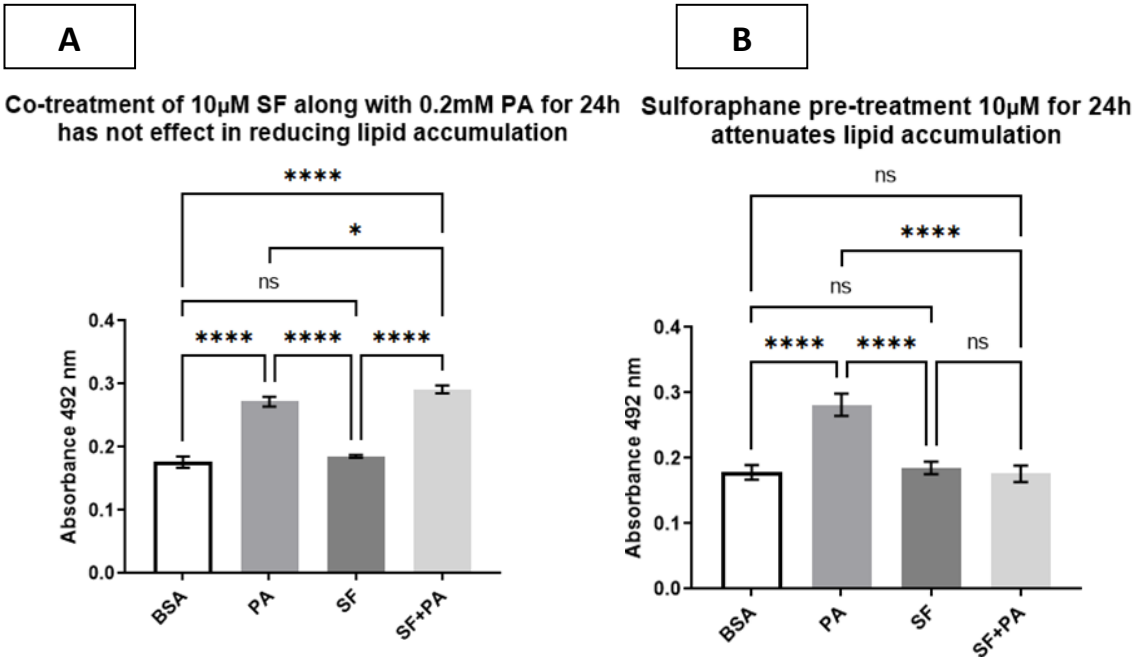

Figure 3.9. **Sulforaphane pre-treatment but not co-treatment suppress lipid accumulation following palmitate treatment determined through Oil Red O Assay.** A) HepG2 were cultured in EMEM, basal glucose media with 0.2 mM palmitate, 10 µM SF only or 10 µM SF and 0.2 mM PA combined for 24 h. B) HepG2 were cultured in EMEM, basal glucose media with 0.2 mM palmitate, 10 µM SF only, or cells were pre-treated with 10 µM SF for 24h. After 24h, SF was removed, and then 0.2 mM PA was added for a subsequent 24h. Lipid accumulation was measured at an absorbance of 492 nM. All values are expressed as mean ± SD from three biological replicates. Statistical analysis was performed through a One way ANOVA followed by Tukey post. A) **BSA vs PA** $p<0.0001$, **PA vs SF** $p<0.0001$, and **PA vs SF+PA** $p=0.035$. B) **PA vs SF+PA** $p<0.0001$.

A)

Control BSA-DMSO

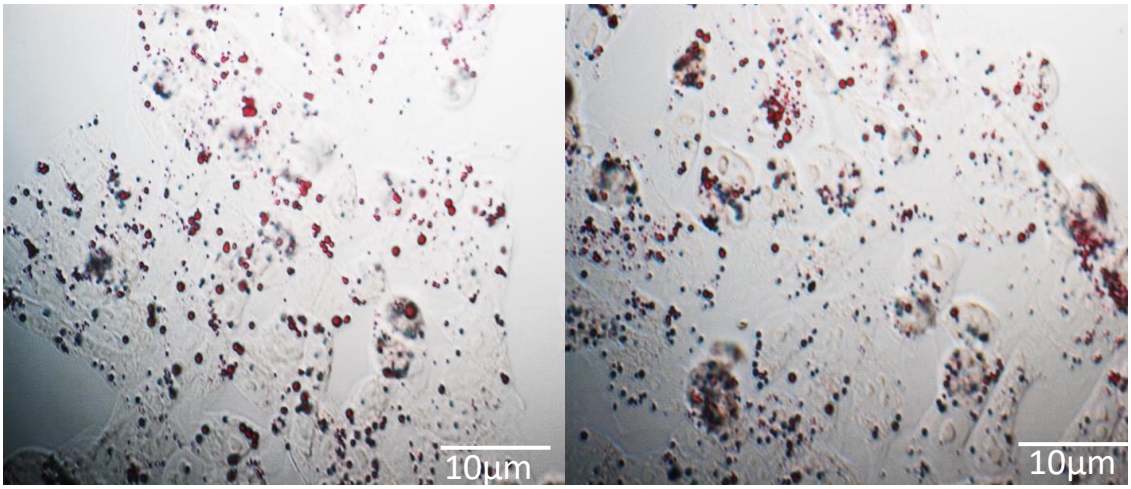

B)

0.2 mM PA

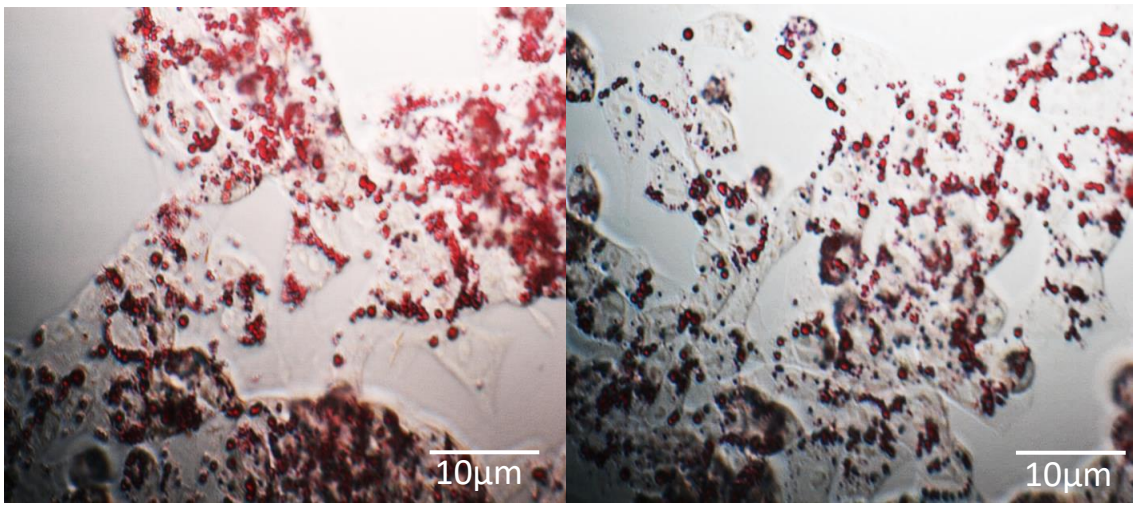

C)

10 µM SF

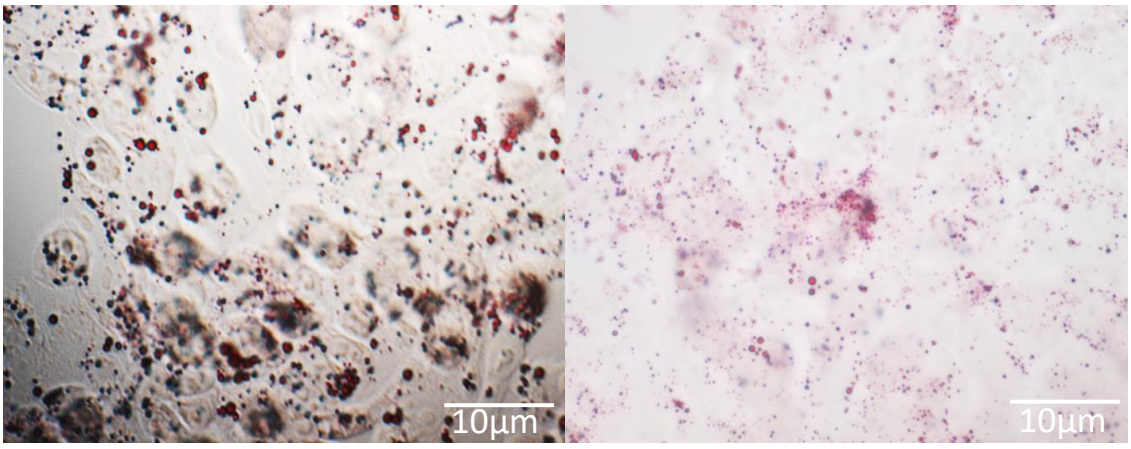

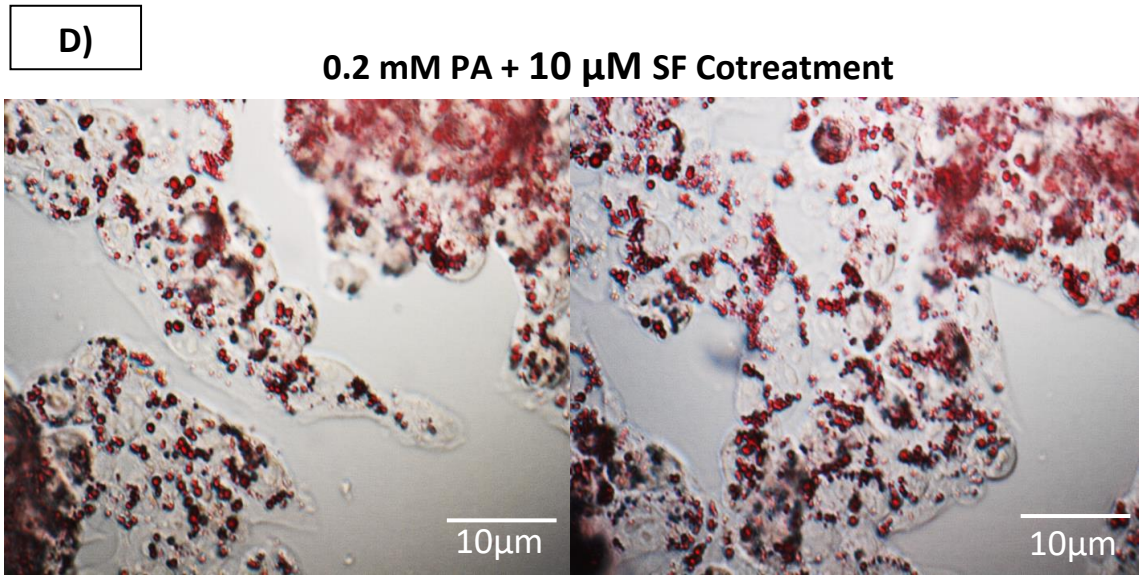

Figure 3.10. **Effect of lipid accumulation determined through microscopy.** A) HepG2 were cultured in EMEM, basal glucose media BSA-PA, the control. B) HepG2 were cultured with 0.2 mM Palmitate. C) HepG2 were cultured with 10 µM SF only. D) HepG2 were cultured with 10 µM SF and 0.2 mM PA combined for 24 h. Scale bar 10 µm.

3.2.3 SF redirects metabolism under different glucose environments

Having assessed how palmitate treatment to HepG2 can lead to mitochondria impairment, the subsequent analysis involved assessing how HepG2 challenged with various glucose concentrations would impact mitochondrial function. In this assay, HepG2, after being cultured in normal basal glucose media on the day of the treatment, media was switched composing of: no glucose, to mimic a state of starvation (no glucose); basal, to represent a healthy liver (basal glucose); or, excessive amounts of glucose (high glucose) to represent a state of hyperglycemia, and therefore mimic a state of metabolic syndrome and pre-diabetes. All of the assays were conducted without the presence of serum. The results are shown in figure 3.11.

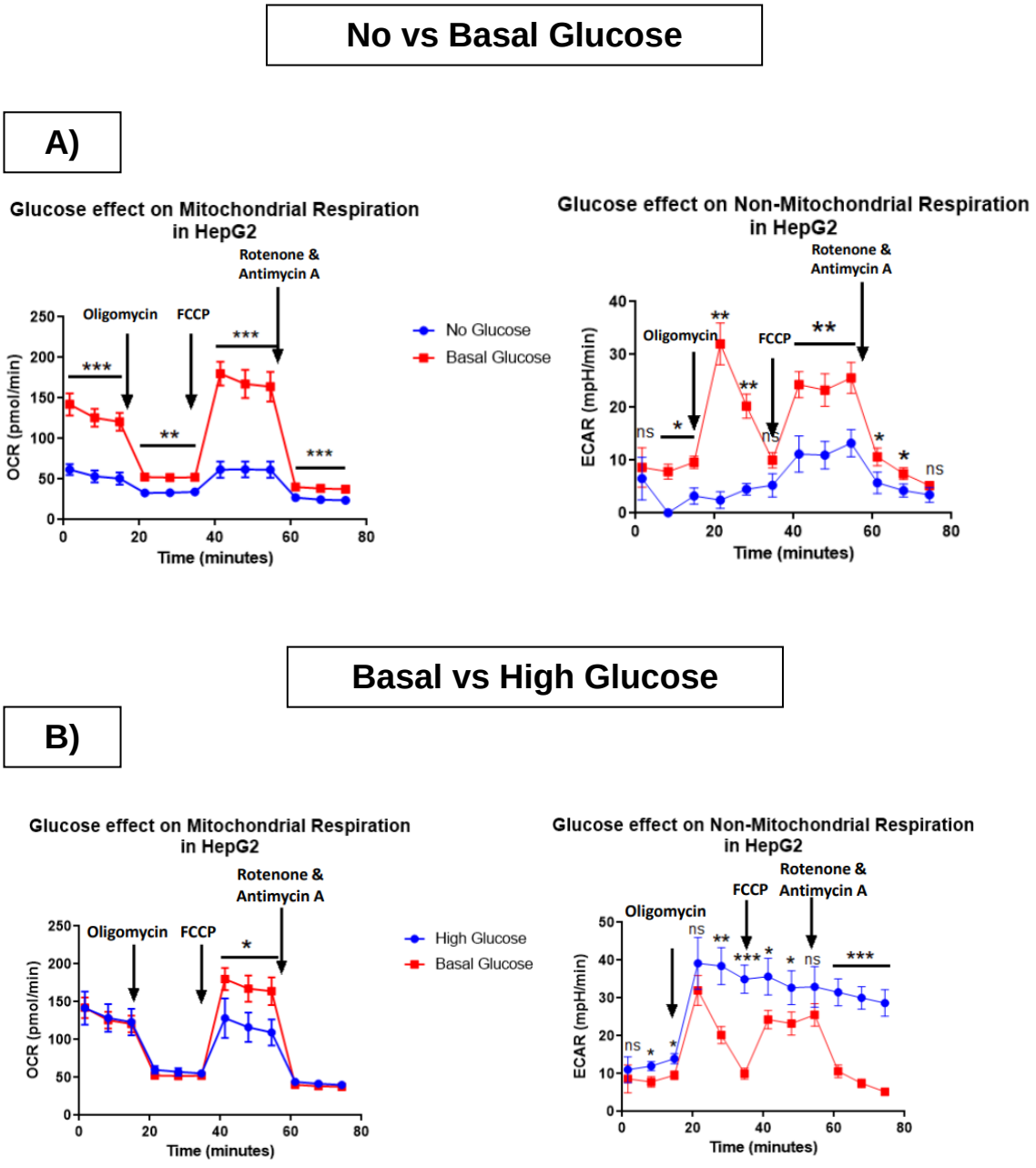

Figure 3.11. **Cell energy phenotype analysis comparing HepG2 cultured in basal glucose vs either a no-glucose or high-glucose environment.** Cells were treated with either (**A**) no glucose (blue 0 mM) vs basal-glucose (red 5.5 mM) or (**B**) basal glucose (red 5.5 mM) vs high-glucose (blue 25 mM) for 24 h. Mitochondrial and non-mitochondrial respiration were measured in the form of oxygen consumption rate (OCR) and extracellular acidification rate (ECAR). Experimental wells are shown in red, and controls are depicted in blue. All values are expressed as mean ± SEM from three biological replicates. For this assay, samples were not normalized to protein.

Cell energy phenotyping using the Seahorse XFp Mito stress assay, **figure 3.11a** revealed that under glucose starvation, compared to basal glucose, the lack of glucose results in suppression of both the oxygen consumption rate (OCR) and extracellular

acidification rate (ECAR), an indirect measurement of glycolysis, potentially implying the inability of cancer cells to produce energy under glucose deprivation. In contrast, when mitochondrial and non-mitochondrial metabolism was assessed in HepG2 cultured with basal compared to high glucose levels, whilst excessive glucose concentrations result in a decrease in OCR, an increase in ECAR was observed (**figure 3.11b**). The results suggest that under excess glucose, HepG2, due to its cancer phenotype, rewire their metabolism to produce energy mainly through glycolysis (the Warburg effect).

Next, the effect of physiological concentrations of SF on mitochondria activity in these two glucose environments was assessed. When HepG2 was exposed to SF for 24 h in basal glucose environments, SF compared to the DMSO control did not affect the mitochondrial activity of the cells (**figure 3.12a**). In contrast, in the presence of a high glucose environment, SF treatment after 24 h compared to the DMSO control resulted in an overall reduction in both mitochondria and non-mitochondrial (glycolysis) metabolism (**figure 3.12b**).

Basal Glucose (5.5 mM)

A)

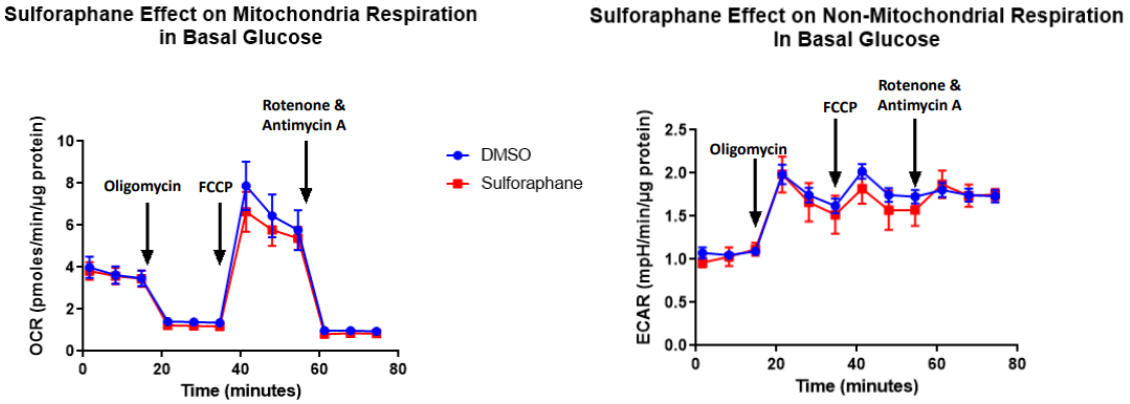

B) High Glucose (25 mM)

B)

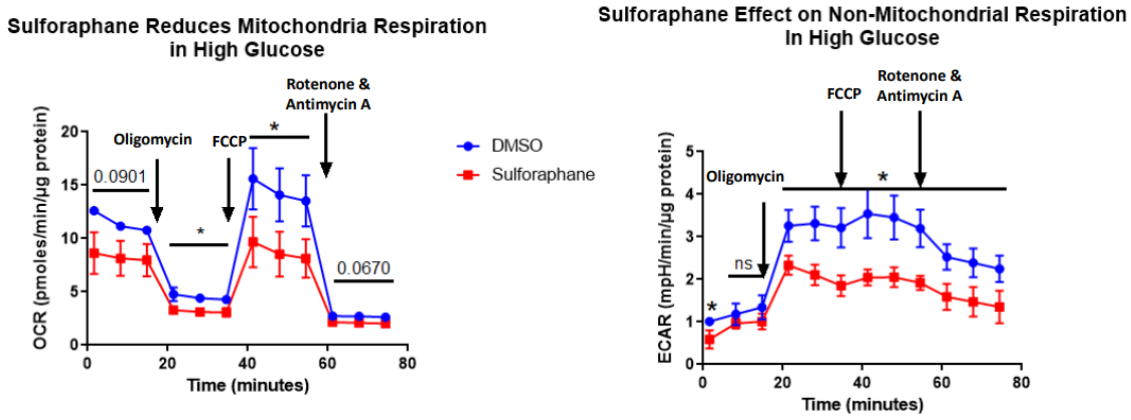

Figure 3.12. **Cell energy phenotype of HepG2 cells following Sulforaphane treatment for 24 h under basal and high glucose conditions**. HepG2 was cultured in A) DMEM basal glucose 5.5 mM media with 10 µM SF for 24 h or B) DMEM High Glucose media 25 mM with 10 µM SF for 24 h. Mitochondrial and non-mitochondrial respiration were measured using oxygen consumption rate (OCR) and extracellular acidification rate (ECAR), respectively. Experimental wells are shown in red, and controls are depicted in blue. All values are expressed as mean ± SEM from three biological replicates.

To assess whether the overall reduction in mitochondrial activity occurs immediately following SF exposure or only after following a long incubation period, the experiment was repeated using a 2 h and 4 h treatment (**figure 3.13 a and b**). Both experiments showed that early point, SF also reduces both mitochondrial and non-mitochondrial respiration compared to the DMSO control.

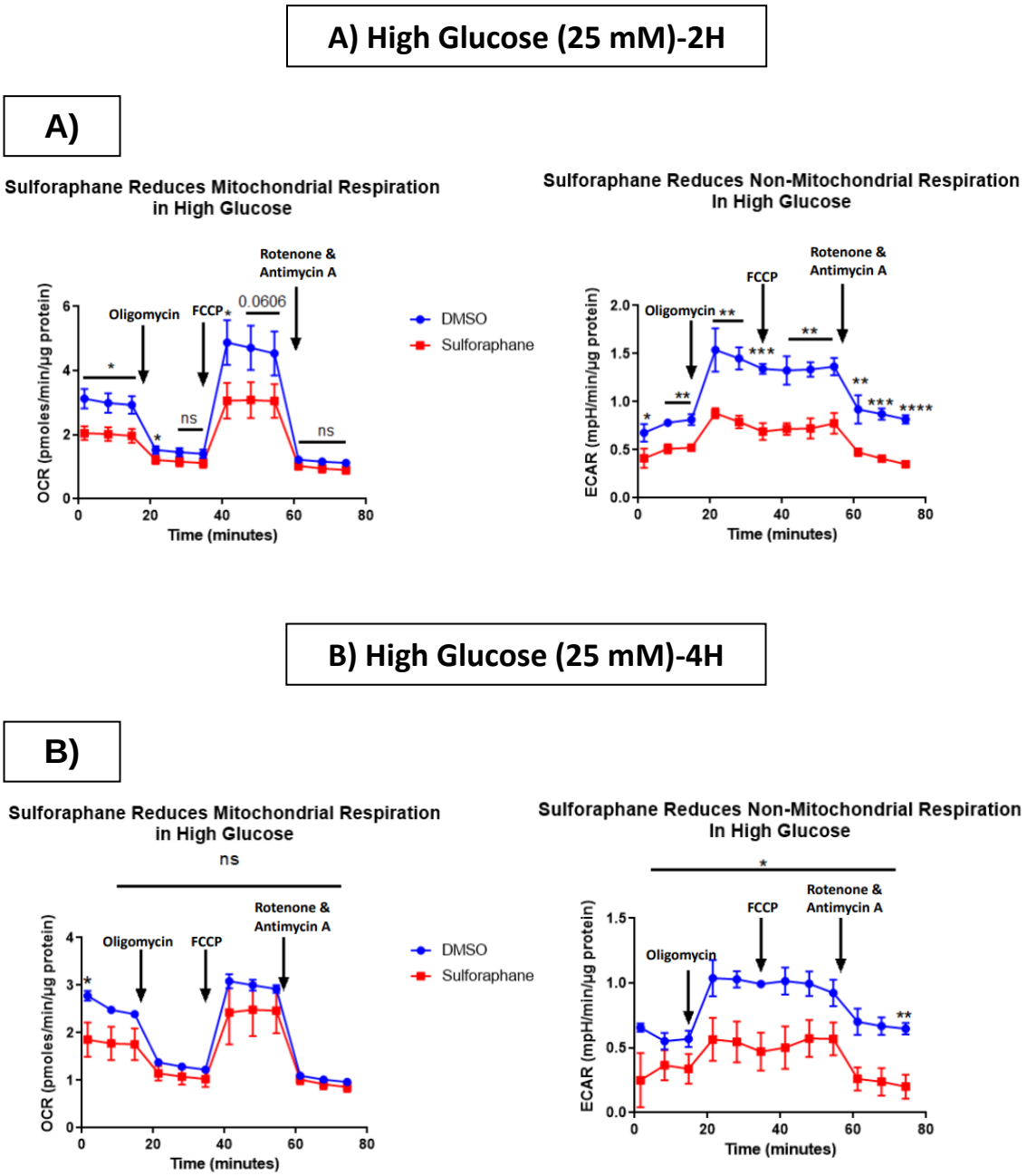

Figure 3.13. **Cell energy phenotype of HepG2 cells following Sulforaphane treatment for 2 and 4 h under basal and high glucose conditions**. HepG2 were cultured in A) DMEM high glucose 25 mM media with 10 µM SF for 2 h or B) DMEM high glucose media 25 mM with 10 µM SF for 4 h. Mitochondrial and non-mitochondrial respiration were measured using oxygen consumption rate (OCR) and extracellular acidification rate (ECAR), respectively. Experimental

wells are shown in red, and controls are depicted in blue. All values are expressed as mean ± SEM from three biological replicates.

As previous studies have shown that constituent NRF2 activation results in glucose and glutamine being redirected towards the PPP, for anabolic programming (Mitsuishi et al., 2012), I hypothesized that the reduction in OCR (**figure 3.12 b**) observed by SF is due to the glucose being redirected towards the PPP. The expression of three key genes in the PPP through qRT-PCR was assessed to test the hypothesis. RNA was extracted from HepG2 cultured in 25 mM glucose following 24 h of continuous SF treatment. SF significantly upregulated G6PD, PGD, and TKT, shown in figure 3.14. These three genes were chosen as they have all been shown to have an ARE sequence and therefore are known to be direct targets of NRF2.

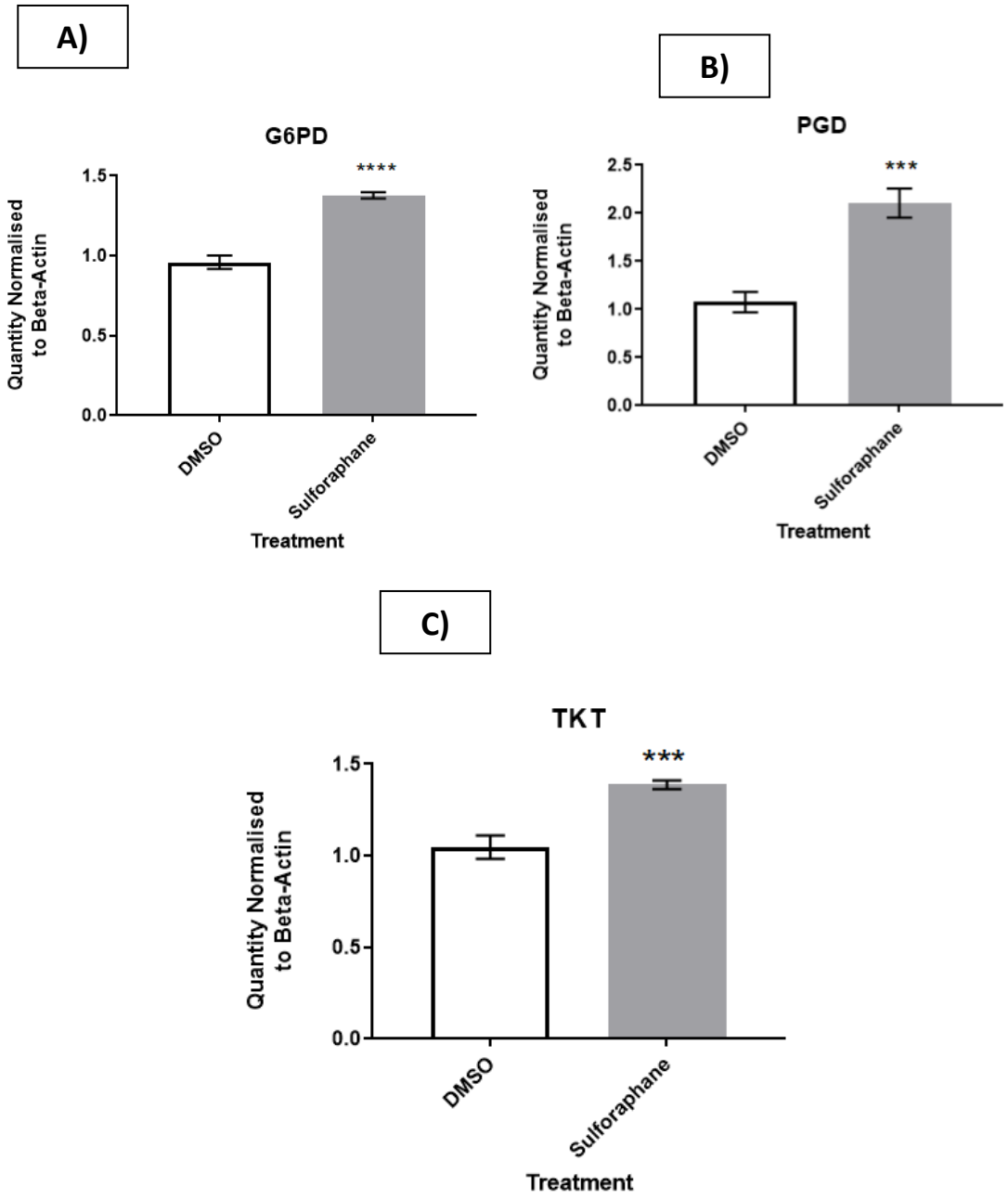

Figure 3.14. **Assessing three genes involved in the Pentose Phosphate Pathway in HepG2 treated continuously with 10 µM SF under high glucose.** HepG2 were cultured in high glucose (25 mM) from three biological replicates, and RNA was extracted at a 24 h time point before gene expression was assayed by qRT-PCR. Samples were normalized to the Housekeeping control beta-actin. All values are expressed as mean ± SD from three independent wells. A t-test between control and treatment determined statistical analysis. A) **G6PD**: (95% CI 0.3437 to 0.493, P<0.0001), B) **PGD**: (95% CI 0.7315 to 1.327, P=0.0007), and C) **TKT**: (95% CI 0.2323 to 0.4495, P< 0.0010).

Given that HepG2 is a carcinoma cell line, despite having a functional mitochondrion, cancer cells tend to rewire their metabolism and produce a large proportion of energy through glycolysis, a phenomenon known as the Warburg effect. It was, therefore, asked what would happen when HepG2 was challenged with either the presence of no glucose or galactose, a monosaccharide that is, however, not metabolized through glycolysis. In a no glucose environment, the two major metabolites used by the cells as an energy sources are pyruvate and the amino acid glutamine. Pyruvate enters the TCA cycle immediately; glutamine, on the other hand, can instead enter the TCA cycle through a two-step process known as glutaminolysis. Firstly, glutamine is lysed to form glutamate by glutaminase. Glutamate is then converted to α-ketoglutarate by glutamate dehydrogenase. Continuous physiological treatments of SF for 24 h in a no glucose environment resulted in a reduction in maximal respiration along with a reduction in non-mitochondrial respiration (**figure 3.15 a and b**).

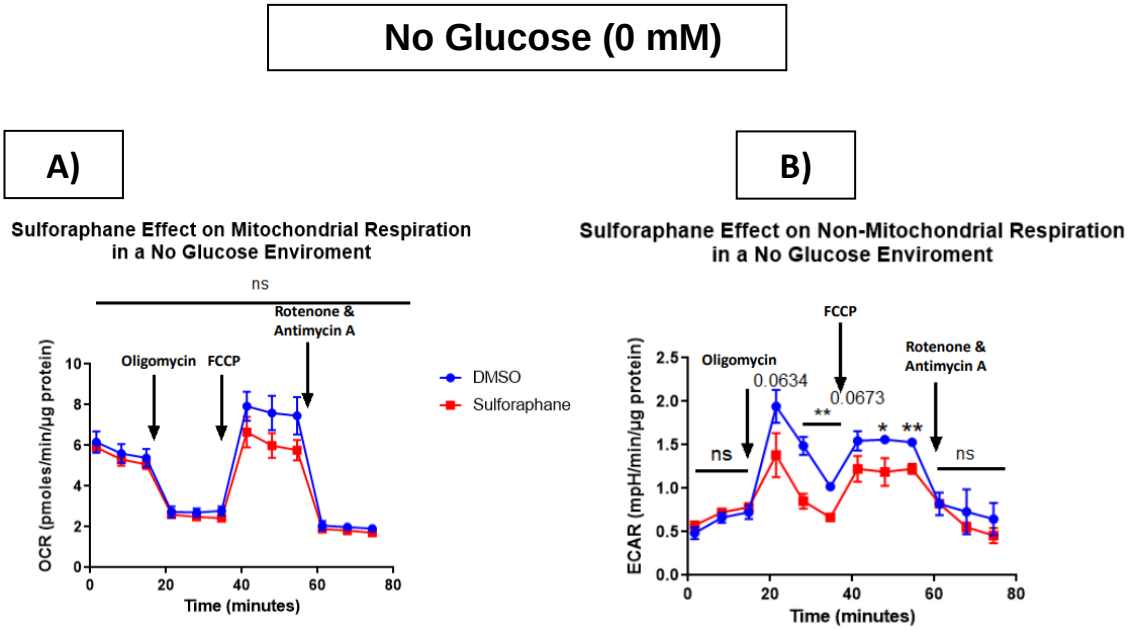

Figure 3.15. Cell energy phenotype of HepG2 cells following Sulforaphane treatment for 24h under no glucose environment. HepG2 were cultured in DMEM no glucose media, 4 mM glutamine with 10 µM SF for 24 h. Mitochondrial and non-mitochondrial respiration were measured in the form of A) oxygen consumption rate (OCR) and B) extracellular acidification rate (ECAR), respectively. Experimental wells are shown in red, and controls are depicted in blue. All values are expressed as mean ± SEM from three biological replicates.

Galactose was chosen as a substrate since the oxidation of galactose to pyruvate through glycolysis produces no ATP (Marroquin *et al*., 2007). When glucose in the media is replaced with galactose and glutamine, cells oxidise pyruvate via oxidative phosphorylation to survive. Figure 3.16 shows, as expected, that in the presence of galactose (rather than glucose), SF does not affect glycolysis. However, in the

presence of galactose, SF reduces maximal mitochondrial respiration (**figure 3.16 a**). The results may imply that this reduction may be due to either SF affecting TCA genes or affecting other entry points in the TCA cycle.

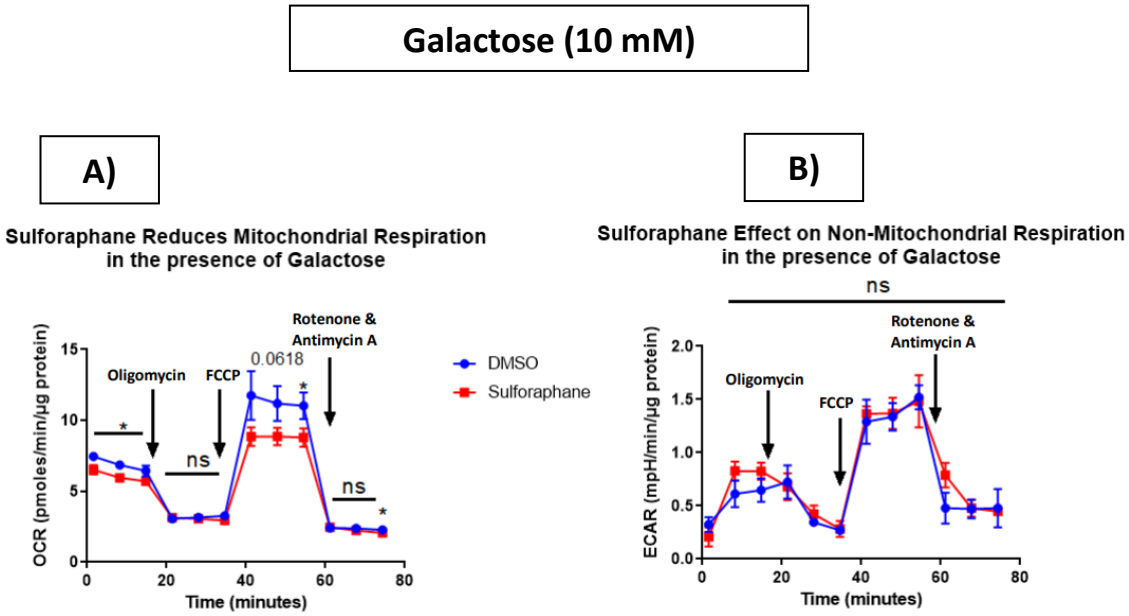

Figure 3.16. Cell energy phenotype of HepG2 cells following Sulforaphane treatment for 24 h under 10 mM Galactose. HepG2 were cultured in DMEM No glucose media, supplemented with 10 mM Galactose and 4 mM Glutamine with 10 µM SF for 24 h. Mitochondrial and non-mitochondrial respiration were measured in the form of A) oxygen consumption rate (OCR) and B) extracellular acidification rate (ECAR), respectively. Experimental wells are shown in red, and controls are depicted in blue All values are expressed as mean ± SEM from three biological replicates.

3.4 Discussion:

One of the main aims of this chapter was to establish a cell culture model of liver dysregulation to assess how SF impacts hepatic metabolism. This was achieved by exposing HepG2 cells to a wide range of substrates in the presence of sulforaphane. To date, only a few *in vitro* studies have shown how physiological concentrations of SF may modulate hepatic metabolism. This chapter is the first that looked at the effect of SF on metabolic regulation using a combination of transcriptional, analytical, and live mitochondrial phenotyping methods, along with providing insights on the timing and duration of treatments and the interaction with fatty acids and glucose metabolism.

3.4.1 SF effects on the antioxidant response and metabolic genes:

The gene expression time course kinetics identified that SF induced the expression of both the antioxidant response genes HMOX1 and NQO1 and two metabolic genes, CPT1a and FASN. For HMOX1, an immediate induction was observed; however, this began to drop after 6 h, returning to basal at 24 h. NQO1, on the other hand, only began to be induced at 4 h and reached 2.5-fold after 24 h SF treatment. The transient SF treatment showed similar findings. My results agree with that reported by (Bergstrom *et al*., 2011). In his study, Bergstrom exposed 15 µM SF to astrocytes and monitored both the mRNA and protein levels of two key NRF2 target genes: HMOX1 and NQO1. Firstly, the group showed that continuous treatment of 15 µM SF at early time points resulted in a large increase in the mRNA of HMOX1 and following 24 h returned to baseline. NQO1, on the other hand, at early time points was not induced, but a large increase was observed after 24 h. Similarly, the same trend was observed when astrocytes were transiently exposed to SF. The protein levels of these two genes also followed a similar pattern, despite the effect not being so profound. Another critical finding carried out in his work was when astrocytes were repeatedly stimulated daily with SF for a short time; although SF did not affect HMOX1, it did result in a persistent accumulation of both mRNA and protein levels of NQO1. The outcome was continuous cell protection against oxidative damage (Bergstrom *et al*., 2011). Nevertheless, it can be argued that 15 µM SF may not represent physiological concentrations of SF for astrocytes and instead may be quite a high dose, thereby not representing a realistic model.

Work from this chapter, builds on the findings of Bergstrom and colleagues by identifying SF regulating the activity of both CPT1a and FASN. One of the interesting findings from this work is that the induction of the metabolic genes CPT1A and FASN occurs at a late time point, thereby suggesting that either NRF2 may be activating an

intermediate protein that regulates the activity of these genes, or SF may simply be inducing other genes and/or transcription factors. However, it was surprising to see that a short high dose of SF (2 h at 25 μM SF) was already able to induce the mRNA of CPT1a, potentially implying that NRF2 may regulate the activity of CPT1a. Although in a real-life scenario obtaining such a high dose of SF would be difficult, it does, nevertheless, raise the question of whether regular intake of broccoli may indeed mitigate the effects of the high fat meal. Future work should also repeat the daily SF treatment such as the one conducted in the study to assess the levels of both CPT1a and FASN, to explore whether over prolonged periods SF can improve hepatic metabolism in individuals suffering from insulin resistance or type 2 diabetes. An additional limitation worth highlighting was that the current work conducted only assessed the mRNA but not the protein levels of these four genes. Protein levels of CPT1a and FASN should have also been assessed to check whether mRNA was indeed translated to the protein as opposed to being sent for ubiquitination.

3.4.2 SF effect on fatty acid metabolism:

Although the work in this chapter, assessing SF impact on fatty acid metabolism, is not novel, the data generated still provides new insights into the role of SF in regulating lipid metabolism. In this chapter, an *in vitro* model of NAFLD was utilised through palmitate treatment. The Oil Red O work that was conducted showed that although co-treatment of sulforaphane and palmitate had no effect in preventing lipid accumulation, SF pre-treatment followed by palmitate was instead able to mitigate the effects of the fatty acids. Therefore, it could be hypothesized that CPT1a upregulation followed by SF treatment allowed the mobilization of the fatty acid to the mitochondria for β-oxidation, rather than instead accumulating on the liver, which could lead to cirrhosis of the liver. The basis of this work originates from the research conducted by (Nagata *et al*., 2017, Axelsson *et al*., 2017), where the study showed that mice and rats challenged a high fat diet along with glucoraphanin and SF supplementation, ameliorated insulin resistance, and markers of fatty liver.

The major limitation of this work was that the cells were exposed to a single fatty acid; although palmitate is the most abundant saturated fatty acid, it does not mimic a high fat meal. Therefore, the assay should have been repeated using a combination of fatty acids such as palmitate, oleic acid (monosaturated fatty acid), and α-linoleic acid (polyunsaturated fatty acid). The Seahorse data (f**igure 3.8**) revealed that treatment of palmitate suppressed mitochondrial respiration. Other studies have shown a similar finding. For example, one study showed that HepG2 treated with palmitate results in the suppression of the activity of several protein complexes of the respiratory chain,

along with increased production of reactive oxygen species (ROS) (García-Ruiz *et al*., 2015). A second study identified that co-treatment of palmitate along with high glucose also results in a 25-40% reduction of Complex IV along with a reduction inhibition of Complex V (Alnahdi *et al*., 2019). The most recent study determined that palmitate treatment on both HepG2 and primary rat hepatocytes resulted in increased necrosis and cell death. This effect was suppressed though by, the anti-diabetic drug metformin as well as resulting in a reduction in the number of ROS induced, through increased superoxide dismutase activity. Seahorse data from the study also revealed that palmitate and metformin co-treatment resulted in an overall reduction in mitochondrial respiration (Geng *et al*., 2020). Whilst in this chapter seahorse analysis of SF and palmitate should have also been carried out, nevertheless, the results obtained by Geng and colleagues are similar to the data of the overall reduction of mitochondrial respiration induced by sulforaphane, following exposure to high glucose. This further highlights the potential of simple lifestyle changes, for example, increasing the number of vegetables in the diet such as broccoli, to mitigate the effects of a high fat meal. The results also raise the possibility that these phytochemicals may provide similar benefits as the drug metformin, challenging the current health care system that general practitioners should perhaps consider start prescribing lifestyle changes and not just medication (Jarbøl *et al*., 2017).

Tian and colleagues also showed that SF treatment to an immortalized human liver cell line HHL5 in the presence of the fatty acids (oleic and palmitic acid) improved lipid metabolism. The group went further by identifying a mechanism through which SF impacts lipid metabolism via two separate ways: endoplasmic reticulum (ER) stress-dependent and independent manners (Tian *et al*., 2018). More specifically, the group found that SF could inhibit both the protein and mRNA level of the transcription factor SREBF1 by blocking the expression of eukaryotic translation initiation factor 2-alpha kinase 3 (PERK). SF also decreased ER stress by attenuating the expression of X-box binding protein 1 (XBP1) (Tian *et al*., 2018). In the second study, the group showed that fatty acid treatment (2:1 mixture of oleic and palmitic acid) led to a decrease in UCP2, whilst SF pre-treatment reversed that effect. SF also increased the expression of two genes involved in hepatic lipid metabolism: hormone sensitive lipase (HSL) and adipose triglyceride lipase (ATGL), both involved in inducing lipolysis (Lei *et al*., 2019). In both studies two different concentrations of SF were utilized: 10 and 20 μM, potentially representing physiological concentrations.

A separate study by Teng *et al* also demonstrated an additional mechanism through which SF could mitigate the effects induced by palmitate. Teng and his team showed that SF regulated the functions of two proteins involved in glucose uptake: the insulin

receptor substrate 1 (IRS-1) and protein kinase B (Kamal *et al*., 2020), both involved in the insulin signaling pathway in a dose-dependent manner (Teng *et al*., 2019). The overall findings from the study identified SF downregulating the transcription factor regulating genes related to ceramide biosynthesis and in doing so ameliorating the onset of metabolic syndrome. In this thesis chapters, 4 and 6 provide further insight into the mechanistic basis for the protective effect of SF in a high glucose environment.

Additional studies have also reported that the effect of SF in improving lipid homeostasis is not limited to the liver, but also present in additional tissues. For example, SF has been shown to impact fatty acid metabolism in prostate cancer cell lines such as LNCAP and castration resistant (22Rv1) and *in vivo*, Transgenic Adenocarcinoma Mouse Prostate (TRAMP). SF treatment to LNCAP and 22Rv1 cells resulted in downregulation of both protein and mRNA levels of both ACC and FASN, but not ACL similar to what has been identified in other studies. The study showed that the downregulation of these proteins was due to SF inhibiting SREBF1 (Singh *et al.,* 2018). It appears that one of the exciting findings worth exploring is whether the inhibition of the transcription factor SREBF1 is mediated through NRF2 or other proteins.

Sulforaphane is regarded as a nutrigenomic activator. Other nutrigenomic activators that are currently under research include certain polyphenols, such as resveratrol found in red wine, lycopene found predominantly in tomatoes, and curcumin found in turmeric (Houghton *et al*., 2016). For example, the polyphenol resveratrol and its metabolites also improved fatty acid metabolism (Trepiana *et al*., 2020). In this study, mouse hepatocytes AML12 were incubated with the presence of resveratrol 1 µM and/or its breakdown products (trans-resveratrol-40 -O-glucuronide (R-4G); trans-resveratrol-3-O-glucuronide (R-3G); trans-resveratrol-3-O-sulfate and dihydro-resveratrol (DH-R)) in the presence of palmitate 0.3 mM. The study showed that resveratrol and its breakdown products resulted in the phosphorylation of ACC, thereby inhibiting its function. Resveratrol treatment for 18h resulted in the activity of FASN returning to that present in non-steatotic cells, whilst cells treated with the breakdown metabolites R-4 and R3-G showed even lower FASN activity (Trepiana *et al*., 2020). Several studies have shown that resveratrol is a powerful activator of Sirtuin 1(NAD-dependent acetylase), a well-established metabolic regulator (Chao *et al*., 2017, Mohar and Malik, 2012). Currently, only a single study has shown that SF influences the activity of sirtuin 1 (Li *et al*., 2016). Therefore an additional mechanism through which SF may affect lipid metabolism is through SF inducing sirtuin1 and other SIRT proteins, thereby potentially explaining a mechanism for the downregulation of genes involved in fatty

acid metabolism such as FASN (Zhang *et al*., 2014). Future research should therefore also assess whether SF affects the activity of SIRT proteins.

3.4.3 SF effect on glucose homeostasis:

When it comes to diet, excessive intake of sugars such as glucose and in particular fructose for prolonged periods has been shown to alter hepatic metabolism leading to metabolic syndrome and its respective complications (Zhao *et al*., 2016). In the current work, an established *in vitro* model of metabolic syndrome was used by challenging, HepG2 with the presence of high levels of glucose (25 mM).

To assess and provide a snapshot of how SF would impact hepatic metabolism in the presence of different glucose environments, the Seahorse Analyzer was used. Without the presence of SF, high glucose led to an increase in glycolysis, seen through the increase in EACR. SF treatment, on the other hand successfully reduced this. Therefore it was hypothesized that this reduction was due to the glucose being redirected to the PPP. Further analysis did identify the induction of glucose-6-phosphate dehydrogenase, 6-phosphogluconate dehydrogenase, and transketolase genes involved in the pathway. The PPP is split into two distinct phases: an oxidative irreversible pathway generating NADPH, and a ribose-5-phosphate molecule. The non-oxidative pathway is made up of several reversible reactions interconverting between ribose phosphates and glycolytic intermediates depending on the cell's requirements for NADPH, ribose phosphates, or ATP (Wamelink *et al.,* 2008). Several additional studies have shown that activation of NRF2 leads to the upregulation of these genes. Yamamoto and colleagues showed that G6PD, PGD, TKT, and TALDO are all direct targets of NRF2 having an ARE sequence (Mitsuishi *et al*., 2012). A second study by Agyeman, where non-cancerous human breast epithelial MCF10A were treated 15 µM SF for 24 hours, also showed a significant increase of at least 1.2-fold in the expression of PGD, G6PD, TALDO1, and TKT (Agyeman *et al*., 2012).

Within the last couple of years, SF has also attracted attention due to its ability to improve glucose homeostasis in type 2 diabetics. A recent study, where T2D supplemented with broccoli sprout extract (BSE), containing a high concentration of glucoraphanin (delivering the equivalent of 150 µM SF), resulted in a significant decrease in fasting blood glucose between the intervention (8.3 ± 0.3 mM) compared to the placebo group (9 ± 0.4 mM) (Axelsson *et al*., 2017). Furthermore, Hb1Ac levels also changed; the placebo group had (57 mmol/mol) whilst the BSE treated was reduced to (53 mmol/mol). What remains unclear is the molecular mechanism through which SF carries this out. One potential mechanism was identified in a recently published study, where SF reduced the activity of several glycolytic genes. This was

also reflected by a reduction in non-mitochondrial metabolism assessed through the Glycolysis Stress Test from the Seahorse BioScience (Carrasco-Pozo *et al*., 2019).

Culturing hepatocytes in a high glucose environment has been shown to result in a wide range of metabolic alterations. One study showed an increased accumulation of triglycerides, along with increased expression of genes involved in fatty acid biosynthesis, such as SREBF1, SCD, and CD36. However, no effect on mitochondrial function was identified (Su *et al*., 2019). An additional study showed that high glucose results in activation of the NF-Κβ pathway, along with increased production of inflammatory cytokines and ROS (Panahi *et al*., 2018). A third study where HepG2 were cultured under various glucose concentrations ranging from 15-57 mM showed that the high concentration of glucose (33 mM) blocked the phosphorylation of the protein AKT, which lies downstream of the insulin receptor. This resulted in inhibiting protein kinases, thereby blocking the signalling pathway and suppressing glycogen synthesis (Nakajima *et al*., 2000). There is increasing evidence showing that whilst ROS plays an important role as a signalling molecule, metabolic syndrome results in ROS overproduction (Ando and Fujita, 2009). The increase in free radicals, in turn, results in increased attack and damage to proteins, nucleic acids, and even lipids. These oxidized products consequently decrease biological activity, leading to altered cell signalling and function (Mahjoub and Masrour-Roudsari, 2012).

The current work was also extended further by culturing HepG2 without glucose for 24 h (a hypoglycemic state). Assessment of the literature revealed that no other studies had carried this out. One study used very low glucose concentrations (0.5 mM); nevertheless, glucose was still added (Deorosan and Nauman, 2011). In this study, Bone-Marrow Derived Mesenchymal Stem Cells cultured in the lowest concentration of glucose experienced increased cell death and slowest proliferation rate (Deorosan and Nauman, 2011). It is worth mentioning, however, that in a real-life scenario, no glucose circulating in the blood would ever occur. Even after having fasted for long periods or following a ketogenic diet, small amounts of glucose would still be circulating in the blood.

This no glucose environment was carried out to determine whether a method could be developed to assess the effect of SF on mitochondrial function only. The Seahorse analysis still revealed that cells were still carrying out glycolysis despite the lack of glucose, highlighting the cancer phenotype of HepG2. The pyruvate was most likely derived from the carbon source glutamine through glutaminolysis and the conversion of malate to pyruvate through the action of malate dehydrogenase. Notably, the presence of SF in the glucose starved HepG2 cells showed a reduction in glycolysis, suggesting

the health benefits of SF also interfering with the glutamine metabolism pathway and suppressing the tumorigenic Warburg effect. The reduction in maximal respiration may also be to SF resulting in decreased activity of the TCA cycle. At the same time, however, deprivation of glucose in cancer cells may result in increased oxidative stress (Gatenby and Gillies, 2007). Therefore, it was hypothesized that the reduction in maximal respiration may also be due to glutamine being redirected for glutathione biosynthesis.

A potentially better model to assess how SF affects the mitochondria only was established by treating the cells with 10 mM galactose (Marroquin *et al*., 2007). Previously, using the universally labelled glucose and galactose $^{13}C_6$ tracers revealed that in the presence of the galactose tracer, no 13C lactate tumortutuunmwas identified, compared with the universal glucose tracer, which resulted in large amounts of 13C lactate (Xu *et al*., 2019). Therefore, the cells can only survive by producing ATP through oxidative phosphorylation (Marroquin *et al*., 2007). Thus, cells switch to an "aerobic" state under galactose treatment. Under the presence of galactose Xu, HepG2 increases glutaminolysis to try and maintain the high ATP production demands (Xu *et al*., 2019). Interestingly, in the current study, when SF was added in galactose treated HepG2 cells, SF could still reduce mitochondrial respiration. This suggests that the reduction in mitochondrial respiration is due to a decrease in glycolysis and the subsequent entry of fewer substrates into mitochondrial respiration and other mechanisms, for example, targeting enzymes involved in the TCA cycle (see chapter 5) or further redirection of metabolic intermediates.

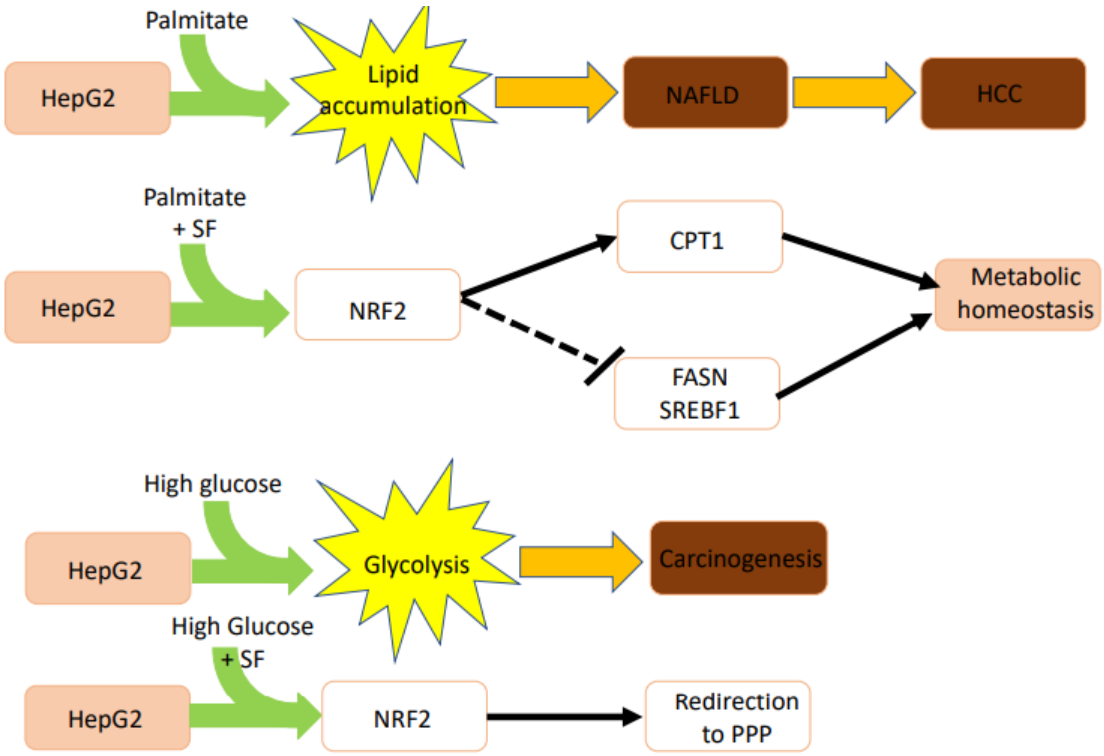

Figure 3.17. Summary of the findings of this chapter, showing SF preliminary effects as a metabolic regulator. When HepG2 are cultured with the presence of palmitate, palmitate accumulates, resulting in NAFLD the latter can develop to HCC. SF treatment instead results in NRF2 activation, resulting in inhibition of FASN along with induction of CTP1. The outcome is inhibition of fatty acid biosynthesis, thereby restoring metabolic homeostasis. When HepG2 are cultured in high glucose, the glucose is mainly metabolized through glycolysis; in contrast, SF addition results in NRF2 activation, which redirects the glucose towards the PPP.

3.5 Conclusion:

The effect of SF as a metabolic regulator has been largely unexplored, yet it provides a huge opportunity to explain some of the beneficial effects observed in populations with high dietary intake and in disease models. In addition, NRF2, one of the targets of SF in the cell, has also been shown to regulate a wide range of metabolic processes. In this current chapter, an *in vitro* model of liver metabolic dysregulation (potentially insulin resistance) was used by treating a well-established carcinoma cell line HepG2 with physiological concentrations of sulforaphane along with the presence of a wide range of substrates. The data obtained from this chapter supports the current findings from the literature that SF activates both the antioxidant response through NRF2 and can also act as a metabolic regulator. Furthermore, it was also identified that short exposure to SF is enough to lead to sustained transcription effects. The data also recalled that SF treatment profoundly affected lipid metabolism by inducing CPT1a and downregulating the activity of FASN, and suppressing the accumulation of lipids on HepG2 challenged with fatty acids. A crucial finding from figure 11 is that there needs to be a “priming” of the cellular machinery ahead of exposure to palmitate for SF to prevent its detrimental effects in lipid accumulation. The Seahorse analysis furthermore showed that when hepatocytes were challenged with high glucose alone, this resulted in increased EACR along with decreased OCR. SF treatment suppresses this effect by reducing overall mitochondrial respiration and re-directing the glucose to other pathways. In the next chapter, this work will be explored further by conducting an RNAseq study, assessing the whole transcriptome of HepG2 with the presence of SF in these three distinct metabolic environments.

Chapter 4: The transcriptional effect of sulforaphane on liver cells at different metabolic states

Chapter 4 Figures

Chapter 4 Tables:

4.1 Introduction:

One of the liver's many functions is maintaining blood glucose concentrations in the 3.9 to 5.5 mM range. This process is highly regulated by balancing the liver's glucose output with the amount of glucose absorbed in the peripheral tissue (Klover and Mooney, 2004). Abnormal glucose homeostasis can result in pre-diabetes, metabolic syndrome, and, if left untreated, ultimately type 2 diabetes. In type 2 diabetes (T2DM), the resulting circulating levels of glucose in the blood can rise into the hyperglycaemic range (greater than 5.5 mM) (Tolman *et al*., 2007). If left untreated, the resulting outcome can have detrimental effects throughout the body. A couple of studies have shown that diets rich in refined/processed carbohydrates (such as monosaccharides and disaccharides) to overweight and obese individuals who already have metabolic

dysfunction were associated with increased *de novo* lipogenesis (Marques-Lopes *et al*., 2001, McDevitt *et al*., 2001). In the liver, the excessive abundance of glucose will first be converted to glycogen. The remaining glucose will be utilized for de novo lipogenesis if the glycogen stores are full. The outcome is lipid accumulation in hepatocytes through insulin. Insulin induces the activation of the mammalian target of rapamycin complex 1 (mTORC1) through the phosphoinositide 3-kinase AKT pathway, and mTORC1 is required for insulin to induce the expression of SREBF1 (Li *et al*., 2010). Hepatic inhibition of AKT2 through deletion of the *rictor* gene results in attenuation of glycolysis and lipogenesis (Hagiwara *et al*., 2012). This results in a phenomenon called steatosis, where the accumulation of lipids in the liver is greater than 5% (Fabbrini *et al*., 2009). The hallmark of non-acholic fatty liver diseases, the leading cause of liver complications, is steatosis. If left untreated, steatosis can progress to cirrhosis/fibrosis and eventually hepatocellular carcinoma (Soto-Angona *et al*., 2020). This accumulation of lipids and the continuous supply of glucose consumption can form chronic reductive stress (Farhana *et al*., 2010, Valadi *et al*., 2004, Teodoro *et al*., 2013). The aerobic breakdown of glucose from glycolysis results in pyruvate: which enters the TCA cycle resulting in the production of electrons stored and transported by NADH/$FADH_2$. Therefore a constant intake of glucose results in the overproduction of NADH, and coupled with the lack of NAD^+, the outcome is an imbalance between the two metabolites leading to a condition referred to as pseudohypoxia (Gomes *et al*., 2013, Ido and Williamson, 1997). Under this state oxygen is not effectively consumed; the outcome is metabolic stress which can result in metabolic syndrome often found in individuals with diabetes (Williamson *et al*., 1993). This reductive stress leads to oxidative stress by overproducing mitochondrial superoxide and other ROS such as hydrogen peroxide and peroxynitrite (Turrens, 1997, Shah *et al*., 2007). These ROS can react and cause the oxidation of proteins, lipids, and DNA (Cai and Yan, 2013). The increased ROS accumulation and NADPH can also inhibit the glycolytic gene glyceraldehyde-3-phosphate dehydrogenase (Rivera-Nieves *et al*., 1999), resulting in the build of glyceraldehyde-3-phosphate, which is redirected towards both the polyol and the glyceraldehyde autoxidation pathways and methylglyoxal production (Lovestone and Smith, 2014). Essentially these pathways further contribute to the production of ROS. The metabolite methylglyoxal has been shown to modify proteins via glycation of the amino groups present on proteins (Queisser *et al*., 2010, Thornalley *et al*., 1999). This glycation process, in addition, results in the production of ROS. The outcome is the activation of several redox-sensitive transcription factors such as the NF-ƙB pathway, activator protein 1 (AP-1) and the early growth response 1 (EGR1), resulting in further inflammation (Muñoz and Costa, 2013).

To counterbalance the build-up of ROS, activation of NRF2 either through pharmacological or dietary means has been shown to play a vital role in resistance to oxidative stress (Ma, 2013). Major antioxidants identified include small molecular molecules such as reduced glutathione, thioredoxin (TRX), glutaredoxin, along with enzymes such as superoxide dismutase (SOD) and glutathione peroxidase (Ma, 2013). In addition to SF regulating the antioxidant response through NRF2, within the last couple of years, increasing evidence has shown that broccoli bioactives such as SF suppresses the effects of a high fat meal in both animals and *in vitro* studies. For example, glucoraphanin supplementation in mice fed a high fat diet suppresses lipid accumulation (Nagata *et al* 2017, Xu *et al* 2020). *In vitro* work showed that SF could protect beta-cells of the pancreas when treated with cholesterol (Carrasco-Ponzo *et al* 2017). To gain a better understanding of the molecular mechanism of how lipid metabolism, central metabolism, and the antioxidant response are interconnected, an RNA-sequencing study was designed.

In this study, differential gene expression was performed through RNA sequencing from HepG2 in no (0 mM), basal (5 mM), and high glucose (25 mM) representing fasting, healthy and insulin-resistant hepatocytes, treated with physiological concentrations (10 µM) SF for 24 h. The current study aimed to determine: the transcriptional effect of SF in different metabolic states in the liver by addressing the following question:

1. Assessing how the NRF2 target genes respond under different metabolic states
2. Characterizing SF effect on genes linked to central metabolism in hepatocytes under different metabolic states

This experiment was designed to explore two hypotheses:

1: Regardless of the levels of glucose, the presence of SF will still induce the antioxidant response.

2: In a high glucose environment (but not basal/no glucose), SF will induce the expression of genes involved in fatty acid metabolism (β-oxidation) to suppress the detrimental effects of high glucose concentration

4.2 Methods:

4.2.1 Processing the raw reads to obtain the differentially expressed genes

The statistical analysis carried out with RNAseq tests whether there is a difference for each gene or differential expression across the two sample groups (control vs treatment). The null hypothesis is no differential expression across the two samples.

The differentially expressed genes were obtained through the limma approach. This method converts the RNA seq counts to log2-counts per million, and the mean variance relationship is modeled either with precision weights or with an empirical Bayes prior trend. Following the processing of the data, StringTie converts the assembled RNAseq reads to potential transcripts. The output of StringTie is a matrix of raw counts. This is usually in the form of binary data. For example, 0 if a gene is not or very low expressed and 1000 or greater if the gene is expressed. This introduces a lot of bias to the data as the gene size, the sample size, and sequencing depths are not considered. Therefore, the data must be transformed. Popular transformation includes counts per million (CPM), which accounts for differences in sequencing depths between samples, log counts per million, or fragments per kilobase of transcript per million (FPKM) (Robinson and Oshlack, 2010, Robinson *et al*., 2010). In this analysis, the counts were converted to log2-counts per million (log CPM) using the cpm function in edgeR, (package in the Statistical software R) where log transformations use a prior count of 0.25 to avoid taking the log of zero (Robison *et al* 2010). Once the counts have been converted, the outcome is a distribution that contains all the genes. Genes that are not expressed at a biologically meaningful level however need to be discarded as they provide little evidence for differential expression. What is hoped to get is a plot for the filtered data that resembles a normal distribution (Law *et al* 2016).

The final step consists of carrying out the differential gene expression to obtain the differentially expressed genes (DEGs). Several options can be used at this stage; either the limma-trend or the voom plot. Which approach is used, very much depends on the quality of the data. The limma-trend works well when the sequencing depth is consistent across all RNA samples. This approach works well if the ratio of the largest library size to the smallest is not more than about 3 fold. When variability is present between samples or library sizes then the voom approach is more powerful/robust than the limma trend (Law *et al*., 2014).

Both the limma-trend and the voom approach calculate the DEG using the same approach. The basis of statistics is ***moderated t-statistics***; this is like a t-statistic test

only that the linear model has been replaced using Bayesian inference (empirical Bayes. With Empirical Bayes the prior distribution is estimated from the data, which is different from a normal Bayesian inference. In normal Bayesian inference, the prior distribution is kept constant and the posterior distribution is utilized to estimate the data. This approach is preferred as the degrees of freedom are increased and the standard error is reduced. For this analysis, the voom using precision weights was carried out.

4.2.2 Gene Set Enrichment Analysis (GSEA)

After obtaining the DEGs, functional analysis was performed with the ranked list of expressed genes using the rank-rank hypergeometric overlap algorithm (RRHO) (Plaisier *et al*., 2010). The RRHO algorithm is used to compare two gene expression profiles as a ranked list, typically using the statistical results from the differential expression analysis. The algorithm uses the complete list of expressed genes instead of using a subset of the top differentially expressed genes, which increases the sensitivity to small but concordant changes. The motivation for using the whole gene expression profile is that groups of genes with small but consistent changes tend to be discarded when taking only the top changing genes as representatives for genome-wide expression profiles. Considering all expressed genes allows for the detection of enriched groups of related genes that would have been considered weakly differential on their own, but with a concordant change in expression.

The results of the differential expression test were represented as the list of expression changes ranked on the statistical significance of differential expression of no glucose SF treated vs no glucose control (group 1), basal glucose SF vs basal glucose control (group 2), and high glucose SF vs high glucose control (group 3). The same genes were ranked using the (negative) -log10-transformed p-value multiplied by the sign of the log2-FC, where the sign denotes the direction of the change: positive for upregulated gene expression in samples in group 1 and negative for downregulated expression in samples in group 1. The most significantly upregulated genes are at the top of the list, the most significantly downregulated genes are at the bottom and those genes with small changes are in the middle. The same was carried out for group 2 and group 3

The list of the ranked genes was then compared against genes sets to search for coordinated changes in the gene expression dataset using Gene Set Enrichment Analysis, GSEA, v4.0.3 (Subramanian *et al*., 2005) and the Kyoto Encylopedia of Genes and Genomes (KEGG) (Kanehisa *et al*., 2017, Kanehisa *et al*., 2015). The KEGG database contains 186 gene sets. These genes sets contain information on the following processes:

- Metabolism- including metabolic pathways and an overall picture of metabolism
- Genetic information processing (transcription, translation, DNA replication, and repair)
- Environmental processing (signal transduction)
- Cellular processes (cell growth, cell death, and cell membrane functions)
- Human diseases
- Drug development
- The immune system, endocrine, and nervous system function.

GSEA was performed using the GSEA Preranked tool with a weighted enrichment statistic and 1000 permutations to correct for multiple hypotheses testing. The normalized enrichment score for each pathway and their associated p-values and FDR-adjusted p-values for the transcriptomic differences between groups are reported.

4.2.3 Network Analysis

The network analysis was constructed using the NRF2ome database (http://nrf2ome.org/) through Cytoscape (https://cytoscape.org/). NRF2ome is a manually curated database. The database contains vast information on how both upstream and downstream targets (both direct and indirect targets of NRF2), influence additional signaling pathways, thereby identifying the possible involvement of NRF2 in various pathways. It also contains information on how NRF2 regulates transcription factors (TF) and miRNAs. The database contains over 8,000 proteins out of which NRF2 directly regulates 225 but over 7,000 are indirectly regulated by NRF2. These interactions have been identified both through manual curation of the literature and have also been experimentally predicted (Papp *et al*., 2012, Turei *et al*., 2013). This analysis by master regulators implied identifying whether NRF2 controlled the activity of any TF. When it comes to biological networks, the most common nomenclature used to describe the network, hence the genes and its interactions, are node and edges. A node can represent, genes, RNA, proteins, etc, whilst an edge represents the interaction occurring between the nodes. These interactions can be directed, this means, for example, a gene or protein is directly binding to another gene/protein, or undirected. These interactions can also tell if it's stimulatory or inhibitory, hence whether the interaction will induce downstream targets or inhibit these targets.

4.3 Results:

4.3.1 RNA-sequencing data analysis and identification of treatment clustering

Figure 4.1 shows the data normalisation, using the trimmed mean of M-values (TMM). From figure 4.1, it can be seen how the normalization was effective as the boxplots of samples after normalization are symmetrical. The data was then analyzed using the edgeR-limma package to obtain the differentially expressed genes.

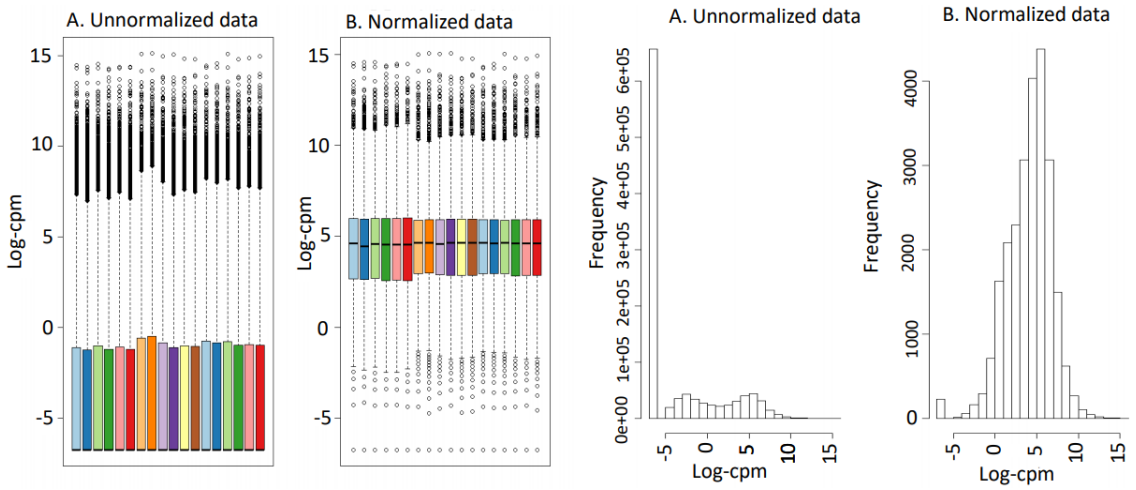

Figure 4.1. Representation through box plots and histograms of counts data before and after normalization. Normalization is essential because to conduct any form of statistical analysis such as a t-test, one assumption is that the data needs to be normally distributed.

In the next step, heteroscedasticity in the count data was removed, shown in figure 4.2. Heteroscedasticity occurs when the variance is no longer constant to the mean, mean=variance. This is shown by the voom plot by the decreasing trend between the mean and variances (**figure 4.2 a**). This results from a combination of both technical variations in the sequencing experiment and biological variation among the replicates. Following transformation, the trend disappears resulting in gene counts with a constant variance, thereby removing heteroscedasticity.

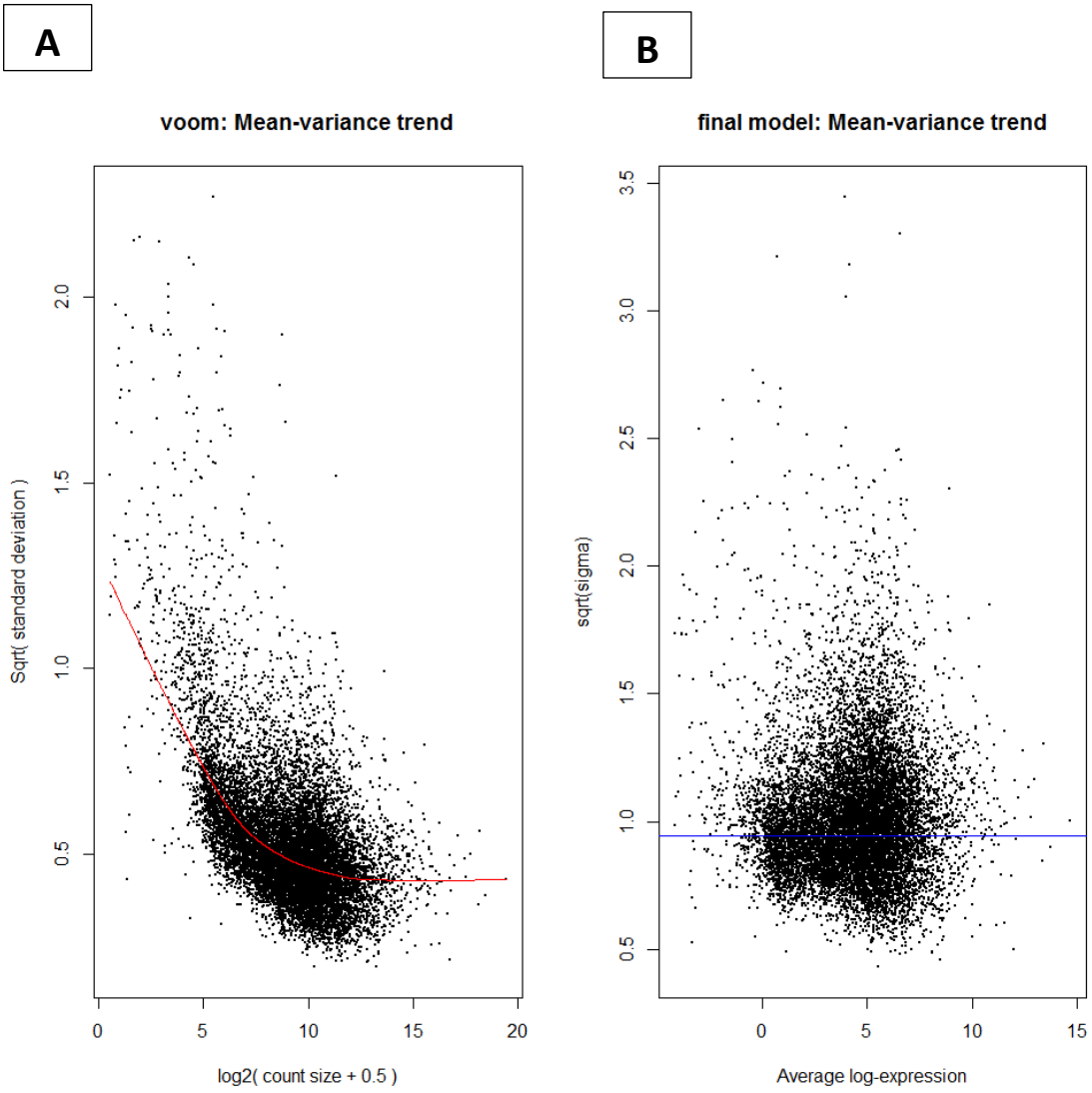

Figure 4.2. **Mean-variance relationship before and after the transformation.** Means (x-axis) and variance (y-axis) between each gene to show the relationship between the two, before the voom precision weights are applied to **A** to transform the data. Notice how after the transformation the trend/pattern in A disappears. Plot A is obtained through the voom function in R and is constructed by extracting the residual variances from the linear regression. The square root of the residual variances is then taken and plotted against the mean expression of each gene. The mean is then $\log_2$ transformed.

In the final step, a pairwise comparison was then conducted between 10μM SF and the untreated control under the various glucose levels to determine the number of differentially expressed genes changed at different adjusted p values. Results are shown in table 4.1.

Table 4.1 Number of genes differentially expressed in response to SF under the various glucose environments under varying adjusted p values

Ctrl vs SF	No glucose DMSO vs no glucose SF	Basal glucose DMSO vs basal glucose SF	High glucose DMSO vs high glucose SF
q < 0.05	**393 (↑139 ↓254)**	**1657 (↑691 ↓966)**	**1250 (↑536 ↓714)**
q < 0.1	**907 (↑369 ↓538)**	**2553 (↑1117 ↓1436)**	**1981 (↑ 846↓1135)**
q < 0.2	**2312 (↑1067 ↓1245)**	**3895 (↑1741 ↓2154)**	**3048 (↑1309 ↓1739)**
q < 0.25	**3174 (↑1500 ↓1674)**	**4505 (↑2022 ↓2483)**	**3556 (↑1540 ↓2016)**

The number of genes in bold is the total number of transcripts changed. In brackets ↑ indicates the number of upregulated genes while ↓ indicates the number of downregulated genes.
q values are adjusted for false discovery rates using the Benjamini-Hochberg correction

Table 4.1 revealed that a total of 393 genes were differentially expressed in response to 10µM SF compared to untreated controls in the no glucose environment, in basal glucose 1657 genes and high glucose 1250 genes were differentially expressed compared to the untreated control (adjusted $p < 0.05$ or $q < 0.05$).

The next question addressed was whether any of the significant genes were expressed in more than one group. A Venn diagram was therefore constructed to investigate the overlap between these three different pairwise comparisons. Interestingly 90 genes were common in all three glucose environments (figure 4.3).

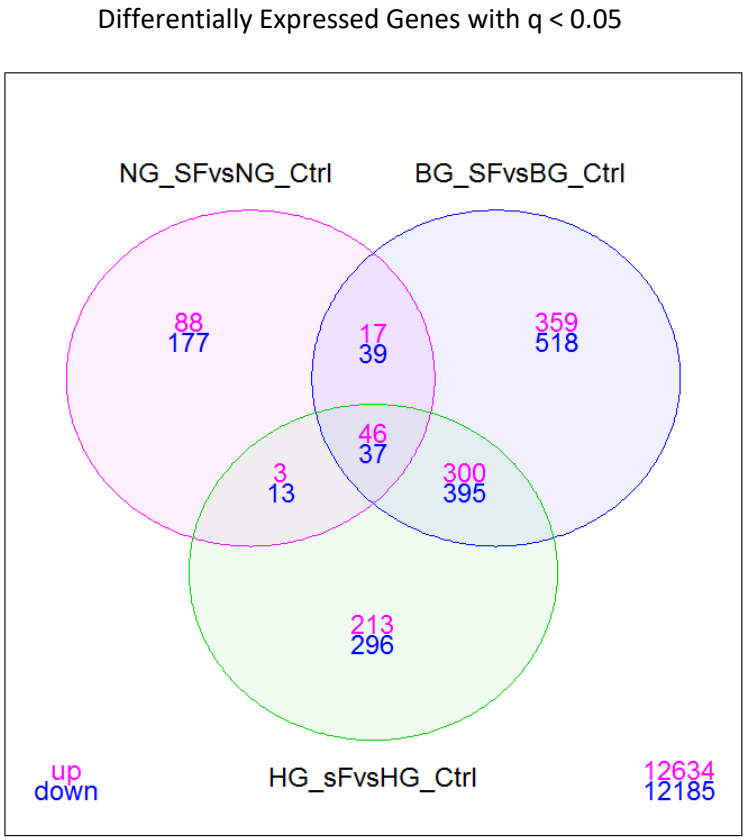

Figure 4.3. Effect of SF in the presence of various glucose environments on gene expression. 83 genes were found to be affected by 10 µM SF in no, basal, and high glucose environments. 16 genes were found to be affected by 10 µM SF in no and high glucose. 56 genes were found to be affected by 10µM SF in no and basal glucose. 695 were found to be affected by 10 µM SF in basal and high glucose

The multidimensional scaling plot (MDS) shown in (figure 4.4) immediately highlights two interesting observations: firstly, the no glucose samples behave completely differently from the samples with glucose, which is to be expected. Interestingly, the basal glucose samples treated with SF responded in a similar manner to the samples in high glucose and behaved differently to their respective control.

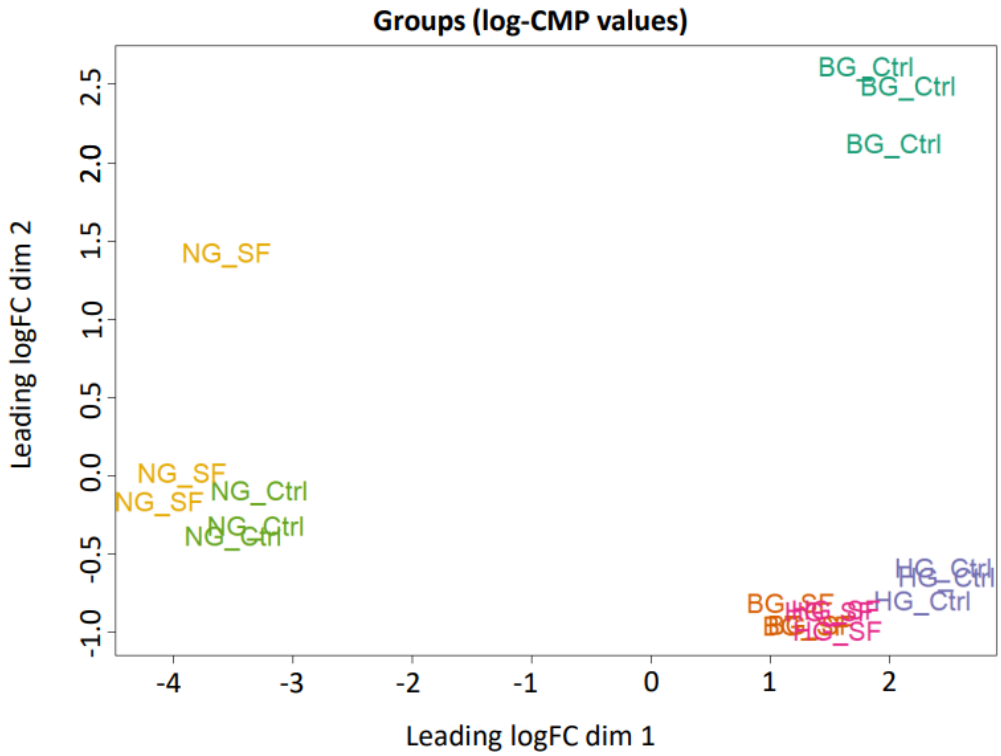

Figure 4.4. Multidimensional scaling analysis (MDS) plot of differential expression data gathered from HepG2 cells cultured under three different glucose environments with the presence of Sulforaphane for 24 h. The distance on the plot corresponds to the leading fold change which is the average log_2-fold change. The first dimension which in this dataset represents the glucose environments, explains the largest proportion of variation of the data (Law et al., 2016). Yellow = NG +SF, Green = NG +DMSO, Blue= BG+ DMSO, Orange = BG + SF, Pink = HG +SF, Purple = HG+ DMSO

4.3.2 Identification of enriched gene sets by SF under different metabolic states obtained through the Gene Set Enrichment Analysis

The output of the limma plot (**figure 4.2**) is a list of differentially expressed genes. A gene is said to be differentially expressed if its expression levels or read counts are different compared to its respective control following statistical analysis. In the next step, the GSEA was conducted. Detailed analysis that includes all of the pathways including those enriched and not enriched by SF has been put in Table S1.0 (Appendix). A summary statistic of the pathway analysis by KEGG is instead shown in table 4.2. Figures 4.5-4.7 represent the enriched gene sets following multiple testing corrections ($q<0.05$) by SF under the different glucose environments

Table 4.2 Summary Statistics of the GSEA analysis using the KEGG Database

Samples	Enriched Pathways	FDR q <0.25	Nominal p-value <0.05	Nominal p-value <0.01
No Glucose	**151** (↑83 ↓68)	**97** (↑56 ↓41)	**56** (↑36 ↓33)	**38** (↑20 ↓18)
Basal Glucose	**151** (↑65↓86)	**21** (↑8 ↓13)	**21** (↑8 ↓13)	**17** (↑7 ↓10)
High Glucose	**151** (↑91 ↓60)	**48** (↑43 ↓5)	**38** (↑30 ↓8)	**16** (↑13 ↓3)

Pathway analysis was carried out using the GSEA software mapped to the KEGG database. 151 total pathways were calculated where ↑ represents upregulated pathway ↓ is downregulated pathway. The bold values under the FDR q value column represent the statistically significant pathways that have been enriched, the p-value that has corrected using Benjamini-Hochberg. The nominal p-value is the p-value normalized to the enrichment score

For the GSEA analysis and the remaining analysis of this chapter, the FDR q-values were chosen over the nominal p-values; as the FDR q-values are an estimated probability that the normalized enrichment score will represent a false positive finding.

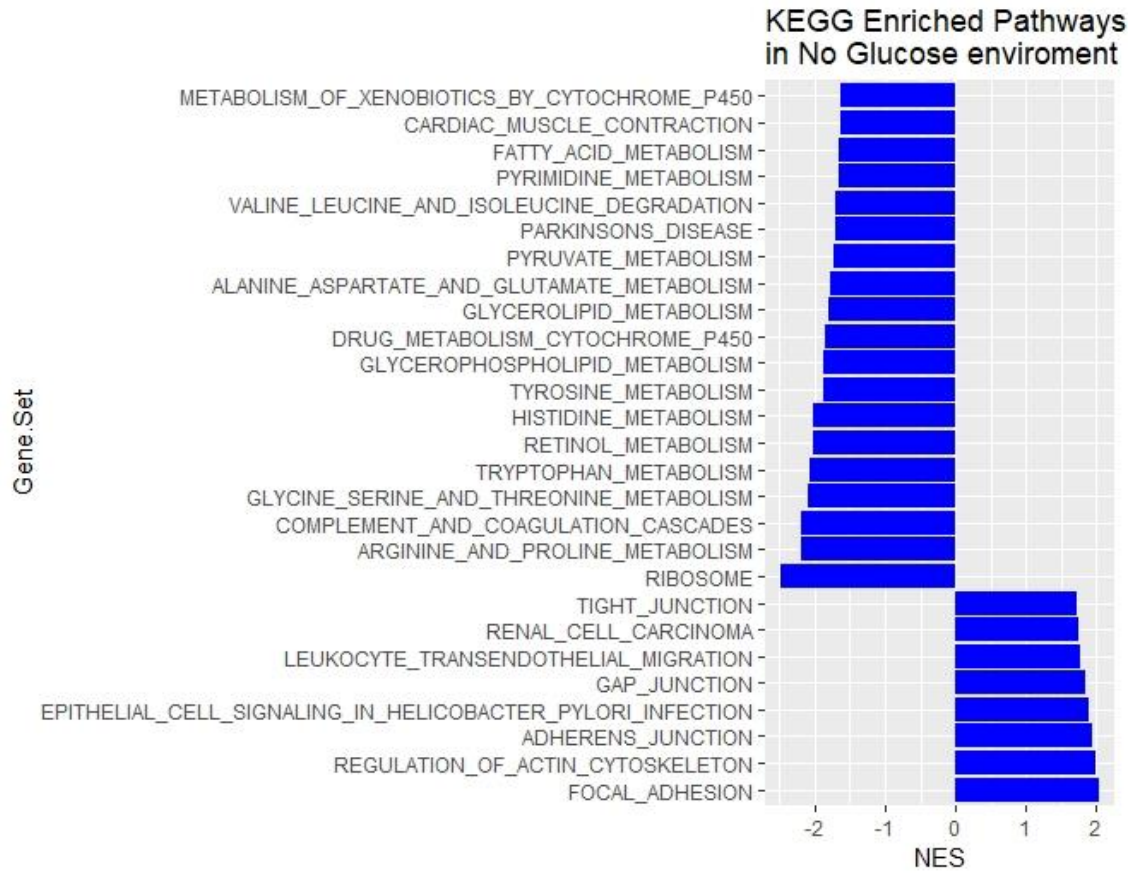

Figure 4.5. Significantly enriched gene sets were identified within the differential expression data of HepG2 cells cultured under a no-glucose environment compared to the sulforaphane treatment. The x-axis represents the normalized enrichment score (NES). The NES is calculated using the GSEA. NES represents an estimation of the significance of the gene set normalized to the size of each gene set. An increase in the gene set shows positive NES, and negative NES denotes an overall decrease in the gene set. The y-axis represents the gene sets. Both treatment and controls are representative of triplicate samples

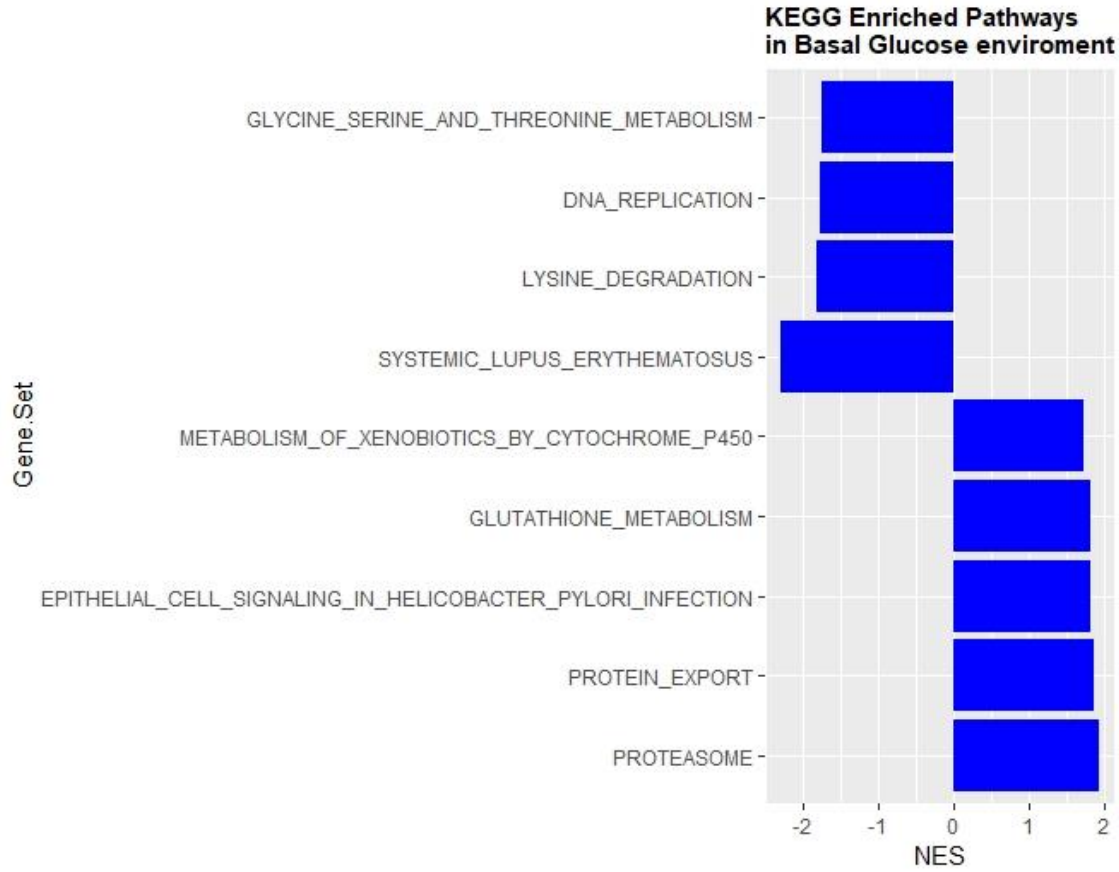

Figure 4.6. Significantly enriched gene sets were identified within the differential expression data of HepG2 cells cultured under a basal glucose environment compared to sulforaphane treatment. The x-axis represents the normalized enrichment score (NES). The NES is calculated using the GSEA. NES represents an estimation of the significance of the gene set normalized to the size of each gene set. An increase in the gene set shows positive NES, and negative NES denotes an overall decrease in the gene set. The y-axis represents the gene sets. Both treatment and controls are representative of triplicate samples

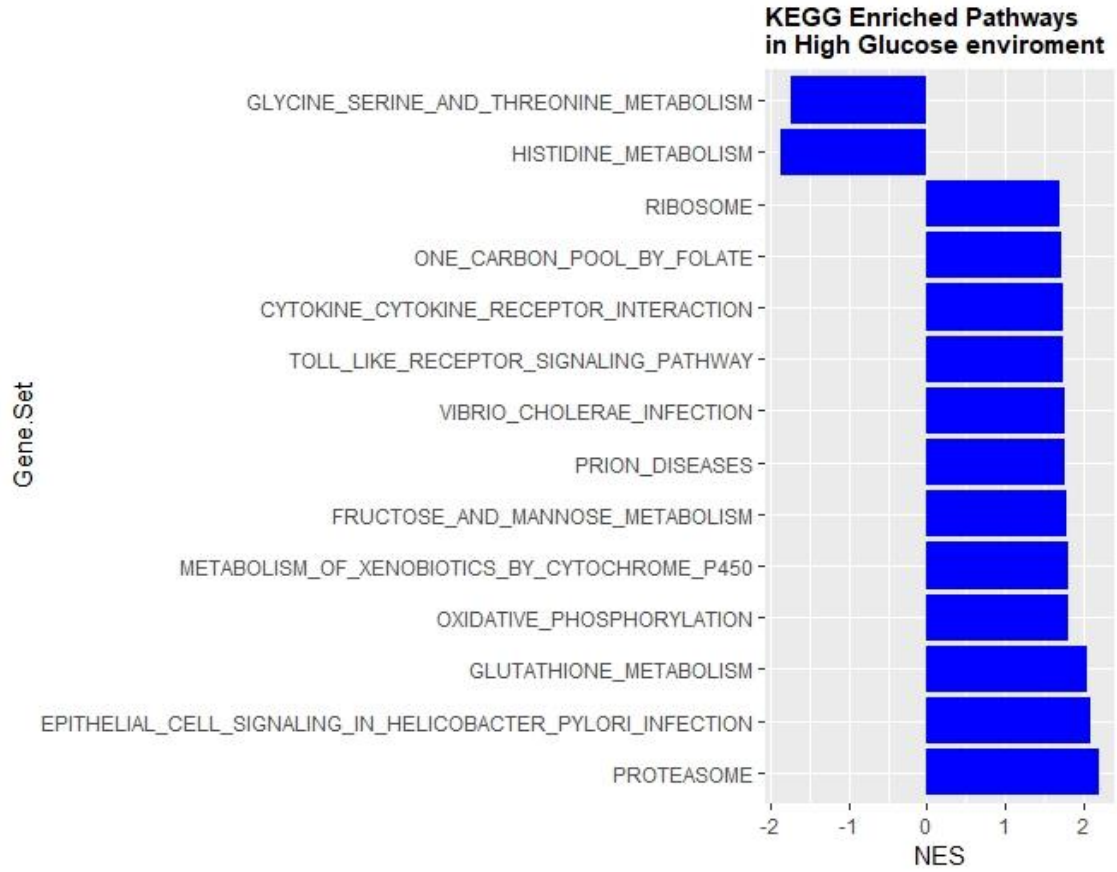

Figure 4.7 Significantly enriched gene sets identified within the differential expression data of HepG2 cells cultured under a high glucose environment when compared to sulforaphane treatment. The x-axis represents the normalized enrichment score (NES). The NES is calculated using the GSEA. NES represents an estimation of the significance of the gene set normalized to the size of each gene set. An increase in the gene set shows positive NES, and negative NES denotes an overall decrease in the gene set. The y-axis represents the gene sets. Both treatment and controls are representative of triplicate samples

4.3.3. Determining the transcriptional effects of SF in different metabolic states in the liver

To ask the question of whether the same transcriptional changes occur under the different glucose conditions, common enriched pathways by sulforaphane in the presence of the various glucose environments were plotted as bar plots to visualize common pathways (figure 4.8).

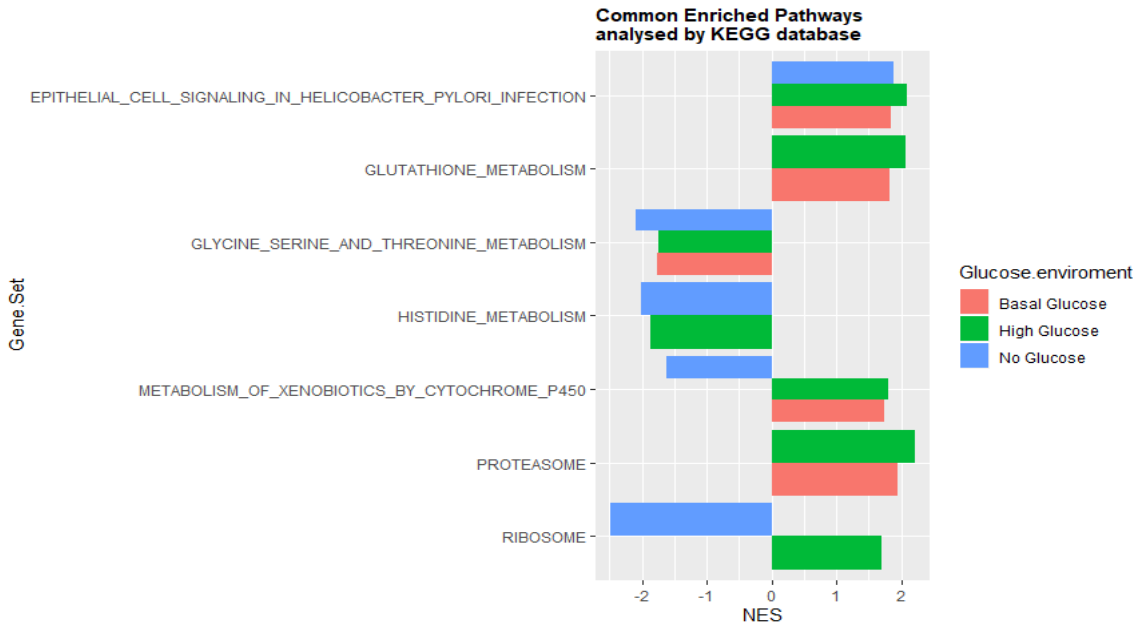

Figure 4.8. Pathways that have significantly been enriched by SF are common in all three glucose environments. The x-axis represents the normalized enrichment score (NES). The NES is calculated using the GSEA. NES represents an estimation of the significance of the gene set normalized to the size of each gene set. Positive NES is shown by an increase in the gene set, and negative NES denotes an overall decrease in the gene set. The y-axis represents the gene sets. Both treatment and controls are representative of triplicate samples.

Figure 4.8 shows that three pathways were enriched in all three glucose environments: upregulation of epithelial cell signaling in *Helicobacter Pylori* infection, in all three sets, downregulation of serine, glycine, and threonine metabolism in all three sets, and upregulation of metabolism of xenobiotics by cytochrome P450 in basal and high glucose along with a downregulation in the no glucose environment. Upregulation of metabolism of xenobiotics by cytochrome P450 along with glutathione metabolism is a marker of NRF2 induction. This consists of genes involved in the antioxidant response and phase II detoxification. The first hypothesis that the study wanted to address is that the presence of SF, regardless of the glucose levels, NRF2 induction would still occur. Downregulation, therefore, of the metabolism of xenobiotics by cytochrome P450 gene set and no induction of glutathione metabolism in the no glucose environment could be

an indicator that NRF2 is not induced in this environment. This hypothesis was validated by assessing a couple of NRF2 target genes, through qPCR (Appendix figure S1.0) The results do seem to support that NRF2 is not induced in glucose deprivation.

A novel finding from the analysis is the downregulation of the serine glycine and threonine metabolism. Serine and glycine are non-essential amino acids. Serine is synthesized from 3-phosphoglycerate a glycolytic intermediate, whilst glycine is derived from serine. Threonine is instead an essential amino acid. A detailed analysis of the enrichment in this pathway can be found in the next chapter (**chapter 5**)

4.3.4 Assessing how the NRF2 target genes respond under different metabolic states

Figure 4.8, identified that in the presence of glucose, upregulation of the gene sets metabolism of xenobiotics by cytochrome P450 along with glutathione metabolism occurred. The analysis was expanded by extracting all the differentially expressed genes from those two enriched pathways. This analysis also included the same set of genes in the no glucose environment, to further assess whether glucose is necessary for the induction of NRF2. These results are shown in figures 4.9 and 4.10. Analysis of the glutathione metabolism gene set revealed strong upregulation of more than 4-fold in genes involved in glutathione biosynthesis such as GCLC/GCLM in both basal and high glucose environments. Under no glucose, GCLC/GCLM induction was attenuated (**table 4.3 and figure 4.9**).

Similarly, SF treatment resulted in a 2-fold increase in glutathione reductase (GSR) in both glucose environments, with glucose deprivation inhibiting GSR induction. GSR is involved in catalyzing the conversion of oxidized glutathione to reduced glutathione in the presence of NADPH. The gene set also revealed that SF treatment induced G6PD, the rate-limiting step of the pentose phosphate pathway, involved in NADPH production (although only statically significant in the high glucose environment q= 0.01). In this gene set, the analysis also revealed SF upregulating the ornithine decarboxylase gene in both glucose environments (ODC1 only statistically significant in basal q <.0.0001, and high glucose q <0.0001). This gene is involved in catalyzing the breakdown of ornithine an intermediate in the urea cycle to putrescine the first step in polyamine synthesis. Putrescine through a series of reactions can be converted to glutathionyl spermidine which is then converted to glutathione. Therefore the results suggest that polyamine biosynthesis may also contribute to the antioxidant response.

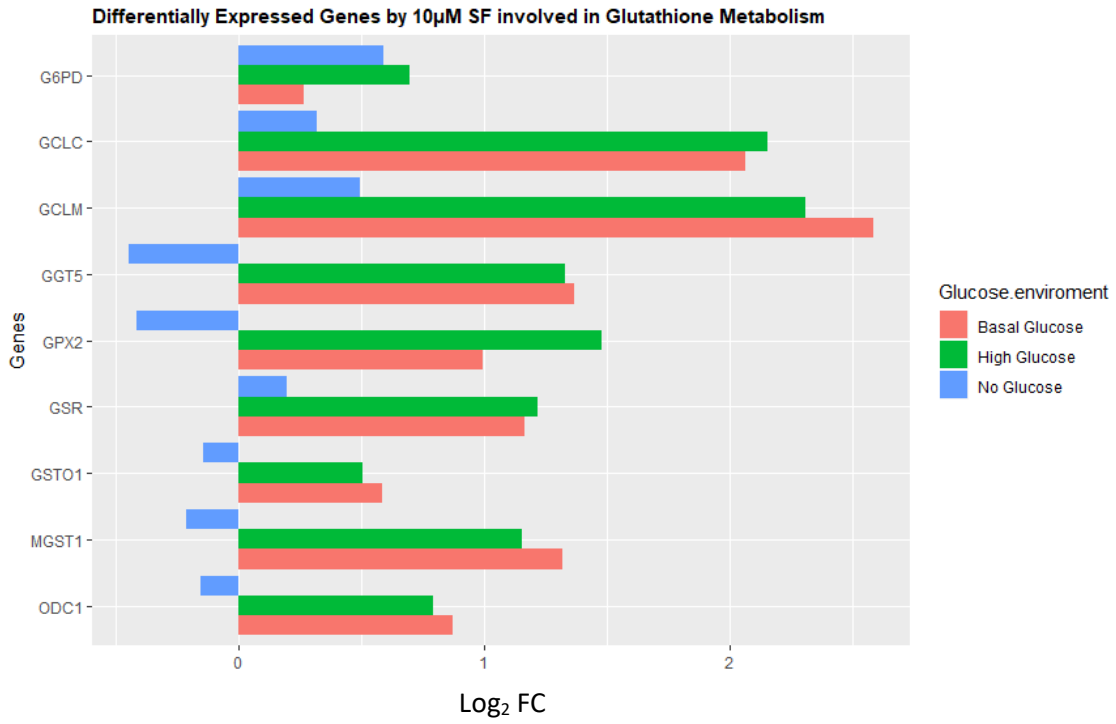

Figure 4.9. Top enriched differentially expressed genes from the glutathione metabolism gene set. These top enriched genes also referred to as the leading edge are defined as those which contributed most to the set enrichment score; reflecting their degree of overrepresentation in a running-sum metric. This is calculated using both the fold enrichment and degree of significance (p-value). Genes were plotted against the $\log_2$ of the fold change under the various glucose environments: no (0 mM), basal (5.5 mM), and high glucose (25 mM). Glucose-6-Phosphate (G6PD), Glutamate-Cysteine Ligase Catalytic Subunit (GCLC), Glutamate-Cysteine Regulatory Subunit (GCLM), Gamma-Glutamyltransferase 5 (GGT5), Glutathione Peroxidase2 (GPX2), Glutathione Reductase (GSR), Glutathione S-Transferase Omega-1 (GSTO1), Microsomal Glutathione S-transferase 1 (MGST1) and Ornithine Decarboxylase 1 (ODC1). All the genes in both the basal and the high glucose environment but not in the no Glucose were statistically significant following multiple testing ($q < 0.05$).

For the metabolism of xenobiotics by cytochrome P450 gene set, (**figure 4.10**) the analysis further reinforced the idea that in the absence of glucose NRF2 activation does not occur, thereby suggesting glucose is necessary for NRF2 activation. The analysis identified that both basal and high glucose SF treatment resulted in a more than 4-fold increase in two genes belonging to the Aldo-Keto reductase family: AKR1C1 and AKR1C2. Again in the presence of no glucose, this effect was not observed. The analysis also identified SF in both basal and high glucose inducing two genes that were also enriched in the glutathione metabolism gene set GSTO1 and MGST1, thereby suggesting a link between the glutathione and metabolism of

xenobiotics by cytochrome P450 gene sets. GSTO1 and MGST1 both are involved in conjugating glutathione to xenobiotics so that they can be detoxified.

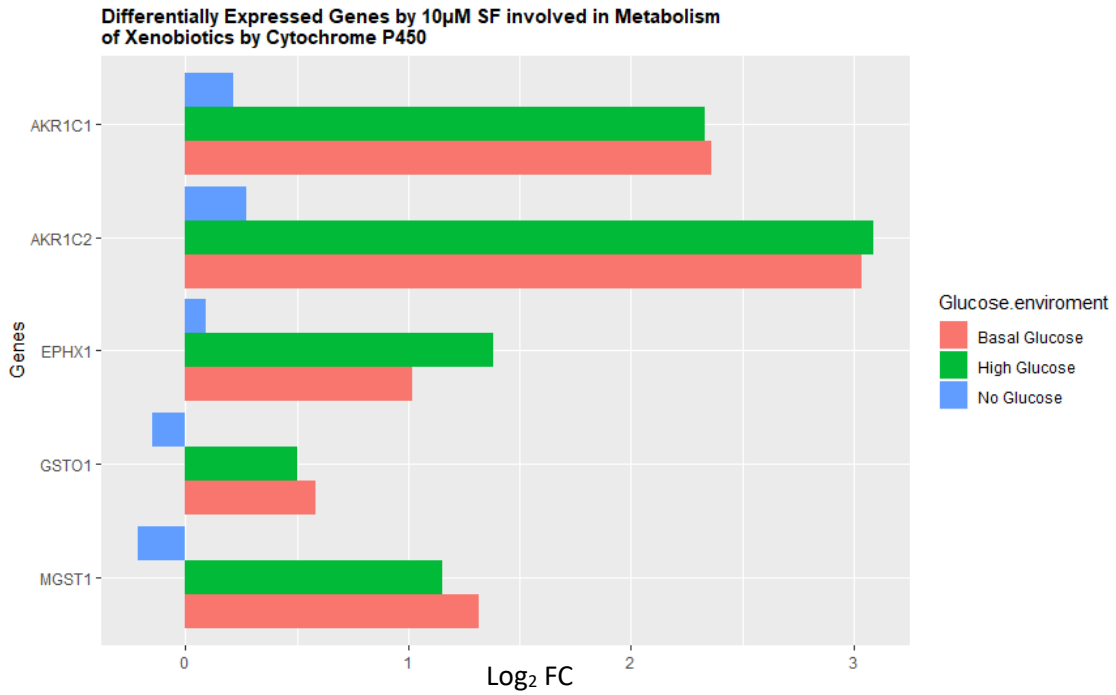

Figure 4.10. Top enriched differentially expressed genes from the metabolism of xenobiotics by cytochrome P450 gene set. These top enriched genes also referred to as the leading edge are defined as those which contributed most to the set enrichment score; reflecting their degree of overrepresentation in a running-sum metric. This is calculated using both the fold enrichment and degree of significance (p-value). The x-axis represents the $\log_2$ fold change whilst, the y-axis represents the genes of interest Aldo-Keto Reductase 1 Family Member C1 (AKR1C1), Aldo-Keto Reductase 1 Family Member C2 (AKR1C2), Epoxide Hydrolase 1 (EPHX1), Glutathione S-transferase Omega-1 (GSTO1), Microsomal Glutathione S-transferase 1 (MGST1). All the genes in both the basal and the high glucose environment but not in the no glucose were statistically significant following multiple testing ($q < 0.05$).

Whilst the analysis from the glutathione metabolism and metabolism of xenobiotics by cytochrome P450 gene sets showed that SF as expected upregulated genes involved in the antioxidant response through NRF2, quite a few of the NRF2 target genes such as NQO1 were however missing from the GSEA predetermined gene sets. Therefore, to make sure that no information is lost, the analysis was further expanded. Additional NRF2 target genes involved in phase 1, 2, and 3 metabolisms along with antioxidant glutathione metabolism, antioxidant TXN-based, all that have reported having an ARE

sequence were also individually assessed from the output table of the voom plot. These genes were selected from the following publications (Hayes and Dinkova-Kostova, 2014, Thimmulappa *et al*., 2002, Tebay *et al*., 2015, Chorley *et al*., 2012, Malhotra *et al*., 2010). The results are displayed in the following table 4.3 and bar plots were also carried out to visualize and compare the results in the different glucose environments shown in figures 4.11-4.14.

Table 4.3 A selection of differentially expressed genes in response to SF under various glucose concentrations involved in detoxification pathways

Ensembl ID	Gene Symbol	Gene	SF Log_2 Fold Change vs Control NG	SF Log_2 Fold Change vs Control HG	SF Log_2 Fold Change vs Control BG
Phase I enzymes					
ENSG00000198074	AKR1B10	Aldo-keto reductase family member 1 B10	0.26	3.58[3]	3.48[3]
ENSG00000187134	AKR1C1	Aldo-keto reductase family member 1 C1	0.21	2.33[3]	2.36[3]
ENSG00000165092	ALDH1A1	Aldehyde dehydrogenase family member 1 A1	-0.21	0.79[2]	1.00[3]
ENSG00000164904	ALDH7A1	Aldehyde dehydrogenase family member 7 A1	-0.41	-0.41[1]	-0.43[1]
ENSG00000159228	CBR1	Carbonyl reductase C1	-0.07	0.84[1]	0.29
ENSG00000019186	CYP24A1	Cytochrome P450, family 24, member A1	-0.13	1.41[1]	1.75[3]
ENSG00000143819	EPHX1	Expoxide hydrolase 1	0.09	1.38[3]	1.02[2]
ENSG00000106853	PTGR1	Prostaglandin reductase 1	0.15	2.39[3]	2.39[3]
ENSG00000198848	CES1	Carboxylesterase 1	0.72[1]	0.73[1]	0.72[1]
Phase II enzymes					
ENSG00000134202	GSTM3	Glutathione-S-transferase M3 brain	-0.22	0.17	-0.20
ENSG00000168765	GSTM4	Glutathione-S-transferase Mu 4	-0.34	-0.55[1]	-0.55[1]
ENSG00000148834	GSTO1	Glutathione-S-transferase omega-1	-0.15	0.50[1]	0.59[1]

ENSG00000008394	MGST1	Microsomal glutathione S-transferase 1	-0.21	1.15[2]	1.32[2]
ENSG00000181019	NQO1	NAD(P)H dehydrogenase, quinone (1)	-0.13	1.64[3]	1.71[3]
ENSG00000196502	SULT1A1	Sulfotransferase 1A1	-0.43	0.61	0.80[1]
ENSG00000197165	SULT1A2	Sulfotransferase 1A2	-0.58[1]	1.09[2]	1.03[2]
Phase III enzymes					
ENSG00000103222	ABCC1	Multidrug resistance-associated protein 1 (MRP1)	0.36	0.68[2]	0.65[2]
ENSG00000023839	ABCC2	Multidrug resistance-associated protein 2 (MRP2)	0.44	1.07[3]	1.18[2]
ENSG00000108846	ABCC3	Canalicular multispecific organic anion transporter 2	-0.1	1.72[3]	1.3[3]
ENSG00000118777	ABCG2	ATP-binding cassette super-family G member 2	-0.21	0.63[3]	0.91[3]
Antioxidant response enzymes					
ENSG00000001084	GCLC	Glutamate-cysteine ligase catalytic subunit	0.32	2.15[3]	2.06[3]
ENSG00000023909	GCLM	Glutamate-cysteine ligase regulatory subunit	0.50	2.31[3]	2.58[3]
ENSG00000173221	GLRX	Glutaredoxin-1	0.075	0.88[2]	0.41[1]
ENSG00000176153	GPX2	Glutathione Peroxidase 2	-0.42	1.48[1]	0.99[1]
ENSG00000104687	GSR	Glutathione Reductase	0.19	1.22[3]	1.17[3]
ENSG00000196517	SLC6A9	Glycine transporter 1	-0.052	-0.93[1]	-0.75[1]
ENSG00000151012	SLC7A11	Cysteine/Glutamate transporter	0.63	1.41	1.45[1]

ENSG00000117450	PRDX1	Peroxiredoxin 1	-0.013	0.63[1]	0.60[1]
ENSG00000271303	SRXN1	Sulfiredoxin 1	0.35	2.43[3]	2.44[3]
ENSG00000136810	TXN	Thioredoxin	0.091	0.93[1]	0.87[1]
ENSG00000198431	TXNRD1	Thioredoxin reductase 1	0.99	2.20[1]	0.99[2]

Adjusted P values of fold change: $p^1<0.05$, $p^2<0.001$, $p^3<0.0001$. The adjusted p-values were obtained through a linear model by the limma function. The gene counts were first converted to log counts per million. Limma then plots the log-cpm for each experimental design control vs treatment. The residual standard deviations for every gene is fit to a global mean-variance trend across all the genes of all samples. In the final step, precision weights are calculated for each gene.

Phase I enzymes which are mainly cytochrome P450 involve the transfer of hydroxyl, carboxyl, or an amino group to the toxic compound (Lin *et al*., 2016). In the analysis shown in figure 4.11, the Aldo-Keto reductase family (AKR) had the largest increase in expression, followed by prostaglandin reductase (PTGR), with SF treatment in both basal and high glucose resulting in a 4-fold increase in PTGR activity. In the no glucose environment, PTGR activity was also abolished. The analysis identified that SF also upregulated in both basal and high glucose several aldehyde dehydrogenases along with several genes from the cytochrome P450 family. These effects were not observed in the no glucose environment (**figure 4.11 and table 4.3**).

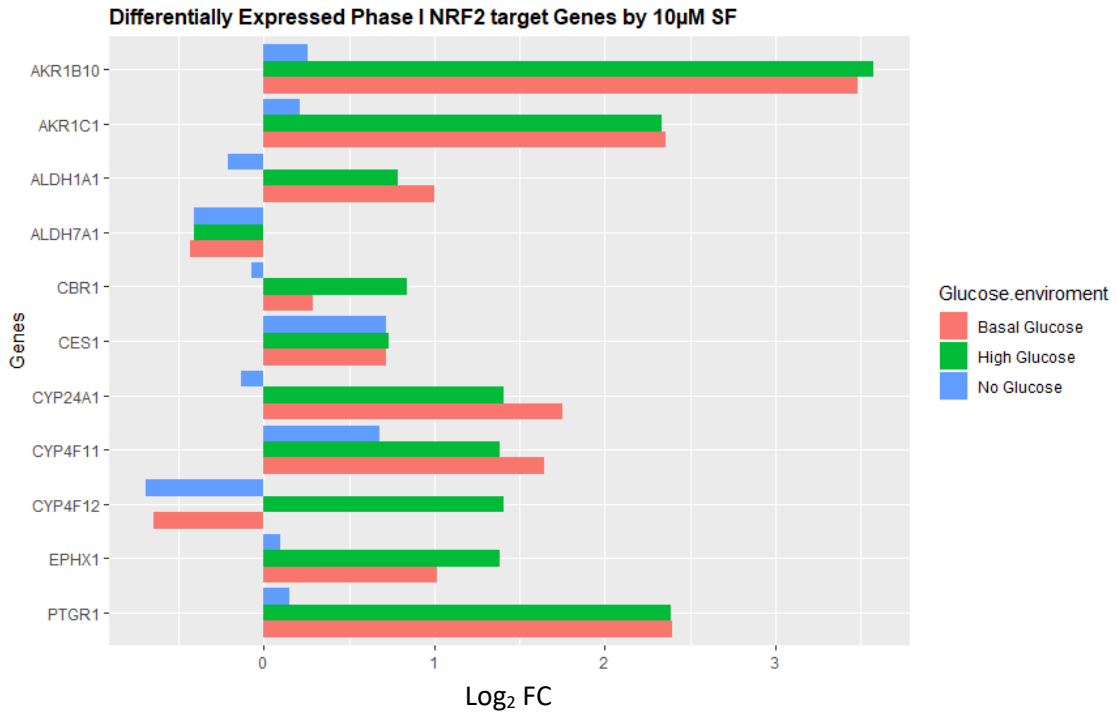

Figure 4.11. Induction of a selection of phase I genes by 10 μM SF in different glucose environments. The x-axis represents the log_2 fold change whilst, the y-axis represents the genes of interest. These include Aldo-Keto Reductase 1 Family Member B10 (AKR1B10), Aldo-Keto Reductase 1 Family Member C1 (AKR1C1), Aldehyde Dehydrogenase 1 Family Member A1, Aldehyde Dehydrogenase 7 Family Member A1 (ALDH7A1), Carbonyl Reductase (CBR1), Carboxylesterase (CES1), Cytochrome P450 Family 24 Subfamily A Member 1 (CYP24A1), Cytochrome P450 Family 4 Subfamily F11 (CYP4F11), Cytochrome P450 Family 4 Subfamily F12 (CYP4F12), Epoxide Hydrolase 1 (EPHX1) and Prostaglandin Reductase (PTGR). The statistical significance of the DEG can be found in table 4.3.

Phase II enzymes are also referred to as transferases as they can transfer the modified metabolite to hydrophilic molecules. From figure 4.12, SF treatment resulted in a large induction, more than 3-fold in both basal and high glucose in NQO1, thereby confirming the qt-PCR data identified in chapter 3 (**figure 3.2b and 3.5b**). In addition, the analysis identified SF upregulating two members of the sulfotransferase family (SULT1A1/A2) involved in the conjugation of a wide range of xenobiotics rendering them more water soluble to facilitate its excretion. The analysis also identified SF downregulating the expression of two glutathione S-transferase genes (GSTM3/M4) whose function is involved in conjugating glutathione to xenobiotics, thereby potentially suggesting that these two GSTMs are not needed for the detoxification of xenobiotics. What is striking is that all of the phase II genes analyzed were instead downregulated in the no glucose environment (**figure 4.12, table 4.3**).

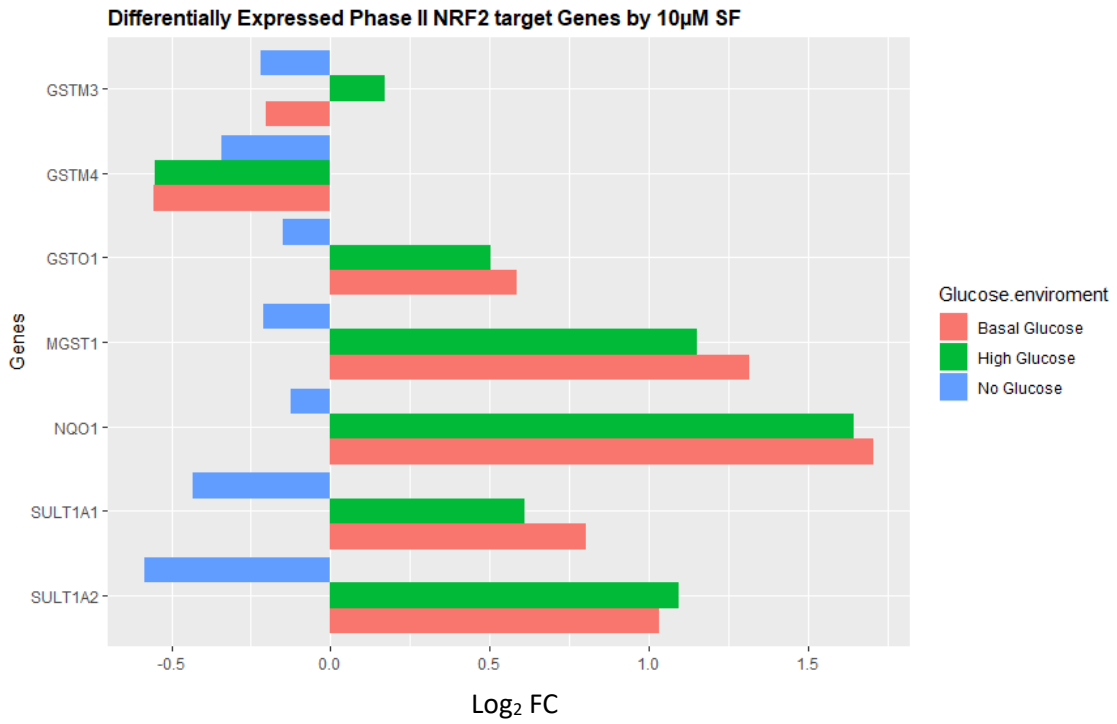

Figure 4.12. Induction of a selection of phase II genes by 10 μM SF in different glucose environments. The x-axis represents the log_2 fold change whilst, the y-axis represents the genes of interest. These include Glutathione-S-transferase Mu 3 (GSTM3), Glutathione-S-transferase Mu 4 (GSTM4), Glutathione-S-transferase Omega 1, (GSTO1), Microsomal Glutathione S-transferase 1 (MGST1), NAD(P)H Dehydrogenase Quinone 1, (NQO1), Sulfotransferase 1A1 (SULT1A1), Sulfotransferase 1A2 (SULT1A2). The statistical significance of the DEG can be found in table 4.3.

After phase II enzymes have increased the hydrophobicity of the xenobiotic, this facilitates the excretion of the toxic compound by phase III enzymes. In the analysis, it was identified that SF in the basal and high glucose environment upregulated several multidrug resistance-associated proteins such as ABCC1, ABCC2, ABCC3, and ABCG2: thereby identifying several different mechanisms on how SF enables liver cells to eliminate toxic substrates (**figure 4.13 and table 4.3**) In the no glucose environment it was identified no induction of the multidrug resistance-associated proteins (**figure 4.13 and table 4.3**).

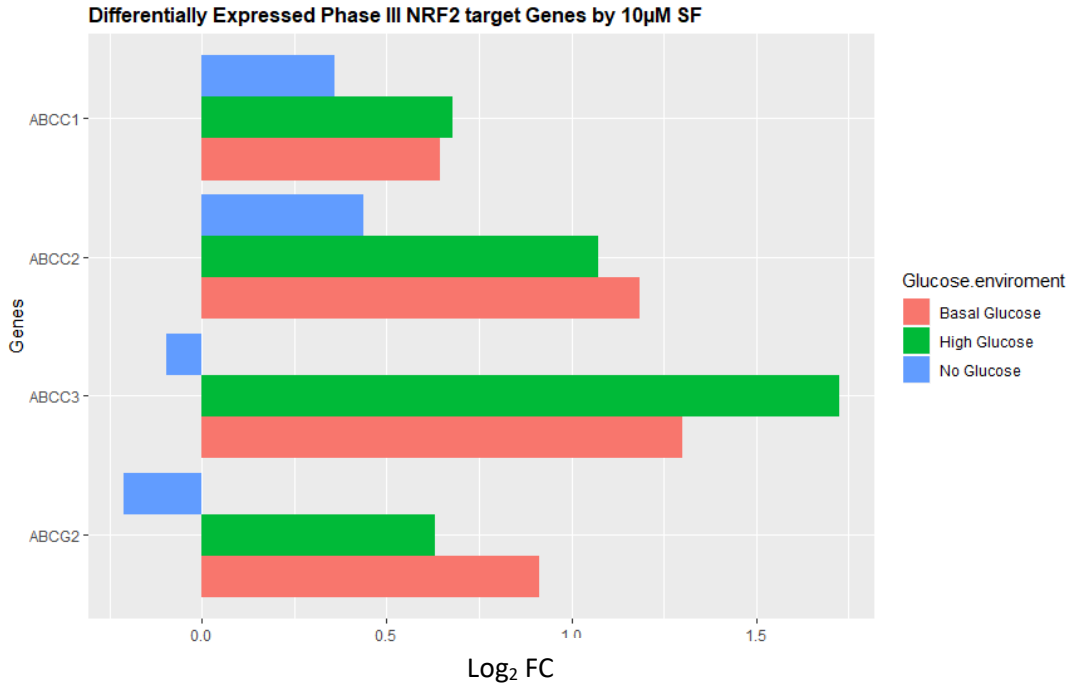

Figure 4.13. Induction of a selection of phase III genes by 10 μM SF in different glucose environments. The x-axis represents the log_2 fold change whilst, the y-axis represents the genes of interest. These include Multidrug resistance-associated protein 1 (ABCC1), Multidrug resistance-associated protein 2 (ABCC2), Canalicular multispecific organic anion transporter 2 (ABCC3), and ATP-binding cassette superfamily G member 2 (ABCG2). The statistical significance of the DEG can be found in table 4.3.

The data from figure 4.14, revealed that SF in the basal and high glucose environments upregulated genes involved in two different mechanisms through which NRF2 induces the antioxidant response: inducing genes involved in glutathione production, as well as thioredoxin reductase (TXNRD1). SF treatment resulted in a 4-fold increase in TXNRD1 compared to a 2-fold increase in both no and basal glucose. TXNRD1 functions in maintaining thioredoxin (TXN) in the reduced state through the reduction of $CySS^-$ to Cys in the presence of NADPH. SF also induced the expression of the SLC7A11 transporter to the same extent in both glucose environments, whose function is importing cysteine from the media into the cell. SF treatment also resulted in a 3-fold increase in the high glucose environment in glutathione peroxidase (GPX) and a 2-fold increase in peroxiredoxin (PRDX1) in both glucose environments whose functions are involved in reducing hydrogen peroxide through the action of reduced glutathione. Finally, SF treatment resulted in a 4-fold increase in both basal and high glucose in sulfiredoxin (SRXN1) involved in reducing the cysteine-sulfinic acid formed under exposure to oxidants. The most prominent finding from figure 4.14 is the identification of a greater induction of the antioxidant genes in the high glucose environment compared to basal and no, thereby identifying a mechanism on how SF increases the antioxidant response, to suppress the increased ROS induced by the excessive glucose.

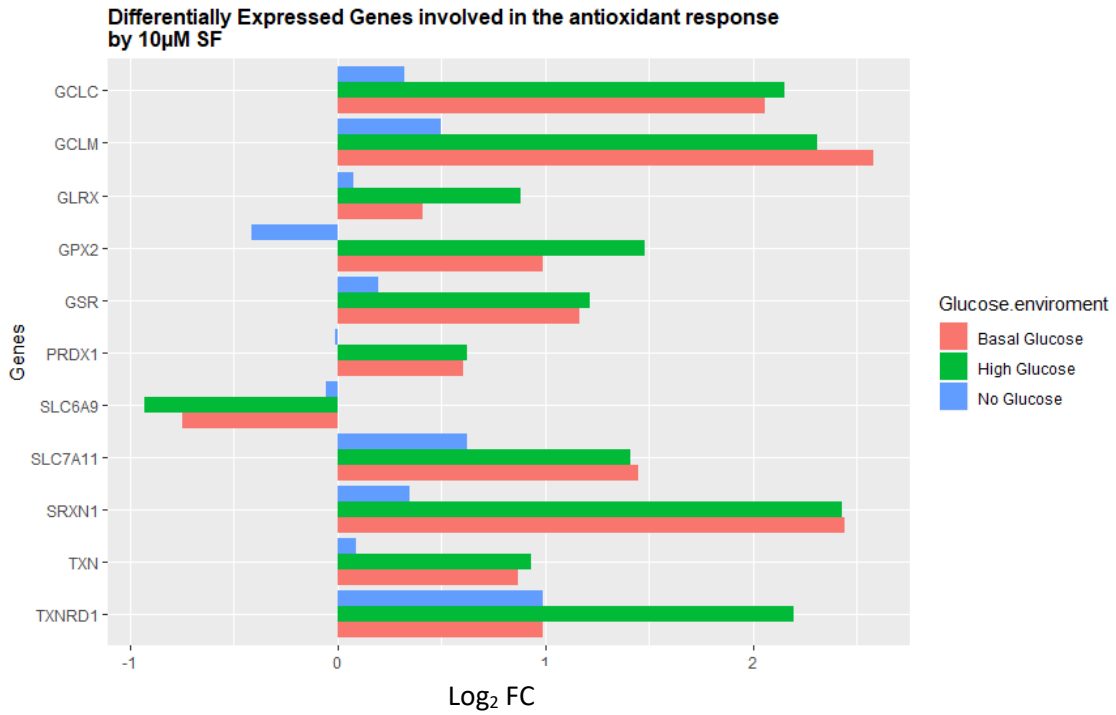

Figure 4.14. Induction of a selection of genes involved in the antioxidant response by 10 μM SF in different glucose environments. The x-axis represents the log_2 fold change whilst, the y-axis represents the genes of interest. These include Glutamate-Cysteine Ligase Catalytic Subunit (GCLC) and the Glutamate-Cysteine Regulatory Subunit (GCLM), Glutaredoxin-1 (GLRX), Glutathione Peroxidase (GPX2), Glutathione Reductase (GSR), Peroxiredoxin-1 (PRDX1), Sodium and Chloride Dependent Glycine Transporter 1 (SLC6A9), Cystine/Glutamate Transporter (SLC7A11), Sulfiredoxin-1 (SRXN1), Thioredoxin (TXN), Thioredoxin Reductase 1 (TXNRD1). The statistical significance of the DEG can be found in table 4.3.

This analysis also revealed that under no glucose, despite the presence of SF NRF2 activation does not occur, as none of the NRF2 target genes are induced and failed to reach statistical significance.

4.3.5. Characterizing SF effect on genes linked to central metabolism in hepatocytes under different metabolic states

In the previous chapter, physiological concentrations of SF resulted in a decrease in lipid accumulation through the Oil Red O assay (**figure 3.9b**), along with upregulation of CPT1a and downregulating the gene responsible for the synthesis of fatty acid synthase FASN (**figure 3.3 a and b**). In addition, the high glucose environment showed the upregulation of three essential genes involved in the PPP. To gain a mechanistic understanding of how these processes are interconnected, the next section of the analysis focused on characterising SF's effect on genes linked to central metabolism in hepatocytes cultured in the different glucose environments.

4.3.5.1 SF impacts key genes involved in lipid metabolism:

GSEA did not identify any pathway related to lipid metabolism being enriched. Perhaps this was due to the limited sample size utilized in the study. To assess, therefore, how SF affects lipid metabolism, genes involved in lipid metabolism (both biosynthesis and oxidation) were consequently carried out manually by selecting genes from the output table of the voom plot. Key selected genes that NRF2 influences were obtained from the following papers (Hayes and Dinkova-Kostova, 2014, Tebay *et al*., 2015). Manual identification revealed that SF in both the basal and the high glucose environment profoundly affected a wide range of genes involved in lipid metabolism (both oxidation and biosynthesis (**table 4.4 and figure 4.15**) therefore providing evidence that SF is interfering in this biological process despite the gene set not passing the enrichment threshold. The most exciting finding is that SF downregulated the mRNA of three crucial transcription factors involved in lipid metabolism: SREBF1 regulates the activity of genes in lipid biosynthesis. SREBF2 regulates the activity of genes in cholesterol homeostasis and CCAAT enhancer-binding protein A (CEBPA), a transcription involved in adipogenesis, the synthesis of new fat cells (**table 4.4 and figure 4.15**). CEBPA was differentially expressed in all three-glucose environments, whilst SREBF1 in basal and high glucose and SREBF2 only in basal glucose. Although FASN was not differentially expressed, the activity of this gene along with FADS1 (involved in adding double bonds to synthesize monounsaturated fatty acids) is regulated by SREBF1.

The other promising finding emerging from this analysis was the downregulation in the activity of acetyl CoA carboxylase (ACACA) (only in the high glucose environment q=0.01) coupled with an increase in malonyl CoA decarboxylase (MLYCD). ACACA is involved in the rate-limiting step in fatty acid biosynthesis by converting acetyl-CoA to malonyl CoA, whilst MLYCD essentially catalyzes the reverse reaction, breaking down

malonyl CoA back to acetyl CoA. Acetyl CoA is an intermediate in a wide range of cellular processes. The analysis also revealed SF interfering with β-oxidation by upregulating CPT1a in both glucose environments, confirming the results in chapter 3 (**figure 3.3a and 3.6a**) but also downregulating the activity of two genes involved in the synthesis of triglycerides: diacylglycerol O-acyltransferase 1/2 (DGAT1/2) (Yen *et al*., 2008). Further analysis revealed that SF downregulated the long-chain-fatty acid-CoA ligase 1/5 (ACSL1) gene, whilst at the same time upregulating the ACSL5 gene. These genes are involved in converting free long-chain fatty acids into fatty acyl-CoA esters. These fatty acyl-CoA esters are then transported to the mitochondrial through the action of CPT1a to fatty acylcarnitine. SF also affected the activity of the fatty-acid binding protein 1/5. These proteins located in the cytoplasm bind long chain fatty acids as well as other hydrophobic ligands.

Table 4.4 Genes differentially expressed in response to SF under various glucose concentrations involved in lipid metabolism

Ensembl ID	Gene Symbol	Gene	SF Log_2 Fold Change vs Control NG	SF Log_2 Fold Change vs Control HG	SF Log_2 Fold Change vs Control BG
Lipid metabolism					
ENSG00000278540	ACACA	Acetyl CoA carboxylase 1	-0.06	-0.51[1]	-0.18
ENSG00000122971	ACADS	Acyl CoA dehydrogenase	-0.45	-0.22	-0.52[1]
ENSG00000151726	ACSL1	Long-chain-fatty acid-CoA ligase 1	0.25	-0.56[1]	-0.35[1]
ENSG00000197142	ACSL5	Long-chain-fatty acid-CoA ligase 5	0.57[1]	0.90[3]	1.14[3]
ENSG00000245848	CEBPA	CCAAT enhancer binding protein A	-0.83[1]	-1.19[3]	-1.44[3]
ENSG00000198848	CES1	Carboxylesterase	0.72[1]	0.74[1]	0.72[1]
ENSG00000110090	CPT1A	Carnitine palmitoyltransferase I	0.20	0.98[2]	0.78[2]
ENSG00000185000	DGAT1	Diacylglycerol O-acyltransferase 1	-0.36	-0.51	-0.85[1]
ENSG00000062282	DGAT2	Diacylglycerol O-acyltransferase 2	-1.09	-0.70	-0.85[1]
ENSG00000163586	FABP1	Fatty Acid Binding Protein 1	-1.23[1]	-0.49	-0.97[1]
ENSG00000164687	FABP5	Fatty Acid Binding Protein 5	-0.83[1]	0.65[1]	0.74[3]
ENSG00000149485	FADS1	Fatty acid desaturase 1	0.20	-0.54[1]	-0.37[1]
ENSG00000103150	MLYCD	Malonyl-CoA decarboxylase	0.02	2.04[3]	1.69[3]
ENSG00000072310	SREBF1	Sterol regulatory element-binding transcription factor 1	-0.36	-0.53[1]	-0.56[1]
ENSG00000198911	SREBF2	Sterol regulatory element-binding transcription factor 2	0.02	-0.3	-0.32[1]

Adjusted P values of fold change: $p^1<0.05$, $p^2<0.001$, $p^3<0.0001$. The adjusted p-values were obtained through a linear model by the limma function. The gene counts were first converted to log counts per million. Limma then plots the log-cpm for each experimental design control vs treatment. The residual standard deviations for every gene is fit to a global mean-variance trend across all the genes of all samples. In the final step, precision weights are calculated for each gene.

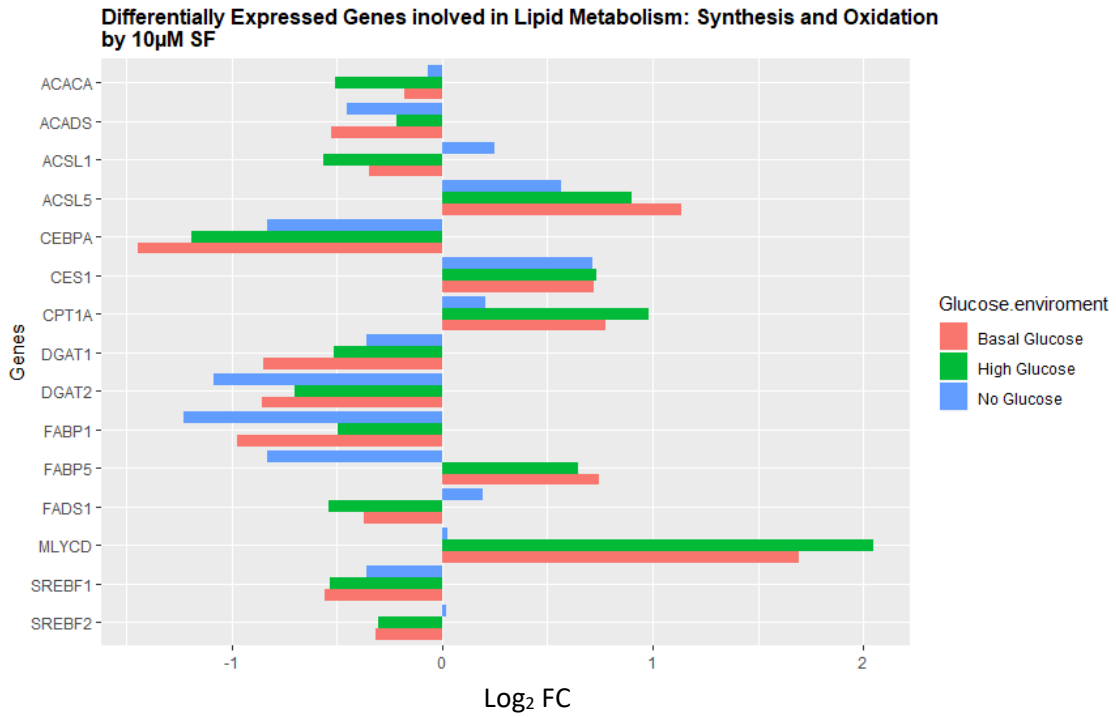

Figure 4.15. Induction of a selection of genes involved in lipid metabolism by 10 μM SF in different glucose environments. The x-axis represents the log_2 fold change whilst, the y-axis represents the genes of interest. These include Acetyl-CoA Carboxylase A (ACACA), Acyl-CoA Dehydrogenase Short Chain (ACADS), Long Chain-Fatty Acid-CoA Ligase 1/Ligase 5 (ASCL1/ASCL5), CCAAT/enhancer Binding Protein Alpha (CEBPA), Carboxylesterase 1 (CES1), Carnitine Palmitoyltransferase I (CPT1a), Diacylglycerol O-acyltransferase 1/2 (DGAT1/2), Fatty Acid Binding Protein 1/5 (FABP1/5), Fatty Acid Desaturase 1 (FADS1), Malonyl-CoA Decarboxylase Mitochondrial (MLYCD), Sterol Regulatory Element Binding Transcription Factor 1/ 2 (SREBF1/2). Statistical significance of the DEG can be found in table 4.4

4.3.5.2 SF affects a wide range of additional metabolic processes.

GSEA in a high glucose environment (**figure 4.7**) revealed SF rewiring hepatic metabolism by affecting a wide range of additional metabolic processes including upregulation of oxidative phosphorylation, fructose, and mannose metabolism, one carbon pool by folate, along with downregulation of histidine and serine, glycine, and threonine metabolism. Detailed analysis on how SF affects each gene set has been explained in the section below and the next chapter 5.

4.3.5.3 SF affects Carbohydrate metabolism and Pentose Phosphate

Table 1 (Appendix) revealed that in the high glucose environment only SF induced genes in the PPP, although following multiple corrections the gene set failed to reach significance (q=0.08). A more detailed analysis of the enriched core genes in the gene set is covered in chapter 5.

4.3.5.4 SF affects oxidative phosphorylation in the high glucose environment

Figure 4.7 identified that in the presence of excess glucose, SF upregulates the gene set oxidative phosphorylation implying SF affects and therefore increases the activity of proteins involved in the Electron Transport Chain. A closer assessment of the pathway revealed that the top two upregulated genes are: ATP6V1E1 and ATP5G1. Both proteins are involved in regulating the activity of complex V, ATP synthase. Despite the reduction in mitochondrial respiration by SF described in (**figure 3.12 b**) individual genes in the OxPhos pathway were upregulated by SF. This could be a consequence/response of the mitochondrial respiration reduction, but the mechanisms are unknown.

4.3.5.5 SF affects both glycine, serine, and threonine along with one carbon metabolism in both basal and high glucose

The analysis from figures 4.5-4.7 stumbled upon a novel finding. SF downregulates the serine, glycine, and threonine gene set in all three glucose environments along with upregulation of one pool by folate, better known as one carbon metabolism.

One carbon metabolism is series of biosynthetic reactions largely derived from two amino acids; serine and glycine. Analysis of both gene sets (serine, glycine, and

threonine along with one carbon pool by folate) has been conducted in the following chapter 5.

4.3.5.6 SF affects histidine metabolism in both high and no glucose.

Another interesting finding that no studies have reported in the literature was SF downregulating genes involved in histidine metabolism. Histidine metabolism involves both its biosynthesis but also its degradation. GSEA revealed that SF downregulated the activity of four genes involved histidine catabolism to glutamate: in the high glucose environment SF led to a 1.7-fold downregulation in the histidine ammonia ligase (HAL) gene. HAL catalyzes the first reaction in histidine catabolism, the nonoxidative deamination of L-histidine to *trans*-urocanic acid or urocanate. In the basal and no glucose environment, HAL was also downregulated but failed to reach significance (**table 4.5 and figure 4.16**). SF also resulted in a 4-fold downregulation in both basal and high glucose in the urocanase (URCO1) gene. URCO1 catalyzes the second step in the degradation of histidine, the hydration of urocanate into imidazolonepropionate. SF also resulted in a 2-fold downregulation in both basal and high glucose environments of the imidazolonepropionase (AMDHD1) gene. AMDHD1 converts 4-imidazolone-5-propanoate to N-formimidoyl-L-glutamate (**table 4.5 and figure 4.16**). The final gene that was found to be downregulated by SF again in both basal and high glucose environments, still involved in histidine catabolism is the aminoacylase 3 (ACY3). ACY3 removes the acetyl group from N-acetyl glutamate to generate glutamate. The acyl group is what provides stability for the amino acid, making it more resistant to degradation. The data therefore may suggest a build of the amino acid histidine and thereby potentially implying that SF is redirecting histidine to other metabolic processes.

The analysis also identified SF downregulating several genes in the family of aldehyde dehydrogenase in the different metabolic states: aldehyde dehydrogenase 1 family member B1 (ALDH1B1), aldehyde dehydrogenase 9 family member A1 (ALDH9A1), and aldehyde dehydrogenase 7 family member A1 (ALDH7A1). Aldehyde dehydrogenase utilizes NADPH to convert aldehydes to carboxylic acids. Therefore downregulation of all these family of enzymes may suggest SF inhibiting these reactions so that the NADPH may be redirected to support the antioxidant response, glutathione production/utilization (**figure 4.14**). Results are shown in table 4.5 and figure 4.16.

Table 4.5 Top enriched differentially expressed genes from the histidine metabolism gene set by 10 μM SF in different glucose environments

Ensembl ID	Gene Symbol	Gene	SF Log_2 Fold Change vs Control NG	SF Log_2 Fold Change vs Control HG	SF Log_2 Fold Change vs Control BG
Histidine metabolism					
ENSG00000132744	ACY3	Aminoacylase 3	-1.95	-1.34[2]	-1.61[3]
ENSG00000137124	ALDH1B1	Aldehyde Dehydrogenase 1 family member B1	-0.87[1]	0.02	-0.14
ENSG00000006534	ALDH3B1	Aldehyde Dehydrogenase 3 family member B1	-0.57	-1.21[2]	-1.33[3]
ENSG00000164904	ALDH7A1	Aldehyde Dehyrogenase 7 family member A1	-0.41	-0.41[1]	-0.43[1]
ENSG00000143149	ALDH9A1	Aldehyde Dehydrogenase 9 family member A1	0.06	-0.46[1]	-0.33[1]
ENSG00000139344	AMDHD1	Imdidazolonepropinase	0.1	-1.25[3]	-1.03[2]
ENSG00000084110	HAL	Histidine ammonia ligase	-0.57	-0.74[1]	-0.49
ENSG00000159650	UROC1	Urocanase	-0.09	-2.63[1]	-2.30[1]

Adjusted P values of fold change: $p^1<0.05$, $p^2<0.001$, $p^3<0.0001$. The adjusted p-values were obtained through a linear model by the limma function. The gene counts were first converted to log counts per million. Limma then plots the log-cpm for each experimental design control vs treatment. The residual standard deviations for every gene is fit to a global mean-variance trend across all the genes of all samples. In the final step, precision weights are calculated for each gene.

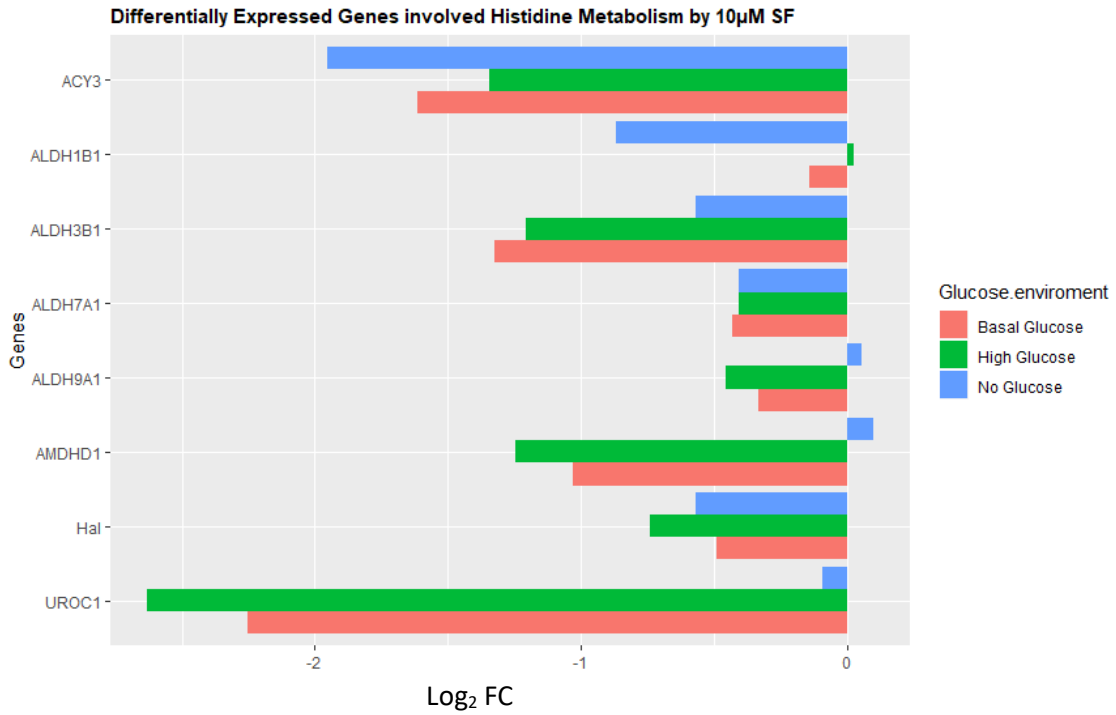

Figure 4.16. Top enriched differentially expressed genes from the histidine metabolism gene set by 10 μM SF in different glucose environments. The -axis represents the log_2 fold change whilst, the y-axis represents the genes of interest. These include Aminoacylae 3 (ACY3), Aldehyde Dehydrogenase 1 Family Member B1(ALDH1B1), Aldehyde Dehydrogenase 3 Family Member B1 (ALDH3B1), Aldehyde Dehydrogenase 7 Family Member A1 (ALDH7A1), Aldehyde Dehydrogenase 9 Family Member A1 (ALDH9A1), Imdidazolonepropinase (AMDHD1), Histidine Ammonia Ligase (Hal), Urocanase (UROC1). Statistical significance of the DEG can be found in table 4.5

4.3.5.7 SF inhibits genes involved in lysine downregulation in basal glucose environments

GSEA identified that in the basal glucose environment, SF downregulated the gene set lysine degradation. Therefore, like with the other gene sets, the DEG were extracted and plotted in bar plots to gain a better understanding, of how SF targets this specific pathway. The analysis revealed that essentially SF downregulated (**table 4.6 figure 4.17** the first two and the last two genes involved in the breakdown of lysine to carnitine, potentially suggesting more lysine in the system to be converted to carnitine for FA metabolism. SF also downregulated greater than 8-fold the histone-lysine-N-methyltransferase (SETD7) gene (**figure 4.17 and table 4.6**). This effect was only identified in the basal glucose environment. SETD7 function is to catalyze the first step in the breakdown of lysine to carnitine,(lysine to N6-ME-lysine). SF also

downregulated by 1.7-fold the euchromatic histone-lysine-N-methyltransferase 2 (EHMT2), involved in converting N6-ME-Lysine to N, N-trimethyl lysine, along with downregulating about 1.5-fold both ALDH7A1 and ALDH9A1 which convert 4-trimethylammoniobutanal to 4-trimethylammoniobutanoate (**figure 4.17 and table 4.6**). SF also led to 1.4-fold downregulation in both basal and high glucose in HADH, involved in the breakdown of S-3-Hydroxy-butanoyl-CoA to Acetoacetyl-CoA (**figure 4.17 and table 4.6**). Acetoacetyl-CoA feeds into the TCA cycle. Finally, my results also showed that SF led to a 1.5-fold downregulation in the 2-oxoglutarate dehydrogenase, mitochondrial (OGDHL) gene, involved in the breakdown of 2-oxoglutarate to succinate and a 128-fold downregulation in the histone-lysine-N-methyltransferase, H3 lysine-36 specific (NSD1) gene, a histone-lysine-N-methyltransferase, potentially implying, that SF was inhibiting the transfer of methyl groups from the lysine to histones. Results can be identified in figure 4.17 and table 4.6.

Table 4.6 Top enriched differentially expressed genes from the lysine degradation gene set by 10 μM SF in different glucose environments

Ensembl ID	Gene Symbol	Gene	SF Log_2 Fold Change vs Control NG	SF Log_2 Fold Change vs Control HG	SF Log_2 Fold Change vs Control BG
Lysine degradation					
ENSG00000145391	SETD7	Histone-lysine-N-Methyltransferase	-0.02	0.40	-3.65[2]
ENSG00000138796	HADH	Hydroxyacyl-Coenzyme A dehydrogenase	-0.03	-0.44[2]	-0.57[1]
ENSG00000204371	EHMT2	Euchromatic histone-lysine-N-methyltransferase 2	-0.65	-0.31	-0.71[1]
ENSG00000165671	NSD1	Histone-lysine-N-methyltransferase, H3 lysine-36 specific	3.63	0.50	-7.53[2]
ENSG00000164904	ALDH7A1	Aldehyde Dehydrogenase 7 family member A1	-0.41	-0.41[1]	-0.43[1]
ENSG00000143149	ALDH9A1	Aldehyde Dehydrogenase 9 family member A1	0.06	-0.46[1]	-0.33[1]
ENSG00000197444	OGDHL	2-Oxoglutrate dehydrogenase like, mitochondrial	-0.91	-0.05	-0.60[1]

Adjusted P values of fold change: $p^1<0.05$, $p^2<0.001$, $p^3<0.0001$. The adjusted p-values were obtained through a linear model by the limma function. The gene counts were first converted to log counts per million. Limma then plots the log-cpm for each experimental design control vs treatment. The residual

standard deviations for every gene is fit to a global mean-variance trend across all the genes of all samples. In the final step, precision weights are calculated for each gene.

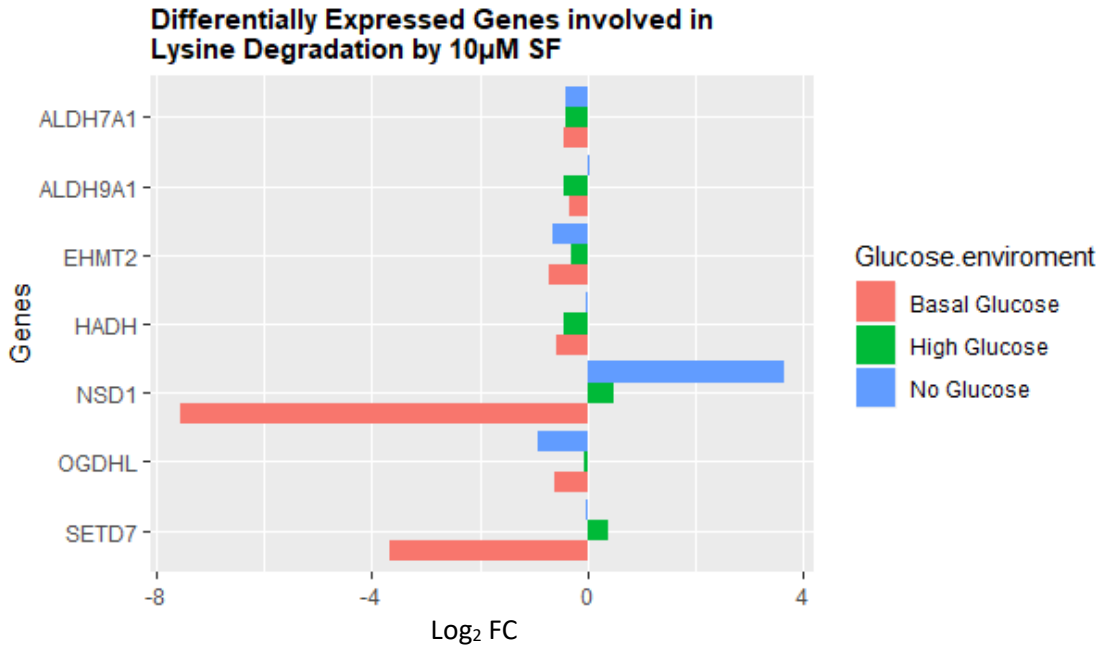

Figure 4.17. Top enriched differentially expressed genes from the lysine degradation gene set by 10 μM SF in different glucose environments. The x-axis represents the log_2 fold change whilst, the y-axis represents the genes of interest. These include Aldehyde Dehydrogenase 7 family member A1, (ALDH7A1), Aldehyde Dehydrogenase 9 family member A1 (ALDH9A1), Euchromatic histone-lysine-N-methyltransferase 2 (EHMT2), Hydroxyacyl Coenzyme A dehydrogenase (HADH), Histone-lysine-N-methyltransferase H3, lysine 36 specific (NSD1), 2-Oxoglutarate dehydrogenase like mitochondrial (OGHDL) and Histone-lysine-N-methyl transferase (SETD7). The statistical significance of the DEG can be found in table 4.6.

4.3.6 SF rewires metabolism in no glucose environment to promote cell survival

Figure 4.5, revealed that in glucose starvation, SF downregulated a wide range of metabolic pathways. Whether downregulation of these metabolic pathways is simply a consequence of the lack of glucose, due to the cancer phenotype of HepG2 requiring glucose to fuel their activity or SF's actual contribution is something to consider. As **table 4.1** identified a small number of genes being downregulated in each metabolic pathway, the analysis has been broken down into the following section and certain gene sets of interest have been analyzed.

4.3.6.1 SF impacts on arginine and proline metabolism

The gene set arginine and proline metabolism consist of a series of reactions which include the following: proline and arginine biosynthesis, creatine metabolism, polyamine biosynthesis either from the breakdown of ornithine or from the breakdown of arginine, and finally arginine succinyltransferase pathway. The analysis revealed four genes in the set were downregulated and differentially expressed after multiple testing corrections. These are ALDH1B1, argininosuccinate synthetase (ASS1), guanidinoacetate N-methyltransferase (GAMT), and creatine kinase (CKM). ALDH1B1 can catalyze two reactions: 4-aminobutanal into 4-aminobutarate and N4-acetylaminobutanal into 4-acetaminobutaonate. ASS1 catalyzes the penultimate step of the urea cycle; the formation of arginosuccinate from, citrulline, aspartate, and ATP. Along with argininosuccinate lysases, these two enzymes are responsible for producing arginine. Downregulation of ASS1 may imply an accumulation of the amino acid aspartate and decreased formation of arginine. GAMT catalyzes the conversion of guanidinoacetate to creatine through the methyl donor S-Adenosylmethionine SAM. Both ASS1 and GAMT genes are both highly specific in the liver. Finally, CKM catalyzes the addition of a phosphate group on creatine. Downregulation of CKM results in a build of creatine.

4.3.6.2 SF impacts on serine glycine and threonine metabolism

The two core enriched genes identified from the serine glycine and threonine pathway in this glucose environment following multiple testing correction were GAMT and glycine C-acetyltransferase (GCAT). GCAT is involved in the degradation of threonine to glycine. Threonine degradation is a two step process: in the first step, L-threonine dehydrogenase breaks down L-threonine to 2-amino-3-ketobutarate. In the second step, GCAT converts this intermediate into glycine and acetyl CoA. Downregulation of

these genes may imply a reduction in the formation of glycine. It was also identified that SF downregulated the activity of methionine S-adenosyltransferase (MAT1A). Whilst this gene is not involved in serine, glycine, and threonine metabolism, it is involved in methionine metabolism. This gene catalyzes the conversion of methionine to S-Adenosylmethionine (SAM). Therefore, downregulation of this gene will result in the accumulation of the amino acid methionine (see chapter 5).

4.3.6.3 SF impacts on tryptophan metabolism

Tryptophan metabolism consists of both its biosynthesis, catabolism, and melatonin synthesis. The two differentially expressed genes identified following multiple testing were glutaryl-CoA dehydrogenase (GCDH) and acetyl-CoA acetyltransferase mitochondrial (ACAT1). Although involved in tryptophan metabolism, these two genes are also involved in a wide range of different metabolic reactions, including fatty acid metabolism. GCDH catalyzes a two-step reaction: firstly, the oxidation of glutaryl-CoA to glutaconyl-CoA. This intermediate remains bound to the enzyme and is then decarboxylated to form crotonyl-CoA. ACAT1 instead catalyzes the breakdown of acetoacetyl-CoA into two molecules of acetyl-CoA. As this reaction is reversible, it could also imply an increase in either the metabolites acetyl-CoA or acetoacetyl-CoA, the latter is the precursor that feeds into the mevalonate pathway for cholesterol biosynthesis. These two genes are also present in the KEGG fatty acid metabolism gene set.

4.3.6.4 SF impacts on retinol metabolism

Retinol metabolism is associated with the metabolism of vitamins and cofactors. Results of the GSEA revealed that three genes were significantly downregulated. These are ADH6, CYP3A5, and DHRS3. Alcohol dehydrogenase 6 (ADH6) and short chain dehydrogenase/reductase 3, (DHSR3) catalyze the reversible reaction of retinol to retinal. The forward reaction retinol to retinal via NADH is produced. Cytochrome P450 family 3 subfamily A member 5 (CYP3A5) belongs to the family of cytochrome P450. CYP3A5 catalyzes the conversion using NADPH of retinoate to all-trans-5-6-Epoxyretinoic acid.

4.3.6.5 SF impacts on glycerolphospholipid, glycerolipid, and fatty acid metabolism:

Since the enriched genes in the tryptophan metabolism gene set were related to fatty acid metabolism, and as glycerolphospholipid glycerolipid gene sets were negatively enriched, the analysis was extended to gain a mechanistic understanding of how SF affects lipid metabolism in glucose deprivation. In the glycerolphospholipid pathway, the following genes were differentially expressed following multiple testing corrections: glycerol-3-phosphate dehydrogenase (GPD1), phospholipase D_1 (CHPT1), lysophospholipid acyltransferase (LPCAT4), glycerol-3-phosphate acyltransferase 1 (GPAM), and group XIIA secretory phospholipase A2 (PLA2G12A). GPD1 catalyzes the reversible reaction of glycerol-3-phosphate to glycerone phosphate utilizing NAD. Glycerone 3 Phosphate, more commonly referred to as dihydroxyacetone phosphate, is then redirected towards triglycerides synthesis metabolism, although it also participates in glycolysis, whereas accumulation of glycerol-3-phosphate can be directed for the *de novo* synthesis of glycolipids. CHPT1 is the diacylglycerol choline phosphotransferase. This enzyme regulates the reversible conversion of CDP-choline to phosphatidylcholine, an essential component of cell membranes. LPCAT4 is the lysophospholipid acyltransferase 4. This gene is also responsible for controlling the synthesis of phosphatidylcholine. GPAM catalyzes the committed step in glycerolipid biosynthesis. This gene controls the levels of cellular triacylglycerol and phospholipid levels. Finally, PLA2G12A, a secretory phospholipase A2, is involved in producing arachidonic acid from phospholipids required to produce eicosanoids.

With regards to the glycerolipid and fatty acid metabolism pathway, the following genes that were differentially expressed following multiple testing included genes that also appear to regulate additional pathways these include: ACAT1, GCDH, ADH6 (see section above) as well as ALDH1B1, sterol O-acyltransferase 2 (SOAT2), malonyl CoA acyl carrier protein transacylase (MCAT), apolipoprotein A-II (APOA2), and apolipoprotein F (APOF). SOAT2 is involved both in steroid and cholesterol metabolism. This enzyme catalyzes the reversible formation of sterol esters (cholesterol esters) from a sterol and a long chain fatty acyl-coenzyme A. Downregulation of this gene could imply the build-up of cholesterol. MCAT is exclusively found in the mitochondria where it catalyzes the transfer of the malonyl group from malonyl-CoA to the mitochondrial carrier protein. APOA2 and APOF both belong to the family of apolipoprotein. APOA2 is the second most abundant protein in high-density cholesterol. APOF is instead involved in binding with lipoproteins and may also be involved in transporting cholesterol. Other DEGs that were identified to play a

role in lipid metabolism are HSD3B7, involved in the biosynthesis of several hormonal steroids, paraoxonase 3 (PON3) which belongs to the family of paraoxonase is involved in inhibiting the oxidation of LDL-cholesterol as well as regulating the activity of HDL protein. It was also identified downregulation of both the fatty acid binding protein 1 and 5 (FABP1/5) and ASCL5 genes, which have already been mentioned in section 3.1. A summary of all the genes that have been downregulated in Lipoprotein metabolism can be found in table 4.7.

Table 4.7 Differentially expressed genes in response to SF in no glucose concentrations involved in Lipoprotein metabolic processes

Ensembl ID	Gene Symbol	Gene	SF Log_2 Fold Change vs Control NG
Lipoprotein metabolic processes			
ENSG00000075239	ACAT1	Acetyl-CoA aceyltransferase mitochondrial	-0.49[1]
ENSG00000158874	APOA2	Apolipoprotein A-II	-0.76[1]
ENSG00000175336	APOF	Apolipoprotein F	-0.90[1]
ENSG00000119927	GPAM	Glycerol-3-phosphate acyltransferase 1	-0.87[1]
ENSG00000099377	HSD3B7	cholest-5-ene-3β,7α-diol 3β-dehydrogenase	-0.84[1]
ENSG00000167780	SOAT2	Sterol O-acyltransferase 2	-0.94[1]
ENSG00000197142	ACSL5	Long-chain-fatty acid-CoA ligase 5	0.57[1]
ENSG00000111666	CHPT1	Phospholipase D_1	-0.44[1]
ENSG00000163586	FABP1	Fatty Acid Binding Protein 1	-1.23[1]
ENSG00000164687	FABP5	Fatty Acid Binding Protein 5	-0.83[1]
ENSG00000105607	GCDH	Glutaryl-CoA dehydrogenase	-0.76[1]
ENSG00000151224	MAT1A	S-adenosylmethionine synthetase 1	-0.87[1]
ENSG00000100294	MCAT	Malonyl CoA acyl carrier protein transacylase	-0.65[1]
ENSG00000105852	PON3	Paraoxnase 3	-0.44[1]

ENSG00000167588	GPD1	Glycerol-3-phosphate dehydrogenase	-1.09[1]
ENSG00000176454	LPCAT4	Lysophospholipid acyltransferase	-0.81[1]
ENSG00000123739	PLA2G12A	Group XIIA secretory phospholipase A2	-0.46[1]

Adjusted P values of fold change: $p^1<0.05$, $p^2<0.001$, $p^3<0.0001$. The adjusted p-values were obtained through a linear model by the limma function. The gene counts were first converted to log counts per million. Limma then plots the log-cpm for each experimental design control vs treatment. The residual standard deviations for every gene is fit to a global mean-variance trend across all the genes of all samples. In the final step, precision weights are calculated for each gene.

4.3.7. Identification of master regulators in the presence of excess glucose from downstream metabolic pathways that are induced by NRF2 activation.

Up to now, it has been identified that SF can modulate, especially in extreme glucose environments a wide range of metabolic processes. To identify whether these enriched gene sets are mediated through NRF2 or other transcription factors, the final analysis that was conducted in the chapter was using regulatory networks. A network usually contains a collection of genes, some of which can act as regulators. These regulators depending on the stimuli will, in turn, control the expression of genes, thereby regulating the mRNA levels and in turn protein of those subsets of genes. The outcome will determine the function of the cell.

For the network analysis, only the high glucose data set was analyzed, as in this environment, SF yielded the most prominent changes in metabolic responses. The analysis first identified NRF2 interacting and potentially regulating a total of 37 other TF. The analysis also revealed that the number of edges, thereby the number of interactions between the different TF was 30. The results are shown in figure 4.18. From the analysis, an important finding was the upregulation of the Sp1. Sp1 has been previously been reported to take part in a wide range of cellular processes including cell differentiation, cell growth, cell differentiation, cell growth, apoptosis, as well as regulating immune response and damages to DNA. This may suggest that NRF2 may be either forming a protein-protein interaction with Sp1 to regulate some of the metabolic processes identified in this chapter. For example, in figure 4.18 the key findings identified from the analysis revealed that a downstream target of Sp1 is SREBF1, a crucial transcription factor involved in fatty acid biosynthesis, thereby getting a better mechanistic understanding of how SF regulates lipid metabolism. A

second TF involved in lipid metabolism is also regulated by Sp1 although this time it is indirect, as it is through EGR1 is CEBPA, involved in adipogenesis.

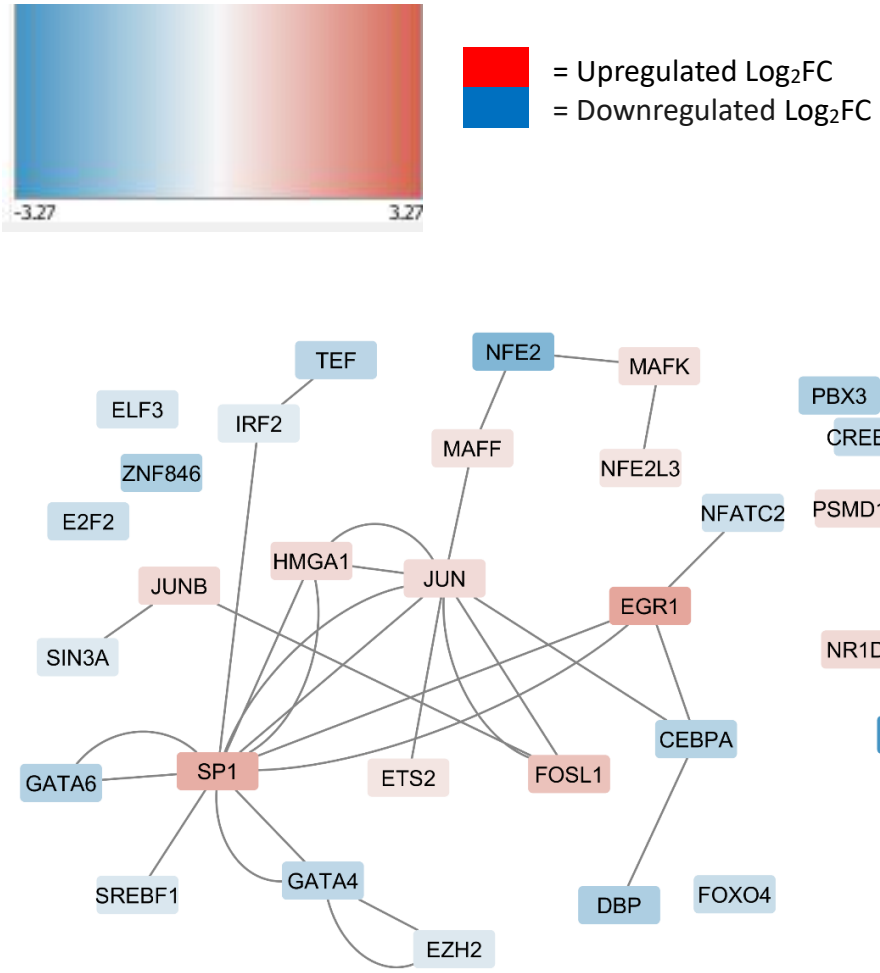

Figure 4.18. Transcription factors activity influenced by NRF2 in the HG dataset. Blue represents downregulation whilst red represents upregulation. The reference database was NRF2ome. The whole database was downloaded as a CSV file. It was then filtered to import a database containing only transcriptional regulation into Cytoscape. The image was constructed using Cytoscape 3.7.1.

4.4 Discussion:

In this study, HepG2 were treated for 24 h with physiological concentrations of SF 10 µM under different glucose conditions: NG, BG, and HG. Transcriptome analysis was conducted to address the transcriptional effect of SF in different metabolic states in HepG2 by mainly assessing, i) how the NRF2 target genes respond under different metabolic states, as well as ii) characterizing the SF effect on genes linked to central metabolism in hepatocytes under different metabolic states. To date, no RNAseq studies have been previously reported in HepG2 with 10 µM SF in different glucose environments. Findings from this detailed study have identified novel pathways that SF targets, and therefore the analysis has shed some light on how SF can act as a metabolic regulator. Whether all these changes in pathways are mediated primarily through NRF2 will be explored in chapter 6. A summary of the findings from this chapter have been presented in figure 4.19

4.4.1 Genes encoding xenobiotic metabolism

SF has been heavily studied both *in vitro* and *in viv*o. Its major effects are inducing Phase II genes and increasing the antioxidant capacity of cells, but also is involved in inducing apoptosis, inhibiting specific cyclin-dependent kinases in the cell cycle, and blocking angiogenesis, thereby preventing tumour growth (Juge *et al*., 2007).

As previously mentioned, in the presence of SF, NRF2, which is usually bound to KEAP1 and sent for proteasomal degradation, is instead released and translocates to the nucleus binding to a specific site on the DNA known as antioxidant response element (ARE). This study, it was shown that 10 µM of SF, in both basal and high glucose, induced several well-characterized NRF2 targets such as NQO1, GCLC, GCLM, etc (**Table 4.3**). This is the first *in vitro* study that indicates that dietary activation of NRF2 by SF is still maintained during excess glucose. As mentioned in the discussion in chapter 3, culturing hepatocytes in supraphysiological concentrations of glucose results in increased production of ROS and inflammatory cytokines (Panahi *et al*., 2018). Two studies on rats showed similar and consistent findings, that following a high-fat diet after 8 and 11 weeks, the mice started to develop mitochondrial dysfunction due to the increased production of ROS, along with inhibition of fatty acid oxidation (Vial *et al*., 2011, Togo *et al*., 2018). Therefore, the data suggests how SF inducing the anti-oxidant response is an important mechanism in preventing diseases of metabolic dysregulation such as type 2 diabetes, and not just simply involved in detoxifying xenobiotics.

Upregulation of the antioxidant response by SF is in agreement with what has been previously published in the literature. For example, SF treatment of 1,2,25 and 50 μM to a colon adenocarcinoma cell line Caco2, also showed induction of genes that were previously been reported to be upregulated by NRF2 (Traka *et al.*, 2005). Moreover, data from non-cancerous primary prostate epithelial and stromal cells treated with 15μM SF for 24 hours showed that 196 genes were found to be altered by more than 1.5-fold in epithelial cells including members of the oxidoreductase family. In stroma cells, only 42 genes were altered by more than 1.5-fold (adjusted p-value < 0.001) (Chambers *et al*., 2009). At the same time cancerous LNCaP prostate cells, treated with 25μM SF had 2579 transcripts differentially expressed and 3061 transcripts differentially expressed in response to 10 μM SF compared to controls ($p < 0.05$) (Bhamre *et al*., 2009). The study by Bhamre and colleagues showed that those genes that were altered to the greatest extent in the LNCaP cells were those that encoded enzymes involved in xenobiotic metabolism and detoxification such as NQO1, TXNRD1, MGST1, and SOD1. In another study using non-cancerous human breast epithelial MCF10A cell line, treatment with 15μM SF for 24 hours resulted in increased expression of many xenobiotic genes: the Aldo-Keto reductases along with the following NQO1, HMOX1, TXNRD1, TXN, SRXN1, EPHX1, MGST1, GCLM, and GSR were all up-regulated at a transcriptional level (Agyeman *et al*., 2012). It is worth highlighting though that in some of the studies conducted, supraphysiological concentrations were used, therefore questioning, the significance of the findings.

In the current study it was revealed through the GSEA, that in the BG data, SF resulted in a downregulation of the DNA replication gene set, further implying SF potentially impacting the cell cycle, and thereby inhibiting cell proliferation. This finding is in agreement with a recent study, showing that SF treatment (11 μM) to the melanoma cell line A375, RNAseq identified that the treatment not only resulted in the upregulation of specific genes involved in the antioxidant response, such as TXNRD1, SRXN1, GCLC/GCLM, etc, but also suppressing the G_2/M cell cycle, causing cell cycle arrest, and promoting apoptosis through the activation of the following caspases 3,8,9. The outcome was inhibition of the melanoma cells to migrate and invade. Some of the pro-apoptotic genes that SF upregulated included were p53, BAX, PUMA, and MDM2 (Arcidiacono *et al*., 2018). Network analysis in the study conducted by Arcidiacono *et al* revealed that the transcription factor EGR1, also identified in the current work was one of the responsible candidates involved in upregulating genes in growth arrest and proliferation. Several additional studies on ovarian and breast cancer cell lines have also reported similar findings; SF treatment resulted in downregulating cyclinD1 and upregulating apoptosis through modulation of the AKT/PI3K pathway (Cheng *et al*., 2019, Pastorek *et al*., 2015).

4.4.2 Genes encoding glucose and lipid metabolism:

In addition to genes encoding proteins involved in xenobiotic metabolism and phase 2 enzymes being differentially regulated in response to SF, it was also identified that SF induced changes in a wide range of different metabolic pathways such as lipid metabolism as well glycine, serine, and threonine metabolism, one carbon metabolism and metabolism of the amino acids lysine and histidine.

Fatty acid metabolism consists of both the synthesis of novel lipids (*de novo* lipogenesis) as well as the breakdown of fatty acids through a process known as beta-oxidation. This current work further supports findings that have been published in the literature. In this study, it was revealed that SF in both basal and high glucose downregulated several genes in fatty acid biosynthesis, including the Transcription Factors SREBF1, CEBPα, along with fatty acid desaturase (FADS), whilst acetyl CoA carboxylase (ACACA), the rate-limiting enzyme in the biosynthesis of fatty acids was only downregulated by SF in the high glucose set. The analysis also showed upregulation of several genes involved in β-oxidation such as CPT1α and MLYCD. Lipid biosynthesis is one of the most NADPH-consuming processes that occur in cells. Thereby downregulation of these genes by SF may suggest that the NADPH might be redirected to support the antioxidant response, especially for the reduction of glutathione and TXNRD1, again to prevent the metabolic dysregulation induced by the excessive glucose (Lin *et al*., 2016).

Dysregulation in lipid metabolism not only contributes to the pathogenesis of CVD, but the increased accumulation of lipids can result in increased metabolic alterations, including obesity, insulin resistance, and metabolic syndrome, to name a few. Obesity is also an initiator and contributor to certain cancers such as prostate, postmenstrual, breast, bladder, ovarian, liver colon, and pancreas (Lega and Lipscombe, 2019). The accumulations of lipids have been shown to initiate carcinogenesis. For example, ovarian cancer relies on lipids provided by adipocytes in the tumour microenvironment for sustained growth, and hypertrophy of adipose tissue diminishes the oxygen levels available, promoting angiogenesis (Butler *et al*., 2020). Whilst tumours have dysregulated glucose metabolism, several tumours also have abnormally active lipid metabolism, allowing them to synthesize, elongate and desaturate fatty acids to support proliferation (Fernández *et al*., 2020). Several genes in *de novo* lipogenesis and cholesterol metabolism have also been identified as biomarkers for cancer prognosis. For example, FASN, which in the previous chapter, SF downregulated its activity (**figure 3.3b**), is upregulated in both prostate and breast cancer (Menendez *et al*., 2016, Menendez and Lupu, 2007). Once synthesized, fatty acids can become

activated by fatty acyl-CoA synthetases (ACSLs), required for the synthesis of phospholipids and triglycerides. In this study, it was identified that SF downregulated the activity of ASCL1 whilst upregulating the activity of ASCL5 in both basal and high glucose environments. This family of genes has also been proposed as biomarkers of cancer. For example, ASCL1/4, overexpression has been associated with poor clinical outcomes in patients with stage II Colon rectal cancer along with lung cancer (Vargas *et al*., 2016, Chen *et al*., 2016a). In contrast breast cancer patients with downregulation of ASCL5 again are associated with poorer prognosis (Yen *et al*., 2017). The analysis also identified SF downregulating two genes involved in triacylglycerol biosynthesis. The final step in the synthesis of triacylglycerol is catalyzed by the gene DGAT, where the diacylglycerol is esterified with a fatty acid. Two humans' DGAT genes have been identified. In this study, SF resulted in a downregulation in the DGAT1 gene in both glucose environments, while DGAT2 was only downregulated in the basal glucose set. Certain studies have found dysregulation of DGAT2 is found in HER2-breast cancer along with endometrial cancer (Gao *et al*., 2020). All these novel findings may suggest new mechanisms on how SF may suppress the formation of cancers.

One mechanism that has been understood on how SF modulates fatty acid metabolism is by inducing pAMPK and changing the pAMPK/AMPK ratio (Chen *et al*., 2018, Li *et al*., 2020b). AMPK acts as a molecular sensor (Herzig and Shaw, 2018). Activation of pAMPK leads to phosphorylation of acetyl-CoA carboxylase, thereby leading to its inhibition and promoting fatty acid oxidation (Viollet *et al.*, 2006). Its activation also results not only in increased energy expenditure through expression PPAR-α; but, PPAR-α interacts with PGC-1α an inducer of mitochondrial biogenesis. pAMPK activation has also been shown to regulate the activity of the CD36 protein which enhances the uptake of fatty acids from the plasma membrane (Xu *et al* 2013).

The analysis, also identified not only SF interfering in lipid metabolism but also with adipogenesis, the synthesis of new fat cells, through downregulation of the transcription factor CEBPα. Two studies using adipocytes have also support this finding. The first study showed, that SF treatment to the adipocyte cell line 3T3-LI resulted in decreased lipid accumulation shown by Oil Red O staining. This reduction was due to SF downregulating the expression of the TF PPARγ and CEBPα, thereby confirming the findings obtained in this chapter (Choi *et al*., 2014). This study also identified, as previously mentioned that SF arrested genes in the cell cycle, along with promoting the expression of the protein p27, thereby preventing the ability of adipocytes to differentiate. The second study showed SF induced adipocyte browning, based on the increased number of mitochondrial and enzymes in the respiratory chain, through NRF2, SIRT1, and PGC1-α pathway. SF also increased the expression of the

uncoupling protein 1 (UCP1), increased glucose uptake, and inhibited gene related to FA synthesis (Zhang *et al*., 2016). In the current work, the expression of UCP1 and downstream targets of the PGC1-α were also assessed, but none of the genes identified were differentially expressed.

Downstream targets of CEBPα include a wide range of genes that code for apolipoprotein. Whilst the network analysis should have been extended further to assess the downstream targets of CEBPα; it is possible to speculate SF is downregulating a wide range of apolipoprotein. The proteins are involved in the binding and transport of lipids in the blood. It has been identified that dysregulation of these proteins can lead to the formation of a wide range of metabolic disorders. For example, elevated levels of APOC3 results in increased accumulation of triglycerides and can contribute to atherosclerosis pathogenesis (Khetarpal *et al*., 2017). Increased levels of ApoD and ApoE have been implicated with the following pathologies: dementia, Alzheimer's disease, and stroke (Dassati *et al*., 2014, Chang *et al*., 2017). Defects in ApoA can result in abnormal cholesterol metabolism, thereby contributing to hypercholesteremia and potential increased risk of developing cardiovascular diseases. Currently, the most common treatment for managing CVDs is through the prescription of the drug statin, with a couple of studies showing that the evidence and benefits of taking statins are currently limited (Armitage *et al*., 2019, Byrne *et al*., 2019). Future studies using *in vivo* models should explore further whether SF can affect these proteins, thereby helping to identify novel strategies to deal with cardiovascular diseases.

4.4.3 Genes encoding additional metabolic processes such as Histidine and Lysine Metabolism:

An additional finding of the GSEA is that SF downregulated the gene set histidine metabolism in the high glucose environment and lysine degradation in the basal glucose environment. Histidine is an essential amino acid, with unique properties; it can act as a buffer by accepting or donating protons, it is involved in metal ion chelation, it can scavenge reactive oxygen and nitrogen species, as well as is involved in erythropoiesis and the histaminergic system (Holeček, 2020). In the current analysis it was identified that SF downregulated the activity of three genes involved in histidine catabolism; histidiase then urocanase (AMDHD1) and finally aminoacylase 3 (ACY3). The current data suggest that SF treatment results in the accumulation of histidine. Literature analysis revealed that this is the first study to report SF affecting these two amino acids. As this was not seen in the absence of NRF2 activation under the glucose-deprived environment, these pathways are likely NRF2 dependent. A couple of

studies have shown a link between histidine metabolism, histidine's catabolism, and one carbon metabolism (see next chapter for SF interfering with one carbon metabolism).

For example, the metabolite forminoglutamate can be converted to glutamic acid by formininotransferase in the presence of tetrahydrofolate. If folate is deficient, FIGLU accumulates, and HIS catabolism is inhibited (Luhby *et a*l 1958). Depletion of THF may lead to a reduction in the ability of cells to synthesize glycine from serine (Holeček and Vodeničarovová, 2019, Meléndez-Hevia *et al*., 2009). Several additional studies have shown that methionine, S-Adenosylmethionine, homocysteine, and S-Adenosylhomocysteine can activate HIS catabolism by increasing the availability of THF (Fell and Steele, 1983, Billings *et al*., 1981). Studies on rats administered with histidine have shown it to improve gastric mucosal damage induced by aspirin (Lim *et al*., 1979), along with inhibiting the development of stroke induced by the occlusion of the middle cerebral artery (Adachi *et al*., 2005), and preventing cardiotoxicity induced by the drugs isoproterenol and doxorubicin (Moradi-Arzeloo *et al*., 2016, Farshid *et al*., 2014). For obese women with metabolic syndrome, histidine supplementation at 4g/day for 12 weeks, resulting in improved insulin resistance, along with a decrease in body mass index, waist circumference, body fat, and markers of systemic inflammation (Niu *et al*., 2012).

This downregulation of catabolic genes potentially leading to increased histidine could be due to the histidine being redirected for carnosine biosynthesis. Carnosine is synthesized using the amino acids histidine and beta-alanine in the presence of ATP (Derave *et al*., 2010). The major source of carnosine can be found in skeletal muscle, with smaller quantities present in cardiac muscle, brain, and other tissues (Abe, 2000, Boldyrev *et al*., 2013). Carnosine is a more efficient proton buffer, metal chelator, and antioxidant compound (anti-glycating agent) than histidine (Holecek 2020). Within the last couple of years, studies on mouse models of diabetes and metabolic syndrome have shown that supplementation with carnosine is effective in suppressing insulin resistance, plasma lipids as well as delayed onset of atherosclerosis (Sun *et al*., 2014, Aldini *et al*., 2011, Brown *et al*., 2014). Similarly, carnosine administration at the same time has been shown to inhibit cognitive decline in a mouse model of Alzheimer’s diseases (Herculano *et al*., 2013), suppress tumorigenesis in a wide range of cancer including human glioblastoma, colorectal, and ovarian carcinoma cells (Rybakova and Boldyrev, 2012, Mikuła-Pietrasik and Książek, 2016, Iovine *et al*., 2014). Human intervention studies have also reported similar findings. For example, prediabetic subjects supplemented with carnosine 200mg/day resulted in a decrease in fasting plasma glucose levels (Liu *et al*., 2015).

In this analysis, SF was also shown to affect lysine metabolism. Lysine is another essential amino acid. For humans, this means that it cannot be synthesized and therefore must be obtained externally either through diet or supplementation. Lysine is involved in several functions: firstly, it is incorporated in the formation of a wide range of proteins. For example, the crosslinks found in collagen, an essential protein involved in the formation of connective tissue, are formed by a triple helix structure consisting of lysine residues. Lysine can also be broken down to carnitine essential for fatty acid metabolism. Finally, it has also been shown that lysine, like methionine, is also involved in histone modification and thus can impact the epigenome (Dambacher *et al*., 2010). The positive side chain along with its long hydrophobic backbone makes lysine somewhat amphipathic. Due to its hydrophilicity, lysine residues are often buried within the protein. The other important role that lysine play is epigenetic regulation. Up to three lysine residues can be methylated or at the same time, acetyl groups can be added to form acetyl-lysine or removed (Dambacher *et al* 2010). In this study, SF was shown to downregulate two key genes involved in epigenetic regulation: SETD7 and NSD1. Over the past couple of years, the SETD7 gene has been identified to regulate at least 30 non-histone proteins, and may therefore be a potential target for several human diseases (Batista and Helguero, 2018). For example, some SETD7 targets include genes involved in the following cellular pathways: cell cycle regulation, DNA damage responses, RNA-polymerase II-dependent gene transcription, chromatin modulation, and cell differentiation (Del Rizzo and Trievel, 2011). Out of these targets, increasing evidence suggests that this gene is mainly involved in regulating cellular differentiation and proliferation. For example, pluripotent stem cells have been shown to exhibit low expression of SETD7 which is thought to be due to the pluripotency maintenance proteins OCT4, NANOG, and SOX2, which bind to the STED7 promoter and suppress its activity (Kamran *et al*., 2013). Similarly, differentiation of embryonic stem cells, as well as smooth muscle, is regulated through STED7 methylation of SOX2, leading to its degradation (Fang *et al.*, 2014) and H3K4 and SRF, which regulate the expression of differentiation genes TAGLN and ACTA2 (Tuano *et al*., 2016). SETD7 activity has also been shown to be tissue specific. For example, inhibition of SETD7 in breast cancer cells results in downregulation of the genes E2F1 and DNMT1. The outcome is downregulation of the signaling cascade that promotes invasion and metastasis (Montenegro *et al*., 2016). In three gastric cell lines (MKN74, MKN45, and AGS), reduced expression of SETD7 is associated with gastric cancer progression (Akiyama *et al*., 2016). In addition, methylation of β-catenin through SETD7 results in reduced proliferation of the HeLa cell line (Shen *et al*., 2015). Perhaps the most promisingly finding is that several hepatocellular carcinoma cell lines have SETD7 overexpressed, resulting in an increased risk of metastasis and

recurrence, along with larger tumor size and increased cell proliferation (Chen *et al*., 2016b). Therefore, the data may indicate a novel mechanism on how SF can act as an anti-carcinogenic agent.

4.4.4 Assessing SF effect in the no glucose environment

One of the major findings in this chapter is that in the absence of glucose antioxidant genes were not induced by SF, which suggests that the NRF2 activation is dependent on the presence of glucose. This is in agreement with Heiss and colleagues were the group showed that activation of NFR2 in fibroblasts leads to increased glucose uptake (Heiss *et al.*, 2013). This glucose is preferably metabolized through the pentose phosphate pathway to produce NADPH. Interference with this process blocks the ability of the cellular antioxidant capacity of the cells to reduce ROS, also leading to reduced expression of antioxidant genes such as glutathione and haem oxygenase (Heiss *et al*., 2013). Therefore, it is possible to hypothesize that the absence of induction of NRF2 genes observed in no glucose is due to the severely diminished levels of NADPH, further supporting a strong link between NRF2, glucose, and NADPH production. Further analysis should therefore assess the levels of NADPH in these three separate glucose environments. Whether in the fasting state NRF2 is induced or not is still not fully understood. For example, in a study where mice were placed on a 24h fast, the mRNA levels of NRF2, GCLC, GCLM, HMOX1, GSR, and GPX4 from the skeletal muscles, were all induced compared to the fed mice. This induction resulted in the inhibition of lipid peroxidation (Lettieri-Barbato *et al*., 2020). The group carried out *in vitro* studies by culturing the muscle cell line C2C12 under 0.5% serum and 5.5 mM glucose to mimic a fasting state and still identified an induction in specific antioxidant genes. The cells were still cultured in glucose and serum in this study, not mimicking a fasted state (Lettieri-Barbato *et al*., 2020). It may be that the lack of glucose could have resulted in cell death; if that was the case, then the study should have considered potentially utilizing lower concentrations of glucose.

In the current data, it was identified that despite NRF2 activation, SF upregulated a wide range of gene sets regulating the cytoskeleton of cells such as tight, gap, and adherents junctions as well as focal adhesion, whilst at the same time downregulating a wide range of genes involved in metabolic processes. Present on the surface of cells are integrin and cadherin receptors. These receptors act as bridges and allow cells to communicate with the external environment. For example, what may occur with the depletion of glucose in these receptors can alter the structure of the actomyosin cytoskeletal network, resulting in changes in downstream signalling pathways (Schlaepfer *et al*., 1994). According to the literature, the cytoskeleton plays a vital role

in regulating three metabolic processes involved in glucose homeostasis: the distribution of the insulin receptor substrate (IRS), translocation of the glucose transporter GLUT4 and the internalization of the insulin receptor (INSR) (Liu *et al*., 2006). At the same time these, components of the cytoskeleton are the first to interact with glycolytic enzymes (Tanner *et al*., 2018). Therefore, upregulation of these gene sets may suggest that SF is allowing the cells to remodel their structure enabling them to utilize additional energy sources, such as glutamine.

A cell culture model without the presence of glucose could also be considered an *in vitro* model for a ketogenic diet. Therefore this no glucose environment may be a good proxy for studying the effects of a ketogenic diet. When levels of glucose in the body are severely diminished, through prolonged fasting, or diet, the major energy source is β-hydroxybutyrate (ketone bodies). In the liver what occurs is that oxaloacetate and citrate are not able to condense to form acetyl-CoA, instead of in these circumstances, the already available acetyl-CoA is broken down to β-hydroxybutyrate and acetoacetate. These are then transported to other tissues where it is converted to acetyl-CoA which enter the citric acid cycle and oxidized in the mitochondria for energy (Rui, 2014). For example, two studies, one on rat glioma cells and the other on pancreatic cancer cells have both shown that in this environment cancers cells are incapable of proliferating and growing as they are unable to utilize ketone bodies as an energy source (Maurer *et al*., 2011, Shukla *et al*., 2014). As research in ketogenic diets is emerging, this is also the first time to assess the effect of food bioactive, therefore opening the opportunities to understand the benefits of how fasting along with plant bioactives may affect health.

4.4.5 Transcription Factor Analysis:

In the final section of the analysis, a network was constructed to gain a better mechanistic understanding of whether the metabolic changes induced by SF in the high glucose environment, were mediated through NRF2 or other transcription factors.

The interesting finding was the upregulation of Sp1. This is contrary to what has been published in other studies, thereby suggesting that Sp1 activity and regulation may be tissue specific. Previous studies have already identified that SF treatment in the prostate cancer cell line LNcaP decreased the activity of Sp1 (Beaver *et al.*, 2014). Sp1 and Sp3 are TF that can enhance or repress genes in a wide range of cellular processes such as cell differentiation, cell growth, apoptosis, immune responses, response to damaged DNA, and chromatin remodeling (Tan and Khachigian, 2009). Several different cancer cells have been reported to have increased levels of Sp1 and its reduction is associated with decreased angiogenesis and increased cancer cell

death (Li and Davie, 2010). In patients with prostate cancer, the increase of both Sp1 and Sp3 predicts the recurrence of the disease (Bedolla *et al*., 2012).

Similarly, siRNA of Sp1 in the prostate cancer cell line DU145 suppresses the proliferation of the cell line (Lu and Archer, 2010). The RNAseq study that Beaver and colleagues conducted and other reported literature identified that up to 25% of genes induced by SF were through both the transcription factors Sp1 and Sp3 (Beaver *et al* 2014). Similarly, in keratinocytes exposed to SF, Sp1 was shown to regulate the expression of p21 (Chew *et al*., 2012). This opens the door to new scientific questions about whether there is a connection between the NRF2 pathway and Sp1 and whether some of the metabolic targets mediated by SF are through Sp1.

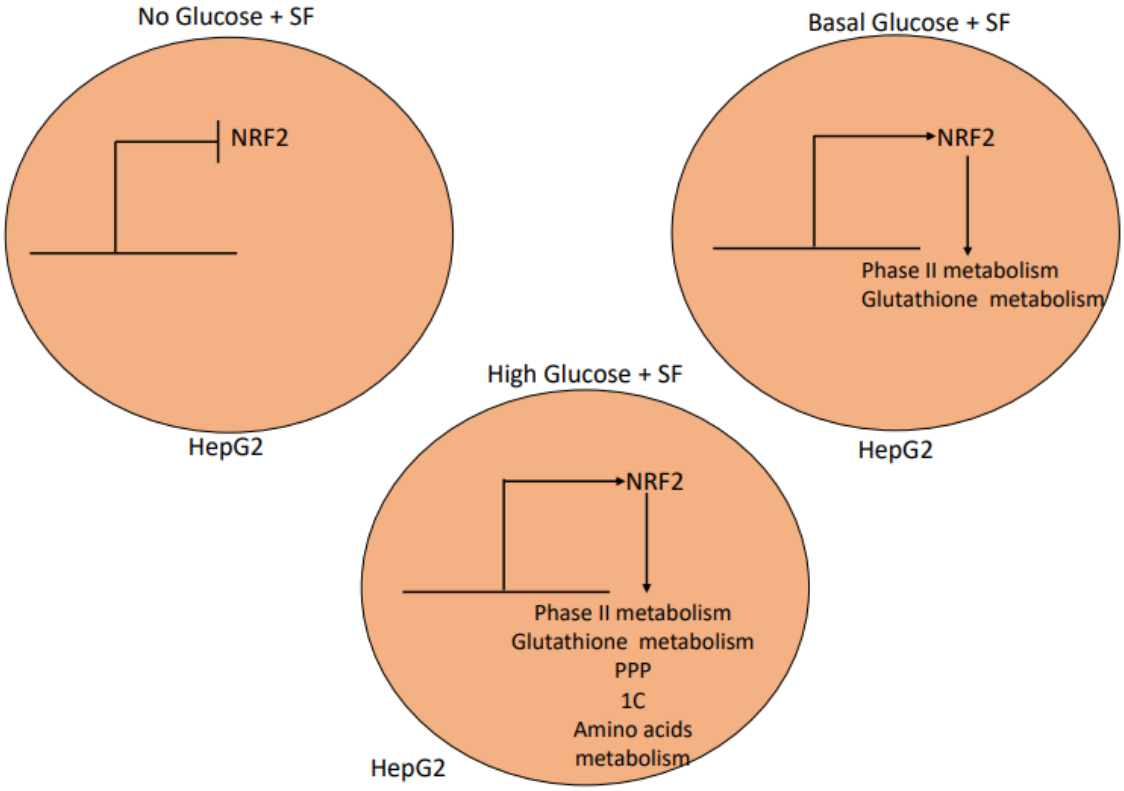

Figure 4.19. **Summary of the findings from this chapter shows how varying glucose concentrations affect NRF2 downstream metabolic processes.** In an environment lacking glucose, NRF2, despite the presence of SF, is not induced. In basal glucose, NRF2 is induced but only regulates the expression of genes involved in Phase II metabolism. In glucose excess, NRF2 regulates the expression of genes involved in Phase II metabolism and a wide range of metabolic genes to cope with the detrimental effects of the excess glucose load.

4.6 Conclusion:

The work that I carried out in this chapter is the first to report the effect of physiological concentrations of SF on liver cells cultured under three different metabolic states (fasting, healthy and insulin-resistant). Firstly through the GSEA, I identified that NRF2 targets are not induced in the absence of glucose. In the presence of glucose, SF upregulated the antioxidant response. This effect was still maintained in the excessive glucose state, thereby suggesting how SF inducing the anti-oxidant response is an important mechanism in preventing diseases of metabolic dysregulation. The focus of the current chapter was to assess the effect of SF at the transcriptional level and identified that glucose availability is key to mediating the metabolic effects of SF. In the next chapter, the use of isotopic tracers such as a fully labeled glucose and glutamine tracer were utilized to assess how SF utilizes these substrates in various metabolic pathways, especially under differing glucose environments.

Chapter 5: Global metabolomic profile of HepG2 cells exposed to sulforaphane in basal and high glucose environments

Chapter 5 Figures:

5.1 Introduction

Metabolic pathways consist of a series of biochemical reactions which are connected by the intermediates; the products of the reaction are the substrate for subsequent reaction. Whilst most chemical reactions are reversible metabolic pathways are considered to flow in one direction. For example, the pathway for the biosynthesis of an amino acid will defer from that of its breakdown. The only exception to the rule is the metabolism of glucose. The breakdown of glucose occurs through glycolysis, but at the same time, several reactions of glycolysis are reversible and participate in the re-synthesis of glucose a process known as gluconeogenesis. These metabolic pathways can act as both anabolic (growth) and catabolic (break down). The best characterized catabolic pathway is the production of ATP. The breakdown of glucose through glycolysis generates pyruvate, which feeds into the TCA cycle to produce the electron carriers nicotinamide adenine dinucleotide (NADH) and flavin adenine dinucleotide (FADH) required for the synthesis of ATP in the mitochondria. An example of an anabolic pathway is gluconeogenesis (Blanco and Blanco, 2017).

A vital pathway regulating glucose metabolism is the pentose phosphate pathway (PPP), which works parallel to glycolysis (Ge *et al*., 2020) (**figure 1.10**). After glucose is phosphorylated to G6P, it continues down the glycolysis pathway to generate fructose-6-phosphate and glyceraldehyde 3-phosphate or can be re-directed to the PPP. The PPP is split into two distinct pathways: the oxidative phase in which NADPH is produced and the non-oxidative synthesis of ribose-5-phosphate (R5P), a five-carbon sugar. Both pathways occur in the cytosol. The two crucial enzymes in the oxidative phase of the PPP are: the G6PD, which catalyzes the conversion of glucose-6-phosphate to 6-phosohogluconolactone, also the rate-limiting step for the PPP, and PGD which catalyzes the conversion of 6-phosphogluconate to R5P. Both reactions are crucial as they produce nicotinamide adenine dinucleotide phosphate (NADPH). The largest proportion of NADPH in cells arises from the PPP, with small amounts also being produced from the malic enzyme (ME1), isocitrate dehydrogenase (IDH1), and the 10-formyltetrahydrofolate dehydrogenase (ALDH1L1) (Ge *et al*., 2020).

NADPH and R5P are two essential metabolites for cell survival and proliferation. R5P is the building block for the synthesis of nucleotides. On the other hand, NADPH is the reducing agent needed for the biosynthesis of fatty acids as well as sterols, nucleotides, and non-essential amino acids (Patra and Hay, 2014, Wamelink *et al*., 2008). NADPH is also required to convert oxidized glutathione to reduced glutathione through the action of glutathione reductase (GSR). Reduced glutathione can act as a cellular antioxidant (Bradshaw, 2019).

Glutathione (GSH) is a tripeptide (synthesized from glycine, cysteine, and glutamate) and is largely synthesized in the liver. The concentration of GSH in most cells is around the 5 mM range, similar to the concentration of glucose in the blood (Pizzorno, 2014). Glutathione can either be synthesized *de novo* via a 2-step process catalyzed by the enzyme glutamate-cysteine ligase (GCL), composed of both a catalytic and regulatory subunit, followed by glutathione synthetase which requires ATP, or it can be regenerated where oxidized glutathione is recycled back to reduced GSH through the action of GSR and NADPH (Pizzorno, 2014). Finally, less common is the recycling of cysteine from oxidized glutathione via gamma-glutamyltransferase (GGTP) through the presence of NADPH. The rate at which glutathione is synthesized as well as recycled and regenerated is dictated by three factors: during *de novo* synthesis, glutathione is primarily regulated by the intracellular concentration of cysteine (Pizzorno, 2014). The buildup of GSH can also inhibit the activity of GCL as direct feedback inhibition. Finally, under increased oxidative stress or inflammation where GSH is depleted, *de novo* synthesis of GSH occurs where the cysteine pool is obtained through the recycling of oxidized form of glutathione through the action of GGTP (Pizzorno, 2014).

Previous literature has identified NRF2 activation as a critical event in glucose redirection towards the PPP. For example, Mitsuishi showed that constituent activation of NRF2 in the A549 cell resulted in the glucose being redirected to the PPP. The group was the first to identify that the three essential genes of the PPP: G6PD, PGD, and TKT contain an antioxidant response element (ARE) sequence, therefore, being direct targets of NRF2 (Mitsuishi *et al*., 2012). A second study by Heiss and colleagues showed that in fibroblast, upon NRF2 activation, glucose is preferentially metabolized through the PPP (Heiss *et al*., 2013). Furthermore, an increase in glutathione synthesis is considered a key outcome of SF treatment. However, aside from transcriptional activation of glutathione biosynthesis genes, the molecular mechanism on how cysteine, glycine, and glutamate are obtained intracellularly for glutathione biosynthesis remains unknown.

In the previous chapter, the role of SF in metabolic regulation, as well as its potential for transcriptional regulation of major metabolic pathways, such as PPP, one carbon (1C) metabolism, as well as regulating amino acids biosynthesis and utilization such as glycine, serine, and threonine along with histidine metabolism, was identified in HepG2 cells for the first time. To provide further insight into the metabolic flux and the changes in metabolite utilization, this chapter focused on providing a better understanding of how glucose and glutamine are utilized by the cells in the presence of sulforaphane. This was undertaken using glucose and glutamine isotopic tracers. This chapter

particularly explored whether SF would affect carbon flux at different concentrations of glucose.

To examine intracellular fluxes, for example, to assess whether the glucose is redirected to the PPP, the most common approach that is currently utilized is using isotope tracers such as ^{13}C. Using GC-MS it is then possible to measure the isotopic distribution of each metabolite of interest. The labeling pattern also referred to as mass isotopomer distribution (MID) vector is represented by metabolite m+n where n is the number of carbon atoms. A metabolite with n carbon atoms can have 0 to n of its carbon atoms labeled with ^{13}C. A fully unlabeled metabolite (all carbon atoms unlabeled) with be represented by M0. In contrast, one labeled carbon atom will be represented by M1 and so on (Buescher *et al*., 2015).

In this chapter the following aims were assessed:

Aims:

1. Does SF redirect the glucose in the high glucose environment towards the pentose phosphate pathway?
2. Similarly, is SF redirecting is the glutamine in the high glucose environment towards glutathione biosynthesis?

5.2 Results:

5.2.1 SF interferes with glycolysis in both basal and high glucose environments:

To gain a mechanistic understanding through which SF reduces mitochondrial respiration in the high glucose environment as demonstrated in chapter 3, through the Seahorse Mito Stress assay (**figure 3.12b**), HepG2 were cultured with the uniformly labeled glucose tracer $13C_6$ as the sole glucose source. The $13C_6$ tracer is metabolized via glycolysis to yield M3 pyruvate and lactate. After 24h, in the basal glucose environment, physiological concentrations of SF did reduce M3 pyruvate ($p<0.0001$), although levels of M3 lactate did not change (**figure 5.1**). This effect was not identified in the high glucose environment. The Seahorse XF analyzer was then applied to measure glycolysis in real-time through the Glycolysis Stress Test, hypothesizing that SF treatment would result in a reduction in glycolysis

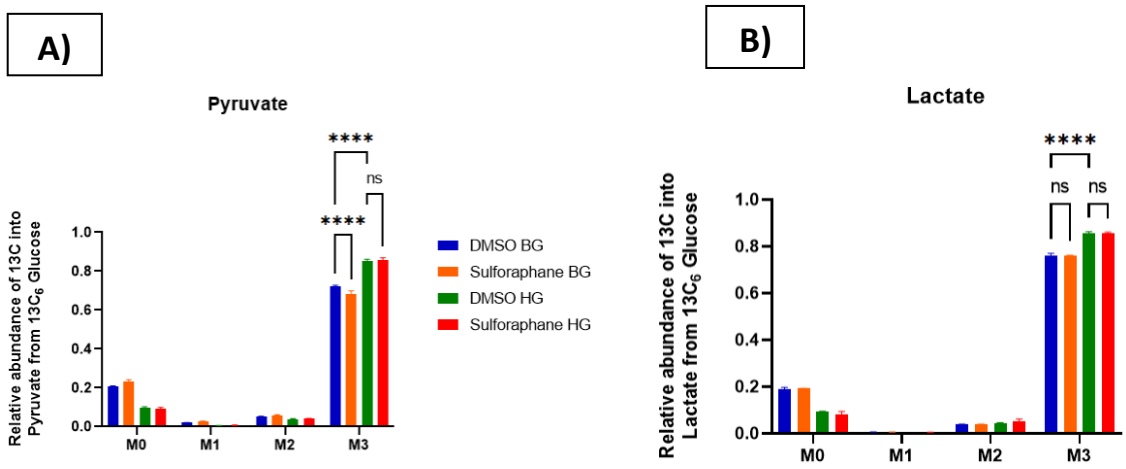

Figure 5.1. **Pyruvate and lactate labelling pattern from the $13C_6$ glucose tracer.** HepG2 cells were treated with 10 µM SF for 24 h in the presence of the fully labelled glucose tracer in basal glucose (5.5 mM) or high glucose (25 mM). After 24 h, metabolites were extracted and quantified using GC-MS. A) Pyruvate, B) Lactate. All values are expressed as mean ± SD from three individual culture wells. The x-axis M0 to M3 represents the relative mass isotopomer (MID). This represents the incorporation of the isotope into the metabolite. M0 means that all the carbon atoms in the metabolite are from carbon-12, whereas M+n all labelled carbon atoms come from the carbon isotope. The MID represents the relative abundances of M+0 to M+n isotopologues (Isotopologues are molecules, in my case, the metabolite of interest with a different number of isotopes). For each particular metabolite. Consequently, the sum of all fractions from M+0 to M+n is 100% or 1. Statistical analysis was conducted by a 2-ANOVA was carried as the two factors are the treatment and glucose levels: **M3 Pyruvate:** DMSO BG vs SF BG $p<0.0001$, DMSO BG vs DMSO HG $p<0.0001$, and DMSO HG vs SF HG $p=0.99$. **M3**

Lactate: DMSO BG vs SF BG p=0.99, DMSO BG vs DMSO HG p<0.0001, and DMSO HG vs SF HG p=0.99.

The glycolysis stress kit revealed a reduction in the extracellular acidification rate (ECAR) by SF in the basal glucose environment (**figure 5.2a**). Glycolytic capacity, which represents maximum energy production from glycolysis following injection of oligomycin and glycolysis, were significantly reduced, while non-acidification glycolytic rate just failed to reach significance (p=0.054) (**Appendix supplementary figure S2**). Although the uniformly glucose tracer in the high glucose environment revealed no difference between the control and the treatment, the Glycolysis Stress Test was also conducted on HepG2 cultured in high glucose to understand how SF regulates glucose homeostasis. It was also identified that SF resulted in a reduction in glycolysis although, assessing the Seahorse data of the two assays together revealed that the cells behaved less glycolytic in the high glucose environment (**figure 5.2b**).

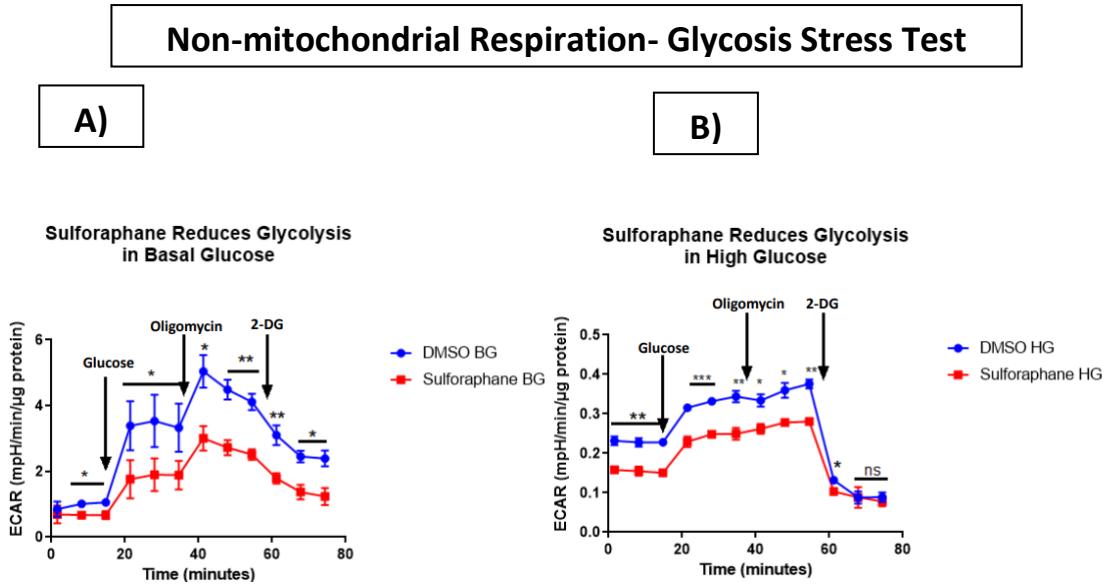

Figure 5.2. **SF effect on glycolysis in basal and high glucose environment through the Seahorse XP_F Analyzer.** A) Extracellular acidification rate (ECAR) of HepG2 treated with 10 µM SF in 5.5 mM glucose. B) Extracellular acidification rate (ECAR) of HepG2 treated with 10 µM SF in 25 mM glucose. All values are expressed as mean ± SD from biological replicates.

Finally, GSEA of RNAseq results in chapter 4 revealed that SF led to a reduction in the glycolysis and gluconeogenesis pathway (q=0.052. **Appendix table 1.0**).

In particular, SF downregulated the carbohydrate-responsive element-binding protein, also referred to as MLXIPL (MLXIPL, BG DMSO vs BG SF q=0.01, HG DMSO vs HG SF q=0.11) (**figure 5.3**). Glucose flux in the liver will induce the MLXIPL gene, which is involved in the induction of glycolysis and lipogenesis. SF also upregulated more than

2-fold the glucokinase regulatory protein (GCKR, BG DMSO vs BG SF q= 5.01e-05, HG DMSO vs HG SF q= 4.61e-05), involved in binding and controlling the function of glucokinase, the first gene in glycolysis (**figure 5.3**). Glucokinase in liver cells will phosphorylate glucose; this allows the glucose to be broken down through glycolysis or converted to glycogen. SF also downregulated several genes along the glycolytic pathway, including phosphofructokinase muscle sub-type by more than 3-fold in the basal glucose environment (PFKM, BG DMSO vs BG SF q=0.002, HG DMSO vs HG SF q= 0.55), whose function is to catalyze the phosphorylation of fructose-6-phosphate to fructose-1-6-bisphosphate (**figure 5.3**). Enolase 3 (ENO3, BG DMSO vs BG SF q= 0.0006, HG DMSO vs HG SF q=0.01) catalyzes the reversible conversion of 2-phosphoglycerate to phosphoenolpyruvate. Phosphoglucomutase-1 (PGM1, BG DMSO vs BG SF q=0.003, HG DMSO vs HG SF q=0.02) catalyzes the interconversion of a phosphate group between positions 1 and 6 in the glucose chain (**figure 5.3**). The data also revealed that SF downregulated two genes acyl-coenzyme A synthetase short-chain 1 and 2 (ACSS1/2, BG DMSO vs BG SF q=0.004, HG DMSO vs HG SF q=0.01) involved in the formation of acetyl-CoA from acetate required for lipid synthesis, thereby identifying an additional mechanism how SF may inhibit lipid biosynthesis. The final genes that were differentially expressed in the data were two aldehyde dehydrogenase genes: ALDH7A1 (BG DMSO vs BG SF q=0.01, HG DMSO vs HG SF q=0.03) and ALDH9A1 (BG DMSO vs BG SF q=0.04, HG DMSO vs HG SF q=0.01), whose function is to catalyze the interconversion of acetaldehyde to acetate in the presence of NAD to generate NADH (**figure 5.3**). In the high glucose environment, it was instead identified that the only glycolytic gene that SF significantly downregulated was ENO3, along with both the ACSS1/2 and both aldehyde dehydrogenase genes (**figure 5.3**).

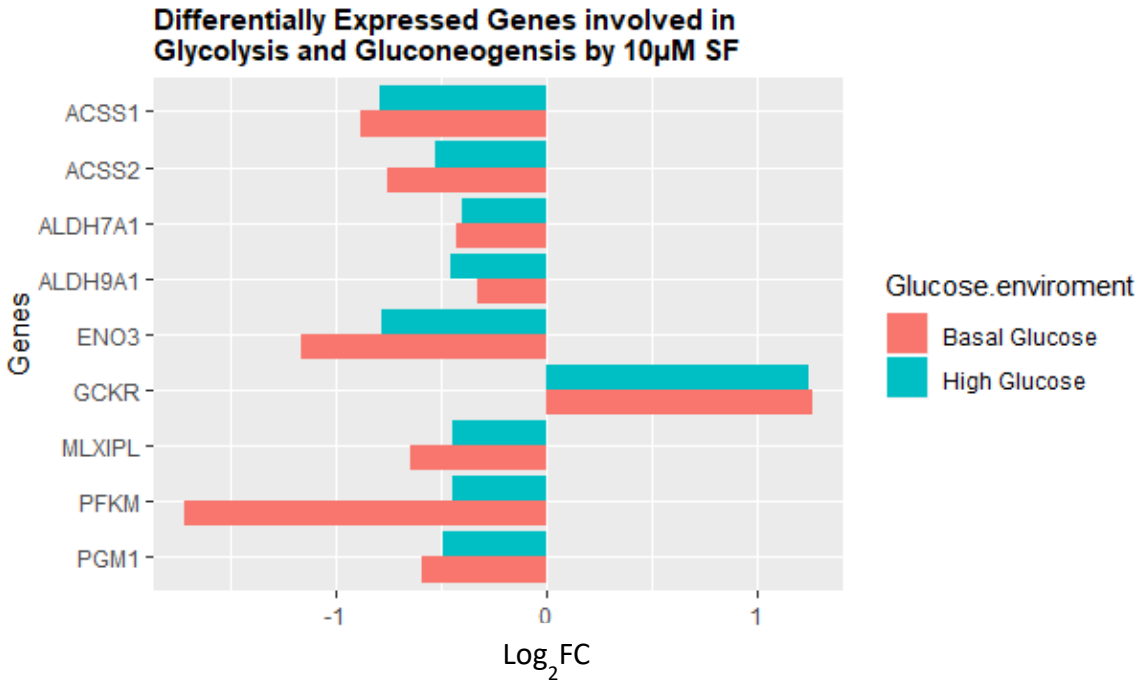

Figure 5.3.SF effect on genes involved in the glycolysis and gluconeogenesis pathway. HepG2 was treated with 10 µM SF for 24 h in basal (5.5 mM) and high glucose (25 mM). After 24 h RNA was extracted and was sent for RNAseq on Illumina. Differentially expressed genes were obtained through edgeR and limma. All genes are statistically significant following Benjamini-Hochberg multiple testing correction q <0.05. Acyl-Coenzyme A Synthetase Short Chain 1 and 2 (ACSS1/2), Aldehyde Dehydrogenase 7 Family Member A1 (ALDH7A1), Aldehyde Dehydrogenase 9 Family Member A1 (ALDH9A1), Enolase 3 (ENO3), Glucokinase Regulatory Protein (GCKR), Carbohydrate-Responsive Element-Binding Protein (MLXIPL), Phospho-Fructo Kinase Muscle subtype (PFKM) and Phosphoglucomutase-1 (PGM1).

5.2.2: SF effect in the PPP using the 1,2-^{13}C-glucose tracer:

One potential explanation for the reduction in glycolysis in figure 5.2b and mitochondrial respiration in the high glucose environment by SF could be the glucose being redirected towards the PPP. In chapter 4, it was identified through the gene set enrichment analysis (GSEA) that the PPP gene set was enriched, although it did not reach significance after correcting multiple testing (**Appendix Table S1**). The fully labelled glucose tracer ($13C_6$) is the commonly used tracer for measuring glycolysis, as all the carbons of intermediates in glycolysis will be labelled. Due to ambiguities in detecting $13C_3$ lactate production from $13C_6$ because lactate can be derived from other pathways (not just glycolysis), the 1,2-13C-glucose is utilised to estimate glycolytic flux better (Brutz *et al*., 2017). The 1,2-13C-glucose, rather than the fully labelled glucose tracer, was utilized to validate further whether the glucose is metabolised through the PPP pathway. The breakdown of the 1,2-^{13}C glucose tracer through PPP detects the accumulation of ribose-5-phosphate (R5P). Flux through the PPP generates M1 lactate (one carbon atom labelled), while glycolysis generates M2 lactate (two carbon atoms labelled) (**figure 5.4**). M1/ M2 lactate ratio reflects PPP overflow to glycolysis (Lee *et al*., 1998). Ribose phosphate labelling instead represents whether oxidative PPP or non-oxidative PPP is occurring (Lee *et al*., 1998). In the current experiment, HepG2 cells were cultured in basal and/or high glucose with the 1,2-^{13}C-glucose tracer as the only glucose source, with the presence of SF for 24h. Figure 5.5 revealed that SF did not lead to M1 lactate accumulation in the high glucose environment, shown by lower M1 labelling compared to the M1 in the basal glucose environment. In addition, M2 levels of lactate were considerably higher than M1 lactate.

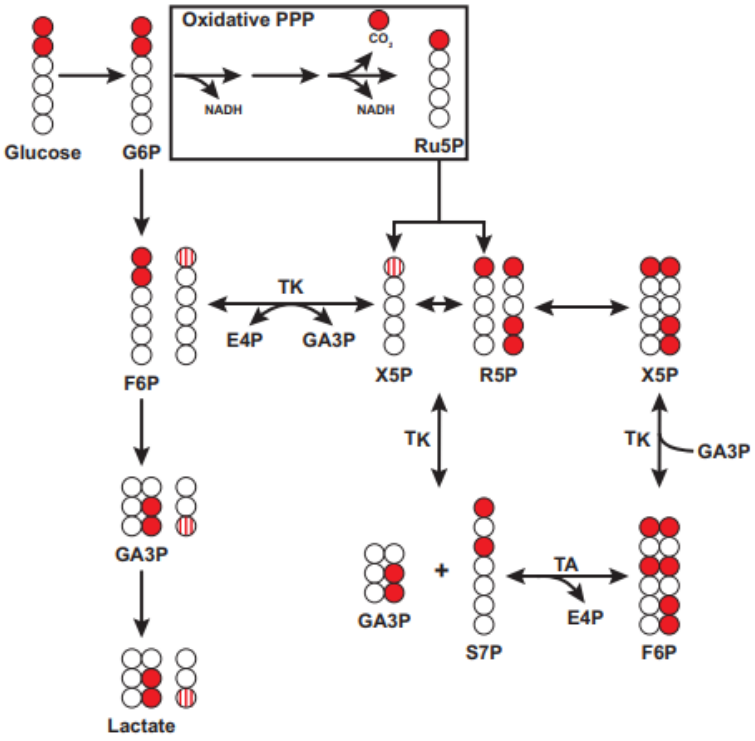

Figure 5.4. Summary of how the 1-2-$^{13}C_2$ glucose tracer is metabolized to assess glycolysis and PPP activity. Following the phosphorylation of glucose through hexokinase to generate glucose-6 phosphate (G6P), the labeled G6P molecule can continue glycolysis producing M2 lactate and pyruvate, or if it metabolized through the oxidative phase of PPP to generate M1 ribulose 5-phosphate (Ru5P), the end product of the oxidative branch of the PPP. Red circles represent the labeled ^{13}C carbon, whilst stripped circles represent the labeled ^{13}C carbon derived from the non-oxidative branch of the PPP. Image has been reproduced from (Bruntz *et al.*, 2017).

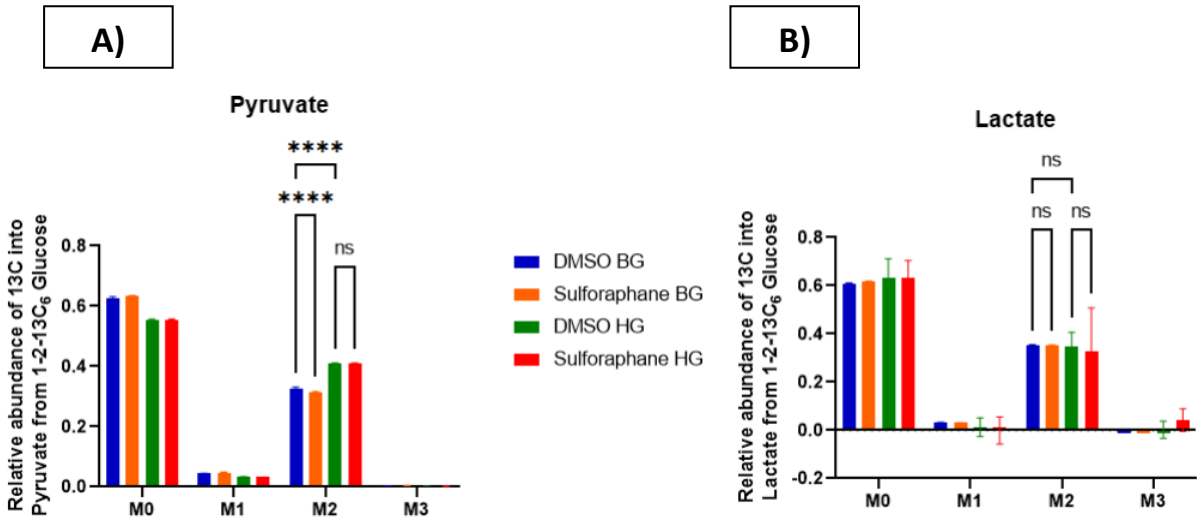

Figure 5.5. Pyruvate and lactate labelling pattern from the 1-2-$^{13}C_6$ glucose tracer. HepG2 cells were treated with 10 µM SF in DMEM media containing basal glucose (BG) 5.5 or high glucose (HG) 25 mM of the 1-2-$^{13}C_6$ glucose tracer along with 4 mM $^{12}C_5$ glutamine -FBS. After 24h, metabolites were extracted and determined by GC-MS. The x-axis M0 to M3 represents the relative mass isotopomer (MID). This represents the incorporation of the isotope into the metabolite. M0 represents that all the carbon atoms in the metabolite are from carbon-12 whereas M+n all labelled carbon atoms come from the carbon isotope. The MID represents the relative abundances of M+0 to M+n isotopologues for each particular metabolite. Consequently, the sum of all fractions from M+0 to M+n is 100% or 1. Statistical analysis was conducted by a 2-ANOVA was carried as the two factors are the treatment and glucose levels. N=3 and the error bars represent standard deviation. **M2 Pyruvate:** DMSO BG vs SF BG p<0.0001, DMSO BG vs DMSO HG p<0.0001, and DMSO HG vs SF HG p=0.99. **M2 Lactate:** DMSO BG vs SF BG p=0.99, DMSO BG vs DMSO HG p=0.99, and DMSO HG vs SF HG p=0.99.

5.2.3 Global untargeted metabolomics reveals that SF interferes with one carbon metabolism:

To gain further insight and to assess the effect of sulforaphane on modulating hepatic metabolism, HepG2 cells were treated with physiological concentrations of SF under both basal and high glucose conditions. After 24 h, metabolites were extracted and untargeted metabolomics was conducted using Gas Chromatography coupled to Mass Spectrometry (GC-MS). Out of a total of 97 metabolites measured, 18 were altered by SF in BG and 15 in HG, shown by the heatmap in figure 5.6a. SF treatment reduced serine ($p < 0.01$) and increased methionine ($p < 0.05$) in both glucose environments (**figure 5.6 a and b**), which are key metabolites of the folate cycle and methionine cycle, respectively, and are part of one carbon (1C) cellular metabolism. The other key finding identified from the untargeted metabolomics data is that SF treatment in the basal glucose environment (**figure 5.6 a**) reduced the two end products of glycolysis, pyruvate ($p = 0.004$) and lactate ($p = 0.01$), thereby supporting the findings from both the fully labelled glucose tracer (**figure 5.1**) and Seahorse Glycolysis Stress Test (**figure 5.2**), (**Appendix supplementary figure S3**). It is also worth reporting that SF treatment in both glucose environments (**figure 5.6 a and b**) was shown to increase the intracellular levels of the following essential amino acids: tryptophan, phenylalanine, methionine, along with leading to a reduction in several non-essential amino acids: alanine, aspartic acid, and serine. The data suggest that SF may be affecting the amination and deamination of the non-essential amino acids. For example, the deamination of alanine with the amine group being incorporated into 2-oxogluartic acid to form glutamate.

A)

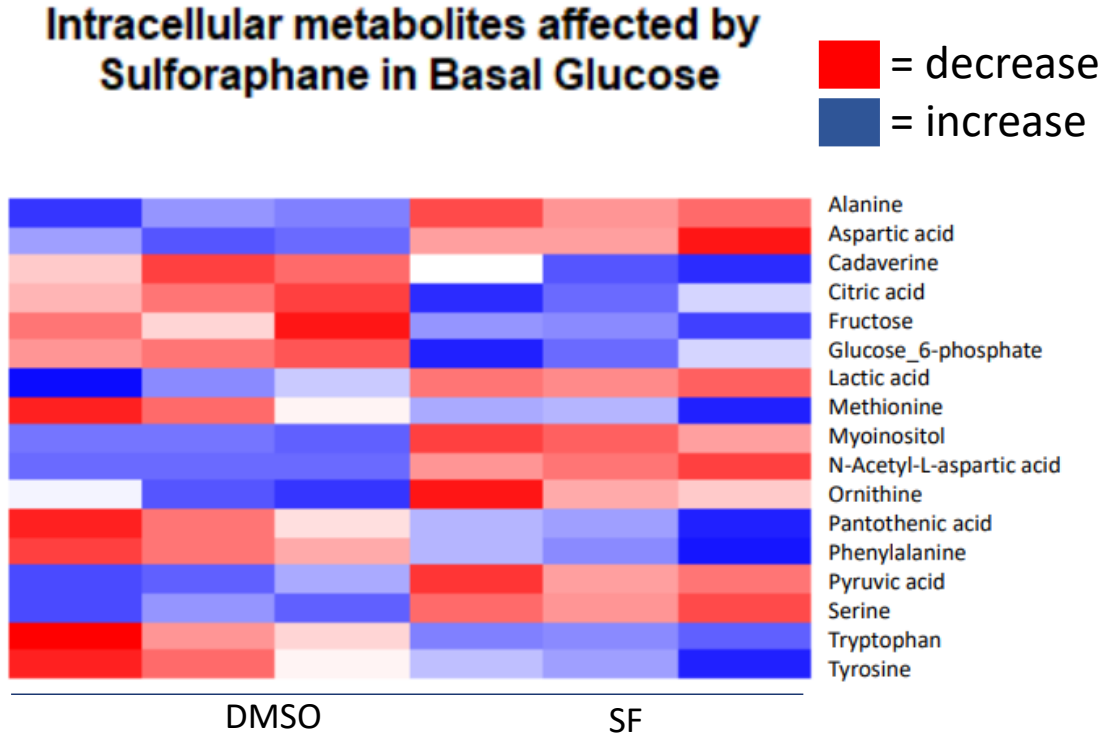
Intracellular metabolites affected by Sulforaphane in Basal Glucose
= decrease
= increase
Alanine
Aspartic acid
Cadaverine
Citric acid
Fructose
Glucose_6-phosphate
Lactic acid
Methionine
Myoinositol
N-Acetyl-L-aspartic acid
Ornithine
Pantothenic acid
Phenylalanine
Pyruvic acid
Serine
Tryptophan
Tyrosine
DMSO
SF

B)

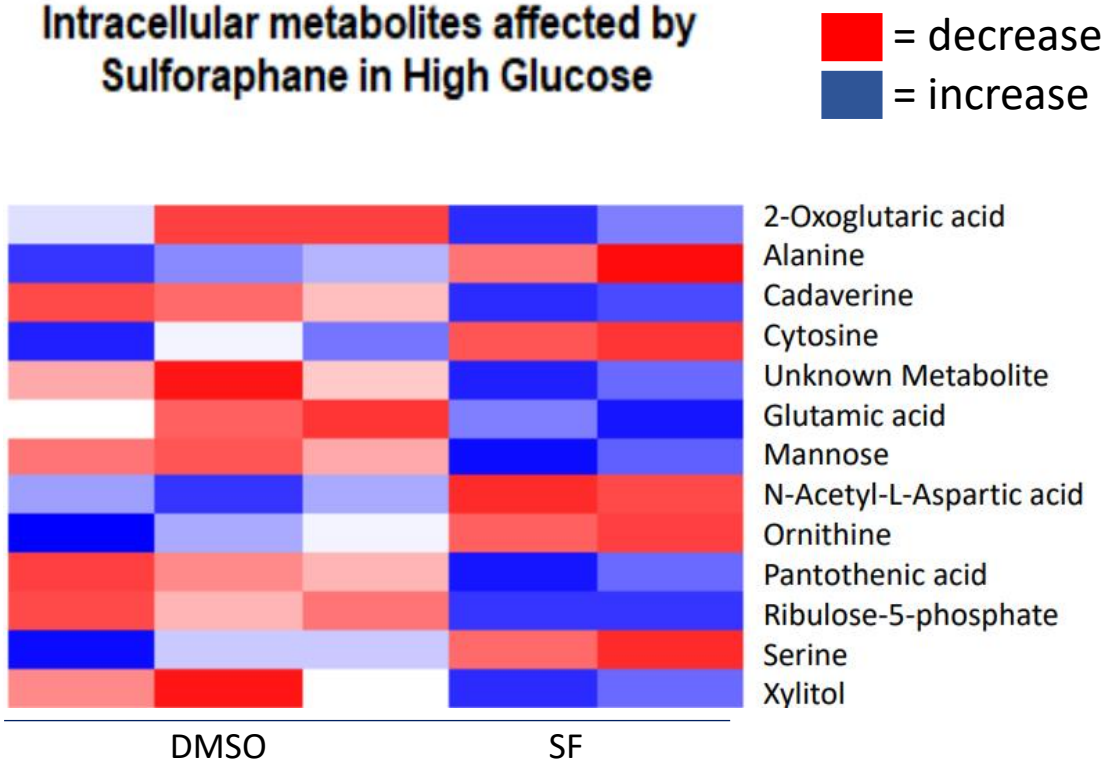
Intracellular metabolites affected by Sulforaphane in High Glucose
= decrease
= increase
2-Oxoglutaric acid
Alanine
Cadaverine
Cytosine
Unknown Metabolite
Glutamic acid
Mannose
N-Acetyl-L-Aspartic acid
Ornithine
Pantothenic acid
Ribulose-5-phosphate
Serine
Xylitol
DMSO
SF

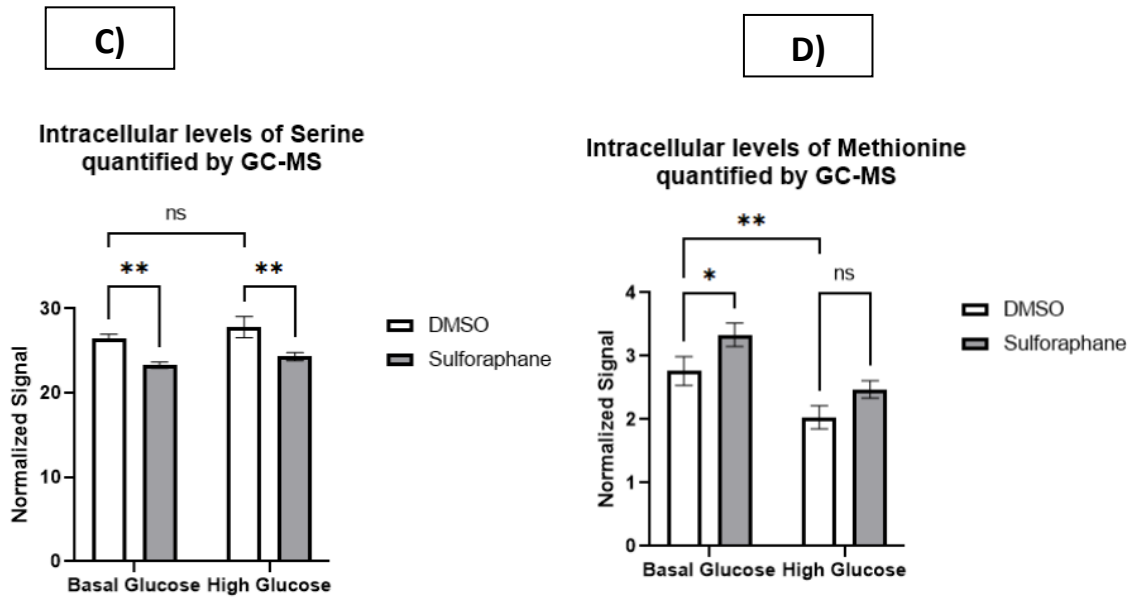

Figure 5.6 Untargeted metabolomics reveals SF interfering with one carbon metabolism. HepG2 cells were treated with 10 µM SF for 24 h in basal glucose (5.5 mM) or high glucose (25 mM). After 24 h, metabolites were extracted and quantified using GC-MS. A) Statistically significant metabolites are displayed in a heatmap, where blue is upregulation and red is downregulation, in the basal glucose environment $p<0.05$, Welch t-test. B) Statistically significant metabolites are displayed in a heatmap, where blue is upregulation and red is downregulation, in a high glucose environment $p<0.05$, Welch t-test. C) Readings from the serine and D) methionine from the heatmap were extracted and plotted into a bar plot. All values are expressed as mean ± SD from three biological replicates. 2-ANOVA was carried as the two factors are the treatment and glucose levels. **Serine: basal glucose DMSO vs basal glucose SF p=0.0047 and high glucose DMSO vs high glucose SF p=0.0059. Methionine: basal glucose DMSO vs basal glucose SF p=0.031 and high glucose DMSO vs high glucose SF p=0.13.**

5.2.4 Uniformly glucose tracer reveals that SF results in serine consumption:

One carbon (1C) metabolism consists of a broad range of biosynthetic reactions that can occur in both the cytoplasm and the mitochondria; to maintain cellular homeostasis, functioning as an integrator of nutrient status. The output of these reactions are metabolites that are used as the building blocks for methylation, redox, and nucleotide biosynthesis. One carbon unit is largely derived from two essential amino acids: serine and glycine, both of which can be either obtained from exogenous sources, such as media in cell culture, or synthesized directly. Serine can be synthesized *de novo* from a glycolytic intermediate 3-phosphoglycerate through a

series of reactions, commonly referred to as the serine synthetic pathway (SSP). To investigate further the effect of SF on the metabolic flux of glucose metabolism, the uniformly glucose tracer $13C_6$ was used in a further experiment. In this experiment, HepG2 was cultured with the $13C_6$ glucose tracer as the only glucose source, with the presence of SF for 24hrs. The uniformly labeled ($13C_6$) tracer can then be metabolized via the glycolytic intermediate 3-phosphoglycerate (3-PG) to serine M3 (with three labeled carbon atoms) and, subsequently, to M2 glycine (with two labeled carbon atoms) through the combined action of the SSP and serine hydroxymethyltransferase (SHTM1/2). A summary figure on how serine is derived from glucose through the serine synthetic pathway is shown in **figure 5.7.**

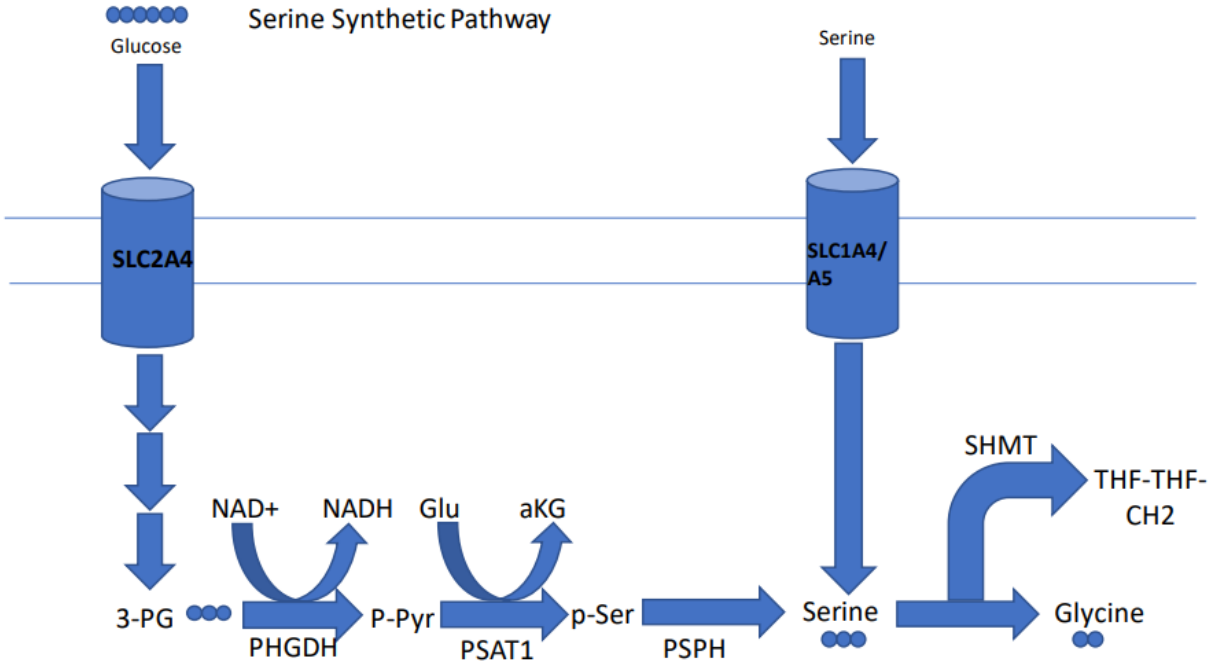

Figure 5.7 Summary of serine biosynthesis from glucose through the serine synthetic pathway. Serine, a non-essential amino acid, can be obtained from the cell culture media or synthesized intracellularly through glucose. As glucose is absorbed into the cell through the SLC2A4 receptor, glucose is metabolized through glycolysis. An intermediate in the glycolytic pathway 3-PG is then redirected towards serine biosynthesis leading to the formation of serine through the action of the following enzymes; PHGDH, PSATI and PSPH.

Using GC-MS, serine and glycine labelling were quantified. It was identified that increasing glucose levels (basal to high) resulted in a significant increase in both M3 serine and M2 glycine (**figure 5.8 a and b**). The addition of SF led to a further slight rise in the abundance of M3 serine ($p= 0.01$) but not M2 glycine ($p=0.7$), suggesting that the biosynthesis of glycine from glucose does not differ within treatments (**figure 5.8 a and b**). The tracer also revealed that SF under the high glucose environment resulted in a decrease in the abundance of both M2 ($p=0.2$) and M1 serine ($p<0.0001$)

(**figure 5.8 a**). A decrease in M1 and M2 serine suggests that the forward reaction in one carbon metabolism is occurring. That means that as serine enters the folate cycle, a methyl group is transferred to generate tetrahydrofolate and glycine by serine hydroxymethyltransferase (**figure 5.7**).

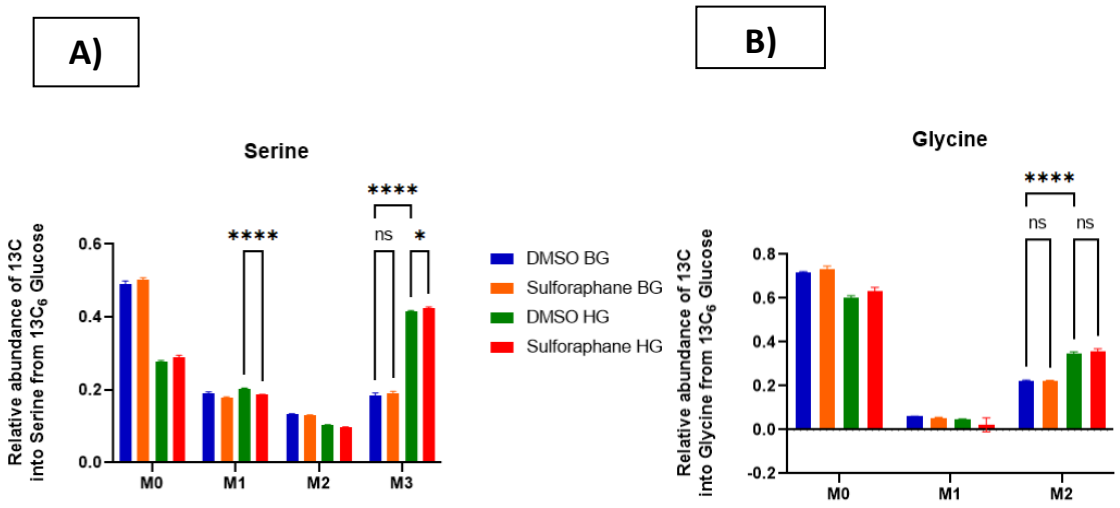

Figure 5.8. Identification of SF interfering with one carbon metabolism using the $13C_6$ glucose tracer. HepG2 was treated with 10 µM SF for 24 h in the presence of either the fully labelled glucose tracer in basal glucose (BG) (5.5 mM) or high glucose (HG) (25 mM) with 4 mM $^{12}C_5$ glutamine. After 24 h, metabolites were extracted and quantified using GC-MS. A) Serine, B) Glycine. The x-axis M0 to M3 and M0 to M2 for glycine represents the relative mass isotopomer (MID). This represents the incorporation of the isotope into the metabolite. M0 represents that all the carbon atoms in the metabolite are from carbon-12 whereas M+n all labelled carbon atoms come from the carbon isotope. The MID represents the relative abundances of M+0 to M+n isotopologues for each particular metabolite. Consequently, the sum of all fractions from M+0 to M+n is 100% or 1. Statistical analysis was conducted by a 2-ANOVA was carried as the two factors are the treatment and glucose levels: A) **Serine M3:** DMSO BG vs SF BG p=0.25, DMSO BG vs DMSO HG p<0.0001, DMSO HG vs SF HG p= 0.0152, **Serine M1:** DMSO HG vs SF HG p <0.0001. B) **Glycine M2:** DMSO BG vs SF BG p=0.99, DMSO BG vs DMSO HG p<0.0001 DMSO HG VS SF HG p = 0.7.

To assess whether the serine in the high glucose environment was derived only from glucose and not other substrates such as glutamine, a separate experiment was conducted where the uniformly glutamine $13C_5$ tracer was used as the only source of glutamine. Data from this experiment confirmed that in the high glucose environment, all the serine and pyruvate are derived from glucose, shown by no labelled M3 serine and pyruvate in the high glucose environment, compared to the basal glucose. This suggests that glutamine does not contribute significantly to the formation of pyruvate

and serine through the action pyruvate carboxylase (PC) and phosphoenolpyruvate carboxykinase (PEPCK) (**figure 5.9 a and b**).

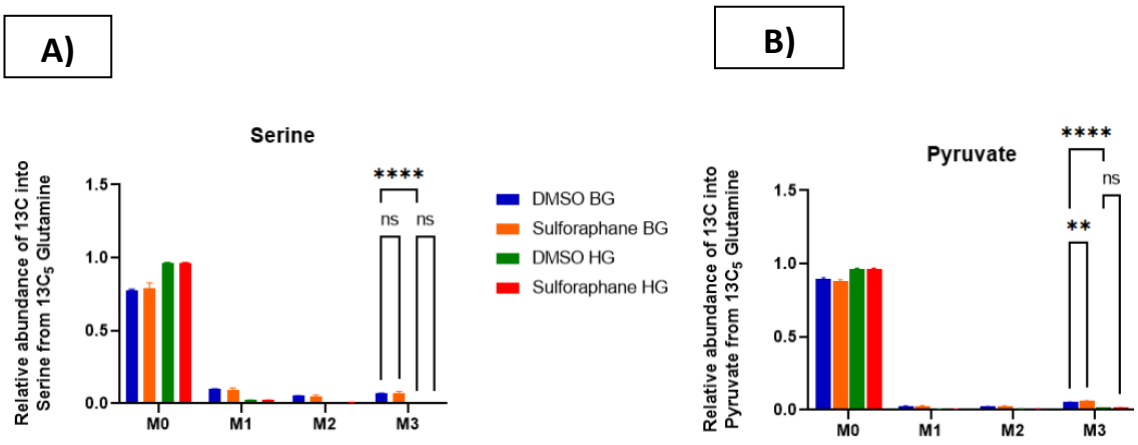

Figure 5.9. The effects of SF interfering on one carbon metabolism using the $^{13}C_5$ glutamine tracer. HepG2 treated with 10µM SF for 24 h in the presence of either the fully labelled glutamine tracer in basal glucose (BG) (5.5 mM) or high glucose (HG) (25 mM) with $^{12}C_6$ glucose. After 24 h, metabolites were extracted and quantified using GC-MS. A) Serine and B) Pyruvate. The x-axis M0 to M3 represents the relative mass isotopomer (MID). This represents the incorporation of the isotope into the metabolite. M0 represents that all the carbon atoms in the metabolite are from carbon-12 whereas M+n all labelled carbon atoms come from the carbon isotope. The MID represents the relative abundances of M+0 to M+n isotopologues for each particular metabolite. Consequently, the sum of all fractions from M+0 to M+n is 100% or 1. Statistical analysis was conducted by a 2-ANOVA was carried as the two factors are the treatment and glucose levels: A) **Serine M3:** DMSO BG vs SF BG p=0.99, DMSO BG vs DMSO HG p<0.0001 DMSO HG vs SF HG p=0.99. B) **Pyruvate M2:** DMSO BG vs SF BG p=0.0028, DMSO BG vs DMSO HG p<0.0001 and DMSO HG vs SF HG p=0.98.

5.2.5 Targeted Metabolomics reveals that SF also depletes glycine pool:

To elucidate whether the depletion of total serine observed in the untargeted metabolomics experiment (**figure 5.6 a-c**) was due to intracellular utilization, or due to a reduction in the cellular import ability from the media, the levels of both serine and glycine in the media, and intracellularly were measured. In this experimental condition, HepG2 cells were cultured in basal and high glucose without the tracers (standard DMEM media). The LC-MS analysis identified that intracellularly SF resulted in a decrease in the serine and glycine pool. In the basal environment, the intracellular concentration of serine in the control samples was 50 µM, with SF decreasing it to 35µM. Shifting to the high glucose, a large depletion was identified where this time the intracellular concentration of serine in the control was 30 µM and SF resulting in a

further decrease to 15 µM, independently supporting both the GC-MS and RNAseq data (**figure 5.10 a**).

Similarly, for glycine, the control intracellular concentration in the basal glucose environment was 100 µM with SF treatment decreasing it to 70 µM, whilst in the high glucose environment, the control concentration dropped to 50 µM with SF further reducing it to 25 µM SF. The decrease in the total glycine pool (**figure 5.10 b**) should not be confused with the no-change observed in M2 glycine in figure 5.5b. The total glycine pool, measured through the LC-MS, represents glycine derived, from a combination of metabolic pathways, such as serine synthetic pathway, along with threonine catabolism. This decrease in total glycine may suggest glycine redirection for glutathione biosynthesis (**figure 5.8 b**). The analysis also identified no difference between control and treatment in the media samples, suggesting that SF reduction was because both serine and glycine were utilized intracellularly (**figure 5.10 c-d**).

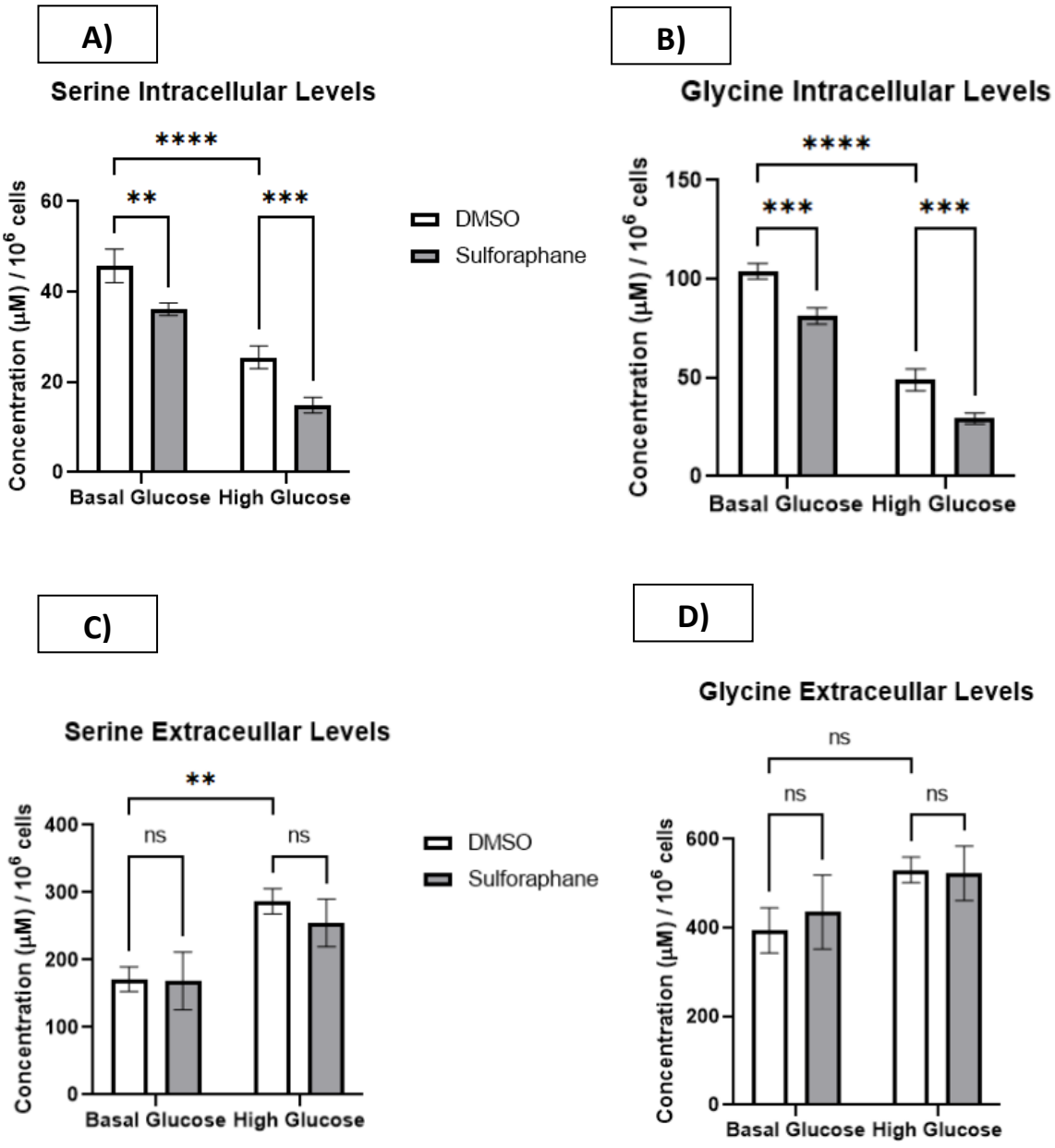

Figure 5.10. LC-MS analysis revealing SF depleting serine and glycine pool. Serine and glycine intracellular and extracellular measurements were quantified using LC-MS. All values are expressed as mean ± SD from three individual culture wells. A) **Serine intracellular levels:** DMSO BG vs SF BG p=0.0024, DMSO BG vs DMSO HG p<0.0001, and DMSO HG vs SF HG p=0.0006, B) **Glycine Intraceullar Levels:** DMSO BG vs SF BG p=0.0003, DMSO BG vs DMSO HG p<0.0001, and DMSO HG vs SF HG p=0.0003 C) **Serine Extraceullar Levels:** DMSO BG vs SF BG p=0.99, DMSO BG vs DMSO HG p=0.0075, and DMSO HG vs SF HG p=0.6. D) **Glycine Extraceullar Levels:** DMSO BG vs SF BG p= 0.82, DMSO BG vs DMSO HG p= 0.08, and DMSO HG vs SF HG p=0.99.

5.2.6 Whole transcriptome analysis reveals that SF affects the activity of genes involved in both one carbon metabolism and glycine, serine metabolism:

In the previous chapter, it was identified through the GSEA that SF in both glucose environments downregulated the glycine, serine, and threonine pathway gene set, along with upregulating genes in the one carbon pool folate gene set (**figure 5.11 a**). To identify the transcriptional mechanism for the decrease in total serine and an increase in total methionine, differentially expressed genes by SF from the two pathways were analyzed. SF downregulated the first and the rate-limiting step in serine biosynthesis, phosphoglycerate dehydrogenase (PHGDH, BG DMSO vs BG SF q=0.0045, HG DMSO vs HG SF q=0.01) (**figure 5.11 b**). The other two genes involved in SSP, phosphoserine aminotransferase 1 (PSAT1) and phosphoserine phosphatase (PSPH) along with SHTM1/2 were not differentially expressed. In addition, SF downregulated the expression of two genes involved in the catabolism of glycine: glycine decarboxylase (GLDC, BG DMSO vs BG SF q=0.005, HG DMSO vs HG SF q=0.03), and glycine-N-methyltransferase (GNMT, BG DMSO vs BG SF q=0.001, HG DMSO vs HG SF q=0.03) (**figure 5.11 b**). GLDC catalyzes the degradation of glycine to H-protein-S-aminomethyldihydrolipoyllysine and carbon dioxide.GNMT instead catalyzes the synthesis of N-methyl glycine (sarcosine) from glycine using S-Adenosyl methionine (SAM) (AdoMet) as the methyl donor. GNMT acts as an enzyme to regulate the ratio of SAM to SAH (AdoHcy) and participates in the detoxification pathway in liver cells. Downregulation of both these genes may suggest that glycine might instead be redirected for glutathione biosynthesis and potentially also for bile acid conjugation.

With regards to the enriched genes from the one carbon pool by folate, SF upregulated the activity of 10-formyltetrahydrofolate dehydrogenase (ALDH1L1, BG DMSO vs BG SF q= 7.12e-04, HG DMSO vs HG SF q= 0.00016), involved regenerating THF from 10-formyl THF, along with monofunctional C1-tetrahydrofolate synthase (MTHFD1L, BG DMSO vs BG SF q=0.01, HG DMSO vs HG SF q= 0.05) both genes involved in producing NADPH, along with two genes: Trifunctional purine biosynthetic protein adenosine-3 (GART, BG DMSO vs BG SF q=0.009, HG DMSO vs HG SF q=0.03) and Inosine monophosphate synthase (ATIC, BG DMSO vs BG SF q=0.03, HG DMSO vs HG SF q=0.009), involved in the first steps in purine biosynthesis. The results, therefore, suggest that the decrease in total serine is due to a combination of both SF inhibiting serine biosynthesis but also SF promoting genes involved in serine catabolism (**figure 5.11 b**).

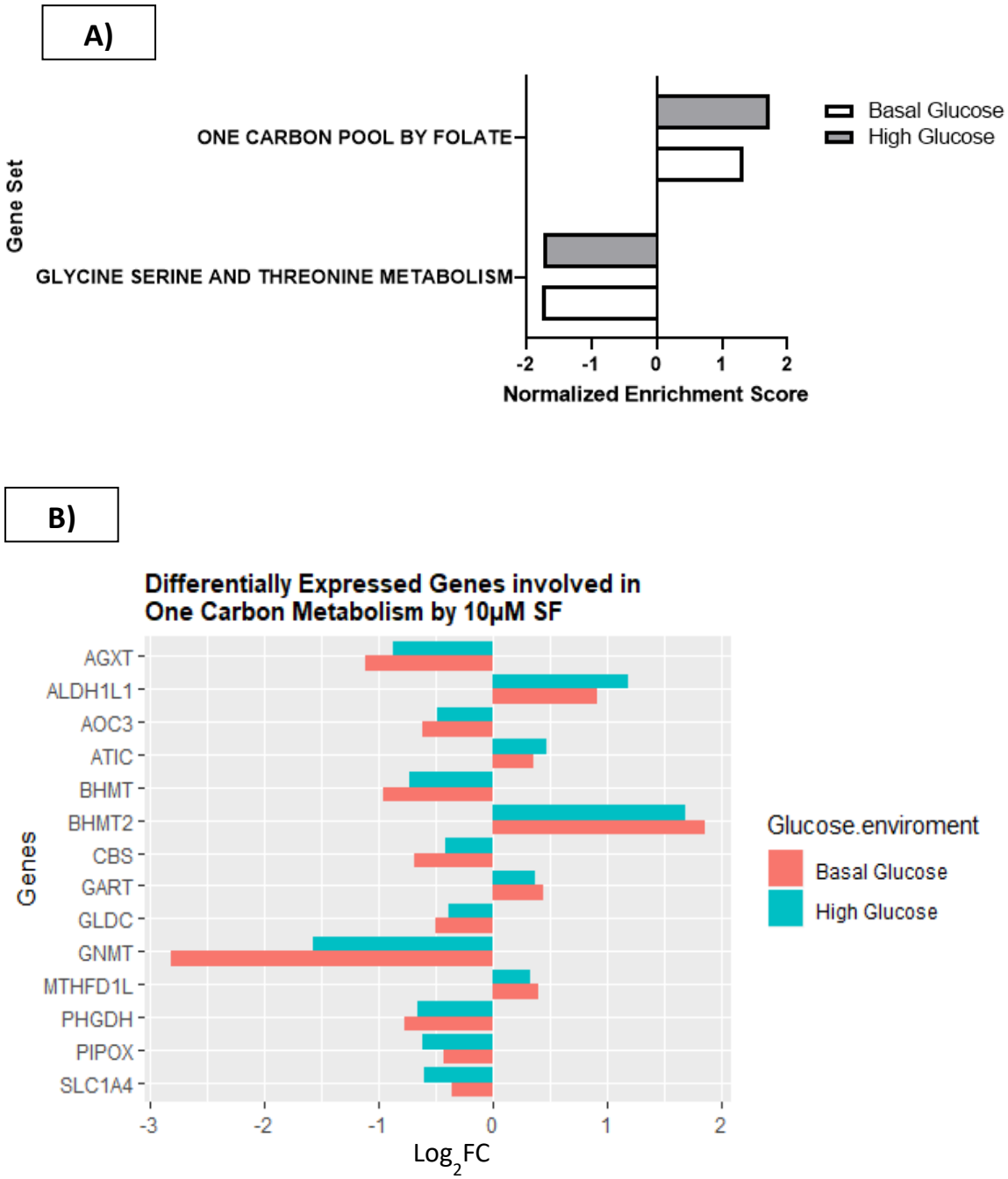

Figure 5.11. **Whole Transcriptome Analysis (RNAseq) reveals that SF interferes with one carbon metabolism.** A) Gene sets were significantly affected by the differential expression in samples treated with sulforaphane in HepG2 cells cultured under basal (5.5 mM) and high glucose (25 mM). Normalized enrichment scores (NES) were determined using the GSEA software. NES represents an estimation of the significance of the gene set normalized to the size of each gene set. Positive NES is shown by an increase in the gene set, and negative NES denotes an overall decrease in the gene set. Both treatment and controls are representative of triplicate samples. **glycine, serine, and threonine metabolism** (**basal glucose**, NES =-1.76, q=0.027), g**lycine, serine, and threonine metabolism** (**high glucose**, NES= -1.74, q=0.047) and o**ne carbon pool folate** (**high glucose** q=0.026, NES= 1.72 B). B) Genes from the glycine, serine, and threonine along with the one carbon pool folate were extracted and plotted using

ggplot (R). All genes are statistically significant following Benjamini-Hochberg multiple testing correction q <0.05. Serine-Pyruvate Aminotransferase (AGXT), 10-Formyltetrahydrofolate Dehydrogenase (ALDH1L1), Amine Oxidase, Copper Containing 3 (AOC3), Inosine Monophosphate Synthase (ATIC), Betaine-Homocysteine S-Methyltransferase/isoform2 (BHMT/BHMT2), Cystathionine Beta-Synthase (CBS) Trifunctional Purine Biosynthetic Protein Adenosine-3 (GART) Glycine Decarboxylase (GLDC), Glycine, N-Methyltransferase (GNMT), Monofunctional C1-tetrahydrofolate synthase (MTHFD1L, Phosphoglycerate Dehydrogenase (PHGDH), Peroxisomal sarcosine oxidase (PIPOX), and Solute Carrier Family 1 Member (SLC1A4).

5.2.7 SF interferes with 1C metabolism to promote the antioxidant response:

Supported by the findings of both the untargeted metabolomics and the glucose tracer, the next step was to determine whether SF was rewiring one-carbon metabolism to support the antioxidant response, mainly through glutathione production. GSEA analysis in the previous chapter revealed that SF upregulated genes involved in glutathione metabolism in both glucose environments. Therefore, in a separate experiment, the levels of oxidized and reduced glutathione were assessed by LC-MS in HepG2 cultured in both glucose environments in the presence of SF for 24h. Firstly it was identified that SF resulted in an increase in both glucose environments in pyroglutamic acid. Pyroglutamic acid is a metabolite derived from the amino group from glutamic acid or glutamine cyclizing to form a lactam ring. It is commonly present in the glutathione cycle, whose main function is glutamate storage (**figure 5.12 a**). The most prominent finding was in the high glucose environment, where SF resulted in a large increase in the intracellular concentration of reduced glutathione; this effect was not identified in the basal glucose environment (**figure 5.12 b**). The analysis also revealed that the intracellular concentration of oxidized glutathione in both glucose environments was not detected, suggesting that all the glutathione is readily and promptly converted to the reduced form.

Using the RNAseq data from the previous chapter, a subset of the differentially expressed genes from the PPP pathway, along with additional genes involved in NADPH production and glutathione metabolism, were assessed. One of the primary functions of the PPP is the production of NADPH. This NADPH can then be used by the cells to convert oxidized glutathione to the reduced form to prevent oxidative stress (Yuan and Kaplowitz, 2009, Lu, 2013). It was identified that in the high glucose compared to basal glucose environment, SF had a stronger effect in upregulating both

transketolase (TKT, BG DMSO vs BG SF q=0.02, HG DMSO vs HG SF q=0.005) and transaldolase1 (TALDO1 BG DMSO vs BG SF q= 0.0005, HG DMSO vs HG SF q= 0.0003), whilst glucose-6-phosphate dehydrogenase the rate-limiting step in the PPP was only upregulated by SF in the high glucose environment (G6PD, BG DMSO vs BG SF q=0.33, HG DMSO vs HG SF q=0.01), (**figure 5.13**). It was also identified that glutathione reductase (GSR) was upregulated by SF, indicating that the glutathione was indeed found in the reduced form.

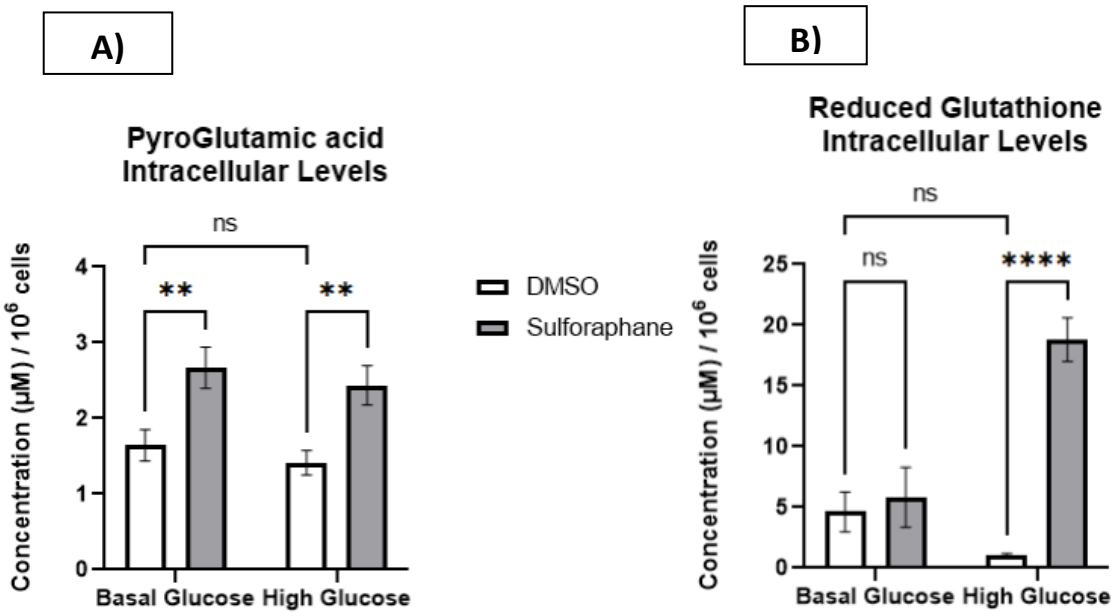

Figure 5.12. SF affects glutathione biosynthesis. HepG2 cells were treated with 10 µM SF for 24 h in basal (5.5 mM) and high glucose (25 mM). A-B) After 24 h metabolites were extracted and quantified using the LC-MS TripleQuad 6490 Agilent. C) PyroGlutamic acid Intracellular Levels. D) Reduced Glutathione Intracellular Levels. All values are expressed as mean ± SD from three individual 10 cm dishes culture dishes. Statistical analysis was carried out using a 2-ANOVA was carried as the two factors are the treatment and glucose levels. Metabolites were normalized to the total number of cells. **Pyroglutamic acid:** DMSO BG vs SF BG p= 0.0027, DMSO BG vs DMSO HG p=0.6, and DMSO HG vs SF HG p=0.0027. **Reduced glutathione:** DMSO BG vs SF BG p= 0.8, DMSO BG vs DMSO HG p= 0.13, and DMSO HG vs SF HG p<0.0001.

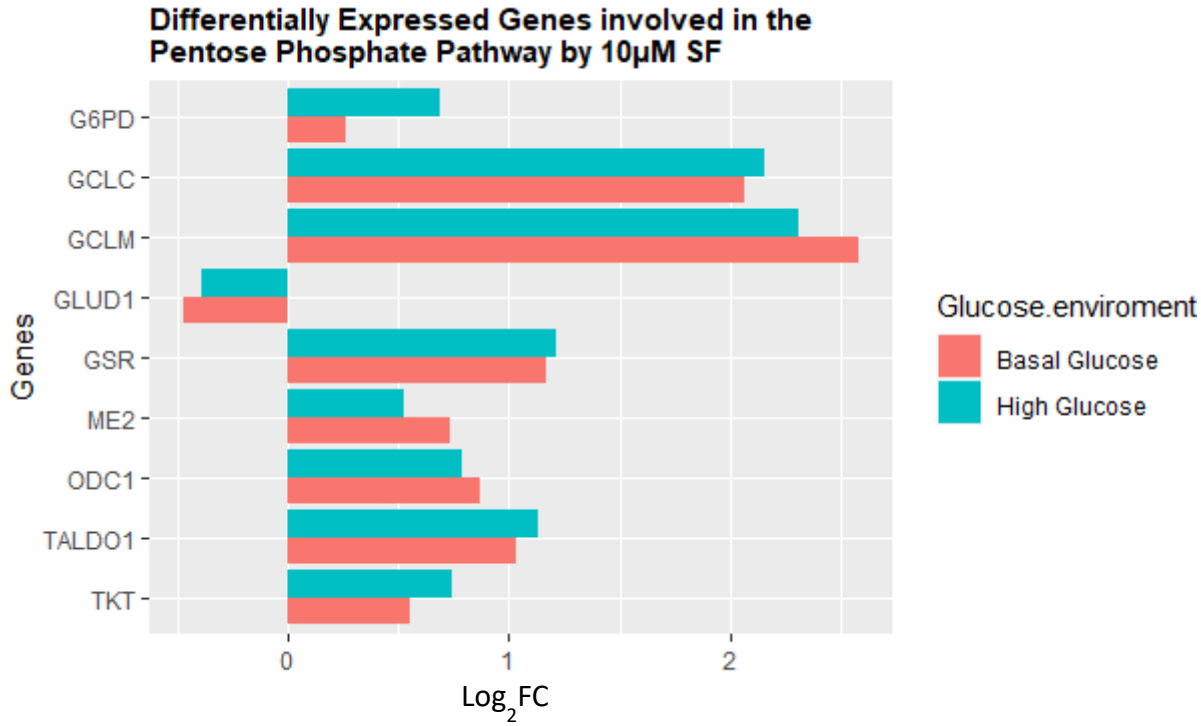

Figure 5.13. **SF effect on genes involved in the NADPH production and glutathione biosynthesis.** HepG2 cells were treated with 10 μM SF for 24 h in basal (5.5 mM) and high glucose (25 mM). After 24 h RNA was extracted and was sent for RNAseq on Illumina. Differentially expressed genes were obtained through EdgeR and limma. All genes are statistically significant following Benjamini-Hochberg multiple testing correction q <0.05. Glucose-6-Phosphate Dehydrogenase (G6PD), Glutamate-Cysteine Ligase Catalytic Subunit (GCLC), Glutamate-Cysteine Regulatory Subunit (GCLM), Glutamate Dehydrogenase 1 (GLDU1, Glutathione Reductase (GSR), Malic Enzyme 2 (ME2), Ornithine Decarboxylase (ODC1), Transaldolase 1 (TALDO1), and Transketolase (TKT).

5.2.8 SF redirects glutamine towards glutathione biosynthesis:

Glutathione biosynthesis occurs in the presence of glutamate, cysteine, and glycine. Glutamate is derived from glutamine, which can also act as an energy source by entering the TCA cycle (Zielke *et al*., 1984). Using the data from the universally labelled glutamine tracer as the only glutamine source (**figure 5.6**), further analysis was carried out to assess whether SF redirected glutamine towards glutathione biosynthesis in the high glucose environment. The glutamine tracer can be converted through the action of glutaminase to M5 glutamate (all five carbon atoms labelled). Glutamate can alternatively feed into the TCA cycle through glutamate dehydrogenase, resulting in M5 α-ketoglutarate. Using GC-MS, the abundance of the metabolites glutamine, glutamate, succinate, and fumarate were quantified. It was identified that SF in a high glucose

environment resulted in an increased abundance of M5 glutamine (p=0.0065), followed by a decrease in M5 glutamate (p=0.0075). The tracer also revealed a profound decrease in M4 succinate (four carbon atoms labelled, due to the release of a molecule of carbon dioxide during the reaction) (p=0.0028), also along with a decrease in M4 fumarate, although failing to reach statistical significance. This decrease in the metabolites of the TCA could be an explanation of the reduction in mitochondrial respiration seen by the Seahorse in the high glucose environments (chapter 3, **figure 3.12b**). The results support the hypothesis that glutamine is indeed re-directed towards glutathione biosynthesis (**figure 5.14**).

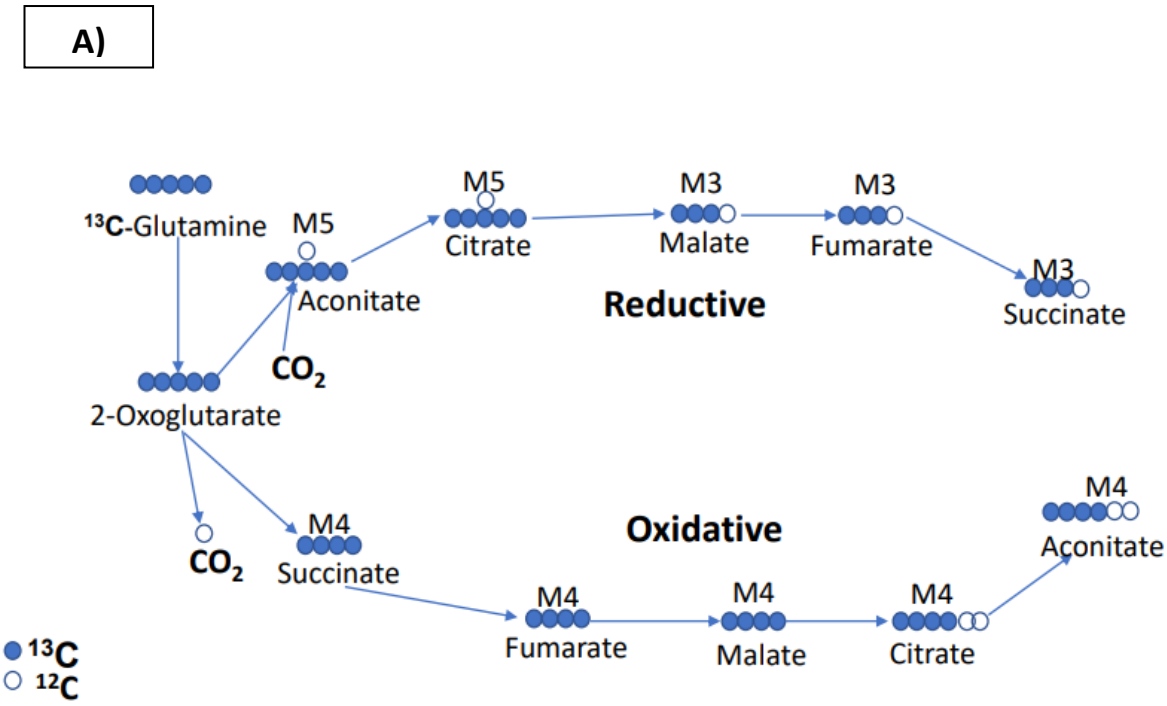

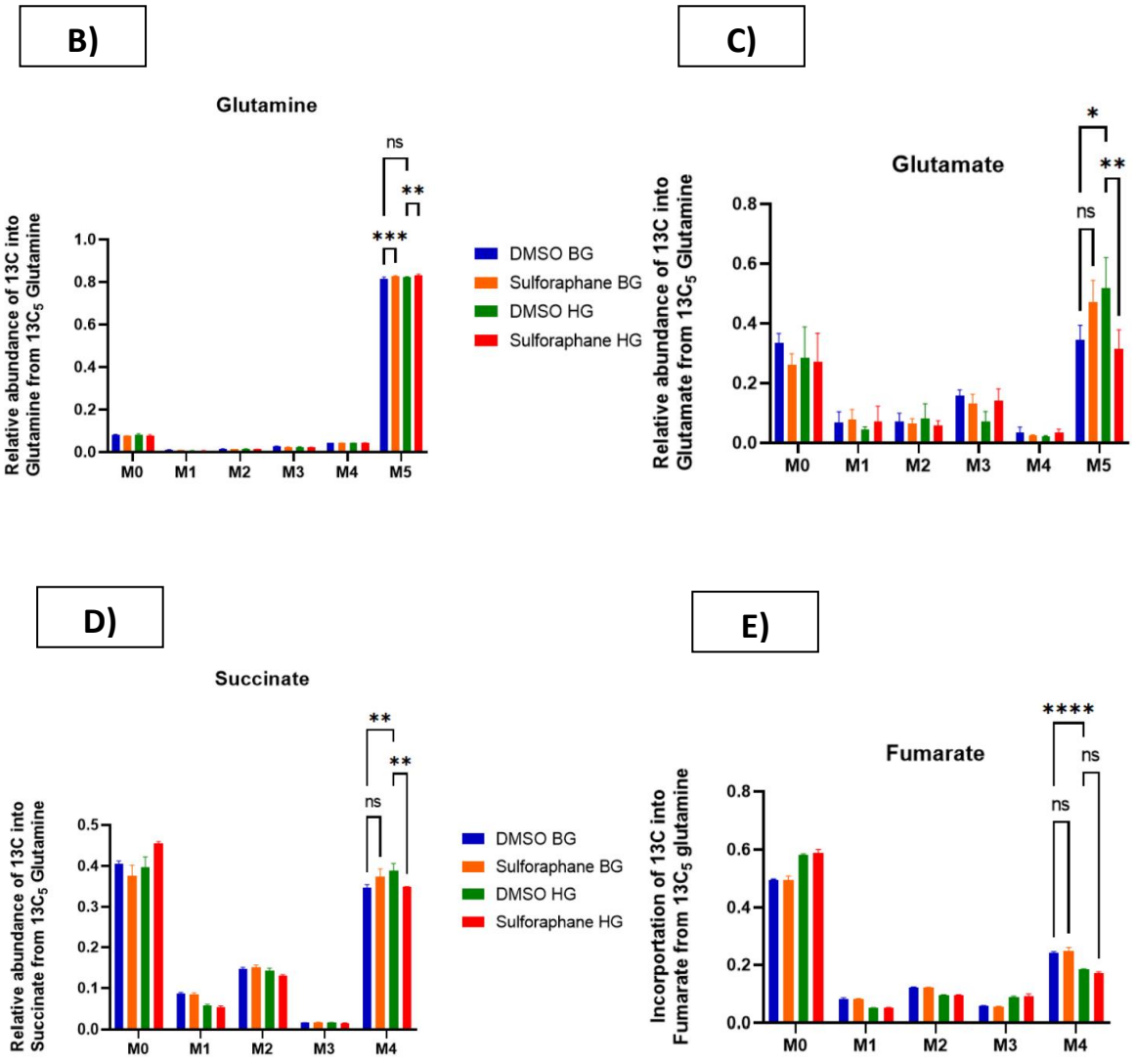

Figure 5.14. Reduction of TCA metabolites through the glutamine tracer suggests SF redirecting glutamine towards a different pathway, possibly glutathione biosynthesis. HepG2 cells were treated with 10 µM SF for 24 h in the presence of the fully labelled glutamine tracer ($13C_5$) in basal glucose (BG, 5.5 mM) or high glucose (HG, 25 mM). After 24 h, metabolites were extracted and quantified using GC-MS. A) Schematic representation of how glutamine is metabolized in the TCA, either through oxidative glutamine metabolism or reductive glutamine metabolism. B) Labelling pattern of glutamine, C) Labelling pattern of glutamate D) Labelling pattern of succinate, and E) Labelling fumarate. All values are expressed as mean ± SD from three individual culture wells. The x-axis M0 to M5 for glutamine and M0 to M4 for succinate and fumarate represent the relative mass isotopomer (MID). This represents the incorporation of the isotope into the metabolite. M0 means that all the carbon atoms in the metabolite are from carbon-12, whereas M+n all labelled carbon atoms come from the carbon isotope. The MID represents the relative abundances of M+0 to M+n isotopologues for each particular metabolite. Consequently, the sum of all fractions from M+0 to M+n is 100% or 1. Statistical analysis was conducted by a 2-ANOVA was carried as the two factors are the treatment and glucose levels. **M5 glutamine:** DMSO BG vs SF BG p= 0.0002, DMSO BG vs DMSO HG p=0.96, and DMSO HG vs DMSO SF p=0.0065. **M5 glutamate:** DMSO BG vs SF BG p=0.2, DMSO BG vs DMSO HG p= 0.01, and DMSO HG vs SF HG p=0.0075. **M4**

succinate: DMSO BG vs SF BG p= 0.19, DMSO BG vs DMSO HG p=0.0016, and DMSO HG vs SF HG p=0.0028. **M4 fumarate:** DMSO BG vs SF BG p= 0.96, DMSO BG vs DMSO HG p<0.0001, and DMSO HG vs SF HG p=0.69.

5.2.9 SF drives Methionine to produce S-Adenosyl Methionine to feed methylation reactions

The untargeted metabolomics (**figure 5.6**) revealed that in both glucose environments SF increased the levels of methionine (**figure 5.6 d**). Since the extracellular levels of methionine were not changed by SF (**Appendix Supplementary S4**), the next question that was assessed was firstly understanding where the methionine was derived from and secondly the purpose of the increase in methionine. As methionine is the only other amino acid, apart from cysteine, to have a sulfur group, it was assessed whether the additional methionine was obtained from cysteine through the backflow of the Transsulfuration pathway. Once in the cell, cysteine can enter the methionine cycle by a two-step process: first, it is converted to cystathionine and eventually to SAH, since these reactions are reversible. Using LC-MS, it was identified that the extracellular levels of cysteine in both glucose environments were indeed largely decreased compared to the controls, suggesting that SF resulted in increased cysteine import into the cell (**figure 5.15a**). Figure 5.15b revealed that the high compared to basal glucose environment, SF treatment decreased the intracellular concentrations of cysteine, suggesting that a part of the cysteine pool was redirected towards glutathione biosynthesis, whilst the other part was redirected into the transsulfuration pathway for eventually the regeneration of methionine. Using the RNAseq data it was recognized that SF upregulated the activity of cystine/glutamate transporter, in both glucose environments transporter (**q < 0.05, figure 5.15c**).

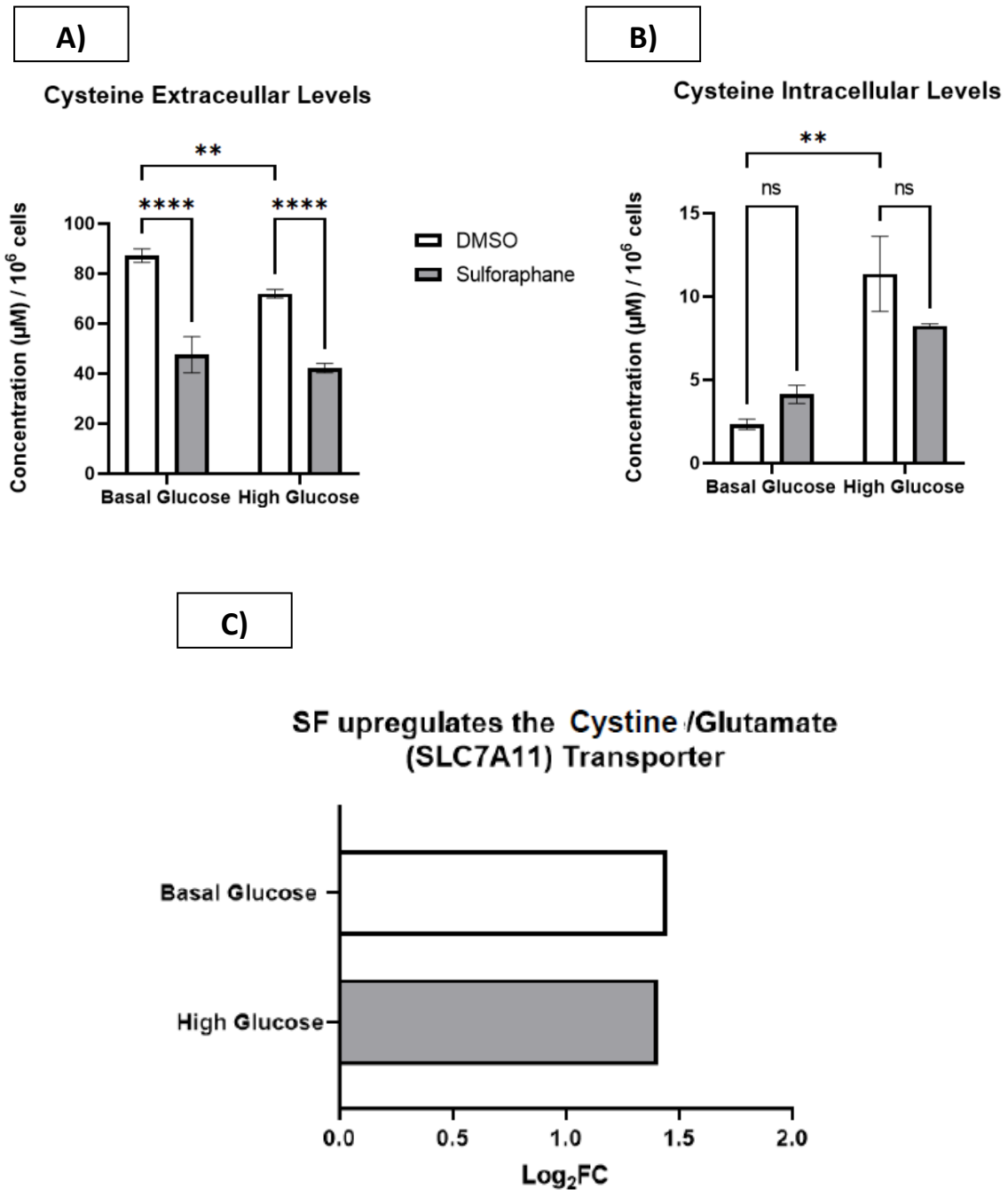

Figure 5.15. SF effect on cysteine metabolism. HepG2 cells were treated with 10 µM SF for 24 h in basal (5.5 mM) and high glucose (25 mM). After 24 h, metabolites were extracted and quantified using the LCMS TripleQuad 6490 Agilent. A) Extracellular levels of cysteine. B) Intracellular levels of cysteine. C) Whole transcriptome analysis on HepG2 looking at the cystine receptor q<0.05 corrected using the Benjamini Hochberg. All values are expressed as mean ± SD from three individual 10cm dishes. For LC-MS data, statistical analysis was carried out using a 2-ANOVA was carried as the two factors are the treatment and glucose levels. Metabolites were normalized to the number of cells. **Cysteine Extraceullar Levels:** DMSO BG vs SF BG p<0.0001, DMSO BG vs DMSO HG p=0.077, and DMSO HG vs SF HG p<0.0001. **Cysteine Intraceullar Levels:** DMSO BG vs SF BG p=0.51, DMSO BG vs DMSO HG p=0.0014, and DMSO HG vs SF HG p=0.15.

As the GSEA analysis revealed no enrichment in genes related to the methionine cycle, a method was developed using the LC-MS to assess all the metabolites in the methionine cycle: methionine, SAM, SAH, and homocysteine. This was done to gain a better understanding of the molecular mechanism of how methionine is metabolized by SF. It was identified that the increased levels of methionine by SF correlated with increased SAM levels, the first step in methionine metabolism, in both basal and high glucose environments (**Fig. 5.16 a,b**). The RNA-seq data was used to assess whether the increased levels of SAM would feed into the methylation reaction (**figure 5.16 e**). It was identified in the high glucose environment, SF resulted in almost a 32-fold upregulation in the DNA (cytosine-5)-methyltransferase 3-like (DNMT3L) gene, along with a small significant downregulation, approximately 2-fold of histone deacetylase 5 (HDAC5), histone deacetylase 6 (HDAC6) and DNA (Cytosine-5)-methyltransferase 3 beta (DNMT3B), by SF in both glucose environments.

The analysis through LC-MS also revealed that in the high glucose environment, SF resulted in a decrease in SAH, further supporting the idea that the reduction in the recovered SAH, was due to SAM being redirected for methylation reaction. The final step in the cycle is the conversion of homocysteine back to methionine. This can occur through two different pathways: either through methionine synthase where the methyl group is obtained from folate through vitamin B12 through the aid of 1C metabolism or through betaine, an amino acid that acts as an important cofactor for methylation reactions. The use of betaine is restricted to the liver and kidney tissue only (Finkelstein, 1998). As it was identified in the RNAseq data a large upregulation of the betaine-homocysteine S-methyltransferase (BHMT2) gene (**figure 5.8 b**), it was postulated that the remethylation of homocysteine was derived through betaine. LC-MS analysis also revealed that physiological concentrations of SF, resulted in a decrease in betaine, supporting the results of the gene expression. The results, therefore, indicate that SF is feeding methylation reactions, as there is a blockage in the top part of the methionine cycle (**figure 5.16**).

A)

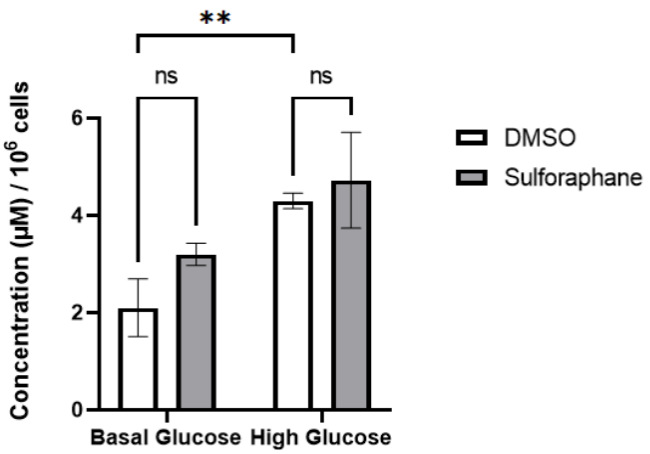
Methionine Intracellular Levels
**
ns
ns
Concentration (µM) / 10^6 cells
6
4
2
0
Basal Glucose
High Glucose
DMSO
Sulforaphane

B)

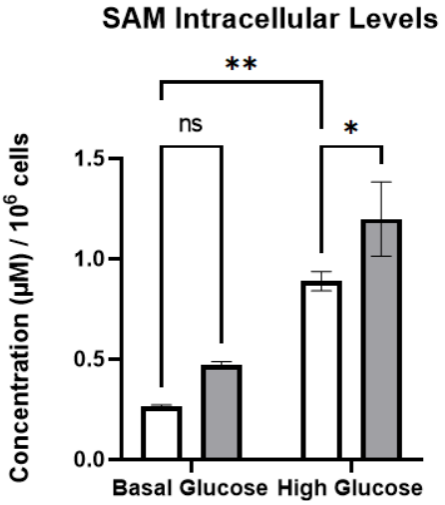
SAM Intracellular Levels
**
ns
*
Concentration (µM) / 10^6 cells
1.5
1.0
0.5
0.0
Basal Glucose
High Glucose

C)

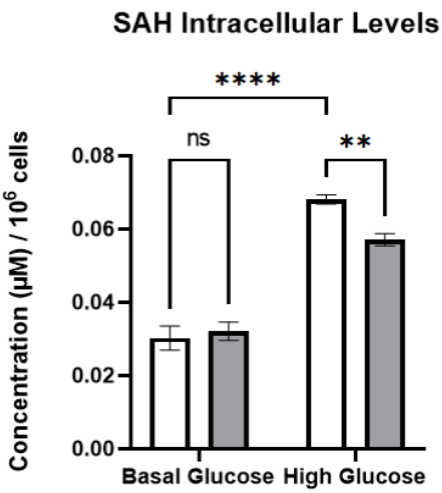
SAH Intracellular Levels
****
ns
**
Concentration (µM) / 10^6 cells
0.08
0.06
0.04
0.02
0.00
Basal Glucose
High Glucose
DMSO
Sulforaphane

D)

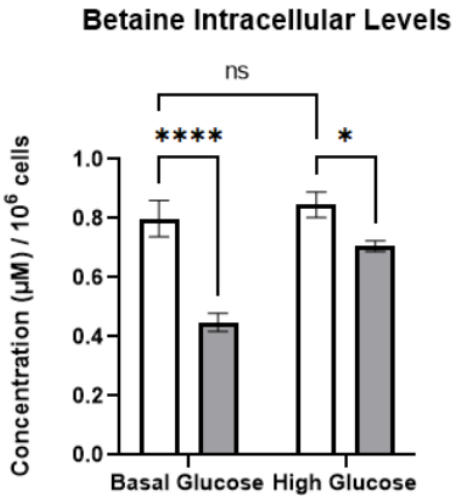
Betaine Intracellular Levels
ns
****
*
Concentration (µM) / 10^6 cells
1.0
0.8
0.6
0.4
0.2
0.0
Basal Glucose
High Glucose

E)

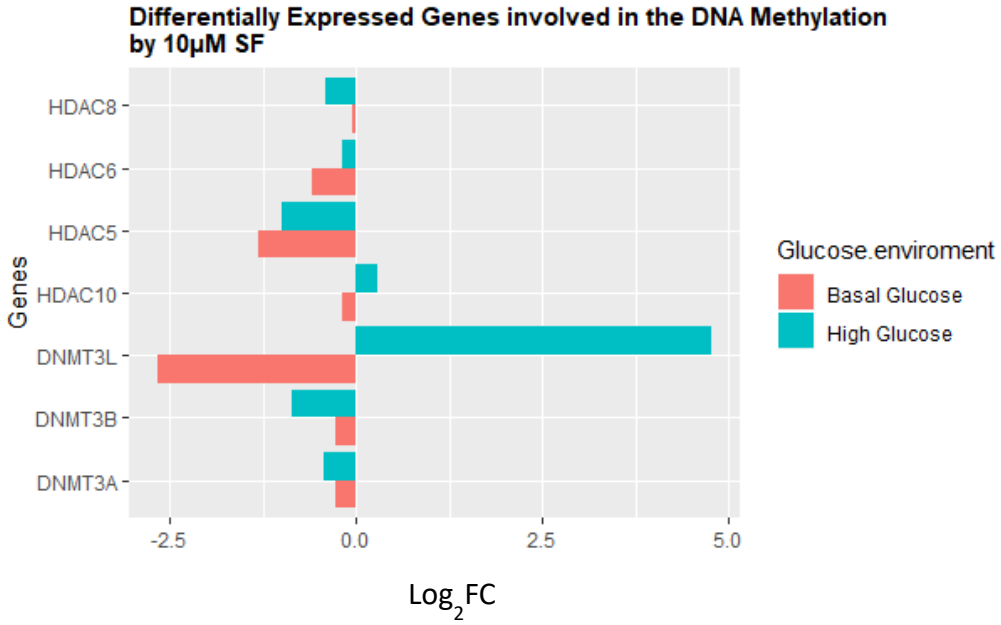

Figure 5.16. SF influence on the methionine cycle. HepG2 cells were treated with 10 µM SF for 24 h in basal (5.5 mM) and high glucose (25 mM). After 24 h, metabolites were extracted and quantified using the LC-MS TripleQuad 6490 Agilent. A) **Methionine:** DMSO BG vs SF BG p=0.18, DMSO BG vs DMSO HG p=0.0082. and DMSO HG vs SF HG p=0.81 B) **S-Adenosyl methionine (SAM)**: DMSO BG vs SF p= 0.14, DMSO BG vs DMSO HG p=0.0011, and DMSO HG vs SF HG p=0.04. C) **S-Adenosyl homocysteine (SAH):** DMSO BG vs SF BG p=0.77, DMSO BG vs DMSO HG p<0.0001, and DMSO HG vs SF HG p=0.0064 D) **Betaine**: DMSO BG vs SF BG p<0.0001, DMSO BG vs DMSO HG p=0.57, and DMSO HG vs SF HG p= 0.01. All values are expressed as mean ± SD from three individual 10 cm dishes culture dishes. Statistical Analysis was carried out using a 2-ANOVA was carried as the two factors are the treatment and glucose levels. Metabolites were normalized to the number of cells. E) Whole transcriptome analysis on HepG2 looking at the Genes involved in DNA methylation. HDAC8 (Histone deacetylase 8), HDAC6 (Histone deacetylase 6), HDAC5 (Histone deacetylase 5), HDAC10 (Histone deacetylase 10), DNMT3L (DNA (cytosine-5)-methyltransferase 3-like), DNMT3B (DNA (Cytosine-5)-methyltransferase 3 beta, DNMT3A (DNA (Cytosine-5-)-methyltransferase 3A. The following genes HDAC5, HDAC6, DNMT3B, and DNMT3L were significant q<0.05 after multiple testing corrections by Benjamini Hochberg.

5.2.10 SF in a high glucose environment contributes to pyruvate anaplerosis through pyruvate carboxylase activity

Pyruvate anaplerosis (anaplerosis is the act of replenishing intermediates of the TCA cycle that have been used up for the biosynthesis of additional pathways) allows the TCA cycle to oxidize acetyl-CoA, providing backbones for biomass production. Using the uniformly glucose tracer it is possible to identify pyruvate anaplerosis by measuring M3 malate, fumarate, or oxaloacetate (OAA). However, since OAA is very unstable, the labeling pattern of aspartate is instead measured as it can serve as a surrogate of oxaloacetate. In the experiment where HepG2 was cultured with the labelled uniformly glucose tracer as the sole glucose source, it was identified that physiological concentrations of SF in a high glucose environment resulted in a significant increase in M3 malate ($p=0.006$), and fumarate although failed to reach significance. The data also revealed a significant increase in M5 citrate ($p <0.0001$) (**figure 5.17 b and c**). Pyruvate carboxylase (PC) can carboxylate $13C_3$ pyruvate with CO2, producing $13C_3$ OAA (Buescher *et al*., 2015). In turn, M3 OAA condenses with M2 acetyl-CoA to generate M5 citrate. The levels of M3 aspartate were therefore also assessed. A decrease in M3 aspartate ($p=0.01$) was identified, potentially suggesting that aspartate was being utilized by reacting with acetyl-CoA to generate citrate (**figure 5.17 d**). Gene expression of pyruvate carboxylase was looked at in the RNA seq data but was not differentially expressed. Untargeted metabolomics in both the basal and glucose environments also revealed an increase in the metabolite Pantothenic acid coupled with a decrease in the metabolite N-acetyl Aspartic acid (NAA) (**figure 5.6 c**). Pantothenic acid is used for the synthesis of coenzyme A. CoA can transfer the acyl group to produce acetyl-CoA. It may be that pyruvate anaplerosis is occurring to allow acetyl-CoA to be transferred to the cytoplasm to allow the synthesis of NAA. NAA has been identified to be the second most abundant metabolite in the human brain after the amino acid glutamate. It is thought to act as a neurotransmitter. Further research is nevertheless needed to understand the function of this metabolite.

A)

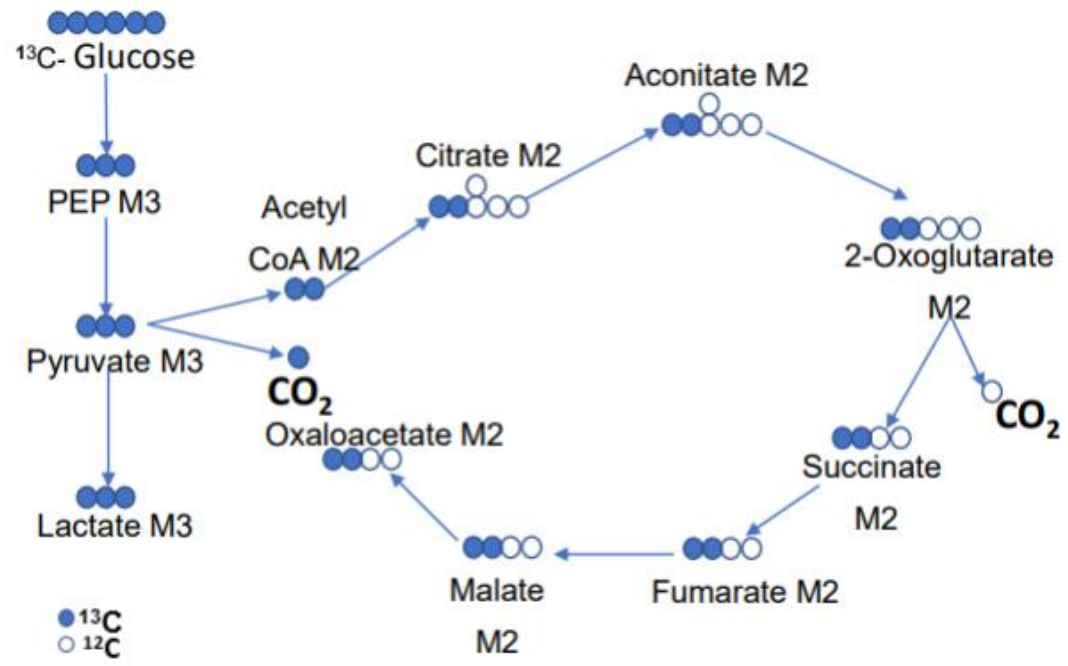
13C- Glucose
PEP M3
Pyruvate M3
Lactate M3
Acetyl
CoA M2
Citrate M2
Aconitate M2
2-Oxoglutarate
M2
CO2
CO2
Oxaloacetate M2
Succinate
M2
Fumarate M2
Malate
M2
13C
12C

B)

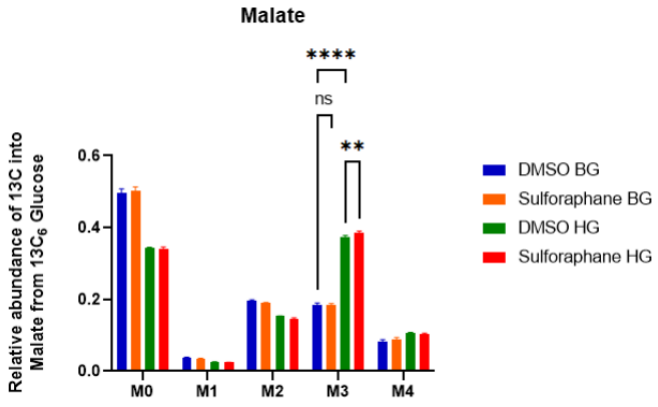
Malate
Relative abundance of 13C into Malate from 13C6 Glucose
****
ns
**
0.6
0.4
0.2
0.0
M0
M1
M2
M3
M4
DMSO BG
Sulforaphane BG
DMSO HG
Sulforaphane HG

C)

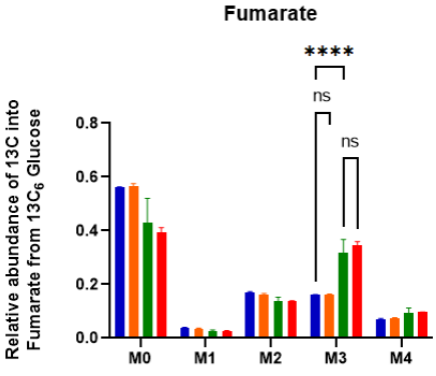
Fumarate
Relative abundance of 13C into Fumarate from 13C6 Glucose
****
ns
ns
0.8
0.6
0.4
0.2
0.0
M0
M1
M2
M3
M4

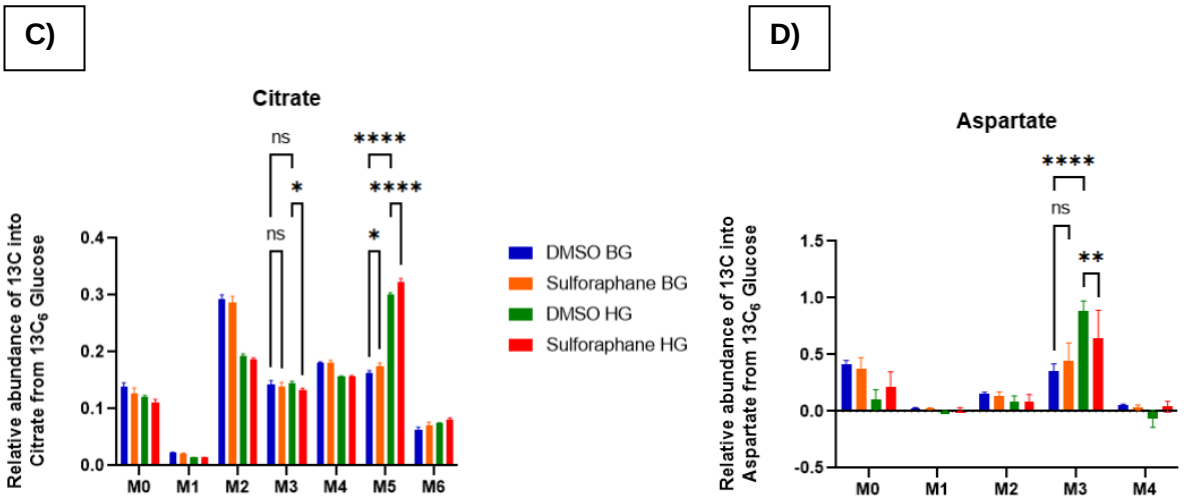

Figure 5.17. SF affects pyruvate anaplerosis in the high glucose environment. HepG2 cells were treated with 10 µM SF in DMEM media containing 5.5 and 25 mM $13C_6$ glucose and 4 mM $^{12}C_5$ glutamine -FBS. After 24 h, metabolites were extracted and determined by GC-MS. The x-axis M0 to M6 for citrate and M0 to M4 for the other metabolites represent the relative mass isotopomer (MID). N=3. A) Schematic representation of how the glucose tracer is metabolized in the TCA. B) Labelling pattern of malate, C) Labelling pattern of fumarate D) Labelling pattern of citrate, and E) Labelling aspartate All values are expressed as mean ± SD from three individual culture wells.

M3 Malate: DMSO BG vs SF BG p=0.99, DMSO BG vs DMSO HG p<0.0001, and DMSO HG vs SF HG p=0.0067. **M3 Fumarate:** DMSO BG vs SF BG p= 0.99, DMSO BG vs DMSO HG p<0.0001, and DMSO HG vs SF HG p=0.59. **M3 Citrate:** DMSO BG vs SF BG p=0.91, DMSO BG vs DMSO HG p=0.88, and DMSO HG vs SF HG p=0.01. **M5 Citrate:** DMSO BG vs SF BG p=0.015, DMSO BG vs DMSO HG p<0.0001, and DMSO HG vs SF HG p<0.0001. **M3 Aspartate:** DMSO BG vs SF p=0.62, DMSO BG vs DMSO HG p<0.0001, and DMSO HG vs SF HG p=0.001.

5.3 Discussion:

In this chapter, HepG2 cells were treated with physiological concentrations of SF, in the presence of glucose and glutamine isotopic tracers. The main aim was to understand how SF affects the metabolism of these substrates in the liver. One of the aims of this chapter was to determine whether the reduction in overall mitochondrial respiration (Seahorse result, chapter 3) was due to the glucose being re-directed towards the PPP. Although the tracer experiment suggests that the glucose is not directed towards the pentose phosphate pathway, there is sufficient evidence to suggest through an increase in the PPP gene set (**Table S1 Appendix**) and reduction in glycolysis and increase in the metabolite ribulose-5-phosphate, the end product of the oxidative branch of the PPP in the HG data by SF (**figure 5.6 b**), that the glucose is still redirected towards the PPP.The research presented in this chapter also stumbled on a novel finding; identifying the molecular mechanism on how SF interferes with 1C metabolism. This is the first study to identify a mechanism on how SF rewires central metabolism to support the antioxidant response. Figure 5.18 summarizes the findings of this chapter on how SF interferes with 1C metabolism.

5.3.1 SF and One Carbon Metabolism:

One carbon (1C) metabolism is a series of biosynthetic reactions consisting of two main pathways: the folate and methionine cycles. 1C metabolism acts as a sensor to regulate the nutrient status of the cells. The main purpose is to catabolize one-carbon (methyl units) required for vital cellular functions such as: providing nucleotides for DNA synthesis, the cell building blocks, as well as reducing agents such as NADH/NADPH (Rosenzweig *et al.*, 2018). These one carbon units are derived mainly from two non-essential amino acids; serine and glycine.

In its long history of research, SF has been referred to as a chemopreventive agent due to its ability to target several different mechanisms within the cell to prevent carcinogenesis (Nandini *et al*., 2020). This is the first study, to identify SF's ability to interfere with 1C metabolism, by decreasing the intracellular levels of serine and glycine, and downregulating genes involved in the serine and glycine biosynthetic pathway, along with upregulating genes in the folate cycle. Although the expression of PSAT1, PSPH, and SHMT1 was not detected, SF did downregulate PHGDH. Reduction of serine may suggest a reduction in the number of methyl units entering the cycle. In turn, this could result in fewer substrates available for DNA synthesis, hence potentially identifying novel mechanisms through which SF may have anticarcinogenic properties. These SSP genes such as PHGDH and SHMT are often upregulated in

certain cancer cell lines, including but not limited to: lung and breast cancer cell lines along with melanoma. The outcome is the ability of the cells to proliferate and metastasize (Mattaini *et al*., 2016, Locasale *et al*., 2011, Ye *et al*., 2014).

Similarly, overexpression of PHGDH in non-tumorigenic breast cells can result in these cells developing a cancer phenotype (Chen *et al*., 2013). Simply inhibiting the activity of PHGDH, either genetically or chemically, inhibits the proliferation of cancer cells. Similarly, deleting or silencing SHMT relies on tumours becoming addicted to exogenous serine, and serine starvation has been shown to reduce tumour growth (Yang and Vousden, 2016). Mutations in the 1C metabolism pathway are often found in tumour cells. For example, mutation of the oncogene KRAS results in increased DNA methylation due to increased levels of SAM obtained via 1C metabolism.

Furthermore, the mechanistic target of rapamycin (mTOR) is a serine/threonine protein kinase that is the core component of two distinct protein complexes: mTORC1 and mTORC2, involved in regulating a wide range of cellular processes (Zou *et al*., 2020b). Within the last couple of years, emerging evidence has shown an oncogenic interplay between mTOR and 1C metabolism. For example, a study showed that mTORC1 activates 1C metabolism in myelopoiesis. It was identified that deletion of mTORC1 impaired cells' ability to uptake glucose, carry out glycolysis, and redirect the glucose towards 1C metabolism (Karmaus *et al*., 2017). A second study identified that primary pancreatic ductal epithelial cells obtained from mice that expressed a mutation in the KRAS gene, along with deletion of the LKB1 gene, results in mTOR activation resulting in increased *de novo* serine biosynthesis along with 1C metabolism (Kottakis *et al*., 2016). It has also been shown that for lung cells to metastases, the resulting pyruvate levels in the environment result in increased mTORC1 signalling; the outcome is amplified serine biosynthesis (Rinaldi *et al*., 2021). A potential mechanism on how SF may inhibit these genes involved in the serine and glycine synthetic pathway that this research did not address is through mTOR inhibition. It has recently been discovered that SF can inhibit mTOR in an NRF2 independent manner (Zhang *et al*., 2019). In addition, a second study also showed that primary hepatocytes obtained from mice placed on a High-Fat diet treated with SF resulted in autophagy through AMPK, resulting in inhibition of mTOR (Yang *et al*., 2016).

Through the GSEA, it was possible to obtain a molecular mechanism on how SF interferes with 1C metabolism. The data identified that SF increased the expression of MTHFD1L. Whilst this gene has also been shown to be upregulated in cancer, (Lee *et al*., 2017, Ducker *et al*., 2016), the reaction catalyzed by MTHFD1L is involved in the production of NADPH. A hypothesis is that the upregulation of MTHFD1L along with additional genes such as ALDH1L1 in the folate cycle occurs to produce NADPH to

support the conversion of oxidized to reduced glutathione. Culturing hepatocytes under high concentrations of glucose results in these cells undergoing a state of inflammation, having increased oxidative stress and increased production of inflammatory cytokines (Panahi *et al*., 2018). Therefore, SF interfering with 1C metabolism in the high glucose environment is a likely mechanism for the cells to increase their antioxidant capacity by synthesizing additional glutathione (Konno *et al*., 2017, Li and Ye, 2020).

When respiration is impaired, serine catabolism becomes the primary source of NADH. If this NADH is not used, its accumulation inhibits the TCA cycle, resulting in decreased cell proliferation (Yang *et al*., 2020a). Whilst the overall reduction in mitochondrial respiration (Seahorse Data) due to the glutamine being redirected to different processes may not necessarily impair respiration, it is likely, though, that the NADH pool from the TCA cycle may be reduced. Therefore, to support glutathione function, the reduction of serine may also be due to an increase in the concentrations of NADH/NADPH. It was also surprising to find that SF treatment upregulated two genes involved in purine metabolism: GART and ATIC. ATIC is involved in the production of inosine monophosphate (Yin *et al*., 2018). Purine metabolism is related to several biochemical reactions, such as maintaining the adenylate and guanylate pool. The primary metabolite in purine metabolism is inosine monophosphate (Yin *et al*., 2018). IMP carries out many functions as it can be used for purine biosynthesis but can also be converted to AMP and/or GMP (Zhao *et al*., 2015). Most specifically, AMP can then be regenerated to ATP through adenosine kinase (AK). It has recently been shown that the reduced form of nicotinamide ribonucleoside (NRH) NRH is phosphorylated to NMNH by AK through ATP, which is then eventually converted to NADH. The final additional step consists of NAD^+ being phosphorylated through the action of NAD^+ kinase in the presence of ATP to produce $NADP^+$ (Yang *et al*., 2020b). Therefore, it is hypothesized that upregulation of GART and ATIC is a mechanism for the cells to regenerate their ATP levels which can then be used either as a feedback loop mechanism to fuel additional NADPH or for the production of additional SAM for methylation reactions (Boison *et al*., 2002).

So far, only one other study identified NRF2 regulating 1C metabolism (DeNicola *et al*., 2015). This study reported that constituent activation of NRF2 in the lung carcinoma A549, along with additional lung carcinoma cell lines through the action of ATF4, resulted in the upregulation of the genes involved in the SSP. This led to increased levels of serine and glycine, allowing the tumour cells to metastasize *(*DeNicola *et al*., 2015). Although this may be tissue specific, it also suggests that constituent NRF2 activation has an adverse effect. The data further highlights that that intermittent and

cyclic NRF2 induction, such as that observed following a diet rich in NRF2 inducers (S-containing metabolites and polyphenols) offers imporved hepatic metabolism.

The other amino acid also critical in 1C metabolism is glycine. It was identified that SF resulted in a decrease in the intracellular levels of glycine. One of the primary genes involved in glycine metabolism is the glycine cleavage pathway, glycine decarboxylase (GLDC). Studies have shown that non-small cell lung cancer and glioblastomas have sustained GLDC hyperactivity, promoting tumorigenesis in these cells (Zhang *et al*., 2012a). In this study, it was identified that SF was also able to suppress the activity of GLDC. This depletion of glycine and the inhibition of the GLDC enzyme are likely due to the glycine being utilized for Glutathione biosynthesis (Ye *et al*., 2014). In regulatory T cells (T_{regs}), a group of immune cells whose function is to prevent autoimmunity and reduce the formation of chronic inflammatory diseases, disruption of glutathione by GCLC deletion in mice results in increased ROS accumulation. This triggers NRF2, resulting in increased serine import. This increase in serine, although it fuels 1C metabolism it, also suppresses T_{regs} ability to scavenge radicals (Kurniawan *et al*., 2020). This stress feedback loop between glutathione and serine that controls T_{regs} function, may also be occurring similarly in hepatocytes.

Targeting 1C metabolism for cancer therapy is not straightforward. Currently, there are two drugs available on the market. The current therapies used to inhibit 1C metabolism in cancer cells include methotrexate and 5-fluorouracil (5-FU). Methotrexate belongs to the family of antifolates, as it inhibits the enzyme DHFR in the folate cycle. 5-FU, on the other hand, has been shown to inhibit the enzyme thymidylate synthase (TYMS), which catalyzes the transfer of a methyl group from methylene-THF onto dUMP to make dTMP (Ducker and Rabinowitz, 2017). The present work provides the first *in vitro* evidence to suggest that a broccoli bioactive and potentially other food bioactives have the capability of inhibiting 1C metabolism.

5.3.2 SF and methionine

Another key finding in this chapter is the consistent increase in the levels of methionine; in both glucose environments. SF has been previously stated to impact epigenetics by affecting the DNA methylation status of cells (Su *et al*., 2018). For example, SF treatment on LnCap prostate cancer cells decreased the expression of specific DNA methyltransferases such as DNMT1 and DNMT3b, but at the same time, SF lowered the methylation in the promoter region of the cyclin D2 gene. This region has been shown to contain multiple binding sites where the transcription factors c-Myc and Sp1 bind onto (Hsu *et al*., 2011). The study showed that reduced methylation of the cyclin D2 promoter resulted in increased expression of the cyclin D2 gene,

contributing to the anti-proliferative effect of SF (Hsu *et al*., 2011). A more recent study on HepG2 showed that varying concentrations of SF from 2-32 µM resulted in SF inhibiting histone deacetylases (HDACs). This resulted in SF altering the methylation status in the promoter region of several oncogenic transcription factors. This resulted in leading to induced cell death through apoptosis and cell cycle arrest, thereby further highlighting its chemopreventive action (Dos Santos *et al*., 2020). Up to now, although it was recognized that SF acted as an epigenetic modulator; the mechanism, however, on how this occurred was not fully understood. In this chapter, a potential mechanism is identified for the first time through which SF leads to the accumulation of methionine, which feeds into the methionine cycle, resulting in increased SAM. This SAM acts as the substrate for the methylation reactions needed to alter the DNA. Research on varying hepatocellular carcinoma cell lines has shown a consistent downregulation in MAT1A; this gene is involved in the synthesis of S-Adenosylmethionine along with an upregulation of the MAT2A gene (Frau *et al*., 2013). The downregulation in MAT1A along with upregulation of MAT2A resulted in decreased levels of SAM. Studies on rodents treated with carcinogens have shown that supplementation with SAM inhibits carcinogenesis, whereas MAT1A-KO mice exhibit steatosis, resulting in the accumulation of mononuclear cells in periportal areas, ultimately leading to hepatocellular carcinoma (Frau *et al*., 2013). This imbalance between MAT1A and MAT2A has also been associated with global DNA hypomethylation, along with a wide range of molecular signalling dysfunctions such as a decrease in DNA repair, increase in polyamine synthesis, etc (Frau *et al*., 2013). The fact that SF increases the levels of SAM in the hepatocellular carcinoma cell line may suggest a different mechanism on how SF can suppress carcinogenesis or improve metabolic functions.

In addition, what remains unclear is whether NRF2 or other proteins mediate the increase in methionine through SF. It has recently been identified through both RNAseq and metabolomics of livers from mice fed a methionine restricted (MR) diet that 6h post-MR resulted in inactivation of both the integrated stress response as well as the anti-oxidant response through the combined action of the PERK/NFE2L2 signalling pathway along with the action ATF4 (Stone *et al*., 2021). This MR did not, however, result in increased ER stress or induced the unfolded protein response. This current study demonstrated that the sulfur group to support increased methionine production by SF was likely derived from the increased import of cysteine from the media. One of the remaining unanswered questions in this chapter is understanding the source of methyl donors for the synthesis of methionine. The data obtained suggest that betaine (trimethylglycine) is the most likely candidate, although it may be through a combination of both serine and betaine. This may also further explain serine depletion and upregulation of genes involved in 1C metabolism. Therefore, future work should

carry out experiments with both the labelled hydroxymethyl group of the serine tracer along a labelled betaine tracer.

5.3.4 SF and its effect on glycolysis:

Due to the increasing amount of evidence from both *in vitro* and *in vivo* studies that SF impacts glucose homeostasis, in chapter 3 the Seahorse Extracellular Flux Analyzer was used to assess whether altering the glucose environment, would impact mitochondrial metabolism; (assessing the TCA cycle and oxidative phosphorylation). In this chapter, data from four separate independent experiments (untargeted metabolomics, glucose tracer, RNAseq, and the Seahorse) all identified a common theme; physiological concentrations of SF had a profound effect in reducing glycolysis, especially in the basal glucose environment. The untargeted metabolomics, revealed a decrease of both end products of glycolysis (lactate and pyruvate), in basal glucose, whilst the glucose tracer revealed a profound decrease in M3 pyruvate in basal but not high. The Seahorse metabolic analysis revealed a decrease in the ECAR (a measurement of glycolysis) in both glucose environments and RNAseq revealed a wide range of genes in the basal glucose environment being downregulated. These findings build on previous findings in the literature, shown by Carrasco-Pozo who identified that SF downregulated the activity of two additional glycolytic genes, hexokinase and pyruvate kinase (Carrasco-Pozo *et al*., 2019). The most common medication given to type 2 diabetics to treat diabetes is the drug metformin (Glucophage). It has been identified that metformin acts to suppress circulating glucose by two separate mechanisms: firstly, it can act directly on the liver by lowering the liver's ability to produce glucose whilst at the same time acts on the gut to increase the utilization of glucose, as well as increasing the levels of GLP-1 and can also alter the microbiome (Rena *et al*., 2017). At the molecular level, metformin seems to have a similar effect to SF, activating pAMPK, increasing insulin sensitivity, reducing the expression of gluconeogenic genes, as well as potentially inhibiting the activity of the glycolytic gene fructose-1,6-bisphosphate (Rena *et al*., 2017). Whilst the data needs to be interpreted with caution, as was carried out in a cancer cell line, which has increased glucose uptake and increased glucose utilization, nevertheless, the data shows SF as a promising bioactive that can regulate glucose homeostasis. Therefore, it is hoped that the output of this research will in the long term support dietary recommendations in diabetes and the pre-diabetic cohort of patients to undertake lifestyle changes.

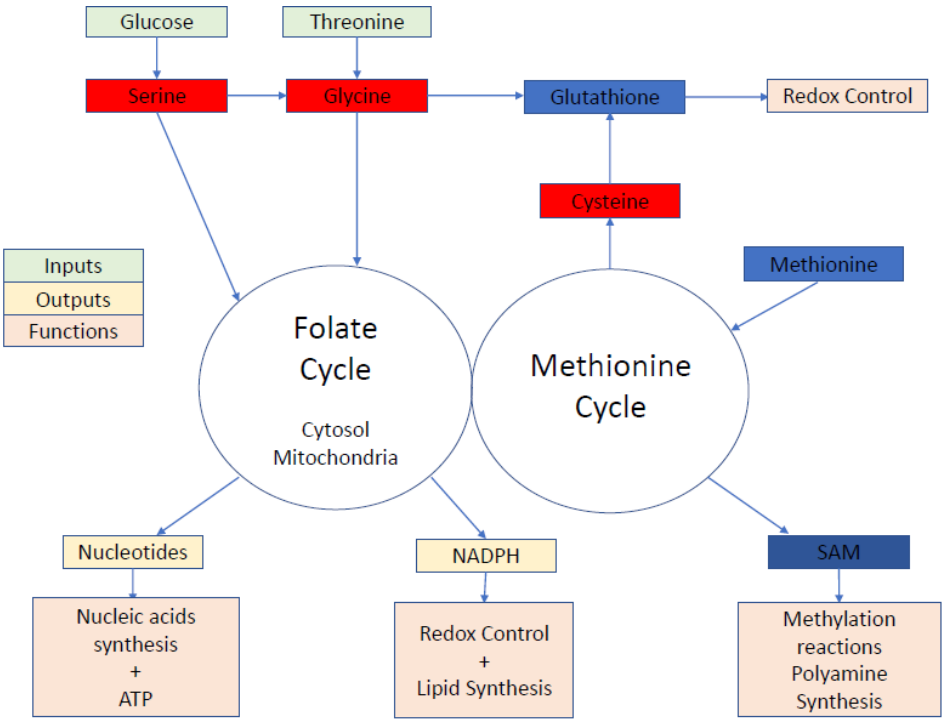

Figure 5.18: Summary of the findings of this chapter, showing how SF interferes with 1C metabolism in the high glucose environment to promote the antioxidant response. The inputs include the starting substrates: these include glucose, and amino acids (threonine). The outputs are the product of the reaction and cycle, which have also been colored red by a decrease and blue increase in those metabolites that have been measured. For example, the output of the serine synthetic pathway is serine, which its intracellular concentration is decreased. Serine feeds into the folate cycle, in which the output is nucleotides. The function of the nucleotides is ATP production and synthesis of nucleic acids.

5.4 Conclusion:

The main question that this chapter aimed to explore was whether SF was redirecting the glucose to the PPP in the high glucose environment. Real-time energy production assessed using the Seahorse Extracellular Flux Analyser demonstrated that SF reduced glycolysis in HepG2 cells in basal and high glucose environments, suggesting the excess glucose is redirected towards the PPP. To support GSH synthesis, SF altered levels of the three amino acids that are the biosynthetic building blocks, namely, increased intracellular utilization of glycine and glutamate, by redirecting the latter away from the TCA cycle, as well as increased the import of cysteine from the media. To support the cellular antioxidant enzyme response, SF also altered pathways generating NADPH, the necessary cofactor for these oxidoreductase reactions, namely pentose phosphate pathway (PPP) and 1C-metabolism. Firstly, SF increased genes in the PPP pathway, including the glucose-6-phosphate dehydrogenase, the rate-limiting step of the PPP, and increased the PPP metabolite ribulose-5-phosphate. Secondly, SF upregulated genes in the folate cycle, namely ALDH1L1 and MTHFD1L, and utilized serine as a methyl donor for THF to support the 1C metabolism, along with SF inhibiting genes involved in the serine and glycine synthetic pathway. The other prominent finding is identifying a mechanism on how SF modulates epigenetics by regulating the levels of methionine and controlling the methionine cycle. Future work could look at methylation status in the presence of methionine and SF? The remaining question that needs to be answered is whether these changes are mediated by NRF2 or through additional proteins. The following chapters will address this question by utilizing the genome-editing technique CRISPR/Cas9.

Chapter 6: Assessing the impact of sulforaphane metabolism in WT and NRF2 KD cells

Chapter 6 Figures

Chapter 6 Tables:

6.1 Introduction:

In 28 years of NRF2 research, the advancements in our understanding of how NRF2 regulates the antioxidant response and its emerging role in central metabolism have been predominantly assessed using NRF2 KO mice models. For example, the first animal study to evaluate the effect of knocking out NRF2 was conducted by Thimmulappa and colleagues. In this study, the transcriptomic profile of WT and NRF2KO mice intestine treated with SF identified that NRF2 was not only involved in regulating the antioxidant response but also the genes involved in cellular NADPH regeneration, such as glucose-6-phosphate dehydrogenase, 6-phosphogluconate dehydrogenase, and the malic enzyme (Thimmulappa *et al*., 2002).

Following this, a wide range of studies assessing a diverse range of tissues has reported NRF2 to be crucial in regulating numerous metabolic functions. One of the initial findings from NRF2KO mice studies showed that the transcriptional factor's loss results in reduced cell proliferation and redox homeostasis becoming compromised. For example, mouse embryonic fibroblasts (MEF), along with macrophages from NRF2KO mice, have a 75% decrease in the intracellular concentrations of glutathione compared to WT MEF (Wakabayashi *et al*., 2004, Higgins *et al*., 2009). This decrease in glutathione is also associated with a reduction in expression several genes involved in the antioxidant response, such as GCLC, GCLM, PRDX1, SLC7A11, TXRND1 (Higgins *et al*., 2009, Ishii *et al.*, 2000, Niso-Santano *et al*., 2010). Livers from NRF2 KO mice have also reported a decrease in the intracellular concentration of glutathione, although this decrease was not as high as that in MEF or macrophages of NRF2KO mice; NRF2KO livers were shown to have a 20% reduction in the intracellular concentration of glutathione (Chowdhry *et al*., 2010, Zhang *et al*., 2013b). In alveoli cells, NRF2KO has been shown to cause a 50% reduction in intracellular concentrations of glutathione (Reddy *et al*., 2007). This decrease in glutathione production results in increased intracellular levels of ROS, as several studies have reported that NRF2KO cells have a 1.6 to 4-fold increase in the levels of ROS compared to WT cells. To name a few, ROS levels in NRF2KO MEF are 2.3-fold higher compared to WT (McDonald *et al*., 2010, Holmstrom *et al*., 2013), and similar cardiomyocytes (heart cells) of NRF2KO mice have 2.5-fold higher ROS compared to the WT cells (He *et al*., 2009). This increase in ROS has detrimental effects, as primary alveolar epithelial cells obtained from NRF2 KO mice, the increased ROS results in activation of the ataxia-telangiectasia mutated DNA damage response pathway, along with the arrest of the cell cycle as fewer cells enter the S-phase of the cell cycle (Reddy *et al*., 2008). The outcome is inhibition of cell proliferation.

Due to the compromised antioxidant response, studies have shown that NRF2 null mice are much more susceptible to a wide range of chemicals such as acetaminophen, benzo[a]pyrene, butylated hydroxytoluene, diesel exhaust fumes, 7,12-dimethylbenz[a]anthracene, nitrosamine, and tobacco smoke (Kensler *et al*., 2007, Xu *et al*., 2006, Becks *et al*., 2010). Moreover, MEF from NRF2 KO mice have reduced expression of the alpha, mu, pi GST isoenzymes, resulting in a decreased ability to bind and conjugate glutathione to the xenobiotic substrate, thereby further impairing the ability to detoxify toxic xenobiotic (Higgins *et al*., 2009). This ability to withstand fewer xenobiotics has also been implicated with NRF2KO mice being more susceptible to developing cancer. For example, NRF2KO mice after four weeks of intraperitoneal injection of the toxin urethane was sufficient to result in a seven-fold increase of nodules in the lungs compared to its WT counterparts, and after 8 weeks, all of the lungs of the NRF2KO mice developed lung tumours, compared to only half of those with/in/of the WT (Higgins and Hayes, 2011).

Identification of NRF2 regulating central metabolic processes such as lipid metabolism and mitochondrial respiration was also identified using animal models. For example, several studies have shown that deletion of NRF2 results in increased mRNA of genes involved in lipid metabolism such as sterol regulatory element-binding proteins 1c and 2 (SREFB1/2), fatty acid synthase (FASN), acetyl-CoA carboxylase 1 (ACACA1) (Tanaka *et al*., 2008, Tanaka *et al*., 2012, Wu *et al*., 2011). Development of non-alcoholic steatohepatitis is also accelerated in mice that lack the transcription factor NRF2, as loss of NRF2 resulted in a 10-fold increase in the p65 protein subunit of the nuclear NF-Ƙb, along with a 5-fold increase in the mRNA levels of the following genes: interleukin 1β, tumour necrosis factor α, and cyclooxygenase 2 compared to WT mice (Chowdhry *et al*., 2010). Loss of the transcriptional factor has also been shown to diminish the activity and bioenergetics of the mitochondrial. MEF and neurons from NRF2KO mice have reduced membrane potential, which results in reduced ATP production and respiration (Holmstrom *et al*., 2013). This attenuation of mitochondrial function also results in the oxidation of long chain fatty acids becoming impaired (Ludtmann *et al*., 2014).

The majority of the studies conducted on NRF2KO mice have been carried out to assess the function of NRF2 rather than assessing the health benefits of SF. In the previous two chapters (4 and 5), it was identified that SF treatment to HepG2 resulted in a wide range of metabolic responses in high glucose environments, particularly rewiring central metabolism, for increased NADPH production, as well as upregulating glutathione metabolism, to induce the antioxidant response. As the work conducted in the thesis was carried out in human cell lines, rather than in NRF2KO mice model, this

chapter aimed to assess whether the metabolic effects of SF in liver cells (SF interfering with 1C metabolism and the serine synthetic pathway) are mediated through NRF2. Therefore a novel liver NRF2 knockdown (NRF2KD) cell line was developed using the CRISPR/Cas9 genome editing technology. Knockdown rather than knockout was favoured as KD results in partial obstruction through the degradation of NRF2 mRNA, thereby resulting in abortive protein translation rather than complete deletion, resulting in complete erasing of downstream targets, which rarely occurs physiologically.

Subsequently, the effect of NRF2 deletion on the bioactivity of SF was assessed through:

1. Metabolic phenotyping (Seahorse and targeted LC-MS analysis)
2. Transcriptional phenotyping (RNAseq technologies)

6.2 Methods:

6.2.1: Processing the raw reads to obtain the differentially expressed genes

In chapter 4, the RNAseq analysis was carried through *edgeR-limma*. *Limma* uses an empirical Bayes, and the test statistics that is used is a t-statistic (F-statistic). The analysis for the RNAseq in this chapter was conducted using DESeq2. The limitation with the *edgeR-limma* model is that its estimates of the variance are lower for weakly expressed genes, and higher for strongly expressed genes compared with DESeq2. Essentially, it is anti-conservative for genes that are low expressed, but this is compensated by being more conservative for strongly expressed genes. Overall, the type I error is maintained (Anders and Huber 2010). Nevertheless, this can still result in some form of bias, as low expressed genes tend to be overrepresented whilst only a few genes that are highly expressed tend to be differentially expressed. Using DESeq2, this limitation is avoided as DEseq2 can control the variance estimation. (Anders and Huber, 2010).

DESeq2's function *estimateSizeFactors* uses the median ratios method to estimate a normalization factor for each sample or *size factor*. These normalization factors are the median ratio of the samples over a "pseudo-sample", where for each gene, is the geometric mean of all samples. Estimating size factors is performed as follows:

1) Calculate a pseudo-reference sample geometric mean for each gene, that is equal to the geometric mean across all samples

2) Calculate the ratio of each sample to the reference: for every gene in a sample, the ratios sample/reference are calculated. This is performed for each sample in the dataset.
3) Calculate the *size factor*, which is the median value of all ratios for a given sample for that sample.
4) Calculate the normalized count values using the normalization factor: this is performed by dividing each raw count value in a given sample by that sample's normalization factor.

Following the construction of the DESeq2 model, before carrying out diagnostic plots to assess the quality of the data, lowly expressed genes were filtered. Genes that had a count of less than ten were discarded as they provide little information for differential expression. Pre filtering, the starting gene count matrix consisted of 60617 counts, and post filtering this number was reduced to roughly 34000 counts. Normally with count data, the Poisson distribution is widely used since it assumes that the mean is equal to the variance. However, with RNAseq data, the common occurrence is that the count data generated results in overdispersion; this means that the assumption of mean=variance is violated. To overcome this limitation, DESeq2 utilizes a negative binomial distribution to model the RNA-seq counts. DESeq2 like edgeR-limma works by building a model or models, depending on the set of parameters to be tested. For this analysis, the two parameters that need to be considered are the time and the line (WT and KD). DESeq2 will fit the normalized count data to the model and coefficients are estimated for each sample group. These coefficients are represented as the $\log_2$ fold change for each sample group, along with various other statistical outputs such as, among others, standard error and p-value.

6.2.2 Negative binomial GLM fitting and Wald statistics (nbinomWaldTest)

For hypothesis testing, the null hypothesis for each gene is that there is no differential expression across groups: *LFC = 0*. DESeq2 uses the Wald test, a hypothesis test, where the estimated standard error of a $\log_2$ fold change is used to test if it is equal to zero. DESeq2 uses the Wald test as follows: takes the LFC and divides it by its standard error, resulting in a z-statistic; the z-statistic is compared to a standard normal distribution, and a p-value is computed reporting the probability that the z-statistic could be observed at random, and if the p-value is small we reject the null hypothesis as there is evidence against that the gene is indeed differentially expressed.

DESeq2 uses independent filtering which helps reduce the number of genes tested by removing genes unlikely to be significantly differentially expressed before testing, such as those with a low number of counts and outliers. A significance cutoff of 0.1 was used to optimize the independent filtering. Independent filtering uses a low mean threshold that is empirically determined from the data. Using this threshold, significantly differentially expressed genes can be increased by reducing the number of genes tested.

The p values from the Wald test are corrected for multiple testing using the False Discovery Rate method based on the Benjamini-Hochberg, BH, algorithm.

6.2.3 Exploratory Analysis of Gene Expression Profiles

Principal Component Analysis (PCA) is a well-known transformation for high-dimensional data. It is used also as an easy visualization to inspect the similarity and dissimilarity of transcriptomics profiles based on a few components that capture most of the variance of the data. For gene expression data, typically the 500 genes with higher variance (after pre-filtering) are included. The high-dimensional data is reduced such that the first principal components (PCs) capture most of the variance in the datasets. Then, the first 2 or 3 principal components can be shown as 2 or 3-dimensional plots.

Methods for exploratory analysis of multi-dimensional data (such as clustering and principal component analysis (PCA)) work best for homoscedastic data, where the variance of a feature (i.e., the expression of a gene) does not depend on the mean. Because variance grows with the mean with RNA-sequenced data, DESeq2 provides two transformations to produce more homoscedastic data: the variance stabilizing transformation (VST) and the rlog. VST attempts to create data that is more approximately normally distributed than the original data (or at least has more constant variance) so that a variable value is not related to the mean value. VST is recommended for medium to large datasets, as it is much faster to compute and is less sensitive to high count outliers than the rlog. These transformations are functions of DESeq2 which are provided for application and visualization of the data only and are not used for differential testing (which uses the raw untransformed counts).

To explore the similarity of transcriptional profiles between samples, heatmaps, hierarchical clustering, and dendrogram are typically used. For this, R and the R library *pheatmap* (version 1.0.12) were used on the count matrix. First, Euclidean distances are calculated according to Equation 1. A larger Euclidean distance represents a smaller similarity. A smaller Euclidean distance represents a higher similarity. Thus, a

Euclidean distance of 0 means the two samples being compared are equal. Heatmaps of the sample-to-sample distances are plotted using dendrograms to give an overview of similarities and dissimilarities between samples. Dendrograms also show how the samples are clustered into groups based on their similarities, where the distance (or height of the dendrogram) represents the similarity between two samples: a shorter height represents more similar samples, while a larger height represents less similar samples.

$$d(p,q) = \sqrt{\sum_{i=1}^{n}(q_i - p_i)^2} \qquad \text{Eq. 1}$$

where

p, q are two points in Euclidean n-space

q_i, p_i are Euclidean vectors, starting from the origin of the space (initial point)

n is the n-space

Finally, extracted differentially expressed genes were used to produce Mean Average (MA) plots. MA plots are 2-D scatter plots used for the visualization of genomic data and provide a useful overview for two-group comparison. They allow the visualization and identification of gene expression changes from two groups in terms of log fold change (M – on Y-axis) and the log of the mean of normalized expression counts over all samples (A – on X-axis). By producing MA plots, we can visualize the degree of differentially expressed genes and in which direction; genes with similar expression in both groups will cluster around M=0 value (i.e. no significant difference in the expression), whereas points away from the M=0 line indicate significantly differentially expressed genes (upregulated or downregulated if above or below the line respectively).

6.3 Results:

6.3.1 Development of a novel NRF2 KD liver cell line

To test the hypothesis that SF interfering with 1C and lipid metabolism along with the serine synthetic pathway identified in chapters (3,4 and 5) are mediated through NRF2, the genome editing technique CRISPR/Cas 9 was employed to develop a novel liver cell line that lacks NRF2. The optimisation's first step consisted of carrying out Genomic Detection Cleavage (GCD) to determine the % of modified cells (how

efficiently the Cas9 has cut the DNA strand). The GCD kit uses genomic DNA isolated from cells transfected with CRISPR/Cas 9 constructs.
Following the CRISPR/Cas 9 transfection, genomic insertions or deletions are created by the cellular repair mechanisms (NHEJ mechanism). The genomic DNA sites where the insertions or deletions occur are amplified by PCR. Next, the PCR product is denatured and reannealed so that mismatches are generated as strands with an indel re-annealed to strands with no indel or a different indel.
The mismatches are subsequently detected, followed by cleavage by an endonuclease enzyme. When running the PCR products on a gel, the cleaved bands will estimate how high the editing efficiency was.

In this GCD protocol, two gRNAs targeting two regions of the NRF2 genome were tested.
For the first gRNA, the editing efficiency after 48 h was 15% of the edited cells had two additional smaller amplicons: one band at 381 bp and the other 267 bp. After 72 h, the % of edited cells increased to 31% (figure 6.1). This suggests that the editing was effective, as shown by the T7 Endonuclease I enzyme identifying and cleaving mismatches in the DNA double strands.
After identifying that the first gRNA was successful in editing the DNA, a second separate experiment was then conducted, testing the efficiency of the second gRNA. Similarly, 48 h and 72 h post transfection, the DNA was extracted and assessed using the GCD Assay. After 48 h, compared to the negative control, which had a single NRF2 amplicon at 550 bp, 75% of the transfected cells were still WT and had a single band at 550bp. In contrast, about 15% of the edited cells yielded two smaller amplicons, one at 380 bp and 170 bp. After 72 h, the transfection efficiency increased to about 31%, figure 6.2.

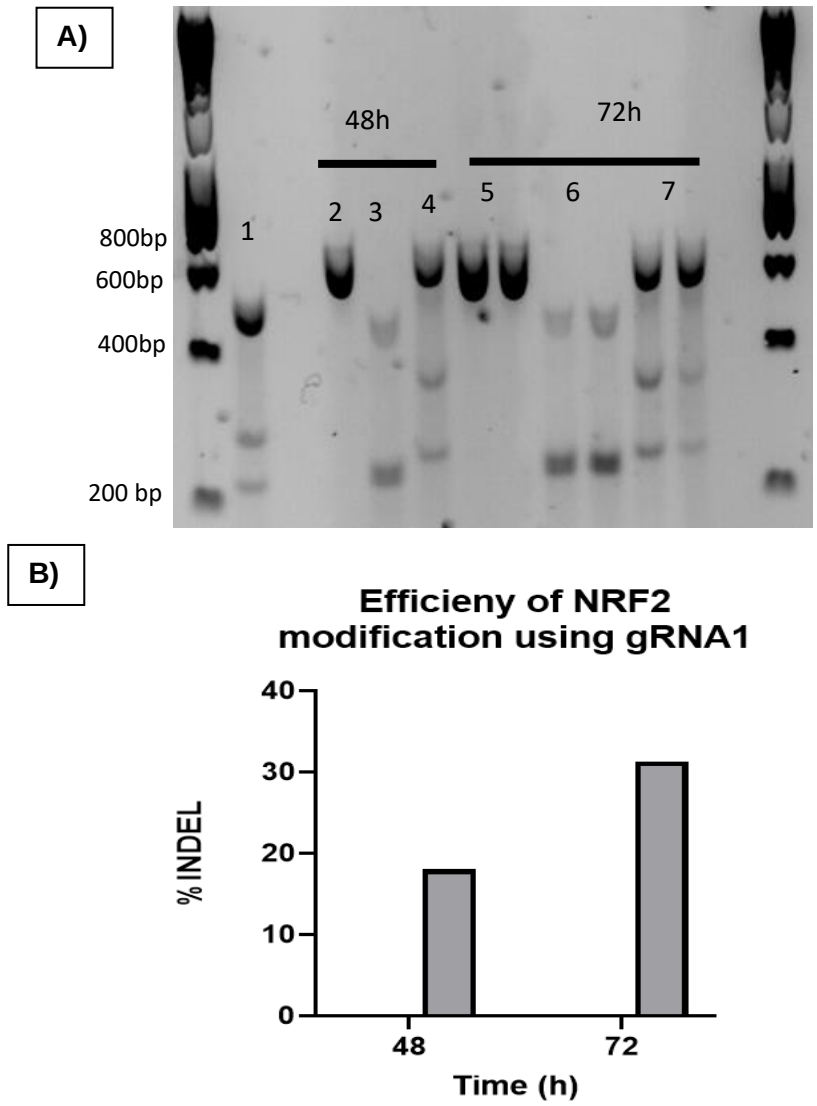

Figure 6.1. Gel image and bands quantification of the genomic detection cleavage assay in transfected cells using the first gRNA, targeting the NRF2 genome. Cells were transfected using the Gene Art Cas 9 protein through lipofectamine transfection. A) Following re-annealing and addition of the T7 Endonuclease I enzyme transfection, the amplified DNA was run of agarose gel to assess transfection efficiency. Samples are the following: 1-Control Template, 2-Negative Control 48 h, 3-Positive Control HPRT1 gene 48 h, 4-NRF2 gene 48 h, 5-Negative Control 72 h, 6-Positive Control HPRT1 gene 72 h, 7-NRF2 gene 72 h. B) The quantified results of the GCD assay. The cleavage product consisting of two bands and the parental band was quantified using Fiji. Gene Modification Efficiency represented by % of INDEL (Insertion/Addition) was calculated through the following equation = [1- ((1-fraction cleaved) 1/2)] × 100.

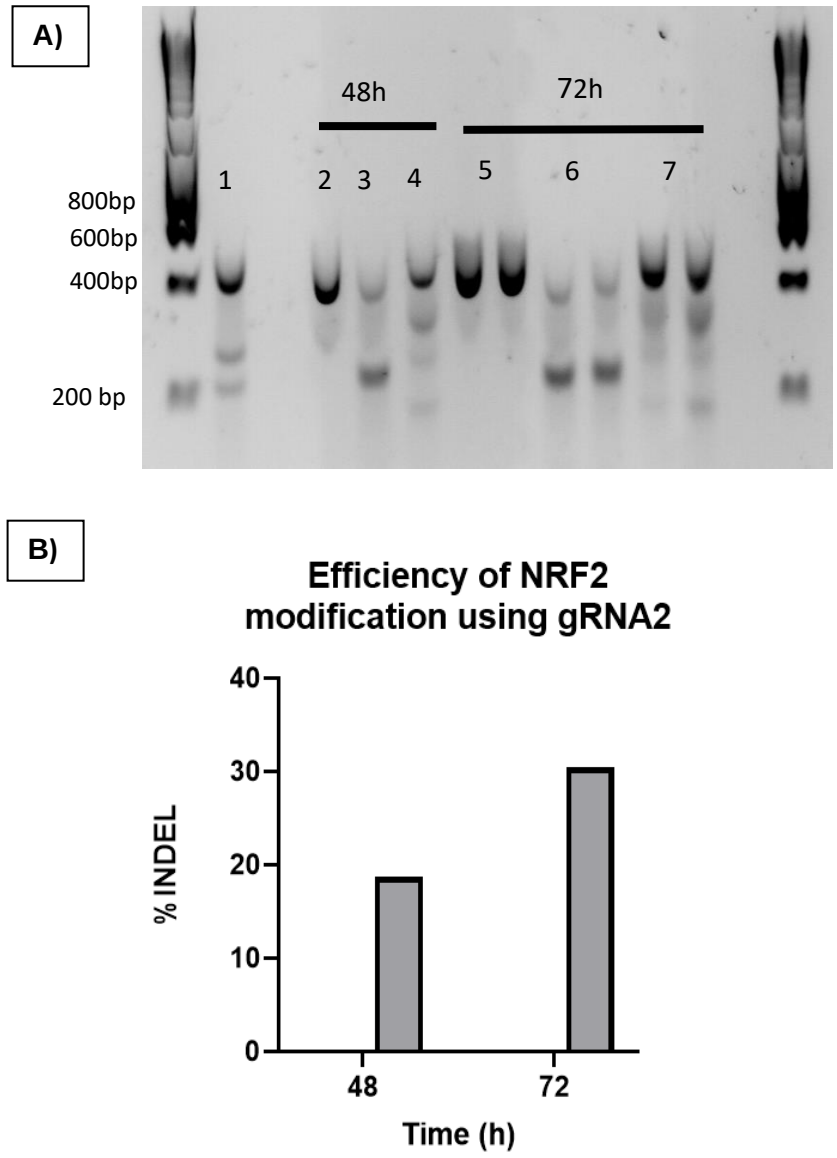

Figure 6.2. Gel image and bands quantification of the genomic detection cleavage assay in transfected cells using the second gRNA, targeting the NRF2 genome. Cells were transfected using the Gene Art Cas 9 protein through lipofectamine transfection. A) Following re-annealing and addition of the T7 Endonuclease I enzyme transfection, the amplified DNA was run of agarose gel to assess transfection efficiency. Samples are the following: 1-Control Template, 2-Negative Control 48 h, 3-Positive Control HPRT1 gene 48 h, 4-NRF2 gene 48 h, 5-Negative Control 72 h, 6-Positive Control HPRT1 gene 72 h, 7-NRF2 gene 72 h. B) The quantified results of the GCD assay. The cleavage product consisting of two bands and the parental band was quantified using Fiji. Gene Modification Efficiency represented by % of INDEL (Insertion/Addition) was calculated through the following equation = [1- ((1-fraction cleaved) 1/2)] × 100

To assess whether the editing in the DNA resulted in a reduction in the protein level of NRF2, the next step in optimization was assessing NRF2 protein through Western Blotting. In this assay, HepG2 was transfected with both gRNA simultaneously. Cell lysates were then collected at 48 and 72 h post transfection. NRF2 under unstressed conditions is heavily regulated by binding to KEAP1 and sent to for proteasomal degradation, both the WT and KO were treated with 10 µM SF for 16/17 h before protein extraction to induce protein NRF2. Figure 6.3 revealed that 48h post-transfection, the editing resulted in a 70 decrease in the NRF2 protein, and 72 h this was even further reduced to 82%.

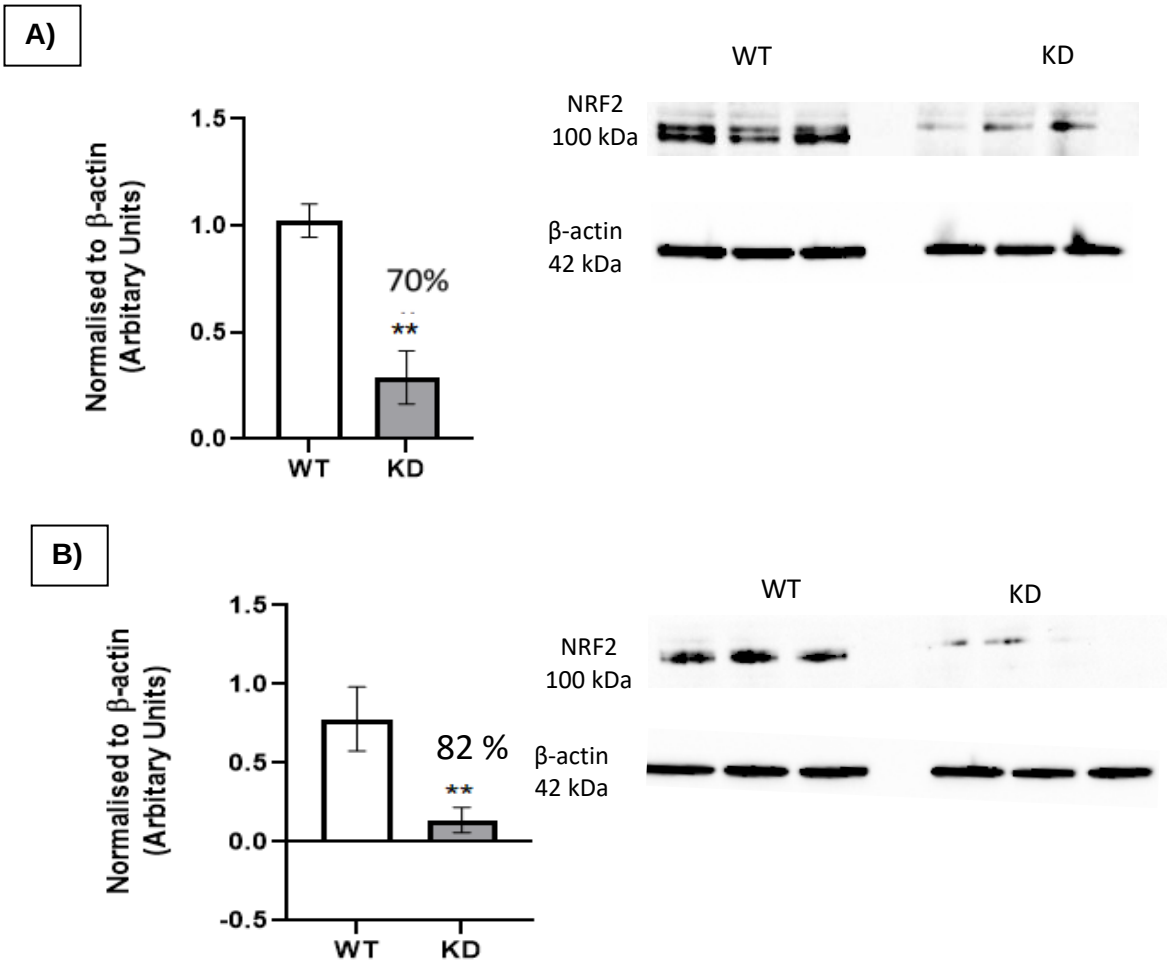

Figure 6.3. Western Blot analysis of transfected HepG2 cells to assess NRF2 protein. Cells were treated with SF, and A) Protein lysates were extracted at 48 h and B) at 72 h post-transfection. Band Intensity was quantified using Fiji, and NRF2 was normalized to beta-actin. Error bars represent the standard deviation. Statistical analysis was performed by independent unpaired two-way t-test p= 0.003 in three biological replicates

In the previous assays (**figures 6.1-6.3**), transfection resulted in forming a heterogenous population (a mixture between WT and KD cells). To fully generate a novel NRF2KO liver cell line, the assay was repeated and 72 h post-transfection single cells were seeded onto 7, 96 well plates. The seeded cells were monitored weekly and images were taken to track colony formation (**figures 6.4-6.6**).

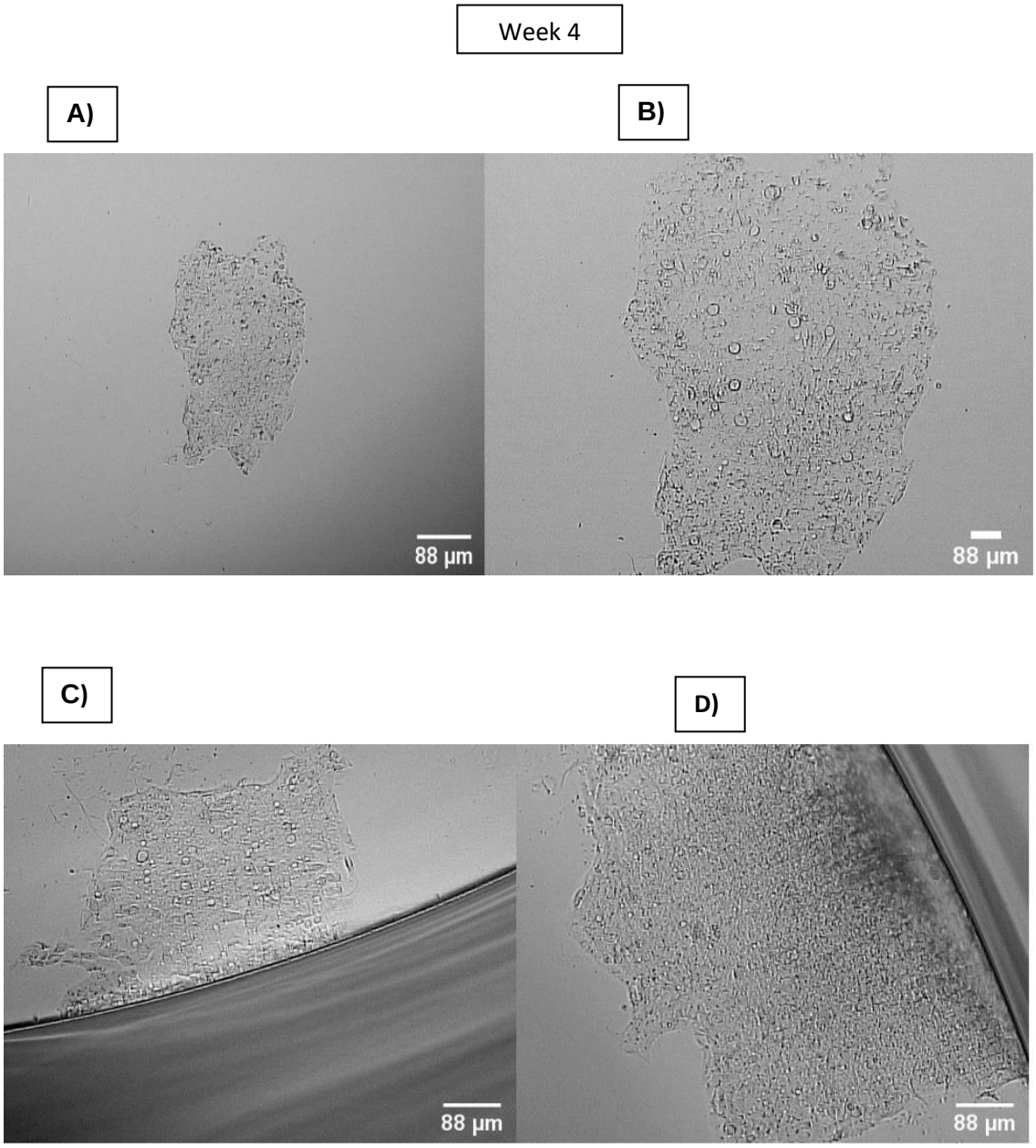

Figure 6.4. Monitoring of clonal expansion of NRF2KO HepG2, four weeks post-transfection. NRF2KO cells were obtained by transfecting with Cas9/gRNA with lipofectamine. Cells were diluted to single cells and were seeded into individual wells of 96 well plates for colonial expansion. A) represents 5 X whilst B) represents the same image as A, only zoomed in 10 X magnification. C/D represents cells from independent wells at 5 X magnification, using the Zeiss Axion Imager. Each picture represents a separate well, therefore a separate colony. Images were taken 4 weeks after seeding.

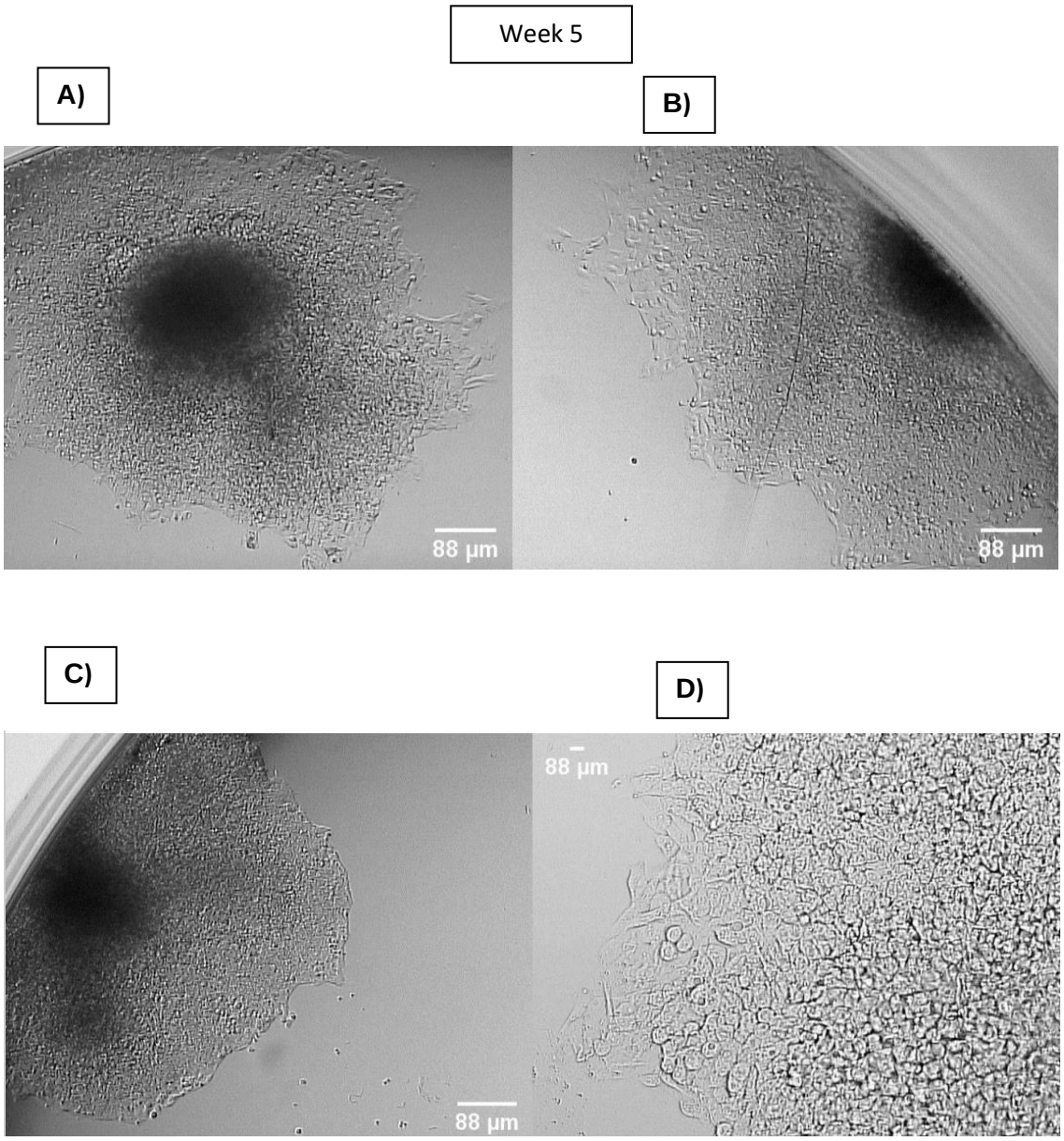

Figure 6.5. Monitoring of clonal expansion of NRF2KO HepG2, five weeks post-transfection. HepG2, NRF2KO cells were obtained by transfecting with Cas9/gRNA with lipofectamine. Cells were diluted to single cells and were seeded into individual wells of 96 well plates, for colonial expansion. A-C) 5 X magnification, D) 20 X magnification. Images were obtained using the Zeiss Axion Imager M2. Each image represents a separate well, therefore a separate colony. Images were taken 5 weeks after seeding.

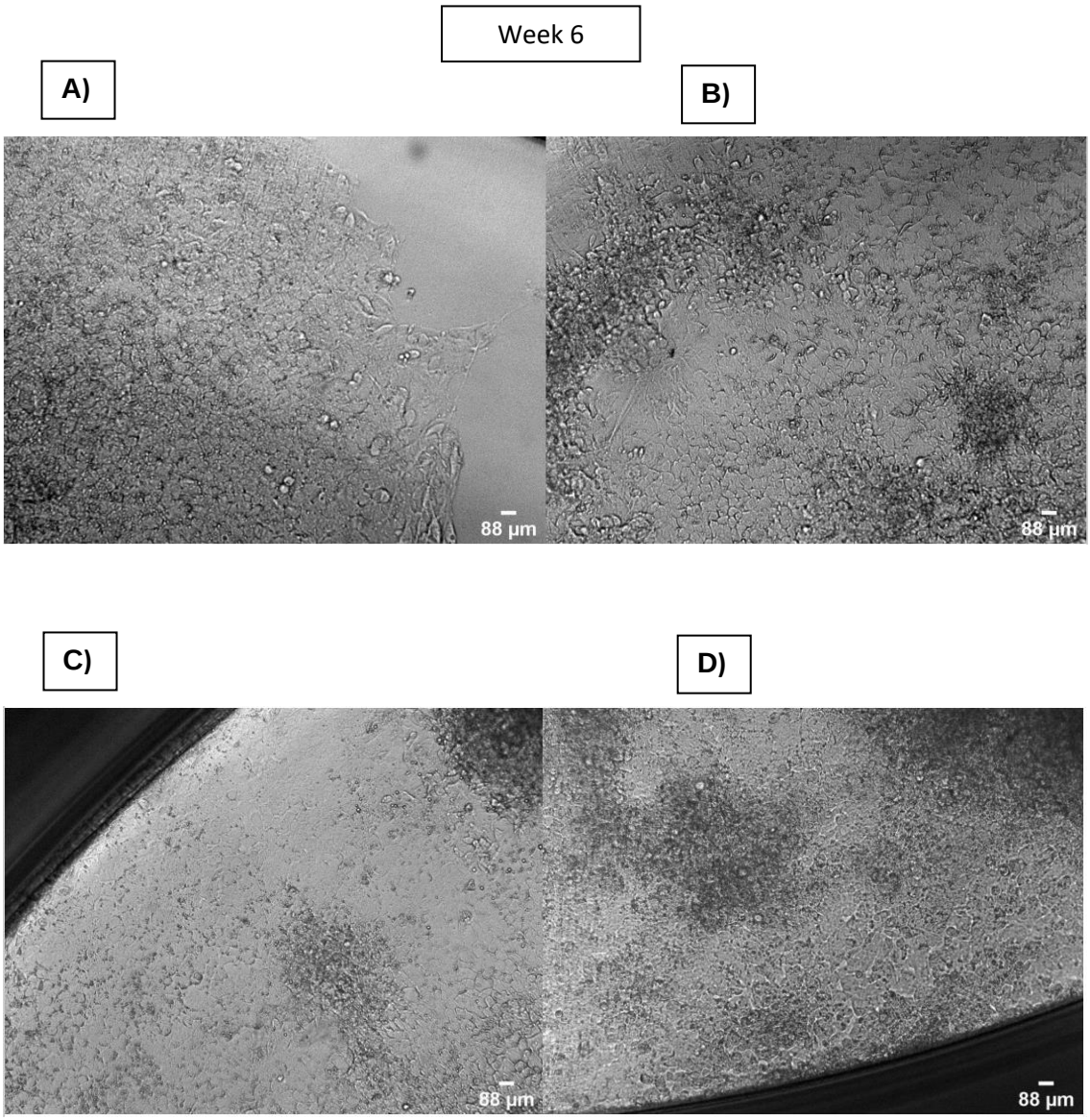

Figure 6.6. Monitoring of clonal expansion of NRF2KO HepG2, six weeks post-transfection. HepG2, NRF2KO cells were obtained by transfecting with Cas9/gRNA with lipofectamine. Cells were diluted to single cells and were seeded into individual wells of 96 well plates for colonial expansion. A-D) All images were taken at 10 X magnification. Images were obtained using the Zeiss Axion Imager. Each image represents a separate well, therefore a separate colony. Images were taken 6 weeks after seeding.

Due to the success of the knock-down, it was deemed that a heterogeneous population of WT and KO cells would be sufficient to address the aims of this chapter. In an independent experiment that also included a third gRNA, the high editing efficiency was further confirmed. In this independent experiment, all three gRNA were transfected simultaneously. DNA modification was only assessed 72h post transfection as it was previously identified that at this time point the greatest amount of editing occurred.

GCD revealed in figure 6.7, that for the first gRNA, whilst the WT cells had only a single band at 648 bp as expected, the edited cells also had two additional amplicons, one at 381 bp and the other 267 bp, although only 10% of the cells were edited. For the second gRNA, the NRF2 band for the WT was 550 bp. Interestingly though it was identified only one amplicon for the edited cells and this band was approximately 400bp, suggesting deletion of 150 bp. For the third gRNA, a similar finding to the editing of the second gRNA was identified. The DNA band for the WT cells was 540bp. For the edited cells only one band was also identified and this band was again 150 bp shorter, at around 400bp. The findings from figure 6.7 may suggest that at two out of three sites the cells might have had 100% editing efficiency.

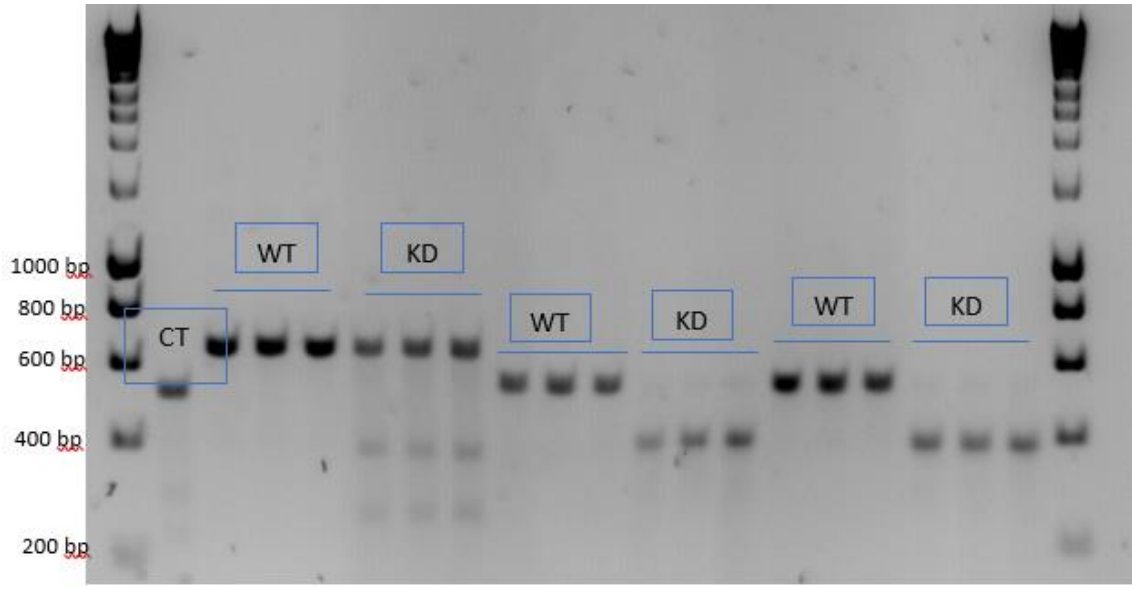

Figure 6.7. Gel image of the genomic detection cleavage assay in transfected cells using all three gRNA simultaneously, targeting the NRF2 genome. HepG2 was transfected through RNP and Lipofectamine. Following re-annealing and addition of the T7Endonuclease I enzyme transfection, the amplified DNA was run on an agarose gel to assess transfection efficiency. Samples are the following: CT= Control Template, WT= Wild type, and KD=NRF2 Knock Down. For the assay, three biological replicates and three technical replicates were used.

The final optimization assay that was carried out was a second Western Blot to assess how the deletion of the 150 bp of the DNA from two sites of the NRF2 gene, identified in figure 6.7 impacted the protein levels of NRF2. It was identified that the editing led to a 60% reduction in NRF2 protein, (**figure 6.8**). Notably, the lower band of the NRF2 was completely deleted.

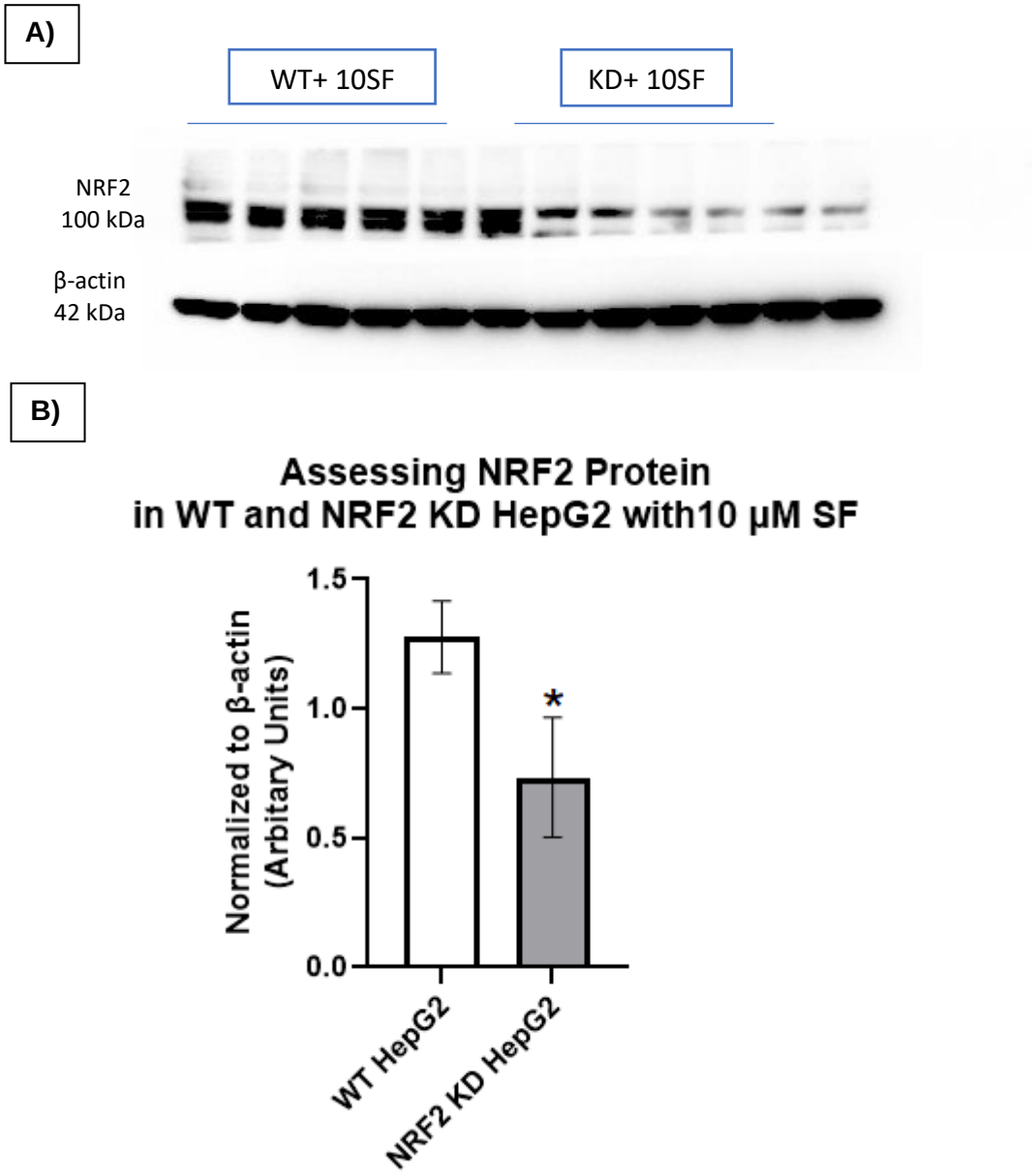

Figure 6.8. Western Blot assessing NRF2 protein in WT and NRF2 KD HepG2 treated with 10 μM SF overnight. Cell lysates were extracted and determined by Western Blotting. Three biological replicates and two technical replicates were run. A) Visualized protein lysates. B) Band Intensity was quantified using Fiji, and NRF2 was normalized to beta-actin. Error bars represent the standard deviation. Statistical analysis was determined through a student t-test p=0.03, comparing three biological replicates.

To assess whether the editing results in loss of function of the downstream targets of NRF2, in a separate experiment, WT and the heterogeneous population of NRF2 edited cells, therefore, NRF2 knockdown (NRF2KD cells), were cultured in a high glucose environment and treated with physiological concentrations of SF at both an early 9 h and late 24 h time point. At these time points, RNA was extracted to quantify

the expression of key NRF2 targets genes, both involved in the antioxidant response, such as NADPH quinone reductase gene (NQO1), glutamate-cysteine ligase catalytic subunit (GCLC), thioredoxin reductase (TXRND1), and heme oxygenase (HMOX1) as well as genes involved in regulating central metabolism such as glucose-6-phosphate dehydrogenase (G6PD) and transketolase (TKT). The analysis also included CPT1a, which up to this point remains unknown whether NRF2 directly regulates its activity or not. Firstly I identified that the expression of NQO1, TXRND1 and GCLC in the NRF2KD control samples was significantly higher compared to the WT control samples, suggestings activation of another NRF2 isoform like NRF1 in the KD samples.

The analysis identified that for NQO1, SF treatment resulted in approximately a 4-fold increase. This effect in the NRF2KD was completely attenuated, as SF treatment resulted in a 1.4-fold change (**figure 6.9 a**). For TXNRD1, SF treatment in the WT cells also resulted in an over 4-fold increase while the effect SF in the NRF2KD cell line resulted in a 1.3-fold change (**figure 6.9 b)**. Induction of GCLC through SF resulted in a 3.5-fold change in the WT, whilst in the knockdown, this was diminished to a 1.5-fold change (**figure 6.9 c**).

For the metabolic genes, SF treatment results in a 1.5-and 2-fold change for G6PD and TKT respectively. In contrast to our surprise, SF treatment did not induce, the expression of G6PD and TKT in the NRF2KD cell line (**figure 6.10 a and b**). It was also identified that regardless of the editing, SF resulted in upregulation of CPT1a, thereby identifying that its activity is unlikely to be mediated by NRF2, (**figure 6.10 c**).

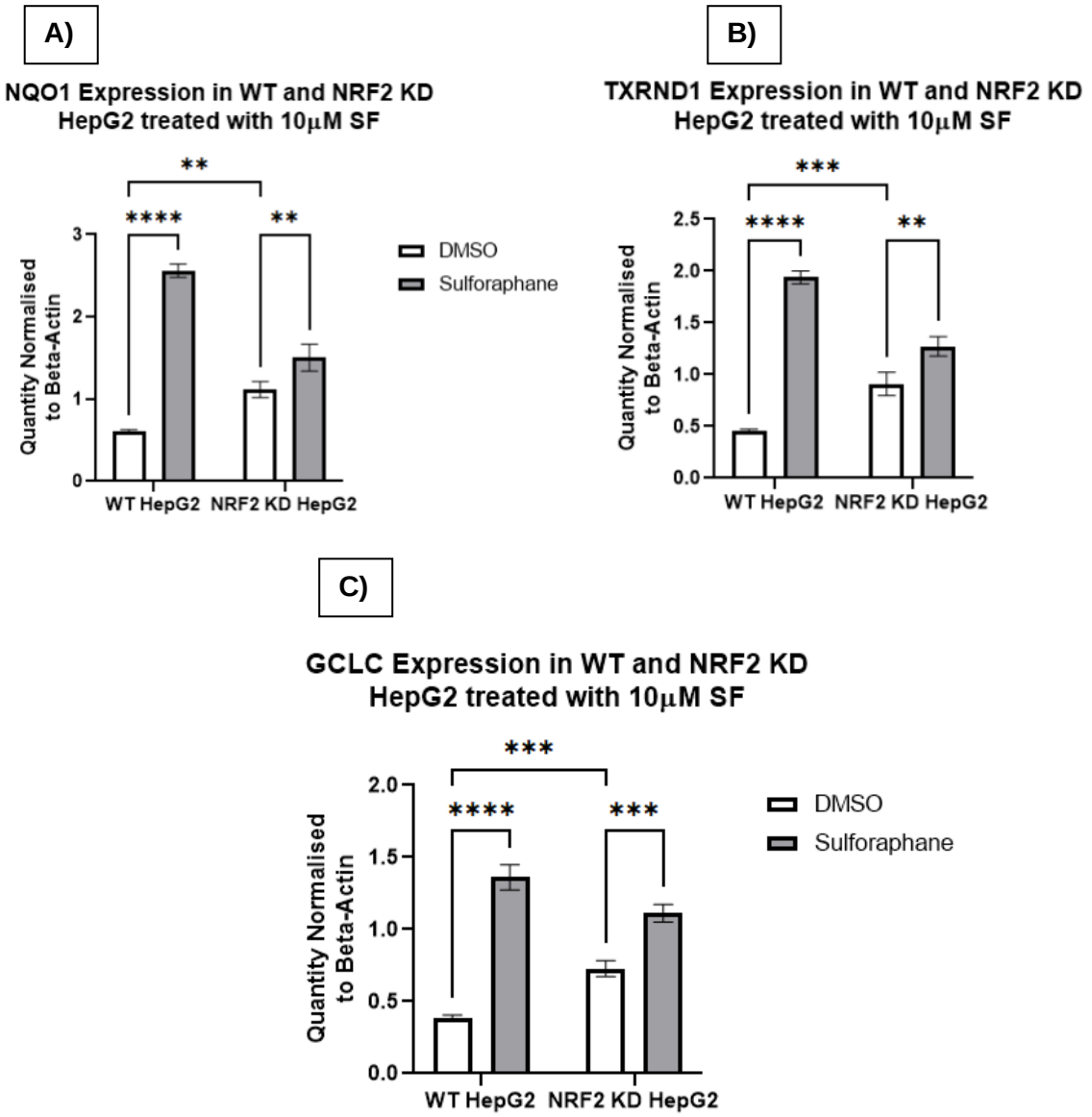

Figure 6.9. qrt-PCR of NRF2 target genes in WT and NRF2KD HepG2. Cells were cultured in high glucose (25 mM) without FBS, and RNA was extracted after 24 h post SF treatment. Gene expression was assessed by qRT-PCR. Samples were normalized to the housekeeping control beta-actin. All values are expressed as mean ± SD from three independent wells. Statistical analysis was determined by a two-way ANOVA between control and treatment and the effect of editing (WT vs NRF2KD). **NQO1:** WT DMSO vs WT SF $p<0.0001$, WT DMSO vs NRF2KD DMSO $p=0.0014$, and NRF2KD DMSO vs NRF2KD SF $p<0.0082$. **TXRND1:** WT DMSO vs WT SF $p<0.0001$, WT DMSO vs NRF2KD DMSO $p=0.0006$, and NRF2KD DMSO vs NRF2KD SF $p=0.0024$. **GCLC:** WT DMSO vs WT SF $p<0.0001$, WT DMSO vs NRF2KD DMSO $p=0.0005$, and NRF2KD DMSO vs NRF2KD SF $p=0.0003$

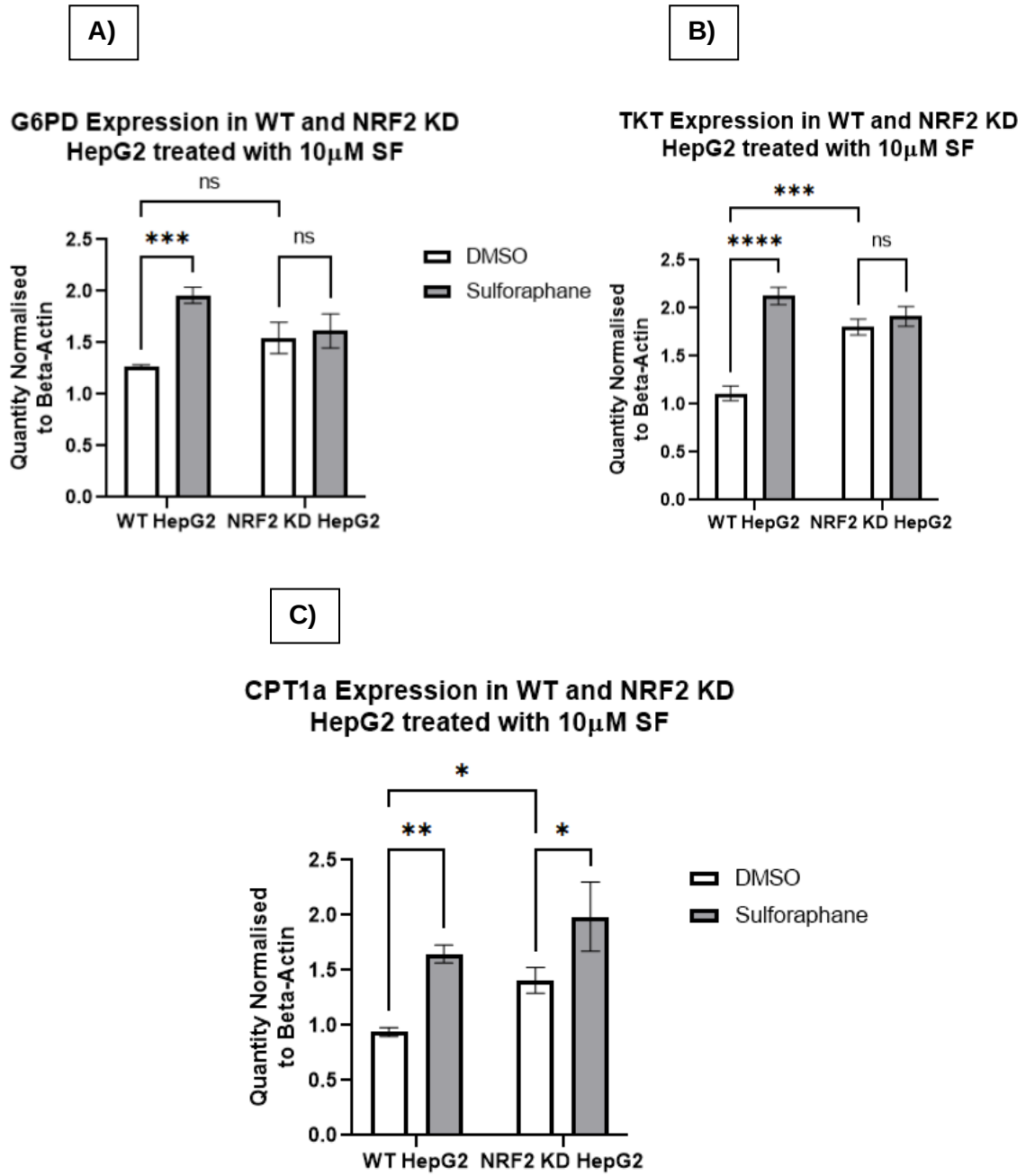

Figure 6.10. qrt-PCR of metabolic genes in WT and NRF2KD HepG2. Cells were cultured in high glucose (25 mM) without FBS and RNA was extracted after 24 h post SF treatment. Gene expression was assessed by qRT-PCR. Samples were normalized to the housekeeping control beta-actin. All values are expressed as mean ± SD from three independent wells. Statistical analysis was determined by a two-way ANOVA between control and treatment and the effect of editing (WT vs NRF2KD). **G6PD:** WT DMSO vs WT SF p=0.0004, WT DMSO vs NRF2KD DMSO p=0.07, and NRF2KD DMSO vs NRF2KD SF p=0.9. **TKT:** WT DMSO vs WT SF p<0.0001, WT DMSO vs NRF2KD DMSO p=0.0001, and NRF2KD DMSO vs NRF2KD SF p=0.52. **CPT1a:** WT DMSO vs WT SF p=0.0047, WT DMSO vs NRF2KD DMSO p=0.043, and NRF2KD DMSO vs NRF2KD SF p=0.015.

Analysis of the early time point also revealed similar findings. HMOX1 and NQO1 expression in the WT stimulated with the presence of SF resulted in a 4-fold increase in HMOX1 and a 3-fold increase in NQO1, respectively. In contrast, SF treatment in the NRF2 KD cells resulted in a 1.5-fold increase in HMOX1 and a 1.3-fold increase in NQO1, thereby further confirming the effectiveness of the editing (**figure 6.11 a and b**).

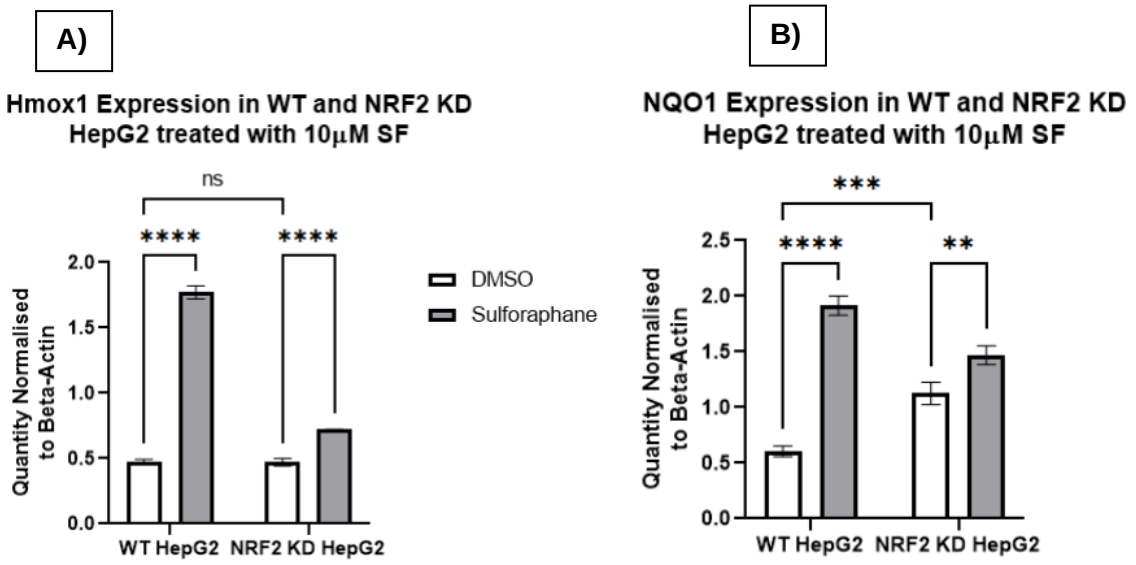

Figure 6.11. qrt-PCR of NRF2 target genes in WT and NRF2KD HepG2. Cells were cultured in high glucose (25 mM) without FBS and RNA was extracted after 9 h post SF treatment. Gene expression was assessed by qRT-PCR. Samples were normalized to the housekeeping control beta-actin. All values are expressed as mean ± SD from three independent wells. Statistical analysis was determined by a two-way ANOVA between control and treatment and the effect of editing (WT vs NRF2KD). **HMOX1:** WT DMSO vs WT SF $p<0.0001$, WT DMSO vs NRF2KD DMSO $p=0.99$, and NRF2KD DMSO vs NRF2KD SF $p<0.0001$. **NQO1:** WT DMSO vs WT SF $p<0.0001$, WT DMSO vs NRF2KD DMSO $p=0.0002$, and NRF2KD DMSO vs NRF2KD SF $p=0.0039$.

6.3.2 Metabolic phenotyping of WT and NRF2KD cells reveals that knockdown of NRF2 affects glycolysis and mitochondrial respiration.

To assess how NRF2 knockdown affects metabolism, both mitochondrial activity and glycolysis were assessed using the Seahorse Bioanalyzer. As previously shown that NRF2 regulates the activity of several genes involved in regulating the TCA cycle (Mitsuishi *et al*., 2012), I hypothesized that KD would reduce the oxygen consumption rate (OCR) an indirect measurement of mitochondrial activity) compared to the WT. In the first assay, mitochondrial activity and glycolysis in WT and NRF2KD cells were assessed without the presence of SF, as shown in figure 6.12. In a separate independent experiment, the assay was repeated, with 24 h SF treatment, to assess what effect SF would have on the cell bioenergetics. Editing of NRF2KD resulted, as expected, in an overall decrease in mitochondrial activity but also a reduction in glycolysis, thereby confirming that also glycolysis is regulated by NRF2 (**figure 6.12 a and c**). When SF was added, the reduction in OCR in the NRF2KD cell compared to the WT was no longer present, suggesting that the reduction in mitochondrial respiration by SF is mediated by NRF2 (**figure 6.13 b**). In contrast, SF was still able to affect/reduce glycolytic function in NRF2KD cells, suggesting that the effect of SF on glycolysis is at least in part mediated through NRF2-independent pathways (**figure 6.12 d**).

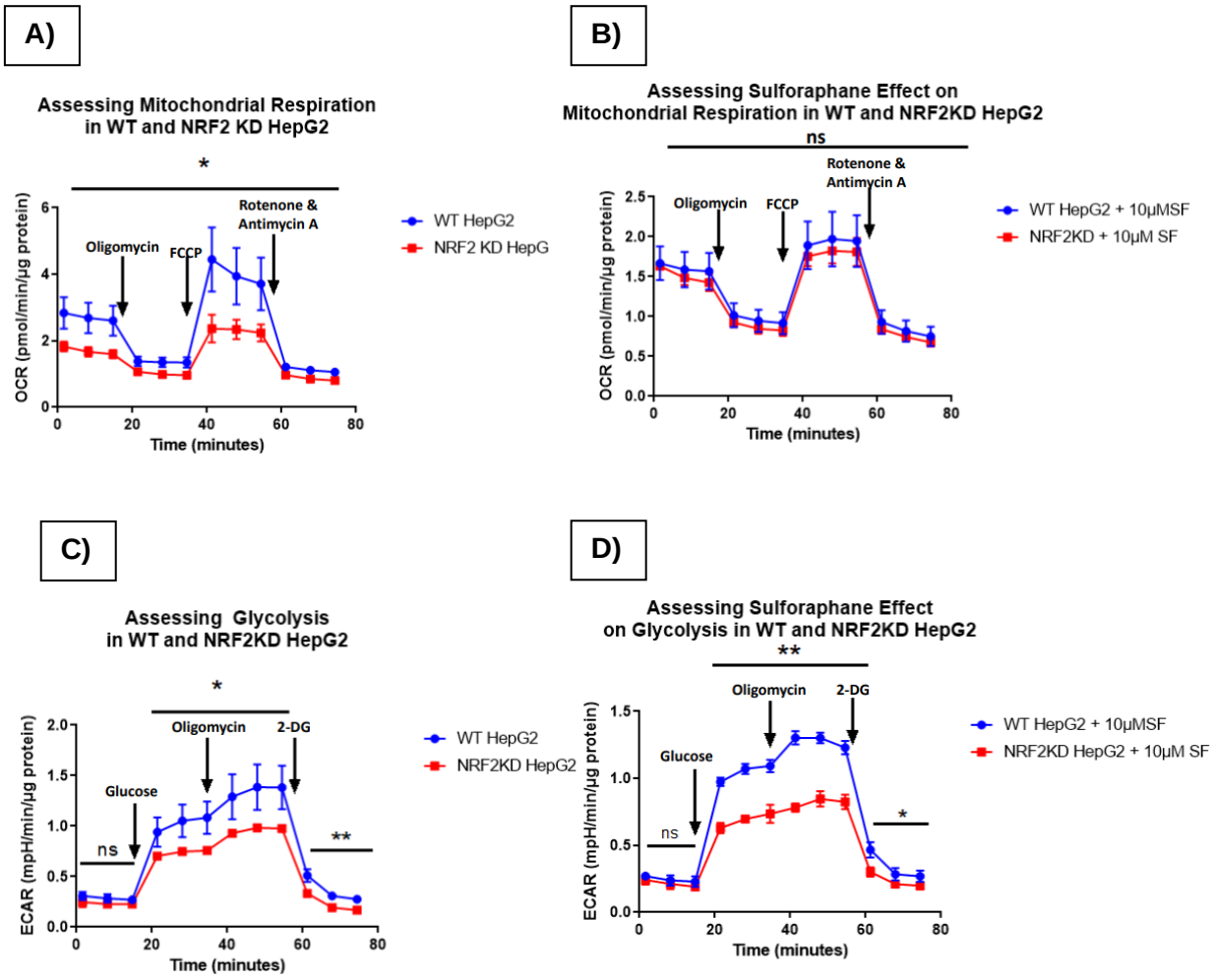

Figure 6.12. Cell energy phenotype of WT and NRF2KD HepG2 cells with and without the presence of SF. A) Oxygen consumption rate (OCR) of the WT (in blue) and NRF2KD cells (in red) only, B) the Oxygen consumption rate of the WT (in blue) and NRF2KD cells (in red) with the presence of 10 µM SF for 24 h without the presence of FBS. C) Extracellular acidification rate (ECAR) of the WT (in blue) and NRF2KD cells (in red) only, D) ECAR of the WT (in blue) and NRF2KD cells (in red) with the presence of 10 µM SF for 24 h without the presence of FBS. All values are expressed as mean ± SEM from three biological replicates.

6.3.3 Targeted metabolomics through LC-MS analysis reveals that SF interference in 1C metabolism is mediated through NRF2

To assess the effect of physiologically relevant concentrations of SF on the intermediary metabolism of WT and NRF2KD HepG2, cells were cultured in 25 mM glucose. Following 9 h and 24 h SF treatment, metabolites were extracted and assessed by LC-MS. Consistent with the findings in chapter 5, 24 h SF treatment led to an approximately 40% reduction in the levels of serine in WT cells. The intracellular concentration of serine in the WT control cells was 120 µM compared with 70 µM of the SF treated WT cells. In contrast, levels of serine in both control and SF treated NRF2KD cells did not change, suggesting that the effect of SF on the amino acid serine is mediated through NRF2 (**figure 6.13 a**). The analysis for glycine also yielded similar results. A 24 h SF treatment also led to a 100 µM decrease in the intracellular concentration of glycine. In the edited cells, this decrease in glycine by SF still occurred, although the effect was not as profound, resulting in a 30 µM decrease in the intracellular concentration of glycine (**figure 6.13 b**). The analysis also revealed that the intracellular concentrations of methionine remained unchanged between the WT control vs SF treated cells. However, comparison of the WT vs NRF2KD control resulted in a significant reduction, potentially implying that also methionine is regulated through NRF2 (**figure 6.13 c**). On the other hand, Betaine revealed that firstly, the WT cells treated with SF had a reduced pool, further confirming the data obtained in chapter 5. The most striking was that the concentration of betaine of both the control and the SF stimulated NRF2KD cells was greater than its respective WT, therefore implying that the SF effect on betaine is not mediated through NRF2 (**figure 6.13 d**).

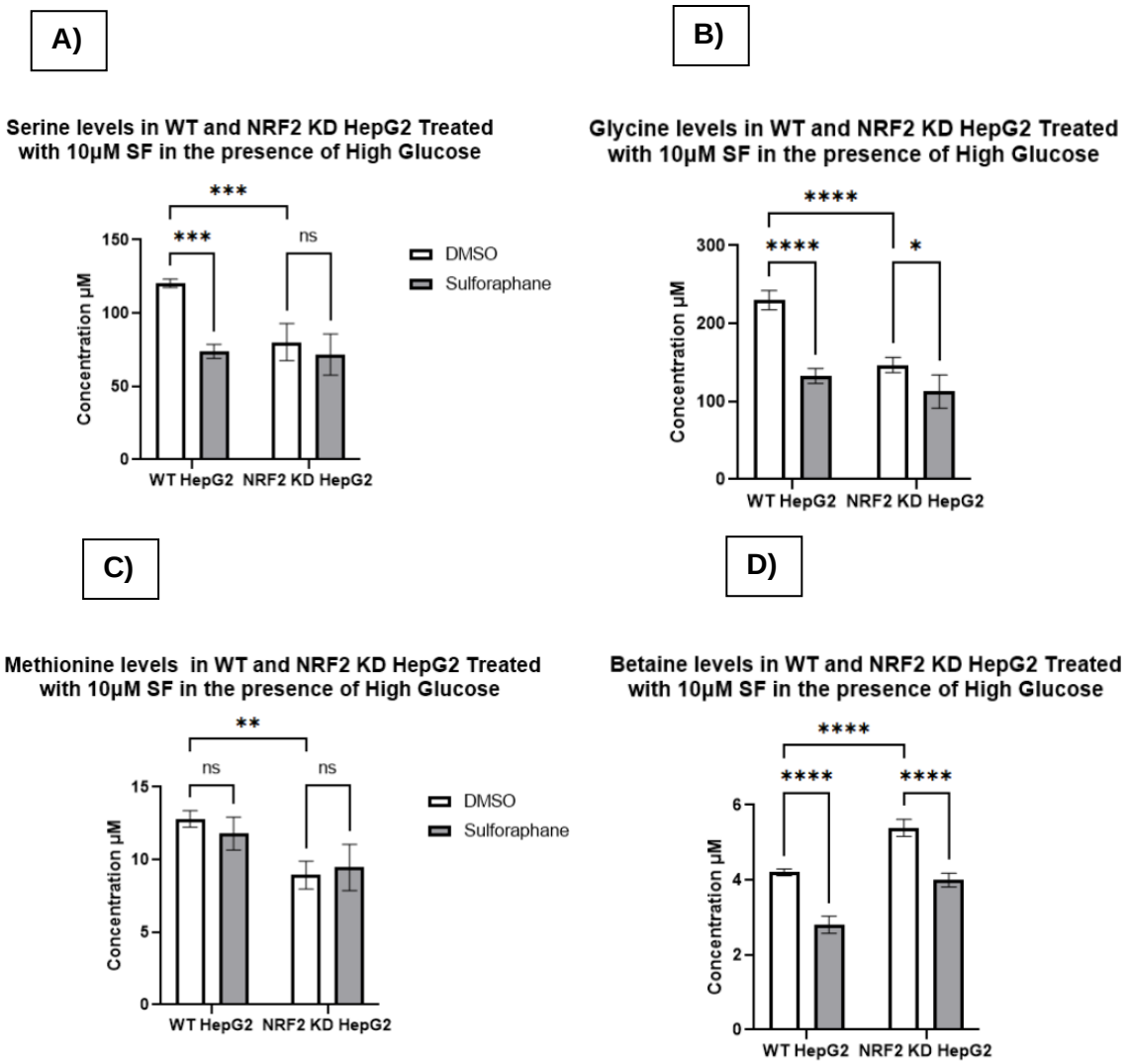

Figure 6.13. **Metabolomic profile of amino acids related to 1C metabolism in WT and NRF2 KD HepG2 cells.** WT and NRF2 KD HepG2 cells were cultured in 25 mM glucose without FBS, and 24 h post SF treatment metabolites were extracted and assessed on the Triple Quad 6490 LC-MS. A) Serine, B) Glycine, C) Methionine, and D) Betaine. All values are expressed as mean ± SD from four independent wells. Statistical analysis was determined by a two-way ANOVA between control and treatment and the editing effect (WT vs NRF2KD) compared to respective controls. **Serine:** WT DMSO vs WT SF p=0.0001, WT DMSO vs NRF2KD DMSO p=0.0005, and NRF2KD DMSO vs NRF2KD SF p=0.63. **Glycine:** WT DMSO vs WT SF p<0.0001, WT DMSO vs NRF2KD DMSO p<0.0001, and NRF2KD DMSO vs NRF2KD SF p=0.02. **Methionine:** WT DMSO vs WT SF p=0.60, WT DMSO vs NRF2KD DMSO p=0.0020, and NRF2KD DMSO vs NRF2KD SF p=0.90. **Betaine:** WT DMSO vs WT SF p<0.0001, WT DMSO vs NRF2KD DMSO p<0.0001, NRF2KD DMSO vs NRF2KD SF p<0.0001.

6.3.4 RNA-seq data analysis and identification of treatment clustering

To gain a molecular understanding of how SF impacts metabolism in the NRF2KD cells and to test the central hypothesis of the thesis that all the metabolic effects identified in chapters 3, 4, and 5 are mediated through NRF2, an RNAseq study was conducted. In this study, WT and NRF2KD cells were treated with physiological concentrations of SF under 25 mM glucose. A time course RNAseq study was conducted for this study, where RNA was extracted after 3, 9, and 24 h SF treatment. This was done to test the following hypotheses

1) The transcriptional changes induced by SF at early time points will affect genes involved in the antioxidant response machinery of the cell.
2) The transcriptional changes induced by SF at 24 h will affect genes involved in central metabolism.

A total of four hepatic mRNA samples per group, at the different time points (four control and four SF treated for WT and same for the NRF2KD), were sent for RNA sequencing (RNAseq). Firstly the data were transformed using principal component analysis (PCA) and Euclidean distance for visualization. In figure 6.14, PC1 explains the biggest variation in the samples (43%) and is likely to be due to the time-course nature of the experiment. PC2 explains an additional 8% of the variation, both the WT and KD samples change as time progresses, but the transcriptional changes observed differ. For the WT, as time progress, the SF treated samples do not change much, whilst the control, however, the samples progressively appear to behave differently. For the KD samples, the clear separation between the treatment and the control is no longer noticeable, clearly highlighting that the transcriptional effects of SF in liver HepG2 cells are primarily mediated through NRF2.

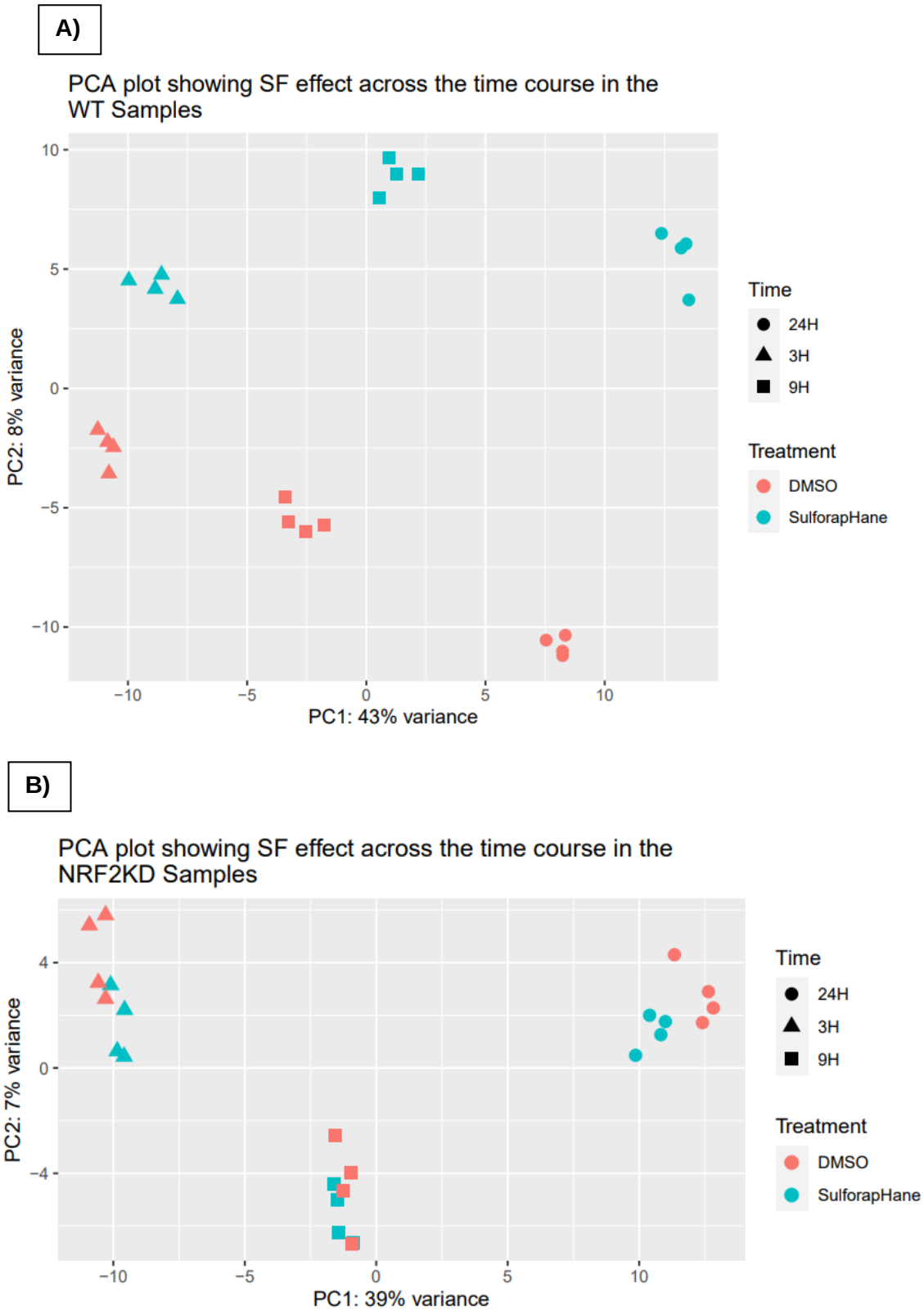

Figure 6.14. Generalized principal component analysis (PCA) plot on raw count data for first and second dimensions. PCA plot showing how throughout the time course SF affects gene expression in HepG2 cultured in a high glucose environment. A) WT samples. B) NRF2KD samples.

The result of the Euclidean distance shows that for both the WT and NRF2KD samples both the control and DMSO are similar among each other and cluster together. In contrast, the SF treated samples cluster separately from their respective control, suggesting the effect of SF on inducing transcriptional changes. Most notably the SF effect in the NRF2KD differs from the WT shown by the reverse heatmap, further implying that the transcriptional effects of SF in liver HepG2 cells are primarily mediated through NRF2 (**figure 6.15**).

A)

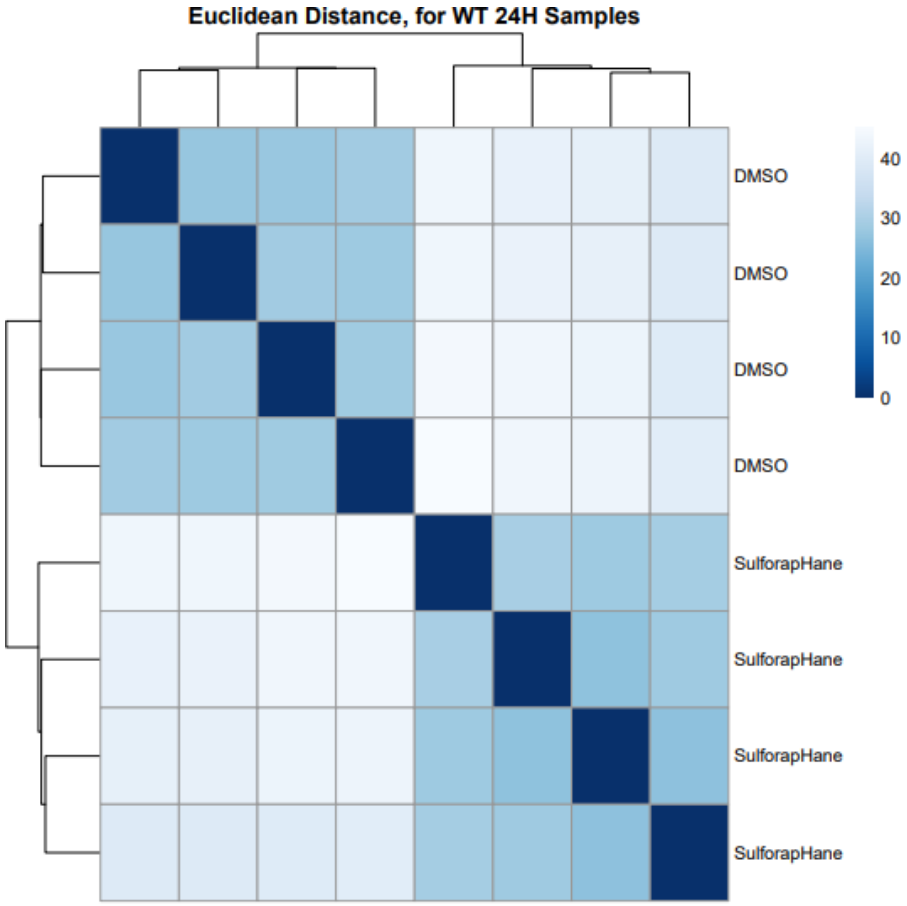

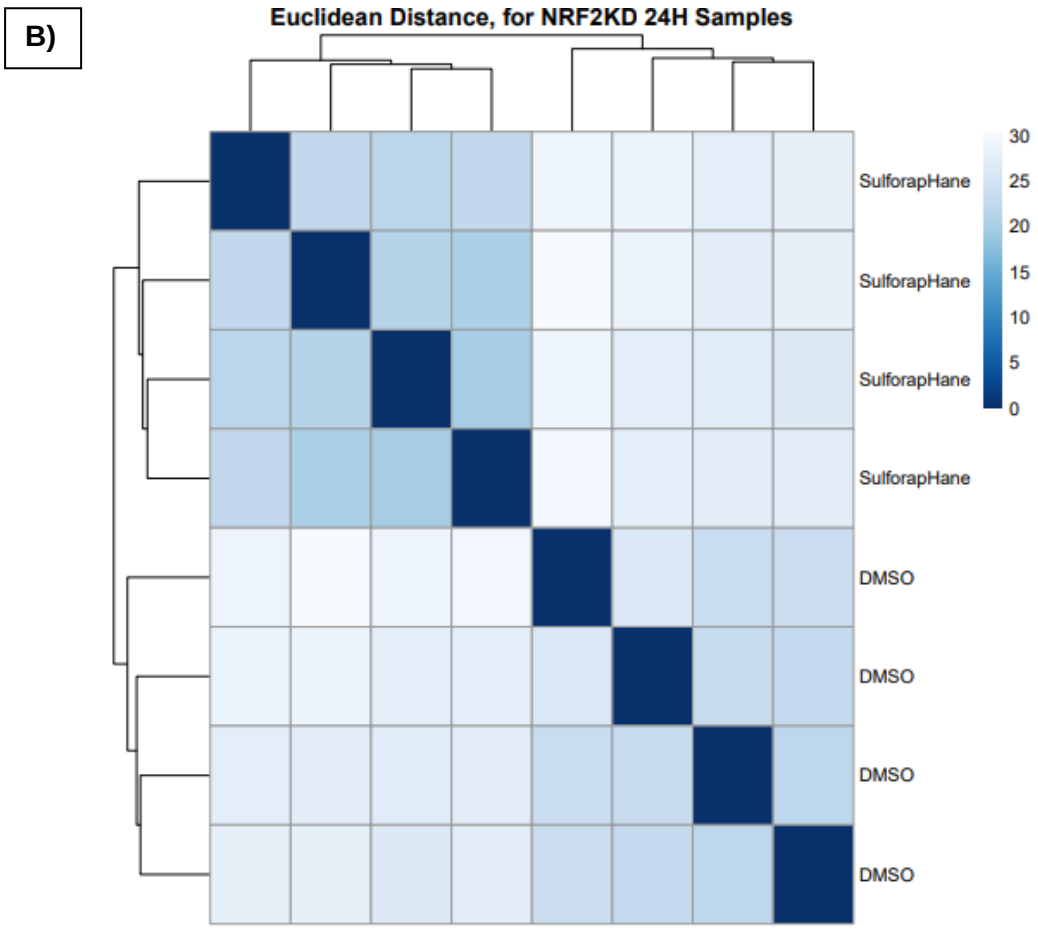

Figure 6.15. **Euclidean distance heatmap for each sample and treatment transformed by rlog.** Euclidean distance plot showing how the WT samples treated with SF behave differently to the NRF2 KD samples in HepG2 cultured in a high glucose environment after 24h treatment. A) WT samples. B) NRF2KD samples.

6.3.5 Differential expression gene testing

Differential expression analysis was performed on the gene counts via DESeq2, and the differentially expressed genes were corrected for multiple testing by Benjamini Hochberg ($q<0.05$). The mean-difference plot shown in figure 6.16 summarises the changes in gene expression induced by SF. A dot represents each gene in the plot, and the blue dots represent the differentially expressed genes, following multiple testing ($q<0.05$). For the WT samples out of the 17346 differentially expressed genes, 7603 were statistically significant ($q<0.05$). Likewise, for the NRF2KD samples out of the 17569 differentially expressed genes, only 4710 were statistically significant ($q<0.05$).

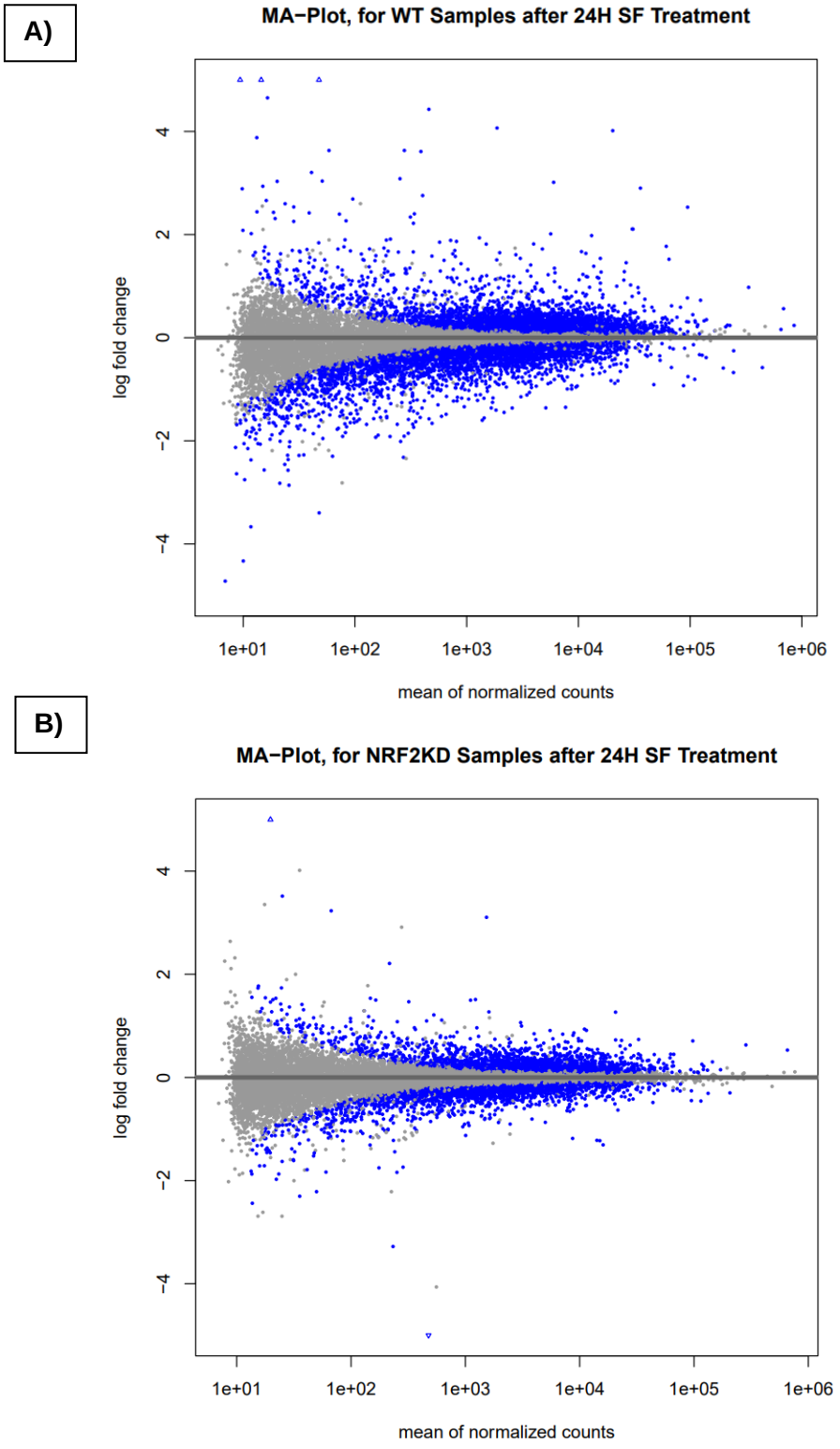

Figure 6.16. **Testing for differential expression between SF vs DMSO for** A) WT samples and B) the NRF2KD samples. Scatter plot of $\log_2$ ratio (fold change) vs mean. The grey color depicts all of the differentially expressed genes, whilst the blue dots represent the differentially expressed genes corrected for multiple testing, False Discovery rate set to 5% (Benjamini-Hochberg). Triangles represent the genes that fall out the y-axis of -5 to 5.

In the final step, the results of the pairwise comparison between 10 µM SF to the control in the WT and KD samples under different levels of the adjusted p-value (Benjamini-Hochberg) were extracted and published in table 6.1. Table 6.1 revealed that a total of 7603 genes were differentially expressed in response to 10µM SF compared to untreated controls in the WT, whilst 4710 genes were differentially expressed compared to the untreated control in the NRF2KD cell line ($q < 0.05$).

Table 6.1. Number of genes differentially expressed in response to SF in the WT and NRF2KD samples following 24h SF treatment

Samples	Num of Genes Expressed	Pass. Wald Test	p.value 0.1	p.value 0.05	q.value 0.1	q.value 0.05
WT	**17351**	**17346**	**9520**	**8511**	**8456**	**7603**
NRF2KD	**17578**	**17569**	**7240**	**6122**	**5561**	**4710**

Differentially expressed genes were obtained using the DESeq2 model. The statistically significant genes were calculated through the Wald test. The Wald test uses a likelihood ratio test which has an asymptotical chi-square test statistic. These statistically significant genes were then corrected for multiple testing for false discovery rates through the Benjamini-Hochberg. The differentially expressed genes corrected by multiple testing are represented by the q value.

6.3.6 Gene Set Enrichment Analysis

GSEA analysis was carried out on all the differentially expressed genes, (all 17351 for WT not just those with $q<0.05$). For the WT samples, it was identified that out of a total of 161 gene sets, 107 were positively enriched and 54 were negatively enriched. Out of these 107, 5 gene sets were enriched with a nominal p-value of <1%, and 23 gene sets were enriched at a nominal p-value of <5%. Similarly, in the negatively enriched sets, 5 gene sets were enriched with a nominal p-value of <1%, and 7 gene sets were enriched at a nominal p-value of <5%. For the NRF2KD samples, instead, it was identified that 105, were positively enriched and 56 were negatively enriched. For the positively enriched genes set, 8 gene sets were enriched with a nominal p-value of <1%, and 21 gene sets were enriched at a nominal p-value of <5%. For negatively enriched genes set 7 gene sets were enriched with a nominal p-value of <1% and 14 gene sets were enriched at a nominal p-value of <5%. Summary of the results can be identified in table 6.2.

Table 6.2. Summary statistics of the pathway analysis using the KEGG database between the WT and NRF2KD samples after SF 24h SF treatment

Samples	Enriched Gene Sets	FDR q <0.25	Nominal p value <0.05	Nominal p value <0.01
WT	**161** (↑107 ↓54)	**21** (↑14 ↓7)	**10** (↑5 ↓5)	**30** (↑23 ↓7)
NRF2KD	**161** (↑105 ↓56)	**39** (↑23 ↓16)	**15** (↑8 ↓7)	**35** (↑21 ↓14)

Pathway analysis was carried out using the GSEA software mapped to the KEGG database. 161 total pathways were calculated where ↑ represents upregulated pathway ↓ is downregulated pathway. The bold values under the FDR q value column represent the statistically significant pathways that have been enriched, the p-value that has corrected using Benjamini-Hochberg. The nominal p-value is the p-value normalized to the enrichment score

For the WT samples, it was identified that out of the positively enriched gene sets five reached a q< 0.05. These are: metabolism of xenobiotics by cytochrome P450 (NES= 1.81, q=0.006) and glutathione metabolism (NES= 1.80, q =0.008), highlighting NRF2 induction in the antioxidant response. Proteasome metabolism (NES= 1.81, q=0.006), was also enriched, thereby identifying NRF2 regulating the activity of several genes involved in the assembly of the proteasome. All these pathways were also identified to be upregulated in the RNASeq study in chapter 4 by 10μM SF in both the basal and high glucose environment (see chapter 4, 4.3.2), as well as being consistent with previously published data. SF also upregulated the pentose phosphate pathway (PPP) gene set (NES= 1.73, q=0.031), and finally, the steroid hormone biosynthesis pathway (NES= 1.71, q=0.038), consisting of additional genes such as the family of Aldo-Keto reductases known to be direct targets of NRF2 (figure 6.17). For the negatively enriched gene sets, the main gene set that SF downregulated was glycine, serine, and threonine metabolism (NES= -1.79, q=0.034), further confirming the findings from chapter 4 and 5, followed by propanoate metabolism (NES= -1.78, q=0.018), complement and coagulation cascades (NES= -1.72, q=0.031) and valine, leucine, and isoleucine degradation (NES= -1.66, q=0.05), while the gene set biosynthesis of unsaturated fatty acids just failed to reach significance (NES= -1.67, q=0.059) (**figure 6.17**).

In the NRF2KD samples, it was identified that the only gene set that was enriched in also the WT samples was the valine, leucine isoleucine degradation set, suggesting that the activity of these genes are likely not mediated by NRF2. Notably, none of the other gene sets found in the WT samples were enriched following SF treatment, suggesting that the role of SF interfering with one carbon metabolism and serine and glycine is mediated through NRF2. The summary results of the GESEA are shown in figure 6.17.

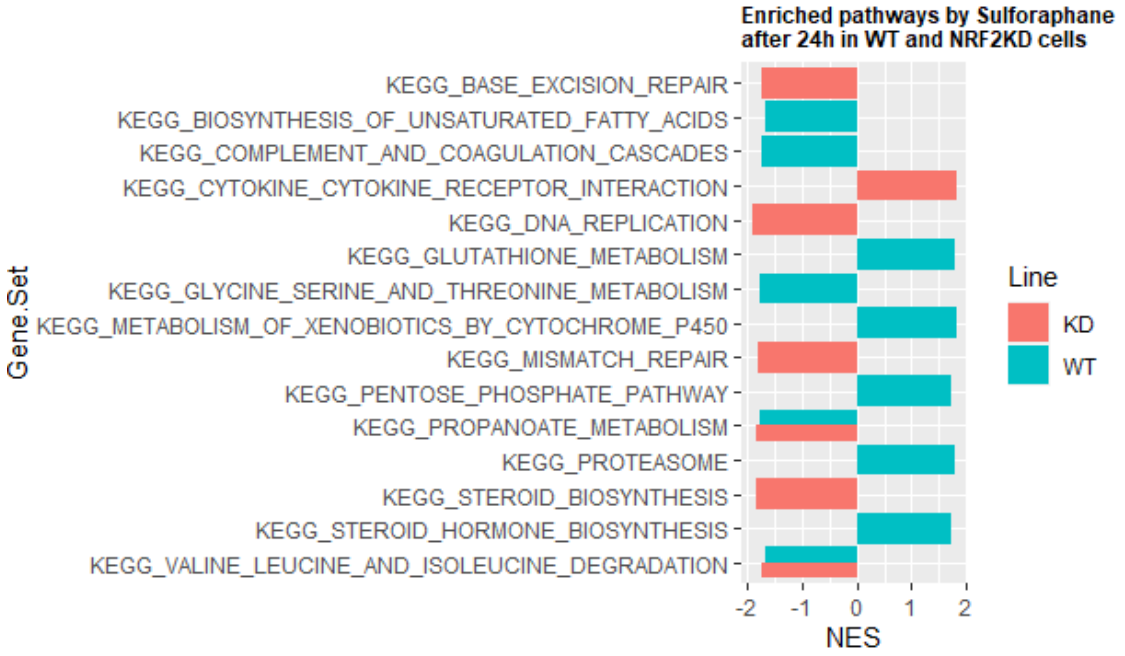

Figure 6.17. Significantly enriched gene sets identified within the differential expression data of WT HepG2 (green) and NRF2KD HepG2 (red) cells cultured under a high glucose environment when compared to sulforaphane treatment. The x-axis represents the normalized enrichment score (NES). The NES is calculated using the GSEA. NES represents an estimation of the significance of the gene set normalized to the size of each gene set. Positive NES is shown by an increase in the gene set, and negative NES denotes an overall decrease in the gene set. The y-axis represents the gene sets. Both treatment and controls are representative of quadruplicate samples.

6.3.7 The metabolic effects induced by SF in the WT cells are abolished in the KD samples

To get some insight into the genes involved in enriched pathways that were changed by SF, the top enriched core genes from each set were analyzed. The enriched core genes are defined as the subset of genes that contribute the most to the enrichment result. For the metabolism xenobiotics by cytochrome P450 gene set, it was identified 11 top enriched core genes. These top core enriched genes included several well-known NRF2 phases I and II targets such as the Aldo-Keto reductase family (AKR) and NQO1 (**figure 6.18**). It was identified from the analysis that the editing had a profound effect, in abolishing the response of genes involved in the antioxidant response in the KD cell line. For example, for the Aldo-Keto reductase genes, AKR1C1, AKR1C2, and AKR1C3 the editing resulted in about a 5- fold decrease in activity compared to the WT cells (AKR1C1 WT DMSO vs WT SF $log_2FC = 2.53$ compared to KD DMSO vs KD SF $log_2FC = 0.15$, **table 6.3 and figure 6.18**). For GSTA1, which is involved in glutathione

metabolism, by conjugating glutathione to xenobiotics, the editing even resulted in a downregulation of its activity compared to the WT (GSTA1, WT DMSO vs WT SF $log_2FC = 1.35$ compared to KD DMSO vs SF KD $log_2FC= -0.36$). It was identified though that the gene, UGT2B10 involved in phase II metabolism, its expression was higher in the KD samples rather than WT, perhaps suggesting that not all of the phase II genes are solely regulated by NRF2 (UGT2B10, WT DMSO vs WT SF $log_2FC = 0.48$ compared to KD DMSO vs SF KD $log_2FC= 0.58$). The results of the core enriched genes in the metabolism of xenobiotics by cytochrome P450 are shown in table 6.3 and figure 6.18.

Table 6.3.Comparison of differentially expressed genes in response to SF in the WT and NRF2KD cell lines involved in the metabolism of xenobiotics pathway by cytochrome P450

Ensembl ID	Gene Symbol	Gene	SF Log_2 Fold Change vs Control WT	SF Log_2 Fold Change vs Control NRF2KD
Metabolism of Xenobiotics by Cytochrome P450				
ENSG00000198099	*ADH4*	Alcohol dehydrogenase 4	0.53[3]	0.23[1]
ENSG00000187134	AKR1C1	Aldo-keto reductase family member 1 C1	2.53[3]	0.15[2]
ENSG00000151632	AKR1C2	Aldo-keto reductase family member 1 C2	2.90[3]	0.261[3]
ENSG00000196139	AKR1C3	Aldo-keto reductase family member 1 C3	1.64[3]	0.40[3]
ENSG00000167600	CYP2S1	Cytochrome P450 family 2 Subfamily S1	1.14[3]	0.44[3]
ENSG00000143819	EPHX1	Expoxide hydrolase 1	1.23[3]	0.44[3]
ENSG00000243955	GSTA1	Glutathione S-transferase alpha 1	1.35[3]	-0.36[3]
ENSG00000148834	GSTO1	Glutathione-S-transferase omega-1	0.67[3]	0.36[3]
ENSG00000008394	MGST1	Microsomal glutathione S-transferase 1	1.19[3]	0.17[3]
ENSG00000181019	NQO1	NAD(P)H dehydrogenase, quinone (1)	1.52[3]	0.27[3]
ENSG00000109181	UGT2B10	UDP glucuronosyltransferase family 2 member B10	0.48[3]	0.56[3]

Adjusted P values of fold change: $p^1<0.05$, $p^2<0.001$, $p^3<0.0001$. The differentially expressed genes were obtained through DESeq2. In the first step, DEseq2 performs an internal normalization, where the geometric mean for each gene across the samples is calculated. The count for each gene is then divided by the geometric mean. This procedure is done to normalize library size and RNA bias composition. In the next step DESeq2 plots a negative binomial for each gene count to obtain the differentially expressed genes. Multiple testing is corrected through Benjamini-Hochberg.

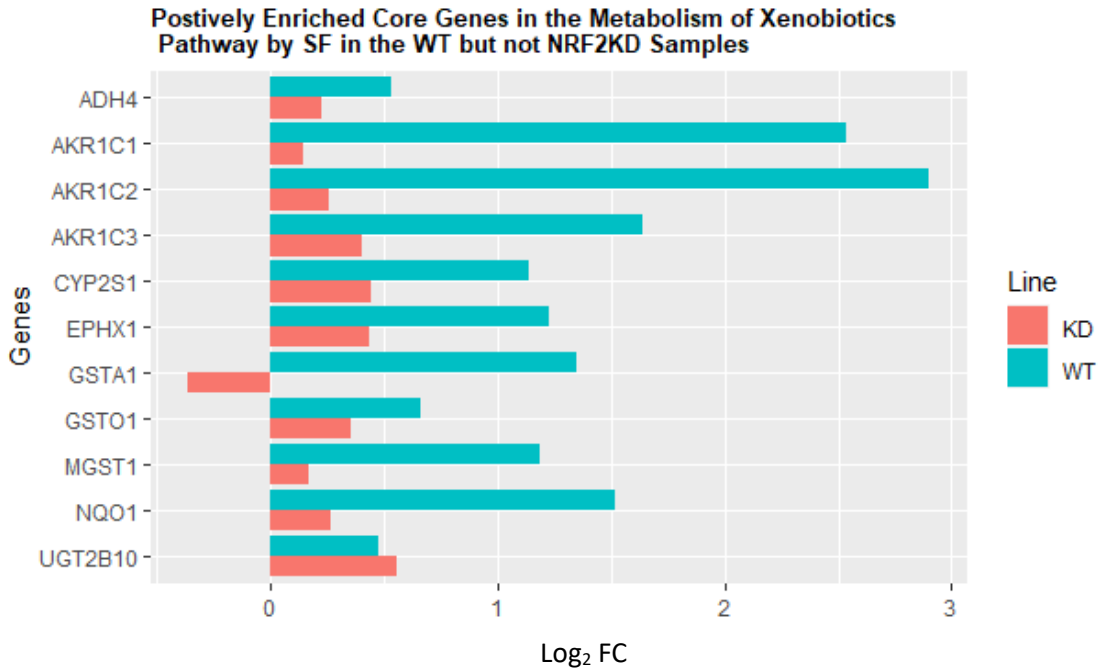

Figure 6.18. **Bar plot of the top enriched core gene, from the metabolism of xenobiotics by cytochrome P450 gene set by 10 µM SF**. These top enriched genes also referred to as the leading edge are defined as those which contributed most to the set enrichment score; reflecting their degree of overrepresentation in a running-sum metric. This is calculated using both the fold enrichment and degree of significance (p-value). Red = KD and Blue= WT samples. The x-axis represents the log_2 fold change whilst, the y-axis represents the genes of interest. These include Alcohol Dehydrogenase 4 (ADH4), Aldo-Keto Reductase 1 family member C1 (AKR1C1), Aldo-Keto Reductase 1 family member C2 (AKR1C2), Aldo-Keto Reductase 1 family member C3 (AKR1C3), Cytochrome P450 Family 2 Subfamily S1 (CYP2S1), Epoxide Hydrolase 1 (EPHX1), Glutathione-S-transferase alpha 1 (GSTA1), Glutathione-S-transferase omega 1, (GSTO1), Microsomal Glutathione S-transferase 1 (MGST1), NAD(P)H Dehydrogenase Quinone 1, (NQO1) and UDP Glucuronosyltransferase family 2 member B10 (UGT2B10). The statistical significance of the DEG can be found in table 6.3.

The next step of the analysis involved assessing the impact of the KD on the enriched core genes from the glutathione metabolism gene set. In chapter 4 it was identified a large increase in expression of the glutathione biosynthetic genes, correlating with an increase in the production of the metabolite reduced glutathione, identified in chapter 5. Therefore, it was expected that the editing would also result in a large reduction in the activity of genes in this set. It was identified that for the GCLC and GCLM, the rate-limiting enzymes involved in glutathione biosynthesis, editing resulted in a 2.5 and over 3-fold decrease in the activity of the genes, whilst GSR, needed for the conversion of oxidized to reduced glutathione editing resulted in about a 2-fold decrease (**table 6.4**

and figure 6.19). The analysis also revealed that G6PD the rate-limiting enzyme in the pentose phosphate pathway and PGD both involved in the pentose phosphate pathway the editing completely abolished the activity of these genes (**table 6.4 and figure 6.19**). Two genes involved in spermidine biosynthesis were also identified to be upregulated by SF: ornithine decarboxylase (ODC1), (previously reported in chapter 4) involved converting ornithine into the biogenic amine putrescine and spermidine synthase (SRM), the latter involved converting putrescine into spermidine, with the editing resulting in a 1.33-fold decrease in both genes compared to the WT. The results of the top 10 core enriched in glutathione metabolism are shown in table 6.4 and figure 6.19.

Table.6.4. Comparison of differentially expressed genes in response to SF in the WT and NRF2KD cell lines involved in glutathione metabolism

Ensembl ID	Gene Symbol	Gene	SF Log_2 Fold Change vs Control WT	SF Log_2 Fold Change vs Control NRF2KD
Glutathione Metabolism				
ENSG00000160211	G6PD	Glucose-6-Phosphate Dehydrogenase	0.55^3	0.02
ENSG00000001084	GCLC	Glutamate-cysteine ligase catalytic subunit	1.67^3	0.42^3
ENSG00000023909	GCLM	Glutamate-cysteine ligase regulatory subunit	2.02^3	0.45^3
ENSG00000176153	GPX2	Glutathione Peroxidase 2	1.00^3	0.002
ENSG00000104687	GSR	Glutathione Reductase	1.16^3	0.21^3
ENSG00000148834	GSTO1	Glutathione-S-transferase omega-1	0.67^3	0.36^3
ENSG00000008394	MGST1	Microsomal glutathione S-transferase 1	1.19^3	0.17^3
ENSG00000115758	ODC1	Ornithine Decarboxylase	0.67^3	0.26^3
ENSG00000142657	PGD	Phosphogluconate dehydrogenase	0.58^3	-0.0001
ENSG00000116649	SRM	Spermidine synthase	0.53^3	0.11^2

Adjusted P values of fold change: $p^1<0.05$, $p^2<0.001$, $p^3<0.0001$. The differentially expressed genes were obtained through DESeq2. In the first step, DEseq2 performs an internal normalization, where the geometric mean for each gene across the samples is calculated. The count for each gene is then divided

by the geometric mean. This procedure is done to normalize library size and RNA bias composition. In the next step DESeq2 plots a negative binomial for each gene count to obtain the differentially expressed genes. Multiple testing is corrected through Benjamini-Hochberg.

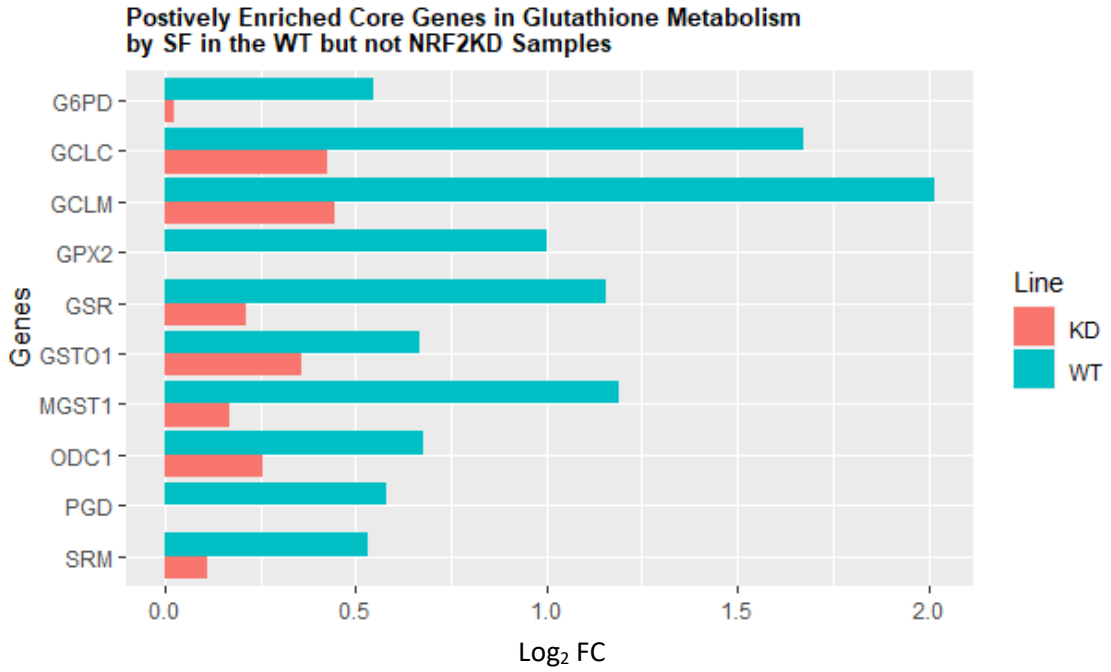

Figure 6.19. Top enriched differentially expressed genes from the Glutathione Metabolism gene set by 10 µM SF. These top enriched genes also referred to as the leading edge are defined as those which contributed most to the set enrichment score; reflecting their degree of overrepresentation in a running-sum metric. This is calculated using both the fold enrichment and degree of significance (p-value). Red = KD and Blue= WT samples. Glucose-6-Phosphate (G6PD), Glutamate-Cysteine Ligase Catalytic Subunit (GCLC), Glutamate-Cysteine Regulatory Subunit (GCLM), Glutathione Peroxidase2 (GPX2), Glutathione Reductase (GSR), Glutathione S-transferase omega-1 (GSTO1), Microsomal Glutathione S-transferase 1 (MGST1), Ornithine Decarboxylase 1 (ODC1), Phosphogluconate Dehydrogenase (PGD) and Spermidine Synthetase (SRM). The statistical significance of the DEG can be found in table 6.4.

The final positively enriched gene set that was analyzed, was the (PPP). In this set, it was identified, nine core enriched genes: the majority involved in the PPP but a couple also involved in glycolysis. Two enriched genes, G6PD and PGD respectively also overlapped with the glutathione metabolism gene set: Analysis of this gene set identified SF upregulating in the WT samples, the activity of the following genes, all belonging to the non-oxidative branch of the PPP: Phosphopentose epimerase (RPE) involved in converting ribulose-5-phosphate to xylulose 5-phosphate, transketolase (TKT) catalyzes the conversion of xylulose 5-phosphate to a 5 carbon atom aldose (D-ribose-5-P) to form a 7 carbon atom molecule (sedoheptulose) and transaldolase

(TALDO) catalyzing the reversible conversion of sedoheptulose to erythrose 4-phosphate and fructose 6-phosphate. When these genes were assessed in the KD samples it was identified that only RPE and TALDO were differentially expressed although had a log_2FC of 0.11 and 0.15, largely implying that the editing abolished the activity of these genes (**table 6.5 and figure 6.20**). From the core enriched genes of the PPP, it was also identified SF upregulating the activity of several glycolytic genes such as glucose phosphate isomerase (PGI), involved in converting glucose-6-phosphate to fructose-6-phosphate, the second step in glycolysis, phosphofrutco kinase (PFKP), catalyzing the conversion of fructose-6-phosphate to fructose-1-6-bisphosphate and aldolase A (ALDOA) or more commonly referred to as fructose-bisphosphate aldolase involved in catalyzing the reversible reaction of breaking fructose-1-6-biphosphate into the triose dihydroxyacetone phosphate (DHAP) and glyceraldehyde 3-phosphate (G3P). Again the editing abolished the activity of PFKP (WT DMSO vs WT SF log_2FC=0.76, compared to KD DMSO vs KD SF log_2FC=0.08) and ALDOA (WT DMSO vs WT SF log_2FC=0.59, compared to KD DMSO vs KD SF log_2FC=0.09), whilst the activity of PGI was severely diminished **(table 6.5 and figure 6.20**). The final gene identified to be enriched in the PPP gene set is phosphoribosyl pyrophosphate synthase (PRPS1). This enzyme is involved in synthesizing several important metabolites: nucleotides (purines and pyrimidines), cofactors NAD and NADP, and the amino acids histidine and tryptophan. The results of the top nine core enriched in the pentose phosphate pathway are shown in table 6.5 and figure 6.20.

Table.6.5. Comparison of differentially expressed genes in response to SF in the WT and NRF2KD cell lines involved in pentose phosphate pathway

Ensembl ID	Gene Symbol	Gene	SF Log_2 Fold Change vs Control WT	SF Log_2 Fold Change vs Control NRF2KD
Pentose Phosphate Pathway				
ENSG00000149925	ALDOA	Aldolase A	0.59[3]	0.09
ENSG00000160211	G6PD	Glucose-6-Phosphate Dehydrogenase	0.55[3]	0.02
ENSG00000105220	PGI	Glucose Phosphate Isomerase	0.40[3]	0.11[2]
ENSG00000067057	PFKP	Phospho Fructo Kinase platelet	0.76[3]	0.08
ENSG00000142657	PGD	Phosphogluconate dehydrogenase	0.58[3]	-0.0001
ENSG00000147224	PRPS1	Phosphoribosyl pyrophosphate synthase 1	0.40[3]	0.06
ENSG00000197713	RPE	ribulose-5-phosphate-3-epimerase	0.32[3]	0.14[1]
ENSG00000177156	TALDO1	Trans Aldolase 1	1.14[3]	0.16[3]
ENSG00000163931	TKT	Trans Ketolase	0.80[3]	0.03

Adjusted P values of fold change: $p^1<0.05$, $p^2<0.001$, $p^3<0.0001$. The differentially expressed genes were obtained through DESeq2. In the first step, DEseq2 performs an internal normalization, where the geometric mean for each gene across the samples is calculated. The count for each gene is then divided by the geometric mean. This procedure is done to normalize library size and RNA bias composition. In the next step DESeq2 plots a negative binomial for each gene count to obtain the differentially expressed genes. Multiple testing is corrected through Benjamini-Hochberg.

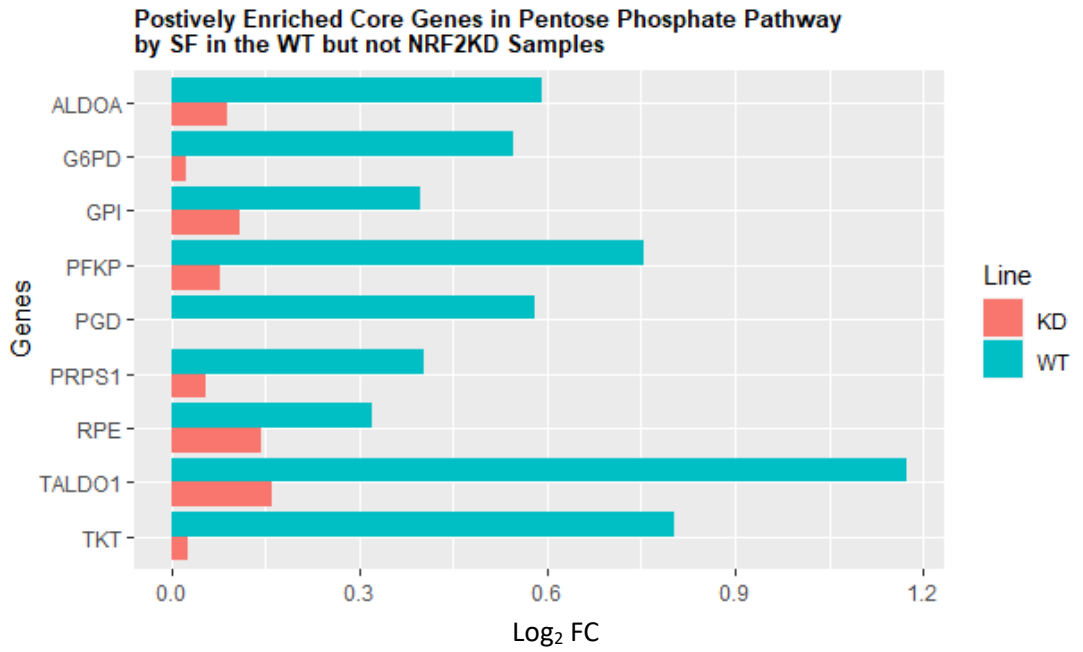

Figure 6.20. Top enriched differentially expressed genes from the pentose phosphate pathway gene set by 10 µM SF. These top enriched genes also referred to as the leading edge are defined as those which contributed most to the set enrichment score; reflecting their degree of overrepresentation in a running-sum metric. This is calculated using both the fold enrichment and degree of significance (p-value). Red = KD and Blue= WT samples. Aldolase A (ALDOA) Glucose-6-Phosphate (G6PD), Glucose Phosphate Isomerase (PGI) Phosphofructo Kinase Platelet (PFKP), Phosphogluconate Dehydrogenase (PGD), Phosphoribosyl Pyrophosphate Synthase (PRSP1), Ribulose-5-Phosphate-3-Epimerase (RPE), Transaldolase 1 (TALDO1), and Transketolase (TKT). The statistical significance of the DEG can be found in table 6.5.

The next step of the analysis focused on assessing the effect of SF in the WT and KD samples on glycine, serine, and threonine metabolism, including 1C metabolism. Focusing on the serine biosynthetic genes SF downregulated both the rate-limiting enzyme of serine biosynthesis phosphoglycerate dehydrogenase (PHGDH) (confirming the findings in chapter 5) as well as the final enzyme involved in serine biosynthesis, phosphoserine phosphatase PSPH. This effect in the KD cells by SF was reduced (PHGDH, WT DMSO vs WT SF log_2FC = -0.30 compared to KD DMSO vs KD SF log_2FC = -0.19) (**table 6.6, figure 6.21**). For glycine metabolism, it was identified a downregulation in both glycine decarboxylase (GLDC) inhibiting the breakdown of glycine and the glycine N-methyltransferase (GNMT) involved in converting glycine to sarcosine, and in doing so functions to regulate levels of SAM and SAH, confirming the findings identified in chapter 5. Again editing, resulted in attenuation of GLDC and GNMT, with the largest effect seen on GNMT (GNMT, WT DMSO vs WT SF log_2FC = -

1.53 compared to KD DMSO vs KD SF log_2FC = -1.00, **table 6.6, figure 6.21**). The analysis also found SF downregulating in two genes not identified in the previous analysis (chapter 5). Sarcosine dehydrogenase (SARDH) by 1.5-fold, is involved in synthesizing glycine from sarcosine, thereby potentially resulting in an increase in the levels of sarcosine and glycerate-2-kinase (GLYCTK) by 1.33-fold, is involved in converting to glycerate to 2-phospho-D-glycerate. Editing resulted in a decrease in expression in both SARDH and GLYCTK with SF resulting in a 1.3-fold and 1.15-fold change. With regards to the genes involved from the one-carbon pool, folate gene set it was identified that the gene with the largest increase in expression is the aldehyde dehydrogenase family 1 member L1, also known as the cytosolic 10-formyltetrahydrofolate (ALDH1L1), with the editing abolishing the activity of ALDH1L1 (WT DMSO vs WT SF log_2FC = 1.19 compared to KD DMSO vs KD SF log_2FC = 0.035, table 6.26, figure 6.21). Like in chapter 5 it was identified that SF upregulated two genes GART and ATIC involved in purine metabolism, along with the methylenetetrahydrofolate dehydrogenase (MTHFD1L), whilst in the edited cells, this effect was diminished. SF also resulted in a 2.3-fold change in BHMT2, whilst the editing resulted in a 1.3-fold change. The only gene that was identified to have increased expression in the KD cell line compared to the WT was the cystathionine beta-synthetase (CBS), which catalyzes the conversion of homocysteine using serine to cystathionine, the first step of the transsulfuration pathway. The results of the glycine, serine, and threonine metabolism along 1C metabolism are shown in table 6.6 and figure 6.21.

Table.6.6. Comparison of differentially expressed genes in response to SF in the WT and NRF2KD cell lines involved in glycine serine and threonine including one carbon pool by folate gene sets.

Ensembl ID	Gene Symbol	Gene	SF Log_2 Fold Chang e vs Contol WT	SF Log_2 Fold Change vs Control NRF2K D
Glycine Serine and Threonine Metabolism				
ENSG00000172482	AGXT	Serine-pyruvate transferase	-1.22[3]	-0.72[3]
ENSG00000144908	ALDH1L1	Aldehyde Dehydrogenase family 1 member L1	1.19[3]	0.035
ENSG00000145020	AMT	Aminomethyl transferase	-0.47[3]	-0.38[3]
ENSG00000138363	ATIC	5-aminoimidazole-4-carboxamide ribonucleotide formyltransferase	0.42[3]	0.15[3]
ENSG00000132840	BHMT2	betaine--homocysteine S-methyltransferase 2	1.21[3]	0.39[3]
ENSG00000160200	CBS	Cystathione beta-synthatse	-0.33[2]	-0.44[3]
ENSG00000110887	DAO	D-amino acid oxidase	-1.52[3]	-0.21
ENSG00000159131	GART	Phosphoribosylglycinamide formyltransferase	0.33[3]	0.09[1]
ENSG00000178445	GLDC	Glycine Decarboxylase	-0.35[3]	-0.24[3]
ENSG00000168237	GLYCTK	Glycerate-2-Kinase	-0.42[3]	-0.17[2]
ENSG00000124713	GNMT	Glycine-N-methyl transferase	-1.53[3]	-1.00[3]
ENSG00000120254	MTHFD1L	Methylenetetrahydrofolate dehydrogenase	0.36[3]	0.11[1]
ENSG00000092621	PHGDH	Phosphoglycerate Dehydrogenase	-0.30[3]	-0.19[3]
ENSG00000179761	PIPOX	Pipecolic acid and sarcosine oxidase	-0.32[3]	-0.13[2]
ENSG00000146733	PSPH	Phosphoserine Phosphatase	-0.47[3]	-0.25[3]
ENSG00000123453	SARDH	Sarcosine Dehydrogenase	-0.57[3]	-0.27[3]

Adjusted P values of fold change: $p^1<0.05$, $p^2<0.001$, $p^3<0.0001$. The differentially expressed genes were obtained through DESeq2. In the first step, DEseq2 performs an internal normalization, where the

geometric mean for each gene across the samples is calculated. The count for each gene is then divided by the geometric mean. This procedure is done to normalize library size and RNA bias composition. In the next step DESeq2 plots a negative binomial for each gene count to obtain the differentially expressed genes. Multiple testing is corrected through Benjamini-Hochberg.

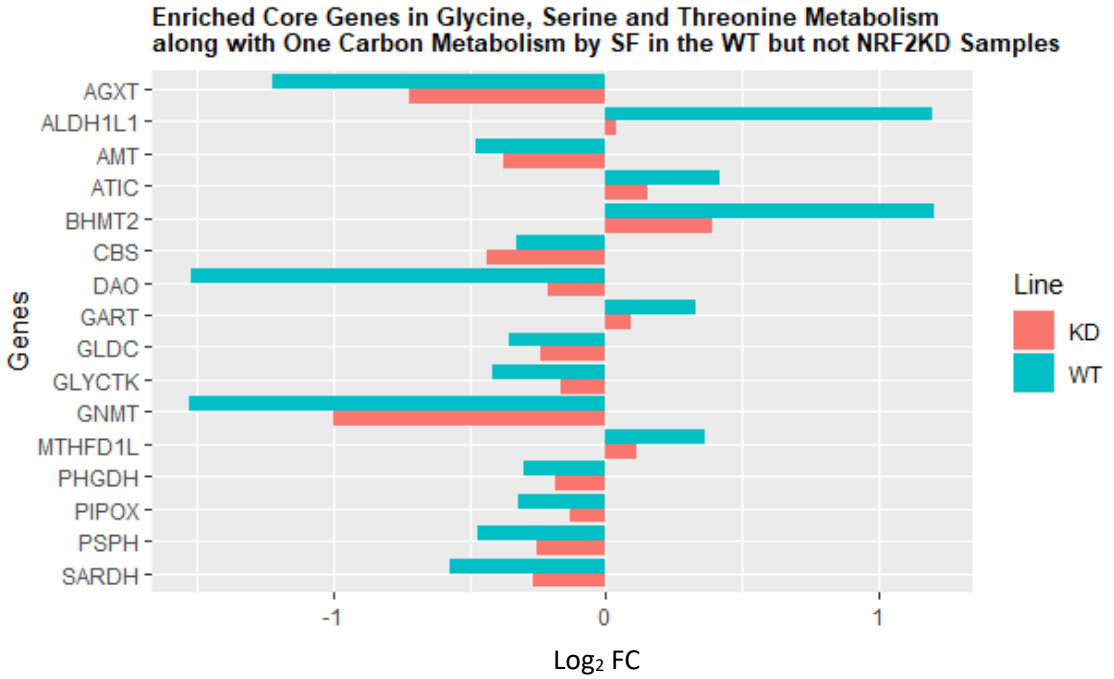

Figure 6.21. Top enriched differentially expressed genes from the glycine serine and threonine metabolism, include one carbon pool by folate gene set by 10 µM SF. These top enriched genes also referred to as the leading edge are defined as those which contributed most to the set enrichment score; reflecting their degree of overrepresentation in a running-sum metric. This is calculated using both the fold enrichment and degree of significance (p-value). Red = KD and Blue= WT samples. Serine-Pyruvate Aminotransferase (AGXT), 10-formyltetrahydrofolate dehydrogenase (ALDH1L1), Aminomethyl Transferase (AMT), Inosine Monophosphate Synthase (ATIC), Betaine-Homocysteine S-Methyltransferase/isoform 2 (BHMT2), Cystathionine Beta-Synthase (CBS), D-amino acid oxidase, Trifunctional Purine Biosynthetic protein adenosine-3 (GART), Glycine Decarboxylase (GLDC), Glycerate-2-Kinase (GLYCTK), Glycine, N-methyltransferase (GNMT), Monofunctional C1-tetrahydrofolate Synthase (MTHFD1L), Phosphoglycerate Dehydrogenase (PHGDH), Peroxisomal Sarcosine Oxidase (PIPOX), Phosphoserine Phosphatase (PSPH), Sarcosine Dehydrogenase (SARDH). The statistical significance of the DEG can be found in table 6.6.

With regards to the biosynthesis of the unsaturated fatty acids gene set, it was identified that the gene with the highest downregulation was the transcription factor sterol regulatory element-binding protein 1 (SREBF1) by 1.8-fold in the WT samples, whilst the editing resulted instead a 1.4-fold change. SREBF1 plays a key role in the initiation of lipogenesis in the liver (**table 6.7, figure 6.22**). SF also downregulated the rate-limiting enzyme involved in the synthesis of unsaturated fatty acids stearoyl-CoA

desaturase (SCD) by 1.3-fold whilst the editing resulted in a 1.2-fold downregulation. SCD is involved in the biosynthesis of the monounsaturated fatty acids oleate (oleic acid) and palmitoleate (**table 6.7, figure 6.22**). Another additional enzymes involved in regulating the synthesis of unsaturated fatty acids are the fatty acid desaturase family. In this analysis, SF was shown to downregulate the activity of both FADS1 and FADS2 by 1.3 and 1.5-fold respectively in the WT samples, whilst FADS3 interestingly in the WT samples was not differentially expressed, but in the NRF2KD, SF resulted in a significant downregulation (**table 6.2.7, figure 6.22**). FADS1, also referred to as delta-5 desaturase is involved in synthesizing omega-3 and omega-6 fatty acids, by catalyzing the formation of eicosapentaenoic acid (EPA) and arachidonic acid. FADS2 also referred to as delta-6 desaturase on the other hand is involved in alpha-linoleic acid metabolism, by converting linoleoyl CoA to gamma-linoleonoyl CoA. SF also downregulated two genes ACOT1 and ACOT2 by 1.4 and 1.14-fold in the WT samples, whilst in the NRF2KD samples SF led a 1.17-fold downregulation in ACOT1, whilst ACOT2 was no longer induced. ACOT1 and 2 both belong to the family acyl-CoA thioesterases, whose function is to catalyze the hydrolysis of various Coenzyme A attached to the fatty acid to generate a free coenzyme A plus the fatty acid (table 6..7, figure 6.2). The final gene that SF downregulated is the elongation of very long-chain fatty acids or more commonly referred to as fatty acid elongase 2 who's role is to synthesize very long polyunsaturated fatty acids by the addition of two carbon atoms. The results of the top seven core enriched in the biosynthesis of unsaturated fatty acids gene set are shown in table 6.7 and figure 6.22.

Table.6.7. Comparison of differentially expressed genes in response to SF in the WT and NRF2KD cell lines involved in the biosynthesis of unsaturated fatty acids

Ensembl ID	Gene Symbol	Gene	SF Log_2 Fold Change vs Control WT	SF Log_2 Fold Change vs Control NRF2KD
Biosynthesis of Unsaturated Fatty Acids				
ENSG00000184227	ACOT1	Acyl-CoA thioesterase 1	-0.47[3]	-0.23[3]
ENSG00000119673	ACOT2	Acyl-CoA thioesterase 2	-0.19[3]	-0.07
ENSG00000197977	ELOVL2	Fatty acid elongase 2	-0.39[3]	-0.21[3]
ENSG00000149485	FADS1	Fatty acid desaturase 1	-0.41[3]	-0.36[3]
ENSG00000134824	FADS2	Fatty acid desaturase 2	-0.62[3]	-0.59[3]
ENSG00000099194	SCD	Stearoyl-CoA Desaturase	-0.38[3]	-0.31[3]
ENSG00000072310	SREBF1	Sterol regulatory element binding protein 1	-0.81[3]	-0.54[3]

Adjusted P values of fold change: $p^1<0.05$, $p^2<0.001$, $p^3<0.0001$. The differentially expressed genes were obtained through DESeq2. In the first step, DEseq2 performs an internal normalization, where the geometric mean for each gene across the samples is calculated. The count for each gene is then divided by the geometric mean. This procedure is done to normalize library size and RNA bias composition. In the next step DESeq2 plots a negative binomial for each gene count to obtain the differentially expressed genes. Multiple testing is corrected through Benjamini-Hochberg.

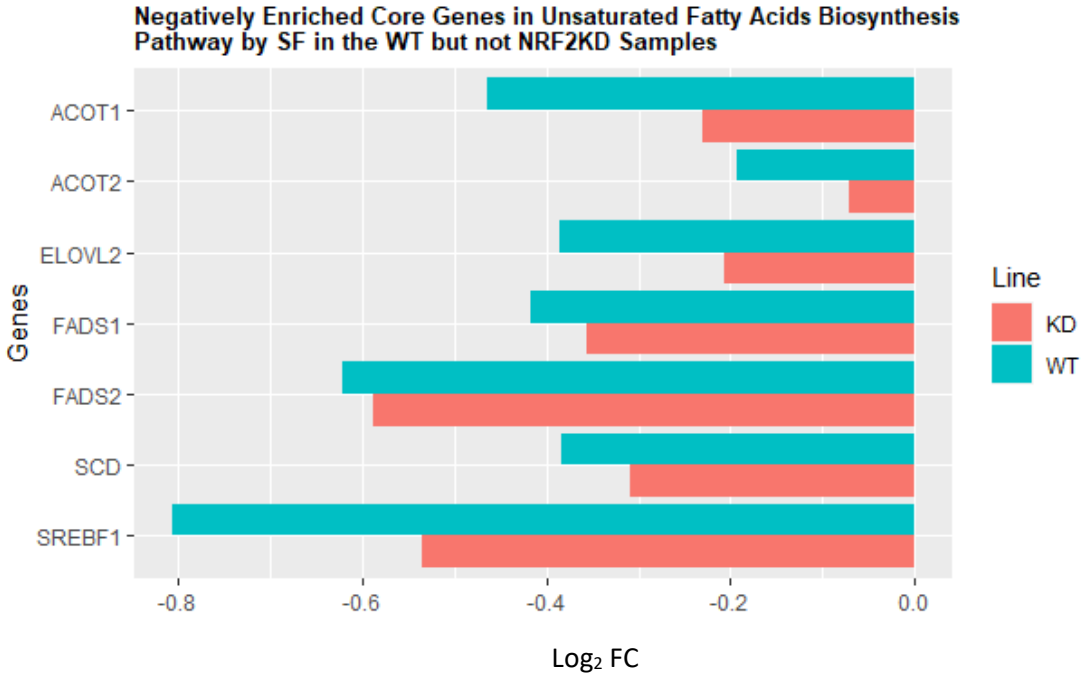

Figure 6.22. Top enriched differentially expressed genes from the biosynthesis of unsaturated fatty acids gene set by 10 μM SF. These top enriched genes also referred to as the leading edge are defined as those which contributed most to the set enrichment score; reflecting their degree of overrepresentation in a running-sum metric. This is calculated using both the fold enrichment and degree of significance (p-value). Red = KD and Blue= WT samples. Acyl-CoA Thioesterase 1 (ACOT1), Acyl-CoA Thioesterase 2 (ACOT2), Fatty acid Elongase 2 (ELVOL2), Fatty acid Desaturase 1 (FADS1), Fatty Acid Desaturase 2 (FADS2), Sterol-CoA Desaturase (SCD), and Sterol Regulatory Element-Binding Protein 1 (SREBF1). Statistical significance of the DEG can be found in table 6.7.

6.3.8 SF impacts DNA metabolism in the NRF2KD cell line

GSEA analysis, of the enriched gene sets by SF in the NR2KD cell line identified that none of the positively enriched gene sets, reached significance (q<0.05) (**figure 6.17**). The two gene sets, that just failed to reach statistical significance were the cytokine-cytokine receptor interaction (NES = 1.82 q=0.052) and the JAK-STAT pathway (NES = 1.73 q =0.063), followed by glycosaminoglycan degradation (NES = 1.72 q= 0.142). It was identified that SF downregulated several gene sets related to DNA Metabolism such as: DNA replication (NES = -1.92 q= 0.005), mismatch repair (NES = -1.79 q=0.019), base excision repair (NES = -1.75 q=0.026), with cell cycle just failing to reach significance (NES = -1.69 q=0.069), along with a couple of additional metabolic process such as propanoate metabolism (NES = -1.85 q=0.012), steroid biosynthesis (NES = -1.83 q=0.013) and valine, leucine and isoleucine degradation (NES =-1.75 q=0.03) (**figure 6.17**).

For the cytokine-cytokine interaction gene set, the analysis identified that although this gene set was enriched in the KD cells only, gene expression activity was still higher in the WT samples, (**figure 6.23**). SF upregulated the expression of the C-C motif chemokine ligand 20 (CCL20) and its receptor (CCR6), by 1.39-fold in the WT and 1.34-fold in the KD samples respectively, whose function is to attract lymphocytes and dendritic cells towards epithelial cells of a specific tissue of interest, in this case, the liver. SF also increased the expression of several genes belonging to the type I cytokine receptor family; the interleukin 6 receptor (IL6R), by 2.2-fold in the WT and 1.7-fold in the KD samples respectively. IL6R is involved in regulating not only cell growth and differentiation, interleukin 13 receptor subunit alpha 1 (IL13RA1), who was only differentially expressed in the KD samples, is involved in inducing activation of the JAK/STAT pathway, mainly through activation of STAT6 and the oncostatin M receptor (OSMR). The analysis also showed SF upregulating three protein receptors belonging to the TNF family; TNFRSF10B/D, and TNFRSF1A. In the WT samples, SF led a 1.7-fold change in both TNFRSF10B/D, compared to 1.2 and 1.39-fold change respectively in the KD samples. Both TNFRSF10B/D are also referred to as the death receptors 5 and 2 are involved in inducing apoptosis. Finally, SF also upregulated the expression of the transforming growth factor, beta receptor II (TGFBR2) by 1.35-fold in the WT sample compared to 1.2 fold in the KD samples. The full results are shown in table 6.8 and figure 6.23.

Table.6.8. Comparison of differentially expressed genes in response to SF in the WT and NRF2KD cell lines involved in cytokine-cytokine interaction pathway

Ensembl ID	Gene Symbol	Gene	SF Log_2 Fold Change vs Contol WT	SF Log_2 Fold Change vs Control NRF2KD
Cytokine-Cytokine Interaction				
ENSG00000115009	CCL20	C-C Motif Chemokine Ligand 20	0.47[1]	0.42[3]
ENSG00000112486	CCR6	C-C Motif Chemokine Receptor 6	0.63[3]	0.58[3]
ENSG00000146648	EGFR	Epidermal growth factor receptor	0.85[3]	0.75[3]
ENSG00000131724	IL13RA1	Interleukin 13 receptor subunit alpha 1	0.11	0.45[3]
ENSG00000160712	IL6R	Interleukin 6 receptor	1.14[3]	0.75[3]
ENSG00000145623	OSMR	Oncostatin M receptor	0.56[3]	0.48[3]
ENSG00000163513	TGFBR2	Transforming growth factor beta receptor 2	0.43[3]	0.28[3]
ENSG00000120889	TNFRSF10B	TNF receptor superfamily member 10b	0.30[3]	0.27[3]
ENSG00000173530	TNFRSF10D	TNF receptor superfamily member 10d	0.78[3]	0.47[3]
ENSG00000067182	TNFRSF1A	TNF receptor superfamily member 1A	0.78[3]	0.40[3]

Adjusted P values of fold change: $p^1<0.05$, $p^2<0.001$, $p^3<0.0001$. The differentially expressed genes were obtained through DESeq2. In the first step, DEseq2 performs an internal normalization, where the geometric mean for each gene across the samples is calculated. The count for each gene is then divided by the geometric mean. This procedure is done to normalize library size and RNA bias composition. In the next step DESeq2 plots a negative binomial for each gene count to obtain the differentially expressed genes. Multiple testing is corrected through Benjamini-Hochberg.

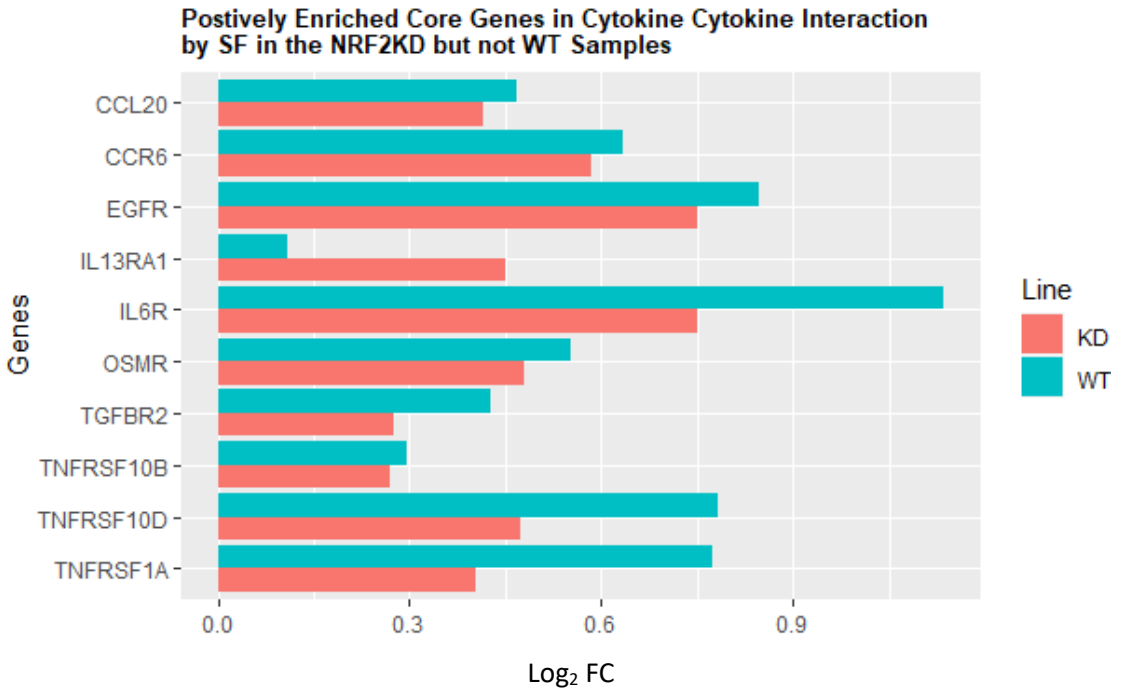

Figure 6.23. Top enriched differentially expressed genes from the cytokine-cytokine interaction gene set by 10 μM SF. These top enriched genes also referred to as the leading edge are defined as those which contributed most to the set enrichment score; reflecting their degree of overrepresentation in a running-sum metric. This is calculated using both the fold enrichment and degree of significance (p-value). Red = KD and Blue= WT samples. C-C motif Chemokine Ligand 20 (CCL20), C-C motif Chemokine Receptor 6 (CCR6), Epidermal Growth Factor Receptor (EGFR), Interleukin 13 Receptor Subunit Alpha 1, (IL13RA1), Interleukin 6 Receptor (IL6R), Oncostatin M Receptor (OSMR), Transforming Growth Factor Beta Receptor 2 (TGFBR2), TNF Receptor Superfamily Member 10B (TNFRSF10B), TNF Receptor Superfamily Member 10D (TNFRSF10D) and TNF Receptor Superfamily Member 1A (TNFRSF1A). The statistical significance of the DEG can be found in table 6.8.

With regards to the negatively enriched gene sets, it was identified that both proliferating cell nuclear antigen (PCNA) and DNA ligase 1 (Lig1) were downregulated in all three gene sets: DNA replication, base excision repair, and DNA mismatch. PCNA acts as a clamp allowing the binding of a specific DNA polymerase, delta, in eukaryotic cells. DNA ligase 1 instead is the only known DNA ligase up to now, that is involved in both DNA replication and base excision repair processes. LIG1 is especially responsible for joining the Okazaki fragments formed on the lagging strand of the DNA (**table 6.9, figure 6.26**). The analysis also revealed that SF downregulated several genes from the family of DNA replication of licensing factor also referred to as minichromosome maintenance complex component (MCM) 2,3,4,5 and 7. All of these proteins are involved with the initiation of DNA replication (**table 6.9, figure 6.26**). SF also downregulated the expression of replication factor 1 (RFC1), one of the five

subunits of the DNA Polymerase and the replication protein A 70 kDa binding subunit, which has been shown to interact with the binding a wide range of proteins including MCM2,4,6 and 7 as well as tumor suppressors genes such as p53 (**table 6.9, figure 6.26**). SF also downregulated the activity of Flap structure specific endonuclease 1 (Flap 1), whose function is to remove 5' overhang hands. The results of the core enriched gene sets in DNA replication are shown in table 6.9 and figure 6.26.

Table.6.9. Comparison of differentially expressed genes in response to SF in the WT and NRF2KD cell lines involved in DNA replication

Ensembl ID	Gene Symbol	Gene	SF Log_2 Fold Change vs Contol WT	SF Log_2 Fold Change vs Control NRF2KD
DNA Replication				
ENSG00000168496	FEN1	Flap structure specific endonuclease 1	-0.14[3]	-0.25[3]
ENSG00000105486	LIG1	DNA Ligase 1	-0.53[3]	-0.47[3]
ENSG00000073111	MCM2	Minichromosome maintenance complex component 2	-0.20[3]	-0.21[3]
ENSG00000112118	MCM3	Minichromosome maintenance complex component 3	-0.21[3]	-0.18[3]
ENSG00000104738	MCM4	Minichromosome maintenance complex component 4	-0.18[3]	-0.20[3]
ENSG00000100297	MCM5	Minichromosome maintenance complex component 5	-0.25[3]	-0.28[3]
ENSG00000166508	MCM7	Minichromosome maintenance complex component 7	-0.13[2]	-0.28[3]
ENSG00000132646	PCNA	Proliferating cell nuclear antigen	-0.29[3]	-0.31[3]
ENSG00000035928	RFC1	Replication factor 1	-0.45[3]	-0.28[3]
ENSG00000132383	RPA1	Replication protein A 70 kDa binding subunit	-0.15[3]	-0.21[3]

Adjusted P values of fold change: $p^1<0.05$, $p^2<0.001$, $p^3<0.0001$. The differentially expressed genes were obtained through DESeq2. In the first step, DEseq2 performs an internal normalization, where the geometric mean for each gene across the samples is calculated. The count for each gene is then divided by the geometric mean. This procedure is done to normalize library size and RNA bias composition. In the next step DESeq2 plots a negative binomial for each gene count to obtain the differentially expressed genes. Multiple testing is corrected through Benjamini-Hochberg

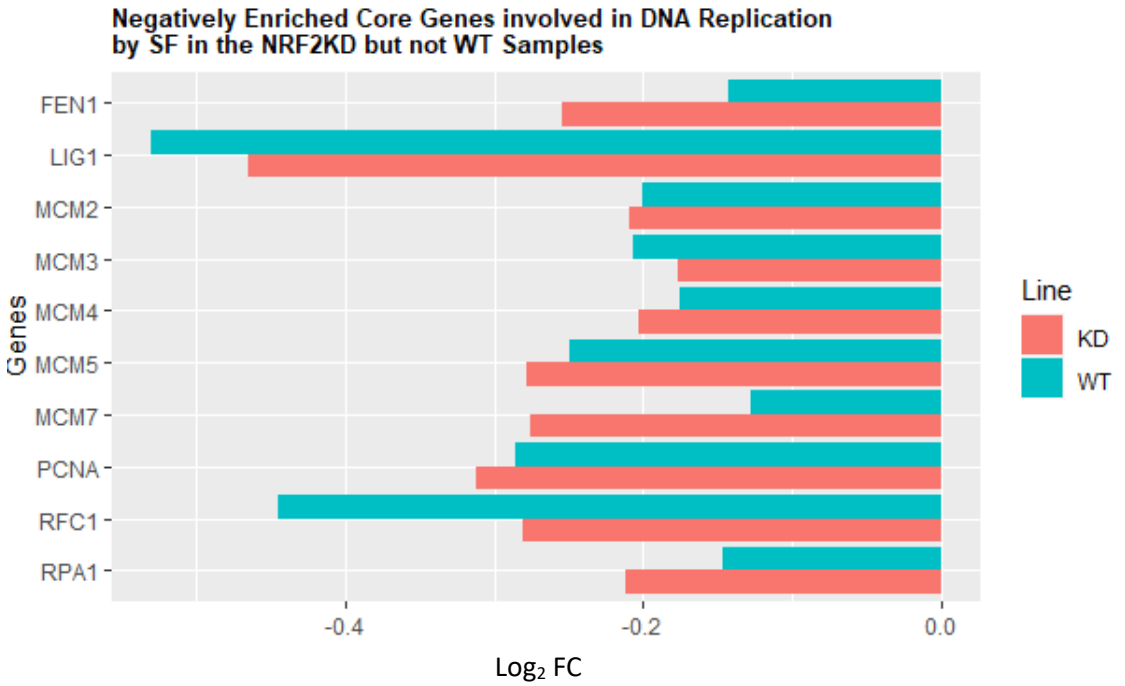

Figure 6.24. Top enriched differentially expressed genes from the DNA Replication gene set by 10 μM SF. These top enriched genes also referred to as the leading edge are defined as those which contributed most to the set enrichment score; reflecting their degree of overrepresentation in a running-sum metric. This is calculated using both the fold enrichment and degree of significance (p-value). Red = KD and Blue= WT samples. Flap Structure Specific Endonuclease 1 (FEN1), DNA Ligase 1 (LIG1), Minichromosome Maintenance Complex Component 2 (MCM2), Minichromosome Maintenance Complex Component 3 (MCM3), Minichromosome Maintenance Complex Component 4 (MCM4), Minichromosome Maintenance Complex Component 5 (MCM5), Minichromosome Maintenance Complex Component 7 (MCM7), Proliferating Cell Nuclear Antigen (PCNA) and Replication Protein A 70 kDa Binding Subunit (RPA1). Statistical significance of the DEG can be found in table 6.9.

In the base excision repair (BER), gene set SF downregulated several genes involved in coding for subunits of both DNA glycosylases involved in the short patch and long patch BER mechanism. SF downregulated, FEN1, PCNA, POLβ, (POLδ1), DNA polymerase epsilon/DNA polymerase epsilon subunit 2 (POLε/POLε2) and LIG1 for the long patch BER along with (XRCC1) and POLβ, that form part of the short-patch BER mechanism (**table 6.2.10, figure 6.25**). It was also identified that SF downregulated an additional two genes, the high mobility group box 1 protein (HMGB1) and uracil-DNA glycosylase (UNG) (**table 6.10, figure 6.25**). UNG functions to remove any uracil bases by cleaving the N-glycosidic bond and thereby initiating the BER pathway, whilst instead, HMGB1 binds the DNA and in doing so bends it thereby allowing the binding

of BER proteins. The results of the core enriched genes in the Base Excision pathway are shown in table 6.10 and figure 6.25.

Table.6.10. Comparison of differentially expressed genes in response to SF in the WT and NRF2KD cell lines involved in base excision repair

Ensembl ID	Gene Symbol	Gene	SF Log_2 Fold Change vs Contol WT	SF Log_2 Fold Change vs Control NRF2KD
Base Excision Repair				
ENSG00000168496	FEN1	Flap structure specific endonuclease 1	-0.14[3]	-0.25[3]
ENSG00000189403	HMGB1	High mobility group box 1 protein	-0.006	-0.15[1]
ENSG00000105486	LIG1	DNA Ligase 1	-0.53[3]	-0.47[3]
ENSG00000132646	PCNA	Proliferating cell nuclear antigen	-0.29[3]	-0.31[3]
ENSG00000070501	POLB	DNA Polymerase Beta	-0.06	-0.22[1]
ENSG00000062822	POLD1	DNA Polymerase Delta subunit 1	-0.11	-0.18[1]
ENSG00000177084	POLE	DNA Polymerase Epsilon	-0.36[3]	-0.22[1]
ENSG00000100479	POLE2	DNA Polymerase Epsilon subunit 2	-0.24[3]	-0.28[1]
ENSG00000076248	UNG	Uracil DNA glycosylase	-0.20[3]	-0.21[3]
ENSG00000073050	XRCC1	X-ray repair cross-complementing protein 1	-0.34[3]	-0.31[3]

Adjusted P values of fold change: $p^1<0.05$, $p^2<0.001$, $p^3<0.0001$. The differentially expressed genes were obtained through DESeq2. In the first step, DEseq2 performs an internal normalization, where the geometric mean for each gene across the samples is calculated. The count for each gene is then divided by the geometric mean. This procedure is done to normalize library size and RNA bias composition. In the next step DESeq2 plots a negative binomial for each gene count to obtain the differentially expressed genes. Multiple testing is corrected through Benjamini-Hochberg.

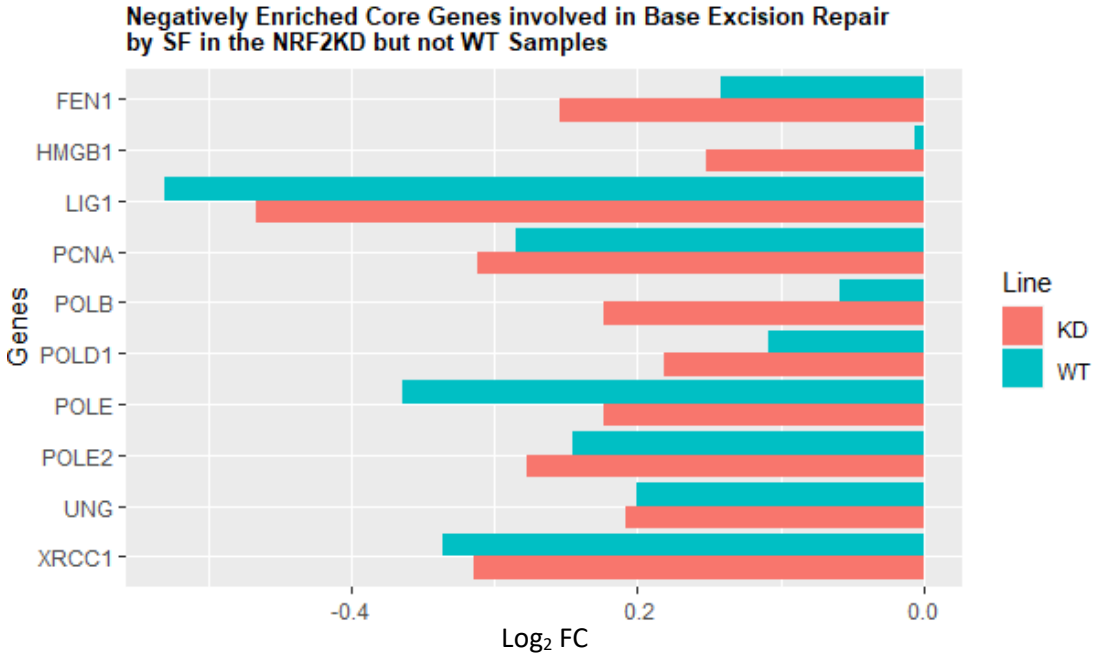

Figure 6.25. Top enriched differentially expressed genes from the Base Excision Repair gene set by 10 μM SF. These top enriched genes also referred to as the leading edge are defined as those which contributed most to the set enrichment score; reflecting their degree of overrepresentation in a running-sum metric. This is calculated using both the fold enrichment and degree of significance (p-value). Red = KD and Blue= WT samples. Flap Structure Specific Endonuclease 1 (FEN1), High Mobility Group Box 1 Protein (HMGB1), DNA Ligase 1 (LIG1), Proliferating Cell Nuclear Antigen (PCNA), DNA Polymerase Beta (POLβ), DNA Polymeraseδ Subunit 1 (POLD1), DNA Polymerase Epsilon (POLε), DNA Polymerase Epsilon Subunit 2 (POLε2), Uracil DNA Glycosylase (UNG) and X-ray Repair Cross-Complementing Protein 1 (XRCC1). The statistical significance of the DEG can be found in table 6.10.

In the DNA mismatch repair (MMR) gene set, SF downregulated both mSH6 and mSH2 along with downregulating several genes belonging to the family replication factor C subunit, RFC1,2 and 4, which allows the binding of PCNA (**table 6.11, figure 6.26**). SF also downregulated the activity of exonuclease 1, EXO1, which binds to MSH2 and in doing so reducing the number of double-stranded breaks that arise during recombination in meiosis. The results of the core enriched genes from the DNA Mismatch repair set are shown in table 6.11 and figure 6.26.

Table.6.11. Comparison of differentially expressed genes in response to SF in the WT and NRF2KD cell lines involved in DNA mismatch repair

Ensembl ID	Gene Symbol	Gene	SF Log_2 Fold Change vs Contol WT	SF Log_2 Fold Change vs Control NRF2KD
DNA Mismatch Repair				
ENSG00000174371	EXO1	Exonuclease 1	-0.23[1]	-0.28[3]
ENSG00000105486	LIG1	DNA Ligase 1	-0.53[3]	-0.47[3]
ENSG00000095002	mSH2	mutS homolog 2	-0.18[1]	-0.22[3]
ENSG00000116062	mSH6	mutS homolog 6	-0.08[1]	-0.13[1]
ENSG00000132646	PCNA	Proliferating cell nuclear antigen	-0.29[3]	-0.31[3]
ENSG00000035928	RFC1	Replication factor C subunit 1	-0.45[3]	-0.28[3]
ENSG00000049541	RFC2	Replication factor C subunit 2	-0.21[1]	-0.25[3]
ENSG00000163918	RFC4	Replication factor C subunit 4	-0.04	-0.19[3]
ENSG00000132383	RPA1	Replication protein A 70 kDa binding subunit 1	-0.15[3]	-0.21[3]
ENSG00000106399	RPA3	Replication protein A 70 kDa binding subunit 3	-0.27[2]	-0.27[2]

Adjusted P values of fold change: $p^1<0.05$, $p^2<0.001$, $p^3<0.0001$. The differentially expressed genes were obtained through DESeq2. In the first step, DEseq2 performs an internal normalization, where the geometric mean for each gene across the samples is calculated. The count for each gene is then divided by the geometric mean. This procedure is done to normalize library size and RNA bias composition. In the next step DESeq2 plots a negative binomial for each gene count to obtain the differentially expressed genes. Multiple testing is corrected through Benjamini-Hochberg.

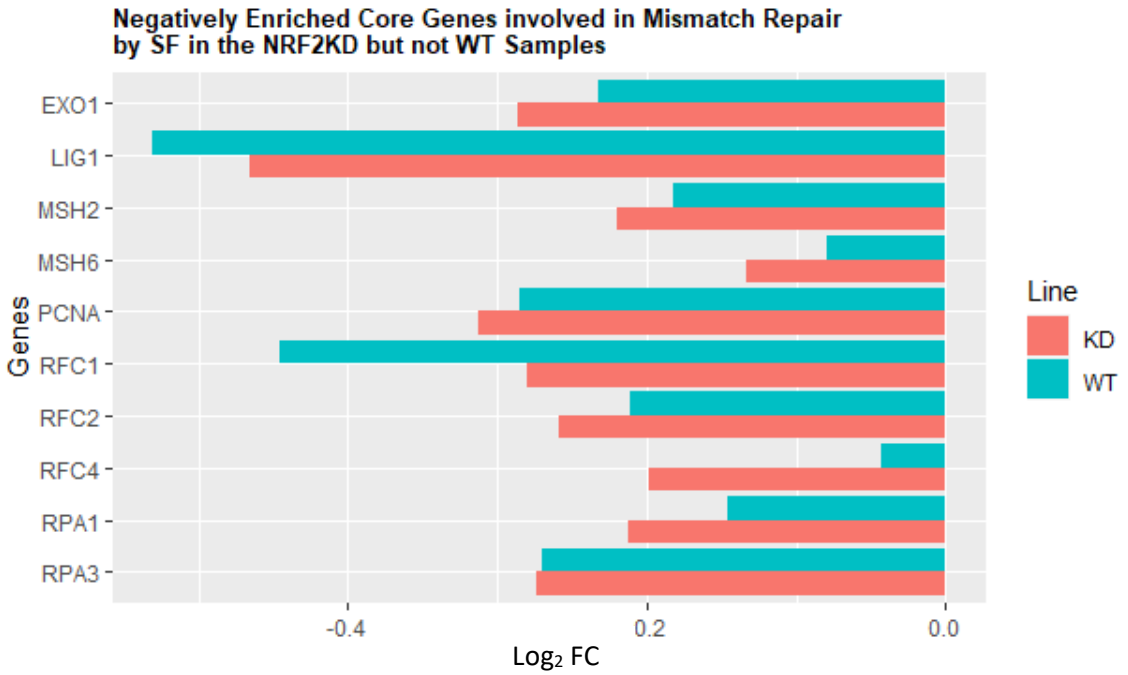

Figure 6.26. Top enriched differentially expressed genes from the DNA mismatch repair gene set by 10 µM SF. These top enriched genes also referred to as the leading edge are defined as those which contributed most to the set enrichment score; reflecting their degree of overrepresentation in a running-sum metric. This is calculated using both the fold enrichment and degree of significance (p-value). Red = KD and Blue= WT samples. Exonuclease 1 (EXO1), DNA Ligase 1 (LIG1), mutS Homolog2 (MSH2), mutS Homolog 6 (MSH6), Proliferating Cell Nuclear Antigen (PCNA), Replication Factor C Subunit 1 (RFC1), Replication Factor C Subunit 2 (RFC2), Replication Factor C Subunit 4 (RFC4), Replication Protein A 70 kDa Binding Subunit 1 (RPA1) and Replication Protein A 70 kDa Binding Subunit 3 (RPA3). The statistical significance of the DEG can be found in table 6.11.

The next step of the analysis involved assessing SF's role on two gene sets that were identified to be downregulated both in the WT and NRF2KD cell line: propanoate metabolism and valine, leucine, and isoleucine degradation (**figure 6.18**). Propanoate metabolism is a subsection of carbohydrate metabolism. In the analysis, it was identified that SF downregulated a couple of genes belonging to the family of aldehyde dehydrogenases: ALDH3A2, ALDH6A1, and ALDH7A1 (**table 6.12, figure 6.27**). It was identified that in this gene set the only two genes that had a stronger downregulation in the KD cells were ALDH3A2 and ACAT2. ALDH3A2 is involved in catalyzing the oxidation of long chain aliphatic aldehydes to fatty acids. ALDH6A1 instead is part of the malonate semialdehyde pathway and functions to catalyze the irreversible decarboxylation of the semialdehydes malonate and methylmalonate to acetyl and propionyl-CoA. ALDH7A1, first identified in chapter 4 is involved in both the detoxification of aldehydes as well in the catabolism of lysine (**table 6.12, figure 6.27**).

SF also downregulated both mitochondrial acetyl-CoA synthetase1/2 ACSS1 and ACSS2, catalyzing the conversion of acetate to acetyl-CoA, along with ACAT2, and acetyl-CoA acetyltransferase involved in a wide range of reactions that require transferring acetyl-CoA groups and ABAT, involved in the breakdown of the neurotransmitter gamma-aminobutyric acid into succinate. The results of the top seven core enriched genes in the propanoate metabolism are shown in table 6.12 and figure 6.27.

Table.6.12. Comparison of differentially expressed genes in response to SF in the WT and NRF2KD cell lines involved in propanoate metabolism

Ensembl ID	Gene Symbol	Gene	SF Log_2 Fold Change vs Contol WT	SF Log_2 Fold Change vs Control NRF2KD
Propanoate Metabolism				
ENSG00000183044	ABAT	4-Aminobutyrate aminotransferase	-0.65[3]	-0.44[3]
ENSG00000120437	ACAT2	Acetyl-CoA acetyltransferase	-0.20[3]	-0.37[3]
ENSG00000154930	ACSS1	Acyl-CoA synthetase short chain family member 1	-0.55[3]	-0.26[3]
ENSG00000131069	ACSS2	Acyl-CoA synthetase short chain family member 2	-0.76[3]	-0.65[3]
ENSG00000072210	ALDH3A2	Aldehyde dehydrogenase 3 family member A2	-0.09[1]	-0.21[3]
ENSG00000119711	ALDH6A1	Aldehyde dehydrogenase 6 family member A1	-0.66[3]	-0.26[3]
ENSG00000164904	ALDH7A1	Aldehyde dehydrogenase 7 family member A1	-0.24[3]	-0.16[3]

Adjusted P values of fold change: $p^1<0.05$, $p^2<0.001$, $p^3<0.0001$. The differentially expressed genes were obtained through DESeq2. In the first step, DEseq2 performs an internal normalization, where the geometric mean for each gene across the samples is calculated. The count for each gene is then divided by the geometric mean. This procedure is done to normalize library size and RNA bias composition. In the next step DESeq2 plots a negative binomial for each gene count to obtain the differentially expressed genes. Multiple testing is corrected through Benjamini-Hochberg.

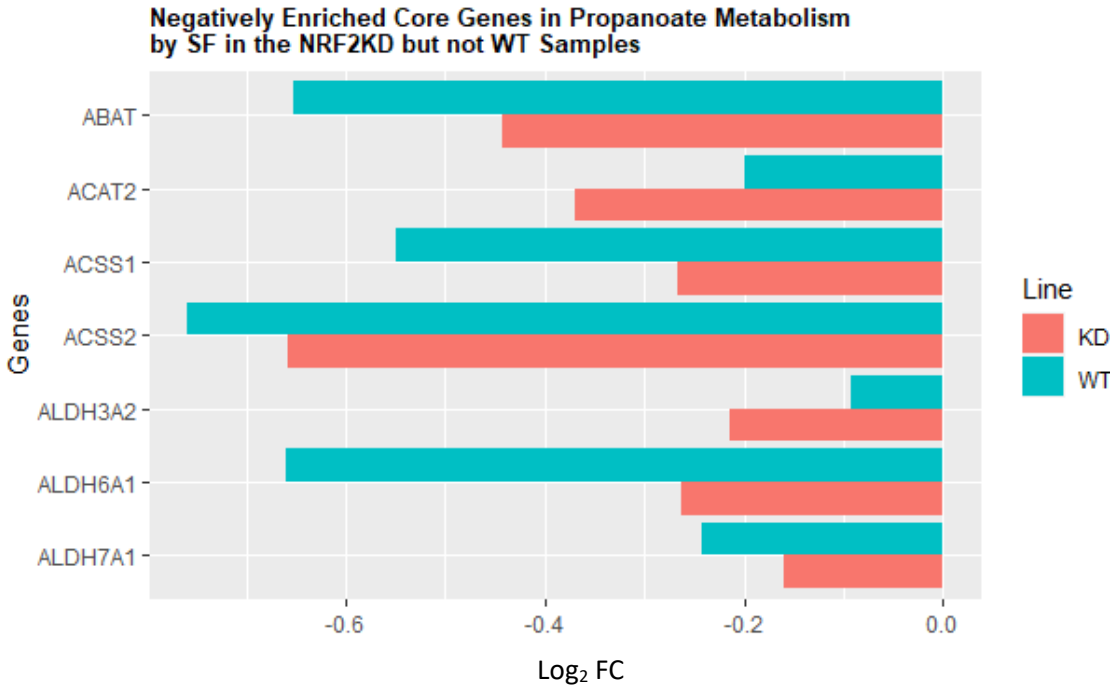

Figure 6.27. Top enriched differentially expressed genes from the propanoate metabolism gene set by 10 μM SF. These top enriched genes also referred to as the leading edge are defined as those which contributed most to the set enrichment score; reflecting their degree of overrepresentation in a running-sum metric. This is calculated using both the fold enrichment and degree of significance (p-value). Red = KD and Blue= WT samples. 4-Aminobutyrate aminotransferase (ABAT), Acetyl-CoA Acetyltransferase (ACAT2), Acyl-CoA Synthetase Short Chain Family Member 1 (ACSS1), Acyl-CoA Synthetase Short Chain Family Member 2 (ACSS2), Aldehyde Dehydrogenase 3 Family Member A2 (ALDH3A2), Aldehyde Dehydrogenase 6 Family Member A1 (ALDH6A1) and Aldehyde Dehydrogenase 7 Family Member A1 (ALDH7A1). The statistical significance of the DEG can be found in table 6.12.

The analysis of the valine, leucine, and isoleucine gene set identified SF downregulating the following genes: ABAT, ACAT2 along with three dehydrogenase ALDH3A2, ALDH6A1, and ALDH7A1 also enriched in this Propanoate gene set, suggesting an overlap between propanoate metabolism and the metabolism of valine, leucine, and isoleucine. The remaining enriched genes in the set that SF downregulated were acetyl-CoA acyltransferase 2 (ACAA2), 3-hydroxyacyl-CoA dehydrogenase (HADH), hydroxymethylglutaryl-CoA synthetase more commonly referred to as HMG-CoA synthetase, and 3-oxoacid CoA-transferase 1 (OXCT1) (**table 6.13, figure 6.28**). ACAA2 and HADH, play a role in regulating β-oxidation; the first catalyzes the last step of β-oxidation, whilst the latter can catalyze both the oxidation of the straight chain 3-hydroxylacyl-CoA dehydrogenase along with medium chain fatty acids. HMG-CoA synthetase, on the other hand, is an intermediary enzyme involved in the biosynthesis of cholesterol and ketogenesis, whilst OXCT1, whose downregulation

was greater in the KD samples compared to the WT is involved in the breakdown of ketone bodies by catalyzing the reversible transfer of coenzyme A from succinyl-CoA to acetoacetate (**table 6.13, figure 6.28**). Thereby the analysis revealed that the degradation of the amino acids valine, leucine, and isoleucine contribute to fatty acid metabolism, and by SF inhibiting these processes, SF through an additional mechanism is inhibiting fatty acid metabolism. The results of the top nine core enriched genes the valine leucine and isoleucine gene set are shown in table 6.2.13 and figure 6.28.

Table.6.13 Comparison of differentially expressed genes in response to SF in the WT and NRF2KD cell line involved in valine, leucine, and isoLeucine degradation

Ensembl ID	Gene Symbol	Gene	SF Log_2 Fold Chang e vs Contol WT	SF Log_2 Fold Change vs Control NRF2K D
Valine, Leucine and Isoleucine Degradation				
ENSG00000183044	ABAT	4-Aminobutyrate aminotransferase	-0.65[3]	-0.44[3]
ENSG00000167315	ACAA2	Acetyl-CoA Acyltransferase 2	-0.26[3]	-0.13[2]
ENSG00000120437	ACAT2	Acetyl-CoA acetyltransferase	-0.20[3]	-0.37[3]
ENSG00000072210	ALDH3A 2	Aldehyde dehydrogenase 3 family member A2	-0.09[1]	-0.21[3]
ENSG00000119711	ALDH6A 1	Aldehyde dehydrogenase 6 family member A1	-0.66[3]	-0.26[3]
ENSG00000164904	ALDH7A 1	Aldehyde dehydrogenase 7 family member A1	-0.24[3]	-0.16[3]
ENSG00000138796	HADH	3-hydroxyacyl-CoA dehydrogenase	-0.39[3]	-0.25[3]
ENSG00000112972	HMGCS1	Hydroxymethylglutaryl -CoA synthetase	-0.43[3]	-0.43[3]
ENSG00000083720	OXCT1	3-oxoacid CoA-transferase 1	-0.22[1]	-0.42[3]

Adjusted P values of fold change: $p^1<0.05$, $p^2<0.001$, $p^3<0.0001$. The differentially expressed genes were obtained through DESeq2. In the first step, DEseq2 performs an internal normalization, where the geometric mean for each gene across the samples is calculated. The

count for each gene is then divided by the geometric mean. This procedure is done to normalize library size and RNA bias composition. In the next step DESeq2 plots a negative binomial for each gene count to obtain the differentially expressed genes. Multiple testing is corrected through Benjamini-Hochberg.

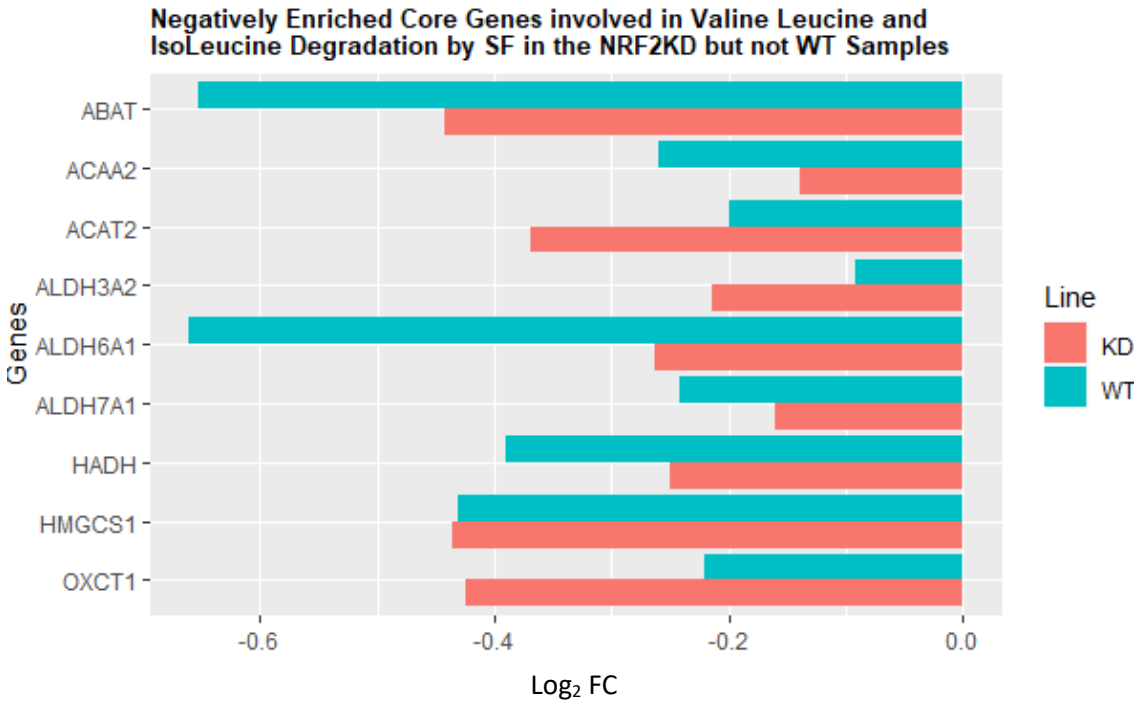

Figure 6.28. Top enriched differentially expressed genes from the valine leucine and isoLeucine degradation gene set by 10 μM SF. These top enriched genes also referred to as the leading edge are defined as those which contributed most to the set enrichment score; reflecting their degree of overrepresentation in a running-sum metric. This is calculated using both the fold enrichment and degree of significance (p-value). Red = KD and Blue= WT samples. 4-Aminobutyrate aminotransferase (ABAT), Acetyl-CoA Acyltransferase 2 (ACAA2), Acetyl-CoA Acetyltransferase (ACAT2), Acyl-CoA Synthetase Short Chain Family Member 1 (ACSS1), Acyl-CoA Synthetase Short Chain Family Member 2 (ACSS2), Aldehyde Dehydrogenase 3 Family Member A2 (ALDH3A2), Aldehyde Dehydrogenase 6 Family Member A1 (ALDH6A1), Aldehyde Dehydrogenase 7 Family Member A1 (ALDH7A1), 3-Hydroxyacyl-CoA Dehydrogenase (HADH), Hydroxymethylglutaryl-CoA Synthetase (HMGCS1) and 3-Oxoacid CoA-Transferase 1 (OXCT1). The statistical significance of the DEG can be found in table 6.13.

The final enriched gene set by SF in the NRF2KD cell line is steroid biosynthesis (**figure 6.18**). SF downregulated the first two genes in the cholesterol biosynthetic process farnesyl diphosphate farnesyltransferase (FDFT1) and squalene monooxygenase (SQLE), the latter is also the rate limiting step in sterol biosynthesis,

with the greatest effect identified in the KD samples. SF also downregulated the activity of lanosterol synthase (LSS) involved in converting squalene-2,3 epoxide to lanosterol (**table 6.14, figure 6.29**). SF was shown to downregulate a couple of genes involved in converting lanosterol to zymosterol: the sterol-4-alpha-carboxylate 3-dehydrogenase (NSDHL), 17beta-estradiol 17-dehydrogenase (HSD17B7), and the delta14-sterol reductase (TM7SF2), with the greatest downregulation of NSDHL and HSD17B7, apart from TM7SF2 been identified in the KD samples (**table 6.14, figure 6.29**). The product zymosterol is used for the synthesis of either cholesterol or Vitamin D_2. The last remaining genes that were downregulated by SF are involved in converting zymosterol to cholesterol. SF downregulated the cholesterol delta isomerase (EBP) along with delta7-dehydrocholesterol reductase (DHCR7), which catalyzes the final step of cholesterol biosynthesis by reducing the double bond in 7-dehydrocholesterol to cholesterol, along with the cholesteryl ester hydrolase (CEL). It was identified that the greatest downregulation of CEL, DHCR7, and EBP was in the KD samples compared to the WT. The results of the top ten core enriched genes in the steroid biosynthesis gene set are shown in table 6.14 and figure 6.29.

Table.6.14. Comparison of differentially expressed genes in response to SF in the WT and NRF2KD cell line involved in steroid biosynthesis

Ensembl ID	Gene Symbol	Gene	SF Log_2 Fold Change vs Contol WT	SF Log_2 Fold Change vs Control NRF2KD
Steroid Biosynthesis				
ENSG00000170835	CEL	Cholesteryl ester hydrolase	-0.55[3]	-0.55[3]
ENSG00000172893	DHCR7	Delta7-dehydrocholesterol reductase	-0.18[3]	-0.24[3]
ENSG00000147155	EBP	Cholesterol Delta isomerase	-0.39[3]	-0.44[3]
ENSG00000079459	FDFT1	Farnesyl diphosphate farnesyltransferase	-0.16[3]	-0.28[3]
ENSG00000132196	HSD17B7	17beta-estradiol 17-dehydrogenase	-0.17[2]	-0.31[3]
ENSG00000160285	LSS	Lanosterol synthase	-0.52[3]	-0.51[3]
ENSG00000052802	MSMO1	Methylsterol monooxygenase 1	-0.15[2]	-0.20[3]
ENSG00000147383	NSDHL	Sterol-4-alpha-carboxylate 3-dehydrogenase	-0.16[2]	-0.21[3]
ENSG00000104549	SQLE	Squalene monooxygenase	-0.13[2]	-0.22[3]
ENSG00000149809	TM7SF2	Delta14-sterol reductase	-0.66[3]	-0.47[3]

Adjusted P values of fold change: $p^1<0.05$, $p^2<0.001$, $p^3<0.0001$. The differentially expressed genes were obtained through DESeq2. In the first step, DEseq2 performs an internal normalization, where the geometric mean for each gene across the samples is calculated. The count for each gene is then divided by the geometric mean. This procedure is done to normalize library size and RNA bias composition. In the next step DESeq2 plots a negative binomial for each gene count to obtain the differentially expressed genes. Multiple testing is corrected through Benjamini-Hochberg.

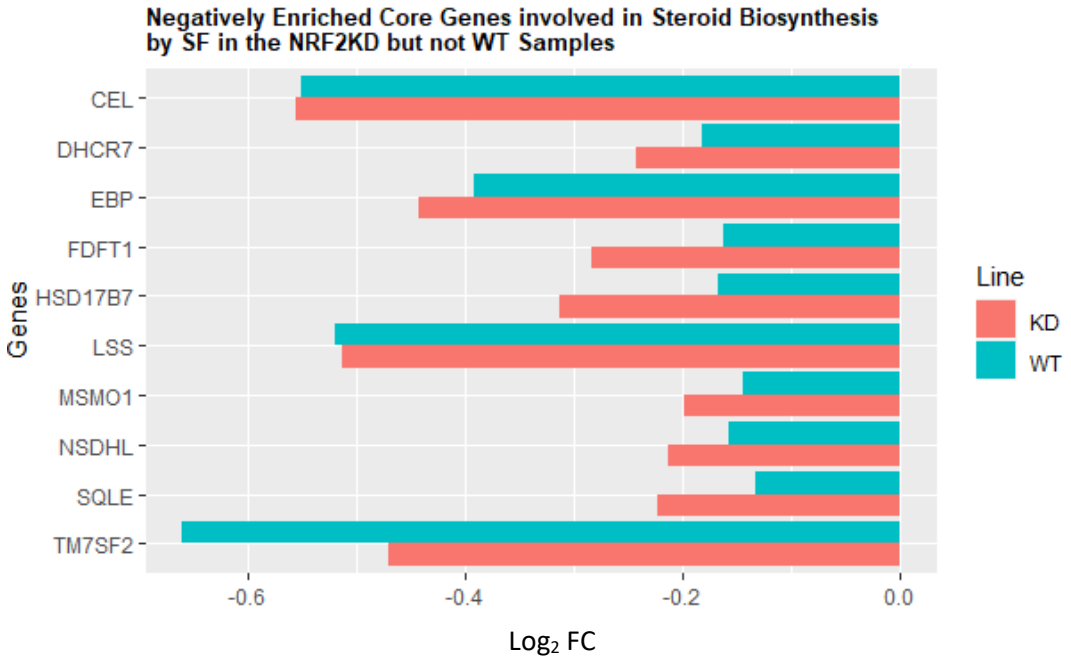

Figure 6.29. Top enriched differentially expressed genes from the steroid biosynthesis gene set by 10 µM SF. These top enriched genes also referred to as the leading edge are defined as those which contributed most to the set enrichment score; reflecting their degree of overrepresentation in a running-sum metric. This is calculated using both the fold enrichment and degree of significance (p-value). Red = KD and Blue= WT samples. Cholesteryl Ester Hydrolase (CEL), Delta7-Dehydrocholesterol Reductase (DHCR7), Cholesterol Delta Isomerase (EBP), Farnesyl Diphosphate Farnesyltransferase (FDFT1), 17Beta-Estradiol 17-Dehydrogenase (HSD17B7), Lanosterol Synthase (LSS), Methylsterol Monooxygenase 1 (MSMO1), Sterol-4-Alpha-Carboxylate 3-Dehydrogenase (NSDHL), Squalene Monooxygenase (SQLE), Delta14-Sterol Reductase (TM7SF2). The statistical significance of the DEG can be found in table 6.14.

6.4 Discussion:

The main aim of this chapter was to test the hypothesis that the metabolic changes observed by SF are all mediated through NRF2. Results from this chapter demonstrated that 70% KD of NRF2 expression through CRISPR/Cas9 editing successfully supported a profound contribution of NRF2 in regulating cellular metabolic processes. Likely, the truncated NRF2 generated through the editing was enough in inhibiting NRF2 activity, thereby identifying that metabolic changes described in detail in previous chapters 4 and 5 are indeed mediated through NRF2.

Chapter 5 it was identified SF interfering with the serine synthetic pathway and 1C metabolism: in particular, inhibiting genes involved in the serine and glycine biosynthesis such as PHGDH and GLDC, along with upregulating genes 1C for NADPH production. This chapter confirmed the data obtained in chapter 5 and identified that SF also downregulates a 2nd gene in the serine biosynthetic pathway PSPH. Results from this chapter have identified that these cellular metabolic processes are regulated through NRF2, consistent with the only published study by (DeNicola *et al*., 2015).

Knocking down NRF2 also resulted in complete inhibition of several genes of the PPP (G6PD, PGD, TALDO, TKT, etc), along with a reduction in the activity of genes involved in the antioxidant response, which matches the data from (Mitsuishi *et al*., 2012). In this study, NRF2 was knocked down using siRNA in the lung cancer cell line A549, resulting in decreased activity of genes involved in the PPP pathway and purine nucleotide biosynthesis (Mitsuishi *et al*., 2012). These genes were also identified in previous microarrays from mouse and human studies to be direct targets of NRF2 (Thimmulappa *et al*., 2002, MacLeod *et al*., 2009). Although the one pool folate gene set was not enriched, looking at the differentially expressed genes, there is still sufficient evidence to show SF affecting this cellular metabolic process. In particular, chapter 5 identified SF upregulating two genes (ATIC and GART) involved in purine biosynthesis. This chapter further supported this evidence by identifying that not only ATIC and GART were upregulated but also PRPS1, with the latter no longer being differentially expressed in the NRF2KD cell line, and the activity of GART and ATIC being severely reduced. All these three genes are involved in purine biosynthesis. Once again, all of the data supports NRF2 role in regulating purine metabolism (Mitsuishi *et al*., 2012, Zou *et al*., 2020a). While NRF2's role in regulating purine biosynthesis is still not fully understood, the upregulation of GART and ATIC may occur for the production of the nucleotide inosine monophosphate so that it can be converted to ATP/ADP/AM. AMP, in particular, can then be reused for the synthesis of novel

NADPH, thereby replenishing the redox regulator NADPH to support glutathione function. Its also worth re-emphasizing that both studies (Mitsuishi and De Nicola) showed that constituent activation of NRF2 results in dysregulated metabolic effects, which allows cancer cells to proliferate continuously, thus further emphasizing that transient activation of NRF2 induced through dietary consumption food bioactive, provides protective effects. Summary figure of the findings obtained in this chapter and the whole thesis is shown in figure 6.30

6.4.1 SF Response in the NRF2 KD cell line

Another important finding in this chapter was SF downregulating several genes involved in the following metabolic processes: genetic information and processing, in particular, DNA replication and repair pathways, including base excision repair (BER) and mismatch repair. The analysis for the first time identified that SF had a more prominent effect in the KD samples, with the majority of genes having greater downregulation. DNA replication consists of a complex network of proteins and enzymes; this includes DNA helicase, which helps to unwind the DNA. BER is instead the main pathway involved in the repair of small lesions present in the DNA induced from either oxidation or alkylation damages. BER is divided into two pathways: short-patch (BER) where only one nucleotide is replaced and long-patch BER where 8 up to 12 nucleotides are replaced. The final gene set enriched by SF was the DNA mismatch repair (MMR) pathway. During replication of DNA, what may occur is the misincorporation of a specific base. As a result, proteins involved in the MMR repair will recognize the newly synthesized DNA strand from the template strand and will bind to it to repair the damaged DNA. In this analysis, it was identified that two genes were downregulated by SF in all three pathways: PCNA and LIG1. Data from this chapter is consistent with what has been published in the literature. For example, several experimental studies have shown that ITCs induce oxidative stress in cancer cell lines, which can contribute to their cytotoxicity. This oxidative stress can arise from two distinct methods: one is through the inhibition of mitochondrial respiratory chain complexes along with depletion of reduced glutathione, resulting in increased levels of ROS (Singh *et al*., 2004, Singh *et al*., 2005, Xiao *et al*., 2009, Sestili *et al*., 2010, Park *et al*., 2014, Liang *et al*., 2018). The second is through the inhibition of genes involved in DNA metabolism, thereby resulting in the formation of DNA breaks. For example, in Ras-transformed cells treated with the ITCs, SF, phenethyl isothiocyanate (PETIC), and benzyl isothiocyanate (BETIC) the ITCs were able to induce thiol modification of topoisomerase 2α resulting in apoptosis (Lin *et al*., 2011). A second study also showed SF to interact and inhibit the proliferating cell nuclear antigen (PCNA), (Mi *et al*., 2011).

Genotoxic stress is one of the many mechanisms through which ITCs have anticancer activities. Several studies have shown that SF and the allyl isothiocyanate (ATIC), induce cell cycle arrest along with the induction of γH2A.X histone, a marker of double-stranded breaks (Singh *et al*., 2004, Sekine-Suzuki *et al*., 2008). Two recent studies, one in the MG-63 osteosarcoma (bone cancer) cell line and a second in a variety of cells lines, have further confirmed these findings. The study using the MG-63 cell showed SF resulting G2/M phase arrest along with an increased number of DNA breaks and nuclear and mitotic abnormalities (Ferreira de Oliveira *et al*., 2014). The second study showed that SF and PETIC treatments to the advanced prostate cancer cell line PC-3, HDF a normal fibroblast cell line along with PNT2 a prostate epithelial cell line, resulted in inhibition of DNA replication in all three cell lines, with the more prominent effect seen in the PC3 cells along with S cell cycle arrest (Hać *et al*., 2020).

At the same time, however, it is likely that the increased DNA damage also resulted from the inflamed state of the cells (due to the high glucose), hence the upregulation of the cytokine-cytokine and JAK-STAT pathways. As previously stated, culturing hepatocytes such as HepG2 in a high glucose environment results in increased inflammation, by promoting inflammatory cytokines such as IL6, TNFα, as well as increased production of ROS (Panahi *et al*., 2018). A possible mechanism to suppress this inflammation, in the WT cells is through SF rewiring central metabolism, by depleting serine and glycine, the latter utilized for the biosynthesis of glutathione and upregulating the production of NADPH through both the PPP and 1C metabolism, providing the reducing agents for glutathione to eliminate the ROS (Wu *et al*., 2011). Whilst the analysis did not measure the levels of reduced glutathione in the KD samples, it was shown though a profound reduction in the activity of glutathione biosynthetic genes such GCLC/GCLM. This may lead to a reduction in the intracellular concentration of reduced glutathione, thereby preventing the cell's ability to suppress the inflammatory status. As the activity of NRF2 in the KD samples is suppressed, the outcome is increased DNA damage, potentially resulting in increased cell death.

A further mechanism that could explain SF downregulation in cellular processes involved in DNA metabolism is epigenetic regulation, potentially through chromatin modification. Although the analysis did not assess various genes involved in histone deacetylation, the previous chapter and other published data have shown SF to inhibit histone deacetylases (HDAC), resulting in increased acetylation of histones H3 and H4 (Myzak *et al*., 2006b). The outcome was upregulation of genes encoding cell cycle inhibition such as p21 and pro-apoptotic proteins (Myzak *et al*., 2006b). Acetylation of histone is an important step during DNA replication, as it facilitates the removal of histones during the unwinding of DNA and forms the DNA template, along with

reintroducing them on the daughter DNA molecule after DNA Replication has occurred (Groth *et al*., 2007). Since SF discovery, several studies using a wide range of cell lines such as acute lymphoblastic leukaemia cells, human colon cancer cells, and lung cancer A549 cells have shown SF interfering and inhibiting various proteins along the cell cycle such as p21, PRAP, and various cyclin kinases (Cdc2, Cyclin B1 complex, and cyclin D1) (Żuryń *et al*., 2016, Suppipat *et al*., 2012, Parnaud *et al*., 2004). Until now, it has remained unknown whether these effects are mediated through NRF2 or if they are independent of it. The GSEA identified that the gene set cell cycle in the KD samples just failed to reach significance (q=0.063), suggesting that NRF2 may not be the only pathway affected; other pathways may also be involved. Therefore, future analysis/experiments should aim to gain a better molecular mechanism understanding of how SF regulates the cell cycle.

Given that this research used NRF2 knockdown instead of a complete NRF2KO cell line, the experiments were kept to a minimum. Moreover, the NRF2 KD cells were treated like primary cells and were passaged only twice after resuscitating them. The reason for this lied in observing whether progressively passaging the cells over time would, firstly, result in the NRF2KO cells dying, and whether, consequently, this would result in the remaining WT cells competing for the NRF2KO cells. Future experiments should also assess the effects of longer passages on the NRF2 status on the cell. This could be achieved by passaging the cell multiple times and after several passages assessing the DNA and protein levels of NRF2. This would provide us with interesting insights into whether the NRF2KD cells would survive and whether the same metabolic responses would be induced upon SF treatment.

Another significant finding worth mentioning is that the qRT-PCR data showed that the expression of the antioxidant genes (such as NQO1) in the control NRF2KD cell line was higher compared to the control WT cell lines. A likely explanation could be that different NRF isoforms may play a role. For example, a study in human bronchial epithelial (HBE1) cells identified that when NRF2 and NRF1 are both present, both can translocate to the nucleus and bind onto the ARE and induce the expression of genes involved the antioxidant response. However, NRF1 recruits a different set of co-activators proteins, causing upregulation of both shared genes with NRF2 and unique NRF1 target genes (Chepelev *et al*., 2013). A second study this time carried out in mice identified that KO NRF1 in mice, microarray analyses revealed that hepatic deletion of NRF1 did not result in downregulation of the NRF2 target genes; on the contrary, these NRF2 target genes were instead upregulated. However, the study identified that NRF1 functions to regulate the expression of genes involved in growth arrest and DNA damage inducible genes, as well as genes involved in glycosylation,

confirming the findings identified in this chapter that the downregulation of the GSEA involved in DNA metabolism may be mediated through NRF1 (Ohtsuji *et al*., 2008).

An additional point worth discussing is the effect of time. Due to time constraints, the GSEA analysis was not conducted at earlier time points. However, from the PCA plot figure 6.14, it can be shown that both in the WT and NRF2KD cells at different time points, the transcriptional profile of the cell differs. To my surprise it was interesting that the PCA plot for the WT samples, SF treatment does not really differ. It is likely that at all three time points, SF is affecting the transcriptional machinery of the cells by inducing genes only involved in influencing different mechanisms of the antioxidant response. At 24 h, induction of genes involved in the antioxidant response is still present along with SF also regulating the activity of genes involved in central metabolism. In the KD cell line, the effect of SF is abolished, and only time becomes the prominent factor.

6.3.3 NRF2 and Fatty acid Metabolism

Lipid synthesis requires high amounts of NADPH, which competes with the detoxification reactions carried out by NRF2. One of the potential consequences of NRF2 inhibiting fatty acid biosynthesis and desaturation is to allow the NADPH to be used for detoxification reactions instead. Throughout the course of the thesis, it was shown that SF downregulated several genes involved in lipid biosynthesis, inducing genes involved in fatty oxidation (chapters 3 and 4) and suppressing lipid accumulation (chapter 3). The analysis carried out in this chapter further confirmed the findings from previously published literature. For example, SF treatment downregulated the activity of both the desaturases (FADS1/2) along with the Stearoyl-CoA desaturase SCD. SCD overexpression has been associated with tumour development and reduced survival in patients with lung adenocarcinoma (Huang *et al*., 2016). It has also recently been identified that specific cancer cells such as murine hepatocellular carcinomas, lung carcinomas, U87 glioblastoma cells, and primary liver cells harbour additional desaturase enzymes such as FADS2 rather than the usual SCD (Vriens *et al*., 2019). This allows to covert the fatty acid palmitate to the unusual fatty acid sapienate, supporting membrane biosynthesis and sustained proliferation (Vriens *et al*., 2019). The ability of SF to suppress both FADS1 and FADS2 is promising, thereby further enhancing the health benefits of SF suppressing lipid metabolism. Therefore, future research should consider carrying out human trials assessing the effect of broccoli bioactives in patients with dyslipidemia and or hypercholesterolemia.

This analysis identified that the expression of the lipid biosynthetic genes such as FADS1/2 and SREBF1 in the NRF2KD were decreased. This is contrary to the

literature where studies using NRF2KO mice have shown that deletion of NRF2KO results in increased expression in the lipid biosynthetic genes. For example, Wu identified through microarrays 36 genes related to lipid metabolism that had higher expression in the NRF2KO mice and lower expression in the Keap1-KO mice. Out of the 21 genes related to fatty acid biosynthesis, 14 were more highly expressed in NRF2KO mice and lower in the Keap1-KO mice. For example, the abundance of FADS1 and FADS2 mRNA was 54% and 52% higher in the NRF2KO mice and 46% and 30% lower in the Keap1-KO mice (Wu *et al*., 2011). A second study showed that 8 weeks old mice with NRF2 deleted, the mRNA of SREBF1 and FASN were also more highly expressed (Zhang *et al*., 2010). were decreased. This is likely due to the effect of SF, suggesting that SF is interfering with lipid metabolism potentially through additional non-NRF2-mediated pathways.

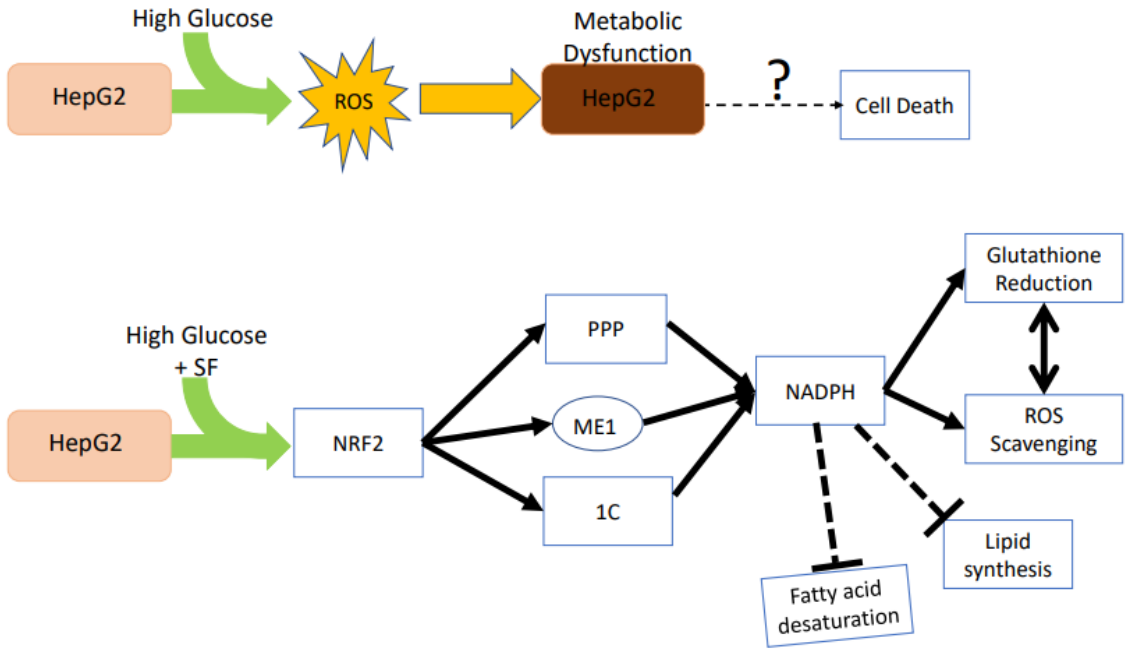

Figure 6.30 Overall summary of the findings of the thesis. A mechanistic understanding of how SF regulates NADPH status within the cell by interfering with various metabolic pathways. The proposed molecular mechanism on how SF acts as a metabolic regulator influencing NADPH production and consumption. In the presence of high glucose without SF, or the NRF2KD samples, the excessive concentration of glucose results in increased reactive oxygen species accumulating. This may result in metabolic dysfunction which in the long term may lead to cirrhosis and even cell death. When SF is instead added, NRF2 is activated. NRF2 will then induce metabolic pathways involved in NADPH production (major ones are the pentose phosphate pathway (PPP) and 1C metabolism (1C) along with some production from the malic enzyme 1 (ME1) as well as inhibiting pathways that consume NADPH such as lipid biosynthesis. Instead, the resulting NADPH is re-directed towards the antioxidant response and acts as a cofactor for glutathione and other oxidoreductases enzymes such as NQO1 to scavenge ROS.

6.5 Conclusion:

Within the last 10 to 15 years, a proliferation of scientific evidence has emerged, showing that both SF and NRF2 can potentially act as metabolic regulators. Nevertheless, whether these metabolic processes affected by SF are mediated through NRF2 is yet to be fully understood. To respond to this ambiguity, this chapter employed the genome editing technique CRISPR Cas 9 to develop a liver cell line that lacked NRF2. As hypothesized, data from this chapter identified that SF regulation in the antioxidant response, through the enrichment of the glutathione metabolism and metabolism of xenobiotics by cytochrome P450 gene sets, is mediated through NRF2. Most importantly, a novel finding was identified: SF regulation of both the serine synthetic pathway and 1C metabolism is mediated through NRF2. Although SF attenuated the expression of genes involved in these pathways, this was not as profound as those involved in the antioxidant response. This may suggest that these genes are regulated through alternative (non-NRF2) pathways, although a small change may have profound downstream effects. Another critical finding is SF's ability to interfere and inhibit through NRF2 the biosynthesis of unsaturated fatty acids. This is likely to allow the NADPH for detoxification reactions instead. In the NRF2KD cells, SF was shown to have genotoxic properties by affecting DNA metabolism, resulting in inhibition of cell proliferation and potentially inducing cell death.

Chapter 7: General Discussion

Chapter 7 Figures

Figure 7.1. The number of publications on sulforaphane research in PubMed.

Chapter 7 Tables

Table 7.1 Animal studies using SF Supplementation

7.1 Summary Findings:

Since its discovery in the early 1990s, the literature on SF and NRF2 has rapidly advanced. In 1992, Zhang and colleagues were the first to show that SF is a potent activator of phase II enzymes, identifying SF inducing both the NAD(P)H dehydrogenase quinone 1 (NQO1), along with the glutathione-S-transferases (GST). Both were involved in the detoxification of steroids and the environmental toxin benzo(a)pyrene (Zhang *et al*., 1992, Prochaska *et al*., 1992, Singletary and MacDonald, 2000). Zhang concluded that the anticarcinogenic properties of broccoli were due to SF. The problem remained that the exact mechanism through which this occurred was still not fully understood. Two years later, the transcription factor NRF2 was discovered (Moi *et al*., 1994). Following the discovery that SF regulates the activity of NRF2, this led the way to discover the presence of an ARE sequence on the promoter region of certain genes, enabling NRF2 to bind and induce the expression of those genes.

A decade later, a study conducted by Thimmulappa resulted in another breakthrough in NRF2 research. SF treatment in the small intestine of WT and NRF2 KO mice identified for the first time that NRF2 was not only involved in regulating previously reported NRF2 genes such as NQO1 and GST but also genes involved in cellular NADPH regeneration such as glucose-6-phosphate dehydrogenase, 6-phosphogluconate dehydrogenase, malic enzyme, along with various xenobiotic metabolizing enzymes, and enzymes involved in the biosynthesis of glutathione and glucuronidation conjugation pathways (Thimmulappa *et al*., 2002). The next breakthrough in NRF2 was provided in two separate studies: (Wu *et al*., 2011) and (Mitsuishi *et al*., 2012) where SF was not used. The study conducted by Wu and colleagues involved microarray analysis on livers from WT, NR2KO, and KEAP1-OVR mice. The study identified NRF2 was not only responsible for upregulating the antioxidant response, and cellular NADPH regeneration pathways but also lipid metabolism. The group was the first to

propose the hypothesis that NRF2 suppression in lipid metabolism, especially lipid biosynthesis is due to NAPDH being redirected for the antioxidant defense to support glutathione ability to scavenge and eliminate reactive oxygen species (Wu *et al*., 2011). On the other hand, Mitsuishi was the first to identify that the genes involved in the PPP have an ARE sequence, and are therefore direct targets of NRF2, along with identifying that NRF2 also regulates purine metabolism (Mitsuishi *et al*., 2012). Figure 7.1 shows the increase in SF research since its first discovery.

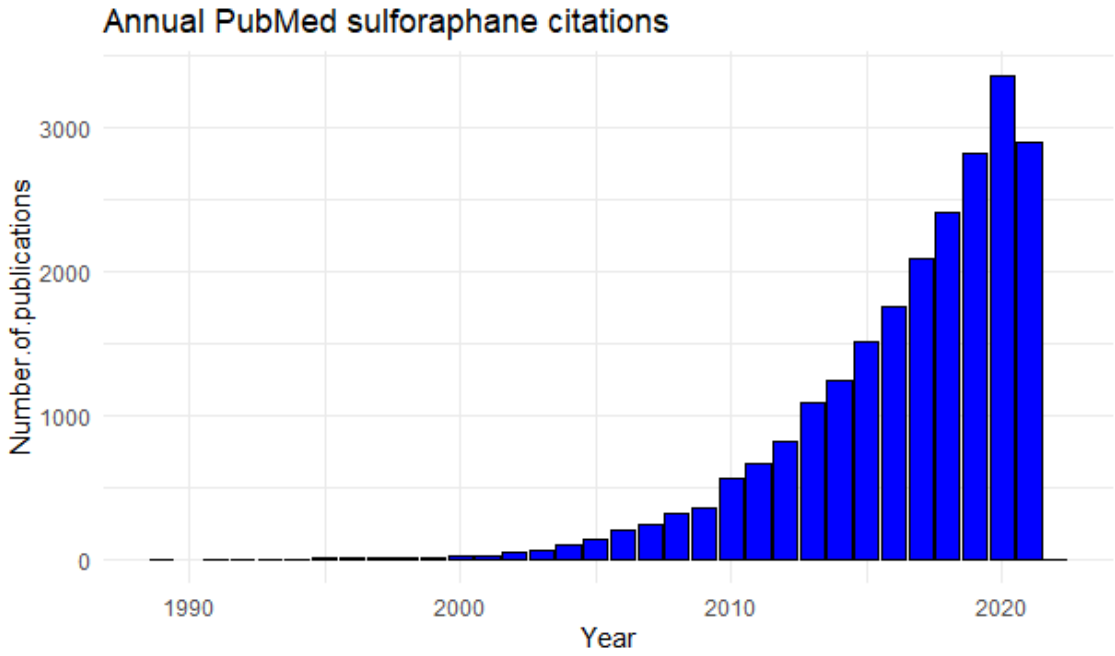

Figure 7.1. The number of publications on sulforaphane research in PubMed.

Due to the increasing evidence that NRF2 could act as a metabolic regulator (Hayes and Dinkova-Kostova, 2014, Lin *et al*., 2016), research on broccoli began to assess whether SF would be able to suppress metabolic dysregulation induced from a poor diet; either from excessive intake of refined/processed carbohydrates or sugars or increasing intake of saturated fats (Du *et al*., 2021). In the following years, four key papers on this topic were published; The first was a human intervention study, showing that consumption of broccoli with 3-5 times higher concentration of the glucosinolate glucoraphanin leads to TCA modulation by restoring the imbalance between the anaplerotic (reactions that form metabolic intermediates) and cataplerotic (reactions that remove or use up metabolic intermediates) reactions necessary to maintain an optimum balance between energy generation as well as the synthesis of fatty acids and other metabolites required for optimal health (Armah *et al*., 2013). The second, also a

human study by Axelsson, demonstrated that high doses of SF obtained from broccoli sprout extracts could improve glucose homeostasis, thereby improving insulin resistance in obese and T2D patients (Axelsson *et al*., 2017). Third, a mouse study by Nagata and colleagues assessed how glucoraphanin supplementation in mice fed a high-fat diet resulted in improved metabolic function by improving insulin resistance as well as reducing obesity and NAFLD (Nagata *et al*., 2017). Finally, an *in vitro* study assessing mitochondrial activity on β-cells of the pancreas stimulated with cholesterol demonstrated that SF could improve and protect the mitochondrial bioenergetics against the dysfunction induced by cholesterol (Carrasco-Pozo *et al*., 2017). These studies collectively supported the role of SF as a metabolic regulator, for example, by suppressing fatty acid biosynthesis and improving glucose utilization, but the underlying mechanistic basis or the contribution of NRF2 remained unclear. The main aim of the current thesis was to provide evidence for the role of SF in regulating critical metabolic pathways in the liver and to identify whether such metabolic effects induced by SF are mediated through NRF2.

The work conducted in the thesis has made a significant contribution to the field of nutrition and cancer metabolism. Furthermore, it has advanced our understanding of how NRF2 regulates cellular metabolism by providing evidence of the specific metabolic targets of SF in hepatocellular cell line and demonstrating that these are primarily mediated through NRF2. A summary of how each chapter has contributed to the scientific literature has been summarized below.

In **chapter 3**, the aim was to understand how SF impacts hepatic metabolism. This was achieved by culturing the hepatocellular cell line (HepG2) with the saturated fatty acid palmitate (the most abundant saturated fatty acid in the body), representing a cell culture model of NAFLD. Firstly, experiments showed that physiological concentrations of SF could suppress lipid accumulation both by inhibiting fatty acid biosynthesis (downregulation of FASN) and inducing fatty oxidation (CPT1a upregulation). I then decided to explore an area on which, to the best of my knowledge, no prior research has been conducted, by characterizing how SF impacted hepatic metabolism when hepatocytes were challenged under various glucose environments: (0 mM) to represent a state of starvation, basal (5.5 mM) a healthy condition and high (25 mM) one of under metabolic dysregulation. Real-time metabolic phenotyping using the Seahorse Extraceullar Analyzer identified that in HepG2 cells exposed to various glucose concentrations, SF was able to alter the mitochondrial bioenergetics by reducing overall mitochondrial respiration in the high but not glucose environment, as well as reducing maximal respiration without the presence of glucose.

Chapter 4 aimed to determine the transcriptional effect of SF in different metabolic states in HepG2. In this chapter, the transcriptional profile identified that in a no glucose environment, in the presence of SF NRF2, induction does not occur. SF induced the antioxidant response by upregulating both glutathione metabolism and metabolism of xenobiotics by cytochrome P450 gene sets both in the basal and high glucose environment. This is the first study showing that SF treatment on NRF2 regulation *in vitro* is still maintained during excess glucose, suggesting that SF inducing the anti-oxidant response is an essential mechanism in preventing diseases of metabolic dysregulation such as type 2 diabetes is not just involved in detoxifying xenobiotics. In the high glucose environment only, SF just failed to upregulate the pentose phosphate pathway gene set required for the production of NADPH. It was also identified in both basal and high glucose that SF interfered in lipid metabolism, despite no gene set being enriched.

Chapter 5 aimed to gain a mechanistic understanding of how SF affects metabolic intermediates in central hepatic metabolism, using untargeted metabolomics and stable isotope tracers for major carbon sources in the cell through glucose, and glutamine. When cells exist in a state of metabolic dysregulation, where HepG2 (human liver cells) were cultured in high levels of glucose, inducing insulin impairment, and increased inflammatory cytokines, I identified SF leading to a substantial increase in the levels of reduced glutathione (GSH). SF induces NRF2 which in turn activates GSH biosynthetic genes, but to support GSH synthesis a sufficient supply of metabolic intermediates is required. Our knowledge of how SF regulates these metabolic intermediates is still poorly studied. Consequently, I set about to understand what metabolic changes occur in the presence of SF that support GSH synthesis by specifically looking at the 3 required amino acids. Firstly I identified a decrease in glutamate through the glutamine tracer. Secondly, following SF treatment, levels of extracellular cysteine were lower, suggesting that more cysteine is imported. Indeed, the expression of the cysteine transporter was increased by SF. However, this increase in cysteine import did not correspond to accumulation intracellularly, which suggests that cysteine is utilized in downstream metabolic pathways (eg GSH biosynthesis). Finally, I identified SF depleting the levels of serine and glycine. Through the use of the glucose tracer, I showed that the reduction in serine is due to an increase in serine utilization. Transcriptomic data (from chapter 4) also identified SF inhibiting the serine synthetic genes. This reduction in serine reflects the reduction in glycine, suggesting redirection of glycine towards GSH biosynthesis. Upregulation of 1C metabolism, therefore, is a novel molecular mechanism of action of SF that is likely supporting the antioxidant response induced by the SF/NRF2 system.

The final results' **chapter 6** probed whether SF interfering in 1C metabolism is mediated through NRF2, using the genome editing technique (CRISPR-Cas 9) for targeting NRF2 in HepG2 cells. Whilst working with a heterogenous edited population, thereby resulting in a 60-70% NRF2KD as opposed to a homogenous NRF2KO cell line, the RNAseq study revealed that SF can act as a powerful metabolic regulator and its effects are mediated through NRF2. Transcriptomics analysis identified that the gene sets, glycine serine, and threonine, along with pentose phosphate pathway, and the various antioxidant response gene sets (glutathione metabolism and metabolism of xenobiotics by cytochrome P450) in the NRF2KD cells were not induced by SF. This positively correlated with SF no longer affecting serine and glycine levels. It was also identified that SF treatment, also mediated through NRF2 downregulated the biosynthesis of unsaturated fatty acids gene set, thereby further suppressing the utilization of NADPH so that it could be utilized for glutathione. On the other hand in the NRF2KD samples, it was observed that SF induced genotoxic stress as well as inhibited cell proliferation, which thus helps us understand how ITCs have anticarcinogenic properties.

7.2 How do the results compare to previously published literature?

In this thesis, HepG2 were used as a proxy for liver model. The liver is the primary organ that governs vital cellular processes such as protein synthesis, glucose homeostasis, and lipid metabolism, along with playing a crucial role in the detoxification of environmental chemicals, drugs, and endogenous toxins (Rui, 2014). NRF2 is a master regulator of encoding genes related to protecting against oxidative and electrophilic stress. Due to the increase in the obesity epidemic, and with several studies over the past 5-10 years with varying experimental designs (mostly mice) identifying SF to govern central metabolism, studying NRF2 activation in the liver is of vital importance. Three studies have reported that the concentration of sulforaphane in the plasma following consumption of standard broccoli ranged from as low as 2 to 6 µM, whilst consumption of the Beneforte broccoli, which contains 3-5 higher concentrations of glucoraphanin, plasma concentrations of SF peaked consistently at 9-11 µM (Gasper *et al*., 2005, Sivapalan *et al*., 2018, Coode-Bate *et al.*, 2019). Therefore, this thesis speculated that the concentration of 10 µM was physiologically relevant.

In chapter 3, I identified that SF was able to significantly suppress lipid accumulation within the cells, by both blocking fatty acid synthesis, through inhibition of FASN and inducing the oxidation of fatty acids through CPT1a. This data is in agreement with several studies done both *in vitro* using a variety of cell lines such as liver (Lei *et al*.,

2019, Tian *et al*., 2018), prostate (Singh *et al*., 2018), and adipocytes (Zhang *et al*., 2016) and *in vivo* including both mouse (Nagata *et al*., 2017) and especially human intervention studies (Armah *et al.*, 2015).

To gain a better mechanistic understanding of what is occurring in the three separate environments, samples were sent for RNAseq. Firstly GSEA (chapter 4) revealed that in the no glucose environment, deprivation of glucose results in no induction of NRF2. This suggests that dietary NRF2 induction by SF is solely reliant on the presence of glucose thereby confirming the results identified by Heiss and colleagues. The study by Heiss and colleagues demonstrated that interfering with glucose uptake in fibroblast inhibits NRF2 ability to induce the PPP, thereby blocking NADPH production, which inhibits NRF2 ability to induce the antioxidant response and suppress the ROS generated (Heiss *et al*., 2013).

The GSEA in chapter 4 also showed that the major role SF played in regulating metabolism was by enriching the gene sets involved in glutathione metabolism, xenobiotic metabolism, protection against oxidative stress, and upregulating the proteasome, needed for the degradation of unwanted/damaged proteins, thereby confirming the abundance of literature. Assessing the literature, the concentrations ranged from 2µM to utilizing supraphysiologic concentrations of SF such as 50µM *(Chambers et al., 2009, Traka et al.*, 2005, Liu *et al*., 2013, Thimmulappa *et al*., 2002, Dinkova-Kostova *et al.*, 2007, Agyeman *et al*., 2012, Bhamre *et al*., 2009). Although the pentose phosphate pathway gene set narrowingly failed to reach significance in this chapter, the second RNA study in chapter 6 identified this set was enriched, providing evidence of SF upregulating cellular NADPH regeneration only in the high glucose environment. This is in agreement with several studies, that have identified NRF2 activation playing a crucial role in inducing genes involved in NADPH production, as well as identifying several of those PPP genes having ARE sequence thereby acting as direct targets of NRF2 (Thimmulappa *et al*., 2002, Wu *et al*., 2011, Mitsuishi *et al*., 2012).

In **chapter 5**, I identified the major finding and the breakthrough of this thesis, by showing SF interfering with several pathways such as 1C metabolism and glycine, serine, and threonine metabolism, which before my research have not been identified. This is because the liver cells that were not challenged by glucose were not metabolically challenged. It is possible that dietary compounds could have minimal effects in normal conditions, but only fully mobilize their protective mechanisms when the cells are in metabolic dysregulation. Firstly, the metabolomics analysis revealed SF depleting the amino acids serine and glycine along with an increase in the amino acids methionine, matching the transcriptomic data set. To date, no previous studies have

identified SF inhibiting serine and glycine biosynthesis. The only other study in the history of the literature of NRF2 regulating serine biosynthesis was by (DeNicola *et al*., 2015). The study by De Nicola and colleagues showed that constitutive activation of NRF2 has adverse metabolic effects, resulting in continuous serine and glycine biosynthesis through upregulation of the serine biosynthetic genes, thus allowing cancer cells to proliferate and metastasize. The main gene involved in serine biosynthesis also the rate limiting enzyme is phosphoglycerate dehydrogenase (PHGDH). In both of the RNAseq chapters 4 and 6, I identified a consistent downregulation of PHGDH along with downregulation of PSPH in chapter 6. All of the serine biosynthetic genes, and in particular PHGDH, are overexpressed in certain cancers such as breast cancer and melanoma. Analysis of large genomic sets obtained from breast cancer patients revealed that overexpression of the serine biosynthetic genes results in poor survival rates (Antonov *et al*., 2014, Pollari *et al*., 2011, Possemato *et al*., 2011, Mullarky *et al*., 2011). Although the result should be interpreted with caution, the results may suggest a novel mechanism through which SF may act as an anticarcinogenic agent. Therefore, the discovery in this thesis that SF could inhibit the serine biosynthetic pathway, which several cancer cells lines have overexpressed, may in the future result in novel therapeutics or better strategies for cancer treatment.

Chapter 5, I also showed a novel mechanism on how the high glucose environment SF rewires central metabolism to support the antioxidant response, thereby linking central metabolism and the antioxidant response. The glutamine tracer revealed in high glucose, the carbon pool of glutamine being redirected to glutathione biosynthesis, shown by reduction in the metabolite succinate of the TCA cycle. The analysis also revealed SF upregulating the activity of the cysteine receptor (SLC7A11), matching previously identified data (Chorley *et al*., 2012, Hirotsu *et al*., 2012). Import of cysteine and glycine, the latter produced from serine, along with glutamate are utilized for the biosynthesis of glutathione (GSH). As the major glutathione pool is found in the liver, it is synthesized by a two-step reaction. The first step is catalyzed by the glutamate-cysteine ligase GCL, the rate limiting enzyme in the reaction. GCL is formed of two subunits: a catalytic and regulatory subunit (GCLC, GCLM). This enzyme combines glutamate and cysteine into a dipeptide. In the second step, glycine is added to the dipeptide catalyzed by glutathione synthetase. In addition to *de novo* biosynthesis of glutathione, reduced glutathione can also be regenerated through oxidized glutathione through glutathione reductase (GSR), along with the presence of NADPH. Both the GCLC/GLCM, GSS, and GSR have all been shown to have an ARE sequence, and in this study, both chapters 4 and 6 also showed strong induction in these genes (Li *et al*., 2009, Chan *et al*., 2001).

Enrichment of the 1C metabolism gene set identified SF upregulating two genes involved in the production of NADPH: ALDH1L1 and MTHF1LD (Yang and Vousden, 2016). NADPH serves as the major reducing agent in the body and many oxidoreduction reactions including reducing oxidized Glutathione and thioredoxin occur through the oxidation of NADPH to $NADP^+$ (Ju *et al*., 2020). Therefore I hypothesized that upregulation of both PPP and 1C metabolism allows the cells ability to maximize NADPH production for the continuous regeneration of GSH, needed to suppress the inflammatory cytokines and ROS produced by the high glucose environment. Before this research, it was known that the majority of the cellular NADPH is generated through the PPP, with small amounts also being produced by the malic enzyme 1 (Mitsuishi *et al*., 2012). The discovery of identifying novel pathways of NADPH production that are regulated by NRF2 will allow future research to develop novel diagnostic or therapeutics for treatments of severe diseases. NRF2 role in regulating cellular detoxification is widely characterized and understood, however, its role in regulating cellular NADPH remains underdeveloped and thus should receive more attention and future research should assess NRF2 and NADPH regulation, as one of the hypotheses generated from this thesis is that NRF2 serves to regulate the NADPH status of the cell. For example, Wu in his microarray analysis of WT, NRF2KO, and KEAP1 KO livers identified that NRF2-null mice have less hepatic NADPH, making them more susceptible to oxidative stress whereas KEAP1 KO mice have higher cellular NADPH (Wu *et al*., 2011).

In chapter 5 I also identified SF downregulating thereby potentially inhibiting the activity of certain histone deacetylase (HDAC), as well as affecting certain DNA methyltransferases (DNMT). This is in agreement with previously published studies showing that SF is a well characterized epigenetic regulator, although the exact molecular mechanism through which this occurred was not fully understood (Su *et al* ., 2019). For example, studies using various prostate cancer cell lines (BPH-1, LnCaP, and PC3) have shown that SF treatment at 15 µM resulted in a 30-40% significant inhibition in HDAC activity, which correlated with G_2M arrest of the cell cycle, resulting in apoptosis (Myzak *et al*., 2006c, Hsu *et al*., 2011). A second study using the prostate cell lines BHP-1, LnCap, and PC3 showed that SF significantly decreased the expression of $DNMT_1$ and $DNMT_{3b}$ (Hsu *et al*., 2011). This effect of SF to affect HDAC and DNMT activity has also been identified in the colon carcinoma CaCo2 (Zhou *et al.*, 2019). The inhibitory effect of SF on HADC activity has also been identified *in vivo* through animal models. For example, treating mice with a concentration of 7.5µM SF daily for 21 days, resulting in a decrease in HADC activity and an increase in global histone acetylation (Myzak *et al*., 2007). Repeated five-day SF treatment to transgenic adenocarcinoma of the mouse prostate, with as low as 1-2.5 µM SF representing more

or less physiological concentrations also resulted in a decrease in the methylation ratio of the first five CpGs of the NRF2 gene promoter (Zhang *et al*., 2013a). The novelty of the work arises by showing that in both glucose environments SF affects the methionine cycle through an increase in the intracellular concentrations of the amino acid methionine, which correlated with an increase in S-Adenosylmethionine (SAM), the universal methyl donor. This SAM is likely the substrate needed to regulate the activity of HADC and DNMTs.

To further validate the role of SF as a metabolic regulator in the final chapter the genome editing technique, CRISPR-Cas9 was applied. Firstly, in this chapter, I also showed that NRF2KD resulted in both a decrease in mitochondrial activity as well as a reduction in glycolysis. This data also agrees with the findings from Holmstrom and colleagues, where deletion on NRF2 in mice embryonic fibroblasts results in mitochondrial depolarization, reduced ATP production, and ultimately impaired respiration (Holmstrom *et al*., 2013). Reduction in glycolysis is also in agreement with published literature, as identified by Carrasco-Pozo and colleagues, sulforaphane treatment to prostate cancer LNCaPcells was found to reduce the activity of two glycolytic genes: hexokinase and pyruvate kinase (Carrasco-Pozo *et al*., 2019). The RNAseq study in chapter 6 also identified a large attenuation in both the antioxidant response genes along with several genes in the PPP pathway that have shown to be NRF2 targets such as G6PD, PGD, TKT, and TALDO. My data is in agreement with two studies. The first one, by Mitsuishi and colleagues, showed using NRF2 siRNA a reduction in the activity of several genes in the PPP along with two genes in the TCA cycle: ME1 and IDH (Mitsuishi *et al*., 2012). The second by Thimmulappa and colleagues identified that SF treatment in the small intestine of NRF2KO mouse did not induce genes in the PPP compared to WT mice (Thimmulappa *et al*., 2002). The analysis also revealed a similar reduction and thereby potential loss of function in several other glycolytic genes such as fructose-bisphosphate aldolase A (ALDOA) phosphoribosylpyrophosphate synthetase (PRPS1), and glucose phosphate isomerase (PGI), potentially identifying novel NRF2 target genes.

Throughout this thesis, SF's ability to affect lipid metabolism has been identified several times. In particular, in chapter 6 the gene set biosynthesis of unsaturated fatty acids just failed to reach significance. Whilst NRF2's role in regulating lipid metabolism is still not fully clear, it is worth highlighting though that lipid biosynthesis, in particular, FASN and SCD are enzymes that utilize NADPH as a cofactor (Kuhajda *et al*., 1994, Koh *et al*., 2004). As a result, NRF2 regulation favors that NADPH is utilized to reduce oxidative stress by supporting the antioxidant response, rather than the biosynthesis of lipids.

Focusing on the downregulated gene sets of the NRF2KD cell line in chapter 6, I showed SF to heavily impact DNA metabolism both by blocking DNA replication and by downregulating, thereby inhibiting the activity of certain repair enzymes. The results match with that from the studies by (Hać *et al*., 2020, Piberger *et al.*, 2014), where the research identified ITC to block DNA replication in both cancer and normal cell lines. The results of the data may explain one of the several mechanisms through which ITCs have antiproliferative effects on cancer cell lines. As a result, these findings may pave the way for future research combining ITCs along with therapeutics that can block DNA replication or damage DNA for identifying novel treatments for cancer.

7.2.1 SF and glucose homeostasis. Can it be used to prevent T2D and its complications?

From the findings identified in this thesis along with the abundance of literature surrounding SF, there is strong evidence to suggest that SF and other plant-derived bioactive compounds have the potential to bring significant therapeutic benefits to human health. The current era of modern medicine is strongly centered around the relief of symptoms, with pharmaceuticals providing a vast number of drugs to address this demand. However, it is becoming increasingly apparent that while these drugs may delay the progression of diseases, they do not target their fundamental upstream cause. Finding the upstream cause of diseases is by far no easy stretch, as homeostasis in cells relies on a wide range of cellular metabolic processes. That is why plant bioactives should be considered as future candidates for therapeutics since they can target a wide range of signaling pathways within cells and organs (Budisan *et al*., 2017, Probst *et al*., 2017, Yoo *et al*., 2018).

Data from this thesis has shown that SF can be used as a potential therapeutic in a wide range of diseases such as T2D, cancer, and potentially other metabolic disorders such as CVD and NAFLD. Data from this thesis showed that in the high glucose environment, SF redirected the excess glucose load to the PPP pathway to suppress. In terms of T2D, accumulating literature is beginning to emerge through various mechanisms on how SF can improve T2D. One human intervention study showed 81 T2D participants after 4 weeks of receiving:

- either 5 grams of broccoli sprout extract (BSE) (equivalent to 112.5 µM SF)
- or 10 grams of BSE (225 µM SF),

SF could reduce, especially at higher doses, lipid peroxidation, in particular a decrease in plasma malondialdehyde (MDA) and oxidized LDL (ox-LDL) (Bahadoran *et al*., 2011). The reduction in ox-LDL is an important factor as this can infiltrate arteries and

form atherosclerotic plaque. In a follow up study where T2D patients were supplemented with 5 or 10 g of BSE, after four weeks of consumption of 10 g of BSE, participants had a significant decrease in serum insulin concentration and homeostatic model assessment of insulin resistance (HOMA-IR) (Bahadoran *et al.*, 2012). Axelsson and colleagues' recent human intervention study showed that SF from broccoli sprout extract could also reduce Hb1Ac and improve gluconeogenesis (Axelsson *et al*., 2017).

From the literature, it has been proposed that oxidative stress is a pathogenic mechanism that can result in insulin resistance through the dysfunction of β-cells of the pancreas and the endothelium (Ceriello and Motz, 2004, Cohen and Tong, 2010). The outcome is diabetes and potentially even cardiovascular disease. For example, plasma levels of thiol-related proteins (such as GSH and thioredoxin (TRX)) needed for the suppression of ROS and lipid peroxides have been reported to be lower in T2D compared to healthy controls (Ceriello *et al.*, 1997). Moreover, levels of GSH are reduced in pre-diabetics compared to controls, and as the diseases progress to diabetes, whilst the levels of GSH slightly rise, they are nowhere near that of healthy individuals resulting in increased cardiovascular complications (Nwose *et al.*, 2006). Simply infusing patients with GSH in a clinical trial was shown to improve endothelial dysfunction increasing vasodilation and enhancing the activity of nitric oxide (Prasad *et al*., 1999). Similarly, a mouse study showed that downregulation of the GCLC-GCLM in ApoE null mice results in reduced levels of GSH, making the mouse more susceptible to developing atherosclerosis (Biswas *et al*., 2005).

The thioredoxin system consists of two proteins: thioredoxin (TXN) and thioredoxin reductase (TXNRD), along with NADPH. Like GSH, TRX has been shown to exhibit a cardioprotective effect. A 7-day human intervention study demonstrated that 100 grams of fresh broccoli sprouts provided cardiovascular benefits (Murashima *et al*., 2004). This cardioprotective effect arises through the glucose being metabolized through the PPP. As glucose is redirected towards the PPP to generate reducing equivalents (NADPH), the NADPH is transferred through a series of cycling redox reactions (Holmgren and Lu, 2010). The outcome is the induction of TRX and TRX reductase by SF that results in the ability of TRX to alleviate much of the metabolic stress associated with T2DM. What's more, it has been identified that TRX influences both the hormone insulin and the activity of the glucocorticoid receptor, as well as other signalling proteins and transcription factors (Houghton, 2019).

It is also recognized that hyperglycemia results in the increased formation of advanced glycation end products (AGE). In endothelial cells, the interaction of the AGE with the receptor RAGE results in increased ROS production and induction and translocation of

NF-Ƙb, inducing a wide range of proinflammatory and procoagulatory molecules (Houghton, 2019).

7.2.2 SF can it be used to delay the onset of cancer?

In this thesis, I reported for the first time a potential novel anticarcinogenic activity of SF by downregulating and thereby inhibiting genes involved in both serine and glycine biosynthesis, which are often overexpressed in cancer cells. This finding and additional data obtained, such as SF inducing genotoxic stress from this thesis, build on the extensive literature on how SF acts as an anticarcinogenic agent. A large number of studies of *in vitro* have shown that SF anticarcinogenic mechanism includes inducing both phase I and phase II enzymes (Clarke *et al*., 2008) as well as disrupting the cell cytoskeleton (tubulin polymerization), thereby causing cell cycle arrest by blocking G2M phase of the cell cycle, along with inducing apoptosis (Hecht, 2000, Kallifatidis *et al*., 2009, Juge *et al*., 2007). Several *in vitro* studies using the breast cancer cell line MCF-7 have shown that an additional mechanism on how SF may prevent or treat breast cancer is by inducing changes in estrogen metabolism. Excessive estrogen can promote purine metabolism, resulting in DNA biogenesis, while estradiol treatment has been shown to induce an increase in the amino acids L-proline and L-arginine. Together these allow nutrients for cancer cells to divide and proliferate (Aumeeruddy and Mahomoodally, 2019).

To translate the *in vitro* findings of SF interfering with various aspects of cancer metabolism, within the last couple of years, human intervention studies have also been conducted on a wide range of tissues such as prostate, and breast cancer as well as melanoma, to assess whether SF could reduce the advancement of the disease. A first study recently identified that men with prostate cancer under surveillance who consumed 5-7 greater amounts of GR had a reduced risk of cancer progression (Traka *et al*., 2019). A second study showed that a single dose of BSE (containing the equivalent of 200 µM) to women with breast cancer, SF, was shown to reduce both tumour size and growth *(Cornblatt et al*., 2007). Simultaneous treatment of SF and docetaxel in mice has been shown to reduce the size of breast tumours up to 92%, compared to the control alone, along with inhibition of cancer proliferation (Burnett *et al*., 2017). An additional study assessing women with abnormal mammograms were randomized and were split into two groups for 2 up to 8 weeks:

- Control, a placebo supplement
- Treatment, GR supplement containing SF

The study identified that SF reduced the levels of the proliferation marker Ki-67 and histone deacetylases 3 but not 6 (HDAC) in the benign tissue. SF was also able to reduce the levels of HDAC in peripheral blood mononuclear cells (PBMC). The study concluded that whilst GR supplementation was safe, the short intervention was not sufficient for producing changes to biomarkers in breast tissue (Atwell *et al*., 2015). An additional human study that was carried out looked at assessing the effect of SF, again from BSE, on seventeen participants diagnosed with melanoma. In this study, participants were randomly allocated to receive the following:

- 50 µM BSE, daily for 28 days
- 100 µM BSE, daily for 28 days
- 200 µM BSE, daily for 28 days

The study identified that all concentrations of BSE and sulforaphane were well tolerated, and that plasma concentration of inflammatory cytokines decreased and levels of the tumor suppressor decorin were also increased (Tahata *et al*., 2018). It is worth highlighting that although the data is promising, all of these trials conducted apart from the study by Traka and colleagues were for short intervention. Future research should not only consider designing longer interventions but also following up with the participants once the trials are over to assess whether indeed SF can increase life span.

7.2.3 SF for the prevention of NAFLD

Data from this thesis is consistent with published data, showing through both *in vitro* in cell culture models and *in vivo* animal studies that SF interferes with a wide range of genes involved in lipid metabolism (Hayes and Dinkova-Kostova, 2014, Lin *et al*., 2016). Only one study has been translated in humans to assess SF impact on individuals with fatty liver. 24 participants received 30 mg of GR from broccoli sprout (BS) extract capsules for 2 months in this study. GR treatment compared to the control significantly reduced serum levels of the following liver function markers: ALT, γ-GTP as well as alkali phosphatase activity. Urinary markers of 8-OHdG, an established oxidative stress marker, was also significantly reduced in participants who had received the BS capsules (Kikuchi *et al*., 2015).

7.2.4 SF anti-inflammatory effects of reducing systemic inflammation

Consumption of a high-fat diet has been shown to alter the gut microbiome composition, resulting in decreased bacteria diversity and increased levels of Firmicutes and decreased relative abundance of *Bacteroides* (Le Chatelier *et al*.,

2013). Shifts in gut microbiota activate the Toll-like receptor signalling pathway, leading to increased intestinal permeability to endotoxin such as lipopolysaccharide (LPS) (Duan *et al*., 2018). Increased LPS and/or free fatty acids may directly affect intestinal cells, resulting in increased production of pro-inflammatory cytokines such as interleukin (IL)-1β, IL-6, and tumour necrosis factor-alpha (TNFα) in the gut. These cytokines circulating in the system will induce the nuclear factor of kappa B (NF-ƙB) signalling pathway. Whilst NF-ƙB does play an important role in the immune systems, sustained activation results in the induction of various cellular stress responses, including oxidative stress, endoplasmic reticulum stress (ERS), and apoptosis (Duan *et al*., 2018).

In endothelial cells, SF has been shown to inhibit NF-ƙB, and the same effect would likely be observed in other epithelial cells such as intestinal, thereby delaying or even preventing the onset of inflammation (Chen *et al*., 2009). Induction of NRF2 by SF allows NRF2 to interact and inhibit NF-ƙB binding to the DNA (Heiss *et al*., 2001). The imbalance between NRF2 and NF-ƙB has been associated with many diseases across various tissues and organs of the body (Ben-Neriah and Karin, 2011). This interplay between NRF2 and NF-ƙB is nevertheless complex, as NF-ƙB has also been shown to regulate the expression of NRF2-ARE genes through several different mechanisms (Yu *et al*., 2011a). It has been suggested that the cross-talk between NRF2 and NF-ƙB allows cells to regulate their response to cellular stressors more finely; as previously stated, gram-negative bacteria result in the release of the endotoxin LPS. LPS can then bind and activate the TLR4 receptor resulting in the generation of inflammatory cytokines (Kent *et al*., 1998). Similarly, saturated fatty acids can act as ligands and bind onto the TLR4 receptor of both macrophages and adipocytes, with these signals regulating a wide range of pro-inflammatory cytokines (Rahman *et al*., 2012). SF has been shown in a thiol-dependent manner to suppress the dimerization of the TLR4 receptor (Folkard *et al*., 2014).

To assess whether SF can reduce the effect of inflammation markers in humans, forty healthy overweight participants consumed 30 grams of fresh broccoli sprouts daily (equivalent to 117 µmol of GR). The study assessed the levels of two critical inflammatory cytokines:

- Interleukin-6 (IL-6)
- C-reactive protein (CRP)

During the 70 days, markers of both IL-6 and CRP declined. At the end of the study, after 90 days, the biomarkers were measured again. Levels of IL-6 continued to decrease, whereas CRP started to increase again. When the final measurements were

taken at day 160, although CRP had risen, it was lower than the value at the start of the study. IL-6 also increased, but it was significantly lower than the baseline measurement (López-Chillón *et al*., 2019). A second study in a cohort of T2D diabetics also showed that SF supplementation after four weeks significantly reduced the following markers IL-6, CRP, and TNF-α (Mirmiran *et al*., 2012).

7.3 Limitation of the Research

The work conducted throughout this thesis was all undertaken through cell culture, *in vitro* cell models, or cell-free systems. Cell culture studies can play an essential role in getting a theoretical and mechanistic understanding of how the compound of interest at a particular point in time affects cell behaviour. In addition, it is easy to use and cheap compared to animal models and not influenced by a range of factors such as age, diet, and, to some extent, gender. In particular, when carrying out knockdown investigations, it is easier to control that the effects are not indirect, as knockdown *in vivo* can affect other off-target organs, although it is possible in mice to target specific tissues and minimize the off-target effects. However, cell culture studies also offer several disadvantages. For example, results from *in vitro* studies are challenging to translate to *in vivo* situations for several reasons. Firstly, as the cells are isolated in the culture, they do not experience the same conditions as encountered *in vivo,* and without existing in circulation, many growth factors may not be experienced. Another consideration is that each time the cell is passaged, the cell will behave slightly differently from the original or previous cell, thereby responding differently to the treatment. Nevertheless, it is worth highlighting that relatively narrow passage numbers were utilized throughout the courses of this research precisely to avoid introducing any anomalies.

In addition, the work carried out throughout this thesis was conducted using a hepatocellular carcinoma cell line (HepG2). Cancer cells can harbour several mutations, which makes them challenging to study. Despite HepG2 being a cancerous cell line, HepG2 is the most commonly studied liver cell line because it metabolically resembles an *in vivo* liver tissue. For example, it has been identified that the expression of gluconeogenic enzymes glucose-6-phosphatase catalytic subunit (G6PC) and phosphoenolpyruvate carboxykinase 1, the latter being the rate-limiting enzyme in gluconeogenesis, although expressed in HepG2, were not expressed in the liver cell lines THLE2 and AML-12 (Sefried *et al*., 2018).

Additional limitations were the concentrations of SF used, along with the supraphysiological concentrations or the lack of glucose introduced throughout the

research. Physiological concentrations of SF in the plasma were shown to range from as low as 2 to 6 µM, whilst consumption of the Beneforte broccoli, which contains 3-5 higher concentrations of glucoraphanin, plasma concentrations of sulforaphane peaked consistently at 9-11 µM (Gasper *et al*., 2005, Sivapalan *et al*., 2018, Coode-Bate *et al.*, 2019). Whilst it was hypothesized that 10 µM SF represents physiological concentrations of SF, it is likely that 10 µM would have been on the higher end, thereby over capturing all of the metabolic effects of SF. Throughout this research, cells were cultured either in glucose excess (25 mM) or lack of glucose for 24 h. It is worth highlighting that even a diabetic person does not experience such excess glucose levels, as these levels would be cytotoxic, leading to permanent damage to several organs and resulting in coma and potentially death in the long term. Similarly, a lack of glucose would also never occur. Even diets severely low in carbohydrates glucose would still be intracellularly synthesized.

In **chapter 3,** it is also worth re-highlighting that in the *in vitro* model of non-acholic fatty liver diseases (NAFLD), high concentrations of the fatty acid palmitate were used. Whilst palmitate is the most commonly consumed saturated fatty acid, our diet, especially common 21st-century diets that include many processed foods, contains several different fatty acids, thereby not representing an accurate picture.

In **chapters 4,5,** and **6,** the RNAseq data analysis identified that SF affected the expression of a wide range of genes. Whilst certain gene sets were enriched, such as the 1C metabolism, glycine, serine, threonine metabolism, etc., other genes in this set had a slight upregulation. For example, the observed fold change was as low as 1.2-1.4. Therefore, it would have been more important to follow up the expression of these genes by looking at the protein level to support the potential functional consequences further. In **chapter 6,** a heterogenous NRF2KD cell population was used. Since NRF2 is a master regulator, by regulating a wide range of cellular processes, perhaps working with a full NRF2KO cell line, the editing would have been lethal, resulting in cell death. RNAseq has become a gold standard to characterise and quantify the transcriptome at a given time, allowing the study of transcriptomic profiles under different conditions. However, the significant limitations of this technology include: it is costly and employs a time-intensive process for both running the assay and data analysis (Alpern *et al*., 2019). Library preparation and generation for RNAseq is a complex and error-prone process, requiring many steps, and after each step, sample loss may occur (Whitley *et al*., 2016).

In the first step, the RNA is reverse transcribed to cDNA, then processed further to generate libraries. If high abundance RNAs are present in the sample, additional steps must be employed to remove or enrich mRNA. Whilst these steps are essential as they

help with the quality of the data (downstream analysis), they add labour cost and reduce the quantity of starting RNA, which may be problematic if you are working with single cells where your starting RNA concentration is low (Whitley *et al*., 2016). To avoid enriching mRNA, the RNA is both pre-amplified and then deeper sequenced to increase the number of reads to overcome this issue. In this thesis, the library preparation method selected in both chapters was Poly-A enrichment. Depending on the goal of the analysis, sample preparation can consist of either undertaking poly-A, which is often the favourable method as it prevents mRNA degradation, requiring less sequencing depth. The disadvantage of poly-A adenylation is that it does not allow the detection of small RNA (microRNAs) and long non-coding RNAs, thereby potentially losing data. (Whitley *et al*., 2016). Again, depending on the study's goal, other methods can be used to preserve the microRNAs in the samples, like using QIAzol lysis reagent instead of using the QIAshredder process.

During the data processing stage, RNAseq is mainly used to measure gene expression, whereas other approaches like whole-exome sequencing are used to identify mutations in the genome. After obtaining the DEGs, these are added to the GSEA to get pathways of interest. Selecting the appropriate database for GSEA is crucial to obtaining relevant results. It is essential to verify and validate the results from the algorithms and parameters used. It is also important to use diagnostic plots to validate any statistical methods used for the data analysis, a critical aspect of ensuring transparency and reproducibility in science (Tamayo *et al*., 2016).

7.4 Future Research

The data presented in this thesis provides evidence that SF can act as a metabolic regulator, and its effects are mediated mainly through NRF2. Several extensions could be made to the experimental design to further this project.

Although NRF2 activation regulates metabolism, few cell line studies have reported that constituent activation of NRF2 has an adverse effect, allowing lung cancer cell lines to proliferate and metastasize (Mitsuishi *et al*., 2012, DeNicola *et al*., 2015), as well as worsening glucose tolerance and lipid metabolism in mice, fed a high-fat diet (More *et al*., 2013). Therefore, continuing the *in vitro* work, the CRISPR-Cas9 system could have been used to develop a constituent active NRF2 hepatic cell line through KEAP1 knockdown/knockout. This cell line would have then been exposed to physiological concentrations of SF, challenged with different concentrations of glucose and or fatty acids. The Seahorse, along with transcriptomics and metabolomics, would

have been used to assess whether intermittent and cyclic NRF2 induction, such as that observed following a diet rich in NRF2 inducers, will improve hepatic metabolism.

If the *in vitro* work were to be continued, a second option would be to use either primary liver cells or a more robust model like liver organoids. Primary liver cells are still considered the gold standard for creating an *in vitro* model of liver cell culture. Due to their origin in the native liver, they reflect the complete functionality of the human organ *in vivo* and thus provide highly predictive results in pharmacological and toxicological *in vitro* research. Furthermore, as each sample is obtained by a different donor, it offers the opportunity to analyze a broad range of genetic polymorphisms using individual cell isolates (Zeilinger *et al*., 2016). The significant limitations of working with primary cells are that interindividual differences and cell alterations due to the isolation procedure will result in variations in experimental results, complicating the standardization of models (Zeilinger *et al*., 2016). Human organoids are formed by human stem cells in a 3D culture system; this system makes it possible to re-create the architecture and physiology of human organs in remarkable detail, enabling them to be essential models for the study of human diseases (Kim *et al*., 2020). An alternative option could be the use of the liver-on-a-chip model. Liver-on-a-chip is a 3D *in vitro* hepatic microphysiological system that aims to recreate the conditions of liver tissue on a microscopic scale (Rennert *et al*., 2015).

One of the main advantages of this system is integrating several different cell types all at once, mimicking liver tissue in real life. For example, the system would incorporate non-parenchymal cells (NPCs) in a vascular layer made of HUVECs, tissue macrophages, Kupffer cells, and an opposing layer of hepatic stellate cells (HSCs) co-cultured with hepatocytes. Luminescence-based sensors in the device allow real-time measurement of oxygen consumption, thereby assessing how SF treatment or challenging the different cells type substrates such as glucose or fatty acids. By seeding hepatics spheroids and establishing a liver-on-chip model, the liver tissue will resemble the native function and the spheroids the native structure (Hassan *et al*., 2020). This, in combination with biosensors integrated into the chips (Kulkeaw and Pengsart, 2021), will help address the static model used and provide a novel biological understanding of the liver function and SF as a therapeutic compound.

The *in vitro* findings of SF affecting the serine biosynthetic pathway and its ability to interfere with 1C metabolism should be scaled up to an *in vivo* model. Several studies described in the review by Kamal have shown that SF can act as an anticarcinogenic agent (Kamal *et al*., 2020). As previously stated, certain cancer cell lines have the serine biosynthetic genes overexpressed, allowing them to become addicted to serine, which is needed for the constant production of nucleotides. To test whether SF may

also inhibit or slow down cancer progression by inhibiting these genes, an *in vivo* study design using mice that have either PHDGH or the serine hydroxymethyltransferase SHTM1/2 in the liver overexpressed could be carried out. Overexpression of PHGDH or SHTM1/2 could be carried out either with a cre knock-in at a tissue-specific locus, allowing the overexpression to be specific only at the liver. The alternative could use the bacterial artificial chromosome (BAC) system to develop transgenic mice (Tsyrulnyk and Moriggl, 2008). The main limitation of BAC is that it is not tissue-specific, but instead, the overexpression is on the whole body. Control and SF or even glucoraphanin (GR) supplemented mice at specific doses (for example, making a dose response) would then be administered for a particular time. The primary outcome would be to assess whether the supplementation results in the mice living longer compared to its respective control and a reduction or even potential inhibition of cancer to metastasize. Based on the findings of the primary outcome, the secondary outcome would be to obtain the liver tissue and potentially other tissues, extract metabolites and RNA from the control and treated samples, and send the samples for metabolomics and transcriptomics to assess and identify how SF targets specific pathways that could inhibit cancer to spread.

Within the last couple of years, there have been several studies assessing how SF impacts lipid metabolism by feeding mice a high-fat diet along with GR or SF supplementation (Axelsson *et al*., 2017, Nagata *et al*., 2017, Li *et al*., 2021, Xu *et al*., 2020). An alternative study to assess how SF impacts hepatic metabolism and not simply focus on lipid metabolism could also be an *in vivo* study where mice are fed a standard chow diet compared to a high-fat diet. In other words, rather than having a diet of 60% in lard or cholesterol, this would be replaced with 30-40% (wt/v) glucose and fructose. Fructose has been suggested since it has been shown to worsen liver metabolism (Softic *et al*., 2017, Geidl-Flueck *et al*., 2021). The glucose and fructose would be supplemented through the water. Both the control and the high sugar diet would also receive SF, GR, or even better whole broccoli (although that would make it more challenging to identify which specific glucosinolate may result in a beneficial impact) for 6 to 8 weeks. After 6-8 weeks, RNA from the liver along with metabolites would be extracted and sent for both RNAseq and metabolomics analysis, to assess whether the broccoli bioactives can mitigate the effects induced by high sugar consumption.

The two limitations of animal studies however include the concentration of SF hoped to be achieved, as well as the choice of the delivery method. For example from table 7.1, it has been identified that several animal studies involving SF supplementation with a

delivery method of either diet supplementation or oral gavage, to ensure SF is still subjected to the digestive tract.

Table 7.1 Animal studies using SF Supplementation

Study	SF dose (µmols/day)*	Duration of supplementation	Broccoli consumption (g/day)**
(Axelsson et al., 2017)	56.4 or 2.82	4 weeks	45.12 or 2.26
(Choi et al., 2014)	28.2	6 weeks	22.6
(Davidson et al., 2013)	3	12 weeks	2.4
(Abbaoui et al., 2012)	7.4	2 weeks	5.6
(Traka et al., 2010)	0.5 or 5	4 or 8 weeks	0.4 or 4
(Myzak et al., 2006a)	2500	16 weeks	2000

* µmols/day was calculated based on two assumptions; the body weight of a mouse is approximately 25g and each mouse consumes around 5g of food per day.

**Using the assumption that there is 0.8µmol of glucoraphanin per g of broccoli fresh weight with 100% conversion to SF (according to the method used within the research group).

The main drawback of mouse models as shown in table 7.1 is the large variation of the concentrations of SF used in animal studies especially compared to the quantity of broccoli that would be needed to be consumed to achieve that concentration. As a result, it is difficult to translate the dose of SF used in the animal to the levels needed for human consumption. In addition, mouse vs human metabolism may also differ, making the result difficult to translate to human clinical applications. Davidson and colleagues were one of the few studies that carried out *in vivo* using physiological concentrations of SF. Davidson found that SF was able to suppress the activity of several cytokines which induced metalloproteinases, thereby decreasing arthritis score in the destabilization of the medial meniscus (DMM) mouse model of osteoarthritis (Davidson *et al.*, 2013).

To overcome the difficulties of a mouse study, a human intervention study could be carried out, thereby making the result much easier to translate and applicable to the general population. Two important factors when designing the experiment for a potential human intervention study include deciding the delivery method of the treatment and the time frame of the intervention (Quirante-Moya *et al*., 2020). SF itself is unstable, and therefore the precursor of SF, glucoraphanin, would be the appropriate source. Glucoraphanin could potentially be delivered as either a supplement, similar to the study conducted by (Nagata *et al*., 2017) or via the use of whole broccoli, such as the study conducted both by (Armah *et al*., 2015) and (Traka *et al*., 2019). Another important factor to consider when designing a human intervention study is sample size to reduce inter-individual variability. It is also essential to control for variables (more commonly referred to as co-variables) that can influence and impact other variables. Covariables such as sex, age, and BMI must be controlled as they greatly influence responses linked to inflammatory processes or gene expression.

In terms of conducting a human intervention study, to assess the effect of broccoli on hepatic metabolism, the experimental design could consist of the following. The first option could be administrating whole broccoli or BSE containing SF capsules to healthy patients (control) vs obese patients, or patients with fatty liver diseases. A second study could consist of recruiting patients with fatty liver diseases and splitting them into different groups. Each group would consume broccoli with different concentrations of the glucosinolates GR, obtained from broccoli with increased expression of the transcription factor Myb-related protein-28 (Myb28) from *Brassica villosa*, enabling increased production of glucoraphanin (Traka *et al*., 2013). In terms of delivery method, one option could be in the form of soups, matching the experimental design from the recently published study by Traka and colleagues (Traka *et al*., 2019). When considering the preparation of the soups, it is important to consider the various cooking processes, since that can affect the final concentration of the glucosinolate, as cooking can rapture cell membranes as well as denature the activity of the myrosinase enzyme. For example, steaming has been shown to lead to a 20% decrease in glucosinolates content, high pressure boiling 33% decrease, conventional boiling 55%, and microwaving up to 74% (Mandrich and Caputo, 2020). An alternative option to avoid preparing the broccoli could be through the use of BSE capsules that also contains high doses of SF. The main limitation of delivery capsules containing SF is that it just focus on a single compound, rather than assessing the synergistic effects of a wide range of different glucosinolates. The length of the study could be a medium length study and could range from four weeks up to 6 months. The review by Quirante-Moya and colleagues identified that medium to long-range studies where SF or other broccoli bioactives given to participants for 2 up to 12 months had the greatest effect in inducing

transcriptional changes as well as reducing inflammatory markers (Quirante-Moya *et al*., 2020). If feasible, liver biopsy ahead of a scheduled surgery at the end of the study would be taken, and transcriptomic/metabolomics analysis would be carried to assess how SF affects hepatic metabolism by assessing SF's effect on lipid metabolism, as well as other metabolic pathways.

Although the gut microbiome, within the last 10 to 15 years has shown to play an important role in preventing the onset of a wide range of diseases, such as obesity, cancer, diabetes, etc. (Fan and Pedersen, 2021), until now limited studies have assessed changes in gut microbiota by broccoli and other cruciferous vegetables from interventions studies. When brassica vegetables are ingested, the GLs are firstly hydrolyzed in the small intestine by active myrosinase in the plant, (provided the myrosinase enzyme is not degraded during the cooking process), but can also be hydrolyzed in the colon by specific bacterial microflora that produces the myrosinase enzyme (Rouzaud *et al*., 2003). In humans, it has been shown that the inter-individual variation in GL hydrolysis is mainly dependent on differences in bacterial microflora between individuals. For example, the probiotic strains *Lactobacillus plantarum* KW30 and *Lactococcus lactis* ssp. lactis KF147 were found to convert 30–33% of glucoraphanin and/or glucoerucin into sulforaphane nitrile, erucin nitrile, and some additional unknown metabolites (Krul *et al*., 2002). A further study found that the *Lactobacillus agilis* R16, another lactic acid bacterial strain, can hydrolyze sinigrin into allyl isothiocyanate (ATIC) (Krul *et al*., 2002). An additional human study identified *Lactobacillus agilis* R16, capable of metabolizing 10% glucoraphanin and glucoiberin. In contrast, though the study identified that *Enterococcus casseliflavus CP1* was able to metabolize 40–50% of glucoiberin and glucoraphanin, producing relatively low concentrations of iberin and sulforaphane. The bacteria that had the highest ability to metabolize both glucoraphanin and glucoiberin was *Escherichia coli* VL8, which was shown to metabolized 80–90% of glucoiberin and glucoraphanin. In the process, the bacteria were able to bioconvert glucoiberin and glucoraphanin to glucoerucin and glucoiberverin, and then further breaking down these compounds, producing erucin, erucin nitriles, iberverin, and iberverin nitriles from the two GSLs (Luang-In *et al*., 2014). The findings that lactic acid bacteria strains along with *E.coli* are capable of metabolizing certain glucosinolates have also been confirmed by Kellingray and colleagues. Their work showed that *in vitro* fermentation of fecal samples from five different participants in combination with broccoli leachate had enhanced growth of *lactobacilli*. This corresponded with increased lactate and short chain fatty acid productions, along with increase *E.coli* required for the bioconversion of glucorphanin to its respective analogue *(*Kellingray *et al.,* 2021*).*

To add further complexity, two recent studies showed that mice supplemented with broccoli seeds or stalks/florets, consumption of broccoli resulted in a shift in the microbiome: one study showed an increase in the number of *Bacteroidetes,* and a significant decrease in *Lachnospiraceae* and the other showed an increase in *Akkermansia muciniphila* and a reduction in *Mucispirillum schaedleri (*Zandani *et al*., 2021, Xu *et al*., 2020*)*. Studies have shown that *Akkermansia* can modulate a wide range of hormones and genes related to both glucose metabolism as well as fatty acids oxidation (Yoon *et al*., 2021); for example, it has been identified that in type 2 diabetic mice treated with *Akkermansia,* the treatment increased the expression of genes related to fatty acid oxidation such as (CPT1, PGC1α, and PPARα) (Everard *et al* 2013). Therefore, with advancements in sequencing technologies, future research should focus on understanding the role of the gut microbiota composition in mediating the effects of SF and other bioactives in systemic metabolic regulation. For example, some questions that could be addressed include: are there specific microbiota profiles that would be more susceptible to SF's action? Is it possible to design personalized interventions that target gut microbiota and diet?

In conclusion, the work of this thesis has contributed to our scientific understanding that SF can act as a metabolic regulator, thereby regulating hepatic metabolism and these effects are largely mediated through NRF2. As there has been an increasing number of *in vivo* studies assessing the effect of SF or its precursor GR on how it can improve metabolic syndrome, moving forward future research should consider the effect of whole broccoli intake on individuals who have metabolic syndrome to investigate whether frequent consumption of broccoli can ameliorate the problematics of obesity and metabolic syndrome. This research could provide further evidence for increasing the levels of standard broccoli consumption or potentially recommending to start consuming the commercially available high-GSL Beneforté broccoli within the diet.

References

<Evaluation of statistical methods for normalization and differential expression in mRNA-Seq experiments.pdf>.

Felix Krueger, Babraham Institute, Trim galore v0.5.0. Available at https://github.com/FelixKrueger/TrimGalore.

https://github.com/FelixKrueger/TrimGalore.

Human assembly and gene annotation, available at http://www.ensembl.org/Homo_sapiens/Info/Annotation.

ABBAOUI, B., RIEDL, K. M., RALSTON, R. A., THOMAS-AHNER, J. M., SCHWARTZ, S. J., CLINTON, S. K. & MORTAZAVI, A. 2012. Inhibition of bladder cancer by broccoli isothiocyanates sulforaphane and erucin: characterization, metabolism, and interconversion. *Mol Nutr Food Res,* 56**,** 1675-87.

ABDEL-MISIH, S. R. & BLOOMSTON, M. 2010. Liver anatomy. *Surg Clin North Am,* 90**,** 643-53.

ABE, H. 2000. Role of histidine-related compounds as intracellular proton buffering constituents in vertebrate muscle. *Biochemistry (Mosc),* 65**,** 757-65.

ADACHI, N., LIU, K. & ARAI, T. 2005. Prevention of brain infarction by postischemic administration of histidine in rats. *Brain Res,* 1039**,** 220-3.

AGERBIRK, N. & OLSEN, C. E. 2012. Glucosinolate structures in evolution. *Phytochemistry,* 77**,** 16-45.

AGHAGOLZADEH, P., RADPOUR, R., BACHTLER, M., VAN GOOR, H., SMITH, E. R., LISTER, A., ODERMATT, A., FEELISCH, M. & PASCH, A. 2017. Hydrogen sulfide attenuates calcification of vascular smooth muscle cells via KEAP1/NRF2/NQO1 activation. *Atherosclerosis,* 265**,** 78-86.

AGYEMAN, A. S., CHAERKADY, R., SHAW, P. G., DAVIDSON, N. E., VISVANATHAN, K., PANDEY, A. & KENSLER, T. W. 2012. Transcriptomic and proteomic profiling of KEAP1 disrupted and sulforaphane-treated human breast epithelial cells reveals common expression profiles. *Breast Cancer Res Treat,* 132**,** 175-87.

AKIYAMA, Y., KODA, Y., BYEON, S. J., SHIMADA, S., NISHIKAWAJI, T., SAKAMOTO, A., CHEN, Y., KOJIMA, K., KAWANO, T., EISHI, Y., DENG, D., KIM, W. H., ZHU, W. G., YUASA, Y. & TANAKA, S. 2016. Reduced expression of SET7/9, a histone mono-methyltransferase, is associated with gastric cancer progression. *Oncotarget,* 7**,** 3966-83.

ALDINI, G., ORIOLI, M., ROSSONI, G., SAVI, F., BRAIDOTTI, P., VISTOLI, G., YEUM, K. J., NEGRISOLI, G. & CARINI, M. 2011. The carbonyl scavenger carnosine ameliorates dyslipidaemia and renal function in Zucker obese rats. *J Cell Mol Med,* 15**,** 1339-54.

ALEKSUNES, L. M., REISMAN, S. A., YEAGER, R. L., GOEDKEN, M. J. & KLAASSEN, C. D. 2010. Nuclear factor erythroid 2-related factor 2 deletion impairs glucose tolerance and exacerbates hyperglycemia in type 1 diabetic mice. *J Pharmacol Exp Ther,* 333**,** 140-51.

ALFARISI, H. A. H., MOHAMED, Z. B. H. & IBRAHIM, M. B. 2020. Basic pathogenic mechanisms of atherosclerosis. *Egyptian Journal of Basic and Applied Sciences,* 7**,** 116-125.

ALNAHDI, A., JOHN, A. & RAZA, H. 2019. Augmentation of Glucotoxicity, Oxidative Stress, Apoptosis and Mitochondrial Dysfunction in HepG2 Cells by Palmitic Acid. *Nutrients,* 11.

ALPERN, D., GARDEUX, V., RUSSEIL, J., MANGEAT, B., MEIRELES-FILHO, A. C. A., BREYSSE, R., HACKER, D. & DEPLANCKE, B. 2019. BRB-seq: ultra-affordable high-throughput transcriptomics enabled by bulk RNA barcoding and sequencing. *Genome Biology,* 20**,** 71.

ANDERS, S. & HUBER, W. 2010. Differential expression analysis for sequence count data. *Genome Biology,* 11**,** R106.

ANDO, K. & FUJITA, T. 2009. Metabolic syndrome and oxidative stress. *Free Radic Biol Med,* 47**,** 213-8.

ANEDDA, A., LOPEZ-BERNARDO, E., ACOSTA-IBORRA, B., SAADEH SULEIMAN, M., LANDAZURI, M. O. & CADENAS, S. 2013. The transcription factor Nrf2 promotes survival by enhancing the expression of uncoupling protein 3 under conditions of oxidative stress. *Free Radic Biol Med,* 61**,** 395-407.

ANTONOV, A., AGOSTINI, M., MORELLO, M., MINIERI, M., MELINO, G. & AMELIO, I. 2014. Bioinformatics analysis of the serine and glycine pathway in cancer cells. *Oncotarget,* 5**,** 11004-13.

ARCIDIACONO, P., RAGONESE, F., STABILE, A., PISTILLI, A., KULIGINA, E., RENDE, M., BOTTONI, U., CALVIERI, S., CRISANTI, A. & SPACCAPELO, R. 2018. Antitumor activity and expression profiles of genes induced by sulforaphane in human melanoma cells. *Eur J Nutr,* 57**,** 2547-2569.

ARMAH, C. N., DERDEMEZIS, C., TRAKA, M. H., DAINTY, J. R., DOLEMAN, J. F., SAHA, S., LEUNG, W., POTTER, J. F., LOVEGROVE, J. A. & MITHEN, R. F. 2015. Diet rich in high glucoraphanin broccoli reduces plasma LDL cholesterol: Evidence from randomised controlled trials. *Molecular nutrition & food research,* 59**,** 918-926.

ARMAH, C. N., TRAKA, M. H., DAINTY, J. R., DEFERNEZ, M., JANSSENS, A., LEUNG, W., DOLEMAN, J. F., POTTER, J. F. & MITHEN, R. F. 2013. A diet rich in high-glucoraphanin broccoli interacts with genotype to reduce discordance in plasma metabolite profiles by modulating mitochondrial function. *The American Journal of Clinical Nutrition,* 98**,** 712-722.

ARMITAGE, J., BAIGENT, C., BARNES, E., BETTERIDGE, D. J., BLACKWELL, L., BLAZING, M., BOWMAN, L., BRAUNWALD, E., BYINGTON, R., CANNON, C., CLEARFIELD, M., COLHOUN, H., COLLINS, R., DAHLÖF, B., DAVIES, K., DAVIS, B., DE LEMOS, J., DOWNS, J. R., DURRINGTON, P., EMBERSON, J., FELLSTRÖM, B., FLATHER, M., FORD, I., FRANZOSI, M. G., FULCHER, J., FULLER, J., FURBERG, C., GORDON, D., GOTO, S., GOTTO, A., HALLS, H., HARPER, C., HAWKINS, C. M., HERRINGTON, W., HITMAN, G., HOLDAAS, H., HOLLAND, L., JARDINE, A., JUKEMA, J. W., KASTELEIN, J., KEAN, S., KEECH, A., KIRBY, A., KJEKSHUS, J., KNATTERUD, G., KNOPP, R., KOENIG, W., KOREN, M., KRANE, V., LANDRAY, M. J., LAROSA, J., LONN, E., MACFARLANE, P., MACMAHON, S., MAGGIONI, A., MARCHIOLI, R., MARSCHNER, I., MIHAYLOVA, B., MOYÉ, L., MURPHY, S., NAKAMURA, H., NEIL, A., NEWMAN, C., O'CONNELL, R., PACKARD, C., PARISH, S., PEDERSEN, T., PETO, R., PFEFFER, M., POULTER, N., PREISS, D., REITH, C., RIDKER, P., ROBERTSON, M., SACKS, F., SATTAR, N., SCHMIEDER, R., SERRUYS, P., SEVER, P., SHAW, J., SHEAR, C., SIMES, J., SLEIGHT, P., SPATA, E., TAVAZZI, L., TOBERT, J., TOGNONI, G., TONKIN, A., TROMPET, S., VARIGOS, J., WANNER, C., WEDEL, H., WHITE, H., WIKSTRAND, J., WILHELMSEN, L., WILSON, K., YOUNG, R., YUSUF, S. & ZANNAD, F. 2019. Efficacy and safety of statin therapy in older people: a meta-analysis of individual participant data from 28 randomised controlled trials. *The Lancet,* 393**,** 407-415.

ASHINO, T., YAMAMOTO, M. & NUMAZAWA, S. 2016. Nrf2/Keap1 system regulates vascular smooth muscle cell apoptosis for vascular homeostasis: role in neointimal formation after vascular injury. *Scientific Reports,* 6**,** 26291.

ASHINO, T., YAMAMOTO, M., YOSHIDA, T. & NUMAZAWA, S. 2013. Redox-Sensitive Transcription Factor Nrf2 Regulates Vascular Smooth Muscle Cell Migration and Neointimal Hyperplasia. *Arteriosclerosis, Thrombosis, and Vascular Biology,* 33**,** 760-768.

ATHALE, J., ULRICH, A., MACGARVEY, N. C., BARTZ, R. R., WELTY-WOLF, K. E., SULIMAN, H. B. & PIANTADOSI, C. A. 2012. Nrf2 promotes alveolar mitochondrial biogenesis and resolution of lung injury in Staphylococcus aureus pneumonia in mice. *Free Radic Biol Med,* 53**,** 1584-94.

ATWELL, L. L., ZHANG, Z., MORI, M., FARRIS, P., VETTO, J. T., NAIK, A. M., OH, K. Y., THUILLIER, P., HO, E. & SHANNON, J. 2015. Sulforaphane Bioavailability and Chemopreventive Activity in Women Scheduled for Breast Biopsy. *Cancer Prev Res (Phila),* 8**,** 1184-1191.

AUMEERUDDY, M. Z. & MAHOMOODALLY, M. F. 2019. Combating breast cancer using combination therapy with 3 phytochemicals: Piperine, sulforaphane, and thymoquinone. *Cancer,* 125**,** 1600-1611.

AVEROUS, J., BRUHAT, A., JOUSSE, C., CARRARO, V., THIEL, G. & FAFOURNOUX, P. 2004. Induction of CHOP expression by amino acid limitation requires both ATF4 expression and ATF2 phosphorylation. *J Biol Chem,* 279**,** 5288-97.

AXELSSON, A. S., TUBBS, E., MECHAM, B., CHACKO, S., NENONEN, H. A., TANG, Y., FAHEY, J. W., DERRY, J. M. J., WOLLHEIM, C. B., WIERUP, N., HAYMOND, M. W., FRIEND, S. H., MULDER, H. & ROSENGREN, A. H. 2017. Sulforaphane reduces hepatic glucose production and improves glucose control in patients with type 2 diabetes. *Sci Transl Med,* 9.

BACK, S. H. & KAUFMAN, R. J. 2012. Endoplasmic reticulum stress and type 2 diabetes. *Annu Rev Biochem,* 81**,** 767-93.

BAHADORAN, Z., MIRMIRAN, P., HOSSEINPANAH, F., HEDAYATI, M., HOSSEINPOUR-NIAZI, S. & AZIZI, F. 2011. Broccoli sprouts reduce oxidative stress in type 2 diabetes: a randomized double-blind clinical trial. *Eur J Clin Nutr,* 65**,** 972-7.

BAHADORAN, Z., TOHIDI, M., NAZERI, P., MEHRAN, M., AZIZI, F. & MIRMIRAN, P. 2012. Effect of broccoli sprouts on insulin resistance in type 2 diabetic patients: a randomized double-blind clinical trial. *Int J Food Sci Nutr,* 63**,** 767-71.

BAINS, O. S., TAKAHASHI, R. H., PFEIFER, T. A., GRIGLIATTI, T. A., REID, R. E. & RIGGS, K. W. 2008. Two allelic variants of aldo-keto reductase 1A1 exhibit reduced in vitro metabolism of daunorubicin. *Drug Metab Dispos,* 36**,** 904-10.

BARTON, P., ANDRONIS, L., BRIGGS, A., MCPHERSON, K. & CAPEWELL, S. 2011. Effectiveness and cost effectiveness of cardiovascular disease prevention in whole populations: modelling study. *BMJ,* 343**,** d4044.

BATISTA, I. D. A. A. & HELGUERO, L. A. 2018. Biological processes and signal transduction pathways regulated by the protein methyltransferase SETD7 and their significance in cancer. *Signal Transduction and Targeted Therapy,* 3**,** 19.

BEAVER, L. M., BUCHANAN, A., SOKOLOWSKI, E. I., RISCOE, A. N., WONG, C. P., CHANG, J. H., LÖHR, C. V., WILLIAMS, D. E., DASHWOOD, R. H. & HO, E. 2014. Transcriptome analysis reveals a dynamic and differential transcriptional response to sulforaphane in normal and prostate cancer cells and suggests a role for Sp1 in chemoprevention. *Molecular nutrition & food research,* 58**,** 2001-2013.

BECKS, L., PRINCE, M., BURSON, H., CHRISTOPHE, C., BROADWAY, M., ITOH, K., YAMAMOTO, M., MATHIS, M., ORCHARD, E., SHI, R., MCLARTY, J., PRUITT, K., ZHANG, S. & KLEINER-HANCOCK, H. E. 2010. Aggressive mammary carcinoma progression in Nrf2 knockout mice treated with 7,12-dimethylbenz[a]anthracene. *BMC Cancer,* 10**,** 540.

BEDOLLA, R. G., GONG, J., PRIHODA, T. J., YEH, I. T., THOMPSON, I. M., GHOSH, R. & KUMAR, A. P. 2012. Predictive Value of Sp1/Sp3/FLIP Signature for Prostate Cancer Recurrence. *PLOS ONE,* 7**,** e44917.

BEN-NERIAH, Y. & KARIN, M. 2011. Inflammation meets cancer, with NF-κB as the matchmaker. *Nat Immunol,* 12**,** 715-23.

BERGSTROM, P., ANDERSSON, H. C., GAO, Y., KARLSSON, J. O., NODIN, C., ANDERSON, M. F., NILSSON, M. & HAMMARSTEN, O. 2011. Repeated transient sulforaphane stimulation in astrocytes leads to prolonged Nrf2-mediated gene expression and protection from superoxide-induced damage. *Neuropharmacology,* 60**,** 343-53.

BHAMRE, S., SAHOO, D., TIBSHIRANI, R., DILL, D. L. & BROOKS, J. D. 2009. Temporal changes in gene expression induced by sulforaphane in human prostate cancer cells. *Prostate,* 69**,** 181-90.

BILLINGS, R. E., NOKER, P. E. & TEPHLY, T. R. 1981. The role of methionine in regulating folate-dependent reactions in isolated rat hepatocytes. *Arch Biochem Biophys,* 208**,** 108-20.

BISWAS, S. K., NEWBY, D. E., RAHMAN, I. & MEGSON, I. L. 2005. Depressed glutathione synthesis precedes oxidative stress and atherogenesis in Apo-E(-/-) mice. *Biochem Biophys Res Commun,* 338**,** 1368-73.

BLAAK, E. E., ANTOINE, J. M., BENTON, D., BJÖRCK, I., BOZZETTO, L., BROUNS, F., DIAMANT, M., DYE, L., HULSHOF, T., HOLST, J. J., LAMPORT, D. J., LAVILLE, M., LAWTON, C. L., MEHEUST, A., NILSON, A., NORMAND, S., RIVELLESE, A. A., THEIS, S., TOREKOV, S. S. & VINOY, S. 2012. Impact of postprandial glycaemia on health and prevention of disease. *Obesity reviews : an official journal of the International Association for the Study of Obesity,* 13**,** 923-984.

BLANCO, A. & BLANCO, G. 2017. Chapter 13 - Metabolism. *In:* BLANCO, A. & BLANCO, G. (eds.) *Medical Biochemistry.* Academic Press.

BLANK, V. 2008. Small Maf proteins in mammalian gene control: mere dimerization partners or dynamic transcriptional regulators? *J Mol Biol,* 376**,** 913-25.

BLAŽEVIĆ, I., MONTAUT, S., BURČUL, F. & ROLLIN, P. 2016. Glucosinolates: Novel Sources and Biological Potential. *In:* MÉRILLON, J.-M. & RAMAWAT, K. G. (eds.) *Glucosinolates.* Cham: Springer International Publishing.

BOISON, D., SCHEURER, L., ZUMSTEG, V., RÜLICKE, T., LITYNSKI, P., FOWLER, B., BRANDNER, S. & MOHLER, H. 2002. Neonatal hepatic steatosis by disruption of the adenosine kinase gene. *Proceedings of the National Academy of Sciences of the United States of America,* 99**,** 6985-6990.

BOLDYREV, A. A., ALDINI, G. & DERAVE, W. 2013. Physiology and pathophysiology of carnosine. *Physiol Rev,* 93**,** 1803-45.

BOLLONG, M. J., LEE, G., COUKOS, J. S., YUN, H., ZAMBALDO, C., CHANG, J. W., CHIN, E. N., AHMAD, I., CHATTERJEE, A. K., LAIRSON, L. L., SCHULTZ, P. G. & MOELLERING, R. E. 2018. A metabolite-derived protein modification integrates glycolysis with KEAP1–NRF2 signalling. *Nature,* 562**,** 600-604.

BRADSHAW, P. C. 2019. Cytoplasmic and Mitochondrial NADPH-Coupled Redox Systems in the Regulation of Aging. *Nutrients,* 11**,** 504.

BREMER, A. A., MIETUS-SNYDER, M. & LUSTIG, R. H. 2012. Toward a Unifying Hypothesis of Metabolic Syndrome. *Pediatrics,* 129**,** 557.

BREWER, A. C., MUSTAFI, S. B., MURRAY, T. V. A., RAJASEKARAN, N. S. & BENJAMIN, I. J. 2013. Reductive Stress Linked to Small HSPs, G6PD, and Nrf2 Pathways in Heart Disease. *Antioxidants & Redox Signaling,* 18**,** 1114-1127.

BROWN, B. E., KIM, C. H., TORPY, F. R., BURSILL, C. A., MCROBB, L. S., HEATHER, A. K., DAVIES, M. J. & VAN REYK, D. M. 2014. Supplementation with carnosine decreases plasma triglycerides and modulates atherosclerotic plaque composition in diabetic apo E(-/-) mice. *Atherosclerosis,* 232**,** 403-9.

BROWNLEE, M. 2001. Biochemistry and molecular cell biology of diabetic complications. *Nature,* 414**,** 813-20.

BRUNTZ, R. C., LANE, A. N., HIGASHI, R. M. & FAN, T. W. 2017. Exploring cancer metabolism using stable isotope-resolved metabolomics (SIRM). *J Biol Chem,* 292**,** 11601-11609.

BUDISAN, L., GULEI, D., ZANOAGA, O. M., IRIMIE, A. I., SERGIU, C., BRAICU, C., GHERMAN, C. D. & BERINDAN-NEAGOE, I. 2017. Dietary Intervention by Phytochemicals and Their Role in Modulating Coding and Non-Coding Genes in Cancer. *Int J Mol Sci,* 18.

BUESCHER, J. M., ANTONIEWICZ, M. R., BOROS, L. G., BURGESS, S. C., BRUNENGRABER, H., CLISH, C. B., DEBERARDINIS, R. J., FERON, O., FREZZA, C., GHESQUIERE, B., GOTTLIEB, E., HILLER, K., JONES, R. G., KAMPHORST, J. J., KIBBEY, R. G., KIMMELMAN, A. C., LOCASALE, J. W., LUNT, S. Y., MADDOCKS, O. D., MALLOY, C., METALLO, C. M., MEUILLET, E. J., MUNGER, J., NOH, K., RABINOWITZ, J. D., RALSER, M., SAUER, U., STEPHANOPOULOS, G., ST-PIERRE, J., TENNANT, D. A., WITTMANN, C., VANDER HEIDEN, M. G., VAZQUEZ, A., VOUSDEN, K., YOUNG, J. D., ZAMBONI, N. & FENDT, S. M. 2015. A roadmap for interpreting (13)C metabolite labeling patterns from cells. *Curr Opin Biotechnol,* 34**,** 189-201.

BURCZYNSKI, M. E., LIN, H. K. & PENNING, T. M. 1999. Isoform-specific induction of a human aldo-keto reductase by polycyclic aromatic hydrocarbons (PAHs), electrophiles, and oxidative stress: implications for the alternative pathway of PAH activation catalyzed by human dihydrodiol dehydrogenase. *Cancer Res,* 59**,** 607-14.

BURCZYNSKI, M. E. & PENNING, T. M. 2000. Genotoxic polycyclic aromatic hydrocarbon ortho-quinones generated by aldo-keto reductases induce CYP1A1 via nuclear translocation of the aryl hydrocarbon receptor. *Cancer Res,* 60**,** 908-15.

BURCZYNSKI, M. E., SRIDHAR, G. R., PALACKAL, N. T. & PENNING, T. M. 2001. The reactive oxygen species--and Michael acceptor-inducible human aldo-keto reductase AKR1C1 reduces the alpha,beta-unsaturated aldehyde 4-hydroxy-2-nonenal to 1,4-dihydroxy-2-nonene. *J Biol Chem,* 276**,** 2890-7.

BURNETT, J. P., LIM, G., LI, Y., SHAH, R. B., LIM, R., PAHOLAK, H. J., MCDERMOTT, S. P., SUN, L., TSUME, Y., BAI, S., WICHA, M. S., SUN, D. & ZHANG, T. 2017. Sulforaphane enhances

the anticancer activity of taxanes against triple negative breast cancer by killing cancer stem cells. *Cancer Lett,* 394**,** 52-64.

BUTLER, L. M., PERONE, Y., DEHAIRS, J., LUPIEN, L. E., DE LAAT, V., TALEBI, A., LODA, M., KINLAW, W. B. & SWINNEN, J. V. 2020. Lipids and cancer: Emerging roles in pathogenesis, diagnosis and therapeutic intervention. *Advanced Drug Delivery Reviews,* 159**,** 245-293.

BYRNE, P., CULLINAN, J. & SMITH, S. M. 2019. Statins for primary prevention of cardiovascular disease. *BMJ,* 367**,** l5674.

CAI, Z. & YAN, L. J. 2013. Protein Oxidative Modifications: Beneficial Roles in Disease and Health. *J Biochem Pharmacol Res,* 1**,** 15-26.

CANNING, P., COOPER, C. D., KROJER, T., MURRAY, J. W., PIKE, A. C., CHAIKUAD, A., KEATES, T., THANGARATNARAJAH, C., HOJZAN, V., AYINAMPUDI, V., MARSDEN, B. D., GILEADI, O., KNAPP, S., VON DELFT, F. & BULLOCK, A. N. 2013. Structural basis for Cul3 protein assembly with the BTB-Kelch family of E3 ubiquitin ligases. *J Biol Chem,* 288**,** 7803-14.

CARLSEN, M. H., HALVORSEN, B. L., HOLTE, K., BØHN, S. K., DRAGLAND, S., SAMPSON, L., WILLEY, C., SENOO, H., UMEZONO, Y., SANADA, C., BARIKMO, I., BERHE, N., WILLETT, W. C., PHILLIPS, K. M., JACOBS, D. R. & BLOMHOFF, R. 2010. The total antioxidant content of more than 3100 foods, beverages, spices, herbs and supplements used worldwide. *Nutrition Journal,* 9**,** 3.

CARRASCO-POZO, C., TAN, K. N., GOTTELAND, M. & BORGES, K. 2017. Sulforaphane Protects against High Cholesterol-Induced Mitochondrial Bioenergetics Impairments, Inflammation, and Oxidative Stress and Preserves Pancreatic beta-Cells Function. *Oxid Med Cell Longev,* 2017**,** 3839756.

CARRASCO-POZO, C., TAN, K. N., RODRIGUEZ, T. & AVERY, V. M. 2019. The Molecular Effects of Sulforaphane and Capsaicin on Metabolism upon Androgen and Tip60 Activation of Androgen Receptor. *Int J Mol Sci,* 20.

CARTA, G., MURRU, E., BANNI, S. & MANCA, C. 2017. Palmitic Acid: Physiological Role, Metabolism and Nutritional Implications. *Frontiers in physiology,* 8**,** 902-902.

CERIELLO, A., BORTOLOTTI, N., FALLETI, E., TABOGA, C., TONUTTI, L., CRESCENTINI, A., MOTZ, E., LIZZIO, S., RUSSO, A. & BARTOLI, E. 1997. Total radical-trapping antioxidant parameter in NIDDM patients. *Diabetes Care,* 20**,** 194-7.

CERIELLO, A. & MOTZ, E. 2004. Is oxidative stress the pathogenic mechanism underlying insulin resistance, diabetes, and cardiovascular disease? The common soil hypothesis revisited. *Arterioscler Thromb Vasc Biol,* 24**,** 816-23.

CHALASANI, N., YOUNOSSI, Z., LAVINE, J. E., CHARLTON, M., CUSI, K., RINELLA, M., HARRISON, S. A., BRUNT, E. M. & SANYAL, A. J. 2018. The diagnosis and management of nonalcoholic fatty liver disease: Practice guidance from the American Association for the Study of Liver Diseases. *Hepatology,* 67**,** 328-357.

CHAMBERS, K. F., BACON, J. R., KEMSLEY, E. K., MILLS, R. D., BALL, R. Y., MITHEN, R. F. & TRAKA, M. H. 2009. Gene expression profile of primary prostate epithelial and stromal cells in response to sulforaphane or iberin exposure. *Prostate,* 69**,** 1411-21.

CHAN, K., HAN, X. D. & KAN, Y. W. 2001. An important function of Nrf2 in combating oxidative stress: detoxification of acetaminophen. *Proc Natl Acad Sci U S A,* 98**,** 4611-6.

CHANDRASEKARAN, K., SWAMINATHAN, K., CHATTERJEE, S. & DEY, A. 2010. Apoptosis in HepG2 cells exposed to high glucose. *Toxicol In Vitro,* 24**,** 387-96.

CHANG, T.-Y., YAMAUCHI, Y., HASAN, M. T. & CHANG, C. 2017. Cellular cholesterol homeostasis and Alzheimer's disease. *Journal of lipid research,* 58**,** 2239-2254.

CHAO, S.-C., CHEN, Y.-J., HUANG, K.-H., KUO, K.-L., YANG, T.-H., HUANG, K.-Y., WANG, C.-C., TANG, C.-H., YANG, R.-S. & LIU, S.-H. 2017. Induction of sirtuin-1 signaling by resveratrol induces human chondrosarcoma cell apoptosis and exhibits antitumor activity. *Scientific Reports,* 7**,** 3180.

CHEN, J., CHUNG, F., YANG, G., PU, M., GAO, H., JIANG, W., YIN, H., CAPKA, V., KASIBHATLA, S., LAFFITTE, B., JAEGER, S., PAGLIARINI, R., CHEN, Y. & ZHOU, W. 2013. Phosphoglycerate

dehydrogenase is dispensable for breast tumor maintenance and growth. *Oncotarget,* 4**,** 2502-2511.
CHEN, W. C., WANG, C. Y., HUNG, Y. H., WENG, T. Y., YEN, M. C. & LAI, M. D. 2016a. Systematic Analysis of Gene Expression Alterations and Clinical Outcomes for Long-Chain Acyl-Coenzyme A Synthetase Family in Cancer. *PLoS One,* 11**,** e0155660.
CHEN, X., JIANG, Z., ZHOU, C., CHEN, K., LI, X., WANG, Z., WU, Z., MA, J., MA, Q. & DUAN, W. 2018. Activation of Nrf2 by Sulforaphane Inhibits High Glucose-Induced Progression of Pancreatic Cancer via AMPK Dependent Signaling. *Cell Physiol Biochem,* 50**,** 1201-1215.
CHEN, X. L., DODD, G. & KUNSCH, C. 2009. Sulforaphane inhibits TNF-alpha-induced activation of p38 MAP kinase and VCAM-1 and MCP-1 expression in endothelial cells. *Inflamm Res,* 58**,** 513-21.
CHEN, Y., YANG, S., HU, J., YU, C., HE, M. & CAI, Z. 2016b. Increased Expression of SETD7 Promotes Cell Proliferation by Regulating Cell Cycle and Indicates Poor Prognosis in Hepatocellular Carcinoma. *PLoS One,* 11**,** e0154939.
CHENG, A.-C., SHEN, C.-J., HUNG, C.-M. & HSU, Y.-C. 2019. Sulforaphane Decrease of SERTAD1 Expression Triggers G1/S Arrest in Breast Cancer Cells. *Journal of medicinal food,* 22**,** 444-450.
CHENG, C., NOORDELOOS, A. M., JENEY, V., SOARES, M. P., MOLL, F., PASTERKAMP, G., SERRUYS, P. W. & DUCKERS, H. J. 2009. Heme oxygenase 1 determines atherosclerotic lesion progression into a vulnerable plaque. *Circulation,* 119**,** 3017-27.
CHENG, F., TORZEWSKI, M., DEGREIF, A., ROSSMANN, H., CANISIUS, A. & LACKNER, K. J. 2013. Impact of glutathione peroxidase-1 deficiency on macrophage foam cell formation and proliferation: implications for atherogenesis. *PLoS One,* 8**,** e72063.
CHEPELEV, N. L., ZHANG, H., LIU, H., MCBRIDE, S., SEAL, A. J., MORGAN, T. E., FINCH, C. E., WILLMORE, W. G., DAVIES, K. J. & FORMAN, H. J. 2013. Competition of nuclear factor-erythroid 2 factors related transcription factor isoforms, Nrf1 and Nrf2, in antioxidant enzyme induction. *Redox Biol,* 1**,** 183-9.
CHEW, Y. C., ADHIKARY, G., WILSON, G. M., XU, W. & ECKERT, R. L. 2012. Sulforaphane induction of p21(Cip1) cyclin-dependent kinase inhibitor expression requires p53 and Sp1 transcription factors and is p53-dependent. *J Biol Chem,* 287**,** 16168-78.
CHIANG, J. Y. L. & FERRELL, J. M. 2018. Bile Acid Metabolism in Liver Pathobiology. *Gene expression,* 18**,** 71-87.
CHO, H.-Y., GLADWELL, W., WANG, X., CHORLEY, B., BELL, D., REDDY, S. P. & KLEEBERGER, S. R. 2010. Nrf2-regulated PPAR{gamma} expression is critical to protection against acute lung injury in mice. *American journal of respiratory and critical care medicine,* 182**,** 170-182.
CHOI, K. M., LEE, Y. S., KIM, W., KIM, S. J., SHIN, K. O., YU, J. Y., LEE, M. K., LEE, Y. M., HONG, J. T., YUN, Y. P. & YOO, H. S. 2014. Sulforaphane attenuates obesity by inhibiting adipogenesis and activating the AMPK pathway in obese mice. *J Nutr Biochem,* 25**,** 201-7.
CHORLEY, B. N., CAMPBELL, M. R., WANG, X., KARACA, M., SAMBANDAN, D., BANGURA, F., XUE, P., PI, J., KLEEBERGER, S. R. & BELL, D. A. 2012. Identification of novel NRF2-regulated genes by ChIP-Seq: influence on retinoid X receptor alpha. *Nucleic Acids Res,* 40**,** 7416-29.
CHOWDHRY, S., NAZMY, M. H., MEAKIN, P. J., DINKOVA-KOSTOVA, A. T., WALSH, S. V., TSUJITA, T., DILLON, J. F., ASHFORD, M. L. & HAYES, J. D. 2010. Loss of Nrf2 markedly exacerbates nonalcoholic steatohepatitis. *Free Radic Biol Med,* 48**,** 357-71.
CHUNG, F. L., JIAO, D., GETAHUN, S. M. & YU, M. C. 1998. A urinary biomarker for uptake of dietary isothiocyanates in humans. *Cancer Epidemiol Biomarkers Prev,* 7**,** 103-8.
CLARKE, J. D., DASHWOOD, R. H. & HO, E. 2008. Multi-targeted prevention of cancer by sulforaphane. *Cancer letters,* 269**,** 291-304.

CNOP, M., WELSH, N., JONAS, J. C., JORNS, A., LENZEN, S. & EIZIRIK, D. L. 2005. Mechanisms of pancreatic beta-cell death in type 1 and type 2 diabetes: many differences, few similarities. *Diabetes,* 54 Suppl 2**,** S97-107.

COHEN, R. A. & TONG, X. 2010. Vascular oxidative stress: the common link in hypertensive and diabetic vascular disease. *J Cardiovasc Pharmacol,* 55**,** 308-16.

COLEMAN, D. L. 1978. Obese and diabetes: Two mutant genes causing diabetes-obesity syndromes in mice. *Diabetologia,* 14**,** 141-148.

COODE-BATE, J., SIVAPALAN, T., MELCHINI, A., SAHA, S., NEEDS, P. W., DAINTY, J. R., MAICHA, J.-B., BEASY, G., TRAKA, M. H., MILLS, R. D., BALL, R. Y. & MITHEN, R. F. 2019. Accumulation of Dietary S-Methyl Cysteine Sulfoxide in Human Prostate Tissue. *Molecular nutrition & food research,* 63**,** e1900461-e1900461.

CORNBLATT, B. S., YE, L., DINKOVA-KOSTOVA, A. T., ERB, M., FAHEY, J. W., SINGH, N. K., CHEN, M. S., STIERER, T., GARRETT-MAYER, E., ARGANI, P., DAVIDSON, N. E., TALALAY, P., KENSLER, T. W. & VISVANATHAN, K. 2007. Preclinical and clinical evaluation of sulforaphane for chemoprevention in the breast. *Carcinogenesis,* 28**,** 1485-90.

COTTON, S. C., SHARP, L., LITTLE, J. & BROCKTON, N. 2000. Glutathione S-transferase polymorphisms and colorectal cancer: a HuGE review. *Am J Epidemiol,* 151**,** 7-32.

CULLINAN, S. B. & DIEHL, J. A. 2004. PERK-dependent activation of Nrf2 contributes to redox homeostasis and cell survival following endoplasmic reticulum stress. *J Biol Chem,* 279**,** 20108-17.

DA COSTA, R. M., RODRIGUES, D., PEREIRA, C. A., SILVA, J. F., ALVES, J. V., LOBATO, N. S. & TOSTES, R. C. 2019. Nrf2 as a Potential Mediator of Cardiovascular Risk in Metabolic Diseases. *Frontiers in Pharmacology,* 10.

DAMBACHER, S., HAHN, M. & SCHOTTA, G. 2010. Epigenetic regulation of development by histone lysine methylation. *Heredity,* 105**,** 24-37.

DASHTI, N. & WOLFBAUER, G. 1987. Secretion of lipids, apolipoproteins, and lipoproteins by human hepatoma cell line, HepG2: effects of oleic acid and insulin. *J Lipid Res,* 28**,** 423-36.

DASSATI, S., WALDNER, A. & SCHWEIGREITER, R. 2014. Apolipoprotein D takes center stage in the stress response of the aging and degenerative brain. *Neurobiol Aging,* 35**,** 1632-42.

DAVID, J. A., RIFKIN, W. J., RABBANI, P. S. & CERADINI, D. J. 2017. The Nrf2/Keap1/ARE Pathway and Oxidative Stress as a Therapeutic Target in Type II Diabetes Mellitus. *J Diabetes Res,* 2017**,** 4826724.

DAVIDSON, R. K., JUPP, O., DE FERRARS, R., KAY, C. D., CULLEY, K. L., NORTON, R., DRISCOLL, C., VINCENT, T. L., DONELL, S. T., BAO, Y. & CLARK, I. M. 2013. Sulforaphane represses matrix-degrading proteases and protects cartilage from destruction in vitro and in vivo. *Arthritis and rheumatism,* 65**,** 3130-3140.

DE LA IGLESIA, R., LORIA-KOHEN, V., ZULET, M. A., MARTINEZ, J. A., REGLERO, G. & RAMIREZ DE MOLINA, A. 2016. Dietary Strategies Implicated in the Prevention and Treatment of Metabolic Syndrome. *International journal of molecular sciences,* 17**,** 1877.

DEBERARDINIS, R. J. & THOMPSON, C. B. 2012. Cellular metabolism and disease: what do metabolic outliers teach us? *Cell,* 148**,** 1132-1144.

DEL RIZZO, P. A. & TRIEVEL, R. C. 2011. Substrate and product specificities of SET domain methyltransferases. *Epigenetics,* 6**,** 1059-1067.

DENICOLA, G. M., CHEN, P.-H., MULLARKY, E., SUDDERTH, J. A., HU, Z., WU, D., TANG, H., XIE, Y., ASARA, J. M., HUFFMAN, K. E., WISTUBA, I. I., MINNA, J. D., DEBERARDINIS, R. J. & CANTLEY, L. C. 2015. NRF2 regulates serine biosynthesis in non-small cell lung cancer. *Nature genetics,* 47**,** 1475-1481.

DENISON, M. S., FISHER, J. M. & WHITLOCK, J. P., JR. 1988. The DNA recognition site for the dioxin-Ah receptor complex. Nucleotide sequence and functional analysis. *J Biol Chem,* 263**,** 17221-4.

DENISON, M. S., FISHER, J. M. & WHITLOCK, J. P., JR. 1989. Protein-DNA interactions at recognition sites for the dioxin-Ah receptor complex. *J Biol Chem,* 264**,** 16478-82.

DEOROSAN, B. & NAUMAN, E. A. 2011. The Role of Glucose, Serum, and Three-Dimensional Cell Culture on the Metabolism of Bone Marrow-Derived Mesenchymal Stem Cells. *Stem Cells International,* 2011**,** 429187.

DERAVE, W., EVERAERT, I., BEECKMAN, S. & BAGUET, A. 2010. Muscle carnosine metabolism and beta-alanine supplementation in relation to exercise and training. *Sports Med,* 40**,** 247-63.

DEVLING, T. W. P., LINDSAY, C. D., MCLELLAN, L. I., MCMAHON, M. & HAYES, J. D. 2005. Utility of siRNA against Keap1 as a strategy to stimulate a cancer chemopreventive phenotype. *Proceedings of the National Academy of Sciences of the United States of America,* 102**,** 7280-7285.

DING, C., LI, Y., GUO, F., JIANG, Y., YING, W., LI, D., YANG, D., XIA, X., LIU, W., ZHAO, Y., HE, Y., LI, X., SUN, W., LIU, Q., SONG, L., ZHEN, B., ZHANG, P., QIAN, X., QIN, J. & HE, F. 2016. A Cell-type-resolved Liver Proteome*. *Molecular & Cellular Proteomics,* 15**,** 3190-3202.

DINKOVA-KOSTOVA, A. T. & ABRAMOV, A. Y. 2015. The emerging role of Nrf2 in mitochondrial function. *Free Radic Biol Med,* 88**,** 179-188.

DINKOVA-KOSTOVA, A. T., FAHEY, J. W., WADE, K. L., JENKINS, S. N., SHAPIRO, T. A., FUCHS, E. J., KERNS, M. L. & TALALAY, P. 2007. Induction of the phase 2 response in mouse and human skin by sulforaphane-containing broccoli sprout extracts. *Cancer Epidemiol Biomarkers Prev,* 16**,** 847-51.

DINKOVA-KOSTOVA, A. T. & TALALAY, P. 2000. Persuasive evidence that quinone reductase type 1 (DT diaphorase) protects cells against the toxicity of electrophiles and reactive forms of oxygen11This paper is dedicated with admiration to the memory of Professor Lars Ernster, whose name will be identified forever with DT diaphorase. *Free Radical Biology and Medicine,* 29**,** 231-240.

DONATO, M. T., TOLOSA, L. & GÓMEZ-LECHÓN, M. J. 2015. Culture and Functional Characterization of Human Hepatoma HepG2 Cells. *In:* VINKEN, M. & ROGIERS, V. (eds.) *Protocols in In Vitro Hepatocyte Research.* New York, NY: Springer New York.

DOS SANTOS, P., MACHADO, A. R. T., DE GRANDIS, R. A., RIBEIRO, D. L., TUTTIS, K., MORSELLI, M., AISSA, A. F., PELLEGRINI, M. & ANTUNES, L. M. G. 2020. Transcriptome and DNA methylation changes modulated by sulforaphane induce cell cycle arrest, apoptosis, DNA damage, and suppression of proliferation in human liver cancer cells. *Food Chem Toxicol,* 136**,** 111047.

DU, K., FAN, Y. & LI, D. 2021. Sulforaphane ameliorates lipid profile in rodents: an updated systematic review and meta-analysis. *Scientific Reports,* 11**,** 7804.

DUAN, Y., ZENG, L., ZHENG, C., SONG, B., LI, F., KONG, X. & XU, K. 2018. Inflammatory Links Between High Fat Diets and Diseases. *Frontiers in immunology,* 9**,** 2649-2649.

DUCKER, G. S., CHEN, L., MORSCHER, R. J., GHERGUROVICH, J. M., ESPOSITO, M., TENG, X., KANG, Y. & RABINOWITZ, J. D. 2016. Reversal of Cytosolic One-Carbon Flux Compensates for Loss of the Mitochondrial Folate Pathway. *Cell Metab,* 24**,** 640-641.

DUCKER, G. S. & RABINOWITZ, J. D. 2017. One-Carbon Metabolism in Health and Disease. *Cell metabolism,* 25**,** 27-42.

EDGERTON, D. S., LAUTZ, M., SCOTT, M., EVERETT, C. A., STETTLER, K. M., NEAL, D. W., CHU, C. A. & CHERRINGTON, A. D. 2006. Insulin's direct effects on the liver dominate the control of hepatic glucose production. *The Journal of clinical investigation,* 116**,** 521-527.

ELMARAKBY, A. A. & SULLIVAN, J. C. 2012. Relationship between oxidative stress and inflammatory cytokines in diabetic nephropathy. *Cardiovasc Ther,* 30**,** 49-59.

EMERSON, S. R., SCIARRILLO, C. M., KURTI, S. P., EMERSON, E. M. & ROSENKRANZ, S. K. 2018. High-Fat Meal–Induced Changes in Markers of Inflammation and Angiogenesis in Healthy Adults Who Differ by Age and Physical Activity Level. *Current Developments in Nutrition,* 3.

ESPOSITO, K., CHIODINI, P., COLAO, A., LENZI, A. & GIUGLIANO, D. 2012. Metabolic syndrome and risk of cancer: a systematic review and meta-analysis. *Diabetes care,* 35**,** 2402-2411.

FABBRINI, E., CONTE, C. & MAGKOS, F. 2009. Methods for assessing intrahepatic fat content and steatosis. *Curr Opin Clin Nutr Metab Care,* 12**,** 474-81.

FAHEY, J. W., ZALCMANN, A. T. & TALALAY, P. 2001. The chemical diversity and distribution of glucosinolates and isothiocyanates among plants. *Phytochemistry,* 56**,** 5-51.

FAN, Y. & PEDERSEN, O. 2021. Gut microbiota in human metabolic health and disease. *Nature Reviews Microbiology,* 19**,** 55-71.

FANG, L., ZHANG, L., WEI, W., JIN, X., WANG, P., TONG, Y., LI, J., DU, J. X. & WONG, J. 2014. A methylation-phosphorylation switch determines Sox2 stability and function in ESC maintenance or differentiation. *Mol Cell,* 55**,** 537-51.

FARHANA, A., GUIDRY, L., SRIVASTAVA, A., SINGH, A., HONDALUS, M. K. & STEYN, A. J. C. 2010. Reductive Stress in Microbes: Implications for Understanding Mycobacterium tuberculosis Disease and Persistence. *In:* POOLE, R. K. (ed.) *Advances in Microbial Physiology.* Academic Press.

FARSHID, A. A., TAMADDONFARD, E., SIMAEE, N., MANSOURI, S., NAJAFI, S., ASRI-REZAEE, S. & ALAVI, H. 2014. Effects of histidine and N-acetylcysteine on doxorubicin-induced cardiomyopathy in rats. *Cardiovasc Toxicol,* 14**,** 153-61.

FAVREAU, L. V. & PICKETT, C. B. 1991. Transcriptional regulation of the rat NAD(P)H:quinone reductase gene. Identification of regulatory elements controlling basal level expression and inducible expression by planar aromatic compounds and phenolic antioxidants. *J Biol Chem,* 266**,** 4556-61.

FELL, D. & STEELE, R. D. 1983. Effect of methionine on in vivo histidine metabolism in rats. *J Nutr,* 113**,** 860-6.

FERNÁNDEZ, L. P., GÓMEZ DE CEDRÓN, M. & RAMÍREZ DE MOLINA, A. 2020. Alterations of Lipid Metabolism in Cancer: Implications in Prognosis and Treatment. *Frontiers in Oncology,* 10.

FERREIRA DE OLIVEIRA, J. M., REMÉDIOS, C., OLIVEIRA, H., PINTO, P., PINHO, F., PINHO, S., COSTA, M. & SANTOS, C. 2014. Sulforaphane induces DNA damage and mitotic abnormalities in human osteosarcoma MG-63 cells: correlation with cell cycle arrest and apoptosis. *Nutr Cancer,* 66**,** 325-34.

FERRICK, D. A., NEILSON, A. & BEESON, C. 2008. Advances in measuring cellular bioenergetics using extracellular flux. *Drug Discov Today,* 13**,** 268-74.

FINKELSTEIN, J. D. 1998. The metabolism of homocysteine: pathways and regulation. *European Journal of Pediatrics,* 157**,** S40-S44.

FLORA, G. D. & NAYAK, M. K. 2019. A Brief Review of Cardiovascular Diseases, Associated Risk Factors and Current Treatment Regimes. *Curr Pharm Des,* 25**,** 4063-4084.

FOLKARD, D. L., MELCHINI, A., TRAKA, M. H., AL-BAKHEIT, A., SAHA, S., MULHOLLAND, F., WATSON, A. & MITHEN, R. F. 2014. Suppression of LPS-induced transcription and cytokine secretion by the dietary isothiocyanate sulforaphane. *Mol Nutr Food Res,* 58**,** 2286-96.

FOURQUET, S., GUEROIS, R., BIARD, D. & TOLEDANO, M. B. 2010. Activation of NRF2 by nitrosative agents and H2O2 involves KEAP1 disulfide formation. *J Biol Chem,* 285**,** 8463-71.

FRAU, M., FEO, F. & PASCALE, R. M. 2013. Pleiotropic effects of methionine adenosyltransferases deregulation as determinants of liver cancer progression and prognosis. *Journal of Hepatology,* 59**,** 830-841.

FRIBERG, E., MANTZOROS, C. S. & WOLK, A. 2007. Diabetes and risk of endometrial cancer: a population-based prospective cohort study. *Cancer Epidemiol Biomarkers Prev,* 16**,** 276-80.

FRIEDMAN, S. L., NEUSCHWANDER-TETRI, B. A., RINELLA, M. & SANYAL, A. J. 2018. Mechanisms of NAFLD development and therapeutic strategies. *Nature Medicine,* 24**,** 908-922.

FRILING, R. S., BENSIMON, A., TICHAUER, Y. & DANIEL, V. 1990. Xenobiotic-inducible expression of murine glutathione S-transferase Ya subunit gene is controlled by an electrophile-responsive element. *Proceedings of the National Academy of Sciences,* 87**,** 6258-6262.

FUJII, S., SAWA, T., IHARA, H., TONG, K. I., IDA, T., OKAMOTO, T., AHTESHAM, A. K., ISHIMA, Y., MOTOHASHI, H., YAMAMOTO, M. & AKAIKE, T. 2010. The critical role of nitric oxide signaling, via protein S-guanylation and nitrated cyclic GMP, in the antioxidant adaptive response. *J Biol Chem,* 285**,** 23970-84.

FUJIMOTO, S., MUKAI, E. & INAGAKI, N. 2011. Role of endogenous ROS production in impaired metabolism-secretion coupling of diabetic pancreatic beta cells. *Prog Biophys Mol Biol,* 107**,** 304-10.

FUKUTOMI, T., TAKAGI, K., MIZUSHIMA, T., OHUCHI, N. & YAMAMOTO, M. 2014. Kinetic, thermodynamic, and structural characterizations of the association between Nrf2-DLGex degron and Keap1. *Mol Cell Biol,* 34**,** 832-46.

FUNTIKOVA, A. N., NAVARRO, E., BAWAKED, R. A., FÍTO, M. & SCHRÖDER, H. 2015. Impact of diet on cardiometabolic health in children and adolescents. *Nutrition journal,* 14**,** 118-118.

GAO, C., ZHUANG, J., LI, H., LIU, C., ZHOU, C., LIU, L., FENG, F., SUN, C. & WU, J. 2020. Development of a risk scoring system for evaluating the prognosis of patients with Her2-positive breast cancer. *Cancer Cell Int,* 20**,** 121.

GAO, X., DINKOVA-KOSTOVA, A. T. & TALALAY, P. 2001. Powerful and prolonged protection of human retinal pigment epithelial cells, keratinocytes, and mouse leukemia cells against oxidative damage: The indirect antioxidant effects of sulforaphane. *Proceedings of the National Academy of Sciences,* 98**,** 15221-15226.

GARCÍA-RUIZ, I., SOLÍS-MUÑOZ, P., FERNÁNDEZ-MOREIRA, D., MUÑOZ-YAGÜE, T. & SOLÍS-HERRUZO, J. A. 2015. In vitro treatment of HepG2 cells with saturated fatty acids reproduces mitochondrial dysfunction found in nonalcoholic steatohepatitis. *Disease models & mechanisms,* 8**,** 183-191.

GASPER, A. V., AL-JANOBI, A., SMITH, J. A., BACON, J. R., FORTUN, P., ATHERTON, C., TAYLOR, M. A., HAWKEY, C. J., BARRETT, D. A. & MITHEN, R. F. 2005. Glutathione S-transferase M1 polymorphism and metabolism of sulforaphane from standard and high-glucosinolate broccoli. *Am J Clin Nutr,* 82**,** 1283-91.

GATENBY, R. A. & GILLIES, R. J. 2007. Glycolysis in cancer: a potential target for therapy. *Int J Biochem Cell Biol,* 39**,** 1358-66.

GE, T., YANG, J., ZHOU, S., WANG, Y., LI, Y. & TONG, X. 2020. The Role of the Pentose Phosphate Pathway in Diabetes and Cancer. *Frontiers in Endocrinology,* 11.

GEIDL-FLUECK, B., HOCHULI, M., NÉMETH, Á., EBERL, A., DERRON, N., KÖFELER, H. C., TAPPY, L., BERNEIS, K., SPINAS, G. A. & GERBER, P. A. 2021. Fructose- and sucrose- but not glucose-sweetened beverages promote hepatic de novo lipogenesis: A randomized controlled trial. *Journal of Hepatology,* 75**,** 46-54.

GENG, Y., HERNÁNDEZ VILLANUEVA, A., OUN, A., BUIST-HOMAN, M., BLOKZIJL, H., FABER, K. N., DOLGA, A. & MOSHAGE, H. 2020. Protective effect of metformin against palmitate-induced hepatic cell death. *Biochimica et Biophysica Acta (BBA) - Molecular Basis of Disease,* 1866**,** 165621.

GLEN, J., FLOROS, L., DAY, C. & PRYKE, R. 2016. Non-alcoholic fatty liver disease (NAFLD): summary of NICE guidance. *BMJ,* 354**,** i4428.

GOMES, ANA P., PRICE, NATHAN L., LING, ALVIN J. Y., MOSLEHI, JAVID J., MONTGOMERY, M. K., RAJMAN, L., WHITE, JAMES P., TEODORO, JOÃO S., WRANN, CHRISTIANE D., HUBBARD, BASIL P., MERCKEN, EVI M., PALMEIRA, CARLOS M., DE CABO, R., ROLO, ANABELA P., TURNER, N., BELL, ERIC L. & SINCLAIR, DAVID A. 2013. Declining NAD+

Induces a Pseudohypoxic State Disrupting Nuclear-Mitochondrial Communication during Aging. *Cell,* 155**,** 1624-1638.
GRANDÉR, D. 1998. How do mutated oncogenes and tumor suppressor genes cause cancer? *Medical Oncology,* 15**,** 20-26.
GROTH, A., ROCHA, W., VERREAULT, A. & ALMOUZNI, G. 2007. Chromatin Challenges during DNA Replication and Repair. *Cell,* 128**,** 721-733.
HAĆ, A., BROKOWSKA, J., RINTZ, E., BARTKOWSKI, M., WĘGRZYN, G. & HERMAN-ANTOSIEWICZ, A. 2020. Mechanism of selective anticancer activity of isothiocyanates relies on differences in DNA damage repair between cancer and healthy cells. *European Journal of Nutrition,* 59**,** 1421-1432.
HAGIWARA, A., CORNU, M., CYBULSKI, N., POLAK, P., BETZ, C., TRAPANI, F., TERRACCIANO, L., HEIM, M. H., RÜEGG, M. A. & HALL, M. N. 2012. Hepatic mTORC2 activates glycolysis and lipogenesis through Akt, glucokinase, and SREBP1c. *Cell Metab,* 15**,** 725-38.
HAIGIS, M. C. & YANKNER, B. A. 2010. The aging stress response. *Mol Cell,* 40**,** 333-44.
HANAHAN, D. & WEINBERG, R. A. 2000. The hallmarks of cancer. *Cell,* 100**,** 57-70.
HANAHAN, D. & WEINBERG, R. A. 2011. Hallmarks of cancer: the next generation. *Cell,* 144**,** 646-74.
HANSEN, R. E., ROTH, D. & WINTHER, J. R. 2009. Quantifying the global cellular thiol–disulfide status. *Proceedings of the National Academy of Sciences,* 106**,** 422-427.
HASSAN, S., SEBASTIAN, S., MAHARJAN, S., LESHA, A., CARPENTER, A.-M., LIU, X., XIE, X., LIVERMORE, C., ZHANG, Y. S. & ZARRINPAR, A. 2020. Liver-on-a-Chip Models of Fatty Liver Disease. *Hepatology,* 71**,** 733-740.
HAWKES, H. J., KARLENIUS, T. C. & TONISSEN, K. F. 2014. Regulation of the human thioredoxin gene promoter and its key substrates: a study of functional and putative regulatory elements. *Biochim Biophys Acta,* 1840**,** 303-14.
HAYES, J. D., CHANAS, S. A., HENDERSON, C. J., MCMAHON, M., SUN, C., MOFFAT, G. J., WOLF, C. R. & YAMAMOTO, M. 2000. The Nrf2 transcription factor contributes both to the basal expression of glutathione S-transferases in mouse liver and to their induction by the chemopreventive synthetic antioxidants, butylated hydroxyanisole and ethoxyquin. *Biochemical Society Transactions,* 28**,** 33-41.
HAYES, J. D. & DINKOVA-KOSTOVA, A. T. 2014. The Nrf2 regulatory network provides an interface between redox and intermediary metabolism. *Trends Biochem Sci,* 39**,** 199-218.
HAYES, J. D., FLANAGAN, J. U. & JOWSEY, I. R. 2005. Glutathione transferases. *Annu Rev Pharmacol Toxicol,* 45**,** 51-88.
HAYES, J. D., MCMAHON, M., CHOWDHRY, S. & DINKOVA-KOSTOVA, A. T. 2010. Cancer Chemoprevention Mechanisms Mediated Through the Keap1–Nrf2 Pathway. *Antioxidants & Redox Signaling,* 13**,** 1713-1748.
HAYES, J. D. & STRANGE, R. C. 2000. Glutathione S-transferase polymorphisms and their biological consequences. *Pharmacology,* 61**,** 154-66.
HE, X., KAN, H., CAI, L. & MA, Q. 2009. Nrf2 is critical in defense against high glucose-induced oxidative damage in cardiomyocytes. *Journal of Molecular and Cellular Cardiology,* 46**,** 47-58.
HECHT, S. S. 2000. Inhibition of carcinogenesis by isothiocyanates. *Drug Metab Rev,* 32**,** 395-411.
HEISS, E., HERHAUS, C., KLIMO, K., BARTSCH, H. & GERHÄUSER, C. 2001. Nuclear factor kappa B is a molecular target for sulforaphane-mediated anti-inflammatory mechanisms. *J Biol Chem,* 276**,** 32008-15.
HEISS, E. H., SCHACHNER, D., ZIMMERMANN, K. & DIRSCH, V. M. 2013. Glucose availability is a decisive factor for Nrf2-mediated gene expression. *Redox Biol,* 1**,** 359-65.
HERCULANO, B., TAMURA, M., OHBA, A., SHIMATANI, M., KUTSUNA, N. & HISATSUNE, T. 2013. β-alanyl-L-histidine rescues cognitive deficits caused by feeding a high fat diet in a transgenic mouse model of Alzheimer's disease. *J Alzheimers Dis,* 33**,** 983-97.

HERIEKA, M. & ERRIDGE, C. 2014. High-fat meal induced postprandial inflammation. *Mol Nutr Food Res,* 58**,** 136-46.
HERR, I. & BUCHLER, M. W. 2010. Dietary constituents of broccoli and other cruciferous vegetables: implications for prevention and therapy of cancer. *Cancer Treat Rev,* 36**,** 377-83.
HERZIG, S. & SHAW, R. J. 2018. AMPK: guardian of metabolism and mitochondrial homeostasis. *Nature Reviews Molecular Cell Biology,* 19**,** 121-135.
HEWLINGS, S. J. & KALMAN, D. S. 2017. Curcumin: A Review of Its Effects on Human Health. *Foods (Basel, Switzerland),* 6**,** 92.
HIGGINS, L. G. & HAYES, J. D. 2011. Mechanisms of induction of cytosolic and microsomal glutathione transferase (GST) genes by xenobiotics and pro-inflammatory agents. *Drug Metabolism Reviews,* 43**,** 92-137.
HIGGINS, L. G., KELLEHER, M. O., EGGLESTON, I. M., ITOH, K., YAMAMOTO, M. & HAYES, J. D. 2009. Transcription factor Nrf2 mediates an adaptive response to sulforaphane that protects fibroblasts in vitro against the cytotoxic effects of electrophiles, peroxides and redox-cycling agents. *Toxicology and Applied Pharmacology,* 237**,** 267-280.
HILLER, K., HANGEBRAUK, J., JÄGER, C., SPURA, J., SCHREIBER, K. & SCHOMBURG, D. 2009. MetaboliteDetector: comprehensive analysis tool for targeted and nontargeted GC/MS based metabolome analysis. *Anal Chem,* 81**,** 3429-39.
HIROTSU, Y., KATSUOKA, F., FUNAYAMA, R., NAGASHIMA, T., NISHIDA, Y., NAKAYAMA, K., ENGEL, J. D. & YAMAMOTO, M. 2012. Nrf2-MafG heterodimers contribute globally to antioxidant and metabolic networks. *Nucleic Acids Res,* 40**,** 10228-39.
HOCHMUTH, C. E., BITEAU, B., BOHMANN, D. & JASPER, H. 2011. Redox Regulation by Keap1 and Nrf2 Controls Intestinal Stem Cell Proliferation in Drosophila. *Cell Stem Cell,* 8**,** 188-199.
HOLEČEK, M. 2020. Histidine in Health and Disease: Metabolism, Physiological Importance, and Use as a Supplement. *Nutrients,* 12**,** 848.
HOLEČEK, M. & VODENIČAROVOVÁ, M. 2019. Effects of histidine load on ammonia, amino acid, and adenine nucleotide concentrations in rats. *Amino Acids,* 51**,** 1667-1680.
HOLMGREN, A. & LU, J. 2010. Thioredoxin and thioredoxin reductase: current research with special reference to human disease. *Biochem Biophys Res Commun,* 396**,** 120-4.
HOLMSTROM, K. M., BAIRD, L., ZHANG, Y., HARGREAVES, I., CHALASANI, A., LAND, J. M., STANYER, L., YAMAMOTO, M., DINKOVA-KOSTOVA, A. T. & ABRAMOV, A. Y. 2013. Nrf2 impacts cellular bioenergetics by controlling substrate availability for mitochondrial respiration. *Biol Open,* 2**,** 761-70.
HOLMSTRÖM, K. M., BAIRD, L., ZHANG, Y., HARGREAVES, I., CHALASANI, A., LAND, J. M., STANYER, L., YAMAMOTO, M., DINKOVA-KOSTOVA, A. T. & ABRAMOV, A. Y. 2013. Nrf2 impacts cellular bioenergetics by controlling substrate availability for mitochondrial respiration. *Biology Open,* 2**,** 761-770.
HOLST, B. & WILLIAMSON, G. 2004. A critical review of the bioavailability of glucosinolates and related compounds. *Nat Prod Rep,* 21**,** 425-47.
HOTA, K. B., HOTA, S. K., CHAURASIA, O. P. & SINGH, S. B. 2012. Acetyl-L-carnitine-mediated neuroprotection during hypoxia is attributed to ERK1/2-Nrf2-regulated mitochondrial biosynthesis. *Hippocampus,* 22**,** 723-36.
HOUGHTON, C. A. 2019. Sulforaphane: Its "Coming of Age" as a Clinically Relevant Nutraceutical in the Prevention and Treatment of Chronic Disease. *Oxid Med Cell Longev,* 2019**,** 2716870.
HOUGHTON, C. A., FASSETT, R. G. & COOMBES, J. S. 2016. Sulforaphane and Other Nutrigenomic Nrf2 Activators: Can the Clinician's Expectation Be Matched by the Reality? *Oxid Med Cell Longev,* 2016**,** 7857186.
HSU, A., WONG, C. P., YU, Z., WILLIAMS, D. E., DASHWOOD, R. H. & HO, E. 2011. Promoter de-methylation of cyclin D2 by sulforaphane in prostate cancer cells. *Clinical Epigenetics,* 3**,** 3.

HUANG, J., FAN, X. X., HE, J., PAN, H., LI, R. Z., HUANG, L., JIANG, Z., YAO, X. J., LIU, L., LEUNG, E. L. & HE, J. X. 2016. SCD1 is associated with tumor promotion, late stage and poor survival in lung adenocarcinoma. *Oncotarget,* 7**,** 39970-39979.

HURRLE, S. & HSU, W. H. 2017. The etiology of oxidative stress in insulin resistance. *Biomedical journal,* 40**,** 257-262.

IDO, Y. & WILLIAMSON, J. R. 1997. Hyperglycemic cytosolic reductive stress 'pseudohypoxia': implications for diabetic retinopathy. *Investigative Ophthalmology & Visual Science,* 38**,** 1467-1470.

INSULL, W. 2009. The Pathology of Atherosclerosis: Plaque Development and Plaque Responses to Medical Treatment. *The American Journal of Medicine,* 122**,** S3-S14.

IOVINE, B., OLIVIERO, G., GAROFALO, M., OREFICE, M., NOCELLA, F., BORBONE, N., PICCIALLI, V., CENTORE, R., MAZZONE, M., PICCIALLI, G. & BEVILACQUA, M. A. 2014. The anti-proliferative effect of L-carnosine correlates with a decreased expression of hypoxia inducible factor 1 alpha in human colon cancer cells. *PLoS One,* 9**,** e96755.

ISHII, M., MAEDA, A., TANI, S. & AKAGAWA, M. 2015. Palmitate induces insulin resistance in human HepG2 hepatocytes by enhancing ubiquitination and proteasomal degradation of key insulin signaling molecules. *Arch Biochem Biophys,* 566**,** 26-35.

ISHII, T., ITOH, K., RUIZ, E., LEAKE, D. S., UNOKI, H., YAMAMOTO, M. & MANN, G. E. 2004. Role of Nrf2 in the Regulation of CD36 and Stress Protein Expression in Murine Macrophages. *Circulation Research,* 94**,** 609-616.

ISHII, T., ITOH, K., TAKAHASHI, S., SATO, H., YANAGAWA, T., KATOH, Y., BANNAI, S. & YAMAMOTO, M. 2000. Transcription factor Nrf2 coordinately regulates a group of oxidative stress-inducible genes in macrophages. *J Biol Chem,* 275**,** 16023-9.

ITOH, K., CHIBA, T., TAKAHASHI, S., ISHII, T., IGARASHI, K., KATOH, Y., OYAKE, T., HAYASHI, N., SATOH, K., HATAYAMA, I., YAMAMOTO, M. & NABESHIMA, Y. 1997. An Nrf2/small Maf heterodimer mediates the induction of phase II detoxifying enzyme genes through antioxidant response elements. *Biochem Biophys Res Commun,* 236**,** 313-22.

ITOH, K., IGARASHI, K., HAYASHI, N., NISHIZAWA, M. & YAMAMOTO, M. 1995. Cloning and characterization of a novel erythroid cell-derived CNC family transcription factor heterodimerizing with the small Maf family proteins. *Mol Cell Biol,* 15**,** 4184-93.

ITOH, K., WAKABAYASHI, N., KATOH, Y., ISHII, T., IGARASHI, K., ENGEL, J. D. & YAMAMOTO, M. 1999. Keap1 represses nuclear activation of antioxidant responsive elements by Nrf2 through binding to the amino-terminal Neh2 domain. *Genes Dev,* 13**,** 76-86.

ITOH, K., YE, P., MATSUMIYA, T., TANJI, K. & OZAKI, T. 2015. Emerging functional cross-talk between the Keap1-Nrf2 system and mitochondria. *J Clin Biochem Nutr,* 56**,** 91-7.

JAISWAL, A. K. 1991. Human NAD(P)H:quinone oxidoreductase (NQO1) gene structure and induction by dioxin. *Biochemistry,* 30**,** 10647-10653.

JARBØL, D. E., LARSEN, P. V., GYRD-HANSEN, D., SØNDERGAARD, J., BRANDT, C., LEPPIN, A., BARFOED, B. L. & NIELSEN, J. B. 2017. Determinants of preferences for lifestyle changes versus medication and beliefs in ability to maintain lifestyle changes. A population-based survey. *Preventive medicine reports,* 6**,** 66-73.

JAVITT, N. B. 1990. Hep G2 cells as a resource for metabolic studies: lipoprotein, cholesterol, and bile acids. *Faseb j,* 4**,** 161-8.

JEE, S. H., KIM, H. J. & LEE, J. 2005. Obesity, insulin resistance and cancer risk. *Yonsei medical journal,* 46**,** 449-455.

JELKMANN, W. 2001. The role of the liver in the production of thrombopoietin compared with erythropoietin. *Eur J Gastroenterol Hepatol,* 13**,** 791-801.

JIANG, F. & DOUDNA, J. A. 2017. CRISPR-Cas9 Structures and Mechanisms. *Annu Rev Biophys,* 46**,** 505-529.

JIN, Y., DUAN, L., CHEN, M., PENNING, T. M. & KLOOSTERBOER, H. J. 2012. Metabolism of the synthetic progestogen norethynodrel by human ketosteroid reductases of the aldo-keto reductase superfamily. *J Steroid Biochem Mol Biol,* 129**,** 139-44.

JOSEPH, M. A., MOYSICH, K. B., FREUDENHEIM, J. L., SHIELDS, P. G., BOWMAN, E. D., ZHANG, Y., MARSHALL, J. R. & AMBROSONE, C. B. 2004. Cruciferous vegetables, genetic polymorphisms in glutathione S-transferases M1 and T1, and prostate cancer risk. *Nutr Cancer,* 50**,** 206-13.

JU, H.-Q., LIN, J.-F., TIAN, T., XIE, D. & XU, R.-H. 2020. NADPH homeostasis in cancer: functions, mechanisms and therapeutic implications. *Signal Transduction and Targeted Therapy,* 5**,** 231.

JUAN, C. A., PÉREZ DE LA LASTRA, J. M., PLOU, F. J. & PÉREZ-LEBEÑA, E. 2021. The Chemistry of Reactive Oxygen Species (ROS) Revisited: Outlining Their Role in Biological Macromolecules (DNA, Lipids and Proteins) and Induced Pathologies. *International Journal of Molecular Sciences,* 22**,** 4642.

JUGE, N., MITHEN, R. F. & TRAKA, M. 2007. Molecular basis for chemoprevention by sulforaphane: a comprehensive review. *Cell Mol Life Sci,* 64**,** 1105-27.

JUNG, K.-A., CHOI, B.-H., NAM, C.-W., SONG, M., KIM, S.-T., LEE, J. Y. & KWAK, M.-K. 2013. Identification of aldo-keto reductases as NRF2-target marker genes in human cells. *Toxicology Letters,* 218**,** 39-49.

KAHN, S. E., HULL, R. L. & UTZSCHNEIDER, K. M. 2006. Mechanisms linking obesity to insulin resistance and type 2 diabetes. *Nature,* 444**,** 840-6.

KALLIFATIDIS, G., RAUSCH, V., BAUMANN, B., APEL, A., BECKERMANN, B. M., GROTH, A., MATTERN, J., LI, Z., KOLB, A., MOLDENHAUER, G., ALTEVOGT, P., WIRTH, T., WERNER, J., SCHEMMER, P., BÜCHLER, M. W., SALNIKOV, A. V. & HERR, I. 2009. Sulforaphane targets pancreatic tumour-initiating cells by NF-κB-induced antiapoptotic signalling. *Gut,* 58**,** 949-963.

KAMAL, M. M., AKTER, S., LIN, C.-N. & NAZZAL, S. 2020. Sulforaphane as an anticancer molecule: mechanisms of action, synergistic effects, enhancement of drug safety, and delivery systems. *Archives of Pharmacal Research,* 43**,** 371-384.

KAMRAN, M. Z., PATIL, P. & GUDE, R. P. 2013. Role of STAT3 in cancer metastasis and translational advances. *Biomed Res Int,* 2013**,** 421821.

KANEHISA, M., FURUMICHI, M., TANABE, M., SATO, Y. & MORISHIMA, K. 2017. KEGG: new perspectives on genomes, pathways, diseases and drugs. *Nucleic acids research,* 45**,** D353-D361.

KANEHISA, M., SATO, Y., KAWASHIMA, M., FURUMICHI, M. & TANABE, M. 2015. KEGG as a reference resource for gene and protein annotation. *Nucleic Acids Research,* 44**,** D457-D462.

KANG, M.-I., KOBAYASHI, A., WAKABAYASHI, N., KIM, S.-G. & YAMAMOTO, M. 2004. Scaffolding of Keap1 to the actin cytoskeleton controls the function of Nrf2 as key regulator of cytoprotective phase 2 genes. *Proceedings of the National Academy of Sciences,* 101**,** 2046-2051.

KARMAUS, P. W. F., HERRADA, A. A., GUY, C., NEALE, G., DHUNGANA, Y., LONG, L., VOGEL, P., AVILA, J., CLISH, C. B. & CHI, H. 2017. Critical roles of mTORC1 signaling and metabolic reprogramming for M-CSF-mediated myelopoiesis. *J Exp Med,* 214**,** 2629-2647.

KATOH, Y., ITOH, K., YOSHIDA, E., MIYAGISHI, M., FUKAMIZU, A. & YAMAMOTO, M. 2001. Two domains of Nrf2 cooperatively bind CBP, a CREB binding protein, and synergistically activate transcription. *Genes Cells,* 6**,** 857-68.

KATSUOKA, F., MOTOHASHI, H., ISHII, T., ABURATANI, H., ENGEL, J. D. & YAMAMOTO, M. 2005. Genetic evidence that small maf proteins are essential for the activation of antioxidant response element-dependent genes. *Mol Cell Biol,* 25**,** 8044-51.

KATZ, E., NISANI, S. & CHAMOVITZ, D. A. 2018. Indole-3-carbinol: a plant hormone combatting cancer. *F1000Research,* 7**,** F1000 Faculty Rev-689.

KELLINGRAY, L., LE GALL, G., DOLEMAN, J. F., NARBAD, A. & MITHEN, R. F. 2021. Effects of in vitro metabolism of a broccoli leachate, glucosinolates and S-methylcysteine sulphoxide on the human faecal microbiome. *European Journal of Nutrition,* 60**,** 2141-2154.

KENNEALLY, S., SIER, J. H. & MOORE, J. B. 2017. Efficacy of dietary and physical activity intervention in non-alcoholic fatty liver disease: a systematic review. *BMJ Open Gastroenterology,* 4**,** e000139.

KENSLER, T. W., WAKABAYASHI, N. & BISWAL, S. 2007. Cell survival responses to environmental stresses via the Keap1-Nrf2-ARE pathway. *Annu Rev Pharmacol Toxicol,* 47**,** 89-116.

KENT, L. W., RAHEMTULLA, F., HOCKETT, R. D., JR., GILLELAND, R. C. & MICHALEK, S. M. 1998. Effect of lipopolysaccharide and inflammatory cytokines on interleukin-6 production by healthy human gingival fibroblasts. *Infection and immunity,* 66**,** 608-614.

KHETARPAL, S. A., ZENG, X., MILLAR, J. S., VITALI, C., SOMASUNDARA, A. V. H., ZANONI, P., LANDRO, J. A., BARUCCI, N., ZAVADOSKI, W. J., SUN, Z., DE HAARD, H., TOTH, I. V., PELOSO, G. M., NATARAJAN, P., CUCHEL, M., LUND-KATZ, S., PHILLIPS, M. C., TALL, A. R., KATHIRESAN, S., DASILVA-JARDINE, P., YATES, N. A. & RADER, D. J. 2017. A human APOC3 missense variant and monoclonal antibody accelerate apoC-III clearance and lower triglyceride-rich lipoprotein levels. *Nature medicine,* 23**,** 1086-1094.

KIKUCHI, M., USHIDA, Y., SHIOZAWA, H., UMEDA, R., TSURUYA, K., AOKI, Y., SUGANUMA, H. & NISHIZAKI, Y. 2015. Sulforaphane-rich broccoli sprout extract improves hepatic abnormalities in male subjects. *World journal of gastroenterology,* 21**,** 12457-12467.

KIM, D., LANGMEAD, B. & SALZBERG, S. L. 2015. HISAT: a fast spliced aligner with low memory requirements. *Nature methods,* 12**,** 357-360.

KIM, J., KOO, B.-K. & KNOBLICH, J. A. 2020. Human organoids: model systems for human biology and medicine. *Nature Reviews Molecular Cell Biology,* 21**,** 571-584.

KIM, S.-Y., JEOUNG NAM, H., OH CHANG, J., CHOI, Y.-K., LEE, H.-J., KIM, H.-J., KIM, J.-Y., HWANG JUNG, H., TADI, S., YIM, Y.-H., LEE, K.-U., PARK, K.-G., HUH, S., MIN, K.-N., JEONG, K.-H., PARK MYOUNG, G., KWAK TAE, H., KWEON GI, R., INUKAI, K., SHONG, M. & LEE, I.-K. 2009. Activation of NAD(P)H:Quinone Oxidoreductase 1 Prevents Arterial Restenosis by Suppressing Vascular Smooth Muscle Cell Proliferation. *Circulation Research,* 104**,** 842-850.

KIM, T. H., HUR, E. G., KANG, S. J., KIM, J. A., THAPA, D., LEE, Y. M., KU, S. K., JUNG, Y. & KWAK, M. K. 2011. NRF2 blockade suppresses colon tumor angiogenesis by inhibiting hypoxia-induced activation of HIF-1alpha. *Cancer Res,* 71**,** 2260-75.

KIM, Y.-C., YAMAGUCHI, Y., KONDO, N., MASUTANI, H. & YODOI, J. 2003. Thioredoxin-dependent redox regulation of the antioxidant responsive element (ARE) in electrophile response. *Oncogene,* 22**,** 1860.

KITTERINGHAM, N. R., ABDULLAH, A., WALSH, J., RANDLE, L., JENKINS, R. E., SISON, R., GOLDRING, C. E. P., POWELL, H., SANDERSON, C., WILLIAMS, S., HIGGINS, L., YAMAMOTO, M., HAYES, J. & PARK, B. K. 2010. Proteomic analysis of Nrf2 deficient transgenic mice reveals cellular defence and lipid metabolism as primary Nrf2-dependent pathways in the liver. *Journal of Proteomics,* 73**,** 1612-1631.

KLOVER, P. J. & MOONEY, R. A. 2004. Hepatocytes: critical for glucose homeostasis. *Int J Biochem Cell Biol,* 36**,** 753-8.

KOBAYASHI, M., LI, L., IWAMOTO, N., NAKAJIMA-TAKAGI, Y., KANEKO, H., NAKAYAMA, Y., EGUCHI, M., WADA, Y., KUMAGAI, Y. & YAMAMOTO, M. 2009. The antioxidant defense system Keap1-Nrf2 comprises a multiple sensing mechanism for responding to a wide range of chemical compounds. *Mol Cell Biol,* 29**,** 493-502.

KOH, H. J., LEE, S. M., SON, B. G., LEE, S. H., RYOO, Z. Y., CHANG, K. T., PARK, J. W., PARK, D. C., SONG, B. J., VEECH, R. L., SONG, H. & HUH, T. L. 2004. Cytosolic NADP+-dependent isocitrate dehydrogenase plays a key role in lipid metabolism. *J Biol Chem,* 279**,** 39968-74.

KOLM, R. H., DANIELSON, U. H., ZHANG, Y., TALALAY, P. & MANNERVIK, B. 1995. Isothiocyanates as substrates for human glutathione transferases: structure-activity studies. *Biochem J,* 311 (Pt 2)**,** 453-9.

KONNO, M., ASAI, A., KAWAMOTO, K., NISHIDA, N., SATOH, T., DOKI, Y., MORI, M. & ISHII, H. 2017. The one-carbon metabolism pathway highlights therapeutic targets for gastrointestinal cancer (Review). *Int J Oncol,* 50**,** 1057-1063.

KOTTAKIS, F., NICOLAY, B. N., ROUMANE, A., KARNIK, R., GU, H., NAGLE, J. M., BOUKHALI, M., HAYWARD, M. C., LI, Y. Y., CHEN, T., LIESA, M., HAMMERMAN, P. S., WONG, K. K., HAYES, D. N., SHIRIHAI, O. S., DYSON, N. J., HAAS, W., MEISSNER, A. & BARDEESY, N. 2016. LKB1 loss links serine metabolism to DNA methylation and tumorigenesis. *Nature,* 539**,** 390-395.

KRUL, C., HUMBLOT, C., PHILIPPE, C., VERMEULEN, M., VAN NUENEN, M., HAVENAAR, R. & RABOT, S. 2002. Metabolism of sinigrin (2-propenyl glucosinolate) by the human colonic microflora in a dynamic in vitro large-intestinal model. *Carcinogenesis,* 23**,** 1009-16.

KUHAJDA, F. P., JENNER, K., WOOD, F. D., HENNIGAR, R. A., JACOBS, L. B., DICK, J. D. & PASTERNACK, G. R. 1994. Fatty acid synthesis: a potential selective target for antineoplastic therapy. *Proc Natl Acad Sci U S A,* 91**,** 6379-83.

KULKEAW, K. & PENGSART, W. 2021. Progress and Challenges in the Use of a Liver-on-a-Chip for Hepatotropic Infectious Diseases. *Micromachines (Basel),* 12.

KURNIAWAN, H., FRANCHINA, D. G., GUERRA, L., BONETTI, L., BAGUET, L. S., GRUSDAT, M., SCHLICKER, L., HUNEWALD, O., DOSTERT, C., MERZ, M. P., BINSFELD, C., DUNCAN, G. S., FARINELLE, S., NONNENMACHER, Y., HAIGHT, J., DAS GUPTA, D., EWEN, A., TASKESEN, R., HALDER, R., CHEN, Y., JAGER, C., OLLERT, M., WILMES, P., VASILIOU, V., HARRIS, I. S., KNOBBE-THOMSEN, C. B., TURNER, J. D., MAK, T. W., LOHOFF, M., MEISER, J., HILLER, K. & BRENNER, D. 2020. Glutathione Restricts Serine Metabolism to Preserve Regulatory T Cell Function. *Cell Metab*.

KWAK, M. K., ITOH, K., YAMAMOTO, M. & KENSLER, T. W. 2002. Enhanced expression of the transcription factor Nrf2 by cancer chemopreventive agents: role of antioxidant response element-like sequences in the nrf2 promoter. *Mol Cell Biol,* 22**,** 2883-92.

LAW, C. W., ALHAMDOOSH, M., SU, S., DONG, X., TIAN, L., SMYTH, G. K. & RITCHIE, M. E. 2016. RNA-seq analysis is easy as 1-2-3 with limma, Glimma and edgeR. *F1000Res,* 5.

LAW, C. W., CHEN, Y., SHI, W. & SMYTH, G. K. 2014. voom: Precision weights unlock linear model analysis tools for RNA-seq read counts. *Genome Biol,* 15**,** R29.

LE CHATELIER, E., NIELSEN, T., QIN, J., PRIFTI, E., HILDEBRAND, F., FALONY, G., ALMEIDA, M., ARUMUGAM, M., BATTO, J.-M., KENNEDY, S., LEONARD, P., LI, J., BURGDORF, K., GRARUP, N., JØRGENSEN, T., BRANDSLUND, I., NIELSEN, H. B., JUNCKER, A. S., BERTALAN, M., LEVENEZ, F., PONS, N., RASMUSSEN, S., SUNAGAWA, S., TAP, J., TIMS, S., ZOETENDAL, E. G., BRUNAK, S., CLÉMENT, K., DORÉ, J., KLEEREBEZEM, M., KRISTIANSEN, K., RENAULT, P., SICHERITZ-PONTEN, T., DE VOS, W. M., ZUCKER, J.-D., RAES, J., HANSEN, T., GUEDON, E., DELORME, C., LAYEC, S., KHACI, G., VAN DE GUCHTE, M., VANDEMEULEBROUCK, G., JAMET, A., DERVYN, R., SANCHEZ, N., MAGUIN, E., HAIMET, F., WINOGRADSKI, Y., CULTRONE, A., LECLERC, M., JUSTE, C., BLOTTIÈRE, H., PELLETIER, E., LEPASLIER, D., ARTIGUENAVE, F., BRULS, T., WEISSENBACH, J., TURNER, K., PARKHILL, J., ANTOLIN, M., MANICHANH, C., CASELLAS, F., BORUEL, N., VARELA, E., TORREJON, A., GUARNER, F., DENARIAZ, G., DERRIEN, M., VAN HYLCKAMA VLIEG, J. E. T., VEIGA, P., OOZEER, R., KNOL, J., RESCIGNO, M., BRECHOT, C., M'RINI, C., MÉRIEUX, A., YAMADA, T., BORK, P., WANG, J., EHRLICH, S. D., PEDERSEN, O. & META, H. I. T. C. 2013. Richness of human gut microbiome correlates with metabolic markers. *Nature,* 500**,** 541-546.

LEE, D., XU, I. M.-J., CHIU, D. K.-C., LAI, R. K.-H., TSE, A. P.-W., LAN LI, L., LAW, C.-T., TSANG, F. H.-C., WEI, L. L., CHAN, C. Y.-K., WONG, C.-M., NG, I. O.-L. & WONG, C. C.-L. 2017. Folate cycle enzyme MTHFD1L confers metabolic advantages in hepatocellular carcinoma. *The Journal of Clinical Investigation,* 127**,** 1856-1872.

LEE, J. Y., CHO, H. K. & KWON, Y. H. 2010. Palmitate induces insulin resistance without significant intracellular triglyceride accumulation in HepG2 cells. *Metabolism,* 59**,** 927-34.

LEE, S., HUR, E. G., RYOO, I. G., JUNG, K. A., KWAK, J. & KWAK, M. K. 2012. Involvement of the Nrf2-proteasome pathway in the endoplasmic reticulum stress response in pancreatic beta-cells. *Toxicol Appl Pharmacol,* 264**,** 431-8.

LEE, W. N., BOROS, L. G., PUIGJANER, J., BASSILIAN, S., LIM, S. & CASCANTE, M. 1998. Mass isotopomer study of the nonoxidative pathways of the pentose cycle with [1,2-13C2]glucose. *Am J Physiol,* 274**,** E843-51.

LEE, Y.-R., CHEN, M., LEE, J. D., ZHANG, J., LIN, S.-Y., FU, T.-M., CHEN, H., ISHIKAWA, T., CHIANG, S.-Y., KATON, J., ZHANG, Y., SHULGA, Y. V., BESTER, A. C., FUNG, J., MONTELEONE, E., WAN, L., SHEN, C., HSU, C.-H., PAPA, A., CLOHESSY, J. G., TERUYA-FELDSTEIN, J., JAIN, S., WU, H., MATESIC, L., CHEN, R.-H., WEI, W. & PANDOLFI, P. P. 2019. Reactivation of PTEN tumor suppressor for cancer treatment through inhibition of a MYC-WWP1 inhibitory pathway. *Science (New York, N.Y.),* 364**,** eaau0159.

LEGA, I. C. & LIPSCOMBE, L. L. 2019. Review: Diabetes, Obesity, and Cancer—Pathophysiology and Clinical Implications. *Endocrine Reviews,* 41**,** 33-52.

LEI, P., TIAN, S., TENG, C., HUANG, L., LIU, X., WANG, J., ZHANG, Y., LI, B. & SHAN, Y. 2019. Sulforaphane Improves Lipid Metabolism by Enhancing Mitochondrial Function and Biogenesis In Vivo and In Vitro. *Mol Nutr Food Res,* 63**,** e1800795.

LELOUP, C., TOURREL-CUZIN, C., MAGNAN, C., KARACA, M., CASTEL, J., CARNEIRO, L., COLOMBANI, A. L., KTORZA, A., CASTEILLA, L. & PENICAUD, L. 2009. Mitochondrial reactive oxygen species are obligatory signals for glucose-induced insulin secretion. *Diabetes,* 58**,** 673-81.

LETTIERI-BARBATO, D., MINOPOLI, G., CAGGIANO, R., IZZO, R., SANTILLO, M., AQUILANO, K. & FARAONIO, R. 2020. Fasting Drives Nrf2-Related Antioxidant Response in Skeletal Muscle. *Int J Mol Sci,* 21.

LI, A. M. & YE, J. 2020. Reprogramming of serine, glycine and one-carbon metabolism in cancer. *Biochimica et Biophysica Acta (BBA) - Molecular Basis of Disease,* 1866**,** 165841.

LI, H. & DURBIN, R. 2009. Fast and accurate short read alignment with Burrows-Wheeler transform. *Bioinformatics (Oxford, England),* 25**,** 1754-1760.

LI, J., LEE, J. M. & JOHNSON, J. A. 2002. Microarray analysis reveals an antioxidant responsive element-driven gene set involved in conferring protection from an oxidative stress-induced apoptosis in IMR-32 cells. *J Biol Chem,* 277**,** 388-94.

LI, L. & DAVIE, J. R. 2010. The role of Sp1 and Sp3 in normal and cancer cell biology. *Ann Anat,* 192**,** 275-83.

LI, M., CHIU, J. F., KELSEN, A., LU, S. C. & FUKAGAWA, N. K. 2009. Identification and characterization of an Nrf2-mediated ARE upstream of the rat glutamate cysteine ligase catalytic subunit gene (GCLC). *J Cell Biochem,* 107**,** 944-54.

LI, P., WANG, T., ZENG, C., YANG, M., LI, G., HAN, J. & WU, W. 2020a. Association between metabolic syndrome and prognosis of breast cancer: a meta-analysis of follow-up studies. *Diabetology & Metabolic Syndrome,* 12**,** 10.

LI, S., BROWN, M. S. & GOLDSTEIN, J. L. 2010. Bifurcation of insulin signaling pathway in rat liver: mTORC1 required for stimulation of lipogenesis, but not inhibition of gluconeogenesis. *Proc Natl Acad Sci U S A,* 107**,** 3441-6.

LI, W., WU, W., SONG, H., WANG, F., LI, H., CHEN, L., LAI, Y., JANICKI, J. S., WARD, K. W., MEYER, C. J., WANG, X. L., TANG, D. & CUI, T. 2014. Targeting Nrf2 by dihydro-CDDO-trifluoroethyl amide enhances autophagic clearance and viability of beta-cells in a setting of oxidative stress. *FEBS Lett,* 588**,** 2115-24.

LI, X., TIAN, S., WANG, Y., LIU, J., WANG, J. & LU, Y. 2021. Broccoli microgreens juice reduces body weight by enhancing insulin sensitivity and modulating gut microbiota in high-fat diet-induced C57BL/6J obese mice. *Eur J Nutr*.

LI, Y.-P., WANG, S.-L., LIU, B., TANG, L., KUANG, R.-R., WANG, X.-B., ZHAO, C., SONG, X.-D., CAO, X.-M., WU, X., YANG, P.-Z., WANG, L.-Z. & CHEN, A.-H. 2016. Sulforaphane prevents rat cardiomyocytes from hypoxia/reoxygenation injury in vitro via activating SIRT1 and subsequently inhibiting ER stress. *Acta Pharmacologica Sinica,* 37**,** 344-353.

LI, Z., GUO, H., LI, J., MA, T., ZHOU, S., ZHANG, Z., MIAO, L. & CAI, L. 2020b. Sulforaphane prevents type 2 diabetes-induced nephropathy via AMPK-mediated activation of lipid metabolic pathways and Nrf2 antioxidative function. *Clin Sci (Lond),* 134**,** 2469-2487.

LIANG, J., JAHRAUS, B., BALTA, E., ZIEGLER, J. D., HÜBNER, K., BLANK, N., NIESLER, B., WABNITZ, G. H. & SAMSTAG, Y. 2018. Sulforaphane Inhibits Inflammatory Responses of Primary Human T-Cells by Increasing ROS and Depleting Glutathione. *Frontiers in Immunology,* 9.

LIM, J. K., NARANG, P. K., OVERMAN, D. O. & JACKNOWITZ, A. I. 1979. Beneficial effects of methionine and histidine in aspirin solutions on gastric mucosal damage in rats. *J Pharm Sci,* 68**,** 295-8.

LIN, R.-K., ZHOU, N., LYU, Y. L., TSAI, Y.-C., LU, C.-H., KERRIGAN, J., CHEN, Y.-T., GUAN, Z., HSIEH, T.-S. & LIU, L. F. 2011. Dietary Isothiocyanate-induced Apoptosis via Thiol Modification of DNA Topoisomerase IIα. *Journal of Biological Chemistry,* 286**,** 33591-33600.

LIN, T.-Y., CANTLEY, L. C. & DENICOLA, G. M. 2016. NRF2 Rewires Cellular Metabolism to Support the Antioxidant Response. *A Master Regulator of Oxidative Stress - The Transcription Factor Nrf2.*

LIU, H., SMITH, A. J., LOTT, M. C., BAO, Y., BOWATER, R. P., REDDAN, J. R. & WORMSTONE, I. M. 2013. Sulforaphane can protect lens cells against oxidative stress: implications for cataract prevention. *Invest Ophthalmol Vis Sci,* 54**,** 5236-48.

LIU, R. H. 2013. Health-promoting components of fruits and vegetables in the diet. *Adv Nutr,* 4**,** 384s-92s.

LIU, Y., COTILLARD, A., VATIER, C., BASTARD, J. P., FELLAHI, S., STÉVANT, M., ALLATIF, O., LANGLOIS, C., BIEUVELET, S., BROCHOT, A., GUILBOT, A., CLÉMENT, K. & RIZKALLA, S. W. 2015. A Dietary Supplement Containing Cinnamon, Chromium and Carnosine Decreases Fasting Plasma Glucose and Increases Lean Mass in Overweight or Obese Pre-Diabetic Subjects: A Randomized, Placebo-Controlled Trial. *PLoS One,* 10**,** e0138646.

LIU, Z., ZHANG, Y. W., CHANG, Y. S. & FANG, F. D. 2006. The role of cytoskeleton in glucose regulation. *Biochemistry (Mosc),* 71**,** 476-80.

LO, E. H., DALKARA, T. & MOSKOWITZ, M. A. 2003. Mechanisms, challenges and opportunities in stroke. *Nature Reviews Neuroscience,* 4**,** 399-414.

LOCASALE, J. W., GRASSIAN, A. R., MELMAN, T., LYSSIOTIS, C. A., MATTAINI, K. R., BASS, A. J., HEFFRON, G., METALLO, C. M., MURANEN, T., SHARFI, H., SASAKI, A. T., ANASTASIOU, D., MULLARKY, E., VOKES, N. I., SASAKI, M., BEROUKHIM, R., STEPHANOPOULOS, G., LIGON, A. H., MEYERSON, M., RICHARDSON, A. L., CHIN, L., WAGNER, G., ASARA, J. M., BRUGGE, J. S., CANTLEY, L. C. & VANDER HEIDEN, M. G. 2011. Phosphoglycerate dehydrogenase diverts glycolytic flux and contributes to oncogenesis. *Nature Genetics,* 43**,** 869-874.

LÓPEZ-CHILLÓN, M. T., CARAZO-DÍAZ, C., PRIETO-MERINO, D., ZAFRILLA, P., MORENO, D. A. & VILLAÑO, D. 2019. Effects of long-term consumption of broccoli sprouts on inflammatory markers in overweight subjects. *Clin Nutr,* 38**,** 745-752.

LOVESTONE, S. & SMITH, U. 2014. Advanced glycation end products, dementia, and diabetes. *Proc Natl Acad Sci U S A,* 111**,** 4743-4.

LOZANO, I., VAN DER WERF, R., BIETIGER, W., SEYFRITZ, E., PERONET, C., PINGET, M., JEANDIDIER, N., MAILLARD, E., MARCHIONI, E., SIGRIST, S. & DAL, S. 2016. High-fructose and high-fat diet-induced disorders in rats: impact on diabetes risk, hepatic and vascular complications. *Nutrition & Metabolism,* 13**,** 15.

LU, S. & ARCHER, M. C. 2010. Sp1 coordinately regulates de novo lipogenesis and proliferation in cancer cells. *Int J Cancer,* 126**,** 416-25.
LU, S. C. 2013. Glutathione synthesis. *Biochimica et Biophysica Acta (BBA) - General Subjects,* 1830**,** 3143-3153.
LUANG-IN, V., NARBAD, A., NUENO-PALOP, C., MITHEN, R., BENNETT, M. & ROSSITER, J. T. 2014. The metabolism of methylsulfinylalkyl- and methylthioalkyl-glucosinolates by a selection of human gut bacteria. *Molecular Nutrition & Food Research,* 58**,** 875-883.
LUDTMANN, M. H. R., ANGELOVA, P. R., ZHANG, Y., ABRAMOV, A. Y. & DINKOVA-KOSTOVA, A. T. 2014. Nrf2 affects the efficiency of mitochondrial fatty acid oxidation. *The Biochemical journal,* 457**,** 415-424.
MA, Q. 2013. Role of nrf2 in oxidative stress and toxicity. *Annual review of pharmacology and toxicology,* 53**,** 401-426.
MACKELLAR, J., CUSHMAN, S. W. & PERIWAL, V. 2010. Waves of adipose tissue growth in the genetically obese Zucker fatty rat. *PLoS One,* 5**,** e8197.
MACLEOD, A. K., MCMAHON, M., PLUMMER, S. M., HIGGINS, L. G., PENNING, T. M., IGARASHI, K. & HAYES, J. D. 2009. Characterization of the cancer chemopreventive NRF2-dependent gene battery in human keratinocytes: demonstration that the KEAP1-NRF2 pathway, and not the BACH1-NRF2 pathway, controls cytoprotection against electrophiles as well as redox-cycling compounds. *Carcinogenesis,* 30**,** 1571-80.
MAGNUSSON, I., ROTHMAN, D. L., KATZ, L. D., SHULMAN, R. G. & SHULMAN, G. I. 1992. Increased rate of gluconeogenesis in type II diabetes mellitus. A 13C nuclear magnetic resonance study. *J Clin Invest,* 90**,** 1323-7.
MAHJOUB, S. & MASROUR-ROUDSARI, J. 2012. Role of oxidative stress in pathogenesis of metabolic syndrome. *Caspian journal of internal medicine,* 3**,** 386-396.
MALHOTRA, D., PORTALES-CASAMAR, E., SINGH, A., SRIVASTAVA, S., ARENILLAS, D., HAPPEL, C., SHYR, C., WAKABAYASHI, N., KENSLER, T. W., WASSERMAN, W. W. & BISWAL, S. 2010. Global mapping of binding sites for Nrf2 identifies novel targets in cell survival response through ChIP-Seq profiling and network analysis. *Nucleic Acids Res,* 38**,** 5718-34.
MANDRICH, L. & CAPUTO, E. 2020. Brassicaceae-Derived Anticancer Agents: Towards a Green Approach to Beat Cancer. *Nutrients,* 12.
MANN, N. 2019. Statins for over 75s: the data don't justify medicalising a whole population. *Bmj,* 365**,** l2311.
MARJOT, T., MOOLLA, A., COBBOLD, J. F., HODSON, L. & TOMLINSON, J. W. 2019. Nonalcoholic Fatty Liver Disease in Adults: Current Concepts in Etiology, Outcomes, and Management. *Endocrine Reviews,* 41**,** 66-117.
MARQUES-LOPES, I., ANSORENA, D., ASTIASARAN, I., FORGA, L. & MARTÍNEZ, J. A. 2001. Postprandial de novo lipogenesis and metabolic changes induced by a high-carbohydrate, low-fat meal in lean and overweight men. *The American Journal of Clinical Nutrition,* 73**,** 253-261.
MARRAFFINI, L. A. 2015. CRISPR-Cas immunity in prokaryotes. *Nature,* 526**,** 55-61.
MARROQUIN, L. D., HYNES, J., DYKENS, J. A., JAMIESON, J. D. & WILL, Y. 2007. Circumventing the Crabtree effect: replacing media glucose with galactose increases susceptibility of HepG2 cells to mitochondrial toxicants. *Toxicol Sci,* 97**,** 539-47.
MARTIN, H.-J. & MASER, E. 2009. Role of human aldo–keto-reductase AKR1B10 in the protection against toxic aldehydes. *Chemico-Biological Interactions,* 178**,** 145-150.
MATTAINI, K. R., SULLIVAN, M. R. & VANDER HEIDEN, M. G. 2016. The importance of serine metabolism in cancer. *The Journal of cell biology,* 214**,** 249-257.
MAURER, G. D., BRUCKER, D. P., BÄHR, O., HARTER, P. N., HATTINGEN, E., WALENTA, S., MUELLER-KLIESER, W., STEINBACH, J. P. & RIEGER, J. 2011. Differential utilization of ketone bodies by neurons and glioma cell lines: a rationale for ketogenic diet as experimental glioma therapy. *BMC cancer,* 11**,** 315-315.

MCAULEY, K. & MANN, J. 2006. Thematic review series: patient-oriented research. Nutritional determinants of insulin resistance. *J Lipid Res,* 47**,** 1668-76.

MCDEVITT, R. M., BOTT, S. J., HARDING, M., COWARD, W. A., BLUCK, L. J. & PRENTICE, A. M. 2001. De novo lipogenesis during controlled overfeeding with sucrose or glucose in lean and obese women. *The American Journal of Clinical Nutrition,* 74**,** 737-746.

MCDONALD, J. T., KIM, K., NORRIS, A. J., VLASHI, E., PHILLIPS, T. M., LAGADEC, C., DELLA DONNA, L., RATIKAN, J., SZELAG, H., HLATKY, L. & MCBRIDE, W. H. 2010. Ionizing radiation activates the Nrf2 antioxidant response. *Cancer Res,* 70**,** 8886-95.

MCEVOY, B., SUMAYAO, R., SLATTERY, C., MCMORROW, T. & NEWSHOLME, P. 2015. Cystine accumulation attenuates insulin release from the pancreatic beta-cell due to elevated oxidative stress and decreased ATP levels. *J Physiol,* 593**,** 5167-82.

MCMAHON, M., LAMONT, D. J., BEATTIE, K. A. & HAYES, J. D. 2010. Keap1 perceives stress via three sensors for the endogenous signaling molecules nitric oxide, zinc, and alkenals. *Proc Natl Acad Sci U S A,* 107**,** 18838-43.

MCMAHON, M., THOMAS, N., ITOH, K., YAMAMOTO, M. & HAYES, J. D. 2004. Redox-regulated turnover of Nrf2 is determined by at least two separate protein domains, the redox-sensitive Neh2 degron and the redox-insensitive Neh6 degron. *J Biol Chem,* 279**,** 31556-67.

MEAKIN, P. J., CHOWDHRY, S., SHARMA, R. S., ASHFORD, F. B., WALSH, S. V., MCCRIMMON, R. J., DINKOVA-KOSTOVA, A. T., DILLON, J. F., HAYES, J. D. & ASHFORD, M. L. 2014. Susceptibility of Nrf2-null mice to steatohepatitis and cirrhosis upon consumption of a high-fat diet is associated with oxidative stress, perturbation of the unfolded protein response, and disturbance in the expression of metabolic enzymes but not with insulin resistance. *Mol Cell Biol,* 34**,** 3305-20.

MEHER, A. K., SHARMA, P. R., LIRA, V. A., YAMAMOTO, M., KENSLER, T. W., YAN, Z. & LEITINGER, N. 2012. Nrf2 deficiency in myeloid cells is not sufficient to protect mice from high-fat diet-induced adipose tissue inflammation and insulin resistance. *Free Radic Biol Med,* 52**,** 1708-15.

MELÉNDEZ-HEVIA, E., DE PAZ-LUGO, P., CORNISH-BOWDEN, A. & CÁRDENAS, M. L. 2009. A weak link in metabolism: the metabolic capacity for glycine biosynthesis does not satisfy the need for collagen synthesis. *J Biosci,* 34**,** 853-72.

MENENDEZ, J. A. & LUPU, R. 2007. Fatty acid synthase and the lipogenic phenotype in cancer pathogenesis. *Nat Rev Cancer,* 7**,** 763-77.

MENENDEZ, J. A., VELLON, L., ESPINOZA, I. & LUPU, R. 2016. The metastasis inducer CCN1 (CYR61) activates the fatty acid synthase (FASN)-driven lipogenic phenotype in breast cancer cells. *Oncoscience,* 3**,** 242-257.

MEYER, C., STUMVOLL, M., NADKARNI, V., DOSTOU, J., MITRAKOU, A. & GERICH, J. 1998. Abnormal renal and hepatic glucose metabolism in type 2 diabetes mellitus. *J Clin Invest,* 102**,** 619-24.

MI, L., HOOD, B. L., STEWART, N. A., XIAO, Z., GOVIND, S., WANG, X., CONRADS, T. P., VEENSTRA, T. D. & CHUNG, F.-L. 2011. Identification of Potential Protein Targets of Isothiocyanates by Proteomics. *Chemical Research in Toxicology,* 24**,** 1735-1743.

MIAO, W., HU, L., SCRIVENS, P. J. & BATIST, G. 2005. Transcriptional regulation of NF-E2 p45-related factor (NRF2) expression by the aryl hydrocarbon receptor-xenobiotic response element signaling pathway: direct cross-talk between phase I and II drug-metabolizing enzymes. *J Biol Chem,* 280**,** 20340-8.

MIKUŁA-PIETRASIK, J. & KSIĄŻEK, K. 2016. L-Carnosine Prevents the Pro-cancerogenic Activity of Senescent Peritoneal Mesothelium Towards Ovarian Cancer Cells. *Anticancer Res,* 36**,** 665-71.

MIRMIRAN, P., BAHADORAN, Z., HOSSEINPANAH, F., KEYZAD, A. & AZIZI, F. 2012. Effects of broccoli sprout with high sulforaphane concentration on inflammatory markers in type 2 diabetic patients: A randomized double-blind placebo-controlled clinical trial. *Journal of Functional Foods,* 4**,** 837-841.

MITSUISHI, Y., TAGUCHI, K., KAWATANI, Y., SHIBATA, T., NUKIWA, T., ABURATANI, H., YAMAMOTO, M. & MOTOHASHI, H. 2012. Nrf2 redirects glucose and glutamine into anabolic pathways in metabolic reprogramming. *Cancer Cell,* 22**,** 66-79.

MIURA, T., SHINKAI, Y., JIANG, H. Y., IWAMOTO, N., SUMI, D., TAGUCHI, K., YAMAMOTO, M., JINNO, H., TANAKA-KAGAWA, T., CHO, A. K. & KUMAGAI, Y. 2011. Initial response and cellular protection through the Keap1/Nrf2 system during the exposure of primary mouse hepatocytes to 1,2-naphthoquinone. *Chem Res Toxicol,* 24**,** 559-67.

MOHAR, D. S. & MALIK, S. 2012. The Sirtuin System: The Holy Grail of Resveratrol? *Journal of clinical & experimental cardiology,* 3**,** 216.

MOI, P., CHAN, K., ASUNIS, I., CAO, A. & KAN, Y. W. 1994. Isolation of NF-E2-related factor 2 (Nrf2), a NF-E2-like basic leucine zipper transcriptional activator that binds to the tandem NF-E2/AP1 repeat of the beta-globin locus control region. *Proc Natl Acad Sci U S A,* 91**,** 9926-30.

MOLINARO, A., BECATTINI, B. & SOLINAS, G. 2020. Insulin signaling and glucose metabolism in different hepatoma cell lines deviate from hepatocyte physiology toward a convergent aberrant phenotype. *Scientific Reports,* 10**,** 12031.

MONTENEGRO, M. F., SÁNCHEZ-DEL-CAMPO, L., GONZÁLEZ-GUERRERO, R., MARTÍNEZ-BARBA, E., PIÑERO-MADRONA, A., CABEZAS-HERRERA, J. & RODRÍGUEZ-LÓPEZ, J. N. 2016. Tumor suppressor SET9 guides the epigenetic plasticity of breast cancer cells and serves as an early-stage biomarker for predicting metastasis. *Oncogene,* 35**,** 6143-6152.

MORADI-ARZELOO, M., FARSHID, A. A., TAMADDONFARD, E. & ASRI-REZAEI, S. 2016. Effects of histidine and vitamin C on isoproterenol-induced acute myocardial infarction in rats. *Vet Res Forum,* 7**,** 47-54.

MORAN-RAMOS, S., LÓPEZ-CONTRERAS, B. E. & CANIZALES-QUINTEROS, S. 2017. Gut Microbiota in Obesity and Metabolic Abnormalities: A Matter of Composition or Functionality? *Arch Med Res,* 48**,** 735-753.

MORE, V. R., XU, J., SHIMPI, P. C., BELGRAVE, C., LUYENDYK, J. P., YAMAMOTO, M. & SLITT, A. L. 2013. Keap1 knockdown increases markers of metabolic syndrome after long-term high fat diet feeding. *Free Radic Biol Med,* 61**,** 85-94.

MULLARKY, E., MATTAINI, K. R., VANDER HEIDEN, M. G., CANTLEY, L. C. & LOCASALE, J. W. 2011. PHGDH amplification and altered glucose metabolism in human melanoma. *Pigment Cell Melanoma Res,* 24**,** 1112-5.

MUÑOZ, A. & COSTA, M. 2013. Nutritionally mediated oxidative stress and inflammation. *Oxid Med Cell Longev,* 2013**,** 610950.

MURASHIMA, M., WATANABE, S., ZHUO, X. G., UEHARA, M. & KURASHIGE, A. 2004. Phase 1 study of multiple biomarkers for metabolism and oxidative stress after one-week intake of broccoli sprouts. *Biofactors,* 22**,** 271-5.

MUTHUKUMAR, K. & NACHIAPPAN, V. 2010. Cadmium-induced oxidative stress in Saccharomyces cerevisiae. *Indian J Biochem Biophys,* 47**,** 383-7.

MYZAK, M. C., DASHWOOD, W. M., ORNER, G. A., HO, E. & DASHWOOD, R. H. 2006a. Sulforaphane inhibits histone deacetylase in vivo and suppresses tumorigenesis in Apc-minus mice. *Faseb j,* 20**,** 506-8.

MYZAK, M. C., DASHWOOD, W. M., ORNER, G. A., HO, E. & DASHWOOD, R. H. 2006b. Sulforaphane inhibits histone deacetylase in vivo and suppresses tumorigenesis in Apcmin mice. *The FASEB Journal,* 20**,** 506-508.

MYZAK, M. C., HARDIN, K., WANG, R., DASHWOOD, R. H. & HO, E. 2006c. Sulforaphane inhibits histone deacetylase activity in BPH-1, LnCaP and PC-3 prostate epithelial cells. *Carcinogenesis,* 27**,** 811-819.

MYZAK, M. C., TONG, P., DASHWOOD, W. M., DASHWOOD, R. H. & HO, E. 2007. Sulforaphane retards the growth of human PC-3 xenografts and inhibits HDAC activity in human subjects. *Exp Biol Med (Maywood),* 232**,** 227-34.

NAGATA, N., XU, L., KOHNO, S., USHIDA, Y., AOKI, Y., UMEDA, R., FUKE, N., ZHUGE, F., NI, Y., NAGASHIMADA, M., TAKAHASHI, C., SUGANUMA, H., KANEKO, S. & OTA, T. 2017. Glucoraphanin Ameliorates Obesity and Insulin Resistance Through Adipose Tissue Browning and Reduction of Metabolic Endotoxemia in Mice. *Diabetes,* 66**,** 1222-1236.

NAKAJIMA, K., YAMAUCHI, K., SHIGEMATSU, S., IKEO, S., KOMATSU, M., AIZAWA, T. & HASHIZUME, K. 2000. Selective Attenuation of Metabolic Branch of Insulin Receptor Down-signaling by High Glucose in a Hepatoma Cell Line, HepG2 Cells*. *Journal of Biological Chemistry,* 275**,** 20880-20886.

NANDINI, D. B., RAO, R. S., DEEPAK, B. S. & REDDY, P. B. 2020. Sulforaphane in broccoli: The green chemoprevention!! Role in cancer prevention and therapy. *Journal of oral and maxillofacial pathology : JOMFP,* 24**,** 405-405.

NIOI, P., MCMAHON, M., ITOH, K., YAMAMOTO, M. & HAYES, J. D. 2003. Identification of a novel Nrf2-regulated antioxidant response element (ARE) in the mouse NAD(P)H:quinone oxidoreductase 1 gene: reassessment of the ARE consensus sequence. *The Biochemical journal,* 374**,** 337-348.

NIOI, P., NGUYEN, T., SHERRATT, P. J. & PICKETT, C. B. 2005. The Carboxy-Terminal Neh3 Domain of Nrf2 Is Required for Transcriptional Activation. *Molecular and Cellular Biology,* 25**,** 10895-10906.

NISO-SANTANO, M., GONZÁLEZ-POLO, R. A., BRAVO-SAN PEDRO, J. M., GÓMEZ-SÁNCHEZ, R., LASTRES-BECKER, I., ORTIZ-ORTIZ, M. A., SOLER, G., MORÁN, J. M., CUADRADO, A. & FUENTES, J. M. 2010. Activation of apoptosis signal-regulating kinase 1 is a key factor in paraquat-induced cell death: Modulation by the Nrf2/Trx axis. *Free Radical Biology and Medicine,* 48**,** 1370-1381.

NIU, Y. C., FENG, R. N., HOU, Y., LI, K., KANG, Z., WANG, J., SUN, C. H. & LI, Y. 2012. Histidine and arginine are associated with inflammation and oxidative stress in obese women. *Br J Nutr,* 108**,** 57-61.

NWOSE, E. U., JELINEK, H. F., RICHARDS, R. S. & KERR, P. G. 2006. Changes in the erythrocyte glutathione concentration in the course of diabetes mellitus. *Redox Rep,* 11**,** 99-104.

O'DONNELL, M. J., CHIN, S. L., RANGARAJAN, S., XAVIER, D., LIU, L., ZHANG, H., RAO-MELACINI, P., ZHANG, X., PAIS, P., AGAPAY, S., LOPEZ-JARAMILLO, P., DAMASCENO, A., LANGHORNE, P., MCQUEEN, M. J., ROSENGREN, A., DEHGHAN, M., HANKEY, G. J., DANS, A. L., ELSAYED, A., AVEZUM, A., MONDO, C., DIENER, H.-C., RYGLEWICZ, D., CZLONKOWSKA, A., POGOSOVA, N., WEIMAR, C., IQBAL, R., DIAZ, R., YUSOFF, K., YUSUFALI, A., OGUZ, A., WANG, X., PENAHERRERA, E., LANAS, F., OGAH, O. S., OGUNNIYI, A., IVERSEN, H. K., MALAGA, G., RUMBOLDT, Z., OVEISGHARAN, S., AL HUSSAIN, F., MAGAZI, D., NILANONT, Y., FERGUSON, J., PARE, G. & YUSUF, S. 2016. Global and regional effects of potentially modifiable risk factors associated with acute stroke in 32 countries (INTERSTROKE): a case-control study. *The Lancet,* 388**,** 761-775.

OGURA, T., TONG, K. I., MIO, K., MARUYAMA, Y., KUROKAWA, H., SATO, C. & YAMAMOTO, M. 2010. Keap1 is a forked-stem dimer structure with two large spheres enclosing the intervening, double glycine repeat, and C-terminal domains. *Proceedings of the National Academy of Sciences,* 107**,** 2842-2847.

OHTSUJI, M., KATSUOKA, F., KOBAYASHI, A., ABURATANI, H., HAYES, J. D. & YAMAMOTO, M. 2008. Nrf1 and Nrf2 play distinct roles in activation of antioxidant response element-dependent genes. *The Journal of biological chemistry,* 283**,** 33554-33562.

OROZCO, L. D., KAPTURCZAK, M. H., BARAJAS, B., WANG, X., WEINSTEIN, M. M., WONG, J., DESHANE, J., BOLISETTY, S., SHAPOSHNIK, Z., SHIH, D. M., AGARWAL, A., LUSIS, A. J. & ARAUJO, J. A. 2007. Heme oxygenase-1 expression in macrophages plays a beneficial role in atherosclerosis. *Circ Res,* 100**,** 1703-11.

PADMANABHAN, B., TONG, K. I., OHTA, T., NAKAMURA, Y., SCHARLOCK, M., OHTSUJI, M., KANG, M.-I., KOBAYASHI, A., YOKOYAMA, S. & YAMAMOTO, M. 2006. Structural Basis for Defects of Keap1 Activity Provoked by Its Point Mutations in Lung Cancer. *Molecular Cell,* 21**,** 689-700.

PANAHI, G., PASALAR, P., ZARE, M., RIZZUTO, R. & MESHKANI, R. 2018. High glucose induces inflammatory responses in HepG2 cells via the oxidative stress-mediated activation of NF-κB, and MAPK pathways in HepG2 cells. *Arch Physiol Biochem,* 124**,** 468-474.

PANG, S., LYNN, D. A., LO, J. Y., PAEK, J. & CURRAN, S. P. 2014. SKN-1 and Nrf2 couples proline catabolism with lipid metabolism during nutrient deprivation. *Nature Communications,* 5**,** 5048.

PAPATHEODOROU, K., BANACH, M., BEKIARI, E., RIZZO, M. & EDMONDS, M. 2018. Complications of Diabetes 2017. *Journal of diabetes research,* 2018**,** 3086167-3086167.

PAPP, D., LENTI, K., MODOS, D., FAZEKAS, D., DUL, Z., TUREI, D., FOLDVARI-NAGY, L., NUSSINOV, R., CSERMELY, P. & KORCSMAROS, T. 2012. The NRF2-related interactome and regulome contain multifunctional proteins and fine-tuned autoregulatory loops. *FEBS Lett,* 586**,** 1795-802.

PARAVICINI, T. M. & TOUYZ, R. M. 2006. Redox signaling in hypertension. *Cardiovasc Res,* 71**,** 247-58.

PARK, H. S., HAN, M. H., KIM, G.-Y., MOON, S.-K., KIM, W.-J., HWANG, H. J., PARK, K. Y. & CHOI, Y. H. 2014. Sulforaphane induces reactive oxygen species-mediated mitotic arrest and subsequent apoptosis in human bladder cancer 5637 cells. *Food and Chemical Toxicology,* 64**,** 157-165.

PARNAUD, G., LI, P., CASSAR, G., ROUIMI, P., TULLIEZ, J., COMBARET, L. & GAMET-PAYRASTRE, L. 2004. Mechanism of sulforaphane-induced cell cycle arrest and apoptosis in human colon cancer cells. *Nutr Cancer,* 48**,** 198-206.

PASTOREK, M., SIMKO, V., TAKACOVA, M., BARATHOVA, M., BARTOSOVA, M., HUNAKOVA, L., SEDLAKOVA, O., HUDECOVA, S., KRIZANOVA, O., DEQUIEDT, F., PASTOREKOVA, S. & SEDLAK, J. 2015. Sulforaphane reduces molecular response to hypoxia in ovarian tumor cells independently of their resistance to chemotherapy. *International journal of oncology,* 47**,** 51-60.

PATRA, K. C. & HAY, N. 2014. The pentose phosphate pathway and cancer. *Trends in Biochemical Sciences,* 39**,** 347-354.

PAUL, MANASH K., BISHT, B., DARMAWAN, DAPHNE O., CHIOU, R., HA, VI L., WALLACE, WILLIAM D., CHON, ANDREW T., HEGAB, AHMED E., GROGAN, T., ELASHOFF, DAVID A., ALVA-ORNELAS, JACKELYN A. & GOMPERTS, BRIGITTE N. 2014. Dynamic Changes in Intracellular ROS Levels Regulate Airway Basal Stem Cell Homeostasis through Nrf2-Dependent Notch Signaling. *Cell Stem Cell,* 15**,** 199-214.

PAULSEN, C. E. & CARROLL, K. S. 2010. Orchestrating redox signaling networks through regulatory cysteine switches. *ACS Chem Biol,* 5**,** 47-62.

PAVLOVA, NATALYA N. & THOMPSON, CRAIG B. 2016. The Emerging Hallmarks of Cancer Metabolism. *Cell Metabolism,* 23**,** 27-47.

PERTEA, G. & PERTEA, M. 2020. GFF Utilities: GffRead and GffCompare [version 2; peer review: 3 approved]. *F1000Research,* 9.

PERTEA, M., KIM, D., PERTEA, G. M., LEEK, J. T. & SALZBERG, S. L. 2016a. Transcript-level expression analysis of RNA-seq experiments with HISAT, StringTie and Ballgown. *Nat Protoc,* 11**,** 1650-67.

PERTEA, M., KIM, D., PERTEA, G. M., LEEK, J. T. & SALZBERG, S. L. 2016b. Transcript-level expression analysis of RNA-seq experiments with HISAT, StringTie and Ballgown. *Nature Protocols,* 11**,** 1650-1667.

PIANTADOSI, C. A., WITHERS, C. M., BARTZ, R. R., MACGARVEY, N. C., FU, P., SWEENEY, T. E., WELTY-WOLF, K. E. & SULIMAN, H. B. 2011. Heme oxygenase-1 couples activation of mitochondrial biogenesis to anti-inflammatory cytokine expression. *J Biol Chem,* 286**,** 16374-85.

PIBERGER, A. L., KÖBERLE, B. & HARTWIG, A. 2014. The broccoli-born isothiocyanate sulforaphane impairs nucleotide excision repair: XPA as one potential target. *Archives of Toxicology,* 88**,** 647-658.

PIZZINO, G., IRRERA, N., CUCINOTTA, M., PALLIO, G., MANNINO, F., ARCORACI, V., SQUADRITO, F., ALTAVILLA, D. & BITTO, A. 2017. Oxidative Stress: Harms and Benefits for Human Health. *Oxidative medicine and cellular longevity,* 2017**,** 8416763-8416763.

PIZZORNO, J. 2014. Glutathione! *Integrative medicine (Encinitas, Calif.),* 13**,** 8-12.

PLAISIER, S. B., TASCHEREAU, R., WONG, J. A. & GRAEBER, T. G. 2010. Rank-rank hypergeometric overlap: identification of statistically significant overlap between gene-expression signatures. *Nucleic Acids Res,* 38**,** e169.

PLOVIER, H., EVERARD, A., DRUART, C., DEPOMMIER, C., VAN HUL, M., GEURTS, L., CHILLOUX, J., OTTMAN, N., DUPARC, T., LICHTENSTEIN, L., MYRIDAKIS, A., DELZENNE, N. M., KLIEVINK, J., BHATTACHARJEE, A., VAN DER ARK, K. C., AALVINK, S., MARTINEZ, L. O., DUMAS, M. E., MAITER, D., LOUMAYE, A., HERMANS, M. P., THISSEN, J. P., BELZER, C., DE VOS, W. M. & CANI, P. D. 2017. A purified membrane protein from Akkermansia muciniphila or the pasteurized bacterium improves metabolism in obese and diabetic mice. *Nat Med,* 23**,** 107-113.

POLLARI, S., KÄKÖNEN, S. M., EDGREN, H., WOLF, M., KOHONEN, P., SARA, H., GUISE, T., NEES, M. & KALLIONIEMI, O. 2011. Enhanced serine production by bone metastatic breast cancer cells stimulates osteoclastogenesis. *Breast Cancer Res Treat,* 125**,** 421-30.

POSSEMATO, R., MARKS, K. M., SHAUL, Y. D., PACOLD, M. E., KIM, D., BIRSOY, K., SETHUMADHAVAN, S., WOO, H.-K., JANG, H. G., JHA, A. K., CHEN, W. W., BARRETT, F. G., STRANSKY, N., TSUN, Z.-Y., COWLEY, G. S., BARRETINA, J., KALAANY, N. Y., HSU, P. P., OTTINA, K., CHAN, A. M., YUAN, B., GARRAWAY, L. A., ROOT, D. E., MINO-KENUDSON, M., BRACHTEL, E. F., DRIGGERS, E. M. & SABATINI, D. M. 2011. Functional genomics reveal that the serine synthesis pathway is essential in breast cancer. *Nature,* 476**,** 346-350.

PRASAD, A., ANDREWS, N. P., PADDER, F. A., HUSAIN, M. & QUYYUMI, A. A. 1999. Glutathione reverses endothelial dysfunction and improves nitric oxide bioavailability. *J Am Coll Cardiol,* 34**,** 507-14.

PRESTERA, T., HOLTZCLAW, W. D., ZHANG, Y. & TALALAY, P. 1993. Chemical and molecular regulation of enzymes that detoxify carcinogens. *Proceedings of the National Academy of Sciences,* 90**,** 2965-2969.

PROBST, Y. C., GUAN, V. X. & KENT, K. 2017. Dietary phytochemical intake from foods and health outcomes: a systematic review protocol and preliminary scoping. *BMJ open,* 7**,** e013337-e013337.

PROCHASKA, H. J., SANTAMARIA, A. B. & TALALAY, P. 1992. Rapid detection of inducers of enzymes that protect against carcinogens. *Proceedings of the National Academy of Sciences of the United States of America,* 89**,** 2394-2398.

QUEISSER, M. A., YAO, D., GEISLER, S., HAMMES, H. P., LOCHNIT, G., SCHLEICHER, E. D., BROWNLEE, M. & PREISSNER, K. T. 2010. Hyperglycemia impairs proteasome function by methylglyoxal. *Diabetes,* 59**,** 670-8.

QUIRANTE-MOYA, S., GARCIA-IBANEZ, P., QUIRANTE-MOYA, F., VILLANO, D. & MORENO, D. A. 2020. The Role of Brassica Bioactives on Human Health: Are We Studying It the Right Way? *Molecules,* 25.

RABAR, S., HARKER, M., O'FLYNN, N. & WIERZBICKI, A. S. 2014. Lipid modification and cardiovascular risk assessment for the primary and secondary prevention of cardiovascular disease: summary of updated NICE guidance. *Bmj,* 349**,** g4356.

RAHMAN, I., GILMOUR, P. S., JIMENEZ, L. A. & MACNEE, W. 2002. Oxidative stress and TNF-alpha induce histone acetylation and NF-kappaB/AP-1 activation in alveolar epithelial cells: potential mechanism in gene transcription in lung inflammation. *Mol Cell Biochem,* 234-235**,** 239-48.

RAHMAN, S. M., JANSSEN, R. C., CHOUDHURY, M., BAQUERO, K. C., AIKENS, R. M., DE LA HOUSSAYE, B. A. & FRIEDMAN, J. E. 2012. CCAAT/enhancer-binding protein β (C/EBPβ) expression regulates dietary-induced inflammation in macrophages and adipose tissue in mice. *J Biol Chem,* 287**,** 34349-60.

RAJASEKARAN, N. S., CONNELL, P., CHRISTIANS, E. S., YAN, L.-J., TAYLOR, R. P., OROSZ, A., ZHANG, X. Q., STEVENSON, T. J., PESHOCK, R. M., LEOPOLD, J. A., BARRY, W. H., LOSCALZO, J., ODELBERG, S. J. & BENJAMIN, I. J. 2007. Human αB-Crystallin Mutation Causes Oxido-Reductive Stress and Protein Aggregation Cardiomyopathy in Mice. *Cell,* 130**,** 427-439.

RANGASAMY, T., GUO, J., MITZNER, W. A., ROMAN, J., SINGH, A., FRYER, A. D., YAMAMOTO, M., KENSLER, T. W., TUDER, R. M., GEORAS, S. N. & BISWAL, S. 2005. Disruption of Nrf2 enhances susceptibility to severe airway inflammation and asthma in mice. *J Exp Med,* 202**,** 47-59.

RAO, M. S., VAN VLEET, T. R., CIURLIONIS, R., BUCK, W. R., MITTELSTADT, S. W., BLOMME, E. A. G. & LIGUORI, M. J. 2019. Comparison of RNA-Seq and Microarray Gene Expression Platforms for the Toxicogenomic Evaluation of Liver From Short-Term Rat Toxicity Studies. *Frontiers in Genetics,* 9.

RAY, P. D., HUANG, B.-W. & TSUJI, Y. 2012. Reactive oxygen species (ROS) homeostasis and redox regulation in cellular signaling. *Cellular signalling,* 24**,** 981-990.

REDDY, N. M., KLEEBERGER, S. R., BREAM, J. H., FALLON, P. G., KENSLER, T. W., YAMAMOTO, M. & REDDY, S. P. 2008. Genetic disruption of the Nrf2 compromises cell-cycle progression by impairing GSH-induced redox signaling. *Oncogene,* 27**,** 5821.

REDDY, N. M., KLEEBERGER, S. R., CHO, H. Y., YAMAMOTO, M., KENSLER, T. W., BISWAL, S. & REDDY, S. P. 2007. Deficiency in Nrf2-GSH signaling impairs type II cell growth and enhances sensitivity to oxidants. *Am J Respir Cell Mol Biol,* 37**,** 3-8.

REED, G. W., ROSSI, J. E. & CANNON, C. P. 2017. Acute myocardial infarction. *The Lancet,* 389**,** 197-210.

RENA, G., HARDIE, D. G. & PEARSON, E. R. 2017. The mechanisms of action of metformin. *Diabetologia,* 60**,** 1577-1585.

RENNERT, K., STEINBORN, S., GRÖGER, M., UNGERBÖCK, B., JANK, A. M., EHGARTNER, J., NIETZSCHE, S., DINGER, J., KIEHNTOPF, M., FUNKE, H., PETERS, F. T., LUPP, A., GÄRTNER, C., MAYR, T., BAUER, M., HUBER, O. & MOSIG, A. S. 2015. A microfluidically perfused three dimensional human liver model. *Biomaterials,* 71**,** 119-131.

RINALDI, G., PRANZINI, E., VAN ELSEN, J., BROEKAERT, D., FUNK, C. M., PLANQUE, M., DOGLIONI, G., ALTEA-MANZANO, P., ROSSI, M., GELDHOF, V., TEOH, S. T., ROSS, C., HUNTER, K. W., LUNT, S. Y., GRÜNEWALD, T. G. P. & FENDT, S. M. 2021. In Vivo Evidence for Serine Biosynthesis-Defined Sensitivity of Lung Metastasis, but Not of Primary Breast Tumors, to mTORC1 Inhibition. *Mol Cell,* 81**,** 386-397.e7.

RIVERA-NIEVES, J., THOMPSON, W. C., LEVINE, R. L. & MOSS, J. 1999. Thiols mediate superoxide-dependent NADH modification of glyceraldehyde-3-phosphate dehydrogenase. *J Biol Chem,* 274**,** 19525-31.

ROBINSON, M. D., MCCARTHY, D. J. & SMYTH, G. K. 2010. edgeR: a Bioconductor package for differential expression analysis of digital gene expression data. *Bioinformatics,* 26**,** 139-40.

ROBINSON, M. D. & OSHLACK, A. 2010. A scaling normalization method for differential expression analysis of RNA-seq data. *Genome Biol,* 11**,** R25.

ROMERO, R., SAYIN, V. I., DAVIDSON, S. M., BAUER, M. R., SINGH, S. X., LEBOEUF, S. E., KARAKOUSI, T. R., ELLIS, D. C., BHUTKAR, A., SANCHEZ-RIVERA, F. J., SUBBARAJ, L., MARTINEZ, B., BRONSON, R. T., PRIGGE, J. R., SCHMIDT, E. E., THOMAS, C. J., GOPARAJU, C., DAVIES, A., DOLGALEV, I., HEGUY, A., ALLAJ, V., POIRIER, J. T., MOREIRA, A. L., RUDIN, C. M., PASS, H. I., VANDER HEIDEN, M. G., JACKS, T. & PAPAGIANNAKOPOULOS, T. 2017. Keap1 loss promotes Kras-driven lung cancer and results in dependence on glutaminolysis. *Nat Med,* 23**,** 1362-1368.

ROSENZWEIG, A., BLENIS, J. & GOMES, A. P. 2018. Beyond the Warburg Effect: How Do Cancer Cells Regulate One-Carbon Metabolism? *Frontiers in Cell and Developmental Biology,* 6.

ROUZAUD, G., RABOT, S., RATCLIFFE, B. & DUNCAN, A. J. 2003. Influence of plant and bacterial myrosinase activity on the metabolic fate of glucosinolates in gnotobiotic rats. *Br J Nutr,* 90**,** 395-404.

RUI, L. 2014. Energy metabolism in the liver. *Compr Physiol,* 4**,** 177-97.

RUNGAPAMESTRY, V., DUNCAN, A. J., FULLER, Z. & RATCLIFFE, B. 2006. Changes in Glucosinolate Concentrations, Myrosinase Activity, and Production of Metabolites of Glucosinolates in Cabbage (Brassica oleracea Var. capitata) Cooked for Different Durations. *Journal of Agricultural and Food Chemistry,* 54**,** 7628-7634.

RUSHMORE, T. H., MORTON, M. R. & PICKETT, C. B. 1991. The antioxidant responsive element. Activation by oxidative stress and identification of the DNA consensus sequence required for functional activity. *J Biol Chem,* 266**,** 11632-9.

RUSHMORE, T. H. & PICKETT, C. B. 1990. Transcriptional regulation of the rat glutathione S-transferase Ya subunit gene. Characterization of a xenobiotic-responsive element controlling inducible expression by phenolic antioxidants. *J Biol Chem,* 265**,** 14648-53.

RUSHMORE, T. H. & PICKETT, C. B. 1993. Glutathione S-transferases, structure, regulation, and therapeutic implications. *J Biol Chem,* 268**,** 11475-8.

RUSHWORTH, S. A., ZAITSEVA, L., MURRAY, M. Y., SHAH, N. M., BOWLES, K. M. & MACEWAN, D. J. 2012. The high Nrf2 expression in human acute myeloid leukemia is driven by NF-κB and underlies its chemo-resistance. *Blood,* 120**,** 5188-98.

RYBAKOVA, Y. S. & BOLDYREV, A. A. 2012. Effect of carnosine and related compounds on proliferation of cultured rat pheochromocytoma PC-12 cells. *Bull Exp Biol Med,* 154**,** 136-40.

SAADEH, M., FERRANTE, T. C., KANE, A., SHIRIHAI, O., CORKEY, B. E. & DEENEY, J. T. 2012. Reactive oxygen species stimulate insulin secretion in rat pancreatic islets: studies using mono-oleoyl-glycerol. *PLoS One,* 7**,** e30200.

SAHA, P. K., REDDY, V. T., KONOPLEVA, M., ANDREEFF, M. & CHAN, L. 2010. The triterpenoid 2-cyano-3,12-dioxooleana-1,9-dien-28-oic-acid methyl ester has potent anti-diabetic effects in diet-induced diabetic mice and Lepr(db/db) mice. *J Biol Chem,* 285**,** 40581-92.

SAKLAYEN, M. G. 2018. The Global Epidemic of the Metabolic Syndrome. *Current hypertension reports,* 20**,** 12-12.

SAKURABA, H., MIZUKAMI, H., YAGIHASHI, N., WADA, R., HANYU, C. & YAGIHASHI, S. 2002. Reduced beta-cell mass and expression of oxidative stress-related DNA damage in the islet of Japanese Type II diabetic patients. *Diabetologia,* 45**,** 85-96.

SANDERSON, L. M., BOEKSCHOTEN, M. V., DESVERGNE, B., MÜLLER, M. & KERSTEN, S. 2009. Transcriptional profiling reveals divergent roles of PPARα and PPARβ/δ in regulation of gene expression in mouse liver. *Physiological Genomics,* 41**,** 42-52.

SATTA, S., MAHMOUD, A. M., WILKINSON, F. L., YVONNE ALEXANDER, M. & WHITE, S. J. 2017. The Role of Nrf2 in Cardiovascular Function and Disease. *Oxidative Medicine and Cellular Longevity,* 2017**,** 9237263.

SCHINDELIN, J., ARGANDA-CARRERAS, I., FRISE, E., KAYNIG, V., LONGAIR, M., PIETZSCH, T., PREIBISCH, S., RUEDEN, C., SAALFELD, S., SCHMID, B., TINEVEZ, J.-Y., WHITE, D. J., HARTENSTEIN, V., ELICEIRI, K., TOMANCAK, P. & CARDONA, A. 2012. Fiji: an open-source platform for biological-image analysis. *Nature Methods,* 9**,** 676-682.

SCHLAEPFER, D. D., HANKS, S. K., HUNTER, T. & VAN DER GEER, P. 1994. Integrin-mediated signal transduction linked to Ras pathway by GRB2 binding to focal adhesion kinase. *Nature,* 372**,** 786-91.

SEFRIED, S., HÄRING, H.-U., WEIGERT, C. & ECKSTEIN, S. S. 2018. Suitability of hepatocyte cell lines HepG2, AML12 and THLE-2 for investigation of insulin signalling and hepatokine gene expression. *Open Biology,* 8**,** 180147.

SEKINE-SUZUKI, E., YU, D., KUBOTA, N., OKAYASU, R. & ANZAI, K. 2008. Sulforaphane induces DNA double strand breaks predominantly repaired by homologous recombination

pathway in human cancer cells. *Biochemical and Biophysical Research Communications,* 377**,** 341-345.

SEOW, A., SHI, C. Y., CHUNG, F. L., JIAO, D., HANKIN, J. H., LEE, H. P., COETZEE, G. A. & YU, M. C. 1998. Urinary total isothiocyanate (ITC) in a population-based sample of middle-aged and older Chinese in Singapore: relationship with dietary total ITC and glutathione S-transferase M1/T1/P1 genotypes. *Cancer Epidemiol Biomarkers Prev,* 7**,** 775-81.

SESTILI, P., PAOLILLO, M., LENZI, M., COLOMBO, E., VALLORANI, L., CASADEI, L., MARTINELLI, C. & FIMOGNARI, C. 2010. Sulforaphane induces DNA single strand breaks in cultured human cells. *Mutation Research/Fundamental and Molecular Mechanisms of Mutagenesis,* 689**,** 65-73.

SHAH, S., IQBAL, M., KARAM, J., SALIFU, M. & MCFARLANE, S. I. 2007. Oxidative stress, glucose metabolism, and the prevention of type 2 diabetes: pathophysiological insights. *Antioxid Redox Signal,* 9**,** 911-29.

SHAPIRO, T. A., FAHEY, J. W., DINKOVA-KOSTOVA, A. T., HOLTZCLAW, W. D., STEPHENSON, K. K., WADE, K. L., YE, L. & TALALAY, P. 2006. Safety, tolerance, and metabolism of broccoli sprout glucosinolates and isothiocyanates: a clinical phase I study. *Nutr Cancer,* 55**,** 53-62.

SHEN, C., WANG, D., LIU, X., GU, B., DU, Y., WEI, F. Z., CAO, L. L., SONG, B., LU, X., YANG, Q., ZHU, Q., HOU, T., LI, M., WANG, L., WANG, H., ZHAO, Y., YANG, Y. & ZHU, W. G. 2015. SET7/9 regulates cancer cell proliferation by influencing β-catenin stability. *Faseb j,* 29**,** 4313-23.

SHEN, G. & KONG, A. N. 2009. Nrf2 plays an important role in coordinated regulation of Phase II drug metabolism enzymes and Phase III drug transporters. *Biopharm Drug Dispos,* 30**,** 345-55.

SHUKLA, S. K., GEBREGIWORGIS, T., PUROHIT, V., CHAIKA, N. V., GUNDA, V., RADHAKRISHNAN, P., MEHLA, K., PIPINOS, I. I., POWERS, R., YU, F. & SINGH, P. K. 2014. Metabolic reprogramming induced by ketone bodies diminishes pancreatic cancer cachexia. *Cancer & Metabolism,* 2**,** 18.

SHUKLA, V., MISHRA, S. K. & PANT, H. C. 2011. Oxidative stress in neurodegeneration. *Adv Pharmacol Sci,* 2011**,** 572634.

SINGH, A., HAPPEL, C., MANNA, S. K., ACQUAAH-MENSAH, G., CARRERERO, J., KUMAR, S., NASIPURI, P., KRAUSZ, K. W., WAKABAYASHI, N., DEWI, R., BOROS, L. G., GONZALEZ, F. J., GABRIELSON, E., WONG, K. K., GIRNUN, G. & BISWAL, S. 2013. Transcription factor NRF2 regulates miR-1 and miR-206 to drive tumorigenesis. *J Clin Invest,* 123**,** 2921-34.

SINGH, K. B., KIM, S.-H., HAHM, E.-R., PORE, S. K., JACOBS, B. L. & SINGH, S. V. 2018. Prostate cancer chemoprevention by sulforaphane in a preclinical mouse model is associated with inhibition of fatty acid metabolism. *Carcinogenesis,* 39**,** 826-837.

SINGH, S. V., HERMAN-ANTOSIEWICZ, A., SINGH, A. V., LEW, K. L., SRIVASTAVA, S. K., KAMATH, R., BROWN, K. D., ZHANG, L. & BASKARAN, R. 2004. Sulforaphane-induced G2/M Phase Cell Cycle Arrest Involves Checkpoint Kinase 2-mediated Phosphorylation of Cell Division Cycle 25C*. *Journal of Biological Chemistry,* 279**,** 25813-25822.

SINGH, S. V., SRIVASTAVA, S. K., CHOI, S., LEW, K. L., ANTOSIEWICZ, J., XIAO, D., ZENG, Y., WATKINS, S. C., JOHNSON, C. S., TRUMP, D. L., LEE, Y. J., XIAO, H. & HERMAN-ANTOSIEWICZ, A. 2005. Sulforaphane-induced Cell Death in Human Prostate Cancer Cells Is Initiated by Reactive Oxygen Species*. *Journal of Biological Chemistry,* 280**,** 19911-19924.

SINGLETARY, K. & MACDONALD, C. 2000. Inhibition of benzo[a]pyrene- and 1,6-dinitropyrene-DNA adduct formation in human mammary epithelial cells bydibenzoylmethane and sulforaphane. *Cancer Lett,* 155**,** 47-54.

SIVAPALAN, T., MELCHINI, A., SAHA, S., NEEDS, P. W., TRAKA, M. H., TAPP, H., DAINTY, J. R. & MITHEN, R. F. 2018. Bioavailability of Glucoraphanin and Sulforaphane from High-Glucoraphanin Broccoli. *Mol Nutr Food Res,* 62**,** e1700911.

SOFTIC, S., GUPTA, M. K., WANG, G. X., FUJISAKA, S., O'NEILL, B. T., RAO, T. N., WILLOUGHBY, J., HARBISON, C., FITZGERALD, K., ILKAYEVA, O., NEWGARD, C. B., COHEN, D. E. & KAHN, C. R. 2017. Divergent effects of glucose and fructose on hepatic lipogenesis and insulin signaling. *J Clin Invest,* 127**,** 4059-4074.

SORMUNEN, R., ESKELINEN, S. & LEHTO, V. P. 1993. Bile canaliculus formation in cultured HEPG2 cells. *Lab Invest,* 68**,** 652-62.

SOTO-ANGONA, Ó., ANMELLA, G., VALDÉS-FLORIDO, M. J., DE URIBE-VILORIA, N., CARVALHO, A. F., PENNINX, B. W. J. H. & BERK, M. 2020. Non-alcoholic fatty liver disease (NAFLD) as a neglected metabolic companion of psychiatric disorders: common pathways and future approaches. *BMC Medicine,* 18**,** 261.

SPITZ, M. R., DUPHORNE, C. M., DETRY, M. A., PILLOW, P. C., AMOS, C. I., LEI, L., DE ANDRADE, M., GU, X., HONG, W. K. & WU, X. 2000. Dietary intake of isothiocyanates: evidence of a joint effect with glutathione S-transferase polymorphisms in lung cancer risk. *Cancer Epidemiol Biomarkers Prev,* 9**,** 1017-20.

STARK, R., GRZELAK, M. & HADFIELD, J. 2019. RNA sequencing: the teenage years. *Nature Reviews Genetics,* 20**,** 631-656.

STECKELBROECK, S., OYESANMI, B., JIN, Y., LEE, S.-H., KLOOSTERBOER, H. J. & PENNING, T. M. 2006. Tibolone Metabolism in Human Liver Is Catalyzed by 3α/3β-Hydroxysteroid Dehydrogenase Activities of the Four Isoforms of the Aldo-Keto Reductase (AKR)1C Subfamily. *Journal of Pharmacology and Experimental Therapeutics,* 316**,** 1300-1309.

STEDMAN, M., LUNT, M., LIVINGSTON, M., FRYER, A. A., MORENO, G., BAILEY, S., GADSBY, R. & HEALD, A. 2019. The costs of drug prescriptions for diabetes in the NHS. *The Lancet,* 393**,** 226-227.

STONE, K. P., GHOSH, S., KOVALIK, J. P., ORGERON, M., WANDERS, D., SIMS, L. C. & GETTYS, T. W. 2021. The acute transcriptional responses to dietary methionine restriction are triggered by inhibition of ternary complex formation and linked to Erk1/2, mTOR, and ATF4. *Scientific Reports,* 11**,** 3765.

SU, R. C., LAD, A., BREIDENBACH, J. D., BLOMQUIST, T. M., GUNNING, W. T., DUBE, P., KLEINHENZ, A. L., MALHOTRA, D., HALLER, S. T. & KENNEDY, D. J. 2019. Hyperglycemia induces key genetic and phenotypic changes in human liver epithelial HepG2 cells which parallel the Leprdb/J mouse model of non-alcoholic fatty liver disease (NAFLD). *PLOS ONE,* 14**,** e0225604.

SU, X., JIANG, X., MENG, L., DONG, X., SHEN, Y. & XIN, Y. 2018. Anticancer Activity of Sulforaphane: The Epigenetic Mechanisms and the Nrf2 Signaling Pathway. *Oxidative medicine and cellular longevity,* 2018**,** 5438179-5438179.

SUBRAMANIAN, A., TAMAYO, P., MOOTHA, V. K., MUKHERJEE, S., EBERT, B. L., GILLETTE, M. A., PAULOVICH, A., POMEROY, S. L., GOLUB, T. R., LANDER, E. S. & MESIROV, J. P. 2005. Gene set enrichment analysis: A knowledge-based approach for interpreting genome-wide expression profiles. *Proceedings of the National Academy of Sciences,* 102**,** 15545.

SUN, X., FENG, R., LI, Y., LIN, S., ZHANG, W., LI, Y., SUN, C. & LI, S. 2014. Histidine supplementation alleviates inflammation in the adipose tissue of high-fat diet-induced obese rats via the NF-κB- and PPARγ-involved pathways. *Br J Nutr,* 112**,** 477-85.

SUN, Y., ZHOU, S., GUO, H., ZHANG, J., MA, T., ZHENG, Y., ZHANG, Z. & CAI, L. 2020. Protective effects of sulforaphane on type 2 diabetes-induced cardiomyopathy via AMPK-mediated activation of lipid metabolic pathways and NRF2 function. *Metabolism,* 102**,** 154002.

SUNG, K. C., JEONG, W. S., WILD, S. H. & BYRNE, C. D. 2012. Combined influence of insulin resistance, overweight/obesity, and fatty liver as risk factors for type 2 diabetes. *Diabetes Care,* 35**,** 717-22.

SUPPIPAT, K., PARK, C. S., SHEN, Y., ZHU, X. & LACORAZZA, H. D. 2012. Sulforaphane induces cell cycle arrest and apoptosis in acute lymphoblastic leukemia cells. *PloS one,* 7**,** e51251-e51251.

SUSSAN, T. E., JUN, J., THIMMULAPPA, R., BEDJA, D., ANTERO, M., GABRIELSON, K. L., POLOTSKY, V. Y. & BISWAL, S. 2008. Disruption of Nrf2, a Key Inducer of Antioxidant Defenses, Attenuates ApoE-Mediated Atherosclerosis in Mice. *PLOS ONE,* 3**,** e3791.

TAHATA, S., SINGH, S. V., LIN, Y., HAHM, E. R., BEUMER, J. H., CHRISTNER, S. M., RAO, U. N., SANDER, C., TARHINI, A. A., TAWBI, H., FERRIS, L. K., WILSON, M., ROSE, A., DIETZ, C. M., HUGHES, E., FAHEY, J. W., LEACHMAN, S. A., CASSIDY, P. B., BUTTERFIELD, L. H., ZAROUR, H. M. & KIRKWOOD, J. M. 2018. Evaluation of Biodistribution of Sulforaphane after Administration of Oral Broccoli Sprout Extract in Melanoma Patients with Multiple Atypical Nevi. *Cancer Prev Res (Phila),* 11**,** 429-438.

TAMAYO, P., STEINHARDT, G., LIBERZON, A. & MESIROV, J. P. 2016. The limitations of simple gene set enrichment analysis assuming gene independence. *Statistical methods in medical research,* 25**,** 472-487.

TAN, N. Y. & KHACHIGIAN, L. M. 2009. Sp1 Phosphorylation and Its Regulation of Gene Transcription. *Molecular and Cellular Biology,* 29**,** 2483.

TANAKA, Y., ALEKSUNES, L. M., YEAGER, R. L., GYAMFI, M. A., ESTERLY, N., GUO, G. L. & KLAASSEN, C. D. 2008. NF-E2-related factor 2 inhibits lipid accumulation and oxidative stress in mice fed a high-fat diet. *J Pharmacol Exp Ther,* 325**,** 655-64.

TANAKA, Y., IKEDA, T., YAMAMOTO, K., OGAWA, H. & KAMISAKO, T. 2012. Dysregulated expression of fatty acid oxidation enzymes and iron-regulatory genes in livers of Nrf2-null mice. *J Gastroenterol Hepatol,* 27**,** 1711-7.

TANITO, M., MASUTANI, H., KIM, Y.-C., NISHIKAWA, M., OHIRA, A. & YODOI, J. 2005. Sulforaphane Induces Thioredoxin through the Antioxidant-Responsive Element and Attenuates Retinal Light Damage in Mice. *Investigative Ophthalmology & Visual Science,* 46**,** 979-987.

TANNER, L. B., GOGLIA, A. G., WEI, M. H., SEHGAL, T., PARSONS, L. R., PARK, J. O., WHITE, E., TOETTCHER, J. E. & RABINOWITZ, J. D. 2018. Four Key Steps Control Glycolytic Flux in Mammalian Cells. *Cell Syst,* 7**,** 49-62.e8.

TEBAY, L. E., ROBERTSON, H., DURANT, S. T., VITALE, S. R., PENNING, T. M., DINKOVA-KOSTOVA, A. T. & HAYES, J. D. 2015. Mechanisms of activation of the transcription factor Nrf2 by redox stressors, nutrient cues, and energy status and the pathways through which it attenuates degenerative disease. *Free Radic Biol Med,* 88**,** 108-146.

TENG, W., LI, Y., DU, M., LEI, X., XIE, S. & REN, F. 2019. Sulforaphane Prevents Hepatic Insulin Resistance by Blocking Serine Palmitoyltransferase 3-Mediated Ceramide Biosynthesis. *Nutrients,* 11.

TEODORO, J. S., DUARTE, F. V., GOMES, A. P., VARELA, A. T., PEIXOTO, F. M., ROLO, A. P. & PALMEIRA, C. M. 2013. Berberine reverts hepatic mitochondrial dysfunction in high-fat fed rats: a possible role for SirT3 activation. *Mitochondrion,* 13**,** 637-46.

THIMMULAPPA, R. K., LEE, H., RANGASAMY, T., REDDY, S. P., YAMAMOTO, M., KENSLER, T. W. & BISWAL, S. 2006. Nrf2 is a critical regulator of the innate immune response and survival during experimental sepsis. *J Clin Invest,* 116**,** 984-95.

THIMMULAPPA, R. K., MAI, K. H., SRISUMA, S., KENSLER, T. W., YAMAMOTO, M. & BISWAL, S. 2002. Identification of Nrf2-regulated genes induced by the chemopreventive agent sulforaphane by oligonucleotide microarray. *Cancer Res,* 62**,** 5196-203.

THINGHOLM, L. B., RÜHLEMANN, M. C., KOCH, M., FUQUA, B., LAUCKE, G., BOEHM, R., BANG, C., FRANZOSA, E. A., HÜBENTHAL, M., RAHNAVARD, A., FROST, F., LLOYD-PRICE, J., SCHIRMER, M., LUSIS, A. J., VULPE, C. D., LERCH, M. M., HOMUTH, G., KACPROWSKI, T., SCHMIDT, C. O., NÖTHLINGS, U., KARLSEN, T. H., LIEB, W., LAUDES, M., FRANKE, A. & HUTTENHOWER, C. 2019. Obese Individuals with and without Type 2 Diabetes Show Different Gut Microbial Functional Capacity and Composition. *Cell host & microbe,* 26**,** 252-264.e10.

THORNALLEY, P. J., LANGBORG, A. & MINHAS, H. S. 1999. Formation of glyoxal, methylglyoxal and 3-deoxyglucosone in the glycation of proteins by glucose. *Biochem J,* 344 Pt 1**,** 109-16.

THURSBY, E. & JUGE, N. 2017. Introduction to the human gut microbiota. *The Biochemical journal,* 474**,** 1823-1836.

TIAN, S., LI, B., LEI, P., YANG, X., ZHANG, X., BAO, Y. & SHAN, Y. 2018. Sulforaphane Improves Abnormal Lipid Metabolism via Both ERS-Dependent XBP1/ACC &SCD1 and ERS-Independent SREBP/FAS Pathways. *Mol Nutr Food Res,* 62**,** e1700737.

TILG, H., MOSCHEN, A. R. & RODEN, M. 2017. NAFLD and diabetes mellitus. *Nature Reviews Gastroenterology & Hepatology,* 14**,** 32-42.

TOGO, M., KONARI, N., TSUKAMOTO, M., KIMOTO, R., YAMAGUCHI, T., TAKEDA, H. & KAMBAYASHI, I. 2018. Effects of a high-fat diet on superoxide anion generation and membrane fluidity in liver mitochondria in rats. *Journal of the International Society of Sports Nutrition,* 15**,** 13.

TOLMAN, K. G., FONSECA, V., DALPIAZ, A. & TAN, M. H. 2007. Spectrum of Liver Disease in Type 2 Diabetes and Management of Patients With Diabetes and Liver Disease. *Diabetes Care,* 30**,** 734-743.

TONG, K. I., KATOH, Y., KUSUNOKI, H., ITOH, K., TANAKA, T. & YAMAMOTO, M. 2006. Keap1 recruits Neh2 through binding to ETGE and DLG motifs: characterization of the two-site molecular recognition model. *Mol Cell Biol,* 26**,** 2887-900.

TORRES, T. P., CATLIN, R. L., CHAN, R., FUJIMOTO, Y., SASAKI, N., PRINTZ, R. L., NEWGARD, C. B. & SHIOTA, M. 2009. Restoration of hepatic glucokinase expression corrects hepatic glucose flux and normalizes plasma glucose in zucker diabetic fatty rats. *Diabetes,* 58**,** 78-86.

TRACHOOTHAM, D., ALEXANDRE, J. & HUANG, P. 2009. Targeting cancer cells by ROS-mediated mechanisms: a radical therapeutic approach? *Nat Rev Drug Discov,* 8**,** 579-91.

TRAKA, M., GASPER, A. V., SMITH, J. A., HAWKEY, C. J., BAO, Y. & MITHEN, R. F. 2005. Transcriptome analysis of human colon Caco-2 cells exposed to sulforaphane. *J Nutr,* 135**,** 1865-72.

TRAKA, M. & MITHEN, R. 2008. Glucosinolates, isothiocyanates and human health. *Phytochemistry Reviews,* 8**,** 269-282.

TRAKA, M. H., MELCHINI, A., COODE-BATE, J., AL KADHI, O., SAHA, S., DEFERNEZ, M., TRONCOSO-REY, P., KIBBLEWHITE, H., O'NEILL, C. M., BERNUZZI, F., MYTHEN, L., HUGHES, J., NEEDS, P. W., DAINTY, J. R., SAVVA, G. M., MILLS, R. D., BALL, R. Y., COOPER, C. S. & MITHEN, R. F. 2019. Transcriptional changes in prostate of men on active surveillance after a 12-mo glucoraphanin-rich broccoli intervention-results from the Effect of Sulforaphane on prostate CAncer PrEvention (ESCAPE) randomized controlled trial. *Am J Clin Nutr,* 109**,** 1133-1144.

TRAKA, M. H., SAHA, S., HUSEBY, S., KOPRIVA, S., WALLEY, P. G., BARKER, G. C., MOORE, J., MERO, G., VAN DEN BOSCH, F., CONSTANT, H., KELLY, L., SCHEPERS, H., BODDUPALLI, S. & MITHEN, R. F. 2013. Genetic regulation of glucoraphanin accumulation in Beneforté® broccoli. *New Phytologist,* 198**,** 1085-1095.

TRAKA, M. H., SPINKS, C. A., DOLEMAN, J. F., MELCHINI, A., BALL, R. Y., MILLS, R. D. & MITHEN, R. F. 2010. The dietary isothiocyanate sulforaphane modulates gene expression and alternative gene splicing in a PTEN null preclinical murine model of prostate cancer. *Molecular Cancer,* 9**,** 189.

TREPIANA, J., KRISA, S., RENOUF, E. & PORTILLO, M. P. 2020. Resveratrol Metabolites Are Able to Reduce Steatosis in Cultured Hepatocytes. *Pharmaceuticals (Basel, Switzerland),* 13**,** 285.

TRUSLER, D. 2011. Statin prescriptions in UK now total a million each week. *Bmj,* 343**,** d4350.

TSAI, J. J., DUDAKOV, J. A., TAKAHASHI, K., SHIEH, J.-H., VELARDI, E., HOLLAND, A. M., SINGER, N. V., WEST, M. L., SMITH, O. M., YOUNG, L. F., SHONO, Y., GHOSH, A., HANASH, A. M., TRAN, H. T., MOORE, M. A. S. & VAN DEN BRINK, M. R. M. 2013. Nrf2 regulates haematopoietic stem cell function. *Nature Cell Biology,* 15**,** 309.

TSYRULNYK, A. & MORIGGL, R. 2008. A detailed protocol for bacterial artificial chromosome recombineering to study essential genes in stem cells. *Methods Mol Biol,* 430**,** 269-93.
TUANO, N. K., OKABE, J., ZIEMANN, M., COOPER, M. E. & EL-OSTA, A. 2016. Set7 mediated interactions regulate transcriptional networks in embryonic stem cells. *Nucleic Acids Res,* 44**,** 9206-9217.
TUREI, D., PAPP, D., FAZEKAS, D., FOLDVARI-NAGY, L., MODOS, D., LENTI, K., CSERMELY, P. & KORCSMAROS, T. 2013. NRF2-ome: an integrated web resource to discover protein interaction and regulatory networks of NRF2. *Oxid Med Cell Longev,* 2013**,** 737591.
TURRENS, J. F. 1997. Superoxide production by the mitochondrial respiratory chain. *Biosci Rep,* 17**,** 3-8.
URUNO, A., FURUSAWA, Y., YAGISHITA, Y., FUKUTOMI, T., MURAMATSU, H., NEGISHI, T., SUGAWARA, A., KENSLER, T. W. & YAMAMOTO, M. 2013. The Keap1-Nrf2 system prevents onset of diabetes mellitus. *Mol Cell Biol,* 33**,** 2996-3010.
VALADI, H., VALADI, Å., ANSELL, R., GUSTAFSSON, L., ADLER, L., NORBECK, J. & BLOMBERG, A. 2004. NADH-reductive stress in Saccharomyces cerevisiae induces the expression of the minor isoform of glyceraldehyde-3-phosphate dehydrogenase (TDH1). *Current Genetics,* 45**,** 90-95.
VANDER HEIDEN, M. G., CANTLEY, L. C. & THOMPSON, C. B. 2009. Understanding the Warburg Effect: The Metabolic Requirements of Cell Proliferation. *Science,* 324**,** 1029.
VARGAS, T., MORENO-RUBIO, J., HERRANZ, J., CEJAS, P., MOLINA, S., MENDIOLA, M., BURGOS, E., CUSTODIO, A. B., DE MIGUEL, M., MARTÍN-HERNÁNDEZ, R., REGLERO, G., FELIU, J. & RAMÍREZ DE MOLINA, A. 2016. 3'UTR Polymorphism in ACSL1 Gene Correlates with Expression Levels and Poor Clinical Outcome in Colon Cancer Patients. *PLoS One,* 11**,** e0168423.
VAZQUEZ, G., DUVAL, S., JACOBS, D. R., JR. & SILVENTOINEN, K. 2007. Comparison of body mass index, waist circumference, and waist/hip ratio in predicting incident diabetes: a meta-analysis. *Epidemiol Rev,* 29**,** 115-28.
VIAL, G., DUBOUCHAUD, H., COUTURIER, K., COTTET-ROUSSELLE, C., TALEUX, N., ATHIAS, A., GALINIER, A., CASTEILLA, L. & LEVERVE, X. M. 2011. Effects of a high-fat diet on energy metabolism and ROS production in rat liver. *J Hepatol,* 54**,** 348-56.
VIOLLET, B., FORETZ, M., GUIGAS, B., HORMAN, S., DENTIN, R., BERTRAND, L., HUE, L. & ANDREELLI, F. 2006. Activation of AMP-activated protein kinase in the liver: a new strategy for the management of metabolic hepatic disorders. *The Journal of Physiology,* 574**,** 41-53.
VRIENS, K., CHRISTEN, S., PARIK, S., BROEKAERT, D., YOSHINAGA, K., TALEBI, A., DEHAIRS, J., ESCALONA-NOGUERO, C., SCHMIEDER, R., CORNFIELD, T., CHARLTON, C., ROMERO-PÉREZ, L., ROSSI, M., RINALDI, G., ORTH, M. F., BOON, R., KERSTENS, A., KWAN, S. Y., FAUBERT, B., MÉNDEZ-LUCAS, A., KOPITZ, C. C., CHEN, T., FERNANDEZ-GARCIA, J., DUARTE, J. A. G., SCHMITZ, A. A., STEIGEMANN, P., NAJIMI, M., HÄGEBARTH, A., VAN GINDERACHTER, J. A., SOKAL, E., GOTOH, N., WONG, K.-K., VERFAILLIE, C., DERUA, R., MUNCK, S., YUNEVA, M., BERETTA, L., DEBERARDINIS, R. J., SWINNEN, J. V., HODSON, L., CASSIMAN, D., VERSLYPE, C., CHRISTIAN, S., GRÜNEWALD, S., GRÜNEWALD, T. G. P. & FENDT, S.-M. 2019. Evidence for an alternative fatty acid desaturation pathway increasing cancer plasticity. *Nature,* 566**,** 403-406.
WAKABAYASHI, N., DINKOVA-KOSTOVA, A. T., HOLTZCLAW, W. D., KANG, M. I., KOBAYASHI, A., YAMAMOTO, M., KENSLER, T. W. & TALALAY, P. 2004. Protection against electrophile and oxidant stress by induction of the phase 2 response: fate of cysteines of the Keap1 sensor modified by inducers. *Proc Natl Acad Sci U S A,* 101**,** 2040-5.
WAKABAYASHI, N., ITOH, K., WAKABAYASHI, J., MOTOHASHI, H., NODA, S., TAKAHASHI, S., IMAKADO, S., KOTSUJI, T., OTSUKA, F., ROOP, D. R., HARADA, T., ENGEL, J. D. & YAMAMOTO, M. 2003. Keap1-null mutation leads to postnatal lethality due to constitutive Nrf2 activation. *Nature Genetics,* 35**,** 238.

WAKABAYASHI, N., SHIN, S., SLOCUM, S. L., AGOSTON, E. S., WAKABAYASHI, J., KWAK, M.-K., MISRA, V., BISWAL, S., YAMAMOTO, M. & KENSLER, T. W. 2010. Regulation of Notch1 Signaling by Nrf2: Implications for Tissue Regeneration. *Science Signaling,* 3**,** ra52-ra52.

WAMELINK, M. M. C., STRUYS, E. A. & JAKOBS, C. 2008. The biochemistry, metabolism and inherited defects of the pentose phosphate pathway: A review. *Journal of Inherited Metabolic Disease,* 31**,** 703-717.

WANG, H., LIU, K., GENG, M., GAO, P., WU, X., HAI, Y., LI, Y., LI, Y., LUO, L., HAYES, J. D., WANG, X. J. & TANG, X. 2013. RXRalpha inhibits the NRF2-ARE signaling pathway through a direct interaction with the Neh7 domain of NRF2. *Cancer Res,* 73**,** 3097-108.

WANG, H., NAGHAVI, M., ALLEN, C., BARBER, R. M., BHUTTA, Z. A., CARTER, A., CASEY, D. C., CHARLSON, F. J., CHEN, A. Z., COATES, M. M., COGGESHALL, M., DANDONA, L., DICKER, D. J., ERSKINE, H. E., FERRARI, A. J., FITZMAURICE, C., FOREMAN, K., FOROUZANFAR, M. H., FRASER, M. S., FULLMAN, N., GETHING, P. W., GOLDBERG, E. M., GRAETZ, N., HAAGSMA, J. A., HAY, S. I., HUYNH, C., JOHNSON, C. O., KASSEBAUM, N. J., KINFU, Y., KULIKOFF, X. R., KUTZ, M., KYU, H. H., LARSON, H. J., LEUNG, J., LIANG, X., LIM, S. S., LIND, M., LOZANO, R., MARQUEZ, N., MENSAH, G. A., MIKESELL, J., MOKDAD, A. H., MOONEY, M. D., NGUYEN, G., NSOESIE, E., PIGOTT, D. M., PINHO, C., ROTH, G. A., SALOMON, J. A., SANDAR, L., SILPAKIT, N., SLIGAR, A., SORENSEN, R. J. D., STANAWAY, J., STEINER, C., TEEPLE, S., THOMAS, B. A., TROEGER, C., VANDERZANDEN, A., VOLLSET, S. E., WANGA, V., WHITEFORD, H. A., WOLOCK, T., ZOECKLER, L., ABATE, K. H., ABBAFATI, C., ABBAS, K. M., ABD-ALLAH, F., ABERA, S. F., ABREU, D. M. X., ABU-RADDAD, L. J., ABYU, G. Y., ACHOKI, T., ADELEKAN, A. L., ADEMI, Z., ADOU, A. K., ADSUAR, J. C., AFANVI, K. A., AFSHIN, A., AGARDH, E. E., AGARWAL, A., AGRAWAL, A., KIADALIRI, A. A., AJALA, O. N., AKANDA, A. S., AKINYEMI, R. O., AKINYEMIJU, T. F., AKSEER, N., LAMI, F. H. A., ALABED, S., AL-ALY, Z., ALAM, K., ALAM, N. K. M., ALASFOOR, D., ALDHAHRI, S. F., ALDRIDGE, R. W., ALEGRETTI, M. A., ALEMAN, A. V., ALEMU, Z. A., ALEXANDER, L. T., et al. 2016. Global, regional, and national life expectancy, all-cause mortality, and cause-specific mortality for 249 causes of death, 1980–2015: a systematic analysis for the Global Burden of Disease Study 2015. *The Lancet,* 388**,** 1459-1544.

WANG, P.-X., DENG, X.-R., ZHANG, C.-H. & YUAN, H.-J. 2020. Gut microbiota and metabolic syndrome. *Chinese medical journal,* 133**,** 808-816.

WASSERMAN, W. W. & FAHL, W. E. 1997. Functional antioxidant responsive elements. *Proceedings of the National Academy of Sciences,* 94**,** 5361-5366.

WEGNER, A., WEINDL, D., JÄGER, C., SAPCARIU, S. C., DONG, X., STEPHANOPOULOS, G. & HILLER, K. 2014. Fragment Formula Calculator (FFC): Determination of Chemical Formulas for Fragment Ions in Mass Spectrometric Data. *Analytical Chemistry,* 86**,** 2221-2228.

WEINGÄRTNER, O., PINSDORF, T., ROGACEV, K. S., BLÖMER, L., GRENNER, Y., GRÄBER, S., ULRICH, C., GIRNDT, M., BÖHM, M., FLISER, D., LAUFS, U., LÜTJOHANN, D. & HEINE, G. H. 2010. The Relationships of Markers of Cholesterol Homeostasis with Carotid Intima-Media Thickness. *PLOS ONE,* 5**,** e13467.

WHITEHEAD, K. J., MUTHUSAMY, V. R., RAJASEKARAN, N. S., KANNAN, S., WANG, L., GOMES, A. V., LITWIN, S. E., KENSLER, T. W., ABEL, E. D. & HOIDAL, J. R. 2013. Nrf2 deficiency prevents reductive stress-induced hypertrophic cardiomyopathy. *Cardiovascular Research,* 100**,** 63-73.

WHITLEY, S. K., HORNE, W. T. & KOLLS, J. K. 2016. Research Techniques Made Simple: Methodology and Clinical Applications of RNA Sequencing. *Journal of Investigative Dermatology,* 136**,** e77-e82.

WILLIAMS, R. J., SPENCER, J. P. & RICE-EVANS, C. 2004. Flavonoids: antioxidants or signalling molecules? *Free Radic Biol Med,* 36**,** 838-49.

WILLIAMSON, J. R., CHANG, K., FRANGOS, M., HASAN, K. S., IDO, Y., KAWAMURA, T., NYENGAARD, J. R., VAN DEN ENDEN, M., KILO, C. & TILTON, R. G. 1993. Hyperglycemic pseudohypoxia and diabetic complications. *Diabetes,* 42**,** 801-13.

WITTSTOCK, U. & BUROW, M. 2010. Glucosinolate Breakdown in Arabidopsis: Mechanism, Regulation and Biological Significance. *The Arabidopsis Book,* 2010.

WONG, R. H. F. & SUL, H. S. 2010. Insulin signaling in fatty acid and fat synthesis: a transcriptional perspective. *Current opinion in pharmacology,* 10**,** 684-691.

WU, K. C., CUI, J. Y. & KLAASSEN, C. D. 2011. Beneficial role of Nrf2 in regulating NADPH generation and consumption. *Toxicol Sci,* 123**,** 590-600.

WU, K. C., CUI, J. Y. & KLAASSEN, C. D. 2012. Effect of graded Nrf2 activation on phase-I and -II drug metabolizing enzymes and transporters in mouse liver. *PloS one,* 7**,** e39006-e39006.

XIAO, D., POWOLNY, A. A., ANTOSIEWICZ, J., HAHM, E.-R., BOMMAREDDY, A., ZENG, Y., DESAI, D., AMIN, S., HERMAN-ANTOSIEWICZ, A. & SINGH, S. V. 2009. Cellular Responses to Cancer Chemopreventive Agent D,L-Sulforaphane in Human Prostate Cancer Cells Are Initiated by Mitochondrial Reactive Oxygen Species. *Pharmaceutical Research,* 26**,** 1729-1738.

XU, C., HUANG, M. T., SHEN, G., YUAN, X., LIN, W., KHOR, T. O., CONNEY, A. H. & KONG, A. N. 2006. Inhibition of 7,12-dimethylbenz(a)anthracene-induced skin tumorigenesis in C57BL/6 mice by sulforaphane is mediated by nuclear factor E2-related factor 2. *Cancer Res,* 66**,** 8293-6.

XU, J., DONEPUDI, A. C., MOSCOVITZ, J. E. & SLITT, A. L. 2013. Keap1-Knockdown Decreases Fasting-Induced Fatty Liver via Altered Lipid Metabolism and Decreased Fatty Acid Mobilization from Adipose Tissue. *PLOS ONE,* 8**,** e79841.

XU, Q., LIU, L., VU, H., KUHLS, M., ASLAMKHAN, A. G., LIAW, A., YU, Y., KACZOR, A., RUTH, M., WEI, C., IMREDY, J., LEBRON, J., PEARSON, K., GONZALEZ, R., MITRA, K. & SISTARE, F. D. 2019. Can Galactose Be Converted to Glucose in HepG2 Cells? Improving the in Vitro Mitochondrial Toxicity Assay for the Assessment of Drug Induced Liver Injury. *Chemical Research in Toxicology,* 32**,** 1528-1544.

XU, X., DAI, M., LAO, F., CHEN, F., HU, X., LIU, Y. & WU, J. 2020. Effect of glucoraphanin from broccoli seeds on lipid levels and gut microbiota in high-fat diet-fed mice. *Journal of Functional Foods,* 68**,** 103858.

YADAV, U. P., SINGH, T., KUMAR, P., SHARMA, P., KAUR, H., SHARMA, S., SINGH, S., KUMAR, S. & MEHTA, K. 2020. Metabolic Adaptations in Cancer Stem Cells. *Frontiers in Oncology,* 10.

YAGISHITA, Y., FAHEY, J. W., DINKOVA-KOSTOVA, A. T. & KENSLER, T. W. 2019. Broccoli or Sulforaphane: Is It the Source or Dose That Matters? *Molecules (Basel, Switzerland),* 24**,** 3593.

YAGISHITA, Y., FUKUTOMI, T., SUGAWARA, A., KAWAMURA, H., TAKAHASHI, T., PI, J., URUNO, A. & YAMAMOTO, M. 2014. Nrf2 protects pancreatic beta-cells from oxidative and nitrosative stress in diabetic model mice. *Diabetes,* 63**,** 605-18.

YAGISHITA, Y., URUNO, A., FUKUTOMI, T., SAITO, R., SAIGUSA, D., PI, J., FUKAMIZU, A., SUGIYAMA, F., TAKAHASHI, S. & YAMAMOTO, M. 2017. Nrf2 Improves Leptin and Insulin Resistance Provoked by Hypothalamic Oxidative Stress. *Cell Rep,* 18**,** 2030-2044.

YAMAMOTO, T., SUZUKI, T., KOBAYASHI, A., WAKABAYASHI, J., MAHER, J., MOTOHASHI, H. & YAMAMOTO, M. 2008. Physiological Significance of Reactive Cysteine Residues of Keap1 in Determining Nrf2 Activity. *Molecular and Cellular Biology,* 28**,** 2758-2770.

YANG, G., LEE, H. E. & LEE, J. 2016. A pharmacological inhibitor of NLRP3 inflammasome prevents non-alcoholic fatty liver disease in a mouse model induced by high fat diet. *Scientific Reports,* 6**,** 24399.

YANG, L., GARCIA CANAVERAS, J. C., CHEN, Z., WANG, L., LIANG, L., JANG, C., MAYR, J. A., ZHANG, Z., GHERGUROVICH, J. M., ZHAN, L., JOSHI, S., HU, Z., MCREYNOLDS, M. R., SU,

X., WHITE, E., MORSCHER, R. J. & RABINOWITZ, J. D. 2020a. Serine Catabolism Feeds NADH when Respiration Is Impaired. *Cell Metabolism,* 31**,** 809-821.e6.
YANG, M. & VOUSDEN, K. H. 2016. Serine and one-carbon metabolism in cancer. *Nat Rev Cancer,* 16**,** 650-62.
YANG, Y., ZHANG, N., ZHANG, G. & SAUVE, A. A. 2020b. NRH salvage and conversion to NAD+ requires NRH kinase activity by adenosine kinase. *Nature Metabolism,* 2**,** 364-379.
YATES, M. S., DOLAN, P. M., SHIN, S., KENSLER, T. W., TRAN, Q. T., SUTTER, T. R., OSBURN, W. O., MCCULLOCH, C. C., SILKWORTH, J. B., TAGUCHI, K., YAMAMOTO, M., WILLIAMS, C. R., LIBY, K. T. & SPORN, M. B. 2009. Genetic versus chemoprotective activation of Nrf2 signaling: overlapping yet distinct gene expression profiles between Keap1 knockout and triterpenoid-treated mice. *Carcinogenesis,* 30**,** 1024-1031.
YE, J., FAN, J., VENNETI, S., WAN, Y.-W., PAWEL, B. R., ZHANG, J., FINLEY, L. W. S., LU, C., LINDSTEN, T., CROSS, J. R., QING, G., LIU, Z., SIMON, M. C., RABINOWITZ, J. D. & THOMPSON, C. B. 2014. Serine Catabolism Regulates Mitochondrial Redox Control during Hypoxia. *Cancer Discovery,* 4**,** 1406.
YEN, C.-L. E., STONE, S. J., KOLIWAD, S., HARRIS, C. & FARESE, R. V., JR. 2008. Thematic review series: glycerolipids. DGAT enzymes and triacylglycerol biosynthesis. *Journal of lipid research,* 49**,** 2283-2301.
YEN, M. C., KAN, J. Y., HSIEH, C. J., KUO, P. L., HOU, M. F. & HSU, Y. L. 2017. Association of long-chain acyl-coenzyme A synthetase 5 expression in human breast cancer by estrogen receptor status and its clinical significance. *Oncol Rep,* 37**,** 3253-3260.
YET, S. F., LAYNE, M. D., LIU, X., CHEN, Y. H., ITH, B., SIBINGA, N. E. & PERRELLA, M. A. 2003. Absence of heme oxygenase-1 exacerbates atherosclerotic lesion formation and vascular remodeling. *Faseb j,* 17**,** 1759-61.
YIN, J., REN, W., HUANG, X., DENG, J., LI, T. & YIN, Y. 2018. Potential Mechanisms Connecting Purine Metabolism and Cancer Therapy. *Frontiers in Immunology,* 9.
YOO, S., KIM, K., NAM, H. & LEE, D. 2018. Discovering Health Benefits of Phytochemicals with Integrated Analysis of the Molecular Network, Chemical Properties and Ethnopharmacological Evidence. *Nutrients,* 10.
YOON, H. S., CHO, C. H., YUN, M. S., JANG, S. J., YOU, H. J., KIM, J.-H., HAN, D., CHA, K. H., MOON, S. H., LEE, K., KIM, Y.-J., LEE, S.-J., NAM, T.-W. & KO, G. 2021. Akkermansia muciniphila secretes a glucagon-like peptide-1-inducing protein that improves glucose homeostasis and ameliorates metabolic disease in mice. *Nature Microbiology*.
YOUNOSSI, Z., ANSTEE, Q. M., MARIETTI, M., HARDY, T., HENRY, L., ESLAM, M., GEORGE, J. & BUGIANESI, E. 2018. Global burden of NAFLD and NASH: trends, predictions, risk factors and prevention. *Nature Reviews Gastroenterology & Hepatology,* 15**,** 11-20.
YU, M., LI, H., LIU, Q., LIU, F., TANG, L., LI, C., YUAN, Y., ZHAN, Y., XU, W., LI, W., CHEN, H., GE, C., WANG, J. & YANG, X. 2011a. Nuclear factor p65 interacts with Keap1 to repress the Nrf2-ARE pathway. *Cell Signal,* 23**,** 883-92.
YU, X., LIANG, X., XIE, H., KUMAR, S., RAVINDER, N., POTTER, J., DE MOLLERAT DU JEU, X. & CHESNUT, J. D. 2016. Improved delivery of Cas9 protein/gRNA complexes using lipofectamine CRISPRMAX. *Biotechnol Lett,* 38**,** 919-29.
YU, Z., SHAO, W., CHIANG, Y., FOLTZ, W., ZHANG, Z., LING, W., FANTUS, I. G. & JIN, T. 2011b. Oltipraz upregulates the nuclear factor (erythroid-derived 2)-like 2 [corrected](NRF2) antioxidant system and prevents insulin resistance and obesity induced by a high-fat diet in C57BL/6J mice. *Diabetologia,* 54**,** 922-34.
YUAN, L. & KAPLOWITZ, N. 2009. Glutathione in liver diseases and hepatotoxicity. *Molecular Aspects of Medicine,* 30**,** 29-41.
ZANDANI, G., KAFTORI-SANDLER, N., SELA, N., NYSKA, A. & MADAR, Z. 2021. Dietary broccoli improves markers associated with glucose and lipid metabolism through modulation of gut microbiota in mice. *Nutrition***,** 111240.

ZEILINGER, K., FREYER, N., DAMM, G., SEEHOFER, D. & KNÖSPEL, F. 2016. Cell sources for in vitro human liver cell culture models. *Experimental biology and medicine (Maywood, N.J.),* 241**,** 1684-1698.

ZHANG, C., SU, Z. Y., KHOR, T. O., SHU, L. & KONG, A. N. 2013a. Sulforaphane enhances Nrf2 expression in prostate cancer TRAMP C1 cells through epigenetic regulation. *Biochem Pharmacol,* 85**,** 1398-404.

ZHANG, D. D. & HANNINK, M. 2003. Distinct cysteine residues in Keap1 are required for Keap1-dependent ubiquitination of Nrf2 and for stabilization of Nrf2 by chemopreventive agents and oxidative stress. *Mol Cell Biol,* 23**,** 8137-51.

ZHANG, H. Q., CHEN, S. Y., WANG, A. S., YAO, A. J., FU, J. F., ZHAO, J. S., CHEN, F., ZOU, Z. Q., ZHANG, X. H., SHAN, Y. J. & BAO, Y. P. 2016. Sulforaphane induces adipocyte browning and promotes glucose and lipid utilization. *Mol Nutr Food Res,* 60**,** 2185-2197.

ZHANG, WEN C., SHYH-CHANG, N., YANG, H., RAI, A., UMASHANKAR, S., MA, S., SOH, BOON S., SUN, LI L., TAI, BEE C., NGA, MIN E., BHAKOO, KISHORE K., JAYAPAL, SENTHIL R., NICHANE, M., YU, Q., AHMED, DOKEU A., TAN, C., SING, WONG P., TAM, J., THIRUGANANAM, A., NOGHABI, MONIREH S., HUEI PANG, Y., ANG, HAW S., MITCHELL, W., ROBSON, P., KALDIS, P., SOO, ROSS A., SWARUP, S., LIM, ELAINE H. & LIM, B. 2012a. Glycine Decarboxylase Activity Drives Non-Small Cell Lung Cancer Tumor-Initiating Cells and Tumorigenesis. *Cell,* 148**,** 259-272.

ZHANG, Y.-K. J., WU, K. C. & KLAASSEN, C. D. 2013b. Genetic Activation of Nrf2 Protects against Fasting-Induced Oxidative Stress in Livers of Mice. *PLOS ONE,* 8**,** e59122.

ZHANG, Y. 2000. Role of glutathione in the accumulation of anticarcinogenic isothiocyanates and their glutathione conjugates by murine hepatoma cells. *Carcinogenesis,* 21**,** 1175-82.

ZHANG, Y., GILMOUR, A., AHN, Y. H., DE LA VEGA, L. & DINKOVA-KOSTOVA, A. T. 2019. The isothiocyanate sulforaphane inhibits mTOR in an NRF2-independent manner. *Phytomedicine***,** 153062.

ZHANG, Y., KOLM, R. H., MANNERVIK, B. & TALALAY, P. 1995. Reversible conjugation of isothiocyanates with glutathione catalyzed by human glutathione transferases. *Biochem Biophys Res Commun,* 206**,** 748-55.

ZHANG, Y. & TALALAY, P. 1998. Mechanism of differential potencies of isothiocyanates as inducers of anticarcinogenic Phase 2 enzymes. *Cancer Res,* 58**,** 4632-9.

ZHANG, Y., TALALAY, P., CHO, C. G. & POSNER, G. H. 1992. A major inducer of anticarcinogenic protective enzymes from broccoli: isolation and elucidation of structure. *Proc Natl Acad Sci U S A,* 89**,** 2399-403.

ZHANG, Y. K., WU, K. C., LIU, J. & KLAASSEN, C. D. 2012b. Nrf2 deficiency improves glucose tolerance in mice fed a high-fat diet. *Toxicol Appl Pharmacol,* 264**,** 305-14.

ZHANG, Y. K., YEAGER, R. L., TANAKA, Y. & KLAASSEN, C. D. 2010. Enhanced expression of Nrf2 in mice attenuates the fatty liver produced by a methionine- and choline-deficient diet. *Toxicol Appl Pharmacol,* 245**,** 326-34.

ZHANG, Z., WANG, S., ZHOU, S., YAN, X., WANG, Y., CHEN, J., MELLEN, N., KONG, M., GU, J., TAN, Y., ZHENG, Y. & CAI, L. 2014. Sulforaphane prevents the development of cardiomyopathy in type 2 diabetic mice probably by reversing oxidative stress-induced inhibition of LKB1/AMPK pathway. *J Mol Cell Cardiol,* 77**,** 42-52.

ZHAO, H., CHIARO, C. R., ZHANG, L., SMITH, P. B., CHAN, C. Y., PEDLEY, A. M., PUGH, R. J., FRENCH, J. B., PATTERSON, A. D. & BENKOVIC, S. J. 2015. Quantitative analysis of purine nucleotides indicates that purinosomes increase de novo purine biosynthesis. *The Journal of biological chemistry,* 290**,** 6705-6713.

ZHAO, L., GUO, X., WANG, O., ZHANG, H., WANG, Y., ZHOU, F., LIU, J. & JI, B. 2016. Fructose and glucose combined with free fatty acids induce metabolic disorders in HepG2 cell: A new model to study the impacts of high-fructose/sucrose and high-fat diets in vitro. *Mol Nutr Food Res,* 60**,** 909-21.

ZHENG, J. 2012. Energy metabolism of cancer: Glycolysis versus oxidative phosphorylation (Review). *Oncol Lett,* 4**,** 1151-1157.

ZHOU, J. W., WANG, M., SUN, N. X., QING, Y., YIN, T. F., LI, C. & WU, D. 2019. Sulforaphane-induced epigenetic regulation of Nrf2 expression by DNA methyltransferase in human Caco-2 cells. *Oncol Lett,* 18**,** 2639-2647.

ZIELKE, H. R., ZIELKE, C. L. & OZAND, P. T. 1984. Glutamine: a major energy source for cultured mammalian cells. *Fed Proc,* 43**,** 121-5.

ZOU, G.-L., ZHANG, X.-R., MA, Y.-L., LU, Q., ZHAO, R., ZHU, Y.-Z. & WANG, Y.-Y. 2020a. The role of Nrf2/PIWIL2/purine metabolism axis in controlling radiation-induced lung fibrosis. *American journal of cancer research,* 10**,** 2752-2767.

ZOU, Z., TAO, T., LI, H. & ZHU, X. 2020b. mTOR signaling pathway and mTOR inhibitors in cancer: progress and challenges. *Cell & Bioscience,* 10**,** 31.

ŻURYŃ, A., LITWINIEC, A., SAFIEJKO-MROCZKA, B., KLIMASZEWSKA-WIŚNIEWSKA, A., GAGAT, M., KRAJEWSKI, A., GACKOWSKA, L. & GRZANKA, D. 2016. The effect of sulforaphane on the cell cycle, apoptosis and expression of cyclin D1 and p21 in the A549 non-small cell lung cancer cell line. *Int J Oncol,* 48**,** 2521-2533.

Appendix

Appendix:

This figure is regarding the data in chapter 4

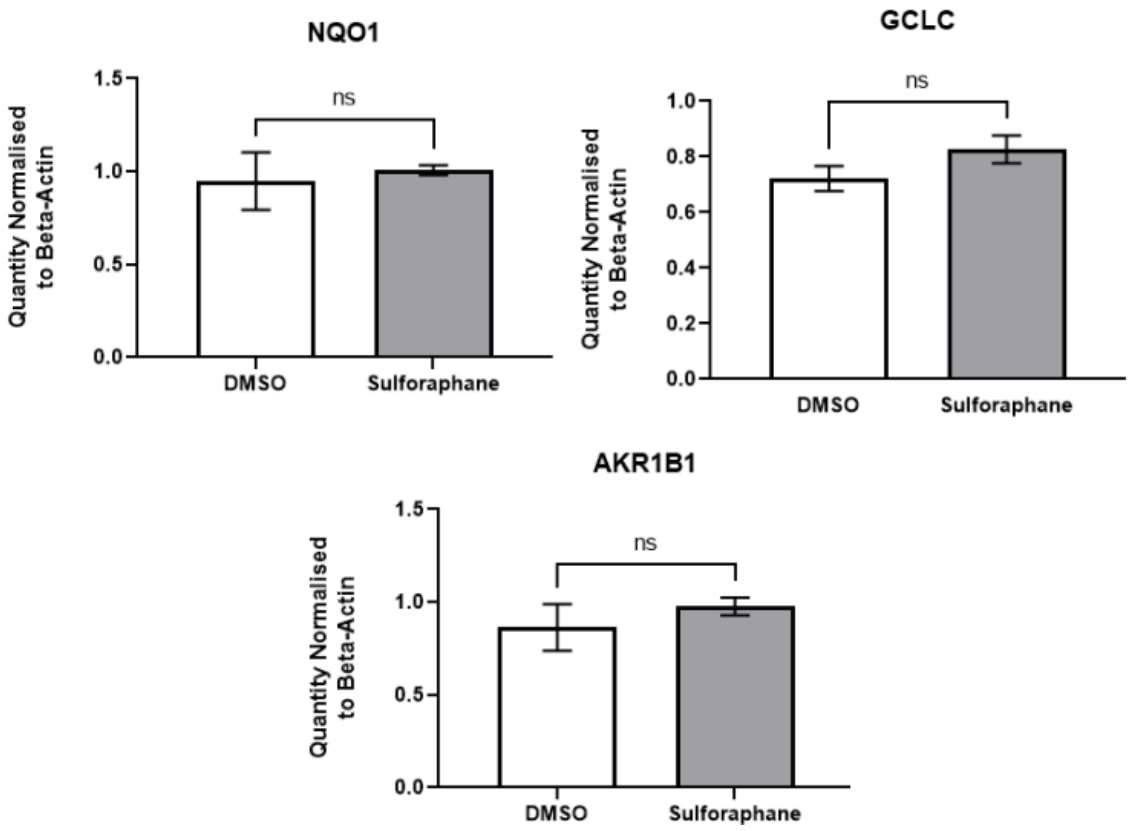

Figure S1.SF does not induce genes related to the antioxidant response in a no glucose environment. HepG2 cells were cultured with 4 mM glutamine and 1 mM pyruvate in a no glucose environment. RNA was extracted after 24 h SF treatment before gene expression was assayed by qRT-PCR. Samples were normalized to the Housekeeping control beta-actin, and mRNA fold change was determined by dividing each normalized treatment by the average of the normalized control. All values are expressed as mean ± SD from three independent wells. Statistical analysis was determined by a t-test between treatment compared to its respective control

This table is regarding the data in chapter 4

Table S1 Pathway analysis of differentially expressed genes in response to SF under various glucose environments analyzed through the KEGG database

	No Glucose Control vs Sulforaphane			Basal Glucose Control vs Sulforaphane			High Glucose Controls vs Sulforaphane		
KEGG	**SIZE**	**NES**	**FDR q value**	**SIZE**	**NES**	**FDR q value**	**SIZE**	**NES**	**FDR q value**
ABC TRANSPORTERS	27	-0.991	0.615	27	1.285	0.380	27	1.540	0.099
ACUTE MYELOID LEUKEMIA	46	1.287	0.174	46	1.119	0.500	46	1.503	0.108
ADHERENS JUNCTION	55	1.960	**0.005**	55	0.932	0.680	55	1.015	0.534
ADIPOCYTOKINE SIGNALING PATHWAY	47	-0.922	0.748	47	1.366	0.317	47	1.530	0.102
ALANINE ASPARTATE AND GLUTAMATE METABOLISM	26	-1.787	**0.008**	26	-1.653	**0.050**	26	-1.522	0.288
ALDOSTERONE REGULATED SODIUM REABSORPTION	23	-0.881	0.817	23	-0.837	0.849	23	-1.089	0.561
ALZHEIMERS DISEASE	114	-1.151	0.349	114	0.841	0.830	114	1.248	0.272
AMINO SUGAR AND NUCLEOTIDE SUGAR METABOLISM	36	-0.880	0.804	36	1.091	0.525	36	1.488	0.107
AMINOACYL TNRA BIOSYNTHESIS	38	-0.622	0.991	38	1.169	0.456	38	1.295	0.238
AMYOTROPHIC LATERAL SCLEROSIS ALS	33	-0.983	0.622	33	-0.760	0.901	33	1.127	0.384
ANTIGEN PROCESSING AND PRESENTATION	36	-1.312	0.170	36	-0.872	0.833	36	1.028	0.513
APOPTOSIS	67	0.973	0.587	67	1.619	0.085	67	1.633	0.059
ARACHIDONIC ACID METABOLISM	22	-1.483	0.073	22	-1.092	0.545	22	-1.106	0.590
ARGININE AND PROLINE METABOLISM	41	-2.192	**0.000**	41	-0.993	0.688	41	1.242	0.275
ARRHYTHMOGENIC RIGHT VENTRICULAR CARDIOMYOPATHY ARVC	36	1.656	0.053	36	0.999	0.596	36	1.571	0.083
AXON GUIDANCE	84	-0.861	0.818	84	-1.558	0.114	84	-1.159	0.658
B CELL RECEPTOR SIGNALLING PATHWAY	45	1.293	0.171	45	0.980	0.616	45	1.192	0.318

BASAL CELL CARCINOMA	30	0.732	0.935	30	-1.295	0.350	30	-1.143	0.650
BASAL TRANSCRIPTION FACTORS	28	0.924	0.674	28	1.003	0.599	28	1.111	0.400
BASE EXCISION REPAIR	31	-0.872	0.810	31	-1.012	0.663	31	-1.092	0.570
BETA ALANINE METABOLISM	15	-1.565	**0.050**	15	-0.889	0.809	15	-0.948	0.645
BLADDER CANCER	33	-0.805	0.881	33	-1.055	0.602	33	-1.103	0.578
BUTANOATE METABOLISM	26	-1.361	0.126	26	-1.306	0.339	26	-1.289	0.475
CALCIUM SIGNALING PATHWAY	66	0.811	0.838	66	-1.333	0.338	66	-1.006	0.582
CARDIAC MUSCLE CONTRACTION	37	-1.634	**0.030**	37	-0.848	0.839	37	1.032	0.534
CELL ADHESION MOLECULES CAMS	59	-1.435	0.089	59	-1.161	0.456	59	-0.859	0.776
CELL CYCLE	114	1.271	0.183	114	-1.196	0.450	114	-1.340	0.397
CHEMOKINE SIGNALING PATHWAY	90	1.417	0.117	90	-1.278	0.351	90	0.801	0.867
CHRONIC MYELOID LEUKEMIA	63	1.304	0.163	63	1.215	0.409	63	1.373	0.196
CITRATE CYCLE TCA CYCLE	29	-1.239	0.247	29	-1.241	0.408	29	0.719	0.952
COLORECTAL CANCER	52	1.189	0.265	52	-0.870	0.826	52	1.114	0.401
COMPLEMENT AND COAGULATION CASCADES	48	-2.182	**0.000**	48	-1.309	0.347	48	-1.322	0.414
CYSTEINE AND METHIONINE METABOLISM	29	1.100	0.380	29	-0.863	0.830	29	1.131	0.384
CYTOKINE CYTOKINE RECEPTOR METABOLISM	86	-1.136	0.360	86	1.704	**0.050**	86	1.748	**0.023**
CYTOSOLIC DNA SENSING PATHWAY	26	-1.366	0.125	26	1.388	0.322	26	1.617	0.066
DILATED CARDIOMYOPAHTY	40	1.355	0.147	40	-0.988	0.676	40	1.359	0.195
DNA REPLICATION	32	-0.800	0.862	32	-1.771	**0.030**	32	-1.516	0.241
DORSO VENTRAL AXIS FORMATION	16	1.661	0.054	16	-0.918	0.765	16	1.015	0.528
DRUG METABOLISM CYTOCHROME P450	23	-1.863	**0.003**	23	0.922	0.691	23	-1.136	0.618
DRUG METABOLISM OTHER ENZYMES	22	-1.475	0.075	22	1.292	0.384	22	1.515	0.103
ECM RECEPTOR INTERACTION	44	1.363	0.143	44	-1.319	0.341	44	1.200	0.309
ENDOCYTOSIS	140	1.577	0.069	140	1.134	0.478	140	0.901	0.713
ENDOMETRIAL CANCER	45	1.369	0.141	45	-1.108	0.529	45	-0.967	0.617

EPITHELIAL CELL SIGNALLING IN HELICOBATER PYLORI INFECTION	51	1.892	**0.011**	51	1.832	**0.018**	51	2.088	**0.001**
ERBB SIGNALING PATHWAY	65	1.558	0.069	65	0.881	0.760	65	0.986	0.582
ETHER LIPID METABOLISM	17	-1.559	**0.048**	17	-1.321	0.351	17	-1.445	0.279
FATTY ACID METABOLISM	31	-1.648	**0.027**	31	-0.989	0.687	31	-0.996	0.569
FC EPSILON R MEDIATED PHAGOCYTOSIS	47	1.273	0.184	47	-1.180	0.454	47	-1.005	0.561
FC GAMMA R MEDIATED PHAGOCYTOSIS	62	1.635	0.059	62	-1.016	0.663	62	-1.053	0.586
FOCAL ADHESION	128	2.043	**0.001**	128	-1.371	0.344	128	1.218	0.293
FRUCTOSE AND MANNOSE METABOLISM	27	1.000	0.542	27	1.154	0.446	27	1.790	**0.022**
GALACTOSE METABOLISM	20	-1.015	0.572	20	-1.125	0.519	20	1.184	0.323
GAP JUNCTION	49	1.860	**0.013**	49	-1.154	0.461	49	-0.765	0.893
GLIOMA	47	1.194	0.263	47	0.958	0.643	47	0.916	0.699
GLUTATHIONE METABOLISM	35	-1.255	0.231	35	1.814	**0.016**	35	2.059	**0.000**
GLYCEROLIPID METABOLISM	27	-1.806	**0.006**	27	-1.436	0.242	27	-1.178	0.628
GLYCEROPHOSPHOLIPID METABOLISM	49	-1.866	**0.003**	49	-1.501	0.181	49	-1.028	0.601
GLYCINE SERINE AND THREONINE METABOLSIM	26	-2.086	**0.000**	26	-1.757	**0.027**	26	-1.738	**0.047**
GLYCOLYSIS GLUCONEOGENSIS	41	-1.438	0.090	41	-1.683	0.054	41	-1.122	0.608
GLYCOSAMINOGLYCAN BIOSYNTHESIS CHONDROITIN SULFATE	16	-0.834	0.842	16	-0.863	0.820	16	-0.838	0.787
GLYCOSAMINOGLYCAN BIOSYNTHESIS HEPARAN SULFATE	16	0.903	0.711	16	-0.957	0.707	16	-0.874	0.762
GLYCOSAMINOGLYCAN DEGRADATION	15	1.149	0.315	15	1.235	0.399	15	1.222	0.294
GLYCOSPHINGOLD BIOSYNTHESIS LACTO AND NEOLACTO SERIES	16	-1.016	0.581	16	1.168	0.443	16	1.478	0.110
GLYCOSPHOSPHATIDYL INOSTIOL GPI ANCHOR BIOSYNTHESIS	23	-0.449	0.999	23	-0.814	0.861	23	-1.057	0.609

GNRH SIGNALLING PATHWAY	61	1.612	0.067	61	-1.439	0.256	61	-1.041	0.586
HEDGEHOG SIGNALLING PATHWAY	25	1.240	0.210	25	-1.092	0.535	25	-1.054	0.600
HEMATOPOIETIC CELL LINAGE	28	-0.776	0.887	28	-1.173	0.459	28	0.943	0.646
HISTIDINE METABOLISM	19	-2.016	**0.001**	19	-1.670	0.052	19	-1.864	**0.010**
HOMOLOGOUS RECOMBINATIO N	22	0.817	0.838	22	-1.223	0.438	22	-1.236	0.508
HUNTINGTONS DISEASES	137	-1.410	0.105	137	-0.527	0.995	137	1.180	0.324
HYPERTROPHIC CARDIOMYOPAT HY HCM	38	1.342	0.145	38	1.391	0.343	38	1.437	0.133
INOSITOL PHOSPHATE METABOLISM	43	1.346	0.147	43	-1.287	0.355	43	-1.149	0.658
INSULIN SIGNALING PATHWAY	102	1.034	0.489	102	-1.108	0.538	102	-1.212	0.550
JAK STAT SIGNALING PATHWAY	76	1.590	**0.066**	76	1.319	0.347	76	1.363	0.202
LEISHMANIA INFECTION	32	1.018	0.514	32	1.266	0.367	32	1.598	0.074
LEUKOCYTE TRANSENDOTHE LIAL MIGRATION	67	1.766	**0.032**	67	-0.963	0.716	67	1.260	0.268
LONG TERM DEPRESSION	33	1.538	0.073	33	-0.998	0.686	33	-0.857	0.767
LONG TERM POTENTIATION	38	1.671	0.058	38	-0.628	0.986	38	0.712	0.947
LYSINE DEGRADATION	36	-1.542	0.053	36	-1.814	**0.026**	36	-1.281	0.467
LYSOSOME	98	1.243	0.211	98	1.020	0.611	98	1.162	0.347
MAPK SIGNALING PATHWAY	166	1.535	0.071	166	-1.080	0.552	166	1.302	0.245
MELANOGENESI S	54	1.416	0.115	54	-1.364	0.340	54	-1.115	0.608
MELANOMA	42	1.119	0.358	42	0.980	0.604	42	0.912	0.697
METABOLISM OF XENOBIOTICS BY CYTOCHROME P450	24	-1.623	**0.031**	24	1.734	**0.041**	24	1.802	**0.021**
MISMATCH REPIAR	21	0.729	0.927	21	-1.262	0.374	21	-1.013	0.607
MTOR SIGNALING PATHWAY	41	1.388	0.127	41	-0.756	0.895	41	0.623	0.977
N GLYCAN BIOSYNTHESIS	38	1.472	0.098	38	1.436	0.304	38	1.348	0.203
NATURAL KILLER CELL MEDIATED CYTOTOXICITY	64	1.105	0.378	64	1.035	0.589	64	1.299	0.237
NEUROACTIVE LIGAND RECEPTOR INTERACTION	35	0.832	0.831	35	1.106	0.515	35	1.225	0.295
NEUROTROPHIN SIGNALING PATHWAY	95	1.393	0.127	95	0.911	0.705	95	0.898	0.711

NITROGEN METABOLISM	16	-1.160	0.343	16	-1.663	0.051	16	-1.468	0.304
NOD LIKE RECEPTOR SIGNALING PATHWAY	35	1.349	0.147	35	1.282	0.351	35	1.401	0.167
NON SMALL CELL LUNG CANCER	45	1.157	0.306	45	-0.927	0.755	45	-1.010	0.586
NOTCH SIGNALING PATHWAY	38	0.899	0.712	38	-1.022	0.662	38	-0.895	0.730
NUCLEOTIDE EXCISION REPAIR	41	0.836	0.834	41	-0.982	0.680	41	0.869	0.756
ONE CARBON POOL BY FOLATE	16	-1.466	0.079	16	1.321	0.364	16	1.722	**0.026**
OOCYTE MEIOSIS	79	1.593	0.068	79	-1.287	0.344	79	-1.349	0.406
OXIDATIVE PHOSPHORYLATION	90	-1.382	0.115	90	0.744	0.925	90	1.821	**0.020**
P53 SIGNALING PATHWAY	58	-1.171	0.338	58	-1.041	0.625	58	-1.053	0.572
PANCREATIC CANCER	57	1.034	0.495	57	0.992	0.601	57	1.104	0.407
PARKINSONS DISEASE	89	-1.702	**0.019**	89	-0.777	0.888	89	1.449	0.132
PATHOGENIC ESCHERICHIA COLI INFECTION	38	1.443	0.101	38	1.217	0.422	38	1.489	0.110
PATHWAYS IN CANCER	220	1.464	0.096	220	-0.944	0.727	220	-0.913	0.706
PENTOSE PHOSPHATE PATHWAY	20	-0.713	0.948	20	1.091	0.538	20	1.582	0.080
PEROXISOME	62	-1.456	0.082	62	-1.164	0.468	62	-1.138	0.637
PHOSPHATIDYLINOSTIOL SIGNALING SYSTEM	54	1.463	0.094	54	-1.212	0.440	54	-1.239	0.529
PORPHRYIN AND CHOLOROPHYLL METABOLISM	23	-1.484	0.075	23	1.079	0.525	23	1.270	0.259
PPAR SIGNALING PATHWAY	46	-1.524	0.059	46	-1.162	0.464	46	-1.089	0.545
PRIMARY IMMUNODEFICIENCY	15	-1.562	**0.049**	15	1.183	0.438	15	1.099	0.404
PRION DISEASES	22	1.527	0.073	22	1.636	0.084	22	1.775	**0.023**
PROGESTERONE MEDIATED OOCYTE MATURATION	64	1.322	0.155	64	-1.348	0.357	64	-1.094	0.582
PROPANOATE METABOLISM	27	-1.512	0.062	27	-1.115	0.532	27	-1.426	0.260
PROSTATE CANCER	72	1.491	0.092	72	-0.835	0.831	72	1.101	0.405
PROTEASOME	35	-0.891	0.810	35	1.935	**0.009**	35	2.204	**0.000**
PROTEIN EXPORT	22	1.566	0.068	22	1.862	**0.015**	22	1.502	0.103
PURINE METABOLISM	98	-1.387	0.114	98	1.012	0.617	98	1.287	0.239

PYRIMIDINE METABOLISM	72	-1.649	**0.029**	72	1.007	0.604	72	1.029	0.525
PYRUVATE METABOLISM	30	-1.730	0.015	30	-1.408	0.281	30	-1.444	0.248
REGULATION OF ACTIN CYTOSKELETON	136	1.990	**0.005**	136	-1.192	0.438	136	0.959	0.619
REGULATION OF AUTOPHAGY	18	1.471	0.095	18	1.282	0.367	18	0.804	0.872
RENAL CELL CARCINOMA	56	1.754	0.031	56	1.247	0.389	56	1.211	0.299
RETINOL METABOLSIM	18	-2.027	**0.000**	18	-0.837	0.840	18	-0.750	0.898
RIBOSOME	77	-2.479	**0.000**	77	-0.813	0.852	77	1.706	**0.030**
RIG I LIKE RECEPTROR SIGNALING PATHWAY	44	-0.847	0.833	44	1.379	0.315	44	1.254	0.269
RNA DEGRADATION	54	1.316	0.158	54	0.813	0.853	54	1.031	0.528
RNA POLYMERASE	24	-1.213	0.278	24	0.951	0.647	24	1.360	0.198
SELNOAMINO ACID METABOLISM	19	-1.402	0.107	19	-0.890	0.817	19	1.028	0.520
SMALL CELL LUNG CANCER	69	1.479	0.097	69	1.008	0.613	69	0.960	0.624
SNARE INTERACTIONS IN VESICULAR TRANSPORT	33	1.078	0.415	33	0.665	0.959	33	0.684	0.959
SPHINGOLIPID METABOLISM	30	1.407	0.119	30	1.198	0.435	30	0.775	0.897
SPLICEOSOME	115	0.954	0.613	115	1.072	0.528	115	1.311	0.238
STARCH AND SUCROSE METABOLISM	23	0.822	0.840	23	1.084	0.526	23	1.290	0.239
STEROID BIOSYNTHESIS	15	-1.141	0.357	15	-1.453	0.248	15	-1.456	0.290
STEROID HORMONE BIOSYNTHESIS	20	-1.169	0.334	20	1.393	0.373	20	1.524	0.102
SYSTEMIC LUPUS ERYTHEMATOSUS	54	-1.109	0.400	54	-2.293	**0.000**	54	-1.249	0.530
T CELL RECEPTOR SIGNALING PATHWAY	67	1.331	0.151	67	1.164	0.437	67	1.443	0.132
TGF BETA SIGNALING PATHWAY	57	1.566	0.071	57	1.195	0.425	57	1.316	0.239
THYROID CANCER	24	0.975	0.591	24	0.727	0.929	24	0.893	0.713
TIGHT JUNCTION	90	1.720	**0.041**	90	-1.193	0.447	90	1.134	0.384
TOLL LIKE RECEPTOR SIGNALING PATHWAY	57	1.668	0.054	57	1.366	0.296	57	1.756	**0.023**
TRYPTOPHAN METABOLISM	26	-2.066	**0.000**	26	-1.344	0.347	26	-1.128	0.616
TYPE II DIBAETES MELLITUS	26	-0.805	0.868	26	-1.107	0.520	26	-1.106	0.610
TYROSINE METABOLISM	23	-1.873	**0.004**	23	0.831	0.835	23	1.302	0.240

UBIQUITIN MEDIATED PROTEOLYSIS	121	1.593	0.073	121	-0.792	0.875	121	-1.018	0.609
VALINE LEUCINE AND ISOLECUINE DEGRADATION	41	-1.697	**0.019**	41	-1.623	0.063	41	-1.593	0.192
VASCULAR SMOOTH MUSCLE CONTRACTION	55	1.556	0.066	55	-1.338	0.342	55	-1.012	0.595
VASOPRESSIN REGULATED WATER REABSORPTION	30	0.960	0.608	30	-1.222	0.426	30	-0.708	0.926
VEGF SIGNALING PATHWAY	47	1.305	0.165	47	-0.959	0.712	47	0.961	0.630
VIBRIO CHOLERAE INFECTION	38	1.454	0.097	38	1.052	0.564	38	1.770	**0.022**
VIRAL MYOCARDITIS	36	0.712	0.931	36	0.799	0.863	36	1.151	0.360
WNT SIGNALING PATHWAY	97	1.342	0.147	97	-1.203	0.448	97	-1.006	0.571

This figure is regarding the data in chapter 5

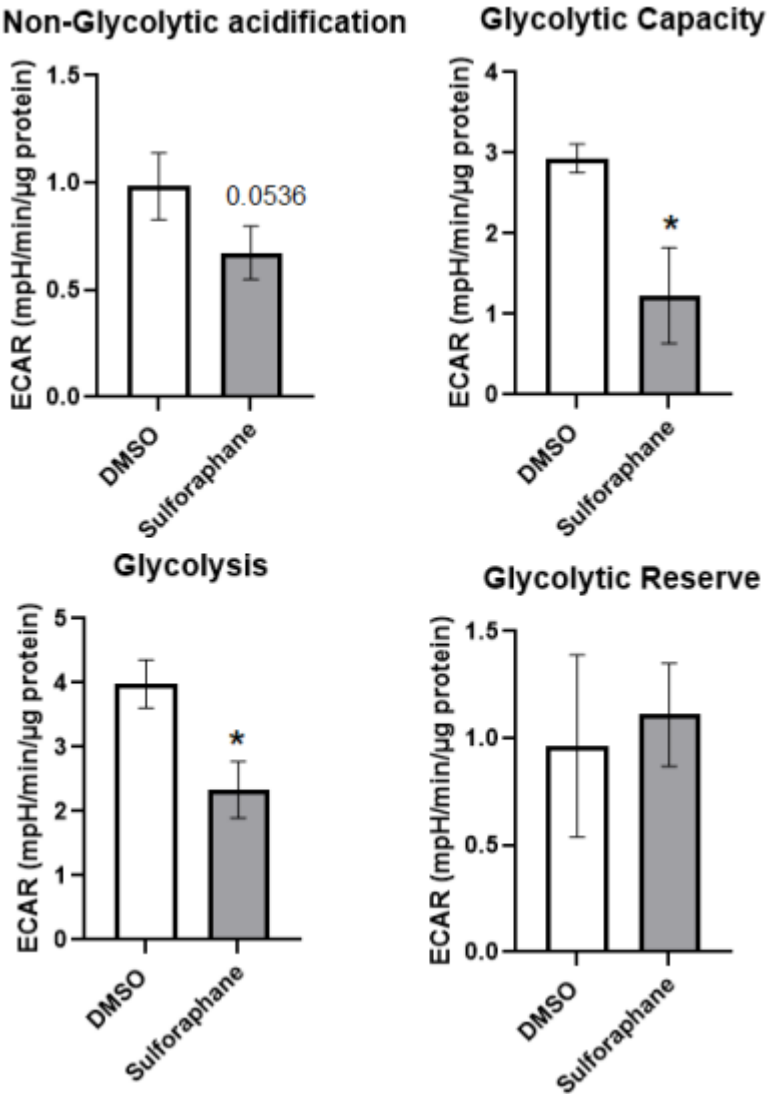

Figure S2. SF interfering with glycolysis in the basal glucose environment. HepG2 cells were treated with 10 µM SF for 24 h in basal (5.5 mM). Data files were generated from Wave software through the Seahorse Glycolysis Stress Test Report Generator. Values were then imported into GraphPad Prism and a t-test between DMSO vs Sulforphane was carried out. All values are expressed as mean ± SEM from three biological replicates. Samples were normalized to protein.

This figure is regarding the data in chapter 5

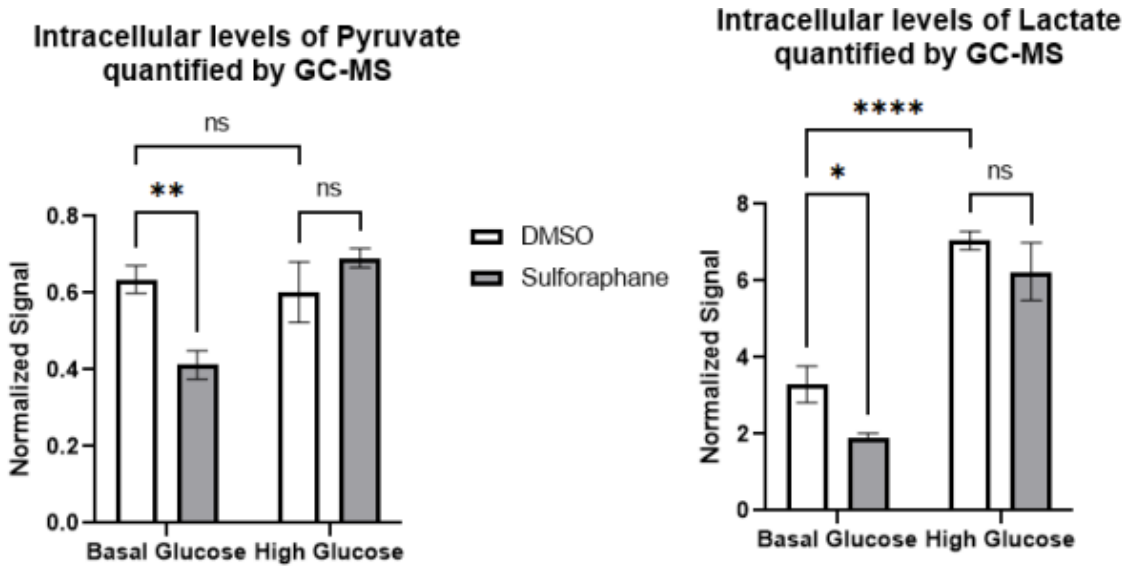

Figure S3. Figure 5.6 Untargeted metabolomics reveals SF interfering with glycolysis. HepG2 cells were treated with 10 µM SF for 24 h in basal glucose (5.5 mM) or high glucose (25 mM). After 24 h metabolites were extracted and quantified using GC-MS. C) Readings from the pyruvate and lactate from the heatmap were extracted and plotted into a bar plot. All values are expressed as mean ± SD from three biological replicates. 2-ANOVA was carried as the two factors are the treatment and glucose levels. **Pyruvate: basal glucose DMSO vs basal glucose SF p=0.047 and high glucose DMSO vs high glucose SF p=0.31. Lactate: basal glucose DMSO vs basal glucose SF p=0.017 and high glucose DMSO vs high glucose SF p=0.21**

This figure is regarding the data in chapter 5

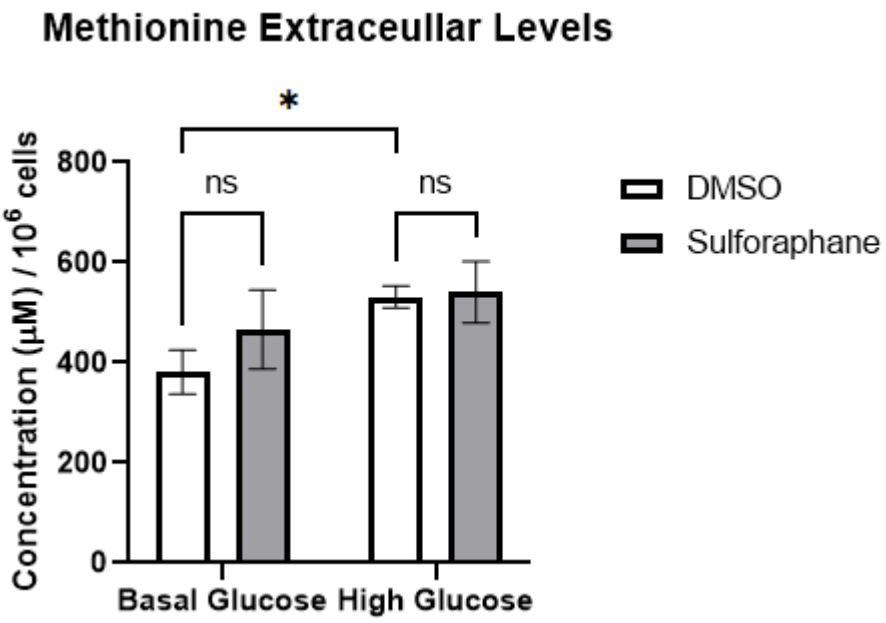

Figure S4. **LC-MS analysis reveals SF does not affect methionine extracellular levels.** HepG2 cells were treated with 10 µM SF for 24 h in basal (5.5 mM) and high glucose (25 mM). After 24 h metabolites were extracted and quantified using the LC-MS TripleQuad 6490 Agilent DMSO BG vs SF BG p=0.31, DMSO BG vs DMSO HG p=0.042, and DMSO HG vs SF HG p=0.99.